Biocontrol of biomolecular systems: polyhedral constraints on binding's regulation of catalysis from biocircuits to metabolism

Thesis by
Fangzhou Xiao

In Partial Fulfillment of the Requirements for the
Degree of
Doctor of Philosophy

CALIFORNIA INSTITUTE OF TECHNOLOGY
Pasadena, California

2022
Defended May 27th, 2022

Fangzhou Xiao
ORCID: 0000-0002-5001-5644

Acknowledgements

I am grateful for the opportunity to have fun and do research at Caltech in the past six years. How amazing my experience has been is best exemplified by the work contained in this thesis. This work is exactly what I hoped to achieve when I started at Caltech. In words from my PhD application: "I aspire to understand biological systems deeply and to develop technologies that enable rational design of biological machines. I view interpretable and predictive modeling of biological systems as the key to this goal." As a result, the ideas in thesis has a continuous trajectory from my first day at Caltech. So let me take this opportunity to thank everyone that inspired me during this journey by tracing chronologically how this work came into being. This makes it long, but fun.

I first thank Michael Dickinson. My chat with him in my first week here at Caltech ended with his suggestion that I should talk to John Doyle. I had no idea who this was, but I soon became captivated by the powerful ideas of John once I met him. Although I had no idea what was control theory or what are constraints and hard limits, I knew that this type of ideas were exactly what I was looking for.

Then I had a great year getting to know chemical reaction networks, control theory, and stochasticity. This was made possible by collaborating with Noah Olsman, who kindly took me in as his minion and passed down to me his great wisdom about research, life, John, and biological art styles. Thanks to the kindness of Erik Winfree, Rob Phillips, and Richard Murray, who later became my thesis committee members, I was able to hang out with their group members and got constant exposure to a wide spectrum of ideas about what theoretical descriptions of biology can be. In particular, I thank Andreés Ortiz Muñoz, William Poole, Rory Williams, and Andy Halleran for all the fun conversations that continue to inspire me, sometimes over great food. I also thank Vahe Galstyan, for his inspiring ideas, meticulous derivations, and beautiful cartoon drawings during our collaborations on taking kinetic proofreading to the wild west of other nonequilibrium mechanisms.

This first year also got me started on my first major work. The idea came from one of John's

frustrations, just like many great ideas. Robust perfect adaptation was well-understood in control theory, but did not seem to map to biocircuits in a straight-forward way. I took on this and did my first paper, which showed that biocircuits has different implementations of robust perfect adaptation compared to electric circuits because variables in biocircuits are molecule concentrations, therefore always positive. This work was my first attempt at using fundamental constraints to understand biological systems. It also shows how biology has distinct structures that are different from other engineering disciplines. I also thank John for suggesting me to go to the Winter Q-Bio conference in Maui, Hawaii that year, where I got to know my wife, Xinying (Cindy) Ren.

Continuing the train of thought from my first work that positivity of variables in biological systems make it distinct from other engineering systems, I wondered what other fundamental differences may exist. Through a joint project between John Doyle and Johan Paulsson, as well as a reading group organized by William Poole, Vipul Singhal and others in the Murray group, I got to know and actually understand Johan's work on the fundamental limit of noise suppression. The limit was based on assuming an input-output structure of biocircuits, while it appeared to me that many simple biocircuits do not satisfy this structure. This became my second work which showed that simple biocircuits violating the input-output structure can suppress noise beyond the fundamental limit. I thank Jiawei Yan for fun conversations during coneferences and collaborations on this project. I also thank Meichen Fang for taking up some complicated algebraic calculations in this work and making the experience of working together during the summer fun and pleasant.

With these two works showing that biology has distinct structures that are different from what is often assumed in existing theories from other disciplines, I became fixated by the idea of developing mathematical theories tailor-made for structures in biology. I thank Johan Paulsson for inspiring me through his many works that strive to capture structures in biology. I also thank Wenlong Ma, a roboticist, who had long and inspiring conversations with me to explain structural constraints of bipedal robots.

In my third year, I became frustrated by the vagueness of my ideas. That my ideas were vague also made it hard to have meaningful conversations with others and get feedback. That was when I had the opportunity to visit Mustafa Khammash group at ETH. I thank Mustafa for this wonderful opportunity that came right on time for me, as well as his care for me and my ideas. I needed a new environment as well as new people to talk to. Ideally, these new people would also care about my vague ideas. I was very lucky to have important feedback from Mustafa and his group members, such as Ankit Gupta and Maurice Filo. I am also grateful that Mustafa invited me to a computational biology workshop in southern

Switzerland, where I had the chance to talk to many other students and professors. These conversations were especially helpful in re-establishing my confidence in the direction I was going into. Among Mustafa's group members at the time, I thank Daniele Cappelletti in particular, for showing great interest in my vague ideas and patiently asking me to formulate my ideas in clearer and clearer languages, ideally mathematical ones. After enduring through a several-hour vague ranting session of me every week during my visit, Daniele has also become a wonderful collaborator on this thesis's work ever since. I again thank Mustafa for the opportunity to visit. The summer in Basel and float trips down the Rhine gave me rejuvenation that lasted a long time.

After I came back to Caltech, I had a much clearer idea in mind, with Daniele as a committed collaborator. In particular, the following ideas were taking shape: the core structure of biomolecular reactions are binding and catalysis, and reaction orders and structural regimes could capture bioregulatory profiles. So everything seemed to be in much better shape. This is when a wonderful collaboration with John Marken began, which made everything from great to fabulous. I thank John for appreciating my ideas, and doing work to infuse them with his own takes, while getting things closer to applications at the bench. The conversations with John has always been fun and inspiring. John's beautiful and thoughtful presentations have also been a great inspiration for me. Thanks to the support from John Doyle and Richard Murray, John Marken and I had the opportunity to bring our work to the winter Q-Bio conference that year. I had helpful feedbacks from other conference attendees, and had fruitful conversations with John Marken and Anish Sarma, facilitated by the Hawaiian breeze.

During the fourth year, despite COVID, I and my collaborators, John Marken and Daniele Cappelletti, carried on with the momentum and generated much work. Along the way, I was also fortunate to have further collaborators. I thank Gabe Salmon, for inspiring collaborations and the conversationsthat are always fun and inspiring, e.g. about average versus bounds. I am grateful for all the food and fun conversations of the KoaLAG team (with John Marken and Gabe Salmon). And some research collaborations, of course.

For most of that year, I was trying to build as wide as possible a foundation based on reaction orders and binding and catalysis to show that the idea is fundamentally important. This was partly due to my fear that these ideas could be completely wrong and practically useless. On the side of reaction orders determining biocircuit stability, I tried to develop a dissipative control theory based on reaction orders to show that the connection between reaction orders and system dynamics is in some sense fundamental. I was lucky to have Riley Murray collaborating with me on this front. In particular, chatting with Riley on my

ideas was important in shaping this work, and Riley's expertise, especially on signomial optimization and entropy-like functions, was central to several directions of the dissipative control work. I am grateful for this collaboration. Around the same time, I was frustrated by failing to understand where the polyhedral shape of the reaction orders in binding networks came from. I thank Joel Tropp's suggestion to look into the Sherman-Morrison formula. This opened up the research direction on decomposition of log derivative operators as the fundamental reason for the polyhedral shape of the set of reaction orders. With these works on dissipativity based on reaction orders and decomposition of log derivative operators, I became more and more confident that the ideas of binding and catalysis and reaction orders were of fundamental importance.

Then came my fifth year. I am thankful that my mentor, John Doyle, motivated me to think about how to upgrade the flux balance analysis method that Tami Khazaei successfully applied to analyze hysteresis in a microbial community, so that it can model metabolism dynamics in addition to steady states. Given that reaction orders from binding's regulation of catalysis were at the center of my mind at the time, I naturally considered maybe fluxes should be controlled through the reaction orders, or exponents. Replacing one exponent with a model predictive controller in the glycolytic oscillations example indeed made it oscillate. This became the proof of concept for the idea of flux exponent control (FEC), that fluxes are controlled through exponents by the cell. When rushing to present this work to meet a grant deadline, I was lucky to have Jingshuang (Lisa) Li and Carmen Alonso helping me on developing FEC. In particular, Lisa was able to formulate the costs in an optimal control problem so that a cell living on glycolysis can exhibit growth arrest behaviors when hit by a shock. I am thankful that Lisa and Carmen were patient with me, since FEC was very messy at the time, and I was disoriented about how to interpret each variable and which constraints were important and which ones were not.

Later, as I continued to develop both the ideas of FEC and binding and catalysis, I am grateful that John Doyle deeply appreciated the FEC idea and supported my work strongly. This support is what made it possible for this thesis to take its current shape. On my (very late) candidacy, I thank Rob Phillips and Erik Winfree for providing me with candid feedback on my work so far. I particularly appreciate the suggestion that I should focus more on understanding and packaging the ideas so that they can be better explained. I am still far away from making these ideas clear and accessible, but I have been making steady efforts on this front.

Outside of this work, there are also lots of great experiences I have had at Caltech. I have always been inspired by the high-quality courses taught by awesome instructors here at

Caltech. I am honored to take the courses by Erik Winfree, Rob Phillips (both physical biology of the cell and the great human experiment), orders-of-magnitude physics by Sterl Phinney, numerous thought-provoking CMS courses by Andrew Start, Joel Tropp, and Venkat Chandrasekaran, and eye-opening biology courses by Joe Parker, Diane Newman, and Elliott Meyerowitz. I also had the fortunate experience of TAing two courses taught by Lior Pachter. I learned much from both TA experiences. Of course John Doyle's courses are also inspiring at the mind-blowing level. This is testified by that these courses, regardless of their numbering and titles, are mostly the same in content, yet I took them more than five times. There remain so many hidden gems in John's lecture slides awaiting heroic graduate students to discover them and make them shine.

During my years at Caltech, I am grateful for the close-knit atmosphere of the CMS and bioengineering departments that enables me to knock on a professor's door and chat about research. I was also able to hang around members of other groups, such as Winfree group, Phillips group, Murray group, Gradinaru group (namely Xinhong Chen and Xiaozhe Ding), and Elowitz group (namely Yitong Ma, Sheng Wang, and Ronghui Zhu). I am thankful to these important mental exchanges that keep me from drifting into the theoretical void and drag me back to the biological reality. The CDS tea every Wednesday afternoon has also been a great occasion, perhaps the only occasion, for me to regularly chat with other members of the Doyle group. This is made possible thanks to Monica Nolasco, to whom I am indebted for much tea-hour happiness and help on trips and reimbursements. I have also been fortunate to have friends sharing my love of food, namely Honglie Ning, Jin Sima, Wenlong Ma, John Marken, and Gabe Salmon.

I thank my family. My parents, Songfeng Bao and Ke Xiao, and my little sister, Fengyi Xiao, have always been supportive of my life and my career, by giving me the maximum freedom when things go well, and the maximum support when I feel frustrated. I also thank my wife, Xinying (Cindy) Ren. I am fortunate to meet you during my years at Caltech. Your humor and ingenuity continue to make my days.

Abstract

One eventual goal of bioengineering is to build complex biological machines that fully realize the unique potential of biotechnology, namely adaptation, survival, growth, and dominance. In order to do so, not only do we need theoretical understanding and reliable manufacturing of biological parts and components, we also need a systems theory that captures fundamental structures to obtain insight about the space of all possible behaviors when parts are put together. This enables us to understand what can and cannot be achieved. Examples from other engineering disciplines are Turing machines for computers, information channels for communication networks, linear input output systems for electrical circuits, and thermodynamics for heat engines. This work is an attempt at developing a systems theory tailored to biomolecular systems in cells. The results form the following statements.

Biomolecular systems are binding and catalysis reactions. Catalysis determines the direction of change, while binding regulates how the catalysis rates vary with reactant concentrations. Given a binding reaction network, the full range of regulatory profiles can be captured by the reaction orders of catalysis, which in turn is constrained in polyhedral sets determined by the stoichiometry of binding. This constitute a rule, that since cells control catalysis by binding, cells control catalysis rates by regulating reaction orders constrained in polyhedral sets. This rule has ramifications in several directions. On metabolism, by incorporating the constraint that reaction orders of metabolic fluxes, not the fluxes themselves, are controlled, we can predict metabolism dynamics directly from network stoichiometry, e.g. glycolytic oscillations and growth arrests. This is a fully dynamic upgrade of flux balance analysis, a popular constraint-based method to model metabolism. On systems biology, this rule derives a method of biocircuit analysis based on the full range of values that reaction orders can take. This allows discovery of necessary and sufficient conditions for a circuit to achieve a certain function, thus revealing regimes hidden by traditional methods of analysis. It also promotes holistic comparisons of different circuit implementations, e.g. activating versus repressing, thur enabling biocircuit design

where we know when a design will work, and when a design will fail. On dynamics and control of biocircuits, reaction order can work as a robust basis for stability, perfect adaptation, multistability, and oscillations. Lyapunov functions and dissipative control theory tailored for biomolecular systems are constructed based on reaction orders. On the mathematics of biology, it relates bioregulation to convex polyhedra, log derivative operator decompositions, and fundamental rules of calculus for positive variables.

TABLE OF CONTENTS

LIST OF ILLUSTRATIONS

Part I

Part 1. Essays on biology

Chapter 1

Introduction: constraints and hard limits, systems theory, and biocontrol

This thesis makes two main contributions to understanding biomolecular systems in cells. One, biomolecular systems consist of two types of reactions, namely binding and catalysis reactions. Like mass and force constitute the core structure of mechanical components, binding and catalysis constitute the core structure of biomolecular reactions in cells. Catalysis determines the direction of change (in molecule concentrations), while binding governs how the catalysis fluxes are regulated (by molecule concentrations). The regulatory profile of catalysis fluxes is therefore determined by the network of binding reactions. Because the regulation of catalysis fluxes by molecule concentrations requires solving intractable systems of polynomial equations from the steady states of binding networks, previously this can only be determined for specific scenarios under restrictive assumptions, e.g. substrate is much more than enzyme in Michaelis-Menten [57] and enzyme state-counting models in statistical physics [35, 88, 91]. However, recent advances in understanding natural biological regulatory circuits and engineering synthetic circuits achieve highly dynamic or combinatorial regulations [9, 10, 32, 83, 103, 122], violating these restrictive assumptions. Therefore a theoretical framework to characterize the full regulatory profile of binding networks on catalysis fluxes, while circumventing the intractability of polynomial equations, is needed. This thesis finds an alternative approach to characterize the full regulatory profile by focusing on the reaction orders of the catalysis fluxes in molecule concentrations, rather than the fluxes themselves. The full regulatory profile of a binding network is then shown to be polyhedral sets of reaction orders, determined directly from the stoichiometry of the binding network. As a result, we can analyze biocircuits in a holistic fashion, revealing hidden functional regimes and predict

when circuits would fail. So the first main contribution is defining the core structure of reactions in biomolecular systems, namely binding and catalysis, and finding a method for its holistic analysis, namely reaction order polyhedra. This is discussed in Chapter 2 and 3.

The other main contribution is a formulation of biomolecular reactions in cells as metabolic machines, where the reaction orders, or exponents, of metabolic fluxes are controlled. This formulation is a logical extension of the previous contribution. Since cells regulate metabolic fluxes by binding reactions, and the regulatory profile of binding reactions is adjusting reaction orders in a polyhedral set, cells control metabolic fluxes by adjusting their reaction orders or exponents. This rule, which we term flux exponent control (FEC), allows us to formulate metabolism dynamics in cells as a problem in control theory on how regulatory mechanisms, e.g. enzyme allostery, control the exponents of fluxes. Similar to how the Langrangian formulation can study the dynamic behavior of any given mechanical system in terms of its response to applied forces, FEC can study the dynamic behavior of any given metabolic system in terms of its response to adjustments of flux exponents. This opens up the frontier to systematically define, categorize, and study metabolic machines in terms of their structures in metabolic stoichiometry and flux exponents.

As a general systems-level formulation of metabolic networks, FEC also makes practical improvement over existing methods to quantitatively study metabolism. Data on metabolic networks are sparse, in the sense that the stoichiometry of metabolic reactions can be reliably understood, but the regulatory mechanisms of the metabolic fluxes, e.g. enzyme allostery, are largely unknown beyond a few well studied pathways. As a result, constraint-based methods, such as flux balance analysis (FBA), that use the sparse reliable data as constraints, and study the set of possible biological behaviors, have been widely applied to understand metabolism. However, existing constraint-based methods such as FBA mainly use metabolic stoichiometry as constraint, while allowing all fluxes to be adjusted. This does not capture intrinsic dynamics of metabolism, such as glycolytic oscillations and growth arrest, that are often the reason for metabolic regulation. FEC serves as an upgrade to existing constraint-based methods by naturally incorporating intrinsic dynamics of metabolism, and therefore can study dynamic properties from hard constraints. This is achieved by including a fundamental constraint on bioregulation of metabolic fluxes in addition to stoichiometry, namely that cells control metabolic fluxes by adjusting their exponents. Another approach to understanding metabolism is by studying hard limits that hold for arbitrary regulatory mechanisms, invented in [25] where limit-on-performance theorems from control theory are applied to explain glycolytic oscillations. FEC also upgrades this approach by formalizing generic metabolic networks into control

systems, where exponents of fluxes are adjusted by regulatory mechanisms. Therefore FEC allows the study of hard limits on metabolism for general systems, e.g. conservation of robustness or accuracy-robustness tradeoffs from feedback control of metabolic fluxes, akin to conservation of energy and the principle of least action from the Lagrangian formulation of classical mechanics. This is discussed in Chapter 4.

In this chapter, I provide broad discussions on the contexts that I am motivated by when developing these results. Readers interested in concrete results and technical contents may skip this and move on to the other chapters. The hope is that the contexts could help the reader understand where I come from, what I aim for, and where I am going next. Ultimately, I cannot make contributions more than what the mental picture of my "pathetic thinking" suggests [56]. Ideally these discussions could serve as a check on the general "mental model" of biomolecular systems in cells with the reader. The discrepancies pointed out in this check could reveal my limitation in reasoning and motivate the reader to make improvements, or at least caution the reader when reading the rest of this thesis.

There are four points about the context that I am motivated by: bioengineering as a potential industry, constraints and hard limits, catalysis at the core of biological activity, and dynamics as the reason for most bioregulatory mechanisms.

One of the eventual goal of bioengineering is to engineer biomolecular systems in cells as biomachines to perform diverse functions, such as adaptation, survival, growth, and dominance. Importantly, to enable an industrial revolution based on technologies from bioengineering, design and manufacture processes of biomachines need to be scaled up so that they become routine, instead of risky, explorative, and requiring experienced craftsmanship. Looking at other mature engineering disciplines, such as classical mechanics, this scaling up requires foundational theoretical understanding on two fronts: elicitation of core structures on the components level, such as Newton's laws of mass and force, and a systems theory on the machine level, such as Lagrangian formulation of mechanical structures subject to applied forces. This is in contrast to the typical trial-and-error, or "model, simulate, fit data" approach currently popular in bioengineering, which does not scale. Therefore, this thesis aspires to build a foundational theory on both components and systems level for biomachines. This is the first perspective taken in this thesis, elaborated in Section 1.1.

Second, against the myth that "anything is possible in biology", this thesis emphasizes the constraints and hard limits on behaviors of biomolecular systems. In other words, I take the view that constraints and hard limits are not in conflict with the diversity of biological behaviors, but rather guides us and enhances our understanding of this diversity. This

means that I strive to capture the space of all behaviors that a system is capable of, and understand its specific behaviors in particular scenarios in this context. This perspective is important because for machines to be useful, they are built to be both restrictive in certain aspects, yet universal in other aspects. For example, electronic computers can only do bit flips, but is capable of general computations; cars can only drive rotational motions on wheels, but can traverse diverse paths on roads. This restrictive yet diverse property of machines is sometimes called "constraints that deconstrain" [38]. To understand it, we see that machines consist of several layers in a hierarchy, characterized by timescales of their modifications. For example, from a machine's defining structures (slowest at the bottom), to its tunable parameters (faster in the middle), to its input-output behaviors in action (fastest at the top). A specific behavior in a particular scenario of one machine is the result of specifying everything in all layers of the hierarchy. To obtain insights on biomachines that hold on longer timescales, we need constraints and hard limits based on information of just lower layers of the hierarchy. This perspective is also discussed in Section 1.1. As an illustration of constraints and hard limits on biomachines, the example of autocatalysis processes is considered in Section 1.4.

Third, this thesis aims to develop rules and principles as well as corresponding mathematical tools tailor-made for structures in biology, rather than straightforward borrowing from other disciplines. In particular, this thesis considers catalysis as the core of bioactivity, since most actions in biology happen through catalysis. On the components level, each catalysis reaction is regulated by binding reactions. So I consider the core structure on the components level of biomolecular systems in cells as catalysis and binding reactions, akin to force and mass for mechanical components. Catalysis, like force, determines the direction of change, while binding, like mass, governs how the change is regulated. On the systems level, again motivated by catalysis as the core of bioactivity, this thesis focuses on biomolecular systems in cells as metabolic machines, serving the function of adjusting metabolic fluxes. This perspective is motivated by a general conception that catalysis, such as in metabolism, is the foundational biological behavior that most other behaviors build on top of. This is discussed in Section 1.3.

Lastly, this work considers dynamics as the major reason for most regulatory mechanisms in biology, therefore takes the perspective of biocontrol. As an example, although homeostasis is one of the hallmarks of biological behavior, a stable steady state is not guaranteed but instead achieved only via elaborate regulatory architectures. This perspective is illustrated by an intuitive inspection of autocatalytic processes in Section 1.4. Autocatalysis is one of the core processes of all life, from energy generation to growth. However, autocatalytic

processes are intrinsically unstable, therefore any homeostasis maintained on top of autocatalysis requires active regulations. Biocontrol can analyze instability and the necessary regulations explicitly, as well as reveal hard limits on system performance. In Section 1.4, hard limits due to instabilty of autocatalysis from the perspective of biocontrol is compared with constraints from stoichiometry and thermodynamics, as an illustration of constraints and hard limits on biomachines.

1.1 Systems theory as foundation of an engineering industry

There are two main contributions of this thesis: one on the components level, and one on the systems level. The main result on the components level is a principled way of formulating and analyzing biomolecular systems, namely as networks of catalysis and binding reactions. By principled, I mean similar to how Newton's laws enable our reasoning of systems with mechanical components: (1) all mechanical components can be specified by force and mass; (2) force and mass interact in a particular way specified by Newton's laws, so that force determines the direction of motion, while mass determines how the force-motion relation is regulated; (3) to analyze or design a mechanical system is to analyze or design a system of force and mass (see Figure 1.1). In other words, Newton's laws formulate force and mass as the core structure of mechanical components in any system, and this serves as the universal protocol (the middle knot of Figure 1.1) that all behaviors of mechanical components (on the left) are converted to, and all methods of analysis and design (on the right) are applied to. In short, one result this thesis strives to deliver is a core structure, namely binding and catalysis, that does the same thing for biomolecular systems in cells. On top of the core structure, just like calculus was invented or adapted to describe the mathematical structure in mechanical systems' behaviors, this thesis also develops reaction order polyhedra as a tool to describe regulatory profiles of binding network on catalysis fluxes.

The other main contribution of this thesis is on the systems level: biomolecular systems in cells is formulated as metabolic machines acting on metabolic fluxes, with external adjustments of fluxes' exponents. This is a systems theory of biomolecular systems, similar to how Lagrangian mechanics formulates mechanical systems as a structure made of mechanical components and subject to applied forces. A systems theory defines an abstract class of machines for a generic purpose or function, and characterizes the space of machines, or systems, in terms of the structures that connect the components into a machine (see Figure 1.2). To come up with a systems theory, we need a formalization of the constrained mathematical structures from the components level. For example, while

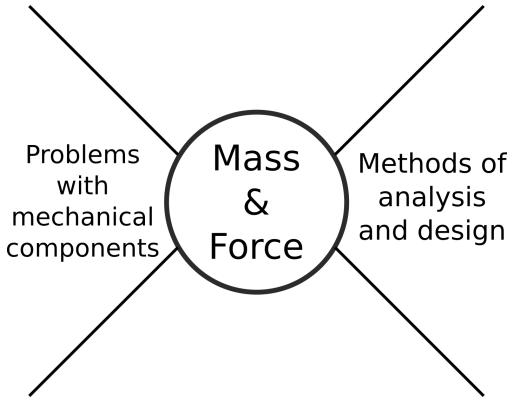

Figure 1.1 Mass and force serve as the core structure of mechanical problems.

each mechanical component has its own position, velocity, and forces, these variables are constrained due to the structural connection that put them together into a machine. The Lagrangian formulation of mechanics, as a systems theory, then builds these constraints as its foundational mathematical structures so we can focus on functions at the machine level.

Once a systems theory is defined, it enables fundamental characterizations of a class of machines that often take the form of hard limits on machine performances. By hard limits, I mean similar to conservation of energy for mechanical systems, and conservation of robustness for control systems, that characterize what these systems can and cannot do in a fundamental way. In particular, conservation of robustness shows that fragility cannot be fully mitigated by control design, but only shifted or re-distributed [104]. This provides a coordinate to view control system design in terms of unavoidable tradeoffs of different performance metrics, guiding the development of the discipline. It also shows that unstable plants (i.e. processes to be controlled) make control problems harder and the resulting system more fragile, in a way that cannot be mitigated by control design. This places control design at the interface with external constraints from physical limitations of hardware, in turn deepening our understanding of control problems at large, beyond just controller design. For example, problems with different physical limitations then constitute control problems with different "hardness", in a fundamental way. This hardness is then to be tackled outside of control design, such as by means of hardware engineering or materials design. In short, the second result that this thesis strives for is a systems theory of biomolecular systems in cells as metabolic machines, defined through constrained structures of bioregulation. The hope is that this provides a systematic way to study generic metabolic systems, enabling the study of hard limits on what biomolecular systems can and cannot do, and guiding the development of biocontrol methods.

To better see why these two types of results, core structures on the components level and a

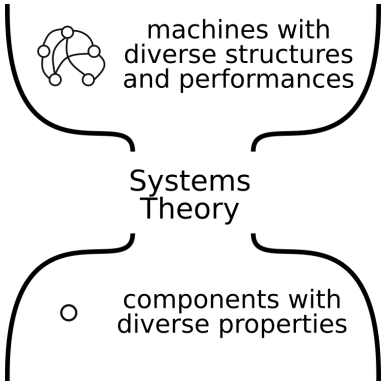

Figure 1.2 A systems theory defines a class of machines for a purpose or function. It takes components with diverse properties, and utilizes core structures on the components level to connect to machines with diverse structures and resulting performances.

systems theory on the machine level, might be useful, let us start with some context for motivations of my research. The goal of my research is to push towards a bio-industry that can tap on the unique capabilities of bio-organisms, namely adaptation, survival, growth, and dominance. Not as a sub-industry or a technique in chemistry, medicine, materials, or health care, but for bio-industry to be an industry with its own unique capabilities that enable other industries, like the rise of digital networks or AI industries. There are examples of employing such unique capabilities in certain fields, such as agriculture, cattle breeding, or tree-growing to reverse desertification. The rise of bio-industry should enable systematic and routine application of engineered bio-organisms that adapt, survive, grow, and dominate to suit societal needs.

To think about how the rise of bio-industry can happen, it is helpful to provide a historical perspective, albeit simplistically. Supposedly an industry is based on some advance in engineering technology, which in turn is based on scientific knowledge. Scientific knowledge about the world is accumulated from a sea of observations (see Figure 1.3). Based on a set of closely-related observations, a phenomenon or a heuristic rule can be summarized, and used as a working knowledge. For example, ancient astronomy was based on heuristic rules of how certain planets seem to move, accumulated from many observations of the sky. From several such heuristic rules, a more general phenomenological model, or mathematical law, can be formulated, e.g. Kepler's law of planet motion. From several such phenomenological laws, the fundamental structure of a large class of problems can be formulated, e.g. Newton's laws of mechanics. This view of scientific progress can be seen as a funneling process from larger and larger sets of observations to smaller and smaller sets of rules that reveal structures of the problem that are more and more fundamental. There are of course further relations among the rules and further dynamics

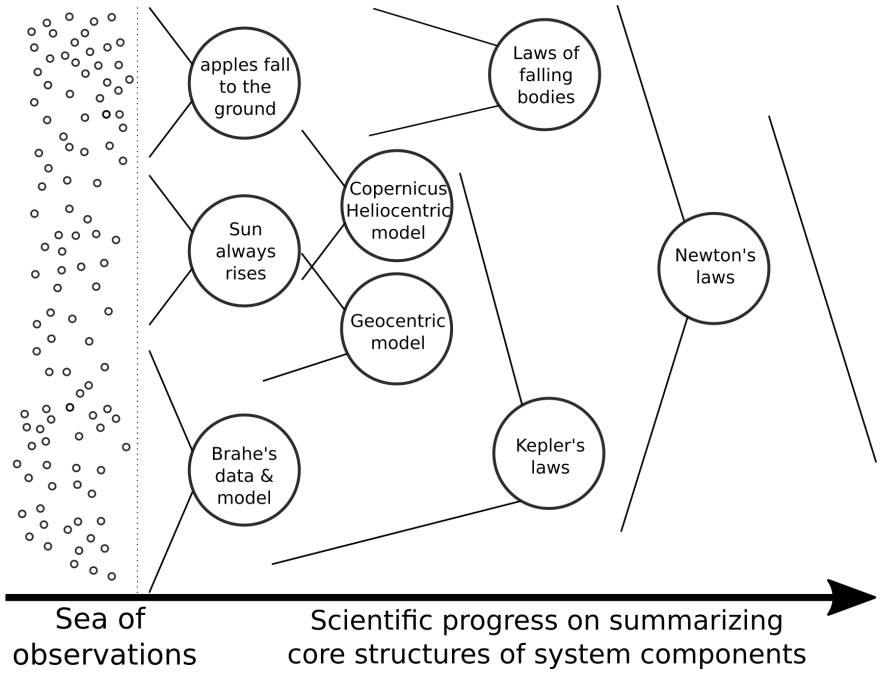

Figure 1.3 Scientific progress as a funneling process of rules that capture the core structures of components.

within this funneling process that we are not going into. One example is the emergence of rules and laws on a larger scale from smaller scale ones, as exemplified in chemistry, statistical physics, and fluid mechanics. Another example is the feedback from a rule as motivation to seek particular kinds of observations, as in hypothesis-driven experiments, and the invalidation of wrong rules.

On top of this scientific progress, from any rule at any stage, it can be used as a basis for engineering (see Figure 1.4). For example, a simplistic engineering directly from observations would be that from several observations of apples falling down from trees, we can use this to harvest apples by waiting for apples to fall. A more fundamental rule capturing the core structure of a wider class of components would yield engineering techniques that can be applied to wider classes of problems and generate more ways to solve a problem. For example, while Kepler's laws can only be applied to planetary systems similar to a planet around a star, Newton's laws can be applied to more complex planetary systems such as three-body problems, as well as other tasks such as calendar keeping, projectiles such as catapults, and fluid motion.

However, when a scientific law is used to solve an engineering problem, it is not as simple as just straightforwardly applying it. The reason is that an engineering problem is often not of analysis, but of design. While the components simply exist, with properties summarized by scientific rules, a machine needs a purpose to be conceived and then built. Given a

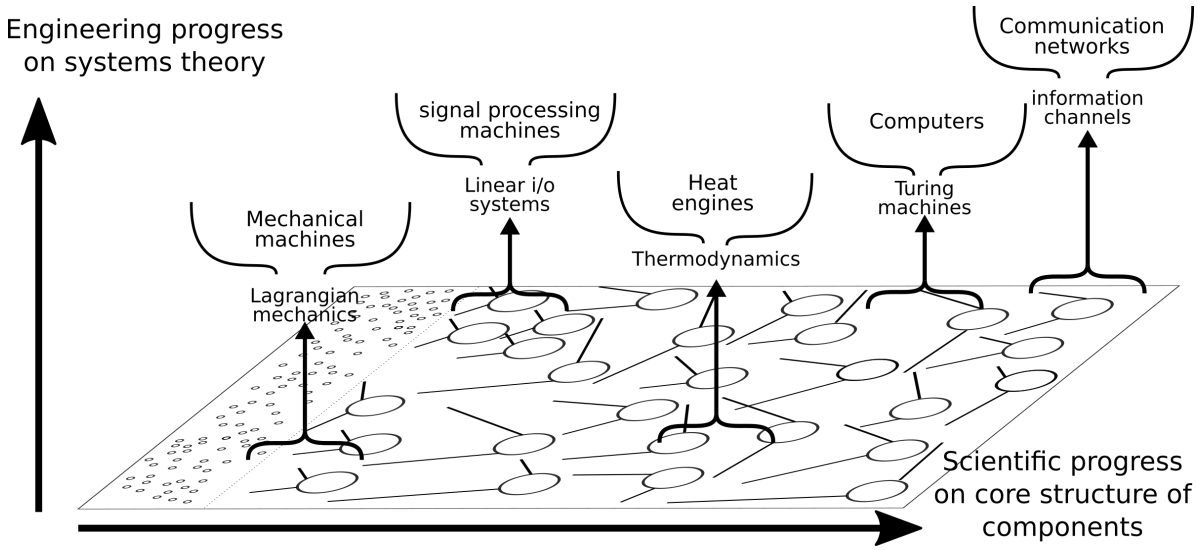

Figure 1.4 On top of core structures of components from scientific progress, engineering progress is made by coming up with systems theories. A systems theory defines a class of machines by formalizing the constrained mathematical structure from the core rules of the components.

mechanical system of mass and force, Newton's laws can analyze it by specifying how the components' position, velocity, force and mass relate. But it is nontrivial to even formulate, let alone answer, a design problem based on Newton's laws. This is because the components' variables have complicated internal constraints, and a purpose or function is not naturally specified in variables of the components. Furthermore, a design problem is not analyzing a given system of components, but rather defining a space of possible systems and then finding one system for an optimizing objective. Given I want a rock to move in a particular motion using some wood sticks, how to put together a machine that is the right mechanical system to do it? We would need to define the general class of machines that can be built from wood sticks, and characterize how each machine design is related to moving a rock, so as to optimize over the designs based on performances. In mechanics, this is approached by alternative formulations of mechanical problems such as the Lagrangian that build internal constraints of component variables from machine structure directly into the formulation and describe machine behavior in terms of system variables rather than components. These formulations also take mechanical control and other domain-specific constraints more explicitly into account. As designs of mechanical machines continue to evolve, new formulations of mechanical machines are still actively invented today, e.g. to tackle cyber-physical systems in robotics.

This points to the need of an engineering systems theory when going from scientific rules to solving engineering problems at scale. Given the core structures for the components that will be used for an engineering purpose, we still need to define a systems theory

characterizing a class of machines by eliciting how the machine architecture of putting components together relates to machine performance on the functional level (see Figure 1.4). This is more apparent from looking at some of the modern engineering fields. Thermodynamics is a systems theory for heat engines on top of gas laws etc. describing system components; Kirchhoff's laws is a systems theory for electrical circuits on top of ohm's law describing resistors and capacitors as components; linear time-invariant input-output systems is a system theory for electronic signal processing on top of op-amps as components; communication channel and its information transmission properties is a systems theory for radio, phone, and internet; and Turing machine is a systems theory for modern computers on top of transistors and band gaps as components (Figure 1.4).

A systems theory often offers two important contributions that make an engineering discipline scale up to an industry. One, it takes the core structure of components from relevant scientific progress and charts out the mathematical space of all possible systems or machines relevant for an engineering problem. This allows systematic explorations in the space of machines for useful designs, especially ones optimal for a certain objective. Second, it can develop hard limits on machine performance based on general features of machine structure. Examples of such hard limits are Carnot's efficiency bound of thermal engines, channel capacity of communication channels, undecidable halting problems for a Turing machine, and Bode's conservation of robustness for control systems. By pointing out fundamental limitations of the class of machines for an engineering problem, this systems theory establishes a central coordinate or direction that aligns and compares all designs and implementations of machines, thereby guiding development of a discipline. In other words, a systems theory charting out the set of engineering systems relevant for a problem and its hard limits is a crucial stage to begin solving an engineering problem at scale.

In the context of biological engineering, this pursuit for scaling up is sometimes not appreciated. There is an implicit but widely accepted notion, especially in bioengineering academia, that theories are useful only to fit and explain experimental data by building models and simulating them. Systems theories, in terms of general rules, axiomatic formulations, and mathematical theorems that characterize the biological systems we deal with, have not been successful, and therefore not necessary for bioengineering. Indeed, most major advances in engineering novel functions in synthetic biology proceed by intuitive reasoning of domain experts aided by model simulations and feedback from experimental data. However, if industrialization of bioengineering is the eventual goal, then scaling up both the design and manufacture processes are necessary. Current design-test-build

cycles of bioengineering highly rely on the experience and craftsmanship of experts, often taking several years of a top-tier PhD student just to have a chance at accomplishing one design. While similar situations are true for the early stages of other mature engineering fields, as discussed above, eventually foundational systems theories were developed to scale up both the education of engineers and the design-build-test process. In other words, systems theories are at the core of enabling industrialization, where works that previously involve high uncertainty and require experienced experts and extensive trial and error now become routine and readily doable at scale. It is this scalability enabled by a systems theory that I hope to achieve in this thesis when developing the systems theory of biomolecular systems in cells as metabolic machines with control input on flux exponents.

From this vantage point of systems theory aiming for scaling up, I note that most ideas in this thesis are not new, but taken more seriously, made systematic, and developed to their logical conclusions. For example, the idea that binding regulates catalysis dates all the way back to Michaelis-Menten [57, 63]. My main contribution is in formalizing that this is the core structure of biomolecular reactions. In other words, I propose that all biomolecular reactions in cells consist of these two types of reactions, with binding regulating catalysis. Placing this at the formal foundation of biomachine components has several implications. On one hand, it claims that we do not need more. Binding and catalysis reactions form a strict subset of all possible chemical reactions. This can avoid some pathology and generality that arise in the study of general chemical reaction networks, which is one obstacle in that discipline [93]. Indeed, without biological restrictions, it has been shown that CRNs can perform Turing complete computations and produce arbitrary steady state distributions [24, 90]. So binding and catalysis can also be seen as a regularization on the space of chemical reaction networks by demanding realistic networks to be "biological", similar to demanding functions to be continuous or smooth in physical solutions of many partial differential equations. This is also facilitated by concretely relating each reaction to a physical process, so that one process always has a detailed and correct way to specifying it, with other specifications corresponding to simplifications with explicit assumptions. On the other hand, binding and catalysis claims that we can not have less. While assumptions such as one species is much more abundant than another is often made for simplifying assumptions in analyzing binding networks, we cannot restrict ourselves to always make such assumptions. Instead, taking binding and catalysis as the components' core structure demands that we characterize the full regulatory profile of binding on catalysis, and analyzing specific scenarios and making restrictive assumptions within the context of the full behavior.

As another example, the idea that the exponents, or reaction orders, are what is important for regulating catalysis fluxes is also not new. It was pioneered by Michael Savageau [97] in his work on S systems in 1970s and has been included in many works on analyzing metabolism, such as metabolic control analysis (see Chapter 13 of [30] for an introduction). However, in those cases, the reaction orders are often taken as empirically useful quantities, such as sensitivities or enzyme efficiency, and used to interpret numerical simulations. This thesis again takes this idea seriously and extends it to its logical conclusions. If reaction orders are truly representative of bioregulation, then what is the space of all possible reaction orders, and how do they relate to underlying regulatory mechanisms, namely binding networks? In other words, what is the mechanistic basis of reaction orders? If reaction orders are truly the quantity regulated when controlling metabolic fluxes, then this is a severe limitation on cells' control of metabolism dynamics. What are the consequences? The answers to these questions, which are logical consequences of the reaction order idea, are important for developing a systems theory that formalize metabolic machines. Through the work of this thesis, surprising properties about reaction orders are revealed when exploring these questions. One is that reaction orders can often take arbitrarily large values in certain directions, which are regimes that corresponds to rays towards infinity (Chapter 3). Biologically, this corresponds to the important phenomenon of hypersensitivity (see Chapter 2). This is rather unexpected from empirical and intuitive notions of reaction orders in previous works, where reaction orders are motivated by saturation phenomenon in Michaelis-Menten type enzymatic activities, so they are often restricted between 0 and some small positive integer. In fact, because Hill functions or other Michaelis-Menten type representations of enzymatic activities cannot naturally handle dependence on multiple total concentrations, reaction orders as vectors in a multi-dimensional space is under studied until this work. Another surprise is that restricting bioregulation of fluxes to adjusting their exponents is actually the natural way to preserve intrinsic dynamics of metabolism (see Section 1.4 and Chapter 4). This observation only becomes clear after confidently taking the FEC rule as a genuine constraint on what cells can do and make it into a constraint-based approach for modeling metabolism.

Our discussion in this section motivates why this thesis aims at formulating the core structure of components and a systems theory of machines for biomolecular systems in cells. Inspired by other engineering disciplines with mature industries, I consider work on these two directions as crucial developments in enabling bioengineering to scale up into an industry. With this in mind, Section 1.3 describes why catalysis is at the center of core structures and systems theory for biomolecular systems in cells. The core structure of binding and catalysis is in terms of how catalysis is regulated, and the systems theory

of metabolic machines is in terms of catalysis fluxes in metabolism as machine function. The next section, Section 1.2, discusses how can systems theory of machines be useful. In particular, how can constraints and hard limits on machines be possible, given that there are examples of machines with extreme diversity in behavior, such as computers, neural networks, and biological organisms.

1.2 Constraints and hard limits characterize properties of machines

In this chapter I provide broad discussions for trying to understand biological behaviors through constraints and hard limits, which is one of the perspectives taken in this thesis. In biological science, there is a general sense that anything is possible in biology, that there is an exception to every rule. However, in traditional quantitative disciplines such as physics and chemistry, we gain fundamental understanding by characterizing what the systems cannot do. The most powerful rules and laws, like the second law of thermodynamics, conservation of energy, or conservation of atoms and charges in chemical reactions, always specify constraints on systems' behavior. This is even more true for engineering, where the class of systems serving a purpose, or machines, are often defined at the very beginning by a complete set of rules governing their basis of behavior. Kirchhoff's current and voltage laws govern electrical circuits; definitions of states, symbols and transitions govern automata and Turing machines; rigid bodies and their holonomic constraints define a mechanical machine such as a tower crane. Even for science or engineering disciplines without a complete set of rules, a major goal, if not the highest priority one, is to uncover such rules.

This appreciation for rules is not completely alien to biology. Rules, such as the central dogma and that bio-organisms are made of cells, are at the foundation of many science and engineering efforts in biology [54, 56]. However, when such biological rules are formulated, it seems they always have exceptions, and often important exceptions. So we have this phenomenon that many useful rules are applicable to different classes of scenarios, but they are brutally violated in many other classes of scenarios. One popular reaction to this, especially given the power of modern molecular biology tools, is that no rules are general; hard limits do not exist; we just have to understand by probing all the details down to the molecules. This view has the strength that some important biological details are well respected, instead of ignored because they do not fit a preconceived theory. I would encourage some optimism on top of it by observing that at least conservation of energy

still holds everywhere in biology, and so does conservation of atoms and charges. In fact, biology is even more constrained than chemistry because the pressure, temperature, and the scale of energy available are quite restricted. So from this line of thinking, we begin to have hope that constraints and hard limits should exist in biology, at least more so than chemistry. However, this immediately reminds us of all the fascinating enzymes, proteins, lipid membranes and other molecular dances that are quintessentially biological, that they seem to defy any summary. I argue that this is not because biology violated the constraints we just described. But on the contrary, it is exactly because of these many severe constraints that life has to evolve and find diverse ways to achieve objectives within the constraints. This is sometimes referred to as "constraints that deconstrain" [38]. Many examples of this phenomenon can be seen in engineered devices. By committing to just 0s and 1s, digital computers are severely constrained in what it can do on this basic level: flipping bits. But on top of this severe constraint, generality and diversity in a totally different sense, namely information storage and processing by software, can be achieved. Below 0s and 1s, another totally different kind of generality and diversity is also achieved by allowing all kinds of hardware to implement bit flips and therefore digital computers. Both the diversity on top and diversity below are achieved without ever violating the constraint of just using 0s and 1s and doing bit flips.

To reconcile all this and reason about how constraints and hard limits can be derived for biology, we need to make a distinction between two kinds of rules: scientific rules on components, and engineering rules on machines. Scientific rules capture the core structures of objects' behavior based on observations. For example, mechanical properties of wood sticks capture how they respond to forces, generally formulated in terms of Newton's laws on mass and force. Engineering rules capture the systems theory describing a class of machines, an abstract conception serving a purpose or function, and characterize it by relating the structures of how components are put together with machine behavior. On top of a systems theory, the class of machines can also be characterized by deriving the hard limits and laws governing this class. For example, catapults, as a class of systems serving the purpose of shooting a projectile, can be described by the systems theory of Lagrangian mechanics on catapult-shape mechanical structures, and has hard limits on the conversion from elastic energy of ropes to kinetic energy of boulders.

These two types of rules also govern systems in reality in different ways. Core structures are empirical summaries of the common properties that many objects share. These are therefore descriptive, and naturally restricted to the systems where the observations were made. So the process of obtaining core structures also includes understanding the boundary where

this core structure holds. When we discover an object that violate a certain core structure, it does not make the core structure useless, but instead just clarifies the boundary within which the core structure applies. Hard limits and laws, on the other hand, are based on a systems theory, where a class of machines to be studied is completely defined, usually in a mathematical sense. A systems theory is often defined via mathematical abstractions of machine architectures, i.e. how components are put together to make up a machine and perform a function. This guarantees that hard limits and laws derived from the systems theory actually govern any machine put together to function in the prescribed way. For example, the systems theory of Turing machines governs any machine with components of states connected by state transitions, performing the function of reading input symbols and writing output symbols. As another example, the systems theory of Lagrangian mechanics govern any machine with components and junctions satisfying mechanical rules subject to externally applied forces. As a further example, Kirchhoff's laws govern any machine made by interconnecting components with current-voltage-like input-output pairs. So a systems theory takes some physical boundaries of core structures on the components level, and integrate it with mathematical boundaries on machine architectures, to form the space of a class of machines. Then hard limits derived on top of a systems theory holds for all machines that satisfy both the abstract machine architecture in a mathematical sense, and the boundary of components' core structures in a physical sense. In other words, if a machine is made by components put together in the same way as prescribed by a systems theory, and the components satisfy the rules of core structures required by the systems theory, then the hard limits governs this machine simply as a logical consequence.

With this distinction made, we see that biology has an exception to every rule in the sense of an exception to every core structure summarized. But this is not surprising, since one of the points of coming up with a core structure is to define the boundary where it applies. The same is true for all known rules from physics and chemistry. Therefore, while any constraints, or scientific rules, from one core structure may not be applicable to all biological systems, there exists core structures that govern wide classes of biological systems. In this thesis, the main constraint from components' core structure is that binding's regulation of catalysis has reaction orders constrained in polyhedral sets. This holds whenever the core structure of binding's regulation of catalysis holds. In quantitative detail, we assumed, and only assumed, time-scale separation that binding reaches steady state and that mass action governs on-off rates of binding reactions. Both are well-tested rules that govern a wide range of biomolecular reactions. It is arguable that more restrictive constraints from further assumptions on the components level, such as Michaelis-Menten approximations, can also be applicable to a wide range of scenarios of interest. However, as discussed at

the beginning of this chapter and in Chapter 2, there are many scenarios of interest in bio-science and engineering that do not satisfy such assumptions. More importantly, even if further assumptions are applicable for a given case, we would like to retain a holistic view so that restricted scenarios can be analyzed in a holistic context. This way, when the system is pushed out of the assumptions, such as in debugging of design-build-test cycles, we always have a holistic view to go back to. This is at the core of how systems theory can scale up design-build-test cycles of an engineering discipline, similar to how fluid dynamics simulations scale up the aviation industry.

Then do there exist hard limits on biological behaviors? While hard limits on all possible observed and yet-to-be observed life may be hard to find, if we define a systems theory based on some component core structures and some class of machine architectures, then hard limits and laws on top of this systems theory holds for all biological machines satisfying the prescriptions as a matter of logic. In this thesis, we consider biomolecular systems in cells as metabolic machines with external adjustments of flux exponents. This formulation combines the constraints from core structure that binding regulates catalysis, and the layered machine architecture from metabolism. The core structure from binding's regulation of catalysis specifies that this regulation is constrained in polyhedral sets in terms of reaction orders. Therefore, since cells regulate catalysis fluxes by binding reactions, and binding reactions regulate fluxes' exponents, we have cells regulate fluxes' exponents. We term this constraint flux exponent control (FEC). The layered architecture of metabolism integrates this constraint into the function of metabolic machines. Metabolism has unchanging and easy-to-characterize metabolic stoichiometry, while metabolic fluxes are quickly varying and hard to measure. So we can consider stoichiometry as the bottom layer with the fluxes regulated by higher layers. Then metabolic fluxes are regulated by binding reactions, which make up the middle layer. Combined with the constraint from core structures that exponents are regulated by binding reactions, the middle layer consists of unchanging structures of binding reactions such as network topology and binding energies, with exponents regulated by higher layers. The top layer then includes all the ways to regulate the exponents, such as protein synthesis and degradation. See Chapter 4 for details. Together, the systems theory of metabolic machines with fluxes exponents adjusted is defined by combining the FEC rule from core structures of binding and catalysis, and the machine architecture from layers of metabolism. As a result, any conclusions such as hard limits derived from this systems theory would hold for a metabolic system as long as it is made of biomolecular reactions satisfying the core structure of binding and catalysis, and has the layered architecture of metabolism described above.

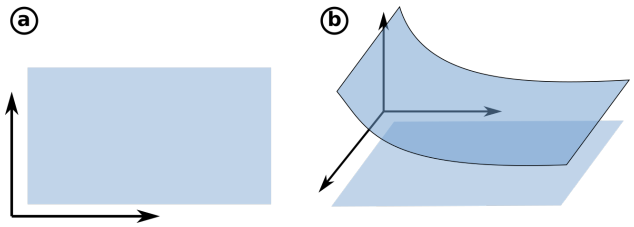

Figure 1.5 A cartoon illustrating how universality of a machine's performance in some metrics (a) can become a tradeoff with additional metrics (b). **(a).** The blue rectangle indicates that all points in the positive orthant can be achieved by a machine. **(b).** With an additional axis, the achievable points in this 3d space is on top of the blue curved surface. While its projection onto the bottom 2d plane is still the blue rectangle as in (a), in 3d space the corner close to the origin is not achievable. This constitutes a hard limit on the machine's performance, or a tradeoff amongst the performance metrics.

Now we have argued that constraints and hard limits are indeed plausible for biomolecular systems in cells, a further question arise: while a machine may be governed by constraints from components and hard limits from system architecture, they may say very little about limits on machine function. For example, a given computer has fixed architecture and processes information using only 0s and 1s and performing bit flips, yet it can achieve universal computations. A car has a fixed architecture and its components are very restricted in their properties, yet it can drive between a wide range of locations. A neural network is defined with a fixed architecture, and its components are just linear threshold units and nonlinear maps such as ReLU, yet it can approximate universal input-output maps.

While it is true that "universality" in certain performance metrics may be achievable despite constraints and hard limits, such universality is often an indication that other practically important performance metrics are ignored. Once a performance metric closer to practice is defined, often hard limits on performance from machine architecture become clear (see Figure 1.5). In fact, while universality in certain metrics is important characterizations of the ideal power of a class of machines, finding additional metrics to turn universality in one metric into a tradeoff in multiple metrics is often more useful in guiding practical improvements for machine design and engineering.

To be explicit about where hard limits on performance may result from machine architecture, let us consider the hierarchy of machine specification that determines a machine's behavior (see Figure 1.6). This hierarchy is defined in terms of the timescales that each layer can be modified. Given a class of machines defined by a systems theory, we specify a particular machine via its architecture. This is slowest to change, because changing architecture is usually considered switching to a new machine. Therefore the machine architecture is the bottom layer. On top of the architecture, we often have parameters of the machine that

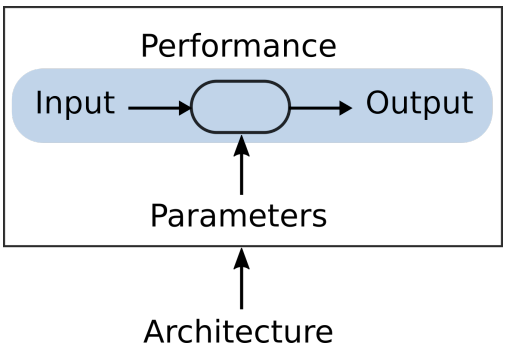

Figure 1.6 The hierarchy of machine behavior defined by timescales of modification. Given a class of machines defined by a systems theory, the architecture specifies a machine. The architecture changes on the slowest timescale, since modifying it is considered switching to a new machine. The parameters of the machine can be tuned on a slower timescale. The performance of a machine is the input-output behavior under fixed parameters and architectures. This changes on the fastest timescale, since the input varies on the functional timescale.

we can tune on a faster timescale than modifying the architecture. The performance of a machine is then defined by the input-output behavior of the machine with parameters and architectures fixed. This is fastest, since inputs vary at the timescale of machine functions.

Let us take neural networks as an example to walk through how architectures may imply hard limits on machine performance. Canonically, a neural network machine is defined by its network architecture, i.e. how the linear threshold units, or neurons, are interconnected. Then, when training a neural network to perform a certain task, say classifying pictures in computer vision, we tune the neural network's parameters so that it approximates the correct picture-to-category map. With the parameters adjusted, or learned from data, the neural network can then perform input-to-output functions that classify any given picture. In this context, it is often considered that this neural network is "universal" in the sense of image classification that by tuning the parameters, the same neural network can learn all kinds of image classification tasks, without modifying the architecture. However, it is also well known that this universality holds even for a neural network with just two hidden layers and a nonlinearity in between, as long as the size of each layer is large enough. But this architecture is rarely used in practice. In fact, diverse architectures of neural networks are invented to adapt to the need for different tasks, such as convolutionary neural networks for computer vision, and recurrent neural networks and transformers for natural language processing. In terms of the performance metric of approximating an input-output map, these architectures all have the same universality, therefore make no difference. These architectures are invented for other performance metrics not included in the previous description of neural networks as machines, such as network size, amount of training data needed, and ease of tuning the parameters.

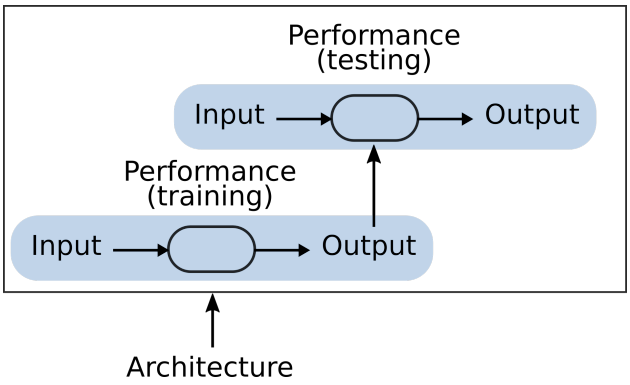

Figure 1.7 A hierarchy of machine behavior with two performance objectives, motivated by training and testing performance of neural networks. The output of the training task is parameters for the testing task.

To incorporate these practically important performance metrics in our systems theory description of neural networks, we need to modify our definition of architecture, parameters, and inputs-outputs. Since training is a large part of practical performance, we need to consider both training and testing performances. For the training task, the input is training data, and the output is parameters of the network. The output of this training task is then fed into the testing task as parameters. This results in the hierarchy of machine behavior with two layered performance objectives. Now, with the performance metrics of both the training and the testing process taken into account, we see quite clearly that architecture significantly limits the machine performance of neural networks. In fact, most important questions of machine learning research concern the training process, rather than the testing process, with many innovations on the architecture layer to improve neural network performance. This is another testament to architectures' limitation on neural networks' machine performance.

We can similarly understand how architecture can limit machine performance for other cases. For example, while cars can universally transport between locations, this universality becomes a tradeoff that promotes diversity of car architectures when other metrics are taken into account, such as speed, ease-of-care, machine longevity, and requirement on road condition. In fact, we can go one step further. Transportation between locations is a performance metric shared by several types of transportation carriers, from walking to cars to trains to airplanes. In this case it becomes even more clear that the universality of transportation between locations for these machines is hiding the necessary diversity promoted by hard limits, or tradeoffs, on multiple performance metrics, such as speed, accuracy, and price. Although we do not discuss it in this work, there are further implications on this necessary diversity due to hard limits or tradeoffs, such as diversity-enabled sweet spots [79, 80].

As a concrete example relevant to biomolecular systems in cells, hard limits on regulation of metabolic fluxes can take the form of a speed-accuracy tradeoff or a tradeoff between steady state error and fragility to disturbances. This is exemplified in the work of [25] that demonstrates how glycolytic oscillation is an inevitable side effect of enzymatic regulations in glycolysis that adapts to steady state metabolite supply and demand. It is based on the general theorem on conservation of robustness from control theory [39, 69, 104]. Furthermore, the autocatalytic stoichiometry of glycolysis worsens the tradeoff so that oscillations are necessarily more severe, due to the intrinsic instability of the system, making it fundamentally harder to control. This is also illustrated in Section 1.4.

From the discussion in this section, we distinguished between constraints from core structures on the components level, and hard limits from systems theories on the machine level. This makes it clear that biology has an exception to every rule is not in conflict with constraints and hard limits can be fruitfully applied to understand biological systems. In terms of hard limits from systems theory, we discussed how a machine's apparent universality in one performance metric may hide hard limits and tradeoffs in multiple practically important metrics by looking at the hierarchy of machine behavior. Together, this discussion motivates the importance of constraints and hard limits in characterizing properties of biomachines.

In Section 1.4, hard limits on cells as metabolic machines from stoichiometry, thermodynamics, and biocontrol are considered in a simple example of autocatalysis. I argue that hard limits from dynamic properties, such as intrinsic instability of certain machine architecture, are especially important. In the next section, I discuss how catalysis is at the core of biomolecular systems' function in cells. As a result, the core structure and the systems theory of biomolecular systems developed in this thesis are formulated around catalysis and its regulation.

1.3 Bioactivity as catalysis, bioregulation as binding

Catalysis is considered the central activity of biology in this work. For biomolecular systems in cells, this thesis formulates the core structure as binding's regulation of catalysis reactions, and the systems theory as machines regulating catalysis fluxes in metabolism. This central position of catalysis in bioactivity is motivated by viewing biomolecular systems in cells from a thermodynamics or statistical mechanics point of view.

A cell, or a biomolecular system inside it, can be viewed as a bag of molecules inside a big environmental bath consisting of many more molecules. For example, think of a

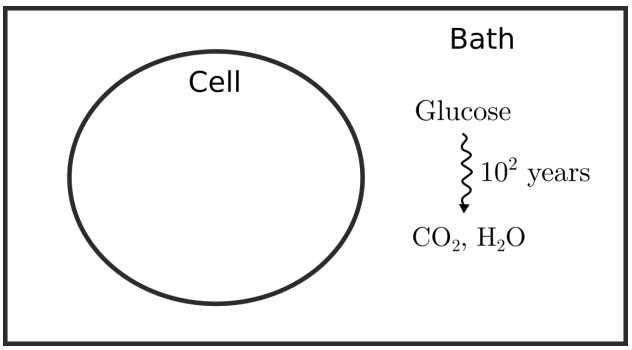

Figure 1.8 A cell in an environmental bath of glucose solution.

vesicle inside an aqueous solution of glucose (see Figure 1.8). The bath is always full of energy, i.e. it is far away from the lowest energy state, so it can serve as the source of energy for life. From thermodynamics, we know such systems' overall behaviors are characterized by bulk parameters, such as pressure / volume, temperature / entropy, and chemical potential / molecule number. There are also more exotic parameters relevant in less-common cases, such as magnetic interactions, but these are not central to our discussion. Based on observations of what typically happen, we assume the cell cannot modify these bulk parameters from the bath, but instead have to take them as given. This is especially true for pressure and temperature. We also assume the environmental bath is relatively stable in itself, therefore the bath is constant for the timescale of the cell. For example, although a lower energy form of glucose is carbon dioxide and water, glucose does not spontaneously degrade in water at a timescale relevant for cells (half life is 96 years [115]). Together, thermodynamics dictates that the long-time dynamics of the cell is to converge towards equilibrium with the bath. This means, in addition to the cell's pressure and temperature tending towards those of the bath, the molecular concentrations in the cell also become equal to the environment, via processes such as diffusion, transport or chemical reactions. In the vesicle in glucose solution example, this means in the long run, the vesicle should become the same glucose solution as the environment. But we don't see this as a typical behavior for cells! We typically expect there is higher pressure inside the cell, the temperature does not necessarily follow the environment, pH in the cell can be drastically different from that out of the cell, and glucose in the cell gets burned into carbon dioxide and water on a very fast time scale. This means although the cell cannot change the bath, it somehow keeps itself away from converging towards equilibrium with the bath. The secret is that cells are able to take reactions that are slow or not possible in the environment and make them happen fast inside the cell (see Figure 1.11). In other words, cells take in molecules that are stable in the environment, and make them unstable through catalysis reactions to unleash the energy in these molecules. To how this is plausible from

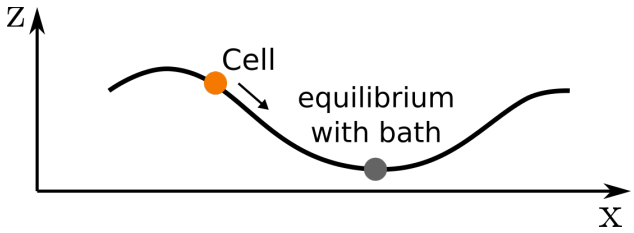

Figure 1.9 An intuitive landscape of the cell with bath fixed.

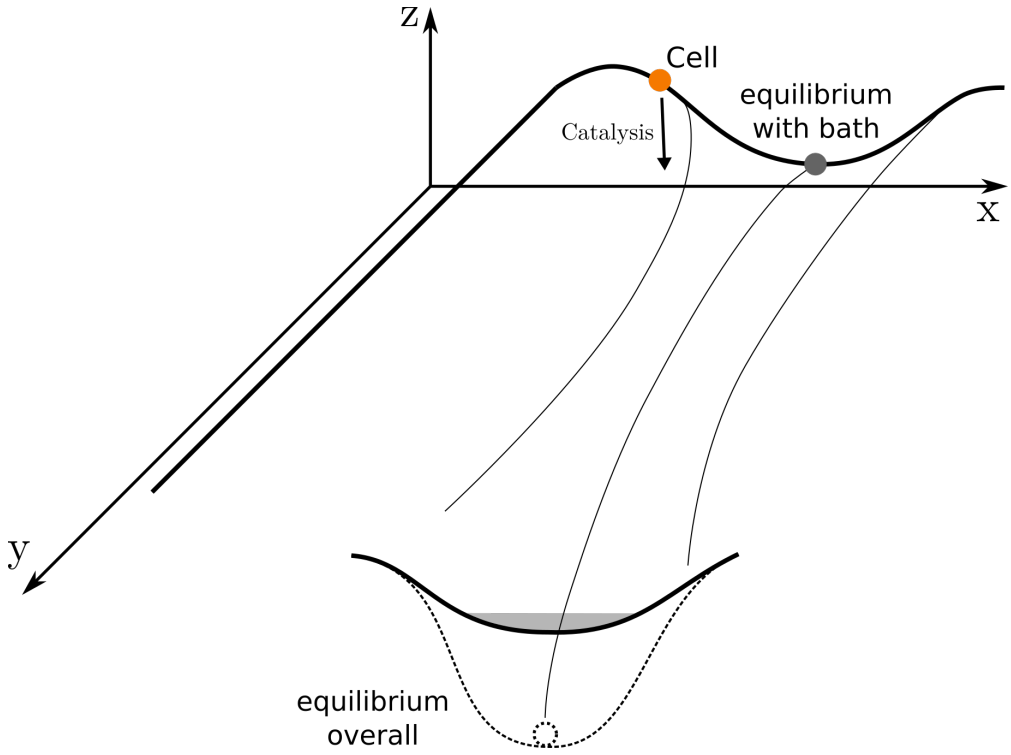

Figure 1.10 The overall landscape of the cell and bath system.

a thermodynamics perspective, let us use an energy landscape analogy.

Intuitively, we can imagine the cell is a point in an energy landscape defined by the bath. Height, or vertical z-axis, corresponds to energy, and x-axis corresponds to varying molecule concentrations of the cell, for example (see Figure 1.9). By default rules from thermodynamics, the cell would tend to the cell-lowest-energy point to be in equilibrium with the bath. In the vesicle in glucose solution example, this means the conditions in the vesicle becoming equal to the solution. We can visualize the landscape along the x-axis as relatively flat to illustrate that skiing down the landscape, or this process towards equilibrium with the bath, happens relatively slowly.

On the very slow time scale, however, we see that the bath is moving towards lower energy states itself. It's just that this is so slow that the bath appears essentially constant. In

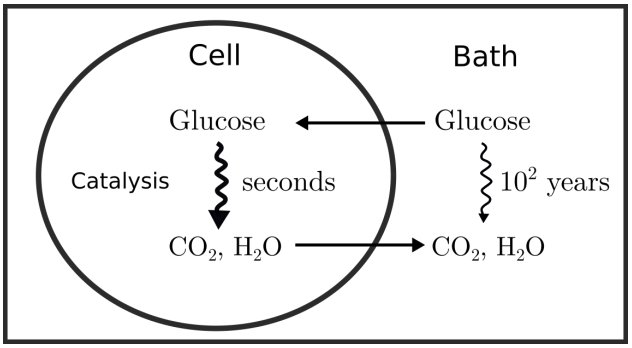

Figure 1.11 By catalysis, the cell makes reactions that are too slow or not possible in the bath happen fast in the cell, to keep it from becoming in equilibrium with the bath.

the example, the glucose in solution is also tending towards carbon dioxide and water, but that is very slowly. This means the energy landscape the cell is in is actually larger than what is defined by the bath, since the state of the bath itself is slowly moving. To visualize this, we can imagine there is a y-axis that the whole (x, z)-axis landscape defined by the bath can move along (see Figure 1.10). The landscape along the y-axis is extremely flat, but going eventually to a very low energy level, illustrating that the natural process towards equilibrium along the y-axis is very slow, but there is lots of energy to dissipate. In the example, the lowest energy state in the (x, z)-axis landscape is that the glucose concentration in the vesicle is the same as in solution, but if moving along the y-axis is included, then the lowest energy state is all glucose decomposed into carbon dioxide and water, both in solution and vesicle.

Now we see that the cell can deviate away from the equilibrium track with the bath if it can go down in energy along the y-axis faster than the bath! That is achieved by catalysis, and keeping catalysis restricted to the cell. Visually, catalysis opens a new track along the y-axis that goes down steeply, allowing the cell to tend towards the cell-bath's overall equilibrium along a path that is not in equilibrium with the bath. Indeed this is steep, bringing processes on hundreds-of-years timescale down to milliseconds! Therefore, although the overall cell-bath system is always going down in energy, the cell can explore the landscape outside the equilibrium-with-bath path and perform versatile behaviors by dissipating energy faster-than-bath through catalysis. In short, cell activities are enabled by catalysis.

Given this, we see the core in understanding the behavior of cells is understanding how catalysis is regulated. This motivates our central focus on catalysis, that the core structure of biomolecular reactions is binding's regulation of catalysis, and the systems theory is machines with inputs and outputs as catalytic fluxes in metabolism.

To formally describe this understanding that catalysis is the core of bioactivity, let us

consider how biological catalysis reactions are different from generic chemical reactions, e.g. in chemical plants. To clearly denote catalysis reactions and their kinetics, we introduce some basic notions from chemistry. Generic chemical reactions are divided into two classes: elementary reactions and non-elementary reactions. We denote elementary reactions with arrow $\longrightarrow$, and non-elementary reactions with squiggly arrow $\rightsquigarrow$. Elementary reactions are where molecules directly react to form products, with no intermediate. In practice, this is defined by either no intermediate is detected, or no intermediate is needed to explain the behavior of the reaction. Elementary reactions almost always are unimolecular (one reactant molecule) or bimolecular (two reactant molecules). The rate of elementary reactions follow the law of mass action. For example, reaction $A \xrightarrow{k} *$ happens with rate kA, where k is rate constant and A denote the concentration of A. Reaction $A + B \xrightarrow{k} *$ happens with rate kAB, and similarly $2A \xrightarrow{k} *$ happens with rate kA^2. This law of mass action can be derived from a collision model of molecules, where reactant molecules move around randomly and by a small chance collides with each other, in which case the reaction happens [109]. Generic chemical reactions then can be considered as arbitrary systems built from such elementary reactions.

In contrast to elementary reactions, reactions in cells are catalysis reactions with negligible spontaneous rates. These catalysis reactions are not elementary, but can be decomposed into several elementary steps, namely binding and conversion steps. This reaction happens via the binding of a catalyst, such as an enzyme, with a substrate, to form an intermediate complex, which is key for the catalyst's effect on lowering energy barrier. For example, a simple enzymatic catalysis reaction in both forward and reverse directions can be written as

$$E + S \underset{k_1^-}{\overset{k_1^+}{\rightleftharpoons}} C \underset{k_2^-}{\overset{k_2^+}{\rightleftharpoons}} C' \underset{k_3^-}{\overset{k_3^+}{\rightleftharpoons}} E + P. \tag{1.1}$$

Here E is enzyme, S is substrate, and P is product. The enzyme E binds with substrate S to form intermediate complex C, which gets converted into the enzyme-product complex C'. The catalysis reactions here, which record the net change in molecules regardless of whether it is in free or bound forms, are

$$t_S \overset{k_2^+ C}{\rightsquigarrow} t_P, \qquad t_P \overset{k_2^- C'}{\rightsquigarrow} t_S. \tag{1.2}$$

Here t_S is the total concentration of the substrate, defined as $t_S = S + C$, the sum of free substrate and the substrate bound in complex C. Similarly, t_P is the total concentration of the product, defined as $t_P = P + C'$. Note that we used squiggly arrows here since catalysis reactions are not elementary and involve more detailed steps of binding reactions. Indeed, their rates do not follow mass action when written as non-elementary reactions.

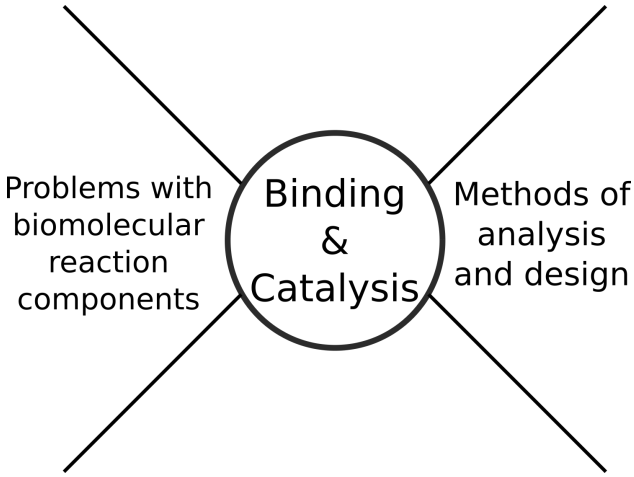

Figure 1.12 The cores structure of biomolecular systems is binding and catalysis.

Instead, their rates follow from mass action on the network of elementary reactions in Eqn (1.1) and the definitions of the totals. We denote the rates or fluxes of the catalysis reactions by the symbols on top of the squiggly arrows in Eqn (1.2). For example, $k_2^+ C$ is the flux of the substrate to product catalysis reaction. The production rate of product from this flux is therefore proportional to the concentration of enzyme-substrate complex C. We often call this complex C the active complex of the substrate to product flux. Similarly, C' is the active complex of the product to substrate flux. How the fluxes of these two catalysis reactions are regulated then corresponds to how the concentration of active complexes depend on the total concentrations, namely total enzyme, total substrate, and total product. In other words, the regulatory profile of the catalysis reactions correspond to the functions $C(t_E, t_S, t_P)$ and $C'(t_E, t_S, t_P)$. Here the total enzyme concentration t_E is defined by $t_E = E + C + C'$. These functions are determined by the steady state equations of the binding reactions:

$$E + S \underset{k_1^-}{\overset{k_1^+}{\rightleftharpoons}} C, \qquad E + P \underset{k_3^+}{\overset{k_3^-}{\rightleftharpoons}} C'. \tag{1.3}$$

In other words, the regulatory profile of catalysis fluxes are determined by the network of binding reactions. This motivates the core structure of biomolecular reactions in cells as consisting of two types of reactions: binding and catalysis (see Figure 1.12). Catalysis determines the direction of change, as in Eqn (1.2). Binding determines how the catalysis fluxes are regulated, as in Eqn (1.3). Therefore, characterizing the regulatory profile of catalysis fluxes, which is the central task of understanding bioactivity, is to characterize the steady states of binding networks. This is the goal of Chapter 3, with introductions and examples in Chapter 2.

To recap, like force and mass form the core structure of mechanical components, I have argued that binding and catalysis form the core structure of biomolecular reactions. So,

binding and catalysis reactions are the knot in the middle of a bowtie (see Figure 1.12). On the left, components of biomolecular reactions in any system can be formulated into binding and catalysis reactions. On the right, analysis and design of biomolecular components corresponds to analyze and design networks of binding and catalysis.

Before we end our discussion on catalysis, I briefly mention an alternative to our focus on catalysis fluxes: the focus on catalytic enzymes. The enzyme state transitions formulation has been popular in biophysics and offers some complimentary insights. The enzyme state transitions formulation focuses on how the state of the enzyme molecule changes over time. From a systems theory perspective, the focus on catalysis fluxes considers molecular concentrations of the whole system, so a biomachine is acts on molecular concentrations through metabolic fluxes. In contrast, the enzyme state transitions formulation focuses on just an enzyme molecule, so a biomachine is just an enzyme molecule cycling in states, ignoring upstream and downstream molecules' concentrations. This enzyme state transitions formulation may not appear as natural for a biomolecular system in cells, but it is the natural view when properties of the enzyme are in focus or when the state of the enzyme carries important information. For example, performance of molecular motors such as ATPase and myosin comes from understanding properties of their cycling through states. For a gene that transition between repressed or activated states, such as in developmental biology, the state itself may be of major importance. Therefore, the enzyme state transitions formulation can be considered as looking at a metabolic machines through magnifying glasses and focusing on each enzyme catalyzing every flux. The properties and constraints on enzyme state transitions can then be incorporated as constraints on fluxes in metabolic machines.

As an example, we can take the binding and catalysis system in Eqn (1.1) and write the following for the enzyme state transitions formulation:

$$E \underset{k_1^-}{\overset{k_1^+ S}{\rightleftharpoons}} C \underset{k_2^-}{\overset{k_2^+}{\rightleftharpoons}} C' \underset{k_3^- P}{\overset{k_3^+}{\rightleftharpoons}} (E). \tag{1.4}$$

Here the last (E) denotes that this is a repeated state, the same as E, the free enzyme state, at the beginning. So this is a 3-state loop. Note two transition steps, namely E to C, and E to C', have non-constant rates that depend on concentrations of substrate and product. If we begin with high amounts of substrate and low amounts of product, the state transitions have a net forward cycling in the direction $E \to C \to C' \to (E)$. With the catalysis in mind, this net cycling converts substrates into product, therefore the rates change over time, with forward cycling slower and slower, eventually balancing with the reverse cycling, reaching an equilibrium. Such equilibrium at the state transition level

satisfy detailed balance. Detailed balance means for each pair of states, the forward and backward transition fluxes balance out, so there is no net cycling on any loop. To analyze enzyme state transitions such as Eqn (1.4), it is often formulated as Markov chains with constant rates, which assumes molecular species other than the enzyme are overabundant in concentration. Methods solving generic Markov chains can then be applied [53, 76], although the resulting solution may be too complicated to extract insight. The enzyme state transitions can also be formulated as a nonequilibrium system with sparse driving at certain transitions, as is often the case in biology, enabling better analytical insight (see [72]). Further simplifications, such as assuming the enzyme states are at equilibrium, can be fruitful for several scenarios, especially transcriptional regulation of gene expression and enzyme allostery [88].

1.4 Constraints and hard limits from stoichiometry, thermodynamics, and biocontrol on simple autocatalysis

Constraints and hard limits are the perspectives this thesis takes to understand biological behaviors. In addition, this thesis considers dynamics as the main reason for many regulatory mechanisms. In particular, homeostasis, one of the hallmarks of biological behavior, is often achieved only via active regulatory mechanisms, due to the intrinsic instability of many biological systems. As developing tools that characterize these require some technical development not important for the discussion here, we illustrate these perspectives using simple examples with short calculations or intuitive arguments here. As an example, we consider simple descriptions of autocatalytic reactions. This is quite worthwhile since catalysis is at the core of biological activity, so autocatalysis is at the core of biological growth. Regarding constraints and hard limits, we show that stoichiometry constrains the steady state fluxes, while thermodynamics relate metabolite concentrations and Gibbs free energies to constraints on flux directions and magnitudes. Regarding dynamics and hard limits from biocontrol, we show that the intrinsic instability of autocatalysis makes regulating it a problem similar to balancing a stick, which is hard from our intuition, and is fundamentally harder than holding a stick downwards. Related methods for calculations are discussed in detail in Chapter 4.

Simple models of autocatalysis

We can begin formulating simple descriptions of autocatalysis by modelling after autocatalytic reactions. One common example of autocatalysis is energy regeneration in glycolysis,

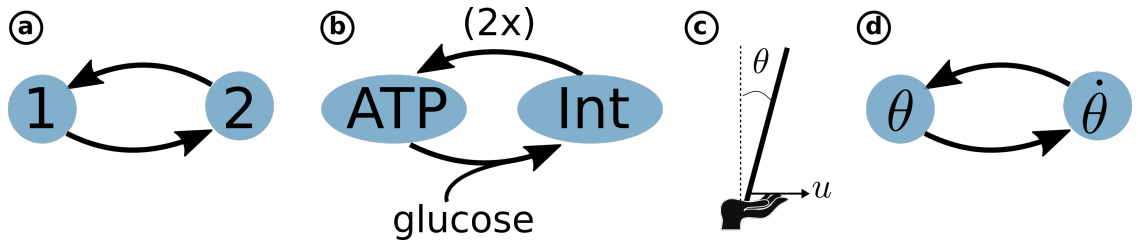

Figure 1.13 Autocatalysis. **(a).** Autocatalysis has a positive feedback interaction between two lumped variables of the system, which is intrinsically unstable. **(b).** A simple model of glycolysis capturing its autocatalytic stoichiometry is described by two species, ATP and intermediate (Int), and two reactions, consuming ATP to produce intermediate by activating glucose, and consuming intermediate to produce more ATP (2-fold in the figure). **(c).** Cartoon illustrating balancing a stick. **(d).** Stick balancing also has a positive feedback interaction between its state variables, angle θ and angular velocity $\dot{\theta}$, therefore intrinsically unstable, just like autocatalysis.

where ATP is used to activate glucose, with more ATP generated eventually (see (b) of Figure 1.13). To model this in a minimal way, we can lump detailed reaction steps together and consider just two reactions, one consuming ATP to activate glucose, resulting in an intermediate, and the other consuming an intermediate, producing more ATP. We can denote the two molecular species involved generically as X_1 and X_2, with X_2 denoting the target species of autocatalysis such as ATP, and X_1 denoting intermediate. If we normalize the unit of concentration for ATP or energy charge such that the net production through an autocatalytic cycle generates one unit of X_2, then we have the following dynamics of the metabolite concentrations:

$$\frac{d}{dt}\begin{bmatrix} x_1 \\ x_2 \end{bmatrix} = \begin{bmatrix} -1 & 1 \\ 1+q & -q \end{bmatrix} \begin{bmatrix} v_1 \\ v_2 \end{bmatrix} + \begin{bmatrix} 0 \\ -1 \end{bmatrix} w. \tag{1.5}$$

Here q denotes the stoichiometry for the amount of ATP needed to activate glucose to produce the intermediate. We also added an external flux w that consumes ATP. This is generic for autocatalytic processes, since the target autocatalytic species is always produced for a consuming goal, such as an energy source or accumulated as part of biomass. Accumulation into biomass is effectively consuming the species under exponential growth.

Other types of autocatalytic processes can be obtained based on whether the target species X_2 and the intermediate X_1 are catalytic or consumed in the reactions. For example, if we write a simple lumped equation for ribosomes catalyzing the production of itself, we may write

$$\frac{d}{dt}\begin{bmatrix} x_1 \\ x_2 \end{bmatrix} = \begin{bmatrix} -q & 1 \\ 1 & 0 \end{bmatrix} \begin{bmatrix} v_1 \\ v_2 \end{bmatrix} + \begin{bmatrix} 0 \\ -1 \end{bmatrix} w. \tag{1.6}$$

Here the second reaction is ribosomes X_2 catalyzing the production of its ribosomal parts or intermediates X_1, and the first reaction is parts assembled into ribosomes. Because

ribosomes work as catalysts, the stoichiometry matrix $\boldsymbol{S}$ has $s_{22} = 0$. The parameter q here correspond to the units of intermediates needed to produce one unit of ribosome. We choose the normalizations so that one autocatalytic cycle still produces one unit of the target species X_2. Here the external consumption w now corresponds to biomass accumulation or growth.

As another example, we can consider ribosomes as X_2 and RNA polymerases as X_1, although in this case both may serve as the autocatalytic target. In this case, ribosomes produce RNA polymerases, while RNA polymerases also produce ribosomes, both through catalysis. Therefore we obtain

$$\frac{d}{dt}\begin{bmatrix} x_1 \\ x_2 \end{bmatrix} = \begin{bmatrix} 0 & q \\ 1 & 0 \end{bmatrix}\begin{bmatrix} v_1 \\ v_2 \end{bmatrix} + \begin{bmatrix} 0 \\ -1 \end{bmatrix} w. \tag{1.7}$$

Here q is used to capture the difference in catalytic activities of RNA polymerase and ribosomes.

Constraints from stoichiometry

With the simple models of autocatalysis defined, we immediately see that the stoichiometry matrices play an important role in writing the dynamics of the system. Physically, we know the stoichiometry governs what reactions can happen in this system. However, it seems unclear whether the stoichiometry constrains what values the metabolite concentrations (x_1, x_2) or the fluxes (v_1, v_2) can take in any way.

One way to clearly see the constraint on biological behavior by stoichiometry is to look at the steady state fluxes. This is the basis for flux balance analysis (FBA), one of the most popular constraint-based approaches in modeling metbolism [60, 85]. We use the glycolysis form of autocatalysis to illustrate this. At steady state, $\frac{d}{dt}x_1 = \frac{d}{dt}x_2 = 0$, so Eqn (1.5) becomes a linear equation, which can be solved in the following way:

$$\begin{bmatrix} -1 & 1 \\ 1+q & -q \end{bmatrix}\begin{bmatrix} v_1^* \\ v_2^* \end{bmatrix} = \begin{bmatrix} 0 \\ 1 \end{bmatrix} w^* \quad \Longrightarrow \quad \begin{bmatrix} v_1^* \\ v_2^* \end{bmatrix} = \begin{bmatrix} q & 1 \\ 1+q & 1 \end{bmatrix}\begin{bmatrix} 0 \\ 1 \end{bmatrix} w^* = \begin{bmatrix} w^* \\ w^* \end{bmatrix}. \tag{1.8}$$

So we see that the internal fluxes (v_1, v_2) are completely determined by the external flux w. To be specific, internal fluxes has 2 degrees of freedom, and the constraint from a rank-2 stoichiometry matrix at steady state eliminates 2 degrees of freedom, resulting in a unique solution. This illustrates how stoichiometry becomes a constraint on how internal and external steady state fluxes are related. The stoichiometry of the reactions involved, when known, act as hard constraints on cell behavior, as unassailable as universal laws such as

conservation of mass. Based on the stoichiometry constraint, we can strongly constrain internal fluxes based on measurements of external fluxes.

That we obtain a unique solution of internal steady state fluxes here is of course not common. Extra degrees of freedom on steady state internal fluxes are necessary for the cell to have "choices" and perform adjustments based on environments at steady state. A unique solution happens here because we used lumped descriptions, while a more detailed stoichiometry matrix is often wide, and therefore not full rank. To illustrate what happens when there are extra degrees of freedom at steady state, consider adding another reaction with flux v_3. We can term this flux growth, which just consumes ATP, but can be regulated by the cell, and therefore constitutes an internal flux.

$$\frac{d}{dt}\begin{bmatrix} x_1 \\ x_2 \end{bmatrix} = \begin{bmatrix} -1 & 1 & 0 \\ 1+q & -q & -1 \end{bmatrix} \begin{bmatrix} v_1 \\ v_2 \\ v_3 \end{bmatrix} + \begin{bmatrix} 0 \\ -1 \end{bmatrix} w.$$

Now the cell has an extra knob v_3 to tune. To make the numbers simple, let us take $q = 1$. The internal steady state fluxes then have one degree of freedom left from the stoichiometry constraint, which we parameterize as follows.

$$\begin{bmatrix} v_1^* \\ v_2^* \\ v_3^* \end{bmatrix} = \frac{1}{3}\begin{bmatrix} 1 \\ 1 \\ -2 \end{bmatrix} w^* + \begin{bmatrix} 1 \\ 1 \\ 1 \end{bmatrix} c = \begin{bmatrix} \frac{1}{3}w^* + c \\ \frac{1}{3}w^* + c \\ -\frac{2}{3}w^* + c \end{bmatrix}, \tag{1.9}$$

where c is a real constant that parameterizes the solution set. So we see that the steady state fluxes v_i^* can be split into two parts: the part determined by external fluxes which depends on w^*, and the part regulated internally which depends on c. In particular, we see that any internal adjustment to increase growth consumption of ATP v_3^* will necessarily require simultaneous increase of ATP and intermediate productions v_1^* and v_2^* in the same amount. This is again hard constraints on all steady state fluxes that can happen, directly from stoichiometry.

One might argue that while the stoichiometry can work as a strong constraint if it is known for sure, but in reality it is hard know the stoichiometry for sure since one reaction stoichiometry we write may actually consists of several detailed steps. This can be studied by considering how much variation in behaviors can be fundamentally caused by changing the stoichiometry in certain ways. Given that detailing one reaction into several steps keep important structures intact, such as the overall autocatalytic structure, some results will hold independent of the changes. Such results can be studied systematically using control theory methods that compare responses between different systems. See discussions in Chapter 4.

Constraints and hard limits from thermodynamics

One pitfall of just considering stoichiometry is that nothing can be said about metabolite concentrations. Indeed, all the discussion above are about steady state fluxes. This is because at steady state the metabolite variables x_i disappear from the equations. In fact, steady state metabolite concentrations are determined by how the fluxes are regulated by detailed mechanisms, such as specified by functions $v_i(\boldsymbol{x})$, where $\boldsymbol{x}$ denote the vector of all metabolite concentrations in the system.

However, without knowing the detailed mechanisms, we can still constrain metabolite concentrations by relating them to irreversibility or energy dissipation of the fluxes. Again taking the glycolysis case to illustrate. Given that ATP at intracellular concentration provides a very strong driving force, we may confidently state that the flux v_1 is irreversible. This in turn becomes a requirement that the free energy change of reaction v_1 is negative, which can be used to bound metabolite concentrations.

For example, we may take reaction v_2 to represent glucose and 2 ATP react to 2 G3P and 2 ADP, the lumped ATP consuming half of glycolysis. We know the free energy change of this lumped reaction under physiological conditions is $\Delta G_2 = -53.73\ \mathrm{kJ\,mol^{-1}}$ (for red blood cell, see page 584 of [48]). Free energy changes vary with concentrations multiplicatively through $2.3RT \log_{10} Q$, where R is molar gas constant, T is temperature, and Q is reaction quotient calculated by fold-change of product and reactant concentrations raised to the power of their stoichiometry. So in this case, $Q = \tilde{\Delta}x_1(\tilde{\Delta}x_2)^{-q}$, with glucose and ADP ignored by assuming they are kept at constant concentrations. Here $\tilde{\Delta}x_i$ means fold-change of x_i's concentration compared to the physiological condition. Since $2.3RT$ is about $5.7\ \mathrm{kJ\,mol^{-1}}$ at $25\ ^\circ\mathrm{C}$, we have estimated that $\tilde{\Delta}x_1(\tilde{\Delta}x_2)^{-q} \leq 10^9$, and that the total variation of intermediates and ATP away from their physiological concentration (in the right direction) cannot be more than 6 orders. This is a rather loose bound, although not completely impossible since ATP to ADP equilibrium ratio is about 10^{-9} while physiological conditions often maintain this at 10.

To get tighter bounds, we need to consider where the negative free energies go. When reactions are kept at negative free energy change ΔG, each net forward reaction dissipates this much energy. A large portion of it goes into driving the reaction forward at a rate much faster than equilibrium kinetics. This is necessary since without driving, the reaction would have an infinitely small net flux. Although not all free energy change is used to drive the reaction because of other dissipation sinks such as enzyme vibrations, we can consider it as an upper bound on how fast the reaction can be driven. To relate this to changes in kinetic

rates out of equilibrium, existing theoretical frameworks take the enzyme view, so that the forward reaction corresponds to the cycling of the enzyme through its states. The driving and dissipation relation often used in nonequilibrium statistical physics is $v\Delta\mu = \sigma T$ ([72], also see Chapter 4), where $\Delta\mu = k_B T \log \frac{q^+}{k^+}$ is the chemical potential required to drive the equilibrium kinetic rate of forward direction k^+ to the out-of-equilibrium rate q^+. k_B the Boltzmann constant is used here because such formula is often used in single enzyme context. σ denote entropy dissipation rate. v denote the net reaction flux. For glucose to G6P, while we do not know the equilibrium kinetic rate k^+, if the catalyzing enzyme hexokinase does not have any activity when there is almost no ATP (at equilibrium ATP to ADP ratio is less than 1 to 10^9), then we can take the spontaneous degradation rate of glucose, which is estimated to be per 100 years [115], or 3×10^9 seconds. To estimate what the driven rate q^+ should roughly be, we can use widely a widely observed number that glucose uptake per gram of dry weight of E. *coli* is on the order of $10\ \mathrm{mmol}$ per hour. Since 1 gram of dry weight has about 10^{12} cells, this means about 6×10^8 molecules per hour per cell. For a rich glucose concentration of $6\ \mathrm{mM}$, there is about 6×10^6 glucose molecules in a cell. So to achieve 6×10^8 molecules per hour per cell, we need conversion of glucose at a rate of 100 per hour, or about one per 30 seconds. If we take this as q^+, then this require 10^8 fold increase from the equilibrium kinetic rates. This correspond to $\Delta\mu = 2.3RT \cdot 8 = 45.6$ $\mathrm{kJ\,mol^{-1}}$ in molar units. To keep ΔG above this number, we can vary concentrations away from physiological conditions without decreasing ΔG more than $53.7 - 45.6 = 8.1\ \mathrm{kJ\,mol^{-1}}$. This corresponds to $\tilde{\Delta} x_1 \tilde{\Delta} x_2^{-q} \leq 10^{\frac{8.1}{5.7}} \approx 26$. So the total fold change cannot be more than 26 fold away from the physiological condition. This is a much tighter bound. Conversely, this very rough estimate can mean deviations of concentrations from the physiological condition in the worsening direction may drastically influence glucose uptake rate.

Hard limits from biocontrol

Previously, for constraints and hard limits from stoichiometry and thermodynamics, we have focused on steady state fluxes and metabolite concentrations. However, we simply assumed steady states exist, without ever checking that they are stable and therefore achievable. If a steady state is not stable, then despite all the steady state analysis, it cannot be achieved, and the metabolic system may have oscillatory or unstable behavior such as some metabolites crashing to zero.

In fact, without active regulations, autocatalytic systems are intrinsically unstable, in the sense that increase in x_1 above the steady state value will cause increase in x_2, which in turn cause increase in x_1, thus an upward spiral blowing up to infinity. Alternatively,

decrease in x_1 below its steady state value will cause decrease in x_2 which in turn cause decrease in x_1, thus forming a downward spiral crashing to zero. As regulatory motifs, we can consider x_1 and x_2 positively influence each other, creating a positive feedback loop (see (a) of Figure 1.13). However, unlike gene regulatory circuits, there is no saturation or safety valve in metabolism, or cells crash before saturation thresholds are reached.

That autocatalytic systems are intrinsically unstable due to the autocatalytic stoichiometry poses hard limits on what regulations on them can do. Requiring stability of the steady state, for example, would pose lower bounds on the steady state error when the demand flux w is varied. More generally, a tradeoff between steady state accuracy and system robustness is unavoidable for such systems. As a result of this, oscillatory behavior is unavoidable when regulations are applied to adapt to changing demands, i.e. minimizing steady state error. This is analyzed in [25] for the case of glycolysis, showing that glycolytic oscillation is a necessary side effect of this tradeoff.

Instead of delving into the technical details to show these hard limits due to intrinsic instability of autocatalysis, as is done in [25] and in Chapter 4, here we instead appeal to the reader's intuition about a familiar intrinsically unstable system: balancing a stick (see (c) of Figure 1.13). Indeed, stick balancing has been used as a tutorial example for system fragility due to intrinsic instability [70]. Below, through standard calculations, we show that the dynamic equations of balancing a stick have a similar form as the autocatalytic equations in Eqn (1.5) and Eqn (1.6). As a result, our intuitions about the hardness in balancing a stick, and the oscillatory movements of hand and stick when disturbed, all pass down to hard limits on dynamics of autocatalytic metabolism.

Balancing a stick. For the sake of clarity, we derive the local dynamics of balancing a stick following standard calculations. Balancing a stick by hand is the same problem as balancing an inverted pendulum on a moving cart. Consider a stick of length ℓ, with mass m at the head, and we control the bottom of the stick on a horizontally moving cart (or hand), which has mass M. Let θ be the angle of the stick, so that $\theta = 0$ is straight up, and $\theta = \pi$ is straight down.

The equations of motion governing an inverted pendulum on a cart, the same as a hand balancing a stick, is

$$\begin{aligned}(M+m)\ddot{x} + m\ell(\ddot{\theta}\cos\theta - \dot{\theta}^2\sin\theta) &= u,\\ m(\ddot{x}\cos\theta + \ell\ddot{\theta} - g\sin\theta) &= 0.\end{aligned}$$

Here x is the position of the cart or hand, with positive x in direction to the right. u is the force applied to the cart or hand horizontally, also to the right. Linearize this around the

static upright position, i.e. around $\theta^* = 0$, so that $\theta = \theta^* + \delta\theta$ for small angle deviation $\delta\theta$, and similarly for all time derivatives such as $\delta\dot{\theta}$, $\delta\ddot{\theta}$ and $\delta\ddot{x}$. We obtain

$$\begin{aligned}(M+m)\delta\ddot{x} + m\ell\delta\ddot{\theta} &= u,\\ \delta\ddot{x} + \ell\delta\ddot{\theta} - g\delta\theta &= 0.\end{aligned}$$

Note the term $\dot{\theta}^2 \sin\theta$ disappears since it is a higher order term. These can be combined to form the dynamics for the stick angle θ:

$$(M+m)g\ \delta\theta - M\ell\ \delta\ddot{\theta} = u.$$

Take the stick angle $\delta\theta$ and its velocity $\delta\dot{\theta}$ as the state variables, we obtain the following system of equations.

$$\frac{d}{dt}\begin{bmatrix}\delta\theta\\ \delta\dot{\theta}\end{bmatrix} = \begin{bmatrix}0 & 1\\ (1+\frac{m}{M})\frac{g}{\ell} & 0\end{bmatrix}\begin{bmatrix}\delta\theta\\ \delta\dot{\theta}\end{bmatrix} + \begin{bmatrix}0\\ -\frac{1}{M\ell}\end{bmatrix}u. \tag{1.10}$$

We see that this stick balancing problem has a similar issue of positive feedback causing downward crashes or blow ups that we anticipated in autocatalysis without active regulation (see (d) of Figure 1.13). An increase in angle $\delta\theta$ causes increase in angular velocity $\delta\dot{\theta}$, while an increase in $\delta\dot{\theta}$ in turn causes $\delta\theta$ to increase. Crashes or blowups in stick balancing corresponds to the stick falling down.

To see the dynamic equation for stick balancing matching with autocatalysis exactly, let us write out the local dynamics of autocatalytic systems without active regulation. The passive dynamics of the reaction fluxes v_1 and v_2 come from their naturally increase with the increase of reactants or catalysts. In other words, the local dynamics of v_1 has positive derivative in x_1, and similarly v_2 has positive derivative in x_2. Denote these derivatives k_1 and k_2 respectively, we have $v_1(\boldsymbol{x}) \approx v_1^* + k_1\delta x_1$, where v_1^* is the steady state flux and δx_1 is small deviation of x_1 from the steady state concentration x_1^*, and similarly $v_2(\boldsymbol{x}) \approx v_2^* + k_2\delta x_2$. So we can write out the local dynamics for the Ribosome-RNAP autocatalytic system in Eqn (1.7).

$$\frac{d}{dt}\begin{bmatrix}\delta x_1\\ \delta x_2\end{bmatrix} = \begin{bmatrix}0 & q\\ 1 & 0\end{bmatrix}\begin{bmatrix}k_1 & 0\\ 0 & k_2\end{bmatrix}\begin{bmatrix}\delta x_1\\ \delta x_2\end{bmatrix} + \begin{bmatrix}0\\ -1\end{bmatrix}\delta w = \begin{bmatrix}0 & qk_2\\ k_1 & 0\end{bmatrix}\begin{bmatrix}\delta x_1\\ \delta x_2\end{bmatrix} + \begin{bmatrix}0\\ -1\end{bmatrix}\delta w. \tag{1.11}$$

We see that the local dynamics is exactly the same as that of the stick balancing system. The other two autocatalytic systems in Eqn (1.5) and (1.6), have the same form of dynamic equation after a slight change of variable. For example, the amino acid-ribosome system in variable $\delta y_1 = \delta x_1 + q\delta x_2$, $\delta y_2 = \delta x_2$, has the same form as the stick balancing system.

In summary, we see the dynamics of an autocatalytic system around a steady state has the same intrinsic instability as balancing a stick around its upright position. Therefore, all the hardness and limitations we intuitively understand about balancing a stick propagates in full to regulating an autocatalytic systems. In particular, active regulatory mechanisms are needed to maintain homeostasis for autocatalysis systems. This is an intuitive and simple example illustrating how considerations on stability and dynamic regulation from biocontrol reveal the necessity of regulatory mechanisms, and can impose hard limits on bioregulation.

Chapter 2

Polyhedral constraints enable holistic analysis of bioregulation

Biomolecular processes in cells happen through catalysis by enzymes. To regulate the rate of these processes, substrates, regulator proteins, cofactors, and other helper molecules bind with or chemically modify the catalytic enzyme to change its activity. Since state transformation by chemical modification can be considered a subcase of binding, we lump them together and call them binding reactions. Understanding the profile of bioregulation therefore constitutes characterization of all the ways that catalysis, or enzyme activities, can be regulated by a network of binding reactions. However, quantitative understanding of how binding regulates catalysis is hard both analytically and computationally, even in the bulk scale where concentrations rather than molecule counts are considered, and assuming binding is fast therefore reaches steady state. This is because the steady state equations from binding reactions relate various bound forms of the enzyme to molecular concentrations through polynomial equations, with degree increasing proportional to the number of binding reactions. Thus analytical or computational methods to find the set of solutions of these systems quickly become infeasible as the binding network increases in size.

Because of this, assumptions are often made to restrict to specific scenarios where simplifications can be made. Michaelis Menten or Hill type simplifications assume molecular species other than the enzyme are in high abundance, and therefore do not change in the binding process. More sophisticated methods to count the single molecule states have also been developed, such as Monod-Wyman-Changeux (MWC) models or general biophysical models with hierarchies of interacting single molecules, e.g. transcription factor states

over gene states. Nevertheless assumptions are made to simplify the problem to counting molecule states, either by overabundance of other species or by assuming experimental settings where species are in equilibrium with an environmental bath. These simplifications have been hugely successful, since many scenarios indeed satisfy the assumptions made. This is especially true for metabolic enzymes where substrate molecules are small and therefore abundant.

Recent advances in understanding regulatory circuits in developmental biology and on RNA and protein level, however, encounter binding regulations that no longer satisfy such assumptions. This is because the "substrate" could be a macromolecule as well, such as a protein phosphorylated by kinases. One example of this is combinatorial behavior, such as in BMP signaling [9], Sox2/Oct4/Sox17 regulation of endodermal differentiation [103], and synthetic multistable circuits based on this principle [122]. A common theme is that each species involved can take both high and low concentrations, with combinatorial regimes corresponding to combinations of high and low concentration of multiple species. Another example is highly dynamic regulations, such as in protein-level circuits [46] and engineered perfectly adapting circuits [10, 58]. The common theme is that large transients from perturbations can push important species out of their typical regimes, such as to a very low concentration.

These combinatorial or highly dynamic scenarios demand a way to characterize bioregulation profiles of binding networks on catalysis that does not make restrictive assumptions. In other words, a method to capture the full bioregulation profile for holistic analysis is needed.

To do so, we need to circumvent the difficult complexity of polynomial equations relating catalysis rate to concentrations. Instead of focusing on rates, we propose to characterize bioregulation through reaction orders. We show that the full landscape of bioregulation in terms of reaction orders can be tractably analyzed and computed for arbitrary binding networks, without any assumptions or restrictions. The small sacrifice is that reaction orders only capture the rates up to a multiplicative constant, so we know the fold-change response of rates to varying concentrations, but not the exact magnitude. This could be trivially resolved in cases where a reference magnitude can be measured or estimated.

In the following sections, we introduce what reaction orders are and describe how to calculate them for binding networks. We show that the full regulatory profile can be captured as polyhedral sets that reaction orders can vary in. These reaction order polyhedra also serve as constraints on bioregulation from the stoichiometry of binding networks. No matter concentrations change with large dynamic transients or in a combinatorial fashion,

bioregulation remain bounded in the polyhedra. We also demonstrate the power of holistic analysis by showing we can recover hidden adaptive regimes in an existing synthetic biocircuit.

2.1 Reaction order captures binding's regulation of catalysis

We illustrate the problem of analyzing binding's regulation of catalysis through a simple enzymatic reaction.

$$E + S \underset{k^-}{\overset{k^+}{\rightleftharpoons}} C \xrightarrow{k^{\text{cat}}} E + P. \tag{2.1}$$

Here E is free enzyme, S is free substrate, C is the complex formed from E and S binding together, and P is the product molecule formed. We note that we call S a substrate only in the sense that enzyme E acts on it, while S could be a molecule large or small. More detailed descriptions of this enzymatic reaction are sometimes used, such as introducing another intermediate complex C' representing E bound with P, or allowing the catalysis step to be reversible. The principle of the calculations we illustrate below generalize to these cases in straightforward ways.

The net catalysis in this enzymatic reaction is that one substrate molecule is converted into a product molecule. The rate or flux of this catalysis is $v = k^{\text{cat}}C$, where C here also denotes the concentration of this species. So we can express the catalysis involved as

$$t_S \overset{k^{\text{cat}}C}{\rightsquigarrow} t_P, \tag{2.2}$$

where $t_S = S + C$ denotes the total concentration of substrate molecules, and $t_P = P$ is the total concentration of product molecules. The squiggly arrow is used here to denote catalysis reactions to emphasize that catalysis is not a simple reaction, with more detailed reaction steps possibly involved such as binding reactions. The reason totals are used here is because we are considering the net effect of the catalysis reaction going forward once. It is clear that the total product has a net increase of one molecule, and the total substrate has the net decrease of one molecule. But because the substrate exists in both bound and free forms C and S, the consumed substrate molecule could come from either free or bound form, and therefore does not correspond to the net decrease of one molecule of S or C.

Binding regulates catalysis. Since the catalysis flux is $v = k^{\text{cat}}C$, the regulation of this flux is varying C when the total enzyme and substrate concentrations are varied. Since we consider the reactions in bulk scale, we write the following deterministic rate equation governing the concentration of C from mass action:

$$\frac{d}{dt}C = k^+ES - (k^- + k^{\text{cat}})C. \tag{2.3}$$

For many scenarios of interest, it is valid to assume that the binding reaction is fast for the timescale we are interested in, so the dynamics of C concentration reach steady state [53, 57, 116]. To add to the argument, we can determine the timescale of binding by looking at the state transition dynamics of the enzyme. That of the substrate molecule is completely analogous. Fixing S, the dynamics of C in the above Eqn (2.3) is transition of enzyme between free state E and bound state C. The rate out of E is k^+S, and the rate out of C is $k^- + k^{\text{cat}}$. So the dynamics can be written as the following using total enzyme $t_E = E + C$.

$$\frac{d}{dt}C = k^+ S t_E - (k^- + k^{\text{cat}} + k^+ S)C. \tag{2.4}$$

Therefore the timescale for enzyme state transition to reach steady state is $(k^- + k^{\text{cat}} + k^+ S)^{-1}$. Hence, although the unbinding rate k^- can be very slow due to a tight binding energy, the timescale of binding is governed by the sum of the three terms, therefore a small k^- does not change the timescale. Specifically, k^+S is often the largest. The diffusion-limited on rate for enzymes often takes value above 10^8 $\text{M}^{-1}\,\text{s}^{-1}$ [75, 107], so for S of 10 molecules per bacterial cell, i.e. 10 nM, we have the k^+S is $1\ \text{s}^{-1}$. So the binding timescale is almost always seconds or faster, and faster with increasing concentrations. For example, S with μM concentration has timescale in milliseconds. If the phenomenon we want to study has timescale longer than seconds, then it is plausible to assume binding is at steady state.

With the binding reaction reaching steady state, we have the following system of equations relating C and total concentrations t_E and t_S.

$$C = \frac{ES}{K}, \quad t_E = E + C, \quad t_S = C + S, \tag{2.5}$$

where the first equation is the steady state expression of complex C, and $K = \frac{k^- + k^{\text{cat}}}{k^+}$. The latter two equations are simply definitions of the total concentrations. These totals are also quantities conserved by the binding reaction. Again, we focus on how C depends on the total concentrations because once the binding network regulating the catalysis reaction is given as in Eqn 2.1 so that no other binding can happen, then cells can only adjust the catalysis rate by producing or degrading the enzyme and substrate molecules. Such production and degradation results in changes of integer numbers of molecules for the totals, but not the free or bound concentrations.

To solve for how C depends on t_E and t_S from Eqn (2.5), we can find the explicit solution in this case by solving the following quadratic equation, obtained by plugging the definitions of totals into the steady state equation.

$$KC = (t_E - C)(t_S - C) \quad \Longrightarrow \quad C = \frac{1}{2}\left(t_E + t_S + K - \sqrt{(t_E + t_S + K)^2 - 4t_E t_S}\right). \tag{2.6}$$

This expression serves as an example for the full profile of bioregulation. All possible responses of the catalysis flux in Eqn (2.1) to total concentrations is characterized by this equation. This is a hard constraint from the binding stoichiometry on how the flux $v = k^{\text{cat}}C(t_E, t_S)$ can be regulated. As long as the binding network is correct with no important binding interactions ignored, this expression captures all possible bioregulation in a holistic fashion. No matter whether or not the cells adjust the concentrations in a highly dynamic or combinatorial fashion, the resulting behavior follows this Eqn (2.6).

While the holistic description by Eqn (2.6) is highly desirable, we caution that the explicit solution can be solved here only because we chose a simple case here with just one binding reaction. With the number of binding reactions increase, the degree of the polynomial equation to be solved increases proportionally, quickly becomes unsolvable without special restrictions on the parameter values. Even for just two binding reactions, the explicit solution is already complicated, while four or more binding reactions results in degree 5 or more, so no algebraic solutions can be found. This hardness propagates to numerical computations as well. Finding specific solutions of a large system of polynomial equations is already hard, let alone scanning for how the solutions vary with the total concentrations.

Reaction orders capture binding's regulation. To circumvent this difficulty, we propose to focus on reaction orders of the flux to the total concentrations, instead of the flux itself. To introduce reaction orders in a simple way, let us consider the typical approach to circumvent the computational difficulty by restricting to specific scenarios. Assuming either the substrate is much more abundant than the enzyme $t_S \gg t_E$, or the free substrate concentration S is kept constant by an external bath, we can simplify the binding dynamics to just state transitions of the enzyme molecule. The steady state equation therefore becomes $KC = ES = (t_E - C)(t_S - C) \approx (t_E - C)t_S$, because complex concentration is much less than total substrate by $C \leq t_E \ll t_S$. Solving for C then yields the classical Michaelis-Menten formula:

$$C_{ES}^{\text{MM}}(t_E, t_S) = t_E \frac{t_S}{t_S + K}. \tag{2.7}$$

If free substrate S is kept constant by an external bath, then we would care about how the flux varies with free substrate S instead of total t_S, so we have the steady state equation in similar form $KC = (t_E - C)S$, simply replacing t_S with S. The resulting expression of C in t_E and S is also of the Michaelis-Menten form. In this simple case, all the methods based on state counting of the enzyme results in the same expression as Michaelis-Menten. In order to go beyond this approximation using state counting methods, the state of the whole system in terms of both enzyme and substrate molecules needs to be counted. But this is simply the discrete and stochastic version of the full explicit solution in Eqn (2.6), which

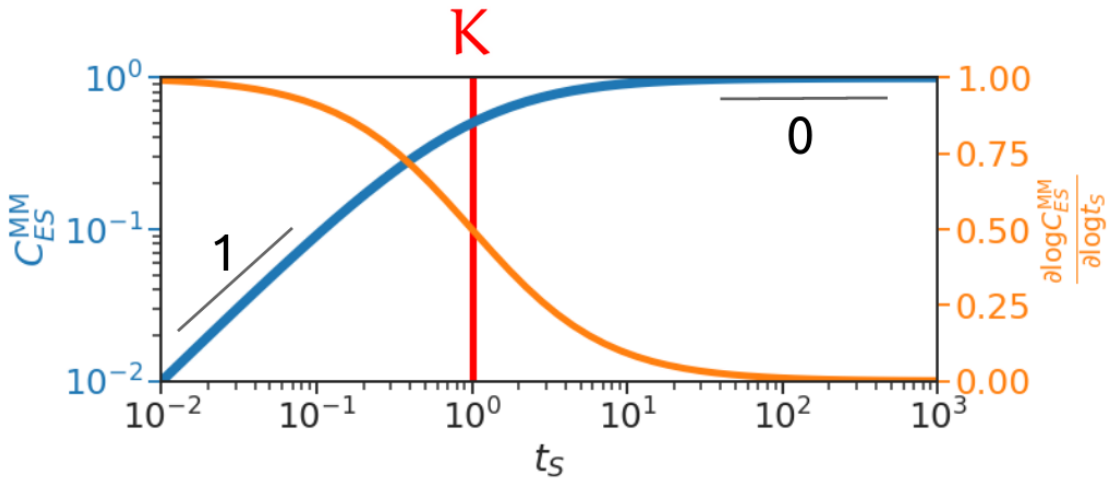

Figure 2.1 Log-log plot of the MM formula (blue and left y-axis) and the its log derivative to total substrate concentration t_S (orange and right y-axis). Parameter values are $t_E = 1$ and $K = 1$ (red vertical line). The two extremes of small and larget_S are highlighted to have slopes of 1 and 0 respectively, captured by the log derivative function.

is even harder to solve than polynomial equations as the number of binding reactions increases.

To see how the flux is regulated by total concentrations, we plotted the Michaelis-Menten formula in Figure 2.1 (blue). The response to total enzyme concentration is imply proportional, so t_E is kept constant in the plot. We see that when t_S is small compared to K, i.e. $t_S \ll K$, the flux increases linearly, or in first order, as seen from the slope in the log-log plot. When t_S is large compared to K, i.e. $t_S \gg K$, the flux becomes flat and saturates, so it does not respond to increases in t_S anymore. This corresponds to a slope of zero in the log-log plot. We see that there are two regimes in how the flux responds to t_s, a linear or first order regime when $t_S \ll K$, and a saturated or zeroth order regime when $t_S \gg K$. We can also see this by applying the asymptotic conditions $t_S \ll K$ or $t_S \gg K$ to the Michaelis Menten formula in Eqn (2.7) to obtain the approximate formula in the two regimes:

$$C_{ES}^{\mathrm{MM}}(t_E, t_S) \approx \begin{cases} \frac{t_S^1 t_E^1}{K}, & t_S \ll K; \\ t_S^0 t_E^1, & t_S \gg K. \end{cases} \tag{2.8}$$

Here we write the order explicitly. We see that the *reaction orders*, defined as the order or exponent of the flux to total concentration changes, capture how the two regimes respond differently. In more detail, the reaction orders capture what fold-change of the flux is caused by fold-changes in the total concentrations. As a result, any multiplicative constants are not described by the reaction orders, just like K is ignored in the order description of the two regimes. We note that this is only because we restricted our attention to the

total concentrations here, while the order in K can be naturally kept in reaction order calculations. See Chapter 3.

Reaction orders, or exponents, nicely capture how the flux responds to concentration changes in the two regimes at the extremes of small and large total substrate concentration t_S. Because the approximate expression of Michaelis Menten formula at these two regimes have monomial form, the exponents naturally correspond to the reaction orders. However, what happens if we do not have monomial forms. More generally, there is a range between the two regimes where the flux also responds to changes in concentrations, how can we describe the reaction orders there? Intuitively, we would think the response should be in between the linear or order 1 regime and the saturated or order 0 regime, so we expect the reaction order to smoothly vary from 1 to 0 as t_S increases. To do so, we need a continuous analogue of exponents, called log derivatives. As a simple example, if $f(x) = kx^a$, then $\frac{\partial \log f(x)}{\partial \log x} = \frac{\partial \log k + a \log x}{\partial \log x} = a$, so we see log derivatives indeed obtain the exponent for monomials. Applying log derivative to the Michaelis-Menten formula, we can calculate

$$\frac{\partial \log C_{ES}^{\mathrm{MM}}}{\partial \log(t_S, t_E)} = \left[\frac{K}{t_S + K} \;\; 1\right]. \tag{2.9}$$

The log derivative of the C's Michaelis-Menten formula to t_S is plotted in Fig 2.1 (orange curve). We see that it smoothly decreases from 1 to 0 as t_S increases, as we desired. The two regimes correspond to vectors of C's reaction order to (t_S, t_E): $(1, 1)$ for the linear regime, and $(1, 0)$ for the saturated regime. When total substrate concentration t_S smoothly increase, we obtain a line segment from $(1, 1)$ to $(1, 0)$ in reaction order space (Figure 2.2). Therefore, log derivative is a differential way to calculate reaction orders beyond the extreme regimes, so that reaction orders can be characterized for all possible concentrations. This paves the way to use reaction orders to capture the full bioregulation profile of binding networks. In particular, the bioregulation profile of the flux restricted to the Michaelis-Menten case is the $(1, 1)$ to $(1, 0)$ line segment.

Full bioregulation profile as reaction order polyhedra. With the full bioregulation profile in mind, we recall that the Michaelis-Menten formula is derived from a simplifying assumption that substrate is much more abundant than enzyme $t_S \gg t_E$. Compare the Michaelis-Menten formula Eqn (2.7) with the explicit solution for full bioregulation profile Eqn (2.6), there are behaviors that the metabolic flux can have that is not captured in the Michaelis-Menten formula. In particular, while there are two regimes captured by the Michaelis-Menten formula, we can take asymptotic conditions in the opposite direction of the $t_S \gg t_E$ assumption to find a third regime not captured by Michaelis-Menten. When $t_E \gg t_S$, the steady state equation becomes $KC = t_E(t_S - C)$. Solve for C we obtain

$C = t_S \frac{t_E}{t_E+K}$. When total enzyme concentration is small, $t_E \ll K$, we recover the linear regime in Michaelis-Menten. When total enzyme concentration is large, $t_E \gg K$, we obtain a new regime that is first order in substrate but zeroth order in enzyme: $C \approx t_S$. We summarize the three regimes as follows.

$$C_{ES}^{\mathrm{MM}}(t_E, t_S) \approx \begin{cases} \frac{t_S^1 t_E^1}{K}, & K \gg t_S, t_E; \\ t_S^0 t_E^1, & t_S \gg t_E, K; \\ t_S^1 t_E^0, & t_E \gg t_S, K. \end{cases} \tag{2.10}$$

In terms of reaction orders of C in (t_S, t_E), this means beyond the two regimes with reaction orders $(1,1)$ and $(0,1)$, there is a third regime with order $(1,0)$. This means the full bioregulation profile in terms of reaction orders goes beyond the $(1,1)$ to $(0,1)$ line segment of Michaelis-Menten to include points like $(1,0)$. So we want to see how the full bioregulation profile is represented in terms of reaction orders.

We could obtain the full set of reaction orders by directly applying log derivatives to the explicit solution Eqn (2.6). However this procedure will not work in general since the explicit solution is not available beyond simple cases. In fact, our goal is to show that reaction orders form intuitive representations of the full bioregulation profile that can be efficiently computed for large binding networks, therefore serve as much better representations of bioregulation than the function of flux in terms of concentrations.

Without relying on the explicit solution, we can directly compute the reaction orders from the steady state equations in Eqn (2.5). To do so, we consider Eqn (2.5) as defining a three-dimensional manifold constraining the six variables involved: (E, S, K, t_E, t_S, K). Then reaction orders, which are differential quantities, can be computed through implicit function theorem (see Chapter 3). The result is the following.

$$\begin{bmatrix} \frac{\partial \log C}{\partial \log t_S} & \frac{\partial \log C}{\partial \log t_E} & \frac{\partial \log C}{\partial \log K} \end{bmatrix} = \begin{bmatrix} \frac{E+K}{S+E+K} & \frac{S+K}{S+E+K} & -\frac{K}{S+E+K} \end{bmatrix}. \tag{2.11}$$

We can visualize this by obtaining points of these reaction orders through uniform sampling of (E, S, K) values, and plotting them onto the 2D space of C's reaction orders to (t_S, t_E). This is plotted in Figure 2.2.

First, we see the that a triangle with vertices $(1,1)$, $(1,0)$ and $(0,1)$ corresponding to the three regimes bounds all the points. It can also be shown analytically that the the set of all possible reaction orders is this triangle by writing Eqn (2.11) into convex combinations (see Chapter 3). The reaction order in K can also be included, which just slants the triangle. Importantly, this triangle is the set of all possible reaction orders that the flux can respond

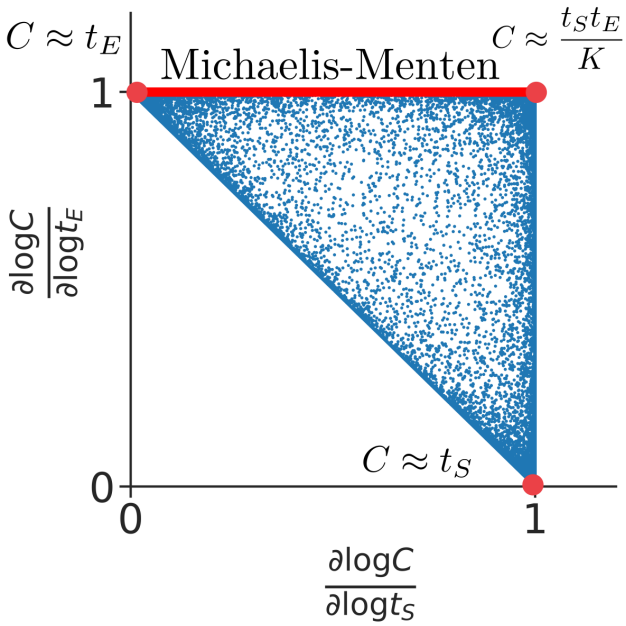

Figure 2.2 The reaction orders of C to t_S and t_E defined by steady state equations in Eq (2.5). A point in this space represents a reaction order vector of the catalysis reaction, which defines how the steady-state C concentration varies due to changes in the total concentration of E and S. The blue points are sampled from Eqn (2.11), with $e = \frac{E}{K}$ and $s = \frac{S}{K}$ log-uniformly sampled between 10^{-6} and 10^{6} for 10^5 points. A triangle with vertices $(1, 1)$, $(1, 0)$, and $(0, 1)$ bounds all the points. These vertices (red dots) correspond to structural regimes with approximate expression for C written next to them. The edge marked by the red line is the range of reaction orders covered by the Michaelis-Menten formula.

to varying concentrations for this simple binding network (Eqn (2.1)). This triangle is therefore the full bioregulation profile of this binding network represented in reaction orders. This triangle is a constraint on all possible bioregulation of the flux, just like the explicit solution Eqn (2.6). No matter the total concentrations t_S and t_E are dynamically regulated with large transients or combinatorially varied, the flux's response in terms of reaction orders is bounded in this triangle. In fact the result is even stronger: when the binding constant K is varied, maybe by different enzyme-substrate pairs, as long as the binding network is still the same, the bioregulation profile is still this triangle of reaction orders.

Next, the triangle is defined by the three vertices, which correspond to the three regimes we discussed before. Each one of them correspond to a region in the space of total concentrations (t_S, t_E) that satisfies an asymptotic condition, such as $t_S \gg t_E, K$. This means, as the total concentrations are varied during regulation, once the concentrations are pushed to extremes, then the flux automatically falls into one of the regimes, and the reaction order is pushed into a vertex. This can be seen in Figure 2.2 through the density of the points as well. We see the points are most dense at the vertices, meaning a large region

of values in (E, S, K) space has a reaction order the same as the vertex. In other words, varying the concentrations in large regions do not vary the reaction orders when they are close to the vertices. This is a measure of robustness, that large variations in concentrations do not change the reaction orders significantly, when the concentrations is already close to the vertices.

These vertices and their corresponding regimes are also structural. Structural here means that they are independent of concentrations, binding constants and kinetic rates. Instead, they are solely determined by the only thing not varied: the stoichiometry or topology of the binding network. The fact that one enzyme and one substrate binds to form a complex determines the vertices and the triangular shape of the reaction order polytope. Therefore we refer to these regimes as structural regimes, to emphasize their independence of parameters. The significant robustness of structural regimes also promotes a view of bioregulation as staying inside a structural regime most of the time, so perturbations that vary concentrations do not change reaction orders. When adjustments need to be done, then the concentrations are strongly varied to push the reaction orders from one structural regime to another, again with high robustness. Although there are intermediate reaction orders between the structural regimes, cells tend to stay in these intermediate regions very little, because they are not robust, therefore any perturbation would push the cells out of them into structural regimes. This description may underlie the observation that biology is robust yet diverse. On one hand, biological systems adapt to large disturbances of all kinds, so it seems they are in such a stable and robust position that nothing will change. On the other hand, when desired, biological systems can perform diverse behaviors in different scenarios. This robust yet diverse property may be rooted in the diverse functions of structural regimes, and the high robustness of each regime.

Now we recall our discussion about Michaelis-Menten. By making the simplifying assumption that substrate is much more abundant than enzyme $t_S \gg t_E$, two structural regimes are retained, and the reaction orders are restricted to the line segment from $(1, 1)$ to $(0, 1)$ (see red line segment in Figure 2.2). This geometrically illustrates how the full bioregulation profile compares to what is allowed by Michaelis-Menten under restricted scenarios. More importantly, we discover that assumptions in the form of asymptotic conditions, e.g. $t_S \gg t_E$, restricts bioregulation profile by projecting to an edge of the triangle. Restricting further with $t_S \ll K$ projects the edge onto the $(1, 1)$ vertex. Therefore more generally we expect asymptotic conditions would project a reaction order polyhedron to its faces. This is very useful since it provides a clear relation between the geometric objects in reaction order polyhedra with conditions in molecule concentrations. In particular,

asymptotic conditions on concentrations correspond to the hierarchical organization of vertices, edges, and faces in a polyhedron.

This correspondence between asymptotic conditions on concentrations and the geometric hierarchy of reaction order polyhedra makes simplifying assumptions transparent. To see this in action, we can consider the edges other than Michaelis-Menten. While the edge symmetric to the Michaelis-Menten one is simply enzyme is over-abundant compared to substrate $t_E \gg t_S$, the diagonal edge between $(1,0)$ and $(0,1)$ is more interesting. It is the tight binding limit, corresponding to asymptotic condition $t_E, t_S \gg K$, so that binding is very tight compared to substrate and enzyme concentrations. Restricting further with $t_E \gg t_S$ or $t_S \gg t_E$ would further project to the $(0,1)$ and $(1,0)$ vertices. Like the edge correspond to a formula in Michaelis-Menten, this edge should also correspond to a formula. By the vertices this edge connects, we already know what form it takes at extremes. To find the full formula, we can simply apply the asymptotic condition to the explicit solution in Eqn (2.6). We obtain that $C^{\mathrm{TB}} = \min\{t_S, t_E\}$, the minimum of enzyme and substrate. This makes intuitive sense, since tight binding implies any free molecule should form a complex unless one of enzyme and substrate is all consumed. Although this tight binding formula is not as popular as Michaelis-Menten, it should be because of its high biological relevance. In [10], a circuit motif achieving robust perfect adaptation is proposed that is based on the strong binding of two molecules, such as sense and anti-sense RNA strands or sigma and anti-sigma factors. This tight binding formula is perfectly appropriate in this situation, and is used in analyzing the circuit motif in [83]. In [92], this tight binding formula taking minimum between enzyme and substrate is used to unify several bacterial growth laws in distinct growth conditions. It is highly likely that the tight binding formula is used and applied in many scenarios that we do no know, simply because of the lack of a common name like Michaelis-Menten or Hill to enthrone the tight binding formula into the canon of quantitative biology.

To summarize, from a simple binding example, we see that binding's regulation of biology can be captured by reaction orders. The set of all reaction orders allowed by a binding network forms a polyhedral set. As a result, this reaction order polyhedra represents the full bioregulation profile of a binding network. The hierarchical geometry of vertices, edges, and faces of reaction order polyhedra correspond to asymptotic conditions on concentrations that are often used as simplifying assumptions in various scenarios. The vertices, in particular, correspond to structural regimes with approximate monomial formula that are highly robust to perturbations in concentrations.

2.2 Reaction order polyhedra can be derived and computed at scale

We proposed to describe bioregulation through reaction orders because the full bioregulation profile in terms of catalysis rates or fluxes' dependence on concentrations require solving high degree polynomial equations, which is intractable analytically and computationally. While previously we illustrated how reaction orders capture binding's regulation of catalysis through a simple binding network where rates can be explicitly solved, in this section we demonstrate that in contrast to rates and fluxes, reaction orders can be computed and derived at scale. We show this by first demonstrating a computational sampling algorithm to obtain reaction order polyhedra through matrix algebra. This is based on a reaction order formula for arbitrary binding networks, generalizing the procedure we used to calculate reaction orders in the simple binding network using implicit function theorem. Then we show that the reaction order polyhedra themselves can also be derived directly through a method called dominance decomposition tree (DDT), based on rules of calculus for positive variables.

Computational sampling of reaction order polyhedra. The computational procedure to sample points of reaction order polyhedra is shown in Figure 2.3. Here we choose the binding network of an induced activator as an illustration. Here G is a gene to be expressed, R is an activating transcriptional regulator, and S is an inducer of the regulator. The two binding reactions are the inducer S binds with the activator R to form a complex C_{RS}, and this induced activator binding with the gene G to form a complex C_{GRS}. C_{GRS} is then the activated gene complex capable of gene expression. So a natural objective for analysis is to understand how the gene expression is regulated by this binding network. We characterize the full bioregulation profile of this binding network by obtaining the reaction order polyhedra, without making any assumption about gene copy number, activator amount, or inducer concentration, or their binding strengths.

To obtain the reaction order polyhedra, one way is to computationally sample points from it. This will visually show the polyhedron because the vertices and edges are robust, therefore naturally have higher density of points. The computational sampling is based on a formula for reaction orders that hold for arbitrary biological binding networks, shown in step 3 of Figure 2.3. This formula is derived using implicit function theorem, through a similar process as in the reaction order calculation of the simple binding network (see Chapter 3 for details).

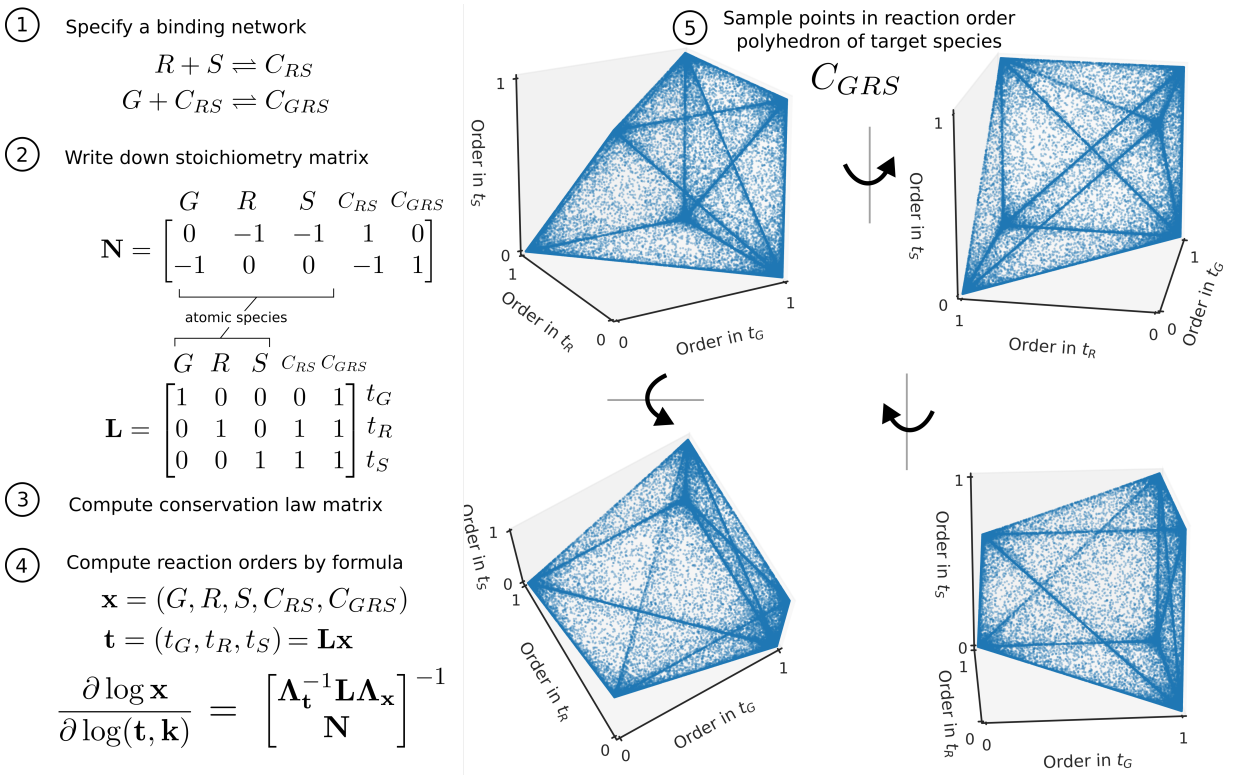

Figure 2.3 The procedure to computationally sample reaction order polyhedra of a binding network, illustrated with the binding network of an induced activator. See Chapter 3 for detailed derivations. Step 1, specify a binding network. Step 2, write down the stoichiometry matrix for the binding reactions. For each binding reaction, use the stoichiometry in the binding direction. For the order of the species, put the free form of the species first. These species are called atomic species, with the special property that conserved quantities represent totals of these species. Step 3, compute the conservation law matrix $\boldsymbol{L}$ from the stoichiometry matrix $\boldsymbol{N}$. Step 4, compute reaction orders using the formula. Here $\mathbf{\Lambda}_{\boldsymbol{t}}$ denote a diagonal matrix with the vector of totals $\boldsymbol{t}$ on the diagonal. Same for $\mathbf{\Lambda}_{\boldsymbol{x}}$. Step 5, for a target species whose reaction order is to be studied, we can sample points of its reaction order polyhedron by taking random values of $\boldsymbol{x}$, calculate $\boldsymbol{t}$ and pass through the formula to compute the reaction order, and then plot the points. The figure listed here shows the reaction order polytope of the induced activator, rotated in four different angles to show the 3D shape. The arrow around a line denotes in which direction the 3D shape is rotated from the upper left figure. Sampling of the C_{GRS} reaction order polytops is done by log-uniformly sampling the values of each variable in $(G, R, S, C_{RS}, C_{GRS})$ between 10^{-6} and 10^{6} with 100000 points in total.

To use the formula, we see it requires the input of the stoichiometry matrix $\boldsymbol{N}$ of dimension $r \times n$ and the conservation law matrix $\boldsymbol{L}$ of dimension $d \times n$, where n is the number of species involved, r is the number of binding reactions with linearly independent stoichiometry, and d is the number of conserved quantities or the number of totals. The stoichiometry matrix can be directly obtained from the binding network once it is specified, as shown in Step 2 of Figure 2.3. It might occur that there are binding reactions with linearly dependent stoichiometry vector. In that case, compute the rank r of the stoichiometry matrix, and select r of the linearly independent reactions to form the stoichiometry matrix $\boldsymbol{N}$. The result is independent of which r linearly independent reactions are selected. Since binding

reactions are reversible, as a convention, we choose the stoichiometry vector of the binding direction to form matrix $\boldsymbol{N}$. When possible, it is helpful if a subset of d of the species, considered atomic species, can be distinguished and arranged first in the ordering of the species. Atomic species often correspond to the free form of the molecules, so that their total amount is conserved through the binding reactions.

The conservation law matrix $\boldsymbol{L}$, which defines the totals, can be computed from the stoichiometry matrix $\boldsymbol{N}$ (see Step 3 of Figure 2.3 for illustration, and Chapter 3 for derivation details). If the atomic species are ordered first, then this computation is simple. We can split $\boldsymbol{L}$ into two submatrices: $\boldsymbol{L} = \begin{bmatrix}\mathbf{I}_d & \boldsymbol{L}_2\end{bmatrix}$, with the first submatrix a $d \times d$ identity matrix. Similarly split $\boldsymbol{N} = \begin{bmatrix}\boldsymbol{N}_1 & \boldsymbol{N}_2\end{bmatrix}$, then the submatrix $\boldsymbol{L}_2$ can be computed as $\boldsymbol{L}_2 = (-\boldsymbol{N}_2^{-1}\boldsymbol{N}_1)^\intercal$. Once $\boldsymbol{L}$ is obtained, the total $\boldsymbol{t}$ of dimension d can be defined as $\boldsymbol{t} = \boldsymbol{L}\boldsymbol{x}$, where $\boldsymbol{x}$, a vector of dimension n, is the concentrations of all the species involved.

With both the stoichiometry matrix $\boldsymbol{N}$ and the conservation law matrix $\boldsymbol{L}$ written down, we can apply the reaction order formula in Step 4 of Figure 2.3. This formula can calculate the reaction orders for any given concentration vector of the species $\boldsymbol{x}$. This allows us to sample points in the reaction order polyhedra for any species of interest. In Step 5 of Figure 2.3, the sampling result for reaction order polyhedron of C_{GRS} to the total gene t_G, total regulator t_R and total substrate t_S is shown. We see a polytope with vertices $(1,0,0)$, $(0,1,0)$, $(0,0,1)$, $(1,1,0)$, $(1,0,1)$, and $(1,1,1)$, where the order is C_{GRS}'s reaction order in (t_G, t_R, t_S). In particular, we see the triangle from the simple binding network is contained as a facet in this polytope. Indeed if inducer concentration is overabundant such that the R is always induced, then the induced activator binding network reduces to $G + R^* \rightleftharpoons C_{GR^*}$, where R^* denote the always induced regulator. This is exactly the same as the simple binding network. Similarly, if the regulator R is overabundant so that the inducer is always bound to regulators, or if the gene is overabundant so that any induced activator is always bound to genes, then we also have reduction to simple binding. This explains the three triangular facets of the polytope. This is another illustration of the geometric hierarchy of reaction order polyhedra, and its correspondence with asymptotic conditions on concentrations.

Lastly, we note that the computation of reaction orders only involves matrix algebra. The most costly step is inverting the matrix. This is much less costly compared to solving polynomial equations. Specifically, inverting a matrix of dimension n has computational complexity $O(n^{2.3})$ to $O(n^3)$, so the cost of computationally sample the polyhedron is $O(Nn^{2.3})$ where N is the number of points in the polyhedra to be sampled. In contrast, a rough complexity for solving systems of polynomial equations is degree to the number of equations [62]. Assuming the number of (linearly independent) binding reactions

r is proportional to the number of species n, we have computational cost $O(N2^n)$ for numerically scanning the full regulatory profile by solving the polynomial equations of binding network steady states. This is indeed much higher cost than sampling reaction order polyhedra. Furthermore, the matrices involved are very sparse for large binding networks, which can further speed up computations.

Dominance decomposition tree (DDT) can derive reaction order polyhedra directly. While the computational sampling algorithm is powerful in obtaining numerical values of reaction orders for large binding networks, to obtain the geometric shape of the reaction order polyhedra requires further analysis on top of the sampled result, such as visual inspection. Here, we describe an analytical procedure that directly obtains the reaction order polyhedra called dominance decomposition tree (DDT). This procedure also provides deeper insight into why the polyhedral shape arise in the first place. See Chapter 3 for details on the relevant concepts and derivations.

In order to obtain the reaction order polyhedra directly, we need to look into why reaction orders form polyhedral sets in the first place. In Chapter 3, we show that convex combinations are part of the fundamental rules of calculus for positive variables. To get a sense of this, we make the following observation, that log derivatives of sums of functions give rise to convex combinations. Consider $f(x) = f_1(x) + f_2(x)$, all are positive functions and x is a positive variable. Then

$$\frac{\partial \log f(x)}{\partial \log x} = \frac{f_1}{f_1 + f_2}\frac{\partial \log f_1(x)}{\partial \log x} + \frac{f_2}{f_1 + f_2}\frac{\partial \log f_1(x)}{\partial \log x}.$$

We see that for reaction orders, or log derivatives, when terms are summed together, the sum's reaction order is the convex combination of each term's reaction order. In other words, terms compete for dominance in their orders. If f_i is large, then the convex coefficient $\frac{f_i}{f}$ is closer to 1, so the order of f_i dominates in f's order. As an application of this, the log derivative of polynomials, or ratios of polynomials, form a polytope from convex combination of each term's exponents. For example, $f(x) = \frac{k_0 x^{a_0}}{k_1 x^{a_1} + k_2 x^{a_2}}$ has log derivative $a_0 - (\lambda_1 a_1 + \lambda_2 a_2)$, where λ_i are convex coefficients defined by $\lambda_1 = \frac{k_1 x^{a_1}}{k_1 x^{a_1} + k_2 x^{a_2}}$ and $\lambda_2 = \frac{k_2 x_2^{a}}{k_1 x^{a_1} + k_2 x^{a_2}}$. Translated into the reaction order context, this means when multiple processes contribute to a flux, the reaction order of the flux is a convex combination of each process's reaction order. Therefore, the flux reaction order takes value in the polytope with each process's reaction order as vertices. The flux reaction order is close to the ith vertex when the ith process is dominant over the other processes.

The reader may have noticed that the rule of competition for order dominance, or convex combinations from sums, is discussed for sums in the quantity to be differentiated. However,

for reaction orders, the sum if in the coordinate variables. For example, in the simple binding network, the reaction order of C to total substrate is $\frac{\partial \log C}{\partial \log t_S} = \frac{\partial \log C}{\partial \log (S+C)}$. So this is the situation of $\frac{\partial \log f}{\partial \log (x_1+x_2)}$, rather than $\frac{\partial \log (f_1+f_2)}{\partial \log x}$ that we discussed above. Without going into details, here we simply state that this rule of competition for order dominance propagates to sums in the coordinate variables as well. To be specific, we have

$$\frac{\partial \log f}{\partial \log x_1 + x_2} = \alpha_1 \frac{\partial \log f}{\partial \log x_1} + \alpha_2 \frac{\partial \log f}{\partial \log x_2}$$

for some convex coefficients α_1 and α_2 with $\alpha_1, \alpha_2 \geq 0$, $\alpha_1 + \alpha_2 = 1$, and α_1 becomes close to 1 when x_1 is dominant in the sum $x_1 + x_2$. Here in order for the log derivatives to make sense, the positive variables x_1 and x_2 are related to each other so that there is only one degree of freedom, e.g. $x_1 + x_2 = 1$ or $x_1 x_2 = 1$, and the function f is a function of this one degree of freedom. This internal relation between the coordinate variables is indeed the case for binding network. For example, the simple binding network has (E, S, C) constrained by the steady state equation to have 2 degrees of freedom, rather than 3.

This rule of competition for dominance is the underlying reason for the polyhedral set of reaction orders. More importantly, this rule can be applied as a calculation procedure to directly obtain the reaction order polyhedra. For example, competition for dominance applied to reaction order of C to (t_S, t_E) in the simple binding network yields the triangle straight-forwardly. When C is dominant in $t_S = S + C$, then $t_S \approx C$, so the reaction order is approximately $\frac{\partial \log C}{\partial \log (t_S, t_E)} \approx \frac{\partial \log C}{\partial \log (C, t_E)}$. Since C appears as a coordinate variable, of course the fold change of C is exactly the same as C itself, independent of t_E when C is held constant. So the reaction order in this dominance condition is $\frac{\partial \log C}{\partial \log (t_S, t_E)} \approx \frac{\partial \log C}{\partial \log (C, t_E)} = \begin{bmatrix} 1 & 0 \end{bmatrix}$. The left-over case is when S is dominant in t_S, so $\frac{\partial \log C}{\partial \log (t_S, t_E)} \approx \frac{\partial \log C}{\partial \log (S, t_E)}$. Now we can consider the next dominance condition of t_E. If C is dominant in t_E, then $\frac{\partial \log C}{\partial \log (t_S, t_E)} \approx \frac{\partial \log C}{\partial \log (S, C)}$, so again C only varies with the t_E coordinate, resulting in a simple reaction order $\begin{bmatrix} 0 & 1 \end{bmatrix}$. Then the left over case is E is dominant in t_E, which gives $\frac{\partial \log C}{\partial \log (t_S, t_E)} \approx \frac{\partial \log C}{\partial \log (S, E)}$. Now we recall the steady state expression that $C = K^{-1} SE$. So the reaction order for this dominance condition is $\begin{bmatrix} 1 & 1 \end{bmatrix}$.

From this simple binding network example, we see that applying the rule of competition for dominance to each coordinate, and ask for which term is dominant, can obtain the vertices of the reaction order polyhedron. Then taking convex combination of the vertices, we obtain the polyhedron itself. This decomposing each coordinate into different dominance conditions reminds us of how the geometric hierarchy of the reaction order polyhedron corresponds to asymptotic conditions on concentrations. Indeed, this competition for

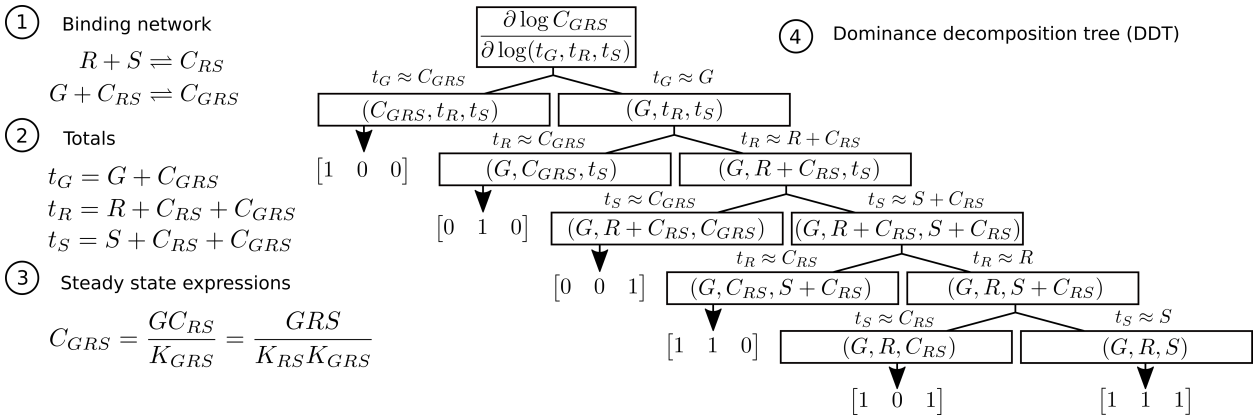

Figure 2.4 Illustration of the dominance decomposition tree (DDT) procedure to obtain reaction order polyhedra directly. The example binding network of an induced activator is used. (1) The binding network for the induced activator. (2) The definitions of the totals in this binding network. (3) The minimal expressions of C_{GRS} in terms of other species through steady state relations. (4) The DDT procedure written out step-by-step for the reaction order of C_{GRS} in (t_G, t_R, t_S). The forked lines denote a decomposition step. The variables in rectangles are coordinates with respect to which the log derivative is to be calculated. The downward black arrow means evaluation of log derivative. After decomposition has finished, all the resulting reaction orders are taken convex combination together to obtain the reaction order polyhedra.

dominance is the deeper reason for why this geometry-to-concentration correspondence can exist.

Putting together the coordinate decomposition steps using the rule of competition for dominance, we obtain the procedure called dominance decomposition tree (DDT) that can directly obtain the reaction order polyhedra. In Figure 2.4, we write out the steps of DDT applied to a more complex example: the binding network of induced activators, whose reaction order polyhedron is also computationally sampled in Figure 2.3. In the DDT procedure, We first write out the binding network, how the totals are expressed in terms of all the species, and the steady state expressions for the target species (parts 1,2 and 3 in Figure 2.4). This is for book-keeping reasons so we do not loose track when performing the decomposition steps. The expression for the totals can be obtained either by inspection or by calculating the conservation law matrix as discussed in the computational sampling procedure. The steady state expressions should include all the distinct ways that the target species can be expressed in the other species. These expressions are important in the DDT procedure to let us know when decomposed coordinates will give a constant reaction order. For example, from the steady state expression $C_{GRS} = GC_{RS}K_{GRS}^{-1}$, we know if decomposed coordinates include G and C_{RS} in them, then we the reaction order of C_{GRS} is constant under this dominance condition.

With these preparations done, in part 4 of Figure 2.4, we begin the decomposition steps for C_{GRS} in the induced activator binding network. In each step, we ask whether one of the

terms in a coordinate is dominant. For example, in the first step, we ask whether C_{GRS} is dominant in total gene $t_G = C_{GRS} + G$. The branch that C_{GRS} is dominant in t_G immediately results in a constant reaction order, while the other branch that G dominant in C_{GRS} need further decompositions. The decomposition steps continue untill all branches have reached a case where the reaction order is constant. Then taking the convex combination of all the resulting constant reaction orders gives us the reaction order polyhedra. Indeed, it can be checked with the visualization in Figure 2.3 that the constant vectors from DDT here are the vertices of the polytope.

We caution that the order in the sequence of decomposition steps taken could be very important. Wrong sequences could build DDT trees with spurious vertices that cannot be reached by reaction orders of the binding network. When performing the sequence of decomposition steps, given the coordinates at the current step, we should search for changes to the coordinates that require fewest number of steps to reach a constant reaction order. Like in Figure 2.4, we take out C_{GRS} from all the coordinates at the first three steps, because this is guaranteed to have a constant reaction order for C_{GRS} itself. We acknowledge that finding the right sequence of decomposition steps requires a bit of the art of problem solving, just like many powerful mathematical techniques. Nonetheless, we have guarantees that any polyhedron we obtain from DDT will always contain the reachable set of reaction orders in it. So we can only overshoot through DDT, and any polyhedron we obtain is an outer bound. This can be used to take a variational view to finding the right sequence of steps in DDT. No matter how we came up with a sequence of decomposition steps, the sequence that results in the smallest polyhedron is always closer to truth. Therefore, in the worse case, we can always search all possible sequences of steps or DDT trees by brute-force computer search. So DDT can be seen as a technique to derive the reaction order polyhedron directly for general binding networks. A generic computational complexity for deriving the reaction order polyhedra directly from DDT is therefore exponential in the number of species, $O(e^n)$. This is perhaps not reducible, since just finding the finite vertices correspond to enumerating the vertices of a polytope given its facets (see Section 3.7 of Chapter 3), which has complexity that is exponential in n. However, DDT directly obtains the full reaction order polyhedra, so this compares favorably to numerical scans when n is much smaller than N the number of points needed in the scan, either from reaction order formula, which has complexity $O(Nn^{2.3})$, or from solving polynomial equations, which has complexity $O(N2^n)$. In practice, it is often the case that N is several orders larger than 2^n so as to sufficiently cover the solution space.

2.3 Reaction order polyhedra reveal hidden adaptive regimes

We have shown that the power of reaction order polyhedra is that it can characterize the full bioregulation profile of how binding networks adjust catalysis fluxes. This holistic characterization make reaction order polyhedra applicable to scenarios previously not amenable to tractable analysis at scale. In particular, no matter how dynamically a system is regulated with large transients or combinatorial changes in concentrations, the system's behavior stays within the bounds of its reaction order polyhedra, therefore amenable to analysis.

Beyond their general applicability to the highly dynamic and combinatorial cases, reaction order polyhedra can also be used for biocircuit designs powered by the holistic nature of this approach. When we have a desired function and a circuit design in mind, holistic analysis based on reaction order polyhedra can reveal all the possible regimes that the function can be achieved. In other words, rather than obtaining sufficient results that a biocircuit under a particular condition can have the desired behavior, holistic analysis can yield necessary statements, that any condition producing desired behavior will satisfy the statements. To illustrate this, we consider an existing biocircuit design from [98] for gene expression that is plasmid number invariant. We re-analyze this circuit to show that there are hidden regimes of the circuit achieving plasmid number invariance that was missed in the paper's original analysis using classical methods such as Michaelis-Menten type analysis.

The biocircuit in [98] is basically a repressor on the same plasmid as the gene of interest. Instead of describing all the detailed parts of the plasmid-number invariance biocircuit in [98], here we focus on a simple model that captures the core of the plasmid number invariance function. Consider a gene of interest G placed on plasmids. On the same plasmid, there is also a constitutively expressed repressor gene encoded, which produces the repressor protein R. This repressor can bind at the gene's location on the plasmid to form a complex C_{GR}, so that the expression of the gene is suppressed. This forms the binding network

$$\text{Binding network: } G + R \rightleftharpoons C_{GR}. \tag{2.12}$$

The plasmid number, which is the same as the total gene from summing repressed and free gene, is $t_G = G + C_{GR}$. Gene expression is proportional to the un-repressed or free gene, G. So the goal of achieving plasmid number invariance is therefore making the steady state of G invariant to changes in t_G. This objective can be simply encoded in terms of reaction

orders as

$$\text{Plasmid number invariance: } G \propto t_G^0, \tag{2.13}$$

that the reaction order of G to t_G should be zero.

Since the plasmid number invariance function here is considered over the time scale of gene expression, the catalysis, or production and degradation of biomolecules, need to be considered. The important dynamics of catalysis here is the production and degradation of the repressor molecule t_R. Again, total is used here because production and degradation causes integer changes in the total number of repressor molecules. The equation for dynamics is

$$\frac{d}{dt}t_R = kt_G - \gamma t_R, \tag{2.14}$$

where production is proportional to plasmid number t_G because the repressor is constitutively expressed on the plasmid, and degradation with rate γ describe dilution from cell growth. At steady state, we have

$$\text{Catalysis steady state: } t_R = \frac{k}{\gamma}t_G. \tag{2.15}$$

As a result of this the repressor amount is proportional to plasmid number.

Now we have described everything in the system. There are three elements, (1) the binding regulation, (2) the desired function of plasmid number invariance, and (3) the steady state relation from catalysis dynamics. All together, they form conditions on reaction orders so that plasmid number invariance is achieved at steady state if and only if this condition on reaction orders is satisfied.

The integration of these three elements into constraints on reaction orders is illustrated in (a) of Figure 2.5. Denote a_R and a_G as the reaction orders of G to t_R and t_G. For intuition and convenience of notation, let us denote that reaction orders roughly mean G has proportional relation $G \propto t_R^{a_R} t_G^{a_G}$. The constraint from binding regulation is then that the reaction orders (a_R, a_G) are bounded in a polyhedral set $\mathcal{P}_{\text{bind}}$. This reaction order polyhedra is both derived via DDT, as shown in (b) of Figure 2.5, and visualized by computer sampling in (d) of Figure 2.5.

Then we incorporate the constraint from catalysis steady state. The steady state relation implies $t_R \propto t_G$, i.e. the repressor amount is proportional to the plasmid number. Therefore, we can write its influence on reaction orders by $G \propto t_R^{a_R} t_G^{a_G} \propto t_G^{a_G + a_R}$. Lastly, we incorporate the constraint from the requirement of plasmid number invariance, that $G \propto t_G^0$. We see that this becomes the constraint $a_G + a_R = 0$ in terms of reaction orders. As a result of all

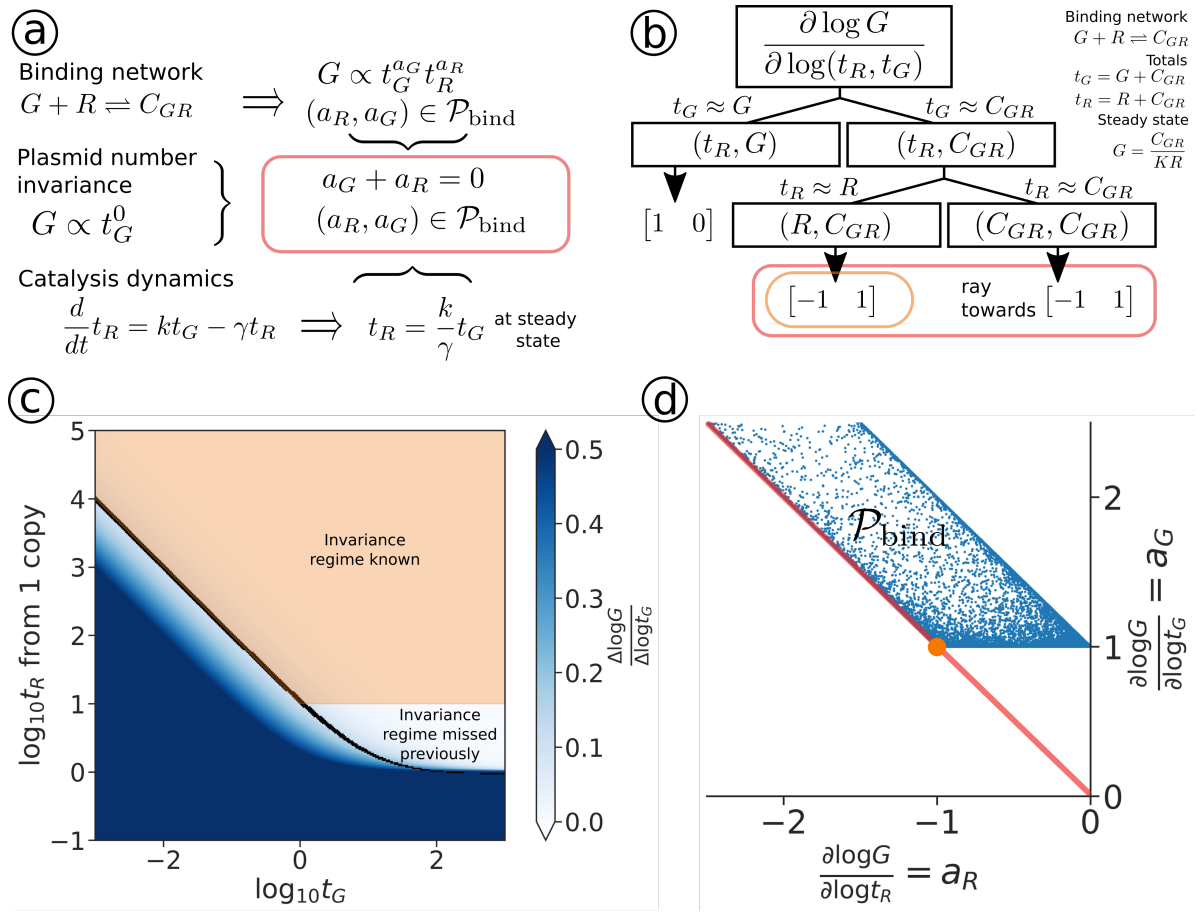

Figure 2.5 Holistic analysis of the plasmid number invariance circuit from [98] reveals invariance regimes previous missed. **(a)** Circuit specifications form constraints on reaction orders. Constraints on reaction orders (a_R, a_G) of gene G's to repressor and plasmid number come from all three parts of the system: binding regulation, catalysis or production-degradation of repressor, and the plasmid number invariance function. Binding network restricts the reaction orders to the reaction order polyhedron $\mathcal{P}_{\text{bind}}$. The steady state of catalysis dynamics requires that the repressor concentration is proportional to the plasmid number, so $G \propto t_G^{a_G} t_R^{a_R} = t_G^{a_G + a_R}$. These together with the constraint from the desired plasmid number invariance function results in the constraints on the reaction orders (circled in red). **(b)** DDT of target species G. The last step of decomposition results in a vertex (circled by orange) and a ray. Both the vertex and the ray satisfy the reaction order constraints, therefore circled in red. The vertex corresponds to the orange region in (c), and the orange dot in (d). The vertex together with the ray, circled red, corresponds to the region above the black line in (c) and the red line's intersection with the polyhedron in (d). Upper right corner of the DDT lists the binding network, definition of totals, and the steady state expression for the target species G for book-keeping. **(c)** Variation in G caused by varying plasmid number t_G. White means plasmid number invariance. y-axis is repressor expression strength k. The orange region is the invariance regime known in [98], corresponds to vertex $(-1, 1)$ in reaction orders. The white region above the black line is a previously missed invariance regime, corresponds to the ray in reaction orders. Above the black line is concentrations where C_{GR} dominate in t_G, so $\frac{C_{GR}}{G} \geq 10$. The orange region is from the above and that R dominates t_R by $\frac{R}{C_{GR}} \geq 10$. **(d)** Reaction order polyhedron of G obtained by computer sampling, with $\frac{G}{K}$ and $\frac{R}{K}$ log-uniformly sampled between 10^{-6} and 10^6 with a total of 10^5 points. The orange dot corresponds to the $(-1, 1)$ vertex in DDT from (b). The red line is the constraint that $\alpha_G + \alpha_R = 0$ from plasmid number invariance and catalysis steady state.

three elements of the system, we have the following necessary and sufficient condition for plasmid number invariance (see (a) of Figure 2.5).

$$\text{Plasmid number invariance at steady state} \iff a_R + a_G = 0, (a_R, a_G) \in \mathcal{P}_{\text{bind}}. \quad (2.16)$$

Visually represented in (d) of Figure 2.5, this is the intersection between the line of $a_R + a_G = 0$ (red) and the polyhedron $\mathcal{P}_{\text{bind}}$. The result is a vertex $(-1, 1)$ with a ray in the $(-1, 1)$ direction. Looking at the DDT in (c) of Figure 2.5, we see that these two together correspond to the dominance condition $t_G \approx C_{GR}$. In other words, most plasmids are bound.

We emphasize that from this holistic analysis based on combining reaction order polyhedra with the functional constraints, this dominance condition $t_G \approx C_{GR}$ that most plasmids are bound is both *necessary and sufficient*. As long as this condition is satisfied, then plasmid number invariance is achieved. Conversely, if plasmid number invariance is achieved, then this condition is for sure satisfied. This conclusion can only be broken if the system specification is wrong. Specifically, either the repressor amount is not proportional to plasmid number at steady state, or the binding network is incorrect that there are other binding reactions involved.

Now we relate to the analysis in the original paper [98] where this design was proposed and implemented in bacteria. Their analysis is based on Hill functions and Michaelis-Menten type assumptions. As a result, they find the $(-1, 1)$ vertex as a functional regime for plasmid number invariance (circled by orange in (b) and the red dot in (d) of Figure 2.5). However, this is a regime contained in the more general conditions necessary for plasmid number invariance, as seen in the DDT (see (c) of Figure 2.5). Specifically, the vertex $(-1, 1)$ requires two dominance conditions, $t_G \approx C_{GR}$ and $t_R \approx R$. In other words, it requires that both most plasmids are bound, and repressor is overabundant so that most repressors are free. The regime missed by this analysis is the ray towards $(-1, 1)$ also contained in the constraint in Eqn (2.16). This hidden regime corresponds to dominance conditions that most plasmids are bound with repressors, but most repressors are bound as well. In other words, the regime where repressors bind tightly with the gene on plasmids, while the repressor amount is low. This means, in addition to the repressor-over-expressed scenario considered in [98] to achieve plasmid number invariance, we could use a low expression for the repressor, as long as the repressor is tight.

To show what the hidden regime looks like when concentrations of gene and repressors are varied, we plotted (c) in Figure 2.5. The invariance regime that is missed previously is

indeed scenarios where the number of repressors expressed per plasmid is low, while the binding is tight.

All this together, we have shown via one example how the application of holistic bioregulation analysis based on reaction order polyhedra can be fruitful in biocircuit design. The power of holistic analysis fundamentally come from its capability to derive necessary and sufficient conditions, rather than just sufficient ones. This allows it to state all possible scenarios a desired function can be achieved. Although this capability is only used here to find a hidden regime, its power in bioengineering is much more profound. Debugging when a design is not performing as desired is part of the foundation for design-build-test cycles in engineering. With only sufficient conditions, debugging can only be done with trial and error. With necessary and sufficient condition for a function in a given circuit design, we can either find how to improve, or conclude that the current circuit design have to be modified.

2.4 Physical and microscopic basis of reaction order

Reaction order is the central object of study in this thesis. In the introduction section, we argue that reaction order should be given high importance because fluxes or rates have to be given up due to intractable computations, while reaction order captures bioregulation and is still tractable. However, beyond this practical argument, it is also worth investigating whether reaction orders are important in themselves, that their high importance in bioregulation is more intrinsic and fundamental. In fact, we argue in this section that reaction orders form the basic map between external and internal chemical potentials of a reaction system.

For this goal, we turn to understanding how reaction orders relate to properties in statistical physics. The reason is that while reaction orders are defined and well understood in dynamics of chemistry empirically for their measurement and utility in calculations, their meaning has remained phenomenonlogical. Work in this thesis is finding reaction orders to be not only a powerful tool, but also a simplifying concept of biological behaviors across scales. It is as if reaction orders is part of the natural architecture of biomolecular systems. This motivates our attempt to find more fundamental physical quantities where reaction orders stem from.

Here I propose that reaction orders can be considered as the natural calculus for chemical potentials. More specifically, the reaction orders we use for binding networks is the order of internal molecular species to variations in total concentrations. These reaction orders are

transformations from external chemical potentials to internal chemical potentials. When external variations change the Gibbs free energy of the system, the reaction orders map this change to changes of internal components of the system. Since chemical potentials measure the tendency to react for species, reaction orders translate external changes into their effect on internal species. In fact, since chemical potentials and Gibbs free energy are quantities more generally defined than log derivatives, e.g. for discrete molecule counts, this physical interpretation of reaction orders can be used as the definition to begin with, and log derivatives emerge as the approximate expression in bulk scale.

We first give a general description of how reaction orders and chemical potentials are related, and then give a concrete example of dimer-monomer mixture to show how the relation works in calculation.

The generic scenario we are considering is a binding network, or any system in reaction equilibrium, that exchanges molecules with external environments. We belabor here that the exchange with the environment is not in equilibrium in general. So in the language of statistical mechanics, this is a canonical ensemble rather than a grand canonical ensemble. Although we allow exchange with the environment to change molecule numbers in the system, this change is slow compared to the system's equilibration. This is akin to tuning temperature when obtaining a phase diagram in thermodynamics. For each point, or each experiment, the temperature is fixed, although the temperature is varied overall.

With this setting of a system that quickly equilibrates while exchanging molecules with external environments in mind, we can have two perspectives on the system. Internally, we see n molecular species $X_1, \ldots, X_n$ with distinct chemical properties. So the state of the system can be described by the number of molecules of each species, $N_1, \ldots, N_n$. The Gibbs free energy is therefore $G(N_1, \ldots, N_n)$. Since our system quickly reaches equilibrium internally, when these numbers change, the Gibbs free energy satisfy $dG = \mu_1 dN_1 + \cdots + \mu_n dN_n$, where μ_i is the chemical potential of X_i. Note that although there are reactions happening inside the system, we do not need to describe them explicitly, since chemical reactions simply cause changes in the numbers $N_1, \ldots, N_n$, hence accounted for in our above description.

Externally, the environment can only distinguish the molecules pushed in or pulled out, but does not have access to the fast reactions inside the system. Therefore, the external description of the system consists of only the exchangeable molecular species, which we denote $N_1^t, \ldots, N_d^t$, so there are d of them, $d \leq n$. Since an exchangeable species can be in multiple forms inside the system through chemical reactions, these N_i^t are total numbers of a species that accounts for different forms the species is in. For example, a species in

monomer or dimer form are not distinguished and summed together in the total.

Just knowing the totals cannot determine the state of the system, since reactions inside the system can change how a given species vary in its various forms. So, to relate the external variables $(N_1^t, \ldots, N_d^t)$ to the internal variables $(N_1, \ldots, N_n)$, we need to find other degrees of freedom to extend $(N_1^t, \ldots, N_d^t)$ so it can describe the state of the system. The degrees of freedom that cannot be tuned externally are the chemical reaction equilibria inside the system, captured by reaction equilibrium constants $(K_1, \ldots, K_r)$, where $r = n - d$. There might be more reactions, but there is always exactly r reactions with linearly independent stoichiometry, so that they determine how the number of species is distributed in its various forms when the total is held fixed. Hence, the Gibbs free energy described from the external view is $G(N_1^t, \ldots, N_d^t, K_1, \ldots, K_r)$. Note that although we included $K_1, \ldots, K_r$ in the description, they cannot be modified externally, and only here to parameterize the states of the system. So the equilibrium relation of Gibbs free energy to external changes in these coordinates is $dG = \mu_1^t dN_1^t + \cdots + \mu_d^t dN_d^t + \kappa_1 dK_1 + \cdots + \kappa_r dK_r$, where μ_i^t is the chemical potential of the ith total species N_i^t, and κ_i is the partial derivative of G with respect to K_i. This nicely splits the part of Gibbs free energy that is adjustable externally, namely the dN_i^t's, and the part that is not adjustable internally, namely the dK_i's determining internal reactions' equilibrium.

Now we have two view of the Gibbs free energy, or more generally the state of the system, via internal variables $(N_1, \ldots, N_n)$ and external variables $(N_1^t, \ldots, N_d^t, K_1, \ldots, K_r)$. How the Gibbs free energy responds to changes in these variables is also characterized differently: internally by chemical potentials $(\mu_1, \ldots, \mu_n)$, and externally by total chemical potentials $(\mu_1^t, \ldots, \mu_d^t)$ and $(\kappa_1, \ldots, \kappa_r)$. Since external exchanges happen through the external variables, while system properties are expressed in internal variables, we would like to map external changes to internal changes. We claim that reaction orders does exactly this, mapping Gibbs free energy changes from external adjustments to internal effects.

We derive this mathematically. Since chemical potentials are partial derivatives of Gibbs free energy to molecule numbers, we have

$$\begin{bmatrix}\mu_1 & \cdots & \mu_n\end{bmatrix} = \frac{\partial G}{\partial(N_1, \cdots, N_n)}, \quad \begin{bmatrix}\mu_1^t & \cdots & \mu_d^t & \kappa_1 & \cdots \kappa_r\end{bmatrix} = \frac{\partial G}{\partial(N_1^t, \ldots, N_d^t, K_1, \ldots, K_r)}.$$

We relate them by a coordinate change:

$$\begin{aligned}\begin{bmatrix}\mu_1^t & \cdots & \mu_d^t & \kappa_1 & \cdots \kappa_r\end{bmatrix} =& \frac{\partial G}{\partial(N_1, \cdots, N_n)} \frac{\partial(N_1, \cdots, N_n)}{\partial(N_1^t, \ldots, N_d^t, K_1, \ldots, K_r)} \\ =& \begin{bmatrix}\mu_1 & \cdots & \mu_n\end{bmatrix} \frac{\partial(N_1, \cdots, N_n)}{\partial(N_1^t, \ldots, N_d^t, K_1, \ldots, K_r)}.\end{aligned}$$

This gives a map between the chemical potentials. However, chemical potentials are per-molecule changes of Gibbs free energy. Therefore we should multiply chemical potentials with molecule numbers to yield free energy changes. This exactly gives log derivatives, or reaction orders.

$$\left[\mu_1^t N_1^t \ \cdots \ \mu_d^t N_d^t \ \kappa_1 K_1 \ \cdots \kappa_r K_r\right] = \left[\mu_1 N_1 \ \cdots \ \mu_n N_n\right] \frac{\partial \log(N_1, \cdots, N_n)}{\partial \log(N_1^t, \ldots, N_d^t, K_1, \ldots, K_r)}. \quad (2.17)$$

Here $\frac{\partial \log N_i}{\partial \log N_j^t}$ is the log derivatives, or reaction orders, of X_i to the jth total, in per-molecule units. This is the same as $\frac{\partial \log x_i}{\partial \log t_j}$ in concentration units, where x_i and t_j are concentrations of X_i and jth total, since the units are ignored in log derivatives, which captures fold changes.

Eqn (2.17) shows that reaction orders, defined as log derivatives, have the natural physical meaning as conversion between external and internal free energy changes. In fact, since free energies are well defined when molecule counts are discrete while log derivatives are not, Eqn (2.17) can be used as a physical definition of reaction orders, and log derivatives emerge as bulk-scale approximation of this definition.

Now we do the calculation in detail for a simple example to illustrate this. We first begin with a system consisting of two types of particles, X_1 and X_2 (see (a) of Figure 2.6). The state of the system is therefore the number of these particles, (N_1, N_2). The Gibbs free energy of the system is described in these coordinates, $G(N_1, N_2)$. To study how the Gibbs free energy of the system would change, we consider that both types of particles can be added or removed externally. Once particles are added or removed, the system equilibrates quickly, so equilibrium relations hold. So we have $dG = \mu_1 dN_1 + \mu_2 dN_2$, where μ_1 and μ_2 are the chemical potentials of the two types of particles. In this setting, all changes to the system are caused by external exchanges. When no particles are added or removed, the state of the system does not change either, so $dN_1 = dN_2 = 0$ resulting in $dG = 0$ in a trivial way.

Next, we allow some internal dynamics to happen through a chemical reaction (see (b) of Figure 2.6). Namely, we have reaction $2X_1 \rightleftharpoons X_2$, that two X_1 form a X_2. This gives us the physical notion that X_2 has two units of X_1. To keep this notion separate from that X_1 and X_2 are two distinct types of particles, we denote X as the unit particle, so X_1 is a monomer of X, and X_2 is a dimer of X. Since the reaction can only happen within the system and quickly reaches equilibrium, the external distinction of X_1 and X_2 becomes trivial, since they inter-convert inside the system. Addition and removal of X_1 and X_2 molecules is then the same as just adding or removing X. Each addition of X_2 can be considered as adding two X, for example. In other words, externally X_1 and X_2 are simply one and two X molecules respectively, and the difference in their chemical properties is no

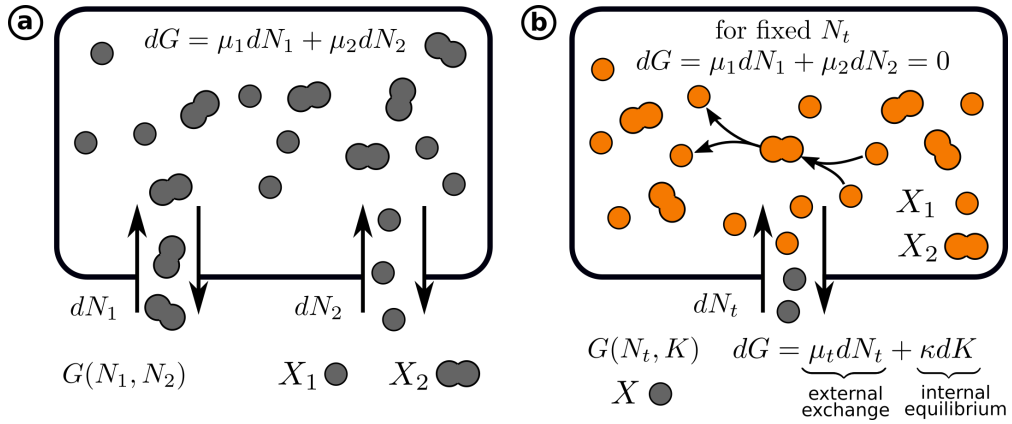

Figure 2.6 Illustration of the biophysical setting considered in connecting chemical potential with reaction orders. (a) A system consisting of two types of particles, X_1 and X_2, in equilibrium within the system. The number of these two particles, N_1 and N_2, can be added or removed via exchange with external environments. Once the particle number changes, the system quickly re-equilibrates. So the Gibbs free energy of the system is described by $G(N_1, N_2)$ and satisfy the equilibrium relation $dG = \mu_1 dN_1 + \mu_2 dN_2$, where μ_i is the chemical potential of particle X_i. (b) A system consisting of two types of particles X_1 and X_2 with internal chemical reaction $2X_1 \rightleftharpoons X_2$ that two X_1 dimerize to form X_2. To distinguish free monomers X_1 and the monomer molecules bound in X_2, we denote X as the generic monomer, so X_1 is monomer of X, and X_2 is dimer of X. The dimerization reaction only happens inside the system, not outside, so we color particles orange as reaction-capable, while grey is not reaction-capable. The exchange with external environment can add or remove monomers. But once a monomer is added or removed externally, the internal reaction quickly equilibrates, therefore causing a net increase or decrease of total monomers, or total X, denoted N_t. The reaction equilibrium internal of the system is therefore $dG = 0$ for fixed N_t, captured by equilibrium constant K for dimer dissociation. From an external point of view, where we can only add or remove X to change N_t, but not modify the equilibrium internal to the system, we want $G(N_t, K)$ expressed in terms of N_t that can be externally modified, and K that cannot be modified. So the equilibrium relation is $dG = \mu_t dN_t + \kappa dK$, where μ_t is chemical potential for a generic X, regardless of monomer or dimer form, and κ is how G changes with K.

longer distinguishable, due to the chemical reaction inside the system. Thus the addition or removal of X externally correspond to changing the total number of X inside the system, which we denote $N_t = N_1 + 2N_2$.

While N_t can be adjusted externally, the reaction equilibrium inside the system can not. Since the system equilibrates quickly, N_t is fixed when reaching towards equilibrium. The condition is therefore $dG = \mu_1 dN_1 + \mu_2 dN_2 = 0$ subject to the constraint that $dN_t = dN_1 + 2dN_2 = 0$. This results in the equilibrium condition $2\mu_1 = \mu_2$. So the system's state variables (N_1, N_2) are no longer completely free to vary, even if N_t can be adjusted. For each value of N_t, N_1 and N_2 are uniquely determined by the equilibrium condition $2\mu_1 = \mu_2$.

To explicitly represent this restriction, we need to relate μ_i with N_i. A simple relation for ideal or dilute solution is that $\mu_i = \mu_i^0 + k_B T \log x_i$, where x_i is the concentration of X_i, proportional to N_i, μ_i^0 is a standard chemical potential for X_i, capturing the internal energies of an X_i molecule, and k_B is Boltzmann's constant. Non-ideal solutions will

have a more sophisticated relationship between chemical potentials and concentrations, which can be captured via linearization of μ_i in $\log x_i$ at a certain concentration to obtain $\mu_i = \mu_i^0 + a(x_i)k_BT\log x_i$. So the ideal behavior can be considered as the case when $a(x_i) \equiv 1$. With this ideal solution formula, we find that the equilibrium condition becomes $2\mu_1^0 + 2k_BT\log x_1 = \mu_2^0 + 2k_BT\log x_2$. This allows us to define the binding constant K so that $\log K = \log \frac{x_1^2}{x_2} = \frac{1}{k_BT}(2\mu_1^0 - \mu_2^0)$. So the relation $Kx_2 = x_1^2$ is an explicit parameterization of the restriction on the numbers or concentrations of X_1 and X_2 from the reaction equilibrium. Note that $Kx_2 = x_1^2$ is the same as what we obtain from the steady state equation in mass-action kinetics of the binding reaction.

Our discussion above yields an alternative description for the state of the system. Given fixed N_t and K, the internal state variables (N_1, N_2) are uniquely determined. In other words, (N_t, K) is an alternative set of state variables. For example, Gibbs free energy can also be considered a state function in these state variables $G(N_t, K)$. This is the natural set of variables for the external view, since N_t is exactly what is adjustable externally, while K describes the internal equilibrium not externally accessible. When we externally add or remove X molecules, therefore, we are changing the system by dN_t. To relate this to Gibbs free energy changes, we have equilibrium relation $dG = \mu_t dN_t + \kappa dK$, where μ_t is the chemical potential of an X molecule, and κ is the partial derivative $\frac{\partial G}{\partial K}$ while keeping N_t constant. When K is not adjustable, as is the case when we are restricted to external exchanges, we have $dG = \mu_t dN_t$.

In order to see how the external adjustment in terms of dN_t causes changes in internal

$$\mu_t = \frac{\partial G}{\partial N_t} = \frac{\partial G}{\partial (N_1, N_2)} \frac{\partial (N_1, N_2)}{\partial N_t} = \begin{bmatrix} \mu_1 & \mu_2 \end{bmatrix} \frac{\partial (N_1, N_2)}{\partial N_t},$$

where the partial derivatives with respect to N_t keeps K constant, since (N_t, K) is the alternative coordinate. To relate to free energy changes, we need to multiply chemical potentials by molecule numbers, so we have

$$\mu_t N_t = \begin{bmatrix} \mu_1 N_1 & \mu_2 N_2 \end{bmatrix} \frac{\partial \log (N_1, N_2)}{\partial \log N_t} = \mu_1 N_1 \frac{\partial \log N_1}{\partial \log N_t} + \mu_2 N_2 \frac{\partial \log N_2}{\partial \log N_t}. \tag{2.18}$$

So we see that log derivatives, or reaction orders, transforms changes in free energy $\mu_t N_t$ from external adjustments to corresponding changes internally, namely $\mu_1 N_1$ and $\mu_2 N_2$.

Since this example is simple, we can calculate this conversion explicitly to see how the transformation is done in detail. Write this in terms of concentration variables, x_i for N_i and t for N_t, we have

$$\mu_t t = \mu_1 x_1 \frac{\partial \log x_1}{\partial \log t} + \mu_2 x_2 \frac{\partial \log x_2}{\partial \log t}. \tag{2.19}$$

We can calculate the reaction orders by brute force using the equilibrium relation $Kx_2 = x_1^2$ and the definition of totals $t = x_1 + 2x_2$.

$$\begin{aligned}\frac{\partial \log x_1}{\partial \log t} =& \frac{\partial \log x_1}{\partial \log(x_1 + 2x_2)} = \left(\frac{\partial \log(x_1 + 2x_2)}{\partial \log x_1}\right)^{-1} \\ =& \left(\frac{x_1}{x_1 + 2x_2} \cdot \frac{\partial \log x_1}{\partial \log x_1} + \frac{2x_2}{x_1 + 2x_2} \cdot \frac{\partial \log 2x_2}{\partial \log x_1}\right)^{-1} \\ =& \left(\frac{x_1}{x_1 + 2x_2} \cdot 1 + \frac{2x_2}{x_1 + 2x_2} \cdot 2\right)^{-1} \\ =& \frac{x_1 + 2x_2}{x_1 + 4x_2}.\end{aligned}$$

We can define $\lambda_1 = \frac{x_1}{x_1+4x_2}$, and $\lambda_2 = \frac{4x_2}{x_1+4x_2}$ so that $\lambda_1 + \lambda_2 = 1$. Then

$$\frac{\partial \log x_1}{\partial \log t} = \lambda_1 \cdot 1 + \lambda_2 \cdot \frac{1}{2}, \quad \frac{\partial \log x_2}{\partial \log t} = 2\frac{\partial \log x_1}{\partial \log t} = \lambda_1 \cdot 2 + \lambda_2 \cdot 1.$$

So we have

$$\mu_t t = \left(\lambda_1 \cdot 1 + \lambda_2 \cdot \frac{1}{2}\right)(\mu_1 x_1 + 2\mu_2 x_2).$$

The change in free energy from external adjustments is propagated to internal ones via a transformation factor $\lambda_1 \cdot 1 + \lambda_2 \cdot \frac{1}{2}$ between 1 and $\frac{1}{2}$. When x_1 is dominant, it is close to 1; when x_2 is dominant, it is close to $\frac{1}{2}$.

In summary, through our generic arguments and this simple example, we see that reaction orders describe how changes in Gibbs free energy from external addition and removal of molecules are mapped to free energy changes of internal components. Importantly, we consider scenarios where a system has internal reactions reaching equilibria that is not adjustable externally, therefore requiring an internal-external split. Hence, reaction orders is a fundamental tool when studying regulations of biomolecular systems where only parts of the species' concentrations are adjustable, and there exists reactions internal to the system.

Part II

Part 2. Mathematical underpinnings

Chapter 3

Polyhedral Representation of Binding Network Steady States

In earlier chapters, we see that binding reaction networks regulate catalysis reactions. In this chapter, we show that the regulatory profiles of a binding network can be characterized as constrained in polyhedral sets in terms of reaction orders (log derivatives). We investigate the mathematical properties of log derivatives from binding networks. In particular, we make the following contributions: (1) we define what the set of binding networks is that makes biological sense; (2) we characterize the manifold of all possible detailed balanced steady states of a binding network; (3) we derive a formula for log derivatives, which can be used for computational sampling; and (4) we show that the polyhedral shape of log derivatives fundamentally comes from decomposition rules of log derivative operators. This further yields a calculus method to analytically obtain log derivative polyhedra, either top-down via dominance-decomposition tree (DDT) or bottom-up via summation of matrix representations.

3.1 Introduction

Biomolecular systems mainly consist of two kinds of reactions: binding and catalysis. Take the simplest enzymatic reaction for example,

$$E + S \underset{k_{ES}^-}{\overset{k_{ES}^+}{\rightleftharpoons}} C_{ES} \xrightarrow{k^{\text{cat}}} C_{EP} \underset{k_{EP}^-}{\overset{k_{EP}^+}{\rightleftharpoons}} E + P. \tag{3.1}$$

Binding reactions are of the form $E + S \rightleftharpoons C_{ES}$, where two molecular species E and S bind together reversibly to form a complex C_{ES}. Catalysis reactions are of the form

$C_{ES} \to C_{EP}$, where one form of molecules is transformed into another form. Here two binding reactions and one catalysis reaction describe this enzymatic reaction with product re-binding. Catalysis governs the direction of net change of the system, namely

$$(t_S, t_P) \xrightarrow{k^{\text{cat}} C_{ES}} (t_S - 1, t_P + 1), \tag{3.2}$$

the total amount of substrate molecule $t_S = S + C_{ES}$ is decreased by one, while the total amount of product molecule $t_P = P + C_{EP}$ is increased by one. Since the speed of the product formation (or the catalysis flux) is governed by the concentration of C_{ES}, understanding the dynamics of biomolecular systems comes down to characterizing how the active complex C_{ES}'s concentration is regulated by the total concentrations of enzymes t_E, substrates t_S, and product t_P.

This problem comes down to solving a system of polynomial equations, with the degree of the problem larger than the number of binding reactions in general. For example, the binding reactions in Eq (3.1) yield the following system of equations at steady state:

$$C_{ES}K_{ES} = ES,\ \ C_{EP}K_{EP} = EP,\ \ t_E = E + C_{ES} + C_{EP},\ \ t_S = S + C_{ES},\ \ t_P = P + C_{EP}, \tag{3.3}$$

where K_{ES} is dissociation constant for the binding of E and S, and K_{EP} is that for E and P. Solving for C_{ES} in terms of $t_E, t_S, t_P, K_{ES}, K_{EP}$, for example, comes down to solving the following polynomial equation of degree 3:

$$C^3(K - K') + C^2(K(K' + t_P - t_S) + t_E(K' - K) + 2K't_S - K^2) - Ct_S(K(K' + t_P) - t_E(K - 2K') + K't_S) + t_EK't_S^2 = 0.$$

Here to make the equation not overly complicated, we used shorthand C and K for C_{ES} and K_{ES}, and C' and K' for C_{EP} and K_{EP}. As the Abel–Ruffini theorem states that polynomial equations of degree more than 5 do not have explicit solution in terms of elementary functions, active complex concentrations are not analytically solvable in general with four or more binding reactions. In fact, even for two binding reactions, the analytical formula is complicated enough that analytical insights are hard to obtain. More importantly, although systems of polynomial equations can be numerically solved to an extent, this is computationally intractable for large systems in general (it is well known to be NP hard), and relaxations such as sum-of-squares [86] or signomials [78] are needed for even moderate-size problems.

Existing approximations are limited in applicable scenarios. Tranditionally, based on the application scenario of interest, approximations are made to trade exactness for tractability. One such example is the Michaelis-Menten (MM) formula, which was developed by Michaelis-Menten [63] and rigorized by Briggs-Haldane [23], and has served as the

foundation of dynamic modeling of biochemical reactions for the past 100 years [31, 57, 65]. Focusing on the case of enzymatic catalysis where substrates are small molecules, the MM formula assumed the substrate concentration is kept much higher than that of the enzyme. Assumptions like this allows simple analytical solutions to the enzymatic catalysis problems. As a result of its powerful simplicity, the MM formula has been fruitfully applied to many biomolecular scenarios, such as bulk enzymatic catalysis, single molecule catalysis, transcription-translation, and chemotaxis phosphorylation [116]. However, as the scientific and engineering study of biomolecular systems ventures forward into more complex and dynamic systems, such as in developmental biology and in post-translational regulations, assumptions of the MM type no longer hold. Instead, full regulatory profile without any assumptions are now needed to understand system behaviors. For example, when the concentrations of chemicals change significantly over time, such as in metabolic shifts and gene regulations, especially *in vivo*, the MM assumption breaks down [2, 28, 108]. Other recent examples are combinatorial regulations in gene circuits that result in promiscuous sensing and multistable cell fate regulations [9, 46, 122].

While MM and related approximations come from the bulk assumption of one species' concentration is much higher than another, another wide class of approximations in biophysics come from microscopic assumptions where the system of study is just one molecule in a bath of other molecules, e.g. one receptor in a bath of ligands [35, 88]. Formula taking the form of rational functions can be analytically obtained for such cases from arguments of thermodynamics [35], statistical mechanics [88, 89], or Markov chain theory [53, 76]. However, when applying results from this analysis to systems with more than one molecules, an implicit assumption of mean-field flavor is made that many molecules' behavior are independent and identical, and therefore approximated as many copies of the same one-molecule system. This is known to cause crucial deviations from experiments in synthetic and systems biology. One term in bioengineering used to describe such phenomenon is retroactivity [32], where transcription factors bound to promoters of genes on plasmids reduce the free transcription factors in solution, so that although the gene regulated is downstream, it "retroactively" acts on its upstream transcription factor. This is an example where the activity of these genes cannot be considered as independent and identical copies of single plasmids, as whether this plasmid will have transcription factors bound depends on whether other plasmids have significantly "absorbed" away transcription factors in solution.

Yet another approach to simplify is to assume that the scenario of interest is similar to an experimental setting where we can control the non-total concentrations directly. This

often holds for "induction curve" experiments, *in vitro* or *in vivo*, where concentrations of small molecules are controlled by a chemical bath, and equilibrium is effectively reached in experiment if the small molecules can freely exchange between solution bath and the system of interest. Hence for the purpose of quantitatively modelling the induction curve obtained, the control variable is the free molecule concentration, instead of total concentration. Each substitution of free concentration as control variable instead of total would simplify the polynomial to be solved by one degree. So if each binding reaction has one species controlled like this, then this reduces to explicit solutions taking rational function forms just like in single-molecule case. For the system in Eq (3.1), if both free substrate concentration S and free product concentration P are controlled via external baths, then the binding reactions are effectively state transitions, which is amenable to a single-molecule or Markov chain interpretation, as is often done in biophysics:

$$E \underset{k_{ES}^-}{\overset{k_{ES}^+ S}{\rightleftharpoons}} C_{ES} \xrightarrow{k^{\text{cat}}} C_{EP} \underset{k_{EP}^- P}{\overset{k_{EP}^+}{\rightleftharpoons}} E.$$

Note that the MM assumption that substrate and product concentrations are much more than the enzyme $t_S, t_P \gg t_E$ produce the same approximation, since the free and the total are approximately the same that $t_S \approx S$ and $t_P \approx P$ in this case. We again see the limitation of this simplifying approach. On one hand, it is only applicable to experimental scenarios where system's internal concentrations are in equilibrium with external bath. On the other hand, the simplification has limited effect for complex systems with significant internal dynamics not accessible to external control. For the binding system in Eq (3.1), if only the free substrate S is externally controlled while product P is not, then to explain the induction curve from experiments, we want active complex C_{ES} in terms of $(S, t_E, t_P, K_{ES}, K_{EP})$, yielding the following polynomial.

$$C_{ES}^2 K_{ES}(K_{ES} + S) + C_{ES} S((K_{EP} + t_P)K_{ES} - t_E K_{ES} + K_{EP} S) - t_E K_{EP} S^2 = 0.$$

This is one degree less than the t_S case, but still not degree one in C_{ES}, therefore not amenable to rational function solution. If there are more internal binding reactions that cannot be externally controlled, then the problem is again increasing in degree and becomes intractable analytically or computationally.

To get a sense for the magnitude of the error made, we consider just one binding reaction $G + R \underset{k^-}{\overset{k^+}{\rightleftharpoons}} G_R$, where G is the concentration or copy number of the gene of interest, and R is that of a regulator such as a transcription factor, and G_R is the complex formed when the gene and the regulator are bound. For this simple system, the same solution $G_R \approx t_G \frac{t_R}{K + t_R}$ with $K = \frac{k^-}{k^+}$, is obtained from the MM approximation that total regulator

is much higher than gene $t_R \gg t_G$, the single molecule states approximation for gene molecules G, and the external bath approximation for a bath of free regulator concentration R. The explicit solution from solving the quadratic equations from the binding reaction is $2G_R = t_G + t_R + K - \sqrt{(t_G + t_R + K)^2 - 4t_G t_R}$. We can hold t_G constant and vary t_R to see big an error does the approximation make compared to the exact solution. See Figure 3.1. Whenever the total regulator concentration t_R gets close to the total gene concentration t_G, we see the exact bound fraction of gene is much less than predicted from approximate solutions.

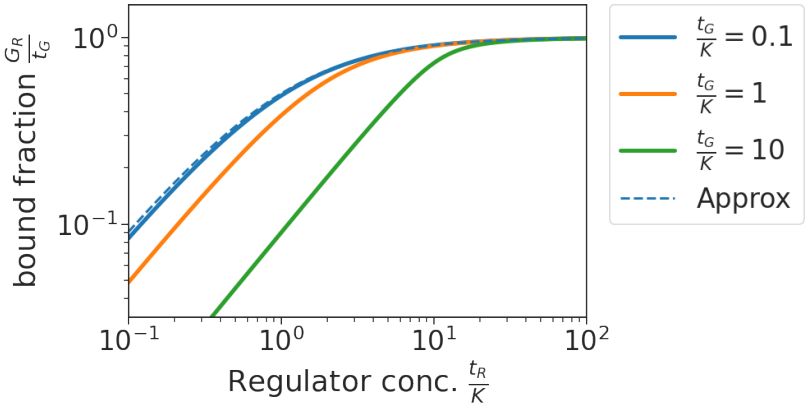

Figure 3.1 Comparison of approximate solution (Approx) to exact solution for a simple binding reaction $R + G \rightleftharpoons G_R$, when different total gene concentration t_G is held fixed. The units of concentrations are K here.

To summarize, MM approximations, single molecule states approximations, and external-bath approximations produce similar simplifications that yield rational-function solutions in ideal cases. There are many scenarios that these simplifications apply, yielding fruitful biological insights. There are also scenarios that go beyond these approximations, such as combinatorial regulations and highly dynamic shifts. Therefore, we would like a method of analysis that can tackle the full regulatory behavior for general scenarios without approximations, and at the same time reduce to simpler cases above when it is reasonable to do so.

As directly solving for the catalysis rate or the active complex concentration is not tractable, we need to find other variables to capture the full regulatory profile. In this work, we focus on the reaction orders, i.e. the order of rates' dependence on total reactant concentrations. We show that the full regulatory profile of catalysis rates can be characterized in terms of polyhedral sets that bound log derivatives, continuous analogues of reaction orders. Since knowing exact log derivatives implies knowing the catalysis rates up to a multiplicative constant, we therefore have a way to capture the full regulatory behavior of rates by giving up the information about exact magnitude, which can often be estimated or measured

experimentally.

In Section 3.3 we formally define binding reaction networks using chemical reaction network theory, and characterize a class of binding networks that are biologically plausible. In Section 3.4 we characterize the manifold of equilibrium or detailed balance steady states of binding networks, and introduce log derivatives as a transform between different parameterizations of the manifold. In Section 3.6, we focus on a binding network with just one binding reaction and fully analyze the reaction orders (one type of log derivatives) and their biological implications. We observe the polyhedral set bounding the full range of values the reaction orders can take. In Section 3.7, given the central importance of vertices of reaction order polyhedra, we characterize the vertices in terms of minimal support vectors of linear subspaces and develop a computational method to obtain them at scale. In Section 3.8, we show that polyhedra arise naturally from decomposition of log derivative operators. Using this, we develop an approach to obtain reaction order polyhedra analytically.

3.2 Illustrative example

Via the example of an enzymatic reaction with product binding, we walk through how reaction orders can be used to parameterize the manifold of binding network's detailed balanced steady states and analyze binding's regulation of catalysis. The concepts and methods developed in this chapter are illustrated by application to this example.

The binding network and catalysis reactions for an enzymatic reaction with product binding is shown in (a) of Figure 3.2. This is also the example discussed in the introduction (Section 3.1). Enzyme E binds with substrate S to form a complex C_{ES}, catalytically converted into a enzyme-product complex C_{EP} can unbind to release enzyme E and product P molecule, or bind from them. The catalysis reaction $C_{ES} \to C_{EP}$ here determines the direction of change to be one substrate molecule converted into a product molecule, $t_S \overset{k^{\text{cat}}C_{ES}}{\rightsquigarrow} t_P$, where $t_S = S + C_{ES}$ is the total amount of substrate and $t_P = P + C_{EP}$ is total amount of prodcut. The catalysis flux is $k^{\text{cat}}C_{ES}$, the catalysis rate constant multiplying the amount of catalytic complex C_{ES}. Therefore, the catalysis flux is governed by how C_{ES} depends on the total amounts of species. This in turn is determined by the binding network, $E + S \rightleftharpoons C_{ES}$ and $E + P \rightleftharpoons C_{EP}$. To understand the regulation of this catalysis flux, i.e. production flux of product, therefore corresponds to characterizing the binding network's regulation.

Some typical trajectories of this catlaysis process is shown in (b) of Figure 3.2, with more opaque trajectories corresponding to tighter enzyme-product binding. We begin the

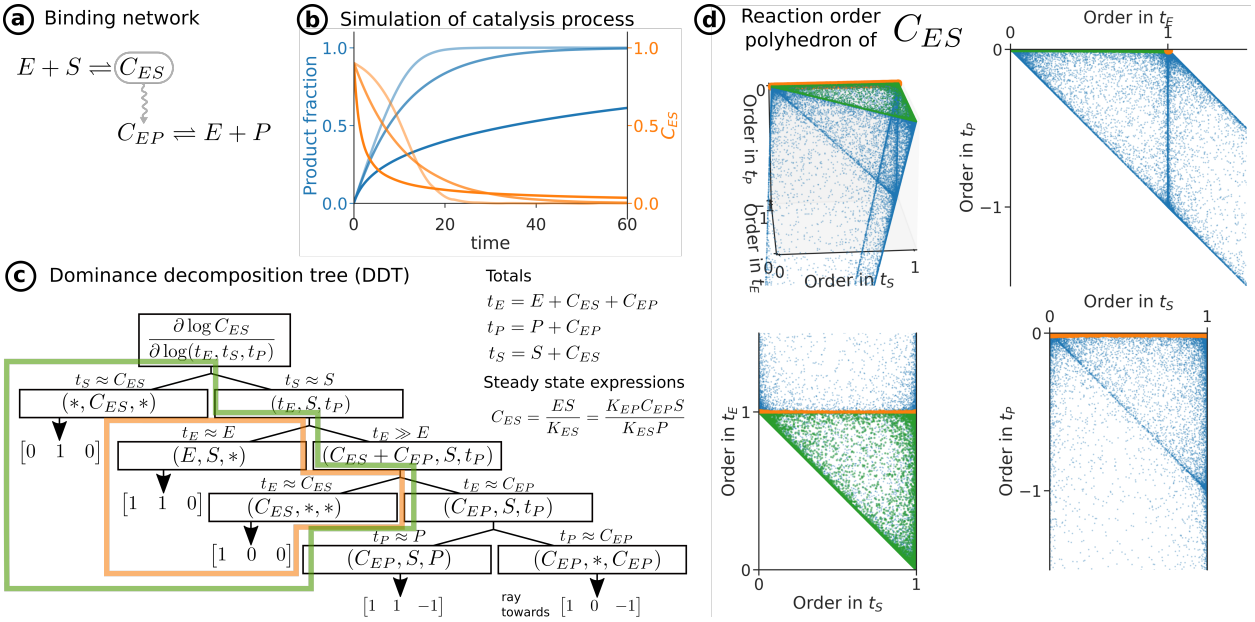

Figure 3.2 Illustration of how methods from this chapter can be used to study the enzymatic reaction with product binding. **(a).** The binding network for enzymatic reaction with product binding. E is enzyme, S is substrate, they bind to form complex C_{ES}, which gets catalyzed to complex C_{EP} which can unbind or bind from E and prouduct molecule P. The catalysis rate of substrate to product conversion is therefore proportional to C_{ES}, which is the target species here (grey cicle). The squiggly arrow denotes catalysis reaction. **(b).** Simulation of this enzymatic reaction with product binding, converting substrates to products. Blue lines are product fraction, defined as total product over the sum of total product and substrate $\frac{t_P}{t_S + t_P}$. Orange lines are the concentration of target species C_{ES}, proportional to catalysis rate. Three different parameter settings are run, with increasing enzyme-product binding strength (i.e. decreasing K_{EP}, graphically represented as increasing opacity). Parameter values are $k^{\text{cat}} = K_{ES} = t_E = 1$, $t_S + t_P = 10$, $K_{EP} \in \{30^{-1}, 1, 10\}$ (smaller K_{EP} is less opaque line). **(c)**. The dominance decomposition tree of the binding network, showing how the vertices and rays of C_{ES}'s reaction order polyhedron can be obtained analytically. Upper right corner lists the definition for totals and the steady state expressions of the target species, to help with keeping track of the decomposition steps. The convex combination of the vertices circled by orange or green corresponds to the orange or green points in (d). **(d).** The reaction order polyhedron of C_{ES}, the target species, by computer sampling. The upper left is a 3D view. The other three panels are projection of the 3D polyhedron to different 2D planes. The green and orange points corresponds to the dominance conditions and vertices in the DDT in (c). 10^5 points are taken by log-uniformly sampling $(E, S, P, C_{ES}, C_{EP})$ with values in $(10^{-6}, 10^6)$. Dominance condition is evaluated for 100-fold difference: orange points is $\frac{t_S}{t_E} \geq 100$, green points is $t_E \gg C_{EP}$ defined by $\frac{C_{EP}}{t_E} \leq 0.01$.

process with no product, so we see the fraction of product in the total of substrate and product continuously increase over time. However, the rate of production decreases as the product accumulates, with a very nonlinear inhibition effect. While the medium binding strength, a 10-fold increase to weak binding strength, causes only negligible increase in the increase of product fraction, the strong binding strength, a 300-fold increase, causes significant effect. This inhibition effect also unevenly influence production rate at different stage of the process. Here, a 300-fold increase in binding strength causes a 5.8-fold increase in time to reach 50% product fraction, but a 20-fold increase in time to reach 90% product

fraction. Another way to look at the inhibition effect is to look at the trajectory for amount of C_{ES}, which is proportional to the rate of production, as shown in orange in Figure 3.2 (b). We see C_{ES} decreases for all three trajectories as the product fraction increases. However, for weak binding, the inhibition does not become significant until product fraction is quite high, while the inhibition kicks in immediately for medium and strong binding. Below, we show that this nonlinearity of inhibition from product binding can be clearly understood by inspecting the full regulatory profile characterized by the reaction order polyhedron.

To understand how the production rate varies with the total concentrations as the catalysis process evolves, we need to characterize the space of regulation on the active complex C_{ES} governed by the two binding reactions. As discussed in the introduction (Eqn (3.3)), solving for C_{ES} in terms of the totals here is solving a degree-3 polynomial equation. This quickly becomes intractable to scan for all possible solutions since the polynomial degree increases with the number of binding reactions. Therefore, we instead focus on characterizing the reaction orders of C_{ES} in the totals. Reaction orders correspond to log derivatives, capturing infinitesimal fold-change variation rather than additive difference in linear derivatives. For monomials, log derivatives yield the exponents, such as $f(x) = kx^a$ with $\frac{\partial \log f}{\partial \log x} = a$. Reaction orders therefore capture how the catalysis flux varies with total concentrations in fold-change, determining the flux magnitude up to a multiplicative constant.

In Section 3.3 and 3.4 we formally define the binding networks studied, and develop a formula for reaction orders, allowing efficient computational sampling at scale. In (d) of Figure 3.2, we show the sampling of the reaction order polyhedron of C_{ES} determined by the binding network of this system, enzymatic reaction with product binding. We see that the set of all possible reaction orders indeed form a polyhedral set. Furthermore, we see the points condense around edges and vertices, implying those are the reaction orders for most concentration values. This motivates the idea of structural regimes corresponding to the vertices. For a large range of concentrations, the reaction orders are kept at one vertex, therefore the regulatory behavior of the binding network governing catalysis fluxes is the same. When very large concentration changes happen, the system would quickly move from one structural regime to another, since the reaction orders would quickly go from one vertex to another. Therefore, we can consider the catalytic process as evolving in the reaction order polyhedron, with different stages of the process corresponding to different regulatory modes in different structural regimes.

To apply the reaction order polyhedron to clearly understand the regulation of the catalysis process, we also want an explicit correspondence between the structural regimes. We

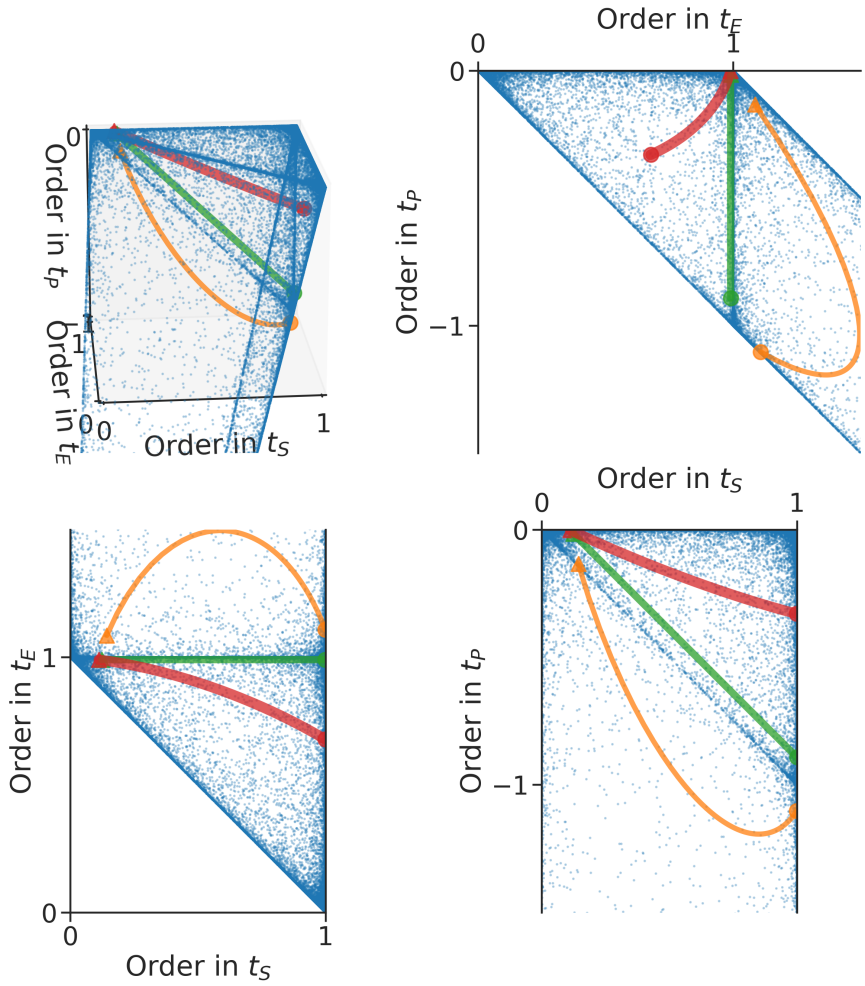

Figure 3.3 Trajectories in reaction order space of the three catalytic processes in (b) of Figure 3.2. The background sampling of the reaction order polyhedron (blue dots) are the same as in (d) of Figure 3.2. The trajectory of the strong enzyme-product binding strength case (most opaque in (b) of Figure 3.2) is orange color, that of the medium binding strength case (medium opacity in (b) of Figure 3.2) is in green color, and that of the weak binding strength (most transparent in (b) of Figure 3.2) is in red. For each trajectory, the triangle end denotes initial point, and the end with a circle denotes end point.

can ask for which part of the reaction order polyhedron corresponds to which part of the concentration space via computer sampling. Indeed, the reaction order polyhedron can be considered as an empowering tool for the classical approach that numerically solves polynomial equations to study bioregulation. Instead of scanning through parameters in the numerical solutions for ad-hoc performance criteria, reaction order polyhedra serves as a structural intermediate between parameters and bioregulatory performance. All effects of parameter variations show up in reaction order polyhedra before influencing bioregulation, and conversely, desired behaviors are definable through reaction orders that can be mapped to parameters.

While visual inspection or further computation on the sampled points in reaction order polyhedra can yield fruitful analysis for bioregulation, we also want to directly tackle the vertices and structural regimes which define the polyhedra and the great majority of bioregulatory behavior. In Section 3.8, we develop a analytical method called dominance decomposition tree (DDT) based on fundamental rules of calculus for positive variables that can directly obtain the vertices of reaction order polyhedra, with corresponding asymptotic conditions on the concentrations. In (c) of Figure 3.2, we show the DDT for this example of enzymatic reaction with product binding. Each vertex corresponds to a dominance condition for the total concentrations, and a structural regime of regulatory behavior. This allows us to go back and force between at a given concentration, what is the structural regime, and for a desirable structural regime, what is the concentration to reach it. These dominance conditions also correspond to faces of the reaction order polyhedron in a direct way. Comparing (c) and (d) of Figure 3.2, the orange vertices and dominance conditions correspond to the orange points in the reaction order polyhedron. This is the classical Michaelis-Menten approximation, where substrate is assumed much higher than the enzyme and product binding is assumed negligible. Indeed, there are two structural regimes contained, the $(1, 1, 0)$ regime that is linearly proportional to total substrate, and the $(1, 0, 0)$ regime that has the enzymes saturated therefore independent of total substrate. Graphically, this corresponds to a line segment, an edge connecting two vertices, in the reaction order polyhedron. The Michaelis-Menten assumption that total substrate is much higher than the enzyme corresponds to the first branching in the DDT, $t_S \approx S$, that free substrate dominates total substrates. Relaxing this assumption to generalize Michaelis-Menten, with only the negligible product binding assumption, we obtain the green region with three structural regimes. These three vertices together form a triangle, with the new regime $(0, 1, 0)$ corresponding to the case where enzymes are overabundant. Lastly, when making no assumption at all, we obtain the full reaction order polyhedron, with the two new regimes, vertex $(1, 1, -1)$ and ray $(1, 0, -1)$, corresponding to inhibition by product binding. Indeed, the reaction order in total production is the negative 3rd entry. Interestingly, this inhibition can be hyper-sensitive in the regime corresponding to the ray towards $(1, 0, -1)$, in the sense that the inhibition effect is more than linear. This happens under the dominance condition $t_P \approx C_{EP}$, when most enzymes and products are bound together.

With all this together, we can fully understand the various production dynamics as shown in (b) of Figure 3.2. For weak enzyme-product binding strength, we expect the enzyme-product complex C_{EP} to not dominate total enzymes, therefore mostly restricted to the green triangular region with the three vertices $(1, 0, 0)$, $(0, 1, 0)$ and $(1, 1, 0)$. Because we

simulated the case with total substrate 10-fold more than total enzyme, the $(0, 1, 0)$ vertex cannot be reached, with just $(1, 0, 0)$ and $(0, 1, 0)$ left. The system begins with abundant substrate, therefore close to the $(1, 0, 0)$ vertex, then as the substrate gets converted into product, moves towards the $(1, 1, 0)$ vertex. This means the flux would proceed mostly at a constant speed, and then when the substrate level finally becomes lower than the binding constant K_{ES}, the inhibition due to low substrate starts to kick in, and the flux decreases proportional to the decrease in substrate concentration. Throughout, the process can be largely explained by the classical Michaelis-Menten approximation. Indeed, as shown in the red trajectory in Figure 3.3, we see although the trajectory goes slightly negative in the order in t_P, and goes slightly below the $(1, 1, 0)$ vertex, the behavior is not far off the Michaelis-Menten edge.

As for the case of medium binding strength, where the enzyme has similar binding affinity to substrate and product molecules, we expect the enzyme to be mostly bound throughout, simply substituting the substrate with product molecule as the production progresses. In detail, we begin again with overabundant substrate, so we are at the $(1, 0, 0)$ vertex where most enzymes are in the form of enzyme-substrate complex C_{ES}. As time progresses, substrate concentration decreases while product concentration increases, but the total of metabolites, substrate plus product, is the same. This means most enzymes are still bound, but instead of enzyme-substrate complex C_{ES}, more and more enzymes are bound in enzyme-product complex C_{EP}. This means going from the $t_E \approx C_{ES}$ dominance condition for the $(1, 0, 0)$ regime, to the $t_E \approx C_{EP}$ dominance condition for the $(1, 1, -1)$ regime. Therefore, as the time goes on, we begin with a constant speed of production to decreasing speed like t_P^{-1} and t_S^1. Indeed, this is what we observe in the green trajectory plotted in Figure 3.3.

Lastly, we consider the strong binding case. When transitioning from substrate-saturating regime $(1, 0, 0)$ to the product-binding regime $(1, 1, -1)$, because of strong enzyme-product binding, the inhibition by product binding requires much less product to be synthesized, therefore kicks in much earlier. In other words, enzyme-product complexes C_{EP} would occupy most product molecules formed, therefore causing C_{EP} to dominate total product t_P, pushing the system in the regime of ray towards $(1, 0, -1)$. This causes hyper-sensitive inhibition of the catalysis flux, stronger than first order inhibition. As a result, we see when binding strength increases, the production rate does not decrease in first order, but faster than first order. Indeed, as shown in the orange trajectory in Figure 3.3, we see although the same end-point is reached in this case as the medium binding strength case, the trajectory reaches into the hypersensitive regime of ray to $(1, 0, -1)$, causing much stronger product

inhibition.

In summary, we see how reaction order polyhedra can holistically capture the regulatory profile of binding's regulation of catalysis fluxes. Hence, we can analyze bioregulatory dynamics in the space of reaction orders, with different regulatory behavior corresponding to shifting between structural regimes as vertices in the reaction order polyhedra. The computational sampling of reaction order polyhedra based on log derivative formula enables large-scale analysis of polyhedra, connecting concentrations and bioregulatory behaviors via reaction orders. Complementing this, the dominance decomposition tree (DDT) relate vertices, or structural regimes of bioregulation, with dominance conditions in concentration space, enabling intuitive understanding that maps dynamic regulations with trajectories through structural regimes.

Below, we begin our formulation and analysis of binding networks, detailed balanced steady states, and their parameterization via reaction orders.

3.3 Binding reaction networks

Here we are concerned with the formal definition of binding reaction networks. We describe biomolecular circuits using the language of chemical reaction networks (CRNs) [44]. In particular, we assume mass-action laws for the kinetics of reaction rates, and focus on the class of binding and catalysis reactions. As binding reactions are fast, we consider the steady states of binding reaction networks. We then define and characterize binding networks that are physical, paving the way for later analysis.

Chemical reaction networks

Let $\mathcal{X}$ be a finite set, denoting the set of molecular species. By assuming a canonical order on the sets of species, we can identify $\mathcal{X}$ with $\{1, \dots, n\}$, where $n = |\mathcal{X}|$. A reaction is a tuple $(\boldsymbol{\alpha}, \boldsymbol{\beta}, k) \in \mathbb{N}^n \times \mathbb{N}^n \times \mathbb{R}_{>0}$, where $\boldsymbol{\alpha}$ and $\boldsymbol{\beta}$ are the counts of reactants and products of this reaction, respectively, and k is its reaction rate constant.

A chemical reaction network (CRN) $\mathcal{C}$ then is a tuple $(\mathcal{X}, \mathcal{R})$, where $\mathcal{X}$ is the set of species and $\mathcal{R} \subset \mathbb{N}^S \times \mathbb{N}^{\mathcal{X}}$ is a finite set of reactions. We denote $n = |\mathcal{X}|$ the number of species, and $m = |\mathcal{R}|$ the number of reactions. Then the jth reaction can be denoted in the following way:

$$\alpha_{j1}X_1 + \cdots + \alpha_{kn}X_n \xrightarrow{k_j} \beta_{j1}X_1 + \cdots + \beta_{jn}X_n,$$

where X_i, $i = 1, \dots, n$ denote chemical species, $j = 1, \dots, m$ index reactions, $\alpha_{ji}, \beta_{ji} \in \mathbb{N}$ denote the number of X_i molecules needed as reactant or produced as product in reaction

j, and $k_j \in \mathbb{R}_{>0}$ is reaction rate constant of reaction j. We denote $\boldsymbol{\alpha}_j = \begin{bmatrix}\alpha_{j1} \cdots \alpha_{jn}\end{bmatrix}^\intercal$ as the reactant stoichiometry vector for reaction j, and similarly define $\boldsymbol{\beta}_j$ for product vector. We define $\boldsymbol{\gamma}_j = \boldsymbol{\beta}_j - \boldsymbol{\alpha}_j$ as the stoichiometric vector of reaction j, and $\boldsymbol{\Gamma} = \begin{bmatrix}\boldsymbol{\gamma}_1 \cdots \boldsymbol{\gamma}_m\end{bmatrix} \in \mathbb{Z}^{n\times m}$ is the stoichiometric matrix.

The deterministic rate equation of the CRN is

$$\frac{d}{dt}\boldsymbol{x}(t) = \boldsymbol{\Gamma}\boldsymbol{v}(\boldsymbol{x}(t)), \tag{3.4}$$

where $x_i(t) \in \mathbb{R}_{\geq 0}$ is the concentration of species X_i at time t, and $\boldsymbol{v}(\boldsymbol{x}) : \mathbb{R}^n_{\geq 0} \to \mathbb{R}^m_{\geq 0}$ denote the rate of reactions, which depends on the concentrations of species.

The stoichiometric subspace of the network is $\mathcal{S} = \operatorname{colspan}\boldsymbol{\Gamma}$. Let r be the dimension of the stoichiometric subspace, i.e. the rank of $\boldsymbol{\Gamma}$. Then we can select r reactions with linearly independent stoichiometry vectors to form matrix $\boldsymbol{N} \in \mathbb{R}^{r\times n}$, where the rows of $\boldsymbol{N}$ are selected columns of $\boldsymbol{\Gamma}$. This way, $\boldsymbol{N}$ is full row rank, and $\operatorname{rowspan}\boldsymbol{N} = \mathcal{S} = \operatorname{colspan}\boldsymbol{\Gamma}$. We call $\boldsymbol{N}$ the **transpose-reduced stoichiometry matrix**.

The mass-action law of rate kinetics specifies that $v_j(\boldsymbol{x}) = k_j\boldsymbol{x}^{\boldsymbol{\alpha}_j}$, where $\boldsymbol{x}^{\boldsymbol{\alpha}_j} := x_1^{\alpha_{j1}} \dots x_n^{\alpha_{jn}}$.

A matrix $\boldsymbol{L} \in \mathbb{R}^{d\times n}$ is a conservation law matrix of the CRN, where $d = n - r$, if $\boldsymbol{L}$ is full row rank with $\operatorname{rowspan}\boldsymbol{L} = \ker\boldsymbol{N} = \mathcal{S}^\perp$.

Binding networks

Since our goal is to study how a catalysis rate is regulated by its binding networks in biomolecular systems, we formally define the binding networks we study. Importantly, we want to characterize a physical class of binding networks that is relevant to biomolecular systems.

Intuitively, a binding reaction is of the form $X_1 + X_2 \rightleftharpoons X_3$ or $2X_1 \rightleftharpoons X_3$, where two of the same or different species bind to form a complex species. A collection of such reactions then form a binding network.

Definition 3.3.1. A CRN $(\mathcal{X}, \mathcal{R})$ is a binding network if it satisfies the following.

1. The CRN is *reversible*.

   A reaction $(\boldsymbol{\alpha}, \boldsymbol{\beta}, k) \in \mathcal{R}$ is reversible if it has a reverse reaction, i.e. there exists $(\boldsymbol{\beta}, \boldsymbol{\alpha}, k') \in \mathcal{R}$ for some k'. A CRN is reversible if all of its reactions are reversible.

2. All of its reactions are *binding reactions*.

A reversible reaction is a binding reaction if exactly one of the forward-reverse pair of reactions satisfies that the product stoichiometry vector $\boldsymbol{\beta}$ has one or two nonzero entries with $\|\boldsymbol{\beta}\|_1 \geq 2$, the reactant stoichiometry vector $\boldsymbol{\alpha} = \boldsymbol{e}_i$ is unit vector at some entry i, and $\boldsymbol{\alpha}$ and $\boldsymbol{\beta}$ have different support. This reaction out of the pair is called the forward reaction, or dissociation reaction.

Since the binding network is reversible and the reactant and product vectors have different support, we can capture all information of the binding network in the stoichiometry matrix of just the forward reactions, which we denote $\boldsymbol{\Gamma}^f \in \mathbb{R}^{n \times \frac{m}{2}}$. Let r be the rank of $\boldsymbol{\Gamma}$. We can formulate a transpose-reduced stoichiometry matrix $\boldsymbol{N} \in \mathbb{R}^{r \times n}$ by selecting r forward reactions with linearly independent stoichiometry vectors. In other words, rows of $\boldsymbol{N}$ are selected columns of $\boldsymbol{\Gamma}^f$.

Based on our physical intuition, the complexes that form in this binding network should be composed of a set of the smallest component species. Whether such sets of smallest component species, or atomic species, exist, constitute the study of atomic CRNs. Below, we extract relevant notions and results from the literature on atomic CRNs, namely the works [1, 36, 37, 50]. For clear exposition, we use a unified notation and frame all results in a linear algebraic fashion, which allows succinct proofs and simple computations. In particular, we define the various atomic notions through a matrix $\boldsymbol{D}$ representing the atomic decompositions of each species.

Definition 3.3.2 ([37])**.** A CRN $(\mathcal{X}, \mathcal{R})$ with stoichiometry matrix $\boldsymbol{\Gamma} \in \mathbb{R}^{n \times m}$ and stoichiometric subspace $\mathcal{S} \subset \mathbb{R}^n$ is **primitive atomic** if there exists a positive integer d and a matrix $\boldsymbol{D} \in \mathbb{N}^{d \times n}$, such that

1. $\boldsymbol{D}\boldsymbol{\Gamma} = 0$, i.e. $\operatorname{rowspan} \boldsymbol{D} \subset \mathcal{S}^\perp$, and
2. no rows or columns of $\boldsymbol{D}$ are all zero.

A CRN is **subset atomic** if it is primitive atomic with a $\boldsymbol{D}$ that has an ordering of the columns, called an atom-first ordering, under which

3. $\boldsymbol{D} = \begin{bmatrix} \mathbf{I}_d & \boldsymbol{D}_2 \end{bmatrix}$, and
4. each column vector of $\boldsymbol{D}_2$ has 1-norm ≥ 2.

A CRN is **stoichiometry-atomic** if it is subset atomic with a $\boldsymbol{D}$ in an atom-first ordering that

5. $\tilde{\boldsymbol{D}} = \begin{bmatrix} \boldsymbol{D}_2 \\ -\mathbf{I}_r \end{bmatrix} \in \mathbb{R}^{n \times r}$ satisfies $\operatorname{colspan} \tilde{\boldsymbol{D}} \subset \mathcal{S}$.

The interpretation behind the definitions are the following. The matrix $\boldsymbol{D}$ can be considered as a map from the set of n species $\mathcal{X}$ to a set of d atoms $\mathcal{A}$, so that the ith species is mapped to the ith column vector of $\boldsymbol{D}$ representing its decomposition in atoms. Condition 1 requires that the sum of the atoms are preserved in reaction dynamics, and condition 2 requires that each atom needs to appear in at least one species and there are no vacuous species that contain no atoms. These two condition constitute primitive atomic CRNs, which is shown to be equivalent to mass conservation in the proposition below. For subset atomic, condition 3 then requires that the atoms $\mathcal{A}$ need to be distinct species already included in the reaction network, i.e. $\mathcal{A} \subset \mathcal{X}$. This allows the split of species into atoms $X_1, \ldots, X_d$ and non-atoms $X_{d+1}, \ldots, X_n$. The jth column of $\boldsymbol{D}$ for $j > d$ can be interpreted as the atomic decomposition of X_j into atoms $X_1, \ldots, X_d$. The ith row of $\boldsymbol{D}$, $i = 1, \ldots, d$, then can be interpreted as the total amount of the ith atomic species X_i in atomic or free form X_i, and in non-atomic or bound forms of $X_{d+1}, \ldots, X_n$. Condition 4 then requires that the non-atomic species contain more than one atom, i.e. atoms have no isomers. For stoichiometry-atomic, we ask that given a non-atomic species, whether the stoichiometry allows the decomposition of the non-atomic species to its atomic compositions. Since the atomic composition of a non-atomic species is a column of $\boldsymbol{D}_2$, this comes down to whether the column vector of $\tilde{\boldsymbol{D}}$ for this species is contained in the stoichiometric subspace $\mathcal{S}$. Note that stoichiometry-atomic only implies that the decomposition from a non-atomic species to its atoms is allowed by the stoichiometry of the reaction, but does not guarantee there exists a sequence of reactions to do so. Requiring such a sequence exists constitute the notion of reachably atomic CRN, which is defined and studied in [37] and is a stronger condition than stoichiometry-atomic.

Below are a few useful characterizations of the various atomic notions.

Proposition 3.3.3 ([37]). *1. A CRN is primitive atomic if and only if it is mass conserving.*

Mass-conserving is defined by there exists a strictly positive vector $\boldsymbol{m} \in \mathbb{R}^n_{>0}$ such that $\boldsymbol{\Gamma}^\intercal \boldsymbol{m} = 0$.

2. For a stoichiometry-atomic CRN, the matrix $\boldsymbol{D}$ is unique.

Proof. Proof for 1 is already transparent in [37].

Proof for 2 (adapted from arguments for reachably atomic of [37]). For a stoichiometry-atomic CRN, we know $\operatorname{rowspan} \boldsymbol{D} \subset \mathcal{S}^\perp$. Take their orthogonal complements, we have

$\mathcal{S} \subset \ker \boldsymbol{D}$. We also have $\operatorname{colspan} \tilde{\boldsymbol{D}} = \ker \boldsymbol{D} \subset \mathcal{S}$ (Lemma 3.3.4). So we have $\mathcal{S} = \ker \boldsymbol{D}$. This fixes the dimension of $\boldsymbol{D} \in \mathbb{N}^{d \times n}$, with $d = n - r$, where r is the rank of $\boldsymbol{\Gamma}$ or dimension of $\mathcal{S}$.

Furthermore, the matrix $\boldsymbol{D}$ itself is unique. We first see that once the set of columns $\mathcal{I}$ that form the identity submatrix is given, then $\boldsymbol{D}$ is uniquely determined. Consider an atom-first ordering such that $\mathcal{I} = \{1, \dots, d\}$. So $\boldsymbol{D}$ can be written as $\boldsymbol{D} = \begin{bmatrix} \mathbf{I}_d & \boldsymbol{D}_2 \end{bmatrix}$. Since rows of $\boldsymbol{D}$ are conservative, we have

$$\boldsymbol{D}\boldsymbol{\Gamma} = \boldsymbol{\Gamma}_1 + \boldsymbol{D}_2\boldsymbol{\Gamma}_2 = \mathbf{0}, \qquad \text{where } \boldsymbol{\Gamma} = \begin{bmatrix} \boldsymbol{\Gamma}_1 \\ \boldsymbol{\Gamma}_2 \end{bmatrix}, \ \boldsymbol{\Gamma}_2 \in \mathbb{Z}^{r \times m},$$

and $\boldsymbol{\Gamma}_2$ has full row rank. So $\boldsymbol{D}_2$ is uniquely determined by $\boldsymbol{D}_2 = -\boldsymbol{\Gamma}_1\boldsymbol{\Gamma}_2^\dagger$, where $\boldsymbol{\Gamma}_2^\dagger$ is the pseudo-inverse of $\boldsymbol{\Gamma}_2$.

Now we are left to show the set of columns $\mathcal{I}$ is unique. Assume there exists two sets of columns $\mathcal{I}, \mathcal{I}' \subset \{1, \dots, n\}$ that determine $\boldsymbol{D}$ and $\boldsymbol{D}'$ respectively. Assume $\mathcal{I} \neq \mathcal{I}'$, then there exists $i^* \in \mathcal{I} \backslash \mathcal{I}'$ or there exists $i^* \in \mathcal{I}' \backslash \mathcal{I}$. Without loss of generality, consider the former case. The vector $\boldsymbol{\sigma} = \boldsymbol{D}^\intercal \mathbf{1}$ satisfies $\sigma_i = 1$ for $i \in \mathcal{I}$, and $\sigma_i \geq 2$ for $i \notin \mathcal{I}$. Since $i^* \in \mathcal{I}$, $\sigma_{i^*} = 1$. Since $i^* \notin \mathcal{I}'$, the ith column of $\boldsymbol{D}'$ is included in $\boldsymbol{D}'_2$. Then stoichiometry-atomic with $\boldsymbol{D}'$ implies $\tilde{\boldsymbol{d}}'_{i^*} := \begin{bmatrix} \boldsymbol{d}'_{i^*} \\ \mathbf{0} \end{bmatrix} - \boldsymbol{e}_{i^*} \in \mathcal{S}$. However, since $\boldsymbol{\sigma} \in \operatorname{rowspan} \boldsymbol{D} = \mathcal{S}^\perp$, we should have $\boldsymbol{\sigma}^\intercal \tilde{\boldsymbol{d}}^*_i = 0$, but we obtain the following contradiction:

$$\boldsymbol{\sigma}^\intercal \tilde{\boldsymbol{d}}^*_i = \boldsymbol{\sigma}^\intercal \left(\begin{bmatrix} \boldsymbol{d}'_i \\ \mathbf{0} \end{bmatrix} - \boldsymbol{e}_i \right) \geq \mathbf{1}^\intercal \boldsymbol{d}'_i - \sigma_i = \mathbf{1}^\intercal \boldsymbol{d}'_i - 1 \geq 2 - 1 = 1,$$

where the first inequality we used $\sigma_i \geq 1$ for all $1 \leq 1 \leq n$, and the second inequality we used $\|\boldsymbol{d}'_i\|_1 \geq 2$. □

Lemma 3.3.4. *Given matrix* $\boldsymbol{D} = \begin{bmatrix} \mathbf{I}_d & \boldsymbol{D}_2 \end{bmatrix} \in \mathbb{R}^{d \times n}$, $d < n$, *define* $\tilde{\boldsymbol{D}} = \begin{bmatrix} \boldsymbol{D}_2 \\ -\mathbf{I}_r \end{bmatrix} \in \mathbb{R}^{n \times r}$, $r = n - d$. *Then* $\operatorname{colspan} \tilde{\boldsymbol{D}} = \ker \boldsymbol{D}$.

Proof. To see this, $\boldsymbol{D}\tilde{\boldsymbol{D}} = \boldsymbol{D}_2 - \boldsymbol{D}_2 = 0$, so $\operatorname{colspan} \tilde{\boldsymbol{D}} \subset \ker \boldsymbol{D}$. Then, since $\ker \boldsymbol{D}$ is of dimension $r = n - d$, since $\boldsymbol{D}$ is full row rank, while $\tilde{\boldsymbol{D}}$ is rank r, by dimensionality $\operatorname{colspan} \tilde{\boldsymbol{D}} = \ker \boldsymbol{D}$. □

The above result enables a simple characterization of stoichiometry-atomic CRNs.

Theorem 3.3.5. *Given a CRN with stoichiometry matrix $\mathbf{\Gamma} \in \mathbb{R}^{n\times m}$ of rank r, it is stoichiometry-atomic if and only if there is a collection of r linearly independent rows of $\mathbf{\Gamma}$, indexed by $\mathcal{I} = \{i_1, \ldots, i_r\} \subset \{1, \ldots, n\}$, such that the matrix $\boldsymbol{L}$ computed from it, as defined below, satisfies that (1) its entries are non-negative and (2) the column sums of $\boldsymbol{L}_2$ are ≥ 2.*

$$\boldsymbol{L} = \begin{bmatrix} \mathbf{I}_d & \boldsymbol{L}_2 \end{bmatrix}, \quad \boldsymbol{L}_2^\intercal := -\mathbf{\Gamma}_1 \mathbf{\Gamma}_2^\dagger, \quad \mathbf{\Gamma} = \begin{bmatrix} \mathbf{\Gamma}_1 \\ \mathbf{\Gamma}_2 \end{bmatrix}, \tag{3.5}$$

where the rows of $\mathbf{\Gamma}$ are re-arranged such that the r linearly indepedent rows of $\mathbf{\Gamma}$ indexed by $\mathcal{I} = \{i_1, \ldots, i_r\}$ now has indices $\{n - r + 1, \ldots, n\}$, i.e. these rows form the submatrix $\mathbf{\Gamma}_2 \in \mathbb{R}^{r\times m}$ in the expression above.

Proof. The forward direction is trivial by the definition of stoichiometry-atomic CRNs. Just set $\boldsymbol{L} := \boldsymbol{D}$ in an atomic ordering. The reverse direction is also clear, and by setting $\boldsymbol{D} := \boldsymbol{L}$ we then recognize that $\boldsymbol{L}$ satisfies all the conditions. □

Note that we can also express $\boldsymbol{L}_2$ in terms of the transpose-reduced stoichiometry matrix $\boldsymbol{N} \in \mathbb{R}^{r\times n}$. Write $\boldsymbol{N} = \begin{bmatrix} \boldsymbol{N}_1 & \boldsymbol{N}_2 \end{bmatrix}$ with $\boldsymbol{N}_2 \in \mathbb{R}^{r\times r}$ a full rank submatrix, then $\boldsymbol{L}_2^\intercal = -\boldsymbol{N}_2^{-1}\boldsymbol{N}_1$.

The characterization in Theorem 3.3.5 shows that the notion of stoichiometry-atomic CRNs is very easy to use. To test whether a given CRN is stoichiometry-atomic with species indexed in $\mathcal{I} = \{i_1, \ldots, i_r\}$ as atoms, take the stoichiometry matrix and compute $\boldsymbol{L}_2$ to check whether it satisfies the two conditions in the theorem. We also know that once we find a set of atomic species that $\boldsymbol{L}_2$ satisfies those conditions, then this is the unique set of atomic species for this CRN, and the columns of $\boldsymbol{L}$ matrix represent the atomic decomposition of each species. On the other hand, to come up with a stoichiometry-atomic CRN from scratch, write out some $\boldsymbol{L}_2$ matrix satisfying the two conditions, then any transpose-reduced stoichiometry matrix $\boldsymbol{N}$ satisfying $\boldsymbol{L}_2^\intercal = -\boldsymbol{N}_2^{-1}\boldsymbol{N}_1$ would specify the independent reactions of a stoichiometry-atomic CRN. For example, take $\boldsymbol{N}_2$ as identify and $\boldsymbol{N}_1 = -\boldsymbol{L}_2^\intercal$ would work.

As a side note, we caution that for a stoichiometry-atomic CRN, although the atomic species are all distinct, the non-atomic species may not have distinct atomic compositions. In other words, the column vectors of $\boldsymbol{L}_2$ may not be all distinct. If two columns $j_1, j_2 > d$ of $\boldsymbol{L}$ are the same, since $\operatorname{colspan} \tilde{\boldsymbol{L}} = \mathcal{S}$, this corresponds to $\boldsymbol{e}_{j_1} - \boldsymbol{e}_{j_2} \in \mathcal{S}$. There is no condition in stoichiometry-atomic CRN that rules this out. For example, this can happen in the following binding network. $3E_1 \rightleftharpoons E_3$, $2E_1 \rightleftharpoons E_2$, $E_1 + E_3 \rightleftharpoons E_4$, $2E_2 \rightleftharpoons E_4'$. Here E_4 and E_4' have the same atomic compositions. It may be appealing from physical intuition that non-atomic species should have distinct atomic compositions. This can be achieved by

imposing further conditions beyond stoichiometry-atomic, such that any two species with the same atomic compositions are identified to be the same species. This would be an interesting and worthwhile investigation if each species in the CRN indeed correspond to distinct atoms or molecules in reality. On the other hand, this may become restrictive, since a common usage of CRN is to use different species to label different states of the same molecule, such as inside or outside of a compartment, or methylation or phosphorylation states when methyl and phosphate groups are ignored in the network description. This highlights that although CRNs can be considered as models of real chemical reactions, they are generic mathematical objects like Markov chains that can have closer connections to very different domains of reality when further structures are imposed.

We examine a few examples to build intuition.

Example 1 (not primitive atomic)**.** Consider the following set of reactions:

$$\begin{aligned} X_1 + X_2 &\rightleftharpoons C_{12}, \\ X_3 + X_4 &\rightleftharpoons C_{34}, \\ C_{12} + C_{34} &\rightleftharpoons C_0, \\ X_2 + X_3 &\rightleftharpoons C_0. \end{aligned} \tag{3.6}$$

We see that there are two ways of forming the complex C_0, one via two-step binding as $C_{12} + C_{34}$, and one via one-step binding as $X_2 + X_3$. Intuitively, from the two-step binding we see C_0 is effectively composed of $X_1 + X_2 + X_3 + X_4$, while C_0 viewed from the one-step binding is effectively composed of only $X_2 + X_3$. So the two paths of decomposition results in different compositions, which is an un-physical result. Indeed, we can show this network does not conserve mass. Therefore, it is not primitive atomic. △

Example 2 (Phosphorylation)**.** Consider the following set of reactions:

$$X_p + Y \rightleftharpoons C \rightleftharpoons X + Y_p. \tag{3.7}$$

The biological context is that X and Y are two proteins, with X_p and Y_p as their phosphorylated forms, respectively. The phosphate group can be transferred between X and Y via the binding reactions. This network is primitive atomic since $X + X_p + Y + Y_p + 2C$ is conserved. With species ordering (X, Y, X_p, Y_p, C), this conserved quantity corresponds to vector $(1, 1, 1, 1, 2)$. To look at whether it has further atomic properties, examine its transpose-reduced stoichiometry matrix below,

$$\boldsymbol{N} = \begin{bmatrix} 1 & 0 & 0 & 1 & -1 \\ 0 & 1 & 1 & 0 & -1 \end{bmatrix}.$$

This CRN has three conserved quantities since $n = 5$, $r = 2$, so $d = n - r = 3$. One choice of conservation law matrix is total X, total Y, and total phosphates $t_p = X_p + C + Y_p$. In matrix form, this is

$$\boldsymbol{L} = \begin{bmatrix} 1 & 0 & 1 & 0 & 1 \\ 0 & 1 & 0 & 1 & 1 \\ 0 & 0 & 1 & 1 & 1 \end{bmatrix}.$$

Intuitively we see this CRN is not subset atomic, because there is no species for phosphate groups. To rigorously show this, we can take all choices of atomic species and check that the conservation law matrix produced cannot have the 3 columns of the atomic species form an identity matrix. △

We can add reactions about phosphate groups to make the phosphorylation network above stoichiometry-atomic.

Example 3 (Phosphorylation, continued)**.** We consider adding the following reactions to the CRN in equation (3.7).

$$X + p \rightleftharpoons X_p, \quad Y + p \rightleftharpoons Y_p. \tag{3.8}$$

With species order (X, Y, p, X_p, Y_p, C), the transpose of the stoichiometry matrix of this binding network is

$$\boldsymbol{\Gamma}^{\intercal} = \begin{bmatrix} 1 & 0 & 1 & -1 & 0 & 0 \\ 0 & 1 & 1 & 0 & -1 & 0 \\ 1 & 0 & 0 & 0 & 1 & -1 \\ 0 & 1 & 0 & 1 & 0 & -1 \end{bmatrix}. \tag{3.9}$$

Now, because the stoichiometry matrix has rank 3, this CRN still has 3 conserved quantities. All of them correspond to conservation of atomic species. The $\boldsymbol{D}$ matrix for atomic species $\{X, Y, p\}$ is

$$\boldsymbol{D} = \left[\begin{array}{ccc|ccc} 1 & 0 & 0 & 1 & 0 & 1 \\ 0 & 1 & 0 & 0 & 1 & 1 \\ 0 & 0 & 1 & 1 & 1 & 1 \end{array}\right]. \tag{3.10}$$

Now this CRN is not only subset atomic, but also stoichiometry-atomic. △

Binding network with state transitions

State transitions correspond to reactions of the form $A \rightleftharpoons B$. This can be interpreted as molecules having two different states A and B, and transitions between them. This interpretation also reflects that for systems with such reactions only, viewing the system as

many independent copies of the same molecule transitioning between states is equivalent to viewing the system as a collection of molecules doing the reactions. Systems with only state transitions therefore come under several different names: first-order chemical reactions, Markov chain dynamics, or Laplacian dynamics on directed graphs. This topic is nicely reviewed in [76]. There are also other views of this, such as random walks and electrical circuits [40].

From the perspective of biomolecular reactions, state transitions can arise from the same biomolecule having multiple states, recording information about location or chemical modifications. In the binding reaction context, state transition can also arise in some simplifying limit of dominance conditions. For the binding reaction $E + S \rightleftharpoons C$ where enzyme E binds with substrate S to form product C, if substrate molecule is overabundant, i.e. the free substrate S dominates in total substrate $t_S = S + C$, then this binding reaction can be viewed as state transition $E \overset{S}{\rightleftharpoons} C$.

Due to above reasons, it is desirable to consider binding networks with state transitions, so that we have a model class closed under reduction by dominance limits. We characterize this below as a slight generalization of binding networks.

Definition 3.3.6. A CRN $(\mathcal{X}, \mathcal{R})$ is a binding network with state transitions if it is reversible, and each pair of forward-backward reactions is either a binding reaction (see Definition 3.3.1), or a *state-transition reaction*.

A reaction $(\boldsymbol{\alpha}, \boldsymbol{\beta}, k) \in \mathcal{R}$ is a state-transition reaction if $\boldsymbol{\alpha} = \boldsymbol{e}_i$ and $\beta = \boldsymbol{e}_j$ for some $i \neq j$ and $i, j \in \{1, \ldots, n\}$.

We also want a physical condition on binding networks with state transitions like the stoichiometry-atomic condition. We see that for the five conditions of stoichiometry-atomic, only condition 4 excludes state transitions (see Definition 3.3.2). Since condition 4 can be interpreted as a no-isomer condition, we give the following definition.

Definition 3.3.7. A CRN is **isomer-atomic** if it satisfies conditions 1, 2, 3, and 5 but not necessarily condition 4 in Definition 3.3.2.

As atoms can have isomers (i.e. different states), an isomer-atomic CRN does not have a unique atomic decomposition $\boldsymbol{D}$ matrix, since it may not have a unique set of atoms to begin with. On the other hand, once a feasible set of atoms are given, then $\boldsymbol{D}$ is still uniquely determined. So we have the following characterization of isomer-atomic CRNs as a corollary of the theorem for stoichiometry-atomic CRNs.

Corollary 3.3.8. *Given a CRN with stoichiometry matrix $\mathbf{\Gamma} \in \mathbb{R}^{n\times m}$ of rank r, it is isomer-atomic if and only if there is a collection of r linearly independent rows of $\mathbf{\Gamma}$, indexed by $\mathcal{I} = \{i_1, \ldots, i_r\} \subset \{1, \ldots, n\}$, such that the matrix $\boldsymbol{L}$ computed from it, as defined in Eq 3.5, satisfies that (1) entries of $\boldsymbol{L}$ are non-negative and (2) no columns of $\boldsymbol{L}_2$ are all zero.*

Proof. Forward direction: by definition, an isomer-atomic CRN yields matrix $\boldsymbol{D}$ that satisfies these conditions. Backward direction: by construction, the $\boldsymbol{L}$ matrix constructed from stoichiometry matrix already satisfy condition 3 and 5 of isomer-atomic, and condition 1 and 2 are assumed for $\boldsymbol{L}$. □

This characterization shows that isomer-atomic CRN simply has less restrictive conditions on the $\boldsymbol{L}$ matrix compared to stoichiometry-atomic. So the condition of isomer-atomic is even easier to check. One implication of this is that an isomer-atomic CRN may have multiple choices for sets of atoms, although there are always $d = n - r$ atomic species in each choice. We illustrate this via an example blow.

Example 4 (MWC)**.** MWC model for receptor-ligand binding captures allosteric effects. Consider a receptor R binds with a ligand L. The receptor has an active state R_a, and an inactive state R_i, with different binding affinities to the ligand. So the binding network is

$$R_i + L \rightleftharpoons C_i, \quad R_a + L \rightleftharpoons C_a, \quad R_i \rightleftharpoons R_a.$$

With species ordering (L, R_i, R_a, C_i, C_a), the stoichiometry matrix is

$$\boldsymbol{N} = \begin{bmatrix} 1 & 1 & 0 & -1 & 0 \\ 1 & 0 & 1 & 0 & -1 \\ 0 & 1 & -1 & 0 & 0 \end{bmatrix}.$$

There are 2 conserved quantities. We can choose them to be total ligand $t_L = L + C_i + C_a$ and total receptor $t_R = R_i + R_a + C_i + C_a$. So the conservation matrix is

$$\boldsymbol{L} = \begin{bmatrix} 1 & 0 & 0 & 1 & 1 \\ 0 & 1 & 1 & 1 & 1 \end{bmatrix}.$$

It is easily checked that this $\boldsymbol{L}$ is also what is obtained by direct computation from $\boldsymbol{N}$ with $\boldsymbol{L}_2^{\intercal} = -\boldsymbol{N}_2^{-1}\boldsymbol{N}_1$, where $\boldsymbol{N}_2$ and $\boldsymbol{L}_2$ are the last 3 columns of $\boldsymbol{N}$ and $\boldsymbol{L}$ respectively. This $\boldsymbol{L}$ treats L and R_i as atomic species. This is not unique, as we can just as well choose $\{L, R_a\}$ as the atomic species. △

Through this example, we can see intuitively that the decomposition matrix $\boldsymbol{L}$ of a stoichiometry-atomic CRN will have exactly d columns with exactly one nonzero entry. These correspond to the atomic species and the column vectors are $\boldsymbol{e}_i\mathbb{R}^d$ for $i = 1, \ldots, d$. For an isomer-atomic CRN, there could be more than one column taking value $\boldsymbol{e}_i$. This correspond to multiple choices for the atomic species.

For convenience, throughout later chapters, unless we explicitly state otherwise, a binding network refers to a binding network with state transitions, and a binding reaction refers to both a binding reaction or a state transition reaction, and the forward reaction is the forward reaction of a binding reaction, or any of the two reactions of a state transition.

The equivalent characterizations of stoichiometry-atomic and isomer-atomic both highlight the relation between conservation law matrix $\boldsymbol{L}$ and the stoichiometry matrix $\boldsymbol{\Gamma}$, or its transpose-reduce $\boldsymbol{N}$. We would like a full description of how conditions on $\boldsymbol{L}$ are related to conditions on $\boldsymbol{N}$. We investigate this next.

Duality between stoichiometry N and conservation L

We see that from atomic requirements on a CRN represented by stoichiometry matrix $\boldsymbol{\Gamma}$, or its transpose-reduce $\boldsymbol{N}$, we obtain conditions on the conservation law matrix $\boldsymbol{L} \in \mathbb{R}^{d\times n}$, which is the atomic decomposition matrix in atomic CRN contexts. What is the relationship between $\boldsymbol{N}$ and $\boldsymbol{L}$ in general? We can view these two matrices as vector configurations to see their combinatorial structures, as is done in the literature of convex polytopes and oriented matroids (see Chapter 6 of [123]).

From this view, $\boldsymbol{L} \in \mathbb{R}^{d\times n}$ is a configuration of n column vectors in $\mathbb{R}^d$, and similarly $\boldsymbol{N} \in \mathbb{R}^{r\times n}$ is a configuration of n column vectors in $\mathbb{R}^r$. Several structures are associated with a vector configuration. We use $\boldsymbol{N}$ as an example. The *linear dependences* of $\boldsymbol{N}$ is $\{\boldsymbol{v} : \boldsymbol{N}\boldsymbol{v} = 0\} = \ker \boldsymbol{N}$. The *covectors* of $\boldsymbol{N}$ are sign vectors $\operatorname{sgn}\ker \boldsymbol{N} = \{\mathrm{v} : \mathrm{v}_i = \operatorname{sgn} v_i, \boldsymbol{v} \in \ker \boldsymbol{N}\} \subset \{+, -, 0\}^n$. Here sgn is sign operation, broadcasted to vectors and vector spaces from its operation on real numbers: $\operatorname{sgn}(x) = 0$ if $x = 0$, $+$ if $x > 0$, and $-$ if $x < 0$, for $x \in \mathbb{R}$. The *cocircuits* of $\boldsymbol{N}$ are minimal sign vectors denoted $\min \operatorname{sgn}\ker \boldsymbol{N} = \{\min \mathrm{v} : \mathrm{v} \in \operatorname{sgn}\ker \boldsymbol{N}\}$. Here "minimal" is defined by a partial order on signs broadcasted to sets of sign vectors: $0 < +$ and $0 < -$. So minimal corresponds to having as many zeros as possible without flipping any sign between $+$ and $-$. Similarly, the set of *value vectors* of $\boldsymbol{N}$ is $\{\boldsymbol{c}^\intercal \boldsymbol{N} : \boldsymbol{c} \in \mathbb{R}^r\} = \operatorname{rowspan} \boldsymbol{N}$. The signed *vectors* of $\boldsymbol{N}$ are $\operatorname{sgn}\operatorname{rowspan} \boldsymbol{N}$. The signed *circuits* of $\boldsymbol{N}$ are $\min \operatorname{sgn}\operatorname{rowspan} \boldsymbol{N}$. Now we connect this back to our CRN context.

For a CRN, we begin with stoichiometry matrix $\boldsymbol{\Gamma} \in \mathbb{R}^{n\times m}$, and the stoichiometric subspace

$\mathcal{S} = \operatorname{colspan} \boldsymbol{\Gamma}$ that species' concentrations can vary in. Let r be the rank of $\boldsymbol{\Gamma}$ or the dimension of $\mathcal{S}$, then we select r linearly independent columns of $\boldsymbol{\Gamma}$ and transpose them to form the transpose-reduced stoichiometry matrix $\boldsymbol{N} \in \mathbb{R}^{r \times n}$. Now $\mathcal{S} = \operatorname{rowspan} \boldsymbol{N}$. The conserved quantities not changed by reactions correspond to vectors in $\mathcal{S}^\perp = \ker \boldsymbol{N} = \ker \boldsymbol{\Gamma}^\intercal$. A $\boldsymbol{L} \in \mathbb{R}^{d \times n}$ with $d = n - r$ is the conservation law matrix if its rows span the space of conserved quantities, i.e. $\operatorname{rowspan} \boldsymbol{L} = \mathcal{S}^\perp$. This condition means $\operatorname{rowspan} \boldsymbol{L} = \ker \boldsymbol{N}$, and conversely $\ker \boldsymbol{L} = \operatorname{rowspan} \boldsymbol{N}$. In the language of vector configurations, the linear dependences of $\boldsymbol{L}$ are the value vectors of $\boldsymbol{N}$, and vice versa. Configurations satisfying this are called *dual configurations*. So $\boldsymbol{L}$ and $\boldsymbol{N}$ are dual configurations. Dual configurations are intimately related in their combinatorial structure beyond linear dependences and value vectors. Namely, the covectors of $\boldsymbol{L}$ are vectors of $\boldsymbol{N}$, and the cocircuits of $\boldsymbol{L}$ are circuits of $\boldsymbol{N}$, and vice versa. This is an example of oriented matroid duality. Below we focus on the notion of primitive atomic as an illustration of this relationship.

From our definition of primitive atomic and Proposition 3.3.3, we see that primitive atomic is equivalent to that the space of conserved quantity has a vector with all entries positive. In terms of $\boldsymbol{L}$, this means there is a strictly positive vector in $\operatorname{rowspan} \boldsymbol{L}$. This is one definition for $\boldsymbol{L}$ is an *acyclic* vector configuration. This is equivalent to a dual condition on $\boldsymbol{N}$ called *totally cyclic*. We write several equivalent conditions in the following, summarizing our discussion above and results in Chapter 6 of [123] on vector configurations.

Proposition 3.3.9. *Let $\boldsymbol{N}$ be the transpose-reduced stoichiometry matrix of a CRN. Let $\boldsymbol{L}$ be a conservation matrix. The following are equivalent.*

1. *This CRN is primitive atomic.*
2. *This CRN conserves mass.*
3. *$\boldsymbol{L}$ is acyclic. This is defined as $\nexists\, \boldsymbol{y} \in \mathbb{R}^n$, $\boldsymbol{y} \geq 0$, $\boldsymbol{y} \neq 0$, $\boldsymbol{L}\boldsymbol{y} = 0$. Another equilvalent definition is $\exists \boldsymbol{c} \in \mathbb{R}^d$, $\boldsymbol{c}^\intercal \boldsymbol{L} > 0$, i.e. every entry of $\boldsymbol{c}^\intercal \boldsymbol{L}$ is positive.*
4. *$\boldsymbol{N}$ is totally cyclic. This is defined as $\nexists \boldsymbol{x} \in \mathbb{R}^r$, $\boldsymbol{N}^\intercal \boldsymbol{x} \geq 0$, $\boldsymbol{N}^\intercal \boldsymbol{x} \neq 0$. An equivalent definition is $\exists \boldsymbol{c} \in (\mathbb{R}^n)^*$, $\boldsymbol{c} > 0$, $\boldsymbol{c}\boldsymbol{N}^\intercal = 0$.*
5. *$\boldsymbol{L}$ has no positive signed circuit, i.e. no positive vector in $\min \operatorname{sgn} \ker \boldsymbol{L} = \min \operatorname{sgn} \mathcal{S} = \min \operatorname{sgn} \operatorname{rowspan} \boldsymbol{N}$. This is equivalent to $\boldsymbol{N}$ has no positive signed cocircuit.*
6. *$\boldsymbol{L}$ has $(++\ldots+)$ as a signed covector, i.e. it is in $\operatorname{sgn} \operatorname{rowspan} \boldsymbol{L} = \operatorname{sgn} \mathcal{S}^\perp = \operatorname{sgn} \ker \boldsymbol{N}$. This is equivalent to $\boldsymbol{N}$ has $(++\ldots+)$ as a signed vector.*
7. *$\boldsymbol{L}$ has every $i = 1, \ldots, n$ contained in a nonnegative cocircuit, i.e. contained in a non-negative sign vector in $\min \operatorname{sgn} \operatorname{rowspan} \boldsymbol{L} = \min \operatorname{sgn} \mathcal{S}^\perp$.*

The above illustrates the dual relationship between $\boldsymbol{N}$ and $\boldsymbol{L}$, and how mass-conservation or primitive-atomic properties of a CRN can be characterized in terms of sign conditions on the stoichiometry subspace. This provides a quick way to check whether a given CRN is primitive-atomic, from sign conditions on either its stoichiometry matrix $\boldsymbol{N}$ or its conservation matrix $\boldsymbol{L}$. Below we show that the isomer-atomic property can be similarly characterized as sign conditions on the conserved quantity space $\mathcal{S}^\perp$, or equivalently on $\operatorname{rowspan} \boldsymbol{L}$. It is an interesting question how this sign condition translates into sign conditions on the stoichiometry subspace $\mathcal{S}$ or on $\operatorname{rowspan} \boldsymbol{N}$.

Proposition 3.3.10. *Given a CRN and its stoichiometry subspace $\mathcal{S}$, the following are equivalent.*

1. *The CRN is isomer-atomic with the first d species as atoms.*
2. $\operatorname{sgn} \mathcal{S}^\perp$ *contains all-positive sign vector* `(++...+)`*, and in* $\operatorname{sgn} \mathcal{S}^\perp$ *there also exists sign vectors $\mathrm{v}^{(i)}$ for $i = 1, \dots, d$, where $\mathrm{v}^{(i)}$ is non-negative and satisfies $\mathrm{v}^{(i)}_i = +$, $\mathrm{v}^{(i)}_j = 0$ for $1 \leq j \leq d$ and $j \neq i$.*

Proof. $(1 \implies 2)$ This direction is obvious since isomer-atomic CRN conserves mass so `(++...+)` is in $\operatorname{sgn} \mathcal{S}^\perp$, and the sign vector of the ith row of $\boldsymbol{L}$ corresponds to $\mathrm{v}^{(i)}$.

$(2 \implies 1)$ For each $\mathrm{v}^{(i)}$, there exists $\boldsymbol{v}^{(i)} \in \mathcal{S}^\perp$ with $\operatorname{sgn} \boldsymbol{v}^{(i)} = \mathrm{v}^{(i)}$. Define $\tilde{\boldsymbol{v}}^{(i)} = (v^{(i)}_i)^{-1} \boldsymbol{v}^{(i)}$. Then concatenating $\tilde{\boldsymbol{v}}^{(i)}$ as rows vectors yields a matrix $\boldsymbol{V} \in \mathbb{R}^{d \times n}$, which satisfies the conditions for $\boldsymbol{L}$ in the definition of isomer-atomic.

□

3.4 Detailed balance steady states of binding networks

Since binding reactions between molecules tend to happen at a faster time scale than the phenomena we are interested in, e.g. production and degradation of molecules, it is natural to assume that the binding reactions have reached a steady state. In fact, we can further assume that the steady states the binding reactions reach are at equilibrium, based on the intuition that nonequilibrium steady states require continuous energy input at the fast time scale of binding reactions, which is costly and therefore unlikely. In other words, although a mathematically specified CRN may not have equilibrium steady states, and may have steady states that are not at equilibrium, it is physically plausible to assume that a binding network on a fast time scale should have equilibrium steady states and practically stay in equilibrium steady states. Therefore, in this work we focus our study of equilibrium steady states in a way that does not concern whether they exist from mathematical specifications.

In this section, we describe the manifold of equilibrium steady states, which are also called detailed balance steady states in chemical reaction network theory.

Let $\boldsymbol{x} \in \mathbb{R}^n_{>0}$ denote a vector of species concentrations in a binding network. Then detailed balance steady states are ones that satisfy the condition that the forward (dissociation) and backward (association) fluxes of each reaction balances out. Let $k_j = \frac{k_j^-}{k_j^+}$, the ratio between the forward (dissociation) and backward (association) reaction rates, be the equilibrium constant of the jth binding reaction (in the dissociation direction, so also called dissociation constants). Assuming mass-action kinetics, then the balancing of forward and backward fluxes corresponds to $k_j^- \boldsymbol{x}^{\boldsymbol{\alpha}_j^f} = k_j^+ \boldsymbol{x}^{\boldsymbol{\beta}_j^f}$, where $\boldsymbol{\alpha}_j^f, \boldsymbol{\beta}_j^f \in \mathbb{Z}^n$ are the reactant and product vectors of the jth forward (dissociation) reaction. This can be written as $\boldsymbol{x}^{\boldsymbol{\gamma}_j^f} = k_j$, where $\boldsymbol{\gamma}_j^f = \boldsymbol{\beta}_j^f - \boldsymbol{\alpha}_j^f \in \mathbb{Z}^n$ is the stoichiometry vector of the jth forward (dissociation) reaction. Let r denote the rank of the stoichiometry matrix $\boldsymbol{\Gamma} \in \mathbb{R}^{n \times m}$, which is also the rank of $\boldsymbol{\Gamma}^f \in \mathbb{R}^{n \times \frac{m}{2}}$, the stoichiometry of only the forward reactions. Then we can always select r forward reactions with linearly independent stoichiometry vector to form the transpose-reduced stoichiometry matrix $\boldsymbol{N}$, whose rows are selected columns of $\boldsymbol{\Gamma}^f$. Similarly, we take the equilibrium constants for the r reactions selected to form vector $\boldsymbol{k} \in \mathbb{R}^r_{>0}$. Taking log and write in matrix form, we have that the detailed balanced condition becomes

$$\boldsymbol{N} \log \boldsymbol{x} = \log \boldsymbol{k}. \tag{3.11}$$

Since there are n variables and r equations, we see the solution $\log \boldsymbol{x}$ of this equation for a fixed $\boldsymbol{k}$ has $d = n - r$ degrees of freedom.

What variables could represent this d degrees of freedom for the detailed balance solutions $\log \boldsymbol{x}$? One natural choice are the conserved quantities. Let $\boldsymbol{L} \in \mathbb{R}^{d \times n}$ be the conservation law matrix, then the conserved quantities are defined as $\boldsymbol{t} = \boldsymbol{L}\boldsymbol{x}$. The conserved quantities are denoted as $\boldsymbol{t}$ for totals since in binding networks they often correspond physically to the total of some species in various forms. So we see the d total concentrations $\boldsymbol{t} \in \mathbb{R}^d_{>0}$ form a natural representation of the remaining d degrees of freedom. If we further require the binding network to be isomer-atomic, then alternatively we can represent the d degrees of freedom as the concentrations of atomic species. We will see this explicitly as alternative coordinate charts for the manifold of detailed balance steady states.

Formally, we define the manifold for the detailed balanced solutions of a binding network. We consider this manifold as the set of all possible values the variables of interest can take for a given binding network. The variables of interest from our above discussion are the species concentration $\boldsymbol{x} \in \mathbb{R}^n_{>0}$, total concentrations $\boldsymbol{t} \in \mathbb{R}^d_{>0}$, and equilibrium constants

$\boldsymbol{k} \in \mathbb{R}^r_{>0}$. The manifold is then defined by the constraint on these variables imposed by the detailed balance condition of a particular binding network.

Definition 3.4.1. Given a binding network with reduced stoichiometry matrix $\boldsymbol{N} \in \mathbb{R}^{r\times n}$. Let $\boldsymbol{k} \in \mathbb{R}^r_{>0}$ be the equilibrium constants for the r reactions selected. Let $\boldsymbol{L} \in \mathbb{R}^{d\times n}$, $d = n-r$ be the unique conservation law matrix of the network. Then the **manifold of detailed balance steady states** of the binding network, also called **equilibrium manifold** of the binding network for short, is

$$\mathcal{M} = \Big\{(\boldsymbol{x}, \boldsymbol{t}, \boldsymbol{k}) \in \mathbb{R}^{2n}_{>0} : \boldsymbol{t} = \boldsymbol{L}\boldsymbol{x}, \boldsymbol{N}\log\boldsymbol{x} = \log\boldsymbol{k}\Big\}. \tag{3.12}$$

Note that $\mathcal{M}$ is n-dimensional and immersed in $\mathbb{R}^{2n}_{>0}$. We denote a point in $\mathcal{M}$ as vector $\boldsymbol{p} \in \mathbb{R}^{2n}_{>0}$. When convenient, we could also consider the $\log$ manifold immersed in $\mathbb{R}^{2n}$.

$$\log\mathcal{M} := \Big\{(\log\boldsymbol{x}, \log\boldsymbol{t}, \log\boldsymbol{k}) \in \mathbb{R}^{2n} : (\boldsymbol{x}, \boldsymbol{t}, \boldsymbol{k}) \in \mathcal{M}\Big\}. \tag{3.13}$$

We caution that this approach of defining $\mathcal{M}$ considers a given binding network as a detailed-balance *constraint* on the values $(\boldsymbol{x}, \boldsymbol{t}, \boldsymbol{k})$ can take. The detailed balance condition takes higher priority than any specification of rates of a CRN. This is different from the typical approaches in CRN theory where the specification of network stoichiometry and rates take precedence, and the existence of detailed balance steady state is then determined later from the CRN specification. Because of our taking detailed balance as higher priority than CRN specifications, several CRNs can be equivalent to the same detailed balance behavior. In other words, if detailed balance is guaranteed, then specifying the full CRN may be redundant. For example, consider 3-state transition $C_1 \rightleftharpoons C_2 \rightleftharpoons C_3 \rightleftharpoons C_1$. With detailed balance given, this network is equivalent to the same network with one reaction deleted. Because of this, any nonequilibrium steady states are also automatically excluded.

Coordinate charts of the equilibrium manifold

With the equilibrium manifold $\mathcal{M}$ defined for a given binding networks, we would like to describe it and characterize its properties. The first thing to do with a smooth manifold is to specify coordinate charts on it, so that we have a parameterization of points on the manifold, and can talk about its tangent bundle for how to move around the manifold.

$\mathcal{M}$ is an n-dimensional manifold. It is naturally immersed in $2n$-dimensional space, where each point is specified as $\boldsymbol{p} = (\boldsymbol{x}, \boldsymbol{t}, \boldsymbol{k}) \in \mathbb{R}^2 n_{>0}$. But these variables are further related by n equations, namely $\boldsymbol{t} = \boldsymbol{L}\boldsymbol{x}$ and $\boldsymbol{N}\log\boldsymbol{x} = \log\boldsymbol{k}$. So we would like a parameterization of $\mathcal{M}$ that maps its points to $\mathbb{R}^n$ in a one-to-one or invertible way, so that the n degrees of freedom

in $\mathcal{M}$ are now explicitly some variable in $\mathbb{R}^n$. Such parameterizations are called *coordinate charts*, and a collection of charts that together cover the whole manifold is called an *atlas*. For $\mathcal{M}$, we will see below that the natural choices of atlas we discuss have just one chart.

The most natural choice to begin with is of course the species concentrations $\log \boldsymbol{x}$. By slight abuse of notation, this corresponds to the map $\log x : \mathcal{M} \to \mathbb{R}^n$ that takes a point specified as $\boldsymbol{p} = (\boldsymbol{x}, \boldsymbol{t}, \boldsymbol{k}) \in \mathcal{M}$ and output the log of the first n variables $\log \boldsymbol{x}$. This map is invertible because given $\log \boldsymbol{x}$, we can find $\boldsymbol{t}$ and $\boldsymbol{k}$ uniquely. Also, this chart is an atlas because every point in $\mathcal{M}$ can be represented in this way. So instead of using a vector $\boldsymbol{p} \in \mathbb{R}^{2n}_{>0}$ to denote a point on $\mathcal{M}$, we could equivalently use $\boldsymbol{x} \in \mathbb{R}^n_{>0}$. We can use the diagram below to represent this mapping:

$$\boldsymbol{p} = (\boldsymbol{x}, \boldsymbol{t}, \boldsymbol{k}) \in \mathcal{M} \underset{(\boldsymbol{x}, \boldsymbol{L}\boldsymbol{x}, \boldsymbol{N} \log \boldsymbol{x})}{\overset{\log \boldsymbol{x}}{\rightleftarrows}} \log \boldsymbol{x} \in \mathbb{R}^n. \tag{3.14}$$

We also want alternative charts for different purposes. For example, if we consider changing the steady states of a given binding network by adjusting the concentrations. In this case, although $\boldsymbol{x}$ varies, the equilibrium constants $\boldsymbol{k}$ are not modified by such changes, therefore should remain constant. So to study changes in concentrations in this case, we would like $\boldsymbol{k}$ to appear explicitly as variables in our parameterization. Another reason we may want this is to study what changes to the system would be caused by modifying the equilibrium constants $\boldsymbol{k}$, which is natural when asking questions about energy of molecules or temperature.

To obtain coordinate charts with $\boldsymbol{k}$ as variables, we first note that $\boldsymbol{k} \in \mathbb{R}^r_{>0}$ is of r dimensions, so to parameterize the n dimensions of $\mathcal{M}$, we need another d variables. A simple choice that is still close to the $\log \boldsymbol{x}$ chart is to take d of the $\boldsymbol{x}$ variables. Assuming our binding network is isomer-atomic, then one natural choice for this is $\boldsymbol{x}^a \in \mathbb{R}^d_{>0}$, concentrations for the d atomic species. This yields chart $(\log \boldsymbol{x}^a, \log \boldsymbol{k})$.

We can investigate properties of this chart by how it is mapped from the $\log \boldsymbol{x}$ chart. To write the map, we re-order the species so that the first d species are atomic. So $\boldsymbol{x} = (\boldsymbol{x}^a, \boldsymbol{x}^c)$ is split into two parts, the d atomic species $\boldsymbol{x}^a \in \mathbb{R}^d$, and r complex species $\boldsymbol{x}^c \in \mathbb{R}^r$. Using detailed balanced condition Eq (3.11), we have

$$\begin{bmatrix} \log \boldsymbol{x}^a \\ \log \boldsymbol{k} \end{bmatrix} = \begin{bmatrix} \mathbf{I}_d & 0 \\ \boldsymbol{N}_1 & \boldsymbol{N}_2 \end{bmatrix} \log \boldsymbol{x}.$$

Invert this expression and use that $\boldsymbol{L}_2^\intercal = -\boldsymbol{N}_2^{-1}\boldsymbol{N}_1$ yields an explicit alternative parameter-

ization of detailed balance steady states:

$$\begin{aligned}
&\{\log \boldsymbol{x} \in \mathbb{R}^n : \boldsymbol{N} \log \boldsymbol{x} = \log \boldsymbol{k}\} \\
=&\left\{ \log \boldsymbol{x} = \boldsymbol{L}^\intercal \log \boldsymbol{x}^a + \begin{bmatrix} 0 \\ \boldsymbol{N}_2^{-1} \end{bmatrix} \log \boldsymbol{k} : \log \boldsymbol{x}^a \in \mathbb{R}^d, \log \boldsymbol{k} \in \mathbb{R}^r \right\} \\
=&\left\{ \log \boldsymbol{x} = \begin{bmatrix} \mathbf{I}_d & 0 \\ \boldsymbol{L}_2^\intercal & \boldsymbol{N}_2^{-1} \end{bmatrix} \begin{bmatrix} \log \boldsymbol{x}^a \\ \log \boldsymbol{k} \end{bmatrix} : \log \boldsymbol{x}^a \in \mathbb{R}^d, \log \boldsymbol{k} \in \mathbb{R}^r \right\}.
\end{aligned} \tag{3.15}$$

So we see that the map between chart $\log \boldsymbol{x}$ and chart $(\log \boldsymbol{x}^a, \log \boldsymbol{k})$ is linear, so we represent this map explicitly as matrices in the following diagram:

$$\log \boldsymbol{x} \underset{\begin{bmatrix} \mathbf{I}_d & 0 \\ \boldsymbol{L}_2^\intercal & \boldsymbol{N}_2^{-1} \end{bmatrix}}{\overset{\begin{bmatrix} \mathbf{I}_d & 0 \\ \boldsymbol{N}_1 & \boldsymbol{N}_2 \end{bmatrix}}{\rightleftharpoons}} (\log \boldsymbol{x}^a, \log \boldsymbol{k}). \tag{3.16}$$

Since this map is invertible, we know $(\log \boldsymbol{x}^a, \log \boldsymbol{k})$ is also a one-chart atlas for $\mathcal{M}$.

Although chart $(\log \boldsymbol{x}^a, \boldsymbol{k})$ contains $\boldsymbol{k}$ as explicit variables, there are still scenarios where we may want an alternative. For one, we need the isomer-atomic assumption to have the atomic species. This may not hold in general. More importantly, in many scenarios when the concentrations in a binding network is adjusted, it is not by adjusting the atomic species' concentration, but by adjusting the conserved quantities or the totals (see Section 3.1). This is especially often the case for time-scale separation for binding and catalysis reactions, where binding reaches equilibrium steady state while catalysis produces or degrades molecules to change concentrations. Here when a molecule is produced or degraded by catalysis, whether it is bound or not, or in which state among the state transitions, is not distinguishable from the slow time scale of catalysis. Once a molecule is produced or degraded in a particular form or state, the binding network quickly equilibrates and the net change of one molecule is then on the total, not any particular form or state.

From this reason, we would like to have the chart $(\log \boldsymbol{t}, \log \boldsymbol{k})$, where $\boldsymbol{t} = \boldsymbol{L}\boldsymbol{x}$ is the totals or conserved quantities. To describe the map between this chart and chat $\log \boldsymbol{x}$ is more involved, as can be seen from the mixing of linear map $\boldsymbol{t} = \boldsymbol{L}\boldsymbol{x}$ and log-linear map $\log \boldsymbol{k} = \boldsymbol{N} \log \boldsymbol{x}$. We delve into this in the next section.

3.5 Log derivative as transform between two coordinate charts

We would like to understand how $\boldsymbol{x}$ changes with respect to $(\boldsymbol{t}, \boldsymbol{k})$ on the manifold $\mathcal{M}$. The map from $\boldsymbol{x}$ to $(\boldsymbol{t}, \boldsymbol{k})$ can be explicitly written as $(\log \boldsymbol{t}, \log \boldsymbol{k}) = (\log \boldsymbol{L}\boldsymbol{x}, \boldsymbol{N} \log \boldsymbol{x})$. However, the inverse map would require us to solve $\boldsymbol{x}$ in terms of $(\boldsymbol{t}, \boldsymbol{k})$. This comes down to solve a system of polynomial equations relating $(\boldsymbol{x}, \boldsymbol{t}, \boldsymbol{k})$, which in general is intractable both analytically and computationally. So we need to characterize the map from $(\boldsymbol{t}, \boldsymbol{k})$ to $\boldsymbol{x}$ through other means. One natural approach for a smooth manifold is to instead characterize how the tangent vectors are mapped between the two charts. This corresponds to study the derivatives.

To show the map $\log \boldsymbol{x} \mapsto (\log \boldsymbol{t}, \log \boldsymbol{k})$ is invertible and study its inverse, we capture the manifold $\mathcal{M}$ as the zero set of the following smooth function:

$$F(\boldsymbol{x}, \boldsymbol{t}, \boldsymbol{k}) = \begin{bmatrix} F_1(\boldsymbol{x}, \boldsymbol{t}) \\ F_2(\boldsymbol{x}, \boldsymbol{k}) \end{bmatrix} = \begin{bmatrix} \boldsymbol{L}\boldsymbol{x} - \boldsymbol{t} \\ \boldsymbol{N} \log \boldsymbol{x} - \log \boldsymbol{k} \end{bmatrix}. \tag{3.17}$$

We can then calculate the differentials by implicit function theorem, at any point $\boldsymbol{x}$ where $\frac{\partial F}{\partial \boldsymbol{x}}$ is invertible.

$$\begin{aligned} \begin{bmatrix} \frac{\partial \boldsymbol{x}(\boldsymbol{t},\boldsymbol{k})}{\partial \boldsymbol{t}} & \frac{\partial \boldsymbol{x}(\boldsymbol{t},\boldsymbol{k})}{\partial \boldsymbol{k}} \end{bmatrix} &= -\left(\frac{\partial F(\boldsymbol{x}, \boldsymbol{t}, \boldsymbol{k})}{\partial \boldsymbol{x}} \right)^{-1} \begin{bmatrix} \frac{\partial F(\boldsymbol{x},\boldsymbol{t},\boldsymbol{k})}{\partial \boldsymbol{t}} & \frac{\partial F(\boldsymbol{x},\boldsymbol{t},\boldsymbol{k})}{\partial \boldsymbol{k}} \end{bmatrix} \\ &= -\begin{bmatrix} \frac{\partial F_1(\boldsymbol{x},\boldsymbol{t})}{\partial \boldsymbol{x}} \\ \frac{\partial F_2(\boldsymbol{x},\boldsymbol{k})}{\partial \boldsymbol{x}} \end{bmatrix}^{-1} \begin{bmatrix} \frac{\partial F_1(\boldsymbol{x},\boldsymbol{t})}{\partial \boldsymbol{t}} & \frac{\partial F_1(\boldsymbol{x},\boldsymbol{t})}{\partial \boldsymbol{k}} \\ \frac{\partial F_2(\boldsymbol{x},\boldsymbol{k})}{\partial \boldsymbol{t}} & \frac{\partial F_2(\boldsymbol{x},\boldsymbol{k})}{\partial \boldsymbol{k}} \end{bmatrix} \\ &= -\begin{bmatrix} \boldsymbol{L} \\ \boldsymbol{N}\boldsymbol{\Lambda}_x^{-1} \end{bmatrix}^{-1} \begin{bmatrix} -\mathbf{I}_d & 0 \\ 0 & -\boldsymbol{\Lambda}_k^{-1} \end{bmatrix} \\ &= \begin{bmatrix} \boldsymbol{L} \\ \boldsymbol{\Lambda}_{\boldsymbol{k}} \boldsymbol{N} \boldsymbol{\Lambda}_x^{-1} \end{bmatrix}^{-1}, \end{aligned} \tag{3.18}$$

where $\mathbf{I}_d$ is the identity matrix of dimension d, and $\boldsymbol{\Lambda}_{\boldsymbol{k}}$ denote the diagonal matrix with $\boldsymbol{k}$ along the diagonal. As for log derivatives, since $\frac{\partial \log \boldsymbol{x}}{\partial \log \boldsymbol{t}} = \boldsymbol{\Lambda}_{\boldsymbol{x}}^{-1} \frac{\partial \boldsymbol{x}}{\partial \boldsymbol{t}} \boldsymbol{\Lambda}_{\boldsymbol{t}}$, we obtain the following result.

Theorem 3.5.1 (Log derivative formula)**.** *Given $\mathcal{M} \subset \mathbb{R}^{2n}_{>0}$, the equilibrium manifold of a binding network with transpose-reduced stoichiometry matrix $\boldsymbol{N}$ and conservation law matrix $\boldsymbol{L}$, at any point $\boldsymbol{p} = (\boldsymbol{x}, \boldsymbol{t}, \boldsymbol{k}) \in \mathcal{M}$, we have*

$$\frac{\partial \log \boldsymbol{x}}{\partial (\log \boldsymbol{t}, \log \boldsymbol{k})} = \begin{bmatrix} \frac{\partial \log \boldsymbol{x}}{\partial \log \boldsymbol{t}} & \frac{\partial \log \boldsymbol{x}}{\partial \log \boldsymbol{k}} \end{bmatrix} = \begin{bmatrix} \boldsymbol{\Lambda}_{\boldsymbol{t}}^{-1} \boldsymbol{L} \boldsymbol{\Lambda}_{\boldsymbol{x}} \\ \boldsymbol{N} \end{bmatrix}^{-1} = \begin{bmatrix} \boldsymbol{L}\boldsymbol{\Lambda}_{\boldsymbol{x}} \\ \boldsymbol{N} \end{bmatrix}^{-1} \begin{bmatrix} \boldsymbol{\Lambda}_{\boldsymbol{t}} & 0 \\ 0 & \mathbf{I}_r \end{bmatrix}, \tag{3.19}$$

where $\mathbf{I}_r$ is the identity matrix of dimension r.

Note that although the theorem states that this log derivative $\frac{\partial \log \boldsymbol{x}}{\partial(\log \boldsymbol{t}, \log \boldsymbol{k})}$ can always be calculated at any point $\boldsymbol{x}$ in this fashion through matrix inversion, we have not proved this, as all previous calculations assumed $\partial_{\boldsymbol{x}} F$ is invertible. To show this, we can prove something stronger, namely the map $f : \log \boldsymbol{x} \mapsto (\log \boldsymbol{t}, \log \boldsymbol{k})$ is a diffeomorphism. This map can be explicitly written as follows:

$$f(\boldsymbol{z}) = \begin{bmatrix} \log \boldsymbol{L} \exp \boldsymbol{z} \\ \boldsymbol{N}\boldsymbol{z} \end{bmatrix}, \tag{3.20}$$

where the exponential map is applied component wise. We can show this map is a diffeomorphism from $\mathbb{R}^n$ to $\mathbb{R}^n$. By Hadamard-Caccioppoli Theorem, f is a diffeomorphism if f is proper and df is bijective at all points. f is proper because for every sequence of $\boldsymbol{z}$ escaping to infinity, $f(\boldsymbol{z})$ also escapes to infinity, since $\boldsymbol{L}$ is non-negative and every column is nonzero. So it is left to show that df is bijective at all points, i.e. df, the log derivative $\frac{\partial(\log \boldsymbol{t}, \log \boldsymbol{k})}{\partial \log \boldsymbol{x}}$ is invertible for all $\boldsymbol{x}$. From (3.19), we see that this is equivalent to the matrix

$$\boldsymbol{M}(\boldsymbol{x}; \boldsymbol{L}) := \begin{bmatrix} \boldsymbol{L}\boldsymbol{\Lambda}_{\boldsymbol{x}} \\ \boldsymbol{N} \end{bmatrix} \tag{3.21}$$

is invertible for all $\boldsymbol{x}$. We prove this in the following proposition.

Proposition 3.5.2. *$\boldsymbol{M}(\boldsymbol{x}; \boldsymbol{L})$ is invertible for all $\boldsymbol{x} \in \mathbb{R}^n_{>0}$.*

Proof. Proof by contradiction. If it is not invertible, then there exists a nonzero vector $\boldsymbol{v}$ s.t. $\boldsymbol{M}(\boldsymbol{x}; \boldsymbol{L})\boldsymbol{v} = 0$. This implies $\boldsymbol{N}\boldsymbol{v} = 0$, i.e. $\boldsymbol{v} \in \operatorname{rowspan} \boldsymbol{L}$, so there exists a nonzero vector $\boldsymbol{c}$ s.t. $\boldsymbol{v} = \boldsymbol{L}^\intercal \boldsymbol{c}$. So $\boldsymbol{L}\boldsymbol{\Lambda}_{\boldsymbol{x}}\boldsymbol{v} = \boldsymbol{L}\boldsymbol{\Lambda}_{\boldsymbol{x}}\boldsymbol{L}^\intercal\boldsymbol{c} = 0$. But this is impossible, since $\boldsymbol{\Lambda}_{\boldsymbol{x}}$ is positive definite, so $\boldsymbol{c}^\intercal \boldsymbol{L}\boldsymbol{\Lambda}_{\boldsymbol{x}}\boldsymbol{L}^\intercal\boldsymbol{c} > 0$. □

Hence, $f : \log \boldsymbol{x} \mapsto (\log \boldsymbol{t}, \log \boldsymbol{k})$ is a diffeomorphism, and the log derivative $\frac{\partial \log \boldsymbol{x}}{\partial(\log \boldsymbol{t}, \log \boldsymbol{k})}$ is well defined on all points in $\mathcal{M}$. The formula 3.19 is always applicable.

We can write the relationship of chart $\log \boldsymbol{x}$ and chart $(\log \boldsymbol{t}, \log \boldsymbol{k})$ in the following diagram:

$$\log \boldsymbol{x} \underset{df^{-1} = \frac{\partial \log \boldsymbol{x}}{\partial(\log \boldsymbol{t}, \log \boldsymbol{k})} = \begin{bmatrix} \boldsymbol{\Lambda}_{\boldsymbol{t}}^{-1}\boldsymbol{L}\boldsymbol{\Lambda}_{\boldsymbol{x}} \\ \boldsymbol{N} \end{bmatrix}^{-1}}{\overset{f(\log \boldsymbol{x}) = (\log \boldsymbol{L}\boldsymbol{x}, \boldsymbol{N} \log \boldsymbol{x})}{\rightleftharpoons}} (\log \boldsymbol{t}, \log \boldsymbol{k}). \tag{3.22}$$

Now we have established that for a generic equilibrium manifold $\mathcal{M}$ of a binding network, in addition to the natural chart $\log \boldsymbol{x}$, we have an alternative chart in terms of totals and equilibrium constants $(\log \boldsymbol{t}, \log \boldsymbol{k})$, which is also a one-chart atlas. Recall that for isomer-atomic binding networks, we have another natural chart using atomic species $(\log \boldsymbol{x}^a, \log \boldsymbol{k})$. We study how this chart relates to the total chart $(\log \boldsymbol{t}, \log \boldsymbol{k})$ below.

Log derivatives and chart transform for isomer-atomic binding networks

Recall that from the previous section, we established that if the binding network is isomer-atomic, then we have another chart using the atomic species, namely $(\log \boldsymbol{x}^a, \log \boldsymbol{k})$, where $\boldsymbol{x} = (\boldsymbol{x}^a, \boldsymbol{x}^c)$ is split into the atomic species and the complex species. To relate this atomic chart to the total chart $(\log \boldsymbol{t}, \log \boldsymbol{k})$, since the equilibrium constants $\boldsymbol{k}$) is kept the same, we just need to study how $\boldsymbol{x}^a$ is mapped to $\boldsymbol{t}$. The chart transform in Eq (3.16) tells us $\log \boldsymbol{x}^c = \boldsymbol{L}_2^\intercal \log \boldsymbol{x}^a + \boldsymbol{N}_2^{-1} \log \boldsymbol{k}$, so we have

$$\boldsymbol{t} = \boldsymbol{L}\boldsymbol{x} = \boldsymbol{x}^a + \boldsymbol{L}_2 \boldsymbol{x}^c = \boldsymbol{x}^a + \boldsymbol{L}_2 \exp(\boldsymbol{L}_2^\intercal \log \boldsymbol{x}^a + \boldsymbol{N}_2^{-1} \log \boldsymbol{k}).$$

The inverse map from $(\log \boldsymbol{x}^a, \log \boldsymbol{k})$ to $(\log \boldsymbol{t}, \log \boldsymbol{k})$ again requires solving an intractible polynomial system, so we resort to differentials.

Theorem 3.5.3 (Isomer-atomic log derivative formula)**.** *Given $\mathcal{M} \subset \mathbb{R}^{2n}_{>0}$, the equilibrium manifold of an isomer-atomic binding network with transpose-reduced stoichiometry matrix $\boldsymbol{N} \in \mathbb{R}^{r\times n}$ and conservation law matrix $\boldsymbol{L} \in \mathbb{R}^{d\times n}$, with an atom-first ordering so that the first d species are atomic species, i.e. $\boldsymbol{L} = \begin{bmatrix}\mathbf{I}_d & \boldsymbol{L}_2\end{bmatrix}$, $\boldsymbol{L}_2 \in \mathbb{R}^{d\times r}$, and $\boldsymbol{N} = \begin{bmatrix}\boldsymbol{N}_1 & \boldsymbol{N}_2\end{bmatrix}$, with $\boldsymbol{L}_2^\intercal = -\boldsymbol{N}_2^{-1}\boldsymbol{N}_1$. Then at any point $\boldsymbol{p} = (\boldsymbol{x}, \boldsymbol{t}, \boldsymbol{k}) \in \mathcal{M}$, we have*

$$\begin{aligned}\frac{\partial \log \boldsymbol{x}^a}{\partial(\log \boldsymbol{t}, \log \boldsymbol{k})} &= \begin{bmatrix}(\boldsymbol{L}\boldsymbol{\Lambda}_{\boldsymbol{x}}\boldsymbol{L}^\intercal)^{-1}\boldsymbol{\Lambda}_{\boldsymbol{t}} & -(\boldsymbol{L}\boldsymbol{\Lambda}_{\boldsymbol{x}}\boldsymbol{L}^\intercal)^{-1}\boldsymbol{L}_2\boldsymbol{\Lambda}_{\boldsymbol{x}^c}\boldsymbol{N}_2^{-1}\end{bmatrix},\\ \frac{\partial \log \boldsymbol{x}^c}{\partial(\log \boldsymbol{t}, \log \boldsymbol{k})} &= \boldsymbol{L}_2^\intercal \frac{\partial \log \boldsymbol{x}^a}{\partial(\log \boldsymbol{t}, \log \boldsymbol{k})} + \begin{bmatrix}0 & \boldsymbol{N}_2^{-1}\end{bmatrix},\end{aligned} \tag{3.23}$$

where $\mathbf{I}_r$ is the identity matrix of dimension r.

Proof. The second formula is immediately obtained by using chain rule and Eq (3.16):

$$\frac{\partial \log \boldsymbol{x}^c}{\partial(\log \boldsymbol{t}, \log \boldsymbol{k})} = \frac{\partial \boldsymbol{L}_2^\intercal \log \boldsymbol{x}^a + \boldsymbol{N}_2^{-1} \log \boldsymbol{k}}{\partial(\log \boldsymbol{t}, \log \boldsymbol{k})} = \boldsymbol{L}_2^\intercal \frac{\partial \log \boldsymbol{x}^a}{\partial(\log \boldsymbol{t}, \log \boldsymbol{k})} + \boldsymbol{N}_2^{-1}\begin{bmatrix}0 & \mathbf{I}_r\end{bmatrix}.$$

The first formula is obtained by block-matrix inversion of Eq (3.19). Block-matrix inversion satisfies

$$\begin{bmatrix}\boldsymbol{A} & \boldsymbol{B}\\ \boldsymbol{C} & \boldsymbol{D}\end{bmatrix} = \begin{bmatrix}(\boldsymbol{A} - \boldsymbol{B}\boldsymbol{D}^{-1}\boldsymbol{C})^{-1} & 0\\ 0 & (\boldsymbol{D} - \boldsymbol{C}\boldsymbol{A}^{-1}\boldsymbol{B})^{-1}\end{bmatrix}\begin{bmatrix}\mathbf{I} & -\boldsymbol{B}\boldsymbol{D}^{-1}\\ -\boldsymbol{C}\boldsymbol{A}^{-1} & \mathbf{I}\end{bmatrix},$$

if blocks $\boldsymbol{A}$ and $\boldsymbol{D}$ are both invertible. So

$$\begin{bmatrix}\boldsymbol{A} & \boldsymbol{B}\end{bmatrix} = (\boldsymbol{A} - \boldsymbol{B}\boldsymbol{D}^{-1}\boldsymbol{C})^{-1}\begin{bmatrix}\mathbf{I} & -\boldsymbol{B}\boldsymbol{D}^{-1}\end{bmatrix}.$$

Applying this to our case,

$$\begin{aligned}\frac{\partial \log \boldsymbol{x}^a}{\partial(\log \boldsymbol{t}, \log \boldsymbol{k})} =& \begin{bmatrix}\mathbf{I}_d & 0\end{bmatrix} \frac{\partial(\log \boldsymbol{x}^a, \log \boldsymbol{x}^c)}{\partial(\log \boldsymbol{t}, \log \boldsymbol{k})} = \begin{bmatrix}\mathbf{I}_d & 0\end{bmatrix} \begin{bmatrix}\boldsymbol{\Lambda}_{\boldsymbol{x}^a} & \boldsymbol{L}_2 \boldsymbol{\Lambda}_{\boldsymbol{x}^c} \\ \boldsymbol{N}_1 & \boldsymbol{N}_2\end{bmatrix}^{-1} \begin{bmatrix}\boldsymbol{\Lambda}_{\boldsymbol{t}} & 0 \\ 0 & \mathbf{I}_r\end{bmatrix} \\ =& (\boldsymbol{\Lambda}_{\boldsymbol{x}^a} - \boldsymbol{L}_2 \boldsymbol{\Lambda}_{\boldsymbol{x}^c} \boldsymbol{N}_2^{-1} \boldsymbol{N}_1)^{-1} \begin{bmatrix}\mathbf{I} & -\boldsymbol{L}_2 \boldsymbol{\Lambda}_{\boldsymbol{x}^c} \boldsymbol{N}_2^{-1}\end{bmatrix} \begin{bmatrix}\boldsymbol{\Lambda}_{\boldsymbol{t}} & 0 \\ 0 & \mathbf{I}_r\end{bmatrix} \\ =& (\boldsymbol{\Lambda}_{\boldsymbol{x}^a} + \boldsymbol{L}_2 \boldsymbol{\Lambda}_{\boldsymbol{x}^c} \boldsymbol{L}_2^\intercal)^{-1} \begin{bmatrix}\boldsymbol{\Lambda}_{\boldsymbol{t}} & -\boldsymbol{L}_2 \boldsymbol{\Lambda}_{\boldsymbol{x}^c} \boldsymbol{N}_2^{-1}\end{bmatrix}.\end{aligned}$$

This is the desired formula by recognizing $\boldsymbol{\Lambda}_{\boldsymbol{x}^a} + \boldsymbol{L}_2 \boldsymbol{\Lambda}_{\boldsymbol{x}^c} \boldsymbol{L}_2^\intercal = \boldsymbol{L} \boldsymbol{\Lambda}_{\boldsymbol{x}} \boldsymbol{L}^\intercal$. □

We remark that the atomic log derivative formula in Eq (3.23) highlights an internal symmetric structure not obviously seen in the more general log derivative formula in Eq (3.19). In particular, the symmetric positive-semidefinite matrix $(\boldsymbol{L} \boldsymbol{\Lambda}_{\boldsymbol{x}} \boldsymbol{L}^\intercal)^{-1}$ constitute the core structure from which all the log derivatives arise.

In addition to characterizing how the atomic chart $(\log \boldsymbol{x}^a, \log \boldsymbol{k})$ is mapped from the total chart $(\log \boldsymbol{t}, \log \boldsymbol{k})$, Eq (3.23) also implies a simpler way to calculate the log derive $\frac{\partial \log \boldsymbol{x}}{\partial(\log \boldsymbol{t}, \log \boldsymbol{k})}$ for isomer-atomic binding entworks. Namely, we can first calculate just the log derivative of $\boldsymbol{x}^a$, then use this to obtain the log derivative of $\boldsymbol{x}^c$. For large scale problems, the bottleneck in log dervative computation would be matrix inversion, which often has $O(n^3)$ complexity to invert a square matrix with dimension n (could be lower by more advanced algorithms, but still larger than $O(n^{2.3})$). We see that in this formula, we can compute all log derivatives by inverting only one matrix with dimension d and one with dimension r, instead of inverting a matrix with dimension n in Eq (3.19), so roughly reducing complexity from n^3 to $d^3 + r^3$. If we are only interested in the log derivative of $\boldsymbol{x}$ with respect to $\boldsymbol{t}$, we only need to compute $\frac{\partial \log \boldsymbol{x}^a}{\partial \log \boldsymbol{t}} = (\boldsymbol{L} \boldsymbol{\Lambda}_{\boldsymbol{x}} \boldsymbol{L}^\intercal)^{-1} \boldsymbol{\Lambda}_{\boldsymbol{t}}$, which only requires to invert a $d \times d$ matrix, and then compute $\frac{\partial \log \boldsymbol{x}^c}{\partial \log \boldsymbol{t}} = \boldsymbol{L}_2^\intercal \frac{\partial \log \boldsymbol{x}^a}{\partial \log \boldsymbol{t}} = \boldsymbol{L}_2^\intercal (\boldsymbol{L} \boldsymbol{\Lambda}_{\boldsymbol{x}} \boldsymbol{L}^\intercal)^{-1} \boldsymbol{\Lambda}_{\boldsymbol{t}}$.

We summarize the three charts studied so far and the transform between them in Figure 3.4.

Other alternative charts

The two alternative charts we have studied so far have equilibrium constants fixed, and the remaining d degrees of freedom are represented as $\boldsymbol{x}^a = \boldsymbol{A}^a \boldsymbol{x}$ where $\boldsymbol{A}^a := \begin{bmatrix}\mathbf{I}_d & 0\end{bmatrix}$ in atomic chart, and $\boldsymbol{t} = \boldsymbol{L} \boldsymbol{x}$ in total chart. This brings the question about what are the other charts of the form $(\log \boldsymbol{A} \boldsymbol{x}, \log \boldsymbol{k})$, for some non-negative matrix $\boldsymbol{A} \in \mathbb{R}^{d \times n}$?

We know $(\log \boldsymbol{A} \boldsymbol{x}, \log \boldsymbol{k})$ is a chart if and only if the map $\log \boldsymbol{x} \mapsto (\log \boldsymbol{A} \boldsymbol{x}, \log \boldsymbol{k})$ is invertible for all $\boldsymbol{x}$. From log derivative formula (3.19), we know this is equivalent to matrix $\boldsymbol{M}(\boldsymbol{x}; \boldsymbol{A})$

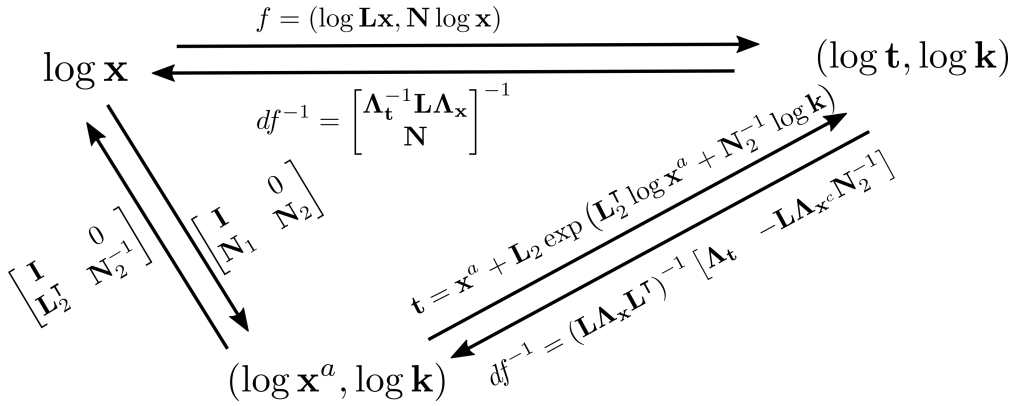

Figure 3.4 The three charts of equilibrium manifold $\mathcal{M}$ of a binding network, and the transform between them.

is invertible for all $\boldsymbol{x}$. Hence we define $\mathcal{A} = \left\{\boldsymbol{A} \in \mathbb{R}^{d\times n}_{\geq 0} : \det \boldsymbol{M}(\boldsymbol{x}; \boldsymbol{A}) \neq 0, \forall \boldsymbol{x}\right\}$, the set of $\boldsymbol{A}$ such that $(\log \boldsymbol{A}\boldsymbol{x}, \log \boldsymbol{k})$ are charts.

Topologically, since determinant is a continuous function, a matrix $\boldsymbol{A} \in \mathcal{A}$ has determinant of $\boldsymbol{M}(\boldsymbol{x}; \boldsymbol{A})$ either positive for all $\boldsymbol{x}$, or negative for all $\boldsymbol{x}$. This separates $\mathcal{A}$ into two connected components,

$$\mathcal{A}^+(\boldsymbol{N}) := \left\{\boldsymbol{A} \in \mathbb{R}^{d\times n}_{\geq 0} : \det \boldsymbol{M}(\boldsymbol{x}; \boldsymbol{A}) > 0, \forall \boldsymbol{x}\right\}, \tag{3.24}$$

and correspondingly $\mathcal{A}^-(\boldsymbol{N})$.

For the atomic chart, $\det \boldsymbol{M}(\boldsymbol{x}; \boldsymbol{A}^a) = \det \boldsymbol{N}_2$. So $\begin{bmatrix}\mathbf{I}_d & 0\end{bmatrix} \in \mathcal{A}^+(\boldsymbol{N})$ if $\det \boldsymbol{N}_2 > 0$. Similarly, we show below that the total chart's sign is determined by the same condition for isomer-atomic CRNs.

Proposition 3.5.4. *Assume isomer-atomic, then $\boldsymbol{L} \in \mathcal{A}^+(\boldsymbol{N})$ if and only if $\det \boldsymbol{N}_2 > 0$.*

Proof. Calculate

$$\begin{bmatrix}\boldsymbol{L} \\ \boldsymbol{N}\end{bmatrix}\begin{bmatrix}\mathbf{I}_d & 0 \\ 0 & \boldsymbol{N}_2^\intercal\end{bmatrix} = \begin{bmatrix}\mathbf{I}_d & -\boldsymbol{N}_1^\intercal \boldsymbol{N}_2^{-\intercal} \\ \boldsymbol{N}_1 & \boldsymbol{N}_2\end{bmatrix}\begin{bmatrix}\mathbf{I}_d & 0 \\ 0 & \boldsymbol{N}_2^\intercal\end{bmatrix} = \begin{bmatrix}\mathbf{I} & -\boldsymbol{N}_1^\intercal \\ \boldsymbol{N}_1 & \boldsymbol{N}_2\boldsymbol{N}_2^\intercal\end{bmatrix}.$$

Take determinant of both sides,

$$\det\left(\begin{bmatrix}\boldsymbol{L} \\ \boldsymbol{N}\end{bmatrix}\right) \det(\boldsymbol{N}_2^\intercal) = \det(\boldsymbol{N}_2\boldsymbol{N}_2^\intercal + \boldsymbol{N}_1\boldsymbol{N}_1^\intercal) > 0.$$

The right hand side is a positive definite matrix, so determinant is positive. Since $\det \boldsymbol{M}(\mathbf{1}; \boldsymbol{L}) > 0$ if and only if $\det \boldsymbol{M}(\boldsymbol{x}; \boldsymbol{L}) > 0$ for all $\boldsymbol{x} \in \mathbb{R}^n_{>0}$ from previous Lemma, we have the desired result. □

So we know the atomic chart with matrix $\boldsymbol{A} = \boldsymbol{A}^a = \begin{bmatrix}\mathbf{I}_d & 0\end{bmatrix}$ and the total chart with $\boldsymbol{A} = \boldsymbol{L}$ both resides in the same connected component of $\mathcal{A}$. Exactly which one depends on the choice of which direction is used for the stoichiometry vectors. Thus, without loss of generality, we assume $\boldsymbol{A}^a, \boldsymbol{L} \in \mathcal{A}^+(\boldsymbol{N})$.

To find other alternative chart, we note that given a $\boldsymbol{A} \in \mathcal{A}^+(\boldsymbol{N})$, then for any $\boldsymbol{S} \in \mathrm{GL}_d^+(\mathbb{R})$ such that $\boldsymbol{SA} \in \mathbb{R}^{d\times n}_{\geq 0}$, then $\boldsymbol{SA} \in \mathcal{A}^+(\boldsymbol{N})$. Here $\mathrm{GL}_d^+(\mathbb{R})$ is the identity component of the general linear group of $d \times d$ matrices, i.e. $d \times d$ matrices with positive determinant. This states that any invertible matrix with positive determinant can be left-multiplied to $\boldsymbol{A}$, and if the resulting matrix is non-negative, then it is in $\mathcal{A}^+(\boldsymbol{N})$. There are several elementary matrices of $\mathrm{GL}_d^+(\mathbb{R})$ worth noting. It includes positive scaling $\boldsymbol{\Lambda}_{\boldsymbol{\alpha}}$, where $\boldsymbol{\alpha} \in \mathbb{R}^d_{>0}$ is a positive vector in $\mathbb{R}^d$. It also includes permutations with positive sign, i.e. consisting of an even number of transpositions. It also includes row additions $\mathbf{I} + a\boldsymbol{E}_{ij}$, where $i \neq j$, $i, j \in \{1, \ldots, d\}$, $\boldsymbol{E}_{ij}$ has 1 at (i, j) entry and zero everywhere else, and $a \in \mathbb{R}$ is a real number. $\mathbf{I} + a\boldsymbol{E}_{ij}$ takes the jth row of $\boldsymbol{A}$, multiply by a, and adds to the ith row of $\boldsymbol{A}$. We caution that combinations of these elementary operations may go out of $\mathrm{GL}_d^+(\mathbb{R})$, and the resulting matrix may no longer be non-negative.

As for right multiplication, given $\boldsymbol{A} \in \mathcal{A}^+(\boldsymbol{N})$, then $\boldsymbol{A\Lambda}_{\boldsymbol{\alpha}} \in \mathcal{A}^+(\boldsymbol{N})$ for any positive vector $\boldsymbol{\alpha} \in \mathbb{R}^n_{>0}$. This is because this multiplication is just a scaling of variables $\boldsymbol{x}$, without changing its domain $\mathbb{R}^n_{>0}$.

These operations give a basic approach to explore other alternative charts of $\mathcal{M}$. It is an interesting question for further research to characterize the set $\mathcal{A}^+(\boldsymbol{N})$.

3.6 Polyhedral shape of log derivatives in one binding reaction

So far we have treated log derivatives as a way to transform between coordinate charts. In this section, we investigate the biological meaning of log derivatives and what biological behaviors can be revealed from properties of log derivatives. The particular log derivatives we investigate is that of some species concentration x_i with respect to the totals $\boldsymbol{t}$ and equilibrium constants $\boldsymbol{k}$, namely $\frac{\partial \log x_i x}{\partial(\log \boldsymbol{t}, \log \boldsymbol{k})}$. Because of their biological significance, we give these log derivatives the special name **reaction orders**. This is because often one species in a binding network is the active catalytic complex that determines the rate of a catalysis reaction. When regulating this reaction rate, the total concentrations of atomic species are varied by the cell. Therefore, how the rate varies with changes in the total concentrations determine behaviors from bioregulation. The order of this change is captured by the

particular log derivative above, $\frac{\partial \log x_i}{\partial(\log \boldsymbol{t}, \log \boldsymbol{k})}$, if x_i is the active catalytic species, hence the name reaction order. Reaction order can also be equivalently interpreted as infinitesimal fold change, or the exponents of a local expression of x_i in terms of $\boldsymbol{t}$ and $\boldsymbol{k}$.

This does not answer the question of why reaction orders are used to study bioregulation though. For example, why the linear direction $\frac{\partial x_i}{\partial(\boldsymbol{t}, \boldsymbol{k})}$ is not used? We demonstrate several useful properties of reaction orders in this section by examining the reaction orders of a single binding reaction in close detail. The key properties we demonstrate are summarized here. (1) Constrained by binding network stoichiometry, reaction orders are bounded within some polyhedral set, with vertices correspond to biologically meaningful regimes. This is in contrast to linear derivatives, which are unbounded in most directions. (2) The polyhedral sets has hierarchical structures corresponding to robustness to variations, so that points concentrate to vertices, edges, and faces under asymptotic limits. This means reaction orders are robust to variations in rates and concentrations, so it can be controlled to precise values using noisy and uncertain actuations, and robust behaviors can be built on top of it.

Explicit reaction order calculation for one binding reaction

We do explicit calculation for one binding reaction to reveal the geometric shape of log derivatives. For transparency, we calculate the log derivatives directly without using any of the formula developed in previous section, although they produce the same result.

A binding network consisting of just one binding reaction can be written as follows:

$$E + S \underset{k^-}{\overset{k^+}{\rightleftharpoons}} C, \tag{3.25}$$

where component species enzyme E and substrate S bind to form complex C, and k^+ and k^- are forward and backward reaction rate constants. Although we used enzyme and substrate to denote the two component species out of tradition, we do not assume they have any special properties, and by symmetry E and S are equivalent by re-labeling.

This binding reaction has the following deterministic dynamics from the law of mass-action:

$$\frac{d}{dt}C(t) = k^+E(t)S(t) - k^-C(t), \tag{3.26}$$

where by slight abuse of notation, the symbol for a species is also used to denote the concentration of that species. This system has steady-state equation

$$ES = KC, \tag{3.27}$$

where $K := \frac{k^-}{k^+}$ is the equilibrium constant in the dissociation direction. As guaranteed, this corresponds to $\boldsymbol{N} \log \boldsymbol{x} = \log \boldsymbol{k}$, where $\boldsymbol{N} = \begin{bmatrix} -1 & -1 & 1 \end{bmatrix}$, $\boldsymbol{x} = (E, S, C)$, and $\boldsymbol{k} = K$. Note that in this particular case, the steady state necessarily satisfy detailed balance, so we do not need to begin with detailed balance condition to define $\mathcal{M}$, but instead derive $\mathcal{M}$ from the specified rates.

The conserved quantities of this binding reaction are the total enzyme and total substrate:

$$\begin{aligned} t_S :=& S + C, \\ t_E :=& E + C. \end{aligned} \tag{3.28}$$

This can be written as $\boldsymbol{t} = \boldsymbol{L}\boldsymbol{x}$ with the conservation matrix below. Here the species ordering is (E, S, C), and the total ordering is (t_E, t_S). We also attach the stoichiometry matrix here for clear comparison.

$$\begin{bmatrix} \boldsymbol{L} \\ \hline \boldsymbol{N} \end{bmatrix} = \left[\begin{array}{ccc} 1 & 0 & 1 \\ 0 & 1 & 1 \\ \hline 1 & 1 & -1 \end{array}\right] \tag{3.29}$$

This in turn defines the equilibrium manifold:

$$\begin{aligned} \mathcal{M} =& \left\{ (\boldsymbol{x}, \boldsymbol{t}, \boldsymbol{k}) \in \mathbb{R}^6_{>0} : \boldsymbol{N} \log \boldsymbol{x} = \log \boldsymbol{k}, \boldsymbol{t} = \boldsymbol{L}\boldsymbol{x} \right\} \\ =& \left\{ (E, S, C, t_E, t_S, K) \in \mathbb{R}^6_{>0} : ES = KC, t_S = S + C, t_E = E + C \right\}. \end{aligned} \tag{3.30}$$

In this case, we can explicitly solve for $\boldsymbol{x} = (E, S, C)$ expressed in $(\boldsymbol{t}, \boldsymbol{k}) = (t_E, t_S, K)$. Namely,

$$2C = t_E + t_S + K - \sqrt{(t_E + t_S + K)^2 - 4 t_E t_S}, \tag{3.31}$$

which is then easily used to derive expressions for E and S. This formula can be used as the exact solution for us to compare with in this case. But for the derivative to follow the workflow in the general case as described in Section 3.4, we do not rely on this formula. Instead, we use the implicit function theorem as we did in the general case to calculate the reaction order, i.e. the log derivative $\frac{\partial \log(E,S,C)}{\partial \log(t_E,t_S,K)}$. Define $F : \mathbb{R}^6_{>0} \to \mathbb{R}^3$ whose zero set is the equilibrium manifold $\mathcal{M}$:

$$F(E, S, C, t_E, t_S, K) = \begin{bmatrix} F_1(E, S, C, t_E, t_S) \\ \hline F_2(E, S, C, K) \end{bmatrix} = \left[\begin{array}{c} E + C - t_E \\ S + C - t_S \\ \hline ES - CK \end{array}\right], \tag{3.32}$$

By implicit function theorem,

$$\frac{\partial(E,S,C)}{\partial(t_E,t_S,K)} = -\begin{bmatrix}1 & 0 & 1\\ 0 & 1 & 1\\ S & E & -K\end{bmatrix}^{-1}\begin{bmatrix}-1 & 0 & 0\\ 0 & -1 & 0\\ 0 & 0 & -C\end{bmatrix}$$
$$= \frac{1}{E+S+K}\begin{bmatrix}E+K & -E & C\\ -S & S+K & C\\ S & E & -C\end{bmatrix}.$$

Since $C = \frac{ES}{K}$, we can express the above in dimensionless quantities $e := \frac{E}{K}$ and $s = \frac{S}{K}$.

$$\frac{\partial(E,S,C)}{\partial(t_E,t_S,K)} = \frac{1}{1+e+s}\begin{bmatrix}1+e & -e & es\\ -s & 1+s & es\\ s & e & -es\end{bmatrix}. \tag{3.33}$$

To calculate log derivative, we note that $\frac{\partial \log g(\boldsymbol{x})}{\partial \log \boldsymbol{x}} = \Lambda_g^{-1}\frac{\partial g(\boldsymbol{x})}{\partial \boldsymbol{x}}\Lambda_{\boldsymbol{x}}$, where $\Lambda_{\boldsymbol{v}} = \mathrm{diag}(\boldsymbol{v})$, since $\frac{\partial \log g_i(\boldsymbol{x})}{\partial \log x_j} = \frac{\partial g_i(\boldsymbol{x})}{\partial x_j}\frac{x_j}{g_i(\boldsymbol{x})}$. Therefore,

$$\frac{\partial \log(E,S,C)}{\partial \log(t_E,t_S,K)} = \frac{1}{E+S+K}\begin{bmatrix}E & 0 & 0\\ 0 & S & 0\\ 0 & 0 & C\end{bmatrix}^{-1}\begin{bmatrix}E+K & -E & C\\ -S & S+K & C\\ S & E & -C\end{bmatrix}\begin{bmatrix}t_E & 0 & 0\\ 0 & t_S & 0\\ 0 & 0 & K\end{bmatrix}$$
$$= \frac{1}{E+S+K}\begin{bmatrix}(1+\frac{S}{K})(E+K) & -t_S & S\\ -t_E & (1+\frac{E}{K})(S+K) & E\\ S+K & E+K & -K\end{bmatrix}.$$

Expressing this in terms of e and s yields the following result.

Theorem 3.6.1 (Reaction orders of a simple binding reaction)**.** *The reaction orders of a simple binding reaction $E + S \underset{k^-}{\overset{k^+}{\rightleftharpoons}} C$ can be expressed as*

$$\frac{\partial \log(E,S,C)}{\partial \log(t_E,t_S,K)} = \frac{1}{1+e+s}\begin{bmatrix}(1+e)(1+s) & -s(1+e) & s\\ -e(1+s) & (1+s)(1+e) & e\\ 1+s & 1+e & -1\end{bmatrix}, \tag{3.34}$$

where $e = \frac{E}{K}$, $s = \frac{S}{K}$, and $K := \frac{k^-}{k^+}$ the equilibrium constant of this binding reaction in the dissociation direction.

Below we re-do the calculation for reaction order using the formula in Eq (3.19) to show that indeed they yield the same result.

Example 5 (Simple binding reaction.). $E + S \rightleftharpoons C$ with binding constant K. Let variables be $\boldsymbol{x} = (E, S, C), \boldsymbol{t} = (t_E, t_S)$ and $\boldsymbol{k} = K$. The corresponding stoichiometry matrix (note we use the forward or dissociation direction), conservation laws, and part of the matrix to be inverted are

$$\boldsymbol{N} = \begin{bmatrix} 1 & 1 & -1 \end{bmatrix}, \quad \boldsymbol{L} = \begin{bmatrix} 1 & 0 & 1 \\ 0 & 1 & 1 \end{bmatrix}, \boldsymbol{\Lambda}_{\boldsymbol{t}}^{-1} \boldsymbol{L} \boldsymbol{\Lambda}_{\boldsymbol{x}} = \begin{bmatrix} \frac{E}{t_E} & 0 & \frac{C_{ES}}{t_E} \\ 0 & \frac{S}{t_S} & \frac{C_{ES}}{t_S} \end{bmatrix}$$

$$\frac{\partial \log(E, S, C)}{\partial \log(t_E, t_S, K)} = \begin{bmatrix} \frac{E}{t_E} & 0 & \frac{C}{t_E} \\ 0 & \frac{S}{t_S} & \frac{C}{t_S} \\ 1 & 1 & -1 \end{bmatrix}^{-1} = \left(\frac{CE + CS + ES}{t_E t_S} \right)^{-1} \begin{bmatrix} 1 & -\frac{C}{t_E} & \frac{CS}{t_E t_S} \\ -\frac{C}{t_S} & 1 & \frac{CE}{t_E t_S} \\ \frac{S}{t_S} & \frac{E}{t_E} & -\frac{ES}{t_E t_S} \end{bmatrix}.$$

Now we express the above in terms of $(e, s) := (\frac{E}{K}, \frac{S}{K})$, we get the same result as Eq (3.34).

We can also utilize the stoichiometry-atomic property of this network, with atomic species $\boldsymbol{x}^a = (E, S)$. This splits the stoichiometry and the conservation law matrix into atomic and non-atomic parts:

$$\boldsymbol{N} = \begin{bmatrix} \boldsymbol{N}_1 & \boldsymbol{N}_2 \end{bmatrix} = \left[\begin{array}{cc|c} 1 & 1 & -1 \end{array}\right], \quad \boldsymbol{L} = \begin{bmatrix} \mathbf{I}_2 & \boldsymbol{L}_2 \end{bmatrix} = \left[\begin{array}{cc|c} 1 & 0 & 1 \\ 0 & 1 & 1 \end{array}\right],$$

and the core symmetric structure is

$$(\boldsymbol{L} \boldsymbol{\Lambda}_{\boldsymbol{x}} \boldsymbol{L}^\intercal)^{-1} = \begin{bmatrix} E + C & C \\ C & S + C \end{bmatrix}^{-1} = \frac{1}{ES + CS + SC} \begin{bmatrix} S + C & -C \\ -C & E + C \end{bmatrix} = \frac{1}{1 + e + s} \begin{bmatrix} 1 + \frac{1}{e} & -1 \\ -1 & 1 + \frac{1}{s} \end{bmatrix}.$$

So $\boldsymbol{N}_2^{-1} = -1$, $-\boldsymbol{L}_2 \boldsymbol{\Lambda}_{\boldsymbol{x}^c} \boldsymbol{N}_2^{-1} = \begin{bmatrix} C \\ C \end{bmatrix}$. From this we can calculate

$$\frac{\partial \log(E, S)}{\partial \log(t_E, t_S)} = (\boldsymbol{L} \boldsymbol{\Lambda}_{\boldsymbol{x}} \boldsymbol{L}^\intercal)^{-1} \boldsymbol{\Lambda}_{\boldsymbol{t}} = \frac{1}{1 + e + s} \begin{bmatrix} (1 + e)(1 + s) & -s(1 + e) \\ -e(1 + s) & (1 + e)(1 + s) \end{bmatrix},$$

$$\frac{\partial \log(E, S)}{\partial \log K} = -(\boldsymbol{L} \boldsymbol{\Lambda}_{\boldsymbol{x}} \boldsymbol{L}^\intercal)^{-1} \boldsymbol{L}_2 \boldsymbol{\Lambda}_{\boldsymbol{x}^c} \boldsymbol{N}_2^{-1} = \frac{1}{1 + e + s} \begin{bmatrix} s \\ e \end{bmatrix},$$

$$\frac{\partial \log C}{\partial \log(t_E, t_S, K)} = \boldsymbol{L}_2^\intercal \frac{\partial \log(E, S)}{\partial \log(t_E, t_S, K)} + \begin{bmatrix} 0 & \boldsymbol{N}_2^{-1} \end{bmatrix} = \frac{1}{1 + e + s} \begin{bmatrix} 1 + s & 1 + e & -1 \end{bmatrix}.$$

△

These calculations have yielded an explicit formula for the reaction orders of one binding reaction (Eq (3.34)). We derived this formula in both ways, one by explicitly step-by-step calculate through the definition of manifold and implicit function theorem, as an illustration of the abstract derivations in Section 3.4, and another by directly applying the resulting log

derivative formula in Eq (3.19) from our general derivations. Below, we use these formula to investigate what properties the reaction orders have, and how are these properties related to biological behaviors.

Polyhedral shape of reaction order and its biological implications

We use the formula Eq (3.34) to study the properties of reaction orders and their biological implications.

We first look at the overall shape of all possible values that the reaction orders can take. In order to visualize in 2D, we can consider the equilibrium constant K as fixed and normalize all the variables so that K is the unit of concentration. This encodes our biological assumption that we focus on changes to reaction orders caused by varying total concentrations t_E, t_S, rather than varying the equilibrium constant K. This makes sense when the biomolecules making up the binding network are already fixed, and we are studying how to regulate it. If instead we are studying what biomolecules to use to achieve a certain behavior in a binding network, then we should allow K to vary and be an explicit variable in the reaction orders. For this particular example, the value that K is fixed at does not matter because Eq (3.34) shows that the value of the reaction orders can take only depends on (e, s), the ratios of E and S to K, so the range of values that the reaction orders can take is independent of what value K is fixed at. Now with K held fixed and normalized away, the reaction orders of interest are reaction order of the complex C to total enzyme and total substrate $\frac{\partial \log C}{\partial \log(t_E,t_S)}$, and reaction order of free enzyme to total enzyme and total substrate $\frac{\partial \log E}{\partial \log(t_E,t_S)}$. Note that S and E are symmetric since we have just one binding reaction. Which species' reaction order is of interest depends on which species is catalytically active. For example, if C is the active complex for downstream catalysis, such as a gene bound with an activating transcription factor or the activated form of an enzyme or receptor, then reaction orders of C corresponds to response of biological activity. On the other hand, if S is a repressive ligand or repressing transcription factor, then the free form E is catalytically active, so the reaction order of E corresponds to biological activity.

We computationally sample the values of reaction orders in Eq (3.34) to obtain Figure 3.5. Several features arise from visual inspection. First, it appears that these sets take a polyhedral shape. Second, the polyhedral shape suggests it can be formed as combinations of simpler shapes, e.g. vertices and edges. Third, the points concentrate at the edges and vertices, suggesting robustness at those locations. Lastly, the reaction order of E is unbounded, going towards infinity in the $(-1, 1)$ direction, suggesting hypersensitivity. We discuss these features in detail below.

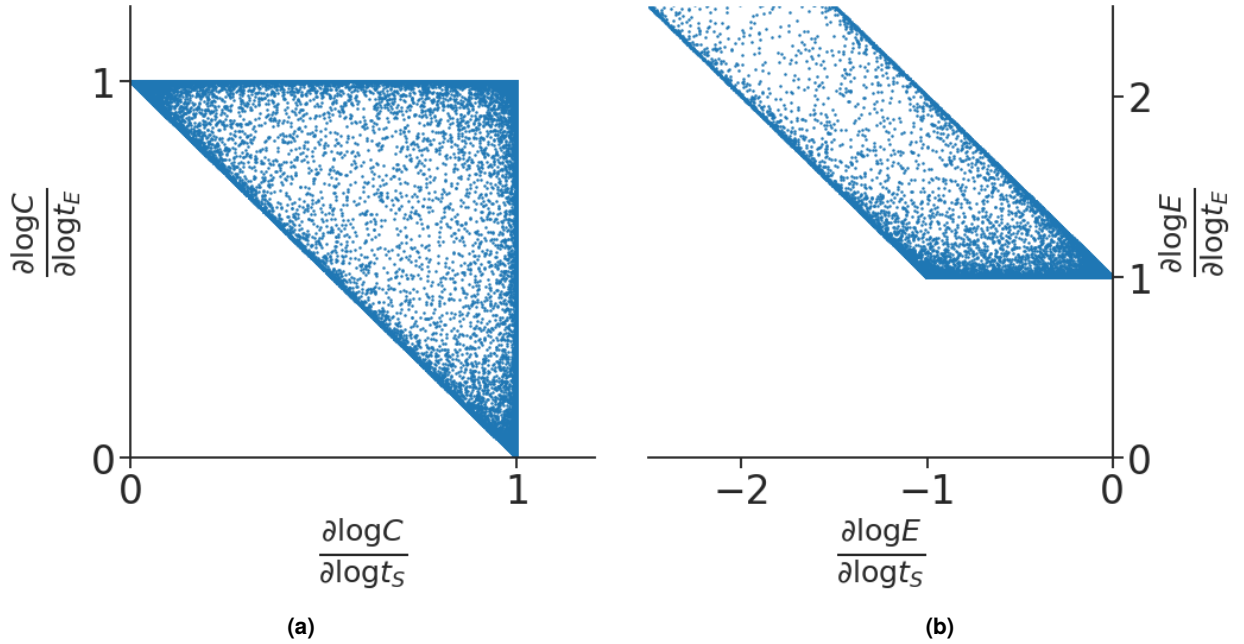

Figure 3.5 Sampling of the log derivative of C (subfigure **(a)**) and E (subfigure **(b)**) with respect to t_E and t_S for the binding network with just one binding reaction $E + S \rightleftharpoons C$. Sampling is via the variables $e = \frac{E}{K}$ and $s = \frac{S}{K}$ taking values between 10^{-6} to 10^{6}, uniformly sampled on the log scale.

Polyhedral shape. The first thing we notice is that the overall shape for both C and E's reaction orders are *polyhedral*. This implies that the full range of reaction orders can be captured as the convex combination of several extreme cases. This can be seen in an explicit and analytical way as follows. Take C's reaction orders for example. We see from the sampled shape that it is the convex combination of vertices $(1, 0)$, $(0, 1)$, and $(1, 1)$. This means any point in the set can be expressed as $\lambda_1(1, 0) + \lambda_2(0, 1) + \lambda_3(1, 1)$ with λ_i non-negative and sum to one $\sum_{i=1}^{3} \lambda_i = 1$. We can then compare this expression with the formula in Eq (3.34) to have the following equation. Note that to be consistent with the figure, we have taken the order for the totals to be (t_S, t_E) instead of (t_E, t_S).

$$\frac{\partial \log C}{\partial \log(t_S, t_E)} = \left[\tfrac{1+e}{1+e+s} \;\; \tfrac{1+s}{1+e+s}\right] = \left[\lambda_1 + \lambda_3 \;\; \lambda_2 + \lambda_3\right]. \tag{3.35}$$

This together with that λ_i's sum to 1 can be used to formulate the following linear system of equations for λ_i's:

$$\begin{bmatrix} 1 & 1 & 1 \\ 1 & 0 & 1 \\ 0 & 1 & 1 \end{bmatrix} \begin{bmatrix} \lambda_1 \\ \lambda_2 \\ \lambda_3 \end{bmatrix} = \begin{bmatrix} 1 \\ \frac{\partial \log C}{\partial \log t_S} \\ \frac{\partial \log C}{\partial \log t_E} \end{bmatrix} = \begin{bmatrix} 1 \\ \frac{1+e}{1+e+s} \\ \frac{1+s}{1+e+s} \end{bmatrix}. \tag{3.36}$$

Solving this linear system of equations yields

$$\begin{bmatrix}\lambda_1\\ \lambda_2\\ \lambda_3\end{bmatrix} = \begin{bmatrix}1 & 0 & -1\\ 1 & -1 & 0\\ -1 & 1 & 1\end{bmatrix}\begin{bmatrix}1\\ \frac{1+e}{1+e+s}\\ \frac{1+s}{1+e+s}\end{bmatrix} = \frac{1}{1+e+s}\begin{bmatrix}e\\ s\\ 1\end{bmatrix}. \tag{3.37}$$

This tells us that we can write the reaction orders of C in an explicit way as convex combinations of a set of vertices:

$$\frac{\partial \log C}{\partial \log(t_S, t_E)} = \frac{e}{1+e+s}(1,0) + \frac{s}{1+e+s}(0,1) + \frac{1}{1+e+s}(1,1). \tag{3.38}$$

As a quick note, although log derivatives are often used to compute "weighted average of exponents" for polynomials in statistical mechanics, and the log derivatives form a convex polytope as well, the polytope for C above is not obtainable from a polynomial. For a polynomial $f(\boldsymbol{x})$ in variables taking positive values $\boldsymbol{x} \in \mathbb{R}^n_{>0}$, the log derivatives are contained in its Newton polytope, which is the polytope formed as a convex combination of the exponents for each monomial term. For example, if $f(\boldsymbol{x}) = 1 + x_1 + x_2$, then the log derivative $\frac{\partial \log f}{\partial \log(x_1,x_2)}$ is contained in polytope with vertices $(0,0)$, $(1,0)$, and $(0,1)$, and the convex coefficients are $\frac{1}{1+x_1+x_2}$, $\frac{x_1}{1+x_1+x_2}$, and $\frac{x_2}{1+x_1+x_2}$ respectively. We see that although these coefficients are the same as the coefficients in Eq (3.38), one of the vertices are different. If we want a polynomial with the $(1,1)$ vertex and similar coefficients, then the polynomial can be $f(\boldsymbol{x}) = x_1 + x_2 + x_1x_2$. But then the coefficient for the $(1,1)$ vertex is $\frac{x_1x_2}{x_1+x_2+x_1x_2}$, a different form compared to that in Eq (3.38). So we see polynomials cannot yield the convex combination in Eq (3.38). Either the vertices are different, or the convex coefficients (i.e. when the vertices are achieved) are different. Indeed, we know Eq (3.38) comes from taking the log derivative of the explicit expression in Eq (3.31) which involves square roots. More generally, reaction order polyhedra come from log derivative of possibly non-analytic expressions that are roots of systems of polynomial equations.

Employing a similar approach we can parameterize a point in the reaction order polyhedron for E as $\lambda_1(0,1) + \lambda_2(-1,1) + \tau(-1,1)$, with $\lambda_1, \lambda_2, \tau \geq 0$ and $\lambda_1 + \lambda_2 = 1$. This expression uses our observation from Figure 3.5b that the polyhedron is defined by two vertices at $(0,1)$ and $(-1,1)$, and a ray in direction $(-1,1)$. The equation relating these coefficients to the reaction order expression in Eq (3.34) is

$$\begin{bmatrix}1 & 1 & 0\\ 0 & -1 & -1\\ 1 & 1 & 1\end{bmatrix}\begin{bmatrix}\lambda_1\\ \lambda_2\\ \tau\end{bmatrix} = \begin{bmatrix}1\\ \frac{\partial \log E}{\partial \log t_S}\\ \frac{\partial \log E}{\partial \log t_E}\end{bmatrix} = \begin{bmatrix}1\\ \frac{-s(1+e)}{1+e+s}\\ \frac{(1+e)(1+s)}{1+e+s}\end{bmatrix} \tag{3.39}$$

Solve this system of linear equations yield

$$\begin{bmatrix}\lambda_1\\ \lambda_2\\ \tau\end{bmatrix} = \begin{bmatrix}0 & 1 & 1\\ 1 & -1 & -1\\ -1 & 0 & 1\end{bmatrix}\begin{bmatrix}1\\ \frac{-s(1+e)}{1+e+s}\\ \frac{(1+e)(1+s)}{1+e+s}\end{bmatrix} = \frac{1}{1+e+s}\begin{bmatrix}1+e\\ s\\ es\end{bmatrix}. \tag{3.40}$$

So we can explicitly write

$$\frac{\partial \log E}{\partial \log(t_S, t_E)} = \frac{1+e}{1+e+s}(0,1) + \frac{s}{1+e+s}(-1,1) + \frac{es}{1+e+s}(-1,1). \tag{3.41}$$

We can also use the above results to write the reaction orders of all species in the form a polyhedron. Define $\lambda_e = \frac{e}{1+e+s}$, $\lambda_s = \frac{s}{1+e+s}$, $\lambda_1 = \frac{1}{1+e+s}$, and $\tau = \frac{es}{1+e+s}$. Then

$$\frac{\partial \log(S,E,C)}{\partial \log(t_S, t_E, K)} = \lambda_e \begin{bmatrix}1 & -1 & 1\\ 0 & 1 & 0\\ 1 & 0 & 0\end{bmatrix} + \lambda_s \begin{bmatrix}1 & 0 & 0\\ -1 & 1 & 1\\ 0 & 1 & 0\end{bmatrix} + \lambda_1 \begin{bmatrix}1 & 0 & 0\\ 0 & 1 & 0\\ 1 & 1 & -1\end{bmatrix} + \tau \begin{bmatrix}1 & -1 & 0\\ -1 & 1 & 0\\ 0 & 0 & 0\end{bmatrix}. \tag{3.42}$$

From the above, we see both through computational sampling and analytical derivations that indeed the range of values that reaction orders can take form a polyhedral set. The mathematical reason for this polyhedral shape is studied in Section 3.8. We investigate the biological implications of the polyhedral shape below.

Vertices and edges as asymptotic approximations. Roughly speaking, a polyhedral set is the set formed by the convex combination of vertices (with vertices generalized to include rays as well). This suggests we can consider the general behavior of a catalysis reaction, i.e. the reaction order of the active species in a binding network, as the "convex combination" of the behaviors at the vertices of reaction order polyhedron. If the behavior is simple at the vertices, then this gives us a way to describe the complicated general behavior through simple extreme-case behavior at the vertices.

We take the C polyhedron to illustrate this. From Eq (3.38), we see each vertex is achieved at a certain extreme of the (e, s) variables. Namely, $(1, 0)$ is achieved when $e \gg 1, s$ (e is much larger than 1 and s), $(0, 1)$ is achieved when $s \gg 1, e$ and $(1, 1)$ is achieved when $1 \gg e, s$. We can relate these vertices' reaction order to the approximate expressions of C in (t_S, t_E, K) at these vertices by applying these asymptotic conditions to the equations defining the equilibrium manifold in Eq (3.30), or to the explicit solution in Eq (3.31). Alternatively, we can include the K variable in the reaction orders to see the vertices are $\frac{\partial \log C}{\partial \log(t_S, t_E, K)}$ taking values $(1, 0, 0)$, $(0, 1, 0)$, and $(1, 1, -1)$, which we can integrate to get C

expressed in (t_S, t_E, K) with a multiplicative constant which we can set to 1. The result is summarized as follows,

$$C \approx \begin{cases} t_E, & \text{reaction order } (0,1), \quad t_S \gg t_E, K; \\ \frac{t_S t_E}{K}, & \text{reaction order } (1,1), \quad K \gg t_E, t_S; \\ t_S, & \text{reaction order } (1,0), \quad t_E \gg t_S, K. \end{cases} \tag{3.43}$$

Each vertex corresponds to a biologically meaningful *regime* that the reaction can operate in. When the total substrate t_S is very large, the enzymes are saturated so that the speed of catalysis is only limited by the enzyme, therefore $C \approx t_E$, corresponding to vertex$(0,1)$. When it is the other way around and the total enzyme is very large and total substrate is limiting, $C \approx t_S$, corresponding to vertex $(1,0)$. When enzyme and substrate are not abundant relative to the binding affinity K, the speed of catalysis is limited by the formation of complex C. In this regime, the complex C is low in number compared to total enzyme and total substrate, and increasing either enzyme and substrate creates more complexes. Therefore $C \approx \frac{t_S t_E}{K}$, corresponding to vertex $(1,1)$. Together, we see that the polyhedral shape highlights the vertices as the *regimes* that a catalysis reaction can operate in, which corresponds to extreme cases of concentrations and equilibrium constants. The asymptotic conditions of these extreme cases in turn yield asymptotic approximations of the active species (C in this case) that are simple monomials and biologically interpretable. The general complicated behavior can then be considered as varying in between these simple extreme-case regimes.

The above extreme-case analysis may remind a reader of the Michaelis-Menten formula (or the Langmuir form more generally), where one asymptotic condition that substrate is overabundant compared to enzyme $t_S \gg t_E$ is used to derive the formula $C \approx t_E \frac{t_S}{t_S + K}$ that spans two regimes. A common description of this formula is that it is responsive when substrate concentration is low $t_S \ll K$, and becomes saturated when substrate concentration is high $t_S \gg K$. This can be viewed as the *edge* connecting vertices $(0,1)$ and $(1,1)$. This is also clear from the asymptotic conditions, as $t_S \gg t_E$ has non-empty intersection with the conditions for these two vertices. We caution that although the Michaelis-Menten formula indeed forms an edge connecting the $(0,1)$ and $(1,1)$ vertices, it does not capture all points on the edge. In other words, the Michaelis-Menten assumption is a sufficient but not necessary condition for the edge. Although the condition $t_S \gg t_E, K$ for the $(0,1)$ vertex is contained in the Michaelis-Menten condition $t_S \gg t_E$, the same does not hold for the $(1,1)$ vertex. The condition $(K \gg t_E, t_S$ of the $(1,1)$ vertex does not require $t_S \gg t_E$, e.g. both $K \gg t_E \gg t_S$ and $K \gg t_S \gg t_E$ can achieve vertex $(1,1)$. The necessary and sufficient condition for the $(0,1)$ to $(1,1)$ edge is $E \ll K$ *or* $t_E \ll t_S$. This is

more general than $t_E \ll t_S$. For example, when $t_S \ll K$, the $(1,1)$ vertex is still achieved by $t_E \ll K$, without assuming $t_E \ll t_S$.

In summary, the polyhedral set for the full range of reaction orders highlights that the Michaelis-Menten formula is a sufficient edge-approximation of the overall behavior. Through one asymptotic condition $t_S \gg t_E$, it captures a behavior spanning the edge connecting two regimes corresponding to vertices $(0,1)$ and $(1,1)$, and misses the regime corresponding to vertex $(1,0)$ and expression $C \approx t_S$.

We can then investigate edge-approximation in general, with Michaelis-Menten approximation (or single molecule states approximations and external-bath approximations, see Section 3.1) as a special case. In the example of C's reaction order, while two asymptotic conditions yield vertices, one asymptotic condition yield edges. In terms of convex coefficients in Eq (3.38), we can yield an edge by eliminating one vertex. For example, to obtain the Michaelis-Menten edge, we can eliminate the $(1,0)$ vertex by letting coefficient $\frac{e}{1+e+s}$ goes to zero, which corresponds to asymptotic condition $e \ll s$ or $e \ll 1$. For simplicity, we follow Michaelis-Menten to use just one of the two conditions to represent an edge approximation. This yields the following summary for edge approximations of C, and the graphical summarize of both edge and vertex approximations in Figure 3.6.

$$C \approx \begin{cases} t_E \frac{t_S}{t_S+K}, & \text{edge from } (0,1) \text{ to } (1,1), \quad t_S \gg t_E; \\ \min\{t_S, t_E\}, & \text{edge from } (0,1) \text{ to } (1,0), \quad K \ll t_E \text{ or } K \ll t_S; \\ t_S \frac{t_E}{t_E+K}, & \text{edge from } (1,0) \text{ to } (1,1), \quad t_E \gg t_S. \end{cases} \tag{3.44}$$

In addition to the edge that is symmetric reflection of Michaelis-Menten, we also obtain an edge approximation connecting $(0,1)$ to $(1,0)$. Importantly, this is another class of approximations just as valid as the Michaelis-Menten or single molecule states or external bath approximations. To derive the formula $C \approx \min\{t_S, t_E\}$, we can apply the asymptotic condition $K \ll t_E$ or $K \ll t_S$, which implies $t_E + t_S + K \approx t_E + t_S$ and $\sqrt{(t_E + t_S + K)^2 - 4t_E t_S} \approx |t_E - t_S|$, to the exact solution of C in Eq (3.31):

$$C(t_E, t_S) \approx \frac{(t_E + t_S) - |t_E - t_S|}{2} = \min\{t_E, t_S\}.$$

The condition $K \ll t_E$ or $K \ll t_S$ corresponds to tight binding between enzyme and substrate. One natural scenario where this is true is in strong sequestrations between molecules, e.g. between sigma and anti-sigma factors, and in nucleic acid circuits. This edge approximation also plays a central role for antithetic integral control motifs for robust perfect adaptation proposed in [22]. Importantly, this edge approximation is an alternative

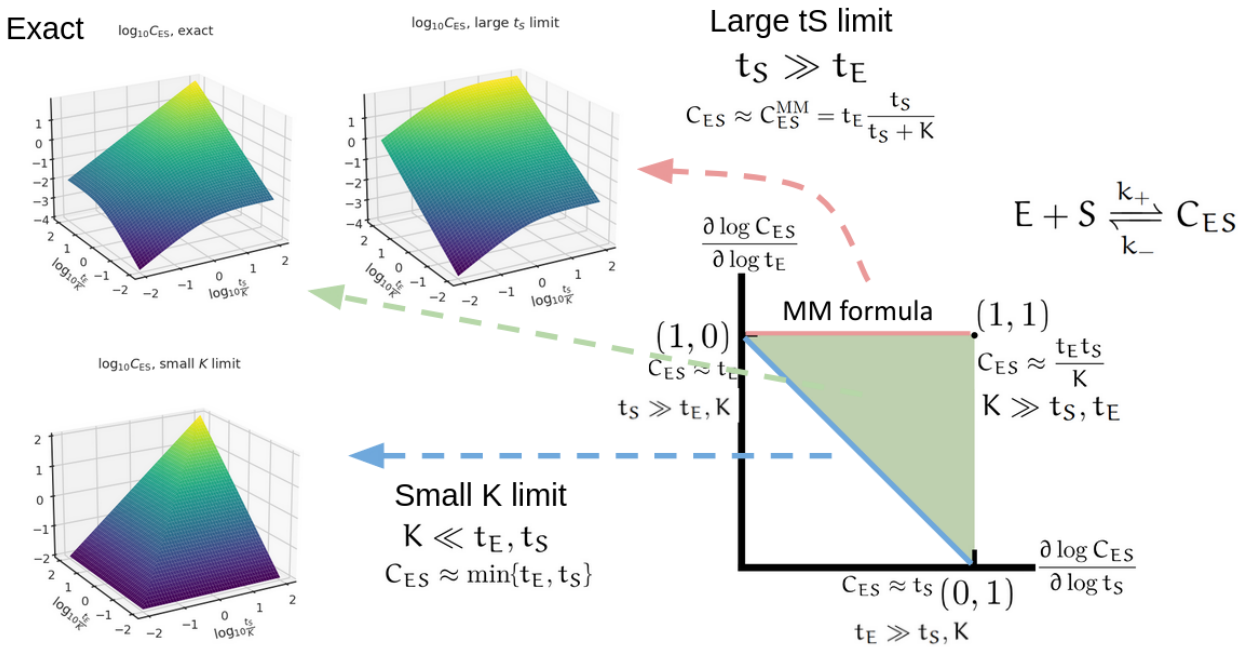

Figure 3.6 Visualization of how the reaction order polyhedron captures the holistic regulatory profile, and how the vertex and edge approximations for C in one binding reaction $E + S \rightleftharpoons C$ compare to the exact solution. Upper left is the exact solution of C in terms of t_E and t_S in Eq (3.31). In the large t_S limit (close to t_S axis in the 3D plot), the Michaelis Menten formula (upper middle) is a good approximation of the exact solution. In the small K limit (when t_E and/or t_S are large), the minimum formula corresponding to the diagonal edge is a good approximation of the exact solution.

to the Michaelis-Menten (or single molecule states or external bath) edge approximations of enzymatic reactions. This edge approximation is valid whenever tight binding is present.

Robustness of vertices and edges. Another prominent feature of the sampling of reaction orders in Figure 3.5 is that the randomly sampled points concentrate at the edges and vertices. Since the points are uniformly sampled in log scale on enzyme and substrate concentrations, if we consider perturbations to the system as multiplicative variations in these concentrations, then the vertices and edges should be robust to such variations.

We can see why the points concentrate at vertices and edges by looking at the convex coefficients in Eq (3.38) and Eq (3.41). Because the coefficients of the vertices all take rational-function form such as $\frac{e}{1+e+s}$, they approach extreme values of 0 or 1 when the variables $(e, s, 1)$ are far apart in values. This means the condition for the reaction order to be in the interior of the polyhedra away from edges and vertices is quite fragile: the concentrations need to be "finely adjusted" so that they are close to each other. Once these concentrations drift apart from each other, we are at the vertices and edges.

Another way to describe this is that we can achieve precise values of reaction orders by very crude control of concentrations. For example, to push the reaction order of C toward

value $(1, 0)$, we just need to drive e large in comparison to s and 1. Such control only needs to be done crudely. However rough the control is, such as an increment of e that varies between ten to ten thousand fold, as long as it can make e large compared to s and 1, the reaction order of C will achieve the precise value $(1, 0)$.

As a way to quantify the robustness or insensitivity at the vertices, we can look at the log derivative, or fold change, of the reaction orders to the concentration variables, which captures the sensitivity. This corresponds to the second order log derivatives, or the log Hessian, of a species' concentration to totals. For example, by chain rule we can calculate

$$\begin{aligned}\frac{\partial^2 \log C}{\partial(\log \boldsymbol{t})(\log \boldsymbol{t})^\intercal} &= \begin{bmatrix} \frac{\partial^2 \log C}{\partial(\log t_E)^2} & \frac{\partial^2 \log C}{\partial(\log t_E)(\log t_S)} \\ \frac{\partial^2 \log C}{\partial(\log t_S)(\log t_E)} & \frac{\partial^2 \log C}{\partial(\log t_E)^2} \end{bmatrix} = \frac{\partial}{\partial \log(t_E, t_S)} \frac{\partial \log C}{\partial \log(t_E, t_S)} \\ &= \left(\frac{\partial \log(e, s)}{\partial \log(t_E, t_S)}\right)\left(\frac{\partial}{\partial \log(e, s)} \frac{\partial \log C}{\partial \log(t_E, t_S)}\right) \\ &= \frac{1}{(1+e+s)^3} \begin{bmatrix} -e^2(1+s)(1+e+s+2es) & 2es(1+e)(1+s) \\ 2es(1+e)(1+s) & -s(1+e)(1+e+s+2es) \end{bmatrix}.\end{aligned}$$

Close to the $(1, 1)$ vertex, for example, we have $1 \gg e, s$. Apply this to the above formula, we have $\frac{\partial^2 \log C}{\partial(\log t_E)^2} \approx -e$, $\frac{\partial^2 \log C}{\partial(\log t_S)^2} \approx -s$, and $\frac{\partial^2 \log C}{\partial(\log t_E)(\log t_S)} \approx 2es$. We see that the closer we are to the vertex, i.e. the smaller e and s are compared to 1, then the smaller the sensitivity to variations in (t_E, t_S), therefore more robust. This highlights the following feature of robustness for edges and vertices in a reaction order polyhedron: the closer we are to a vertex or edge, the more robust we are to variations.

One implication of this robustness is that when we or a cell want to control biomolecular circuits to perform precise and robust regulations, but the control actions are sloppy or noisy or unreliable due to technological limitations or noise and uncertainty in the circuit and environment, then by crudely pushing the concentrations and equilibrium constants toward extreme regimes corresponding to vertices and edges or reaction order polyhedra, we can still achieve precise and robust performance. This motivates analysis and design of biomolecular system dynamics via reaction orders, as investigated in Chapter 5.

Hypersensitivity in reaction order of E. One prominent feature from Figure 3.5 is that while the reaction orders of C are bounded, those of E are not. In fact, the reaction order of E to t_E can reach toward $+\infty$, and that of E to t_S can reach toward $-\infty$. A reaction order higher than 1 corresponds to fold change response sharper than linear, which is often called hypersensitivity. We provide an analysis below relating the hypersensitivity we see from computational sampling in Figure 3.5b to the regimes achieving it in terms of asymptotic conditions on concentrations.

To analyze the reaction orders of E, we employ a similar extreme-case analysis as we did for C. There are three regimes. (1) If almost all enzymes are bound $t_E \approx C$, and almost all substrates are free $t_S \approx S$, then $E = \frac{CK}{S} \approx \frac{t_E K}{t_S}$, with reaction order $(-1, 1)$ in t_S and t_E. (2) If almost all enzymes are unbound $t_E \approx E$, then $E \approx t_E$, with reaction order $(0, 1)$. So it seems natural that the reaction order would be bounded in the line segment between $(-1, 1)$ and $(0, 1)$, so that the sensitivity of E to t_S is always between -1 and 0. Indeed, this corresponds to what we typically obtain from Michaelis-Menten approximation applied to this case, which is $E \approx t_E \frac{K}{t_S + K}$. However, this ignores the third extreme case, (3) when both enzyme and substrate are mostly in bound form, $t_E \approx C$ and $t_S \approx C$. This is a relatively restrictive scenario and require t_E and t_S to be close in addition to tight binding. But this can happen. As t_E and t_S are symmetric, without loss of generality, let us inspect the case with $t_S \geq t_G$. Using $t_E \approx C$, we have $E = \frac{CK}{S} = \frac{CK}{t_S - C} \approx \frac{t_E K}{t_S - t_E}$. We can calculate the log derivative of this formula with respect to t_E and t_S to obtain the result

$$\frac{\partial \log E}{\partial \log(t_S, t_E)} \approx \left[-\frac{t_S}{t_S - t_E} \;\; \frac{t_S}{t_S - t_E}\right] = \frac{t_S}{t_S - t_E}\left[-1 \;\; 1\right].$$

So as t_S approach t_E from above, we see that this goes to infinity in the direction $(-1, 1)$. We can summarize the three regimes as follows

$$\text{Reaction order of } E \text{ in } (t_S, t_E) = \begin{cases} (-1, 1), & t_E \approx C, t_S \approx S; \\ (0, 1), & t_E \approx E; \\ \text{ray towards } (-1, 1), & t_E \approx C, |t_E - t_S| \to 0. \end{cases} \tag{3.45}$$

Therefore, in contrast to bound complex C, the free enzyme E can obtain very high sensitivity to total substrate concentration t_S. The high sensitivity regime is achieved when $t_E \approx C$, i.e. binding is tight, and $|t_S - t_E| \to 0$, i.e. total substrate concentration is close to total enzyme concentration.

One implication of this is in comparing between an activator and a repressor. If S is an activating substrate (or transcription factor), the catalytically active form of the enzyme (or gene) is C. We see that the response of C to change in total substrate concentration t_S in terms of reaction order is bounded between $(0, 1)$ in Figure 3.5a. On the other hand, if S is a repressive substrate, the catalytically active form of the enzyme is E, the free form. The response of E to change in substrate concentration can become hypersensitive and reach toward $-\infty$ in the tight-binding regime, where most of enzymes are in respressed (bound) form C, and the substrate concentration and enzyme concentration are close in magnitude.

Joint variation in reaction orders. Although our discussion above focuses on the reaction order polyhedron of individual species, such as C or E, it should be kept in mind that the

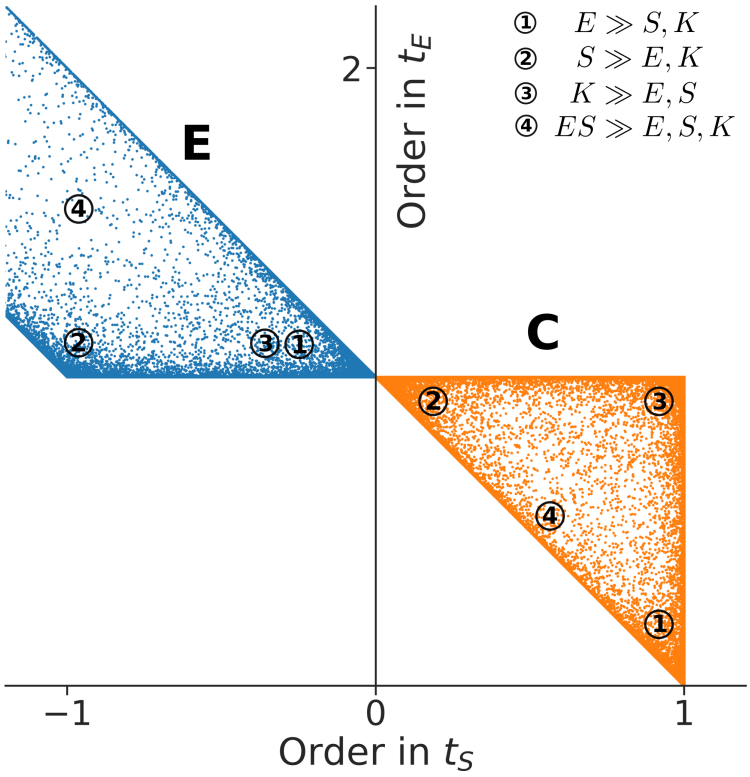

Figure 3.7 Sampling of the reaction order of C (orange) and E (blue) with respect to total substrate t_S and total enzyme t_E from one binding reaction $E + S \rightleftharpoons C$, plotted on the same axis. Different extreme scenarios are labeled by numbers, with corresponding asymptotic conditions listed on the upper right corner. For example, in regime 1, C is close to vertex $(1, 0)$, while E is close to vertex $(0, 1)$.

full reaction order polyhedron is over the matrix of log derivatives (see Eqn (3.42)). This means, when the reaction order of C reaches toward a vertex in its triangular reaction order polyhedron, that could correlate with E reaching toward a vertex in its own polyhedron. This joint variation in reaction orders is precisely described by Eqn (3.42). To provide a visual representation relating the vertices of C and E that we discussed above, see Figure 3.7 where the two polyhedra are plotted together. Such join variations are important to consider in cases where multiple species are catalytically active, or when we want to design regulatory behavior on top of a binding network.

Summary

In this section, we computationally sampled and analytically calculated the reaction orders in one binding reaction. We find that the full range of values that the reaction orders can take form a polyhedral set. The vertices and edges can be robustly achieved when concentrations and equilibrium constants take values that are far apart. In turn, vertex- and edge-approximations can be used as general methods to find simpler approximations

when asymptotic conditions for the vertices and edges are satisfied, with Michaelis-Menten approximation and strong-sequestration approximation as examples in the simple case studied. The vertices and edges are also robust operating regimes for this binding reaction's regulation of downstream catalysis. Other than these common features, different species' reaction orders form different polyhedral sets, revealing their distinct biological activities, such as hypersensitivity.

Given the central importance of vertices in reaction order polyhedra, we study how to characterize vertices mathematically in the next chapter.

3.7 Vertices of binding polyhedra as minimal representations

From the previous section's thorough analysis of one binding reaction, we observed that one central feature of the range of values that the reaction orders can take is that it forms a polyhedral set. The polyhedral set has vertices that correspond to constant reaction orders. Before studying how the polyhedral shape arise in the next section, in this section we focus on just the vertices. We show that vertices in a species' reaction order polyhedra correspond to minimal expressions of a species in terms of others. We then investigate how these minimal expressions can be found in a systematic way, using zonotopes from the theory of convex polytopes and oriented matroids (Chapter 6 and 7 of [123]).

Vertices and minimal representations

For reaction orders, we are interested in the log derivative of one species x_{j^*} considered to be catalytically active, for some $j^* \in \{1, \dots, n\}$, with respect to the totals $\boldsymbol{t} \in \mathbb{R}^d_{>0}$. In the one binding reaction example $E + S \rightleftharpoons C$, if we take the active species x_{j^*} to be C, then the reaction order of interest is $\frac{\partial \log C}{\partial \log(t_S, t_E)}$. From our investigation of this example, we see that vertices correspond to extreme cases where one term dominates the totals. The vertex with reaction order $(1, 1)$ corresponds to approximate expression $C \approx \frac{t_E t_S}{K}$ is achieved when $K \gg E, S$ so that most of enzyme and substrate are in free form. In other words, free enzyme E dominates total enzyme so that $t_E \approx E$, and free substrate dominates total substrate $t_S \approx S$. In this case, we have approximate expression $C = \frac{ES}{K} \approx \frac{t_E t_S}{K}$. Then the log derivative of $\frac{t_E t_S}{K}$ to (t_S, t_E) is just their exponents, namely $(1, 1)$. Let us inspect another vertex. The vertex $(1, 0)$ corresponds to $C \approx t_S$ with condition $t_E \gg t_S, K$. This is a scenario where enzymes are overabundant so most substrates are bound. So bound substrate C dominates t_S, i.e. $t_S \approx C$. Then $C \approx t_S$, and of course the log derivative of t_S to (t_S, t_E) is $(1, 0)$.

This provides a reasoning for what the vertices are. The totals $\boldsymbol{t} = \boldsymbol{L}\boldsymbol{x}$ come from summing the concentration of several species in $\boldsymbol{x}$. When some of the totals $\boldsymbol{t}$ are dominated by one of the species in the sum and the active species x_{j^*} can be expressed as a monomial in these species, then the reaction orders are just the exponents of this monomial. Let us write down exactly what this means. We assume x_j^* can be written as a monomial in terms of variables in $\boldsymbol{x}$ and $\boldsymbol{k}$. This corresponds to $x_{j^*} = \boldsymbol{x}^{\boldsymbol{a}}\boldsymbol{k}^{\boldsymbol{b}}$ for some vector $\boldsymbol{a} \in \mathbb{R}^n$, $\boldsymbol{b} \in \mathbb{R}^r$. Here the notation $\boldsymbol{x}^{\boldsymbol{a}}$ means $\boldsymbol{x}^{\boldsymbol{a}} = x_1^{a_1} \dots x_n^{a_n} = e^{\boldsymbol{a}^\intercal \log \boldsymbol{x}}$. Since the totals $\boldsymbol{t}$ has just d variables, if the variables in this monomial expression are all from dominant species of each total, then there can be at most d different variables of $\boldsymbol{x}$ involved. This corresponds to the exponent vector $\boldsymbol{a}$ has at most d nonzero entries, i.e. its support size is no larger than d. Let $\mathcal{J} \subset \{1, \dots, n\}$ denote the support of $\boldsymbol{a}$, i.e. $\mathcal{J} = \{j : a_j \neq 0\}$. The support of $\boldsymbol{a}$ has no more than d nonzero entries means $|\mathcal{J}| \leq d$. Then if there exists t_{i_j} for each $j \in \mathcal{J}$ such that $t_{i_j} \approx x_j$, then $x_{j^*} = \boldsymbol{x}^{\boldsymbol{a}}\boldsymbol{k}^{\boldsymbol{b}} = \boldsymbol{k}^{\boldsymbol{b}} \prod_{j\in\mathcal{J}} x_j^{a_j} \approx \boldsymbol{k}^{\boldsymbol{b}} \prod_{j\in\mathcal{J}} (t_{i_j})^{a_j}$. So the log derivative of x_{j^*} with respect to $(\boldsymbol{t}, \boldsymbol{k})$ is just $(\boldsymbol{a}, \boldsymbol{b})$.

From this observation, we see finding vertices comes down to finding monomial expressions of x_{j^*} in terms of $\boldsymbol{x}$ and $\boldsymbol{k}$ of the form $x_{j^*} = \boldsymbol{x}^{\boldsymbol{a}}\boldsymbol{k}^{\boldsymbol{b}}$, such that $\boldsymbol{a}$ has no more than d nonzero entries. Taking log, the monomial expression becomes $\log x_{j^*} = \boldsymbol{a}^\intercal \log \boldsymbol{x} + \boldsymbol{b}^\intercal \log \boldsymbol{k}$. The space of such expressions for a binding network is naturally given by the steady state equations defining the equilibrium manifold $\boldsymbol{N} \log \boldsymbol{x} = \log \boldsymbol{k}$ (see Eq (3.12)). The condition on the support of $\boldsymbol{a}$ motivates us to find vectors with minimal support yield a monomial representation. The desire for minimal support is also motivated by the mathematical reason that all other monomials expressions can be written as linear sums of minimal support ones (see Lemma 6.7 in [123] for example). Therefore, we would like to find the minimal representations of x_{j^*} in terms of variables $\boldsymbol{x}$ for a given binding network. This is what we study next.

Minimal representations in binding networks

To begin with, we define precisely what we mean by minimal. In words, a vector $\boldsymbol{v} \in V \subset \mathbb{R}^n$ is minimal in a set of vectors V if there is no nonzero vector in V with smaller support vectors. Support vector is defined as $\boldsymbol{u} := \operatorname{supp} \boldsymbol{v}$ has $u_j = 1$ if $v_j \neq 0$, and $u_j = 0$ if $v_j = 0$. The partial order on support vectors is the canonical one: $0 < 1$ applied component-wise. For convenience, we slightly abuse notation and use $\operatorname{supp} \boldsymbol{v}$ to also denote the set of support indices $\mathcal{J} = \{j = 1, \dots, n : v_j \neq 0\}$. This is identifying the space of subsets of $\{1, \dots, n\}$ with space $\{0, 1\}^n$.

Definition 3.7.1. Given set of vectors $V \subset \mathbb{R}^n$. $\boldsymbol{v}^* \in V$ is a **vector of minimal support** in V

if it is nonzero and there does not exist nonzero vector $\boldsymbol{v} \in V$, such that $\operatorname{supp} \boldsymbol{v} < \operatorname{supp} \boldsymbol{v}^*$. In other words, for any nonzero $\boldsymbol{v} \in V$, either $\operatorname{supp} \boldsymbol{v}^* \leq \operatorname{supp} \boldsymbol{v}$ or they are not comparable. We denote the set of minimal vectors of a set V by $\operatorname{MINSUPP}(V)$.

We note that if V is a vector space, then $\boldsymbol{v}^*$ has minimal support in V implies $\alpha \boldsymbol{v}^*$ has minimal support in V for all nonzero scalar α, since they all have the same support.

Now we consider the minimal representations of x_{j^*} in terms of variables $\boldsymbol{x}$ for detailed balanced solutions of an isomer-atomic network, so $\boldsymbol{x}$ is in equilibrium manifold (see Eq (3.12)). A (monomial) representation of x_{j^*} in terms of $\boldsymbol{x}$ and $\boldsymbol{k}$ can be written as $\log x_{j^*} = \boldsymbol{a}^\intercal \log \boldsymbol{x} + \boldsymbol{b}^\intercal \log \boldsymbol{k}$ for some vector $\boldsymbol{a} \in \mathbb{R}^n$ and $\boldsymbol{b} \in \mathbb{R}^r$. This can be re-written as

$$(\boldsymbol{e}_{j^*} - \boldsymbol{a})^\intercal \log \boldsymbol{x} = \boldsymbol{b}^\intercal \log \boldsymbol{k}.$$

Since $\boldsymbol{x}$ and $\boldsymbol{k}$ are in equilibrium manifold $\mathcal{M}$, it satisfies $\boldsymbol{N} \log \boldsymbol{x} = \log \boldsymbol{k}$. So the above condition can be satisfied for some $\boldsymbol{b} \in \mathbb{R}^r$ if and only if $(\boldsymbol{e}_{j^*} - \boldsymbol{a}) \in \operatorname{rowspan} \boldsymbol{N}$. Indeed, this condition implies there exists some $\boldsymbol{b} \in \mathbb{R}^r$ such that $(\boldsymbol{e}_{j^*} - \boldsymbol{a}) = \boldsymbol{b}^\intercal \boldsymbol{N}$, so we can calculate that $(\boldsymbol{e}_{j^*} - \boldsymbol{a})^\intercal \log \boldsymbol{x} = \boldsymbol{b}^\intercal \boldsymbol{N} \log \boldsymbol{x} = \boldsymbol{b}^\intercal \log \boldsymbol{k}$. In terms of set equivalence,

$$\begin{aligned}
&\{ \text{ representations of } x_{j^*} \text{ in } \boldsymbol{x}\} \\
=&\{\boldsymbol{a} \in \mathbb{R}^n : \text{ there exists } \boldsymbol{b} \in \mathbb{R}^r, \text{ such that } (\boldsymbol{e}_{j^*} - \boldsymbol{a})^\intercal \log \boldsymbol{x} = \boldsymbol{b}^\intercal \log \boldsymbol{k}\} \\
=&\{\boldsymbol{a} : (\boldsymbol{e}_{j^*} - \boldsymbol{a}) \in \operatorname{rowspan} \boldsymbol{N}\} = \boldsymbol{e}_{j^*} - \operatorname{rowspan} \boldsymbol{N} = \boldsymbol{e}_{j^*} + \mathcal{S}.
\end{aligned}$$

The last step we used that $\operatorname{rowspan} \boldsymbol{N} = \mathcal{S}$ is a linear subspace, so $-\mathcal{S} = \mathcal{S}$. The minimal representations of x_{j^*} in terms of all species then comes down to finding the vectors of minimal support in the affine subspace $\boldsymbol{e}_{j^*} + \mathcal{S}$. In other words, we define

$$\{\text{minimal representations of } x_{j^*} \text{ in } \boldsymbol{x}\} := \operatorname{MINSUPP}(\boldsymbol{e}_{j^*} + \mathcal{S}). \tag{3.46}$$

We would like to express minimal support vectors on the affine subspace $\boldsymbol{e}_{j^*} + \mathcal{S}$ in terms of minimal support vectors of linear subspaces. This requires taking $\boldsymbol{e}_{j^*}$ and $\mathcal{S}$ out of the minimal support operator. We do so below by inspecting how the minimal support vectors in $\boldsymbol{e}_{j^*} + \mathcal{S}$ relate to those in $\mathcal{S}$.

Proposition 3.7.2.

$$\operatorname{MINSUPP}(\boldsymbol{e}_{j^*} + \mathcal{S}) = \boldsymbol{e}_{j^*} + \{0\} \cup \operatorname{MINSUPP}_{j^*}(\mathcal{S}), \tag{3.47}$$

where we define $\operatorname{MINSUPP}_{j^*}(\mathcal{S}) := \{\boldsymbol{u} \in \operatorname{MINSUPP}(\mathcal{S}) : u_{j^*} = -1\}$.

Proof. We first note that $\boldsymbol{e}_{j^*}$ has minimal support in this affine subspace. This is simply expressing x_{j^*} as itself, corresponding to the zero vector $\mathbf{0}$ in $\mathcal{S}$.

Now consider any vector of minimal support $\boldsymbol{v} \in \boldsymbol{e}_{j^*} + \mathcal{S}$ that is not $a\boldsymbol{e}_{j^*}$ for some nonzero constant a. $\boldsymbol{v}$ should have $v_{j^*} = 0$. This is because if $v_{j^*} \neq 0$, then we can always divide out x_{j^*} to get a vector with smaller support, contradicting that $\boldsymbol{v}$ is minimal. Seen in another way, if $v_{j^*} \neq 0$, then $\operatorname{supp} \boldsymbol{e}_{j^*} < \operatorname{supp} \boldsymbol{v}$. Therefore, $\boldsymbol{v}$ satisfies $\boldsymbol{v} = \boldsymbol{e}_{j^*} + \boldsymbol{u}$, $\boldsymbol{u} \in \mathcal{S}$ and $u_{j^*} = -1$. In other words, we have shown

$$\operatorname{MINSUPP}(\boldsymbol{e}_{j^*} + \mathcal{S}) \subset \{\boldsymbol{e}_{j^*}\} \dot{\cup} (\boldsymbol{e}_{j^*} + \{\boldsymbol{u} \in \mathcal{S} : u_{j^*} = -1\}),$$

where $\dot{\cup}$ denote disjoint union, or union of disjoint sets. If this $\boldsymbol{u}$ with $u_{j^*} = -1$ has minimal support in $\mathcal{S}$, then the corresponding $\boldsymbol{v} = \boldsymbol{e}_{j^*} + \boldsymbol{u}$ has minimal support in $\boldsymbol{e}_{j^*} + \mathcal{S}$. This is because $\operatorname{supp} \boldsymbol{v} = \operatorname{supp} \boldsymbol{u} \backslash \{j^*\}$.

We then show that this is also necessary. If $\boldsymbol{u}$ is not of minimal support in $\mathcal{S}$, then there exists nonzero vector $\boldsymbol{u}' \in \mathcal{S}$ with smaller support than $\boldsymbol{v}$. Consider the case $u'_{j^*} = 0$. Since $\boldsymbol{u}'$ is nonzero, there exists another $j' \neq 0$ so that $u'_{j'} \neq 0$. Since $\boldsymbol{u}'$ has smaller support than $\boldsymbol{u}$, $u_{j'} \neq 0$ as well. Now consider

$$\boldsymbol{u}'' := \boldsymbol{u} - \frac{u_{j'}}{u'_{j'}} \boldsymbol{u}'.$$

This is linear combination of $\boldsymbol{u}$ and $\boldsymbol{u}'$, so $\boldsymbol{u}'' \in \mathcal{S}$. By construction, $u''_{j'} = 0$, so $\operatorname{supp} \boldsymbol{u}'' \subset \operatorname{supp} \boldsymbol{u} \backslash \{j'\}$. Also, since $u'_{j^*} = 0$, we have $u''_{j^*} = u_{j^*} = -1$. Therefore, $\boldsymbol{v}'' := \boldsymbol{e}_{j^*} + \boldsymbol{u}''$ has smaller support than $\boldsymbol{v}$.

Now consider the case $u'_{j^*} \neq 0$. Since $\boldsymbol{u}'$ has smaller support, there exists j so that $u'_j = 0$ while $u_j \neq 0$. Define $\boldsymbol{u}'' = -(u'_{j^*})^{-1} \boldsymbol{u}' \in \mathcal{S}$. Then $u''_{j^*} = -1$, while $u''_j = 0$. So $\operatorname{supp} \boldsymbol{u}'' \subset \operatorname{supp} \boldsymbol{u} \backslash \{j\}$, and $\boldsymbol{v}'' := \boldsymbol{u}'' + \boldsymbol{e}_{j^*}$ has smaller support than $\boldsymbol{v}$. □

With the above result, we have characterized the vertices of reaction order polyhedra in terms of minimal vectors of linear subspace. When the binding network gets large, we would like a way to compute these vertices in a systematic fashion. Below, we use the tool of zonotopes to compute the minimal vectors of linear subspaces, and therefore vertices of reaction order polyhedra.

Computation of minimal representations through zonotopes

Vectors of minimal support in $\mathcal{S}$ can be explicitly computed through zonotopes. For this, we utilize the theory of polytopes and oriented matroids (see Chapter 6 and 7 of [123]).

Some of the basic tools below may be well known in the fields of polytopes, oriented matroids, and matroid theory. But for completeness, exposition, and accessibility to readers not familiar with those fields, I provide a streamlined development of necessary tools nonetheless. To begin with, instead of the partial order on vectors' support, we consider the partial order on sign vectors, where $0 < +$ and $0 < -$ is applied component-wise. Note that smaller in sign implies smaller in support, but not vice versa in general. For example, `(++)` and `(+-)` are not comparable in the sign order, but their support are both `(11)`, and therefore equal in support order.

Since we consider vectors in a linear subspace, the correspondence between vectors of minimal sign and vectors of minimal support is simple.

Lemma 3.7.3. *For a vector $\boldsymbol{v}$ in linear subspace $\mathcal{V} \subset \mathbb{R}^n$, it is of minimal sign iff it is of minimal support.*

Proof. ($\Longleftarrow$). Contrapositive is not minimal sign implies not minimal support. This is obvious because smaller in sign order implies smaller in support order.

($\Longrightarrow$). Contrapositive is not minimal support implies not minimal sign. $\boldsymbol{v}$ is not minimal support implies there exists $\boldsymbol{u} \in \mathcal{V}$ so that $\operatorname{supp} \boldsymbol{u} < \operatorname{supp} \boldsymbol{v}$, so there exists j_0, $u_{j_0} = 0$ while $v_{j_0} \neq 0$. Let u and v denote $\boldsymbol{u}$ and $\boldsymbol{v}$'s sign vectors. Let $S(\mathrm{u}, \mathrm{v}) = \{j : \mathrm{u}_j = -\mathrm{v}_j \neq 0\}$ be the separation set of u and v. If $S(\mathrm{u}, \mathrm{v}) = \emptyset$, then $\mathrm{u} < \mathrm{v}$. If $S(\mathrm{u}, \mathrm{v}) \neq \emptyset$, let $q = |S(\mathrm{u}, \mathrm{v})|$. Take $j_1 \in S(\mathrm{u}, \mathrm{v})$. We can eliminate j_1 between u and v to obtain $\mathrm{w}^1 \in \operatorname{sgn} \mathcal{V}$. By definition, $\mathrm{w}^1_{j_1} = 0$, and $\mathrm{w}^1_{j_0} = \mathrm{v}_{j_0}$. Since u has smaller support ahtn v, we also have $\operatorname{supp} \mathrm{w}^1 < \operatorname{supp} \mathrm{v}$, but now $|S(\mathrm{w}^1, \mathrm{v})| \leq q - 1$, since they have the same sign at j_1 now. If $|S(\mathrm{w}^1, \mathrm{v})| > 0$, we take its element j_2 and perform the same process. Then after q' steps, $q' \leq q$, we reach a sign vector $\mathrm{w}^{q'} \in \operatorname{sgn} \mathcal{V}$ with $\operatorname{supp} \mathrm{w}^{q'} < \operatorname{supp} \mathrm{v}$ while $S(\mathrm{w}^{q'}, \mathrm{v}) = \emptyset$. This implies $\mathrm{w}^{q'} < \mathrm{v}$. □

In fact, the correspondence between vectors of minimal support and minimal sign in a linear subspace goes even further to have a natural bijection between pairs of minimal sign vectors $\{\mathrm{v}, -\mathrm{v}\}$ and their support vector $\operatorname{supp} \mathrm{v}$.

Lemma 3.7.4. *For a linear subspace $\mathcal{V} \subset \mathbb{R}^n$, consider the support map on sign vectors*

$$\operatorname{supp} : \{+, -, 0\}^n \to \{0, 1\}^n.$$

The pre-image of any minimal support vector in $\operatorname{supp} \mathcal{V} \subset \{0, 1\}^n$ through the support map is a pair $\{v, -v\}$ for some minimal sign vector v in $\operatorname{sgn} \mathcal{V} \subset \{+, -, 0\}^n$.

Proof. Let $\operatorname{supp} \boldsymbol{v}$ denote a minimal support vector in $\operatorname{supp} \mathcal{V}$. Let $\mathrm{v} = \operatorname{sgn} \boldsymbol{v}$, and then $\operatorname{supp} \mathrm{v} = \operatorname{supp}(-\mathrm{v}) = \operatorname{supp} \boldsymbol{v}$. Now we are left to show there are no other sign vectors in $\operatorname{sgn} \mathcal{V}$ with the same support. Let u be any sign vector in $\operatorname{sgn} \mathcal{V}$ with the same support, i.e. $\operatorname{supp} \mathrm{u} = \operatorname{supp} \mathrm{v}$. Because they have the same support, $\mathrm{u} \in \{\mathrm{v}, -\mathrm{v}\}$ is equivalent to $S(\mathrm{u}, \mathrm{v}) = \emptyset$ or $S(\mathrm{u}, -\mathrm{v}) = \emptyset$. Assume not, then there exists $j_+ \in S(\mathrm{u}, \mathrm{v})$ and $j_- \in S(\mathrm{u}, -\mathrm{v})$, $j_+ \neq j_-$. This implies $\mathrm{u}_{j_+} = -\mathrm{v}_{j_+} \neq 0$, while $\mathrm{u}_{j_-} = \mathrm{v}_{j_-} \neq 0$. Then we can form $\mathrm{w} \in \operatorname{sgn} \mathcal{V}$ that eliminates j_+ between u and v. This means $\operatorname{supp} \mathrm{w} \leq \operatorname{supp} \mathrm{u} = \operatorname{supp} \mathrm{v}$, while at the same time, $\mathrm{w}_{j_+} = 0$, so it has strictly smaller support. At the same time, it is not zero, because $\mathrm{w}_{j_-} = \mathrm{u}_{j_-} = \mathrm{v}_{j_-} \neq 0$. This contradicts that u and v are of minimal support. □

Now we show how to explicitly construct vectors with minimal sign in the stoichiometry subspace $\mathcal{S} = \operatorname{rowspan} \boldsymbol{N}$. Consider $\boldsymbol{N} \in \mathbb{R}^{r \times n}$ as a vector configuration of n column vectors $\{\boldsymbol{y}_1, \ldots, \boldsymbol{y}_n\}$ in $\mathbb{R}^r$. Then the (centered) zonotope of $\boldsymbol{N}$ can be equivalently defined in the following ways: as combinations of vectors, Minkowski sum of line segments, or linear image of a cube.

$$Z(\boldsymbol{N}) := \left\{ \boldsymbol{z} \in \mathbb{R}^r : \boldsymbol{z} = \sum_{i=1}^{n} \lambda_i \boldsymbol{y}_i, -1 \leq \lambda_i \leq 1 \right\} = \oplus_{i=1}^{n} [-\boldsymbol{y}_i, \boldsymbol{y}_i] = \boldsymbol{N} C_n,$$

where $\oplus$ denote Minkowski sum, $[-\boldsymbol{y}_i, \boldsymbol{y}_i]$ denote the line segment between $-\boldsymbol{y}_i$ and $\boldsymbol{y}_i$, and C_n denote the n-cube.

As shown in Corollary 7.17 of [123], there is a bijection between the facets of $Z(\boldsymbol{N})$ and the minimal sign vectors (called cocircuits) in $\operatorname{rowspan} \boldsymbol{N}$ (also see end of Section 3.3). Explicitly, any vector $\boldsymbol{u}$ in $\operatorname{rowspan} \boldsymbol{N}$ has unique coefficient vector $\boldsymbol{c} \in \mathbb{R}^r$ so that $\boldsymbol{N}^\intercal \boldsymbol{c} = \boldsymbol{u}$. We associate with $\boldsymbol{c}$, therefore $\boldsymbol{u}$, a face of $Z(\boldsymbol{N})$ defined by

$$Z(\boldsymbol{N})^{\boldsymbol{c}} := \left\{ \boldsymbol{z} \in Z(\boldsymbol{N}) : \boldsymbol{c}^\intercal \boldsymbol{z} = \max_{\boldsymbol{z}' \in Z(\boldsymbol{N})} \boldsymbol{c}^\intercal \boldsymbol{z}' \right\}.$$

The vector $\boldsymbol{u}$ has a minimal sign vector, therefore minimal support, if and only if the face $Z(\boldsymbol{N})^{\boldsymbol{c}}$ is a facet of $Z(\boldsymbol{N})$. This comes from the bijection between the face lattice of $Z(\boldsymbol{N})$ with the partial order of set inclusion, and the sign vectors of $\operatorname{rowspan} \boldsymbol{N}$ with the partial order on sign vectors. See Chapter 7.3 of [123] for details.

We can then obtain the minimal vectors as the vertices of the polar dual of the zonotope: $\operatorname{vert}\left\{ Z(\boldsymbol{N})^\Delta \right\}$, where Δ denote polar dual, because polar dual maps facets of $Z(\boldsymbol{N})$ to vertices of $Z(\boldsymbol{N})^\Delta$. Indeed, the polar dual of the face $Z(\boldsymbol{N})^{\boldsymbol{c}}$ is defined as

$$(Z(\boldsymbol{N})^{\boldsymbol{c}})^\diamond := \{\boldsymbol{y} \in \mathbb{R}^r : \boldsymbol{y}^\intercal \boldsymbol{z} \leq 1, \forall \boldsymbol{z} \in Z(\boldsymbol{N}); \text{ and } \boldsymbol{y}^\intercal \boldsymbol{z} = 1, \forall \boldsymbol{z} \in Z(\boldsymbol{N})^{\boldsymbol{c}}\}.$$

We see that

$$a^{-1}\boldsymbol{c} \in (Z(\boldsymbol{N})^c)^\diamond, \quad a := \max_{\boldsymbol{z}' \in Z(\boldsymbol{N})} \boldsymbol{c}^\intercal \boldsymbol{z}'.$$

For the case where $Z(\boldsymbol{N})^c$ is a facet, its polar dual $(Z(\boldsymbol{N})^c)^\diamond$ is a vertex. So it is a singleton set $\{a^{-1}\boldsymbol{c}\}$. Since the vector $a^{-1}\boldsymbol{c}$ is proportional to the coefficient vector of the minimal vector $\boldsymbol{u} \in \operatorname{rowspan} \boldsymbol{N}$, we can explicitly calculate the minimals vectors by

$$\operatorname{MINSUPP}(\mathcal{S}) = \operatorname{MINSUPP}(\operatorname{rowspan} \boldsymbol{N}) = \boldsymbol{N}^\intercal \operatorname{vert}\Big\{ Z(\boldsymbol{N})^\Delta \Big\}. \tag{3.48}$$

Now we combine this result with (3.47) to find minimal representations of x_{j^*} in terms of $\boldsymbol{x}$:

$$\begin{aligned} \operatorname{MINSUPP}(\boldsymbol{e}_{j^*} + \mathcal{S}) =& \boldsymbol{e}_{j^*} + \{0\} \cup \operatorname{MINSUPP}_{j^*}(\mathcal{S}) \\ =& \boldsymbol{e}_{j^*} + \{0\} \cup \Big\{ \boldsymbol{u} : \boldsymbol{u} \in \boldsymbol{N}^\intercal \operatorname{vert}\Big\{ Z(\boldsymbol{N})^\Delta \Big\}, u_{j^*} = -1 \Big\}. \end{aligned} \tag{3.49}$$

The above constitute the proof of the following theorem.

Theorem 3.7.5. *The minimal representations of x_{j^*} in terms of $\boldsymbol{x}$ in the equilibrium manifold $\mathcal{M}$ of a binding network with transpose-reduce stoichiometry matrix $\boldsymbol{N} \in \mathbb{R}^{d \times n}$ can be written as $\boldsymbol{x}_{j^*} = \boldsymbol{x}^{\boldsymbol{a}} \boldsymbol{k}^{\boldsymbol{b}}$, where $\boldsymbol{a}$ is contained in the set defined in (3.49), and for a given $\boldsymbol{a}$ vector, $\boldsymbol{b} \in \mathbb{R}^r$ can be computed from $(\boldsymbol{e}_{j^*} - \boldsymbol{a}) = \boldsymbol{N}^\intercal \boldsymbol{b}$.*

With this result, we can compute minimal representations of a given species simply by computing the vertices of a zonotope constructed from the transpose-reduced stoichiometry matrix $\boldsymbol{N}$. This can be implemented via linear programming for example, or using off-the-shelf packages such as SageMath [94] and the multi-parameteric toolbox [61]. In terms of computational complexity, we are asking for the vertices of a polytope given its facets, which has a computational complexity that is exponential in the number of facets (see page 80 of [20] and [14]). Since the polytope of concern here is the zonotope of the stoichiometry matrix $\boldsymbol{N}$, the number of facets is roughly n the number of species, therefore the complexity is exponential in n. This is intractable when n is large, but is a significant improvement over numerically scanning all solutions of polynomial systems of equations. A rough generic computational complexity for solving polynomial systems of equations is $O(\text{degree}^{\text{num.eqn.}})$, where degree is the degree of each equation and num.eqn. is the number of equations [62]. If there are r binding reactions, each corresponding to a degree 2 polynomial equation, then this is $O(2^r)$. It is often the case that r scales proportionally with n, so each numerical solution has exponential in n complexity. Let N denote the number of points to scan in the solution space, which satisfy $N \gg 2^n$ always so as to obtain the full regulatory

profile numerically. Then obtaining the full regulatory profile via numerical solutions of polynomial equations has complexity $O(N2^n)$. This is costly compared to $O(e^n)$ of solving for the vertices of the reaction order polyhedra directly using zonotopes. Recall that inverting a matrix of n dimensions has a cost of roughly $O(n^{2.3})$. Then numerically sampling the reaction order polyhedra using the log derivative formula incur a cost of $O(Nn^{2.3})$. This also improves over numerically solving the polynomial equations.

Minimal representations yield vertices

Recall that for a given (monomial) representation of x_{j^*} in terms of $\boldsymbol{x}$ of the form $x_{j^*} = \boldsymbol{x}^{\boldsymbol{a}}\boldsymbol{k}^{\boldsymbol{b}}$ to become a vertex, we also need $\boldsymbol{a}$ to have no more than d nonzero entries. Is this satisfied for all minimal representations we defined in previous subsections? The answer is yes by the following lemma for isomer-atomic binding networks.

Lemma 3.7.6. *Given an isomer-atomic binding network with d atomic species. Vectors of minimal support in $\mathcal{S}$ have at most $d+1$ nonzero entries. The minimal representations of x_{j^*} in terms of $\boldsymbol{x}$ have at most d nonzero entries.*

Proof. Argument via stoichiometrically atomic and then dimensionality counting. The second statement is implied by the first statement, because if a vector $\boldsymbol{u}$ in $\mathrm{MINSUPP}_{j^*}(\mathcal{S})$ has q nonzero entries, then $\boldsymbol{e}_{j^*} + \boldsymbol{u}$ has $q-1$ nonzero entries, since $u_{j^*} = -1$. So suffice to show $\mathrm{MINSUPP}(\mathcal{S})$ has at most $d+1$ nonzero entries.

$\boldsymbol{v} \in \mathcal{S}$ if and only if $\boldsymbol{L}\boldsymbol{v} = 0$, i.e. $\boldsymbol{v}^1 + \boldsymbol{L}_2\boldsymbol{v}^2 = 0$, where we split vector $\boldsymbol{v} \in \mathbb{R}^n$ into its first d entries $\boldsymbol{v}^1 \in \mathbb{R}^d$ and its last r entries $\boldsymbol{v}^2 \in \mathbb{R}^r$. So we have bijection between $\mathbb{R}^r$ and $\mathcal{S}$, which maps $\boldsymbol{c} \in \mathbb{R}^r$ to $\boldsymbol{v} \in \mathcal{S}$ defined by $\boldsymbol{v}^1 = -\boldsymbol{L}_2\boldsymbol{c}$ and $\boldsymbol{v}^2 = \boldsymbol{c}$. In other words,

$$\mathcal{S} = \left\{ \begin{bmatrix} -\boldsymbol{L}_2\boldsymbol{c} \\ \boldsymbol{c} \end{bmatrix} : \boldsymbol{c} \in \mathbb{R}^r \right\}.$$

We specify the zero pattern of a vector $\boldsymbol{v} \in \mathcal{S}$ by indices of zeros in $\boldsymbol{v}^1$, $\mathcal{I} = \{i = 1, \ldots, d : v_i^1 = 0\}$, and indices of nonzeros in $\boldsymbol{v}^2$, $\mathcal{J} = \left\{j = 1, \ldots, r : v_j^2 \neq 0\right\}$. Enforcing $v_i^1 = 0$ for $i \in \mathcal{I}$ then corresponds to $\boldsymbol{c}$ satisfying the system of linear equations $\boldsymbol{0} = \boldsymbol{L}_2^{\mathcal{I}}\boldsymbol{c}$, where $\boldsymbol{L}_2^{\mathcal{I}}$ is the submatrix with $\mathcal{I}$ rows from $\boldsymbol{L}_2$. Since $\boldsymbol{v}^2 = \boldsymbol{c}$, enforcing the zero pattern $\boldsymbol{v}_j^2 = 0$ for $j \notin \mathcal{J}$ then corresponds to restricting $\boldsymbol{c}$ to subspaces, so that the linear system of equations becomes $\boldsymbol{0} = \boldsymbol{L}_{2,\mathcal{J}}^{\mathcal{I}}\boldsymbol{c}_{\mathcal{J}}$, where $\boldsymbol{L}_{2,\mathcal{J}}^{\mathcal{I}}$ denote the submatrix of $\boldsymbol{L}_2$ with $\mathcal{I}$ rows and $\mathcal{J}$ columns, and $\boldsymbol{c}_{\mathcal{J}}$ denote the subvector of $\boldsymbol{c}$ with $\mathcal{J}$ entries. This problem has unique solution ($\boldsymbol{c}_{\mathcal{J}} = \boldsymbol{0}$) if $\boldsymbol{L}_{2,\mathcal{J}}^{\mathcal{I}}$ is full column rank, i.e. $|\mathcal{J}|$. It has infinitely many solutions, and therefore a nonzero solution, if $\boldsymbol{L}_{2,\mathcal{J}}^{\mathcal{I}}$ is not full column rank.

The above can be summarized into the following statement. There exists nonzero $\boldsymbol{v} \in \mathcal{S}$ such that $v_i^1 = 0$ for $i \in \mathcal{I}$ and $v_j^2 = 0$ for $j \notin \mathcal{J}$ if and only if $\boldsymbol{L}_{2,\mathcal{J}}^{\mathcal{I}}$ is not full column rank.

Note that for any $\mathcal{I}, \mathcal{J}$ such that $|\mathcal{J}| = |\mathcal{I}| + 1$, we have more columns than rows, which guarantees $\boldsymbol{L}_{2,\mathcal{J}}^{\mathcal{I}}$ is not full column rank, so there exists a nonzero vector $\boldsymbol{v} \in \mathcal{S}$ with the zero patterns specified by $\mathcal{I}$ and $\mathcal{J}$. Hence, vector $\boldsymbol{v} \in \mathcal{S}$ has minimal support implies its $\mathcal{I}$ and $\mathcal{J}$ satisfy $|\mathcal{J}| \leq |\mathcal{I}| + 1$.

For any vector $\boldsymbol{v} \in \mathcal{S}$ with zero pattern described by $\mathcal{I}$ and $\mathcal{J}$, the number of zeros in $\boldsymbol{v}^1$ is $|\mathcal{I}|$, and the number of zeros in $\boldsymbol{v}^2 = \boldsymbol{c}$ is $r - |\mathcal{J}|$. Together, the number of zeros of $\boldsymbol{v}$ is $r + |\mathcal{I}| - |\mathcal{J}|$. The number of nonzeros of $\boldsymbol{v}$ is $\mathrm{nnz}_v = d + |\mathcal{J}| - |\mathcal{I}|$, by $n = r + d$. If $\boldsymbol{v}$ has minimal support, then $|\mathcal{J}| \leq |\mathcal{I}| + 1$, so $\mathrm{nnz}_v \leq d + 1$. □

Note that $\boldsymbol{v}$ is minimal also implies $|\mathcal{J}| = q + 1$, where q is rank of $\boldsymbol{L}_{2,\mathcal{J}}^{\mathcal{I}}$. Because if not then $\boldsymbol{v}$ is nonzero, which implies $|\mathcal{J}| \geq q + 1$, so $|\mathcal{J}| \geq q + 2$. Eliminating a linearly dependent column yields $\mathcal{J}'$, which together with $\mathcal{I}$ corresponds to a vector $\boldsymbol{v}'$ that has smaller support than $\boldsymbol{v}$.

Examples

We illustrate our way of finding vertices developed in this section via one example.

Example 6 (two paths)**.**

$$A + B \rightleftharpoons C_{\mathrm{AB}}, \quad A + C \rightleftharpoons C_{\mathrm{AC}}, \quad C_{\mathrm{AB}} + C_{\mathrm{AC}} \rightleftharpoons C_{2\mathrm{ABC}} \tag{3.50}$$

Here A participates in the formation of $C_{2\mathrm{ABC}}$ through two paths, one through C_{AB}, and another through C_{AC}.

This network is stoichiometrically atomic. With the following species order, we have the stoichiometry and conservation law matrices as the following:

$$\boldsymbol{x} = (A, B, C, C_{\mathrm{AB}}, C_{\mathrm{AC}}, C_{2\mathrm{ABC}}),$$

$$\begin{bmatrix} \boldsymbol{L} \\ \boldsymbol{N} \end{bmatrix} = \left[\begin{array}{ccc|ccc} 1 & 0 & 0 & 1 & 1 & 2 \\ 0 & 1 & 0 & 1 & 0 & 1 \\ 0 & 0 & 1 & 0 & 1 & 1 \\ \hline -1 & -1 & 0 & 1 & 0 & 0 \\ -1 & 0 & -1 & 0 & 1 & 0 \\ 0 & 0 & 0 & -1 & -1 & 1 \end{array}\right]. \tag{3.51}$$

Consider species A for example. By inspection, we have $A \propto A$, $\frac{C_{\mathrm{AB}}}{B}$, $\frac{C_{\mathrm{AC}}}{C}$, $\left(\frac{C_{2\mathrm{ABC}}}{BC}\right)^{1/2}$, $\frac{C_{2\mathrm{ABC}}}{C_{\mathrm{AB}}C}$ and $\frac{C_{2\mathrm{ABC}}}{C_{\mathrm{AC}}B}$. We can find these minimal expressions from zonotope computation. The following is a implementation of the zonotope computation using SageMath in python.

```
import numpy as np
from sage.all import *
n_mat=np.array([[-1,-1,0,1,0,0],
            [-1,0,-1,0,1,0],
            [0,0,0,-1,-1,1]])
d,n=n_mat.shape
P1 = polytopes.parallelotope(n_mat.T)
P1dual = P1.polar()
cs=np.array(P1dual.Vrepresentation())
vs=cs.dot(n_mat)
idx=0 # index of A
ei=np.zeros(n)
ei[idx]=1
vs_idx=[i for i in range(len(vs)) if vs[i,idx]>0]
[ei-vs[i]/vs[i,idx] for i in vs_idx]
```

This code outputs the following vectors.

```
[array([ 0. , -0.5, -0.5,  0. ,  0. ,  0.5]),
 array([ 0., -1.,  0.,  0., -1.,  1.]),
 array([ 0., -1.,  0.,  1.,  0.,  0.]),
 array([ 0.,  0., -1., -1.,  0.,  1.]),
 array([ 0.,  0., -1.,  0.,  1.,  0.])]
```

We can check that indeed these correspond to the minimal representations we obtained by inspection. △

Vertices for the matrix of reaction orders

As we see in the analysis for one binding reaction in Section 3.6, especially Eq (3.42), that instead of studying the reaction order polyhedra of one species of interest for $\frac{\partial \log x_{j^*}}{\partial \log(\boldsymbol{t},\boldsymbol{k})}$, we can also obtain the reaction order polyhedra on the matrix for all species together for

$\frac{\partial \log \boldsymbol{x}}{\partial \log(\boldsymbol{t},\boldsymbol{k})}$. We provide a preliminary investigation into this using a similar approach as before. This problem is worth further investigation.

Similar to the case of reaction order vector of one species, a vertex happen for the reaction order matrix when d species of $\boldsymbol{x}$ dominates the totals $\boldsymbol{t}$, and there is a monomial relation of $\boldsymbol{x}$ in terms of the dominant $\boldsymbol{x}$ and $\boldsymbol{k}$. We can represent the condition that d species of $\boldsymbol{x}$ are dominant in $\boldsymbol{t}$ by the expression

$$\boldsymbol{P}_t \log \boldsymbol{x} \approx \log \boldsymbol{t}, \tag{3.52}$$

where $\boldsymbol{P}_t \in \mathbb{R}^{d\times n}$ is a projection matrix, with the ith row a basis vector $\boldsymbol{e}_{j_i} \in \mathbb{R}^n$ for some $j_i \in \{1,\dots,n\}$ and $i = 1,\dots,d$. The condition for the monomial relation then can be written as

$$\log \boldsymbol{x} = \boldsymbol{A}^\intercal \boldsymbol{P}_t \log \boldsymbol{x} + \boldsymbol{B}^\intercal \log \boldsymbol{k}, \tag{3.53}$$

where $\boldsymbol{A} \in \mathbb{R}^{d\times n}$, and $\boldsymbol{B} \in \mathbb{R}^{r\times n}$. We see that with these two conditions, we have

$$\frac{\partial \log \boldsymbol{x}}{\partial \log(\boldsymbol{t},\boldsymbol{k})} = \frac{\partial \log \boldsymbol{A}^\intercal \boldsymbol{P}_t \log \boldsymbol{x} + \boldsymbol{B} \log \boldsymbol{k}}{\partial \log(\boldsymbol{t},\boldsymbol{k})} \approx \frac{\partial \boldsymbol{A}^\intercal \log \boldsymbol{t} + \boldsymbol{B}^\intercal \log \boldsymbol{k}}{\partial(\log \boldsymbol{t}, \log \boldsymbol{k})} = \begin{bmatrix}\boldsymbol{A}^\intercal & \boldsymbol{B}^\intercal\end{bmatrix}.$$

So if these two conditions are satisfied, then we obtain a constant log derivative.

So to find vertices for reaction order matrix comes down to restricting what $\boldsymbol{A}$ and $\boldsymbol{P}_t$ can be. We note that Eq (3.7) can be written as

$$(\mathbf{I}_n - \boldsymbol{A}^\intercal \boldsymbol{P}_t) \log \boldsymbol{x} = \boldsymbol{B}^\intercal \log \boldsymbol{k} = \boldsymbol{B}^\intercal \boldsymbol{N} \log \boldsymbol{x},$$

where the last step used $\log \boldsymbol{k} = \boldsymbol{N} \log \boldsymbol{x}$ from conditions of equilibrium manifold. So we have

$$\mathbf{I} - \boldsymbol{A}^\intercal \boldsymbol{P}_t = \boldsymbol{B}^\intercal \boldsymbol{N}.$$

If we denote $\boldsymbol{V} = \boldsymbol{A}^\intercal \boldsymbol{P}_t$, then there exists some $\boldsymbol{B} \in \mathbb{R}^{r\times n}$ such that $\boldsymbol{V} = \boldsymbol{B}^\intercal \boldsymbol{N}$ corresponds to each row of $\mathbf{I} - \boldsymbol{V}$ is in $\operatorname{rowspan} \boldsymbol{N} = \mathcal{S}$. In other words,

$$\begin{aligned}&\Big\{\boldsymbol{V} \in \mathbb{R}^{n\times n} :\ \text{there exists } \boldsymbol{B} \in \mathbb{R}^{r\times n} \text{ such that } \mathbf{I} - \boldsymbol{V} = \boldsymbol{B}^\intercal \boldsymbol{N}\Big\}\\ =&\Big\{\boldsymbol{V} \in \mathbb{R}^{n\times n} : \boldsymbol{v}_j \in \boldsymbol{e}_j + \mathcal{S},\ \ j = 1,\dots,n\Big\},\end{aligned}$$

where $\boldsymbol{v}_j$ is the jth row of $\boldsymbol{V}$.

Now, what is the restriction on $\boldsymbol{V}$ from the fact that $\boldsymbol{V}$ actually $\boldsymbol{V} = \boldsymbol{A}^\intercal \boldsymbol{P}_t$ for some choice of $\boldsymbol{A}$ and projection matrix $\boldsymbol{P}_t^\intercal$. Since $\boldsymbol{P}_t$ is a projection matrix with ith row taking value $\boldsymbol{e}_{j_i}$, we have $\boldsymbol{A}^\intercal \boldsymbol{P}_t$ is just taking the row vectors of $\boldsymbol{A}$ and place them as column vectors, namely the ith row vector of $\boldsymbol{A}$ denoted $\boldsymbol{a}_i$ is mapped to the j_ith column of $\boldsymbol{A}^\intercal \boldsymbol{P}_t$. So there are

exactly d nonzero columns of $\boldsymbol{A}^\intercal \boldsymbol{P}_t$. In other words, each row vector of $\boldsymbol{A}^\intercal \boldsymbol{P}_t$ has at most d nonzero entries, and this choice of d columns are the same for all rows. The converse is also true. If $\boldsymbol{V}$ has only d nonzero columns, then those columns define the projection matrix $\boldsymbol{P}_t$, and the submatrix formed by those columns as row vectors yield $\boldsymbol{A}$. So,

$$\begin{aligned}&\Big\{\boldsymbol{V} : \mathbf{I} - \boldsymbol{V} = \boldsymbol{B}^\intercal \boldsymbol{N}, \boldsymbol{V} = \boldsymbol{A}^\intercal \boldsymbol{P}_t, \text{ for some } \boldsymbol{B} \in \mathbb{R}^{r\times n}, \boldsymbol{A} \in \mathbb{R}^{d\times n}, \text{ projection } \boldsymbol{P}_t \in \mathbb{R}^{d\times n}\Big\}\\ =&\Big\{\boldsymbol{V} \in \mathbb{R}^{n\times n} : \boldsymbol{V} \text{ has } \leq d \text{ nonzero columns and } \boldsymbol{v}_j \in \boldsymbol{e}_j + \mathcal{S},\ \ j = 1, \ldots, n\Big\}.\end{aligned}$$

Since $\boldsymbol{v}_j \in \boldsymbol{e}_j + \mathcal{S}$, we can consider choices of $\boldsymbol{v}_j$ as minimal vectors of $\boldsymbol{e}_j + \mathcal{S}$. From the previous subsections we know how to compute $\mathrm{MINSUPP}(\boldsymbol{e}_j + \mathcal{S})$. From there, we can computationally search for $\boldsymbol{V}$ by trying all possible combinations of the minimal vectors.

As an example, consider the polyhedron from one binding reaction shown in Eq (3.42). We can find all the matrix vertices from scratch using the method developed here. Note that in this case $\mathrm{MINSUPP}\,\mathcal{S} = (1, 1, -1)$. So $\mathrm{MINSUPP}(\boldsymbol{e}_1 + \mathcal{S}) = \{(1, 0, 0), (0, -1, 1)\}$, $\mathrm{MINSUPP}(\boldsymbol{e}_2 + \mathcal{S}) = \{(0, 1, 0), (-1, 0, 1)\}$, and $\mathrm{MINSUPP}(\boldsymbol{e}_3 + \mathcal{S}) = \{(0, 0, 1), (1, 1, 0)\}$. So each row $\boldsymbol{v}_i$ has two choices, yielding eight possible combinations to form the $\boldsymbol{V}$ matrix, listed below:

$$\begin{bmatrix}1&0&0\\0&1&0\\0&0&1\end{bmatrix}, \begin{bmatrix}0&-1&1\\0&1&0\\0&0&1\end{bmatrix}, \begin{bmatrix}1&0&0\\-1&0&1\\0&0&1\end{bmatrix}, \begin{bmatrix}1&0&0\\0&1&0\\1&1&0\end{bmatrix}, \begin{bmatrix}0&-1&1\\-1&0&1\\0&0&1\end{bmatrix}, \begin{bmatrix}0&-1&1\\0&1&0\\1&1&0\end{bmatrix}, \begin{bmatrix}1&0&0\\-1&0&1\\1&1&0\end{bmatrix}, \begin{bmatrix}0&-1&1\\-1&0&1\\1&1&0\end{bmatrix}.$$

Requiring that no more than two columns of $\boldsymbol{V}$ are nonzero eliminates all but the 2nd to 4th. These are exactly the vertices in Eq (3.42).

An interesting question worth further studying is whether we can capture the rays as well.

Relation to other problems

Our analysis in this section showed that the problem of finding minimal representations of a species x_{j^*} in terms of other species on the equilibrium manifold comes down to finding the minimal (sparsest) vectors of a linear subspace. This problem of finding sparse vectors of a linear subspace is also studied in numerical linear algebra and other biological applications such as stoichiometry computation of metabolism. The problem of finding sparse vectors of a matrix's null space is studied in [29] and [52]. They studied the complexity and equivalent formulations of this problem, as well as finding optimal solutions by greedy algorithms. [19] applied this problem to the study of metabolic network stoichiometry and computed the solution via mixed integer linear programs. In

this context, sparse basis vectors of the metabolic stoichiometry matrix can be considered as biologically meaningful pathways within the network. The general use of pathways in metabolic analysis is also discussed in Chapters 12, 13 and Part III of [85]. Our analysis in this section provided new contributions to this problem by linking it to vertices and facets of zonotopes, therefore revealing the combinatoric and geometric structure underlying this problem. The zonotopes also provide a direct geometric algorithm to compute such problems.

3.8 Polyhedra from decomposition of log derivative operators

Here we show that the range of reaction orders in a binding network can be mapped to relations among log derivative operators, enabling a direct calculus for reaction order polyhedra. This also reveals that the reason reaction orders take polyhedral shape is deeply rooted in the calculus rules for positive variables.

Motivation and demonstration through a scalar variable example

To illustrate the main ideas and techniques in the process of calculation done below, here we first motivate and demonstrate through a simple example in the scalar case.

Consider a dimerization reaction, $2X_1 \rightleftharpoons X_2$, two molecules of X-monomer, X_1, form a X-dimer molecule X_2. So the total number of X molecules is $t_X = X_1 + 2X_2$. Assume the dimer has useful catalytic functions, we would like to study how adding or removing X molecules would change the number of X_2 molecules. This could be characterized in terms of reaction order, or log derivative, or X_2 in t_X.

Since this is a scalar case, we could calculate this by brute force. Let k be the dimerization binding constant, so the steady state equation from the binding reaction is $kx_2 = x_1^2$, where x_1 denote the concentration of X monomer. Geometrically, this steady state equation can be considered as restricting the two variables (x_1, x_2) on a one-dimensional manifold parameterized by a variable x, such that $x_1 = x$ and $x_2 = k^{-1}x^2$. Apply this parameterization to the calculation of reaction order, we have

$$\begin{aligned}\frac{d\log x_2}{d\log t_X} =& \frac{d\log k^{-1}x^2}{d\log(x+2k^{-1}x^2)} = 2\frac{d\log x}{d\log(x+2k^{-1}x^2)} = 2\left(\frac{d\log(x+2k^{-1}x^2)}{d\log x}\right)^{-1}\\ =& 2\left(\frac{x}{x+2k^{-1}x^2}\frac{d\log x}{d\log x} + \frac{2k^{-1}x^2}{x+2k^{-1}x^2}\frac{d\log 2k^{-1}x^2}{d\log x}\right)^{-1}\\ =& 2\left(\frac{x}{x+2k^{-1}x^2} + 2\frac{2k^{-1}x^2}{x+2k^{-1}x^2}\right)^{-1} = 2\frac{x+2k^{-1}x^2}{x+4k^{-1}x^2}.\end{aligned}$$

We see that as x increases from 0 to $+\infty$, this reaction order goes from 2 to 1. This makes intuitive sense as well. The dimer fraction in this monomer-dimer mixture is $\frac{x_2}{t_X} = \frac{k^{-1}x^2}{x+2k^{-1}x^2} = \frac{x}{k+2x}$, which increases monotonically with x. So as x increases, the dimer fraction becomes higher. When x is very low, almost all of t_X, the total of X molecules, are in monomer form. Therefore the added X molecules almost all goes into monomer form, with dimer increasing according to the steady state equation $x_2 = k^{-1}x^2 \approx k^{-1}t_X^2$. As a result, the reaction order is 2, so 10-times higher t_X causes 100-times higher x_2. When x is very high, almost all of t_X is in dimer form already. So added X molecules directly go into dimer form, resulting in $x_2 \approx \frac{1}{2}t_X$. Hence reaction order is 1, with 10-times higher t_X causing 10-times higher x_2.

Although we obtained a sensible result after the calculations of the reaction order, we see that the intuition should be directly representable in the calculation. Even without knowing the details, we see that reaction order should be in the interval $[1, 2]$, with 2 reached with low dimer fraction, and 1 reached in high dimer fraction, with in-between dimer fraction reaching in-between reaction order values. In other words, we should be able to write

$$\frac{d\log x_2}{d\log t_X} = \frac{d\log x_2}{d\log x_1 + 2x_2} = \alpha_1 \frac{d\log x_2}{d\log x_1} + \alpha_2 \frac{d\log x_2}{d\log x_2} = \alpha_1 \cdot 2 + \alpha_2 \cdot 1,$$

for some convex coefficients α_1 and α_2, with α_1 close to 1 when the mixture is mostly monomers, and α_2 close to 1 when the mixture is mostly dimers.

In order to accomplish this kind of calculation, we are decomposing a sum in the coordinate variable to be differentiated with respect to. Namely, in the above case, we want to write a log derivative with respect to $t_X = x_1 + 2x_2$ into a convex combination of log derivative to x_1 and log derivative to x_2. This corresponds to a *decomposition of log derivative operators*. A decomposition operation like this is different from the typical interaction between sums and differentiation, where the sum is in the function to be differentiated. For example, we know derivative exchange with sums by linearity: $D(f_1 + f_2) = Df_1 + Df_2$, for some derivative operator D. We also know for log derivative operators $\tilde{D}$, we have simple convex combinations from sums: $\tilde{D}(f_1+f_2) = \frac{f_1}{f_1+f_2}\tilde{D}f_1 + \frac{f_2}{f_1+f_2}\tilde{D}f_2$. But in the case discussed above, we are decomposing sums in the coordinate variable instead. For linear derivatives, the behavior of decomposing functions is drastically different from decomposing coordinates. For log derivatives, they both results in convex combinations, although with different convex coefficients. This is discussed in more detail in Theorem 3.8.2 and the following remarks, where we show how to do this decomposition in multivariate case.

Here, we continue to think about how to perform this decomposition in this scalar, or one-dimensional manifold case.

For a positive scalar function f on a one dimensional manifold embedded in $\mathbb{R}^2_{>0}$, with x_1 and x_2 as the basis variables for $\mathbb{R}^2_{>0}$, we have

$$\frac{\partial \log f}{\partial \log(x_1+x_2)} = \left(\frac{\partial \log(x_1+x_2)}{\partial \log f}\right)^{-1} = \left(\frac{x_1}{x_1+x_2}\frac{\partial \log x_1}{\partial \log f} + \frac{x_2}{x_1+x_2}\frac{\partial \log x_2}{\partial \log f}\right)^{-1}.$$

Denote $H_1 = \frac{\partial \log f}{\partial \log x_1}$ and $H_2 = \frac{\partial \log f}{\partial \log x_2}$, $\lambda_1 = \frac{x_1}{x_1+x_2}$ and $\lambda_2 = \frac{x_2}{x_1+x_2}$, then

$$\frac{\partial \log f}{\partial \log(x_1+x_2)} = \left(\lambda_1 H_1^{-1} + \lambda_2 H_2^{-1}\right)^{-1} = \left(H_1^{-1} + \lambda_2\left(H_2^{-1} - H_1^{-1}\right)\right)^{-1}.$$

We see from this expression that there is a regularity condition required for the reaction orders H_1 and H_2 to guarantee our calculation above is valid: they must have the same sign, so that the $H_1^{-1} + \lambda_2\left(H_2^{-1} - H_1^{-1}\right)$ can be inverted for all λ_2 between 0 and 1. We assume this for the the discussion here, although this condition is slightly relaxed in our general result later to include the singular case, which corresponds to reaction order 0 here.

Recall that the goal is to obtain a formula like

$$\frac{\partial \log f}{\partial \log(x_1+x_2)} = \alpha_1 \frac{\partial \log f}{\partial \log x_1} + \alpha_2 \frac{\partial \log f}{\partial \log x_2} = \alpha_1 H_1 + \alpha_2 H_2.$$

Therefore we are facing a problem of relating $\left(H_1^{-1} + \lambda_2\left(H_2^{-1} - H_1^{-1}\right)\right)^{-1}$ with $\alpha_1 H_1 + \alpha_2 H_2$ for some convex coefficients α_1 and α_2. One nice result on this is the Sherman-Morrison formula, which we use to prove the general case. Here in the scalar case, the formula can be shown by a simple direct calculation. Denote $b = H_2^{-1} - H_1^{-1}$, then

$$\frac{1}{H_1^{-1} + \lambda_2 b} = \frac{H_1}{1+\lambda_2 b H_1} = \frac{H_1 + \lambda_2 b H_1^2 - \lambda_2 b H_1^2}{1+\lambda_2 b H_1} = H_1 - \frac{\lambda_2 b H_1^2}{1+\lambda_2 b H_1}.$$

Now this is in a form closer to our goal to write it as $\alpha_1 H_1 + \alpha_2 H_2$. Note that when we take $\lambda_2 = 1$, we have $H_2 = (H_1^{-1} + (H_2^{-1} - H_1^{-1}))^{-1} = (H_1^{-1} + b)^{-1} = H_1 - \frac{bH_1^2}{1+bH_1}$. Now apply this to have

$$\alpha_1 H_1 + \alpha_2 H_2 = \alpha_1 H_1 + \alpha_2\left(H_1 - \frac{bH_1^2}{1+bH_1}\right) = H_1 - \alpha_2 \frac{bH_1^2}{1+bH_1},$$

where we used α_1 and α_2 should be convex coefficients, therefore sum to 1. Now compare this form to what we just obtained, we see how the coefficients should be related to λ_1 and λ_2:

$$\alpha_1 = \frac{\lambda_1}{\lambda_1 + \lambda_2 \frac{H_1}{H_2}}, \quad \alpha_2 = \lambda_2 \frac{1+bH_1}{1+\lambda_2 b H_1} = \frac{\lambda_2(1+bH_1)}{\lambda_1 + \lambda_2(1+bH_1)} = \frac{\lambda_2 \frac{H_1}{H_2}}{\lambda_1 + \lambda_2 \frac{H_1}{H_2}}.$$

Here we used $1 + bH_1 = \frac{H_1}{H_2} =$. This completes our derivation for how to decompose a log derivative operator, or write $\frac{\partial \log f}{\partial \log(x_1+x_2)}$ in terms of a convex combination of $\frac{\partial \log f}{\partial \log x_1}$ and $\frac{\partial \log f}{\partial \log x_2}$.

Now we can apply this to the motivating example of monomer-dimer mixture. We have justified writing the following formula directly,

$$\frac{d\log x_2}{d\log t_X} = \frac{d\log x_2}{d\log x_1 + 2x_2} = \alpha_1 \frac{d\log x_2}{d\log x_1} + \alpha_2 \frac{d\log x_2}{d\log x_2} = \alpha_1 \cdot 2 + \alpha_2 \cdot 1,$$

with the α_1 and α_2 specified as follows:

$$\alpha_1 = \frac{x_1}{x_1 + 4x_2} = \frac{x}{x + 4k^{-1}x^2}, \qquad \alpha_2 = \frac{4x_2}{x_1 + 4x_2} = \frac{4k^{-1}x^2}{x + 4k^{-1}x^2},$$

by applying the formula we obtained, and recalling that in this monomer-dimer case $\lambda_1 = \frac{x_1}{t_X} = \frac{x_1}{x_1+2x_2}$, and $\lambda_2 = \frac{x_2}{t_X} = \frac{2x_2}{x_1+2x_2}$. A quick check shows that this is indeed a convex combination expression for the reaction order formula we obtained by brute-force calculation.

This motivating example shows why we would want to do log derivative operator decomposition: to directly obtain reaction orders with respect to totals as convex combination of simpler reaction orders, without complicated calculations. In other words, the goal of log derivative operator decomposition is to reveal the inherent polyhedral structure in reaction orders. The decomposition method shown in this scalar case is also a walk-through of the ideas used to prove the formula in the multivariate case below: using Sherman-Morrison formula to write inverses as convex combinations. The regularity condition on the reaction orders also carry through. Recall that we required H_0 and H_1 to have the same sign to make the reaction order decomposition possible. Indeed, if this is not satisfied, such as when $x_1x_2 = 1$, then the decomposition does not result in a convex combination. Namely, the coefficient α_1 can become negative. Now we are well prepared to tackle the multivariate case.

Multivariate case

We begin with one lemma on matrix inversion that shows inverting the line segment between two invertible matrices that differ by a rank-one change results in a line segment between the inverse of the two matrices. In the singular case, this results in a ray.

Lemma 3.8.1 (Inverse of a rank-1 change to identity matrix)**.** *Consider* $\boldsymbol{A}(\lambda) := \mathbf{I} + \lambda \boldsymbol{u}\boldsymbol{v}^\intercal$ *for* $\lambda \in [0, 1]$*, so* $\boldsymbol{A}(0) = \mathbf{I}$*,* $\boldsymbol{A}(1) = \mathbf{I} + \boldsymbol{u}\boldsymbol{v}^\intercal$*.*

1. *If* $\det \boldsymbol{A}(1) = 1 + \boldsymbol{v}^\intercal \boldsymbol{u} > 0$, *then*

$$\boldsymbol{A}(\lambda)^{-1} = \alpha_0 \boldsymbol{A}(0)^{-1} + \alpha_1 \boldsymbol{A}(1)^{-1}, \quad \alpha_0 = \frac{\lambda_0}{\lambda_0 + \lambda(1 + \boldsymbol{v}^\intercal \boldsymbol{u})}, \ \alpha_0 + \alpha_1 = 1, \tag{3.54}$$

   where $\lambda_0 = 1 - \lambda$, $\lambda \in [0, 1]$.

2. *If* $\det \boldsymbol{A}(1) = 1 + \boldsymbol{v}^\intercal \boldsymbol{u} = 0$, *then*

$$\boldsymbol{A}(\lambda)^{-1} = \boldsymbol{A}(0)^{-1} - \beta \boldsymbol{u}\boldsymbol{v}^\intercal, \quad \beta = \frac{\lambda}{1 - \lambda}, \tag{3.55}$$

   where $\lambda \in [0, 1)$.

Proof. Note that $\det \boldsymbol{A}(1) = 1 + \boldsymbol{v}^\intercal \boldsymbol{u} \geq 0$ guarantees $\det \boldsymbol{A}(\lambda) = 1 + \lambda \boldsymbol{v}^\intercal \boldsymbol{u} > 0$ for all $\lambda \in [0, 1)$. Therefore for every $\lambda < 1$, the matrix $\boldsymbol{A}(\lambda)$ is invertible.

For 1. If $\det \boldsymbol{A}(1) > 0$, we can apply Sherman-Morrison formula to obtain

$$\begin{aligned}
\boldsymbol{A}(\lambda)^{-1} &= \mathbf{I} - \frac{\lambda}{1 + \lambda \boldsymbol{v}^\intercal \boldsymbol{u}} \boldsymbol{u}\boldsymbol{v}^\intercal = \alpha_0 \mathbf{I} + \alpha_1 \mathbf{I} - \frac{1}{1 + \boldsymbol{v}^\intercal \boldsymbol{u}} \frac{\lambda(1 + \boldsymbol{v}^\intercal \boldsymbol{u})}{\lambda_0 + \lambda(1 + \boldsymbol{v}^\intercal \boldsymbol{u})} \boldsymbol{u}\boldsymbol{v}^\intercal \\
&= \alpha_0 \mathbf{I} + \alpha_1 \Big(\mathbf{I} - \frac{1}{1 + \boldsymbol{v}^\intercal \boldsymbol{u}} \boldsymbol{u}\boldsymbol{v}^\intercal \Big) = \alpha_0 \mathbf{I} + \alpha_1 \boldsymbol{A}(1)^{-1}.
\end{aligned}$$

For 2. Again apply Sherman Morrison formula and notice that $1 + \lambda \boldsymbol{v}^\intercal u = (1 - \lambda) + \lambda(1 + \boldsymbol{v}^\intercal \boldsymbol{u}) = 1 - \lambda$,

$$\boldsymbol{A}(\lambda)^{-1} = \mathbf{I} - \frac{\lambda}{1 + \lambda \boldsymbol{v}^\intercal \boldsymbol{u}} \boldsymbol{u}\boldsymbol{v}^\intercal = \mathbf{I} - \frac{\lambda}{1 - \lambda} \boldsymbol{u}\boldsymbol{v}^\intercal.$$

□

The previous lemma on matrix inversion has immediate implications in terms of change of coordinates for log derivative operators. For convenience, we denote $\tilde{D}_{\boldsymbol{\xi}}$ as the log derivative operator with respect to positive variables $\boldsymbol{\xi}$. For example, a positive function $f(\boldsymbol{\xi})$'s log derivative is $\tilde{D}_{\boldsymbol{\xi}} f := \frac{\partial \log f}{\partial \log \boldsymbol{\xi}}$. We also denote $\frac{\tilde{\partial}}{\tilde{\partial} \boldsymbol{\xi}} := \frac{\partial \log}{\partial \log \boldsymbol{\xi}}$ as the log derivative operator, same as $\tilde{D}_{\boldsymbol{\xi}}$.

Theorem 3.8.2 (Decomposition of log derivative operators)**.** *Consider positive variables* $(a, b, \boldsymbol{\xi}) \in \mathbb{R}^{n+1}_{>0}$ *on a* n*-dimensional smooth manifold. Define* $c_b = \frac{\tilde{\partial} b}{\tilde{\partial}_{a,\boldsymbol{\xi}}} \boldsymbol{e}_1$, $c_a = \frac{\tilde{\partial} a}{\tilde{\partial}_{b,\boldsymbol{\xi}}} \boldsymbol{e}_1$.

1. *If* $c_b > 0$, *then* $\tilde{D}_{a+b,\boldsymbol{\xi}} = \alpha_a \tilde{D}_{a,\boldsymbol{\xi}} + \alpha_b \tilde{D}_{b,\boldsymbol{\xi}}$, *where* $\alpha_a = \frac{a}{a + bc_b} = \frac{ac_a}{b + ac_a} > 0$, $\alpha_a + \alpha_b = 1$. *Also,* $c_a c_b = 1$.
2. *If* $c_b = 0$, *then* $\tilde{D}_{a+b,\boldsymbol{\xi}} = \tilde{D}_{a,\boldsymbol{\xi}} \Big(\mathbf{I} + \tau_b \boldsymbol{e}_1 \frac{\tilde{\partial} a/b}{\tilde{\partial}_{a,\boldsymbol{\xi}}} \Big)$, *where* $\tau_b = \frac{b}{a}$.

Proof. By chain rule,

$$\tilde{D}_{a+b,\boldsymbol{\xi}} = \tilde{D}_{a,\boldsymbol{\xi}}\left(\frac{\tilde{\partial} a+b, \boldsymbol{\xi}}{\tilde{\partial} a, \boldsymbol{\xi}}\right)^{-1} = \tilde{D}_{a,\boldsymbol{\xi}}\left(\frac{a}{a+b}\frac{\tilde{\partial} a, \boldsymbol{\xi}}{\tilde{\partial} a, \boldsymbol{\xi}} + \frac{b}{a+b}\frac{\tilde{\partial} b, \boldsymbol{\xi}}{\tilde{\partial} a, \boldsymbol{\xi}}\right)^{-1}$$
$$= \tilde{D}_{a,\boldsymbol{\xi}}\left(\mathbf{I} + \lambda_b \boldsymbol{e}_1 \frac{\tilde{\partial} b/a}{\tilde{\partial} a, \boldsymbol{\xi}}\right)^{-1},$$

where we defined $\lambda_b = \frac{b}{a+b}$. Consider $\boldsymbol{A}(\lambda_b) = \mathbf{I} + \lambda_b \boldsymbol{e}_1 \frac{\tilde{\partial} b/a}{\tilde{\partial} a, \boldsymbol{\xi}}$, we see $c_b = 1 + \frac{\tilde{\partial} b/a}{\tilde{\partial} a, \boldsymbol{\xi}} \boldsymbol{e}_1 = \det\left(\mathbf{I} + \boldsymbol{e}_1 \frac{\tilde{\partial} b/a}{\tilde{\partial} a, \boldsymbol{\xi}}\right)$. So $c_b > 0$ and $c_b = 0$ corresponds to the cases in the previous lemma. Applying the lemma gives the desired result. □

Theorem 3.8.2 shows that when the log derivative to the sum of two variables is decomposed into the log derivative to individual variables, convex combinations naturally arise. This is a surprising fact that is special about the calculus of positive variables. The variables are linearly summed, but the derivatives are in log scale. Without this exact combination, we do not have this nice convex decomposition. In the following remark, we show that happens if we do this decomposition for linear derivatives.

Remark 3.8.3 (Decomposition of linear derivatives). A similar but less clean decomposition is possible for linear derivatives. $\frac{\partial a+b, \boldsymbol{\xi}}{\partial a, \boldsymbol{\xi}} = \mathbf{I} + \boldsymbol{e}_1 \frac{\partial b}{\partial a, \boldsymbol{\xi}}$, so $\left(\frac{\partial a+b, \boldsymbol{\xi}}{\partial a, \boldsymbol{\xi}}\right)^{-1} = \mathbf{I} - \frac{1}{1+d}\boldsymbol{e}_1 \frac{\partial b}{\partial a, \boldsymbol{\xi}}$, where $d = \frac{\partial b}{\partial a, \boldsymbol{\xi}} \boldsymbol{e}_1$ is assumed to be positive. Similarly, since $\frac{\partial b, \boldsymbol{\xi}}{\partial a, \boldsymbol{\xi}} = \frac{\partial a+b, \boldsymbol{\xi}}{\partial a, \boldsymbol{\xi}} - \boldsymbol{E}_{11} = \mathbf{I} + \boldsymbol{e}_1\left(\frac{\partial b}{\partial a, \boldsymbol{\xi}} - \boldsymbol{e}_1\right)$, we obtain $\left(\frac{\partial b, \boldsymbol{\xi}}{\partial a, \boldsymbol{\xi}}\right)^{-1} = \mathbf{I} - \frac{1}{d}\left(\boldsymbol{e}_1 \frac{\partial b}{\partial a, \boldsymbol{\xi}} - \boldsymbol{E}_{11}\right)$. So $\left(\frac{\partial a+b, \boldsymbol{\xi}}{\partial a, \boldsymbol{\xi}}\right)^{-1} = \frac{1}{1+d}\mathbf{I} + \frac{d}{1+d}\left(\mathbf{I} - \frac{1}{d}\boldsymbol{e}_1 \frac{\partial b}{\partial a, \boldsymbol{\xi}}\right) = \frac{1}{1+d}\mathbf{I} + \frac{d}{1+d}\left(\left(\frac{\partial b, \boldsymbol{\xi}}{\partial a, \boldsymbol{\xi}}\right)^{-1} - \frac{1}{d}\boldsymbol{E}_{11}\right) = \frac{1}{1+d}(\mathbf{I} - \boldsymbol{E}_{11}) + \frac{d}{1+d}\left(\frac{\partial b, \boldsymbol{\xi}}{\partial a, \boldsymbol{\xi}}\right)^{-1}$.

Therefore, the decomposition for linear derivatives is

$$D_{a+b,\boldsymbol{\xi}} = D_{a,\boldsymbol{\xi}}\left(\frac{\partial a+b, \boldsymbol{\xi}}{\partial a, \boldsymbol{\xi}}\right)^{-1} = \frac{1}{1+d} D_{a,\boldsymbol{\xi}}(\mathbf{I} - \boldsymbol{E}_{11}) + \frac{d}{1+d} D_{b,\boldsymbol{\xi}}.$$

So we have the extra term $\boldsymbol{E}_{11}$. So linear derivative operators decompose into the convex combination of component derivative operators with an extra term. △

We apply the decomposition method in Theorem 3.8.2 to the example of one binding reaction and compare with our previous results in Section 3.6.

Example 7. Consider a binding network consisting of just one binding reaction, labeled as $E + S \rightleftharpoons C$. See Section 3.6 for earlier analysis and more details on this network's

behaviors. We apply Theorem 3.8.2 to first decompose $t_S = S + C$, then $t_E = E + C$.

$$\begin{aligned}\frac{\tilde{\partial} C}{\tilde{\partial} t_E, t_S, K} &= \alpha_{\frac{S}{t_S}} \frac{\tilde{\partial} C}{\tilde{\partial} t_E, S, K} + \alpha_{\frac{C}{t_S}} \frac{\tilde{\partial} C}{\tilde{\partial} t_E, C, K} \\ &= \alpha_{\frac{S}{t_S}} \left(\alpha_{\frac{E}{t_E}, \frac{S}{t_S}} \frac{\tilde{\partial} C}{\tilde{\partial} E, S, K} + \alpha_{\frac{C}{t_E}, \frac{S}{t_S}} \frac{\tilde{\partial} C}{\tilde{\partial} C, S, K} \right) + \alpha_{\frac{C}{t_S}} \frac{\tilde{\partial} C}{\tilde{\partial} t_E, C, K} \\ &= \frac{1}{1 + e^{\frac{1}{1+s}}} \left(\frac{1}{1+s} \begin{bmatrix} 1 & 1 & -1 \end{bmatrix} + \frac{s}{1+s} \begin{bmatrix} 1 & 0 & 0 \end{bmatrix} \right) + \frac{e^{\frac{1}{1+s}}}{1 + e^{\frac{1}{1+s}}} \begin{bmatrix} 0 & 1 & 0 \end{bmatrix},\end{aligned}$$

where the last step used the steady state condition $C = \frac{ES}{K}$, α's are convex coefficients, $\alpha_{\frac{S}{t_S}} + \alpha_{\frac{C}{t_S}} = 1$, and $\alpha_{\frac{E}{t_E}, \frac{S}{t_S}} + \overset{\alpha_C t_E, \frac{S}{t_S}}{=} 1$. c_b for splitting E in t_E is $\frac{\tilde{\partial} C}{\tilde{\partial} E, S, k} \boldsymbol{e}_1 = 1$; c_b for splitting S in t_S is $\frac{\tilde{\partial} C}{\tilde{\partial} t_E, S, k} \boldsymbol{e}_2 = \frac{1}{1+s}$, since $C = \frac{S/k}{1+S/k} t_E$.

Similarly, we could decompose the t_E coordinate first, and then t_S.

$$\begin{aligned}\frac{\tilde{\partial} C}{\tilde{\partial} t_E, t_S, K} &= \alpha_{\frac{E}{t_E}} \frac{\tilde{\partial} C}{\tilde{\partial} E, t_S, K} + \alpha_{\frac{C}{t_E}} \frac{\tilde{\partial} C}{\tilde{\partial} C, t_S, K} \\ &= \alpha_{\frac{E}{t_E}} \left(\alpha_{\frac{S}{t_S}, \frac{E}{t_E}} \frac{\tilde{\partial} C}{\tilde{\partial} E, S, K} + \alpha_{\frac{C}{t_S}, \frac{E}{t_E}} \frac{\tilde{\partial} C}{\tilde{\partial} E, C, K} \right) + \alpha_{\frac{C}{t_E}} \frac{\tilde{\partial} C}{\tilde{\partial} C, t_S, K} \\ &= \frac{1}{1 + s^{\frac{1}{1+e}}} \left(\frac{1}{1+e} \begin{bmatrix} 1 & 1 & -1 \end{bmatrix} + \frac{e}{1+e} \begin{bmatrix} 0 & 1 & 0 \end{bmatrix} \right) + \frac{s^{\frac{1}{1+e}}}{1 + s^{\frac{1}{1+e}}} \begin{bmatrix} 1 & 0 & 0 \end{bmatrix}.\end{aligned}$$

Although the coefficients generated in the process are not necessarily the same, for example $\alpha_{\frac{S}{t_S}, \frac{E}{t_E}} \neq \alpha_{\frac{E}{t_E}, \frac{S}{t_S}}$, both decomposition processes simplify to the same expression, which is also the same as Eq (3.38).

$$\frac{\tilde{\partial} C}{\tilde{\partial} t_E, t_S, k} = \frac{1}{1+e+s} \begin{bmatrix} 1 & 1 & -1 \end{bmatrix} + \frac{e}{1+e+s} \begin{bmatrix} 0 & 1 & 0 \end{bmatrix} + \frac{s}{1+e+s} \begin{bmatrix} 1 & 0 & 0 \end{bmatrix}.$$

Such decomposition procedures can be interpreted as considering one at a time which species is dominant in the total. This is graphically illustrated in Figure 3.8. In each step, we perform a binary split according to Theorem 3.8.2 that considers one species is dominant in one of the totals, or the rest of the total are dominant. △

More generally, Theorem 3.8.2 enables a procedure to obtain the reaction order polyhedra through decomposition of log derivative operators. Since each decomposition corresponds to asking a coordinate variable $(a + b)$ whether a is dominant or b is dominant, we call this procedure the **dominance decomposition tree (DDT)**. The above example (and Figure 3.8) is one illustration of the DDT procedure.

Next we illustrate DDT with a more complicated example of two binding reactions.

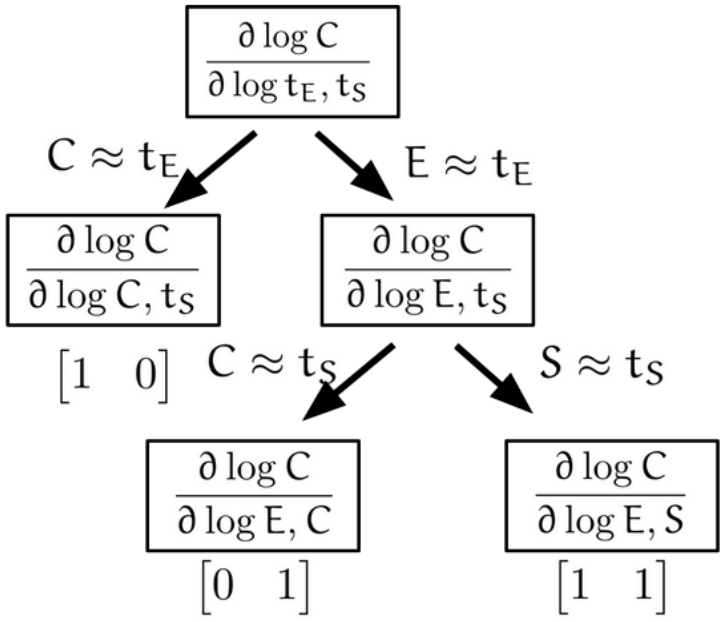

Figure 3.8 Graphical illustration of the dominance decomposition tree (DDT) procedure applied to the binding network of just one binding reaction.

Example 8 (stacked binding.)**.** Consider the following binding network with two binding reactions.

$$A + B \rightleftharpoons C_{AB}, \quad B + C \rightleftharpoons C_{ABC}.$$

This network is stoichiometry-atomic. With an atom-first ordering $(A, B, C, C_{AB}, C_{ABC})$, the atomic decomposition matrix $\boldsymbol{L}$ and transpose-reduced stoichiometry matrix $\boldsymbol{N}$ are

$$\begin{bmatrix} \boldsymbol{L} \\ \boldsymbol{N} \end{bmatrix} = \left[\begin{array}{ccccc} 1 & 0 & 0 & 1 & 1 \\ 0 & 1 & 0 & 1 & 1 \\ 0 & 0 & 1 & 0 & 1 \\ \hline 1 & 1 & 0 & -1 & 0 \\ 0 & 0 & 1 & 1 & -1. \end{array}\right]$$

We can biologically interpret this binding network as an activator's regulation of a gene. For example, A is a gene, with activating transcription factor B binding to it. The activator-gene complex C_{AB} then recruits the RNA polymerase C to form transcriptionially active complex C_{ABC}. From this interpretation, the active species is C_{ABC}, so we would like to know the reaction order of C_{ABC} to totals (t_A, t_B, t_C). This can be done via DDT as illustrated in Figure 2.4 in Chapter 2. △

While the DDT procedure, based on Theorem 3.8.2, guarantees that the polyhedron obtained from log derivative decompositions always contains the set of reaction orders,

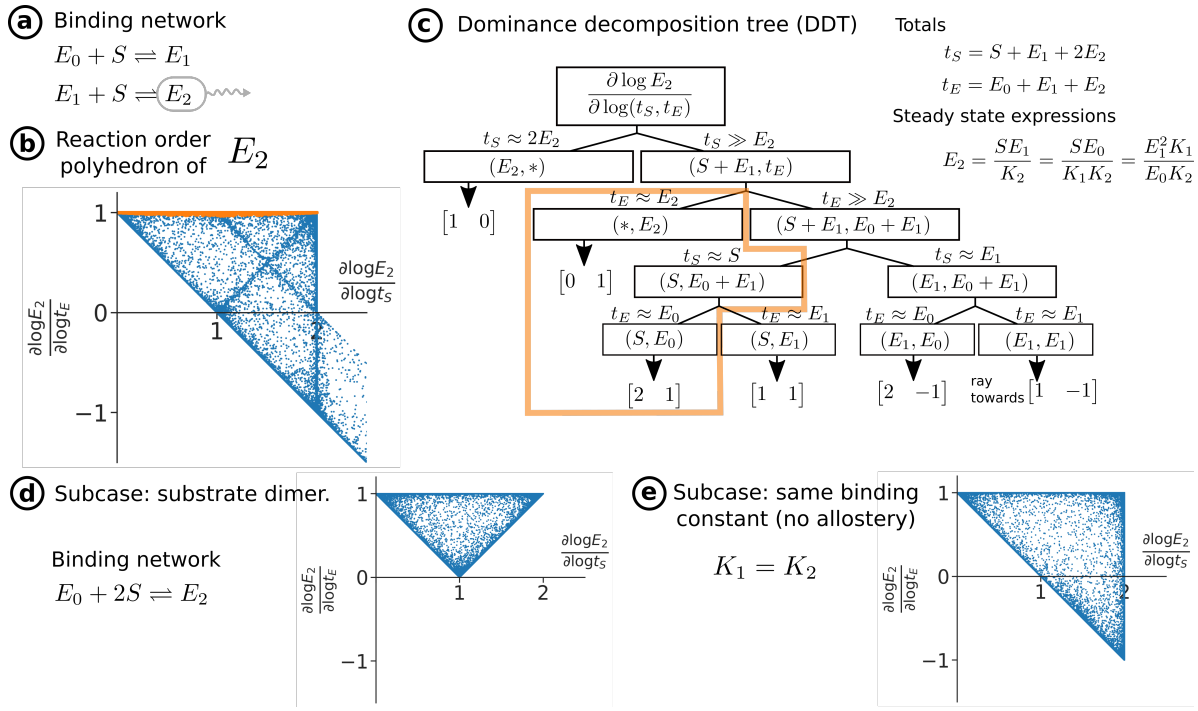

Figure 3.9 Enzyme allostery. **(a)** The binding network of this enzyme allostery example. **(b)** Computational sampling of the reaction order polyhedron of E_2. The edge colored orange corresponds to points with total substrate much higher than total enzyme. This edge corresponds to approximations from enzyme state counting, such as MWC models. **(c)** The DDT of E_2. The vertices circled by orange corresponds to the orange edge in (b). **(d)** The case where the two substrate molecules binds to the enzyme in one step is considered, with the computational sampling of the reaction order polyhedron of E_2 plotted. We see it is a strict subset of the reaction order polyhedron in (b). **(e)** Another subcase, where the same binding network as (a) is considered, but the binding constants are restricted to be the same. We see the resulting polyhedron is again a strict subset of (b), with only the ray disappeared. This implies the ray in (b) is only achievable through allostery, where the two binding constants are different.

it does not guarantee all points in the polyhedron from decomposition are reachable as reaction order at some point of the equilibrium manifold. In fact, the set of all possible reaction orders may not have a polyhedral shape to begin with, although it is always bounded in some polyhedron. We illustrate this with an example motivated by allostery.

Example 9 (allostery)**.** See Figure 3.9 for the binding network (a), sampled reaction order polyhedra (b), and DDT (c). We see that the system has a ray towards the $(1, -1)$ direction, but this ray does not extend from the $(2, 1)$ vertex for example, resulting in a "wedge" on the right side of the $(2, 0)$ and $(2, 1)$ edge that is not achievable. Because of this, the set of achievable reaction orders is a strict subset of the polyhedron obtained from taking convex combination of the vertices and rays from DDT. We can gain some intuitive understanding about this by inspecting the DDT. We see that the ray towards $(1, -1)$ corresponds to the $t_E \approx E_1$ dominance condition, which is the same as the $(1, 1)$ vertex and contradicts with the $(2, 1)$ vertex. This comes from the fact that the same substrate species S is used in

both binding reactions. If these two are distinct species, then we get back the polyhedron from the stacked binding, or activator example, which is fully achievable. We therefore conjecture that if each binding reaction adds a new species, then the achievable reaction orders form a polyhedral set. △

While the DDT procedure works well for small to medium sized examples, the decomposition could become complicated very quickly for larger problems. Also, there are more structures used in our log derivative decomposition than Theorem 3.8.2 included. Namely, we are decomposing positive linear combinations of the form $\boldsymbol{t} = \boldsymbol{L}\boldsymbol{x}$, instead of generic positive variables. Therefore, we would like to include this matrix structure into the problem to see whether we can solve larger problems.

Log derivative decomposition as a matrix operation

In our context of reaction orders in binding networks, the variables that we take log derivative with respect to are always positive combinations of chemical concentrations of the form $\boldsymbol{A}\boldsymbol{x}$, where $\boldsymbol{A}$ is a matrix with non-negative entries. Therefore we would like a clear association between log derivative decomposition and matrix operations. First, let us re-write Theorem 3.8.2 in our matrix context.

Lemma 3.8.4. *Given $\boldsymbol{A} \in \mathbb{R}^{d\times n}_{\geq 0}$, $d < n$, full row rank. Also given a row index $i \in \{1, \dots, d\}$ and a non-negative nonzero vector $\boldsymbol{b} \in \mathbb{R}^n_{\geq 0}$. Then, let $c = \frac{\tilde{\partial}\boldsymbol{b}^\intercal\boldsymbol{x}}{\tilde{\partial}\boldsymbol{A}\boldsymbol{x}}\boldsymbol{e}_i$.*

$$\tilde{D}_{(\boldsymbol{A}+\boldsymbol{e}_i\boldsymbol{b}^\intercal)\boldsymbol{x}} = \begin{cases} \alpha\tilde{D}_{\boldsymbol{A}\boldsymbol{x}} + \overline{\alpha}\tilde{D}_{(\boldsymbol{A}_{\setminus i}+\boldsymbol{e}_i\boldsymbol{b}^\intercal)\boldsymbol{x}}, & \text{if } c > 0; \\ \tilde{D}_{\boldsymbol{A}\boldsymbol{x}} + \tau\left(\tilde{D}_{\boldsymbol{A}\boldsymbol{x}}\right)_i\left(\boldsymbol{e}_i^\intercal - \frac{\tilde{\partial}\boldsymbol{b}^\intercal\boldsymbol{x}}{\tilde{\partial}\boldsymbol{A}\boldsymbol{x}}\right), & \text{if } c = 0, \end{cases} \tag{3.56}$$

where $\tau = \frac{\boldsymbol{b}_i^\intercal\boldsymbol{x}}{\boldsymbol{a}_i^\intercal\boldsymbol{x}}$, $\alpha = \frac{1}{1+\tau c}$, $\overline{\alpha} = 1 - \alpha$, and $\left(\tilde{D}_{\boldsymbol{A}\boldsymbol{x}}\right)_i$ denote the ith row of the matrix obtained when applied to a function.

One issue with the above lemma is that whether $c > 0$ or $c = 0$ seems to depend on $\boldsymbol{x}$ in general. To study when this is independent of $\boldsymbol{x}$, we have the following results.

Lemma 3.8.5. *Given $\boldsymbol{A} \in \mathbb{R}^{d\times n}$ a non-negative full-row-rank matrix, and $\boldsymbol{b}$ a nonzero nonnegative vector in $\mathbb{R}^n_{\geq 0}$. For each $\boldsymbol{x} \in \mathbb{R}^n_{>0}$, assume $\begin{bmatrix}\boldsymbol{A} \\ \frac{\partial \boldsymbol{k}}{\partial \boldsymbol{x}}\end{bmatrix}$ is invertible. Then*

$$\operatorname{sgn} c = \operatorname{sgn}\det\begin{bmatrix}\boldsymbol{B} \\ \frac{\partial \boldsymbol{k}}{\partial \boldsymbol{x}}\end{bmatrix},$$

where $\boldsymbol{B} = \boldsymbol{A}_{\setminus i} + \boldsymbol{e}_i\boldsymbol{b}^\intercal$.

Proof. We can calculate that

$$c = \frac{\tilde{\partial}\boldsymbol{b}^\intercal \boldsymbol{x}}{\tilde{\partial}\boldsymbol{A}\boldsymbol{x}, \boldsymbol{k}}\boldsymbol{e}_i = \frac{1}{\boldsymbol{b}^\intercal \boldsymbol{x}}\frac{\partial \boldsymbol{b}^\intercal \boldsymbol{x}}{\partial \boldsymbol{A}\boldsymbol{x}, \boldsymbol{k}}\begin{bmatrix}\boldsymbol{\Lambda}_{\boldsymbol{A}\boldsymbol{x}} & \boldsymbol{0}_{d\times r} \\ \boldsymbol{0}_{r\times d} & \boldsymbol{\Lambda}_{\boldsymbol{k}}\end{bmatrix}\boldsymbol{e}_i = \frac{\boldsymbol{a}_i^\intercal \boldsymbol{x}}{\boldsymbol{b}^\intercal \boldsymbol{x}}\boldsymbol{b}^\intercal \frac{\partial \boldsymbol{x}}{\partial \boldsymbol{A}\boldsymbol{x}, \boldsymbol{k}}\boldsymbol{e}_i$$
$$= \frac{\boldsymbol{a}_i^\intercal \boldsymbol{x}}{\boldsymbol{b}^\intercal \boldsymbol{x}}\boldsymbol{b}^\intercal \begin{bmatrix}\boldsymbol{A} \\ \frac{\partial \boldsymbol{k}}{\partial \boldsymbol{x}}\end{bmatrix}^{-1}\boldsymbol{e}_i,$$

because $\frac{\partial \boldsymbol{A}\boldsymbol{x}, \boldsymbol{k}}{\partial \boldsymbol{x}} = \begin{bmatrix}\boldsymbol{A} \\ \frac{\partial \boldsymbol{k}}{\partial \boldsymbol{x}}\end{bmatrix}$. Since $\boldsymbol{a}_i$ (the ith row of $\boldsymbol{A}$) and $\boldsymbol{b}$ are non-negative nonzero, $\frac{\boldsymbol{a}_i^\intercal \boldsymbol{x}}{\boldsymbol{b}^\intercal \boldsymbol{x}} > 0$. So $\operatorname{sgn} c = \operatorname{sgn} \boldsymbol{b}_i^\intercal \begin{bmatrix}\boldsymbol{A} \\ \frac{\partial \boldsymbol{k}}{\partial \boldsymbol{x}}\end{bmatrix}^{-1}\boldsymbol{e}_i$.

Now, $\begin{bmatrix}\boldsymbol{B} \\ \frac{\partial \boldsymbol{k}}{\partial \boldsymbol{x}}\end{bmatrix} = \begin{bmatrix}\boldsymbol{A} \\ \frac{\partial \boldsymbol{k}}{\partial \boldsymbol{x}}\end{bmatrix} + \boldsymbol{e}_i(\boldsymbol{b}_i^\intercal - \boldsymbol{a}_i^\intercal)$, so we have

$$\det \begin{bmatrix}\boldsymbol{B} \\ \frac{\partial \boldsymbol{k}}{\partial \boldsymbol{x}}\end{bmatrix} = (\boldsymbol{b}_i^\intercal - \boldsymbol{a}_i^\intercal)\begin{bmatrix}\boldsymbol{A} \\ \frac{\partial \boldsymbol{k}}{\partial \boldsymbol{x}}\end{bmatrix}^{-1}\boldsymbol{e}_i + 1 = \boldsymbol{b}_i^\intercal \begin{bmatrix}\boldsymbol{A} \\ \frac{\partial \boldsymbol{k}}{\partial \boldsymbol{x}}\end{bmatrix}^{-1}\boldsymbol{e}_i,$$

by noticing $1 = \boldsymbol{e}_i^\intercal \begin{bmatrix}\boldsymbol{A} \\ \frac{\partial \boldsymbol{k}}{\partial \boldsymbol{x}}\end{bmatrix}\begin{bmatrix}\boldsymbol{A} \\ \frac{\partial \boldsymbol{k}}{\partial \boldsymbol{x}}\end{bmatrix}^{-1}\boldsymbol{e}_i = \boldsymbol{a}_i^\intercal \begin{bmatrix}\boldsymbol{A} \\ \frac{\partial \boldsymbol{k}}{\partial \boldsymbol{x}}\end{bmatrix}\boldsymbol{e}_i$. □

Lemma 3.8.6. *For $\boldsymbol{x}$, a point in $\mathcal{M}$, the detailed balance steady state manifold of a binding network with rate constants vector $\boldsymbol{k}$,*

$$\operatorname{sgn} c = \operatorname{sgn} \det \begin{bmatrix}\boldsymbol{B}\boldsymbol{\Lambda}_{\boldsymbol{x}} \\ \boldsymbol{N}\end{bmatrix}.$$

Proof. A detailed balance binding network implies $\boldsymbol{N}\log \boldsymbol{x} = \log \boldsymbol{k}$, so $\frac{\tilde{\partial}\boldsymbol{k}}{\tilde{\partial}\boldsymbol{x}} = \boldsymbol{N}$. We get $\frac{\partial \boldsymbol{k}}{\partial \boldsymbol{x}} = \boldsymbol{\Lambda}_{\boldsymbol{k}}\frac{\tilde{\partial}\boldsymbol{k}}{\tilde{\partial}\boldsymbol{x}}\boldsymbol{\Lambda}_{\boldsymbol{x}}^{-1} = \boldsymbol{\Lambda}_{\boldsymbol{k}}\boldsymbol{N}\boldsymbol{\Lambda}_{\boldsymbol{x}}^{-1}$. So that $\begin{bmatrix}\boldsymbol{B} \\ \frac{\partial \boldsymbol{k}}{\partial \boldsymbol{x}}\end{bmatrix} = \begin{bmatrix}\boldsymbol{B} \\ \boldsymbol{\Lambda}_{\boldsymbol{k}}\boldsymbol{N}\boldsymbol{\Lambda}_{\boldsymbol{x}}^{-1}\end{bmatrix}$. Since $\begin{bmatrix}\boldsymbol{B} \\ \frac{\partial \boldsymbol{k}}{\partial \boldsymbol{x}}\end{bmatrix} = \begin{bmatrix}\boldsymbol{B} \\ \boldsymbol{\Lambda}_{\boldsymbol{k}}\boldsymbol{N}\boldsymbol{\Lambda}_{\boldsymbol{x}}^{-1}\end{bmatrix} = \begin{bmatrix}\mathbf{I} & 0 \\ 0 & \boldsymbol{\Lambda}_{\boldsymbol{k}}\end{bmatrix}\begin{bmatrix}\boldsymbol{B}\boldsymbol{\Lambda}_{\boldsymbol{x}} \\ \boldsymbol{N}\end{bmatrix}\boldsymbol{\Lambda}_{\boldsymbol{x}}^{-1}$, we get the desired conclusion. □

Now we know whether the sign of c is independent of $\boldsymbol{x}$ depends on properties of the matrix $\boldsymbol{B}$. Recall from end of Section 3.4 on alternative charts. We see that exactly $\operatorname{sgn} c = \operatorname{sgn} \det \boldsymbol{M}(\boldsymbol{B})$. So $\operatorname{sgn} c = +$ is equivalent to $\boldsymbol{B} \in \mathcal{A}^+(\boldsymbol{N})$, i.e. $\boldsymbol{B}$ could form an alternative chart of $\mathcal{M}$, on the same connected component as $\boldsymbol{L}$.

Recall from end of Section 3.4 on alternative charts that given $\boldsymbol{A} \in \mathcal{A}^+(\boldsymbol{N})$, then any $\boldsymbol{S} \in \mathbb{R}^{d\times d}$ with positive determinant yields $\boldsymbol{S}\boldsymbol{A} \in \mathcal{A}^+(\boldsymbol{N})$ if $\boldsymbol{S}\boldsymbol{A}$ is non-negative in all of its

entries. Next we show that the matrix operation representing the step of changing one coordinate in log derivative coordinates are included in this case, so such operations do not go out of $\mathcal{A}^+(\boldsymbol{N})$.

Proposition 3.8.7. *Given $\boldsymbol{A} \in \mathcal{A}^+(\boldsymbol{N})$. Define $\boldsymbol{A}' = \boldsymbol{A} + \boldsymbol{e}_i\boldsymbol{b}^\intercal$. Consider $\boldsymbol{B} = \boldsymbol{A}_{\setminus i} + \boldsymbol{e}_i\boldsymbol{b}^\intercal$. If $\boldsymbol{B}$ is not full row rank, or $\boldsymbol{B} \in \mathcal{A}^+(\boldsymbol{N})$, then $\boldsymbol{A}' \in \mathcal{A}^+(\boldsymbol{N})$.*

Proof. For simplicity of notation, let us fix $i = 1$ without loss of generality. If $\boldsymbol{B}$ is not full row rank, i.e. $\boldsymbol{b}^\intercal = \boldsymbol{\alpha}^\intercal\boldsymbol{A}$ for coefficient vector $\boldsymbol{\alpha}$ with $\alpha_1 = 0$, then $\boldsymbol{A}' = \boldsymbol{A} + \boldsymbol{e}_1\boldsymbol{b}^\intercal = (\mathbf{I} + \boldsymbol{e}_1\boldsymbol{\alpha}^\intercal)\boldsymbol{A}$. Since $\alpha_1 = 0$, we have $\det(\mathbf{I} + \boldsymbol{e}_1\boldsymbol{\alpha}^\intercal) = 1$. So $\boldsymbol{A}' \in \mathcal{A}^+(\boldsymbol{N})$.

If $\boldsymbol{B} \in \mathcal{A}^+(\boldsymbol{N})$. Then for each $\boldsymbol{x}$, we have coefficient vectors $\boldsymbol{\alpha}(\boldsymbol{x}) \in \mathbb{R}^d$ and $\boldsymbol{\beta}(\boldsymbol{x}) \in \mathbb{R}^r$, so that $\boldsymbol{b}^\intercal\boldsymbol{\Lambda}_{\boldsymbol{x}} = \boldsymbol{\alpha}^\intercal(\boldsymbol{x})\boldsymbol{A}\boldsymbol{\Lambda}_{\boldsymbol{x}} + \boldsymbol{\beta}^\intercal(\boldsymbol{x})\boldsymbol{N}$. This is because $\boldsymbol{A} \in \mathcal{A}^+(\boldsymbol{N})$, so rows of $\boldsymbol{A}\boldsymbol{\Lambda}_{\boldsymbol{x}}$ and rows of $\boldsymbol{N}$ form a basis of $\mathbb{R}^n$. Since $\boldsymbol{B} \in \mathcal{A}^+(\boldsymbol{N})$, we have $\alpha_1(\boldsymbol{x}) > 0$ for all $\boldsymbol{x}$. Indeed,

$$\begin{bmatrix} \boldsymbol{B}\boldsymbol{\Lambda}_{\boldsymbol{x}} \\ \boldsymbol{N} \end{bmatrix} = \begin{bmatrix} \boldsymbol{A}_{\setminus 1}\boldsymbol{\Lambda}_{\boldsymbol{x}} + \boldsymbol{e}_1\boldsymbol{b}^\intercal\boldsymbol{\Lambda}_{\boldsymbol{x}} \\ \boldsymbol{N} \end{bmatrix} = (\mathbf{I} - \boldsymbol{E}_{11} + \boldsymbol{e}_1\begin{bmatrix}\boldsymbol{\alpha}(\boldsymbol{x})^\intercal & \boldsymbol{\beta}(\boldsymbol{x})^\intercal\end{bmatrix})\begin{bmatrix} \boldsymbol{A}\boldsymbol{\Lambda}_{\boldsymbol{x}} \\ \boldsymbol{N} \end{bmatrix},$$

where $\boldsymbol{A}_{\setminus 1}$ is the matrix obtained by seting the first row of $\boldsymbol{A}$ to zero, and $\det(\mathbf{I} - \boldsymbol{E}_{11} + \boldsymbol{e}_1\begin{bmatrix}\boldsymbol{\alpha}(\boldsymbol{x})^\intercal & \boldsymbol{\beta}(\boldsymbol{x})^\intercal\end{bmatrix}) = \alpha_1(\boldsymbol{x})$.

The condition $\alpha_1(\boldsymbol{x}) > 0$ for all $\boldsymbol{x}$ then implies $\boldsymbol{A}' \in \mathcal{A}^+(\boldsymbol{N})$ with $\boldsymbol{A}' = \boldsymbol{A} + \boldsymbol{e}_1\boldsymbol{b}^\intercal$ because

$$\begin{bmatrix} \boldsymbol{A}'\boldsymbol{\Lambda}_{\boldsymbol{x}} \\ \boldsymbol{N} \end{bmatrix} = \begin{bmatrix} \boldsymbol{A}\boldsymbol{\Lambda}_{\boldsymbol{x}} + \boldsymbol{e}_1\boldsymbol{b}^\intercal\boldsymbol{\Lambda}_{\boldsymbol{x}} \\ \boldsymbol{N} \end{bmatrix} = (\mathbf{I} + \boldsymbol{e}_1\begin{bmatrix}\boldsymbol{\alpha}(\boldsymbol{x})^\intercal & \boldsymbol{\beta}(\boldsymbol{x})^\intercal\end{bmatrix})\begin{bmatrix} \boldsymbol{A}\boldsymbol{\Lambda}_{\boldsymbol{x}} \\ \boldsymbol{N} \end{bmatrix},$$

and $\det(\mathbf{I} + \boldsymbol{e}_1\begin{bmatrix}\boldsymbol{\alpha}(\boldsymbol{x})^\intercal & \boldsymbol{\beta}(\boldsymbol{x})^\intercal\end{bmatrix}) = 1 + \alpha_1(\boldsymbol{x}) > 1$. □

Right multiplications by positive diagonal matrices also leaves $\mathcal{A}^+(\boldsymbol{N})$ invariant.

Lemma 3.8.8. *$\boldsymbol{A} \in \mathcal{A}^\sigma(\boldsymbol{N})$, then $\boldsymbol{A}\boldsymbol{\Lambda}_{\boldsymbol{v}} \in \mathcal{A}^\sigma(\boldsymbol{N})$ for any positive diagonal matrix $\boldsymbol{\Lambda}_{\boldsymbol{v}}$ with diagonal vector $\boldsymbol{v} \in \mathbb{R}^n_{>0}$.*

Proof. For each $\boldsymbol{x}$, the matrix $\boldsymbol{A}\boldsymbol{\Lambda}_{\boldsymbol{v}}\boldsymbol{\Lambda}_{\boldsymbol{x}}$ can be expressed as $\boldsymbol{A}\boldsymbol{\Lambda}_{\boldsymbol{x}'}$, where $x'_j = v_j x_j > 0$. □

In summary, operations closed in $\mathcal{A}^+(\boldsymbol{N})$ include left multiplication by invertible matrix with positive determinant and right multiplication by positive diagonal matrices. In particular, this includes adding a vector from $\operatorname{rowspan}\boldsymbol{A}_{\setminus i}$ to the ith row of $\boldsymbol{A}$.

The above decomposition has shown that putting two matrices together in the decomposition steps preserves the regularity condition $c > 0$ for all $\boldsymbol{x}$.

Lemma 3.8.9. *Matrix addition $\boldsymbol{A} + \boldsymbol{e}_i\boldsymbol{b}$ has an equivalent log derivative interpretation. Define $c = \frac{\tilde{\partial}\boldsymbol{b}^\intercal\boldsymbol{x}}{\tilde{\partial}\boldsymbol{A}\boldsymbol{x}}\boldsymbol{e}_i$, $\tau = \frac{\boldsymbol{b}^\intercal\boldsymbol{x}}{\boldsymbol{a}_i^\intercal\boldsymbol{x}}$, $\alpha = \frac{1}{1+\tau c}$.*

1. *If $\boldsymbol{B} \in \mathcal{A}^+(\boldsymbol{N})$, then $c > 0$ for all $\boldsymbol{x}$, and $\boldsymbol{A} + \boldsymbol{e}_i\boldsymbol{b}$ means*

$$\tilde{D}_{(\boldsymbol{A}+\boldsymbol{e}_i\boldsymbol{b}^\intercal)\boldsymbol{x}} = \alpha\tilde{D}_{\boldsymbol{A}\boldsymbol{x}} + \overline{\alpha}\tilde{D}_{\boldsymbol{B}\boldsymbol{x}}. \tag{3.57}$$

2. *If $\boldsymbol{B}$ is not full row rank, then $c = 0$ for all $\boldsymbol{x}$, and $\boldsymbol{A} + \boldsymbol{e}_i\boldsymbol{b}$ means*

$$\tilde{D}_{(\boldsymbol{A}+\boldsymbol{e}_i\boldsymbol{b}^\intercal)\boldsymbol{x}} = \tilde{D}_{\boldsymbol{A}\boldsymbol{x}}\left(\mathbf{I} + \tau\boldsymbol{e}_i\frac{\tilde{\partial}\boldsymbol{a}_i^\intercal\boldsymbol{x}/\boldsymbol{b}^\intercal\boldsymbol{x}}{\tilde{\partial}\boldsymbol{A}\boldsymbol{x}}\right). \tag{3.58}$$

3.9 Summary

To build a mathematical foundation for equilibrium steady states of binding networks, we defined isomer-atomic binding networks that are biologically plausible and characterized their manifold of equilibrium steady states. When transforming between the different charts of the equilibrium manifold, we introduced log derivatives, which turned out to have significant biological meaning. Importantly, reaction orders, i.e. the log derivatives of active species with respect to totals, are bounded in polyhedral sets, with vertices and edges corresponding to robust regulatory regimes of catalysis activities. We then characterized the vertices in terms of vectors with minimal support in the stoichiometry subspace, and developed a computational method to compute them at scale using zonotopes. Lastly, we showed that polyhedral sets arise in reaction orders due to the fundamental reason that decomposition of log derivative operators yield convex combinations. This enables an analytical method called dominance decomposition tree (DDT) to obtain reaction order polyhedra.

Chapter 4

Flux exponent control in metabolism: biological regulation as control of flux exponents

4.1 Introduction

Microbial communities, from the gut microbiome to the soil rhizosphere, play a critical role in human health and well-being [67, 74, 82, 100]. In particular, we now understand that many pathologies are associated with undesired variations in the composition of the microbiome community [18, 101, 120]. It is therefore important that we understand the principles governing the dynamics of microbial community structure.

Despite the wealth of information cataloguing the composition of these communities, we are still far from understanding the governing principles of community dynamics. This is because the microbiomes relevant to human health and agriculture are extremely complex, consisting of many interactions across hierarchical spatiotemporal scales [68, 110]. The combinatorial space of possible interactions is so large that a purely phenomenological approach cannot succeed without a rigorous theoretical framework in which to interpret the data. It is therefore unsurprising that many microbiome scientists feel that they are 'drowning in data' [95, 114], as there is no unified conceptual framework in which to contextualize any given observation.

A theoretical framework that aims to provide such a conceptual basis, as well as to make predictions that can drive further understanding, must span interactions across hierarchical scales, from the molecular to the cellular to the ecological. In microbial communities,

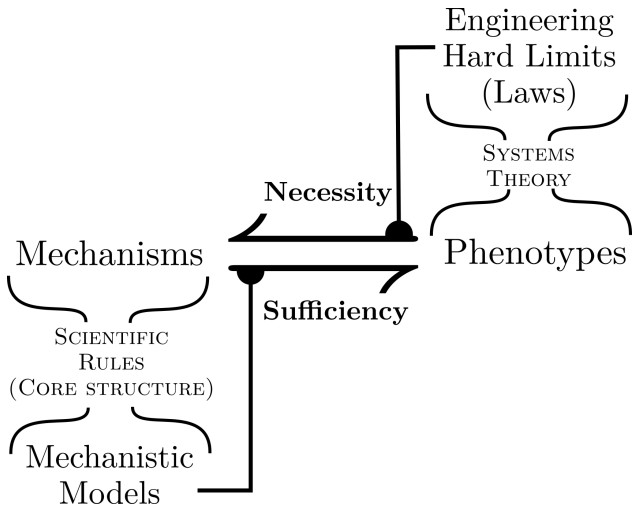

Figure 4.1 Diagram showing knowledge of biological systems split into mechanisms and phenotypes, and how they are mapped to each other. Mechanisms are system properties not varying for the timescale of concern, while phenotypes are system properties that are varying. From our knowledge about mechanisms, scientific rules can be summarized, often using the language of mathematics, to capture the core mechanistic structures. Such core structures can be used to systematically create models from knowledge about mechanisms. By analysis or simulation of these models we can demonstrate that a given mechanism is sufficient for phenotypes it exhibits. To map phenotypes back to mechanisms, mathematical abstractions for the class of systems is needed since phenotypes are behaviors on the system level. Systems theory captures the core structures on the system level, and derive hard limits or laws for given phenotypes. Such laws can then be used to capture necessary conditions on mechanisms for given phenotypes, providing a map via necessity in the reverse direction from phenotypes to mechanisms.

metabolism is the core process that bridges these scales. As an example, Terence Hwa and coworkers have used simple metabolic models to quantitatively explain dynamical phenomena in the growth of single-strain populations encountering various types of nutrient stress [42]. Recently, [66] showed that metabolic interactions can explain a bistable phenotype in a microbial community. Therefore, aiming towards understanding principles of microbial communities, we need a theoretical framework to understand the rules of metabolic regulation in a systematic fashion.

To understand rules of metabolic regulation, we could begin with modeling its dynamics. Metabolism dynamics is fundamentally hard to describe using the traditional mechanistic model approach such as Michaelis-Menten, where explicit equations are written down with many parameters to be identified through experiments. The complication is that while we can experimentally measure bulk metabolic fluxes at scale and characterize metabolite stoichiometry robustly, we lack systematic ways to observe the dynamic fluxes of intermediates in cells which depend on the concentrations of regulatory proteins [7].

To elaborate on the generality of this difficulty, we can consider our knowledge about biological systems as consisting of two types: mechanisms and phenotypes (see Figure

4.1), split according to timescale for a problem of concern. Mechanisms are physical and biochemical knowledge about a system that do not vary at the timescale of concern. Typical examples are size of a cell, elasticity of a tissue, atomic composition and structure of a protein molecule, and binding free energy of a receptor-ligand pair. Phenotypes are behaviors of a particular system in a specific scenario, which varies at the timescale of concern. Most experimental observations on an overall system is of this type, such as metabolic flux, metabolite concentration, gene expression profile, and enzyme numbers in a cell. I quickly emphasize that the split between mechanism and phenotype depends on the timescale of concern, with varying properties considered as phenotypes and non-varying ones as mechanisms. For example, cell size is mechanistic information for metabolism on minutes time scale, but it is a phenotype for cell growth or differentiation on hours to days time scale.

We usually determine that something about a specific system is understood when a phenotype can be clearly mapped to some mechanisms, and the mechanisms can clearly explain phenotypes. In other words, a necessary and sufficient (or if and only if) correspondence between phenotypes and mechanisms is established. Experimental investigations that connects the mechanisms and phenotypes, as in mechanistic perturbations such as gene knockouts, can provide a point-to-point correspondence between mechanisms and phenotypes. But this is all for a particular system, a particular mechanism, and a particular phenotype. When the mechanism involved has more sophisticated architecture or the phenotype has a large number of dimensions, this point-to-point mapping is insufficient. Also, we often want to understand rules governing a class of phenotypes that exists in many systems. To understand this then requires establishing a set-to-set correspondence that a set of mechanisms are necessary and sufficient for a class of phenotypes. Typically, the sufficiency is easier, since it can be obtained from accumulation of point-to-point investigations, while necessity is much harder, since this constitute statements that for a class of phenotypes, only certain mechanistic features matter, while all other details can be ignored.

Classically, set-to-set maps start with sufficient conditions for phenotypes that are obtained by building models based on mechanisms. Mechanistic knowledge are generalizable in the sense that it applies when this component is used in arbitrary contexts at the timescale of concern, even ones not observed before. Therefore, mechanisms can be used to build models that sufficiently demonstrate certain phenotypes, connecting mechanisms to phenotypes in the forward direction. To do so, scientific rules about these mechanisms can be summarized by formalizing the core structures involved, often in a mathematical

language. For example, biological organisms are often made of interacting cells, force and mass are core structures of mechanical systems, and stoichiometry and rate laws are core structures of chemical reactions. These scientific rules then can be viewed as the waist of an hourglass that systematically convert knowledge about mechanisms on the top into models on the bottom. Then by simulation or analysis, these models take a mechanism and demonstrate sufficient conditions for phenotypes this mechanism exhibits.

This forward approach providing sufficient maps from mechanisms to phenotypes via mechanistic models was often considered the major success in classical scientific research. This is because mechanistic knowledge is generalizable while phenotypic knowledge is less so. If they are accumulated at approximately the same rate, then mechanistic knowledge could yield more predictions and apply to more scenarios than just relying on phenotypes. However, the general difficulty of experimental investigations nowadays is the opposite: increasingly large data sets can be obtained for phenotypes by massively parallel methods, but knowledge about mechanisms accumulate slowly, forming a bottleneck. This is especially prevalent in biology, where massive screening, various kinds of omics (transcriptomics, proteomics and metabolomics), and other sequencing and droplets based methods have become the powerhouse of scientific progress. This makes phenotype data accumulate several orders faster than mechanism data, which is based on physical and biochemical approaches that does not yet scale. As a result, there is a shift from placing higher weight on mapping mechanism data to phenotypes in classical times to placing higher weight on mapping phenotype data back to understand mechanisms in recent decades. Another major driving force to this change is engineering. The foundation for engineering is a set of alternatives, or possible designs, to achieve a given system behavior, or phenotype. The desire for a large design space therefore places significant priority on the necessary conditions that mechanisms need to satisfy to achieve a phenotype, which can be used to bound the design space. However, the reverse direction, mapping phenotypes back to mechanisms through necessary conditions, requires a system level understanding that is distinct from the core structures or scientific rules. In particular, since phenotypes are behaviors on the system level, this requires a systems theory that captures the core system level structures and formulate hard limits, or laws, on system performance independent of component level details.

A system theory can be considered as the waist of an hourglass, that connects systems' phenotypes below to the hard limits and laws on top. One example is mechanical movements formulated as phenotypes of Hamiltonian or Lagrangian dynamical systems, deriving conservation of energy, mass, and momentum as hard limits or laws governing

these systems. Other examples are message transmission viewed as information channels with hard limits in terms of channel capacity, computation viewed as Turing machines with hard limits in terms of complexity and decidability, signal processing viewed as linear input output systems with hard reconstruction limits by Nyquist theorem, feedback control viewed as linear control systems with hard limits such as Bode's conservation of robustness, and exchange between work and heat viewed as thermal engines with hard limits such as Carnot's theorem and entropy maximization. These hard limits, or laws, obtained by the formulation of a systems theory, connect phenotypes or system behaviors with mechanisms in the reverse direction. For a given phenotype, the laws explain what properties of mechanisms are important, and what details do not matter. A phenotype can also be mapped back to mechanisms by laws to eliminate implausible mechanisms. In light of the explosion of phenotype data or the demand of engineering, we need more hard limits and laws to do the reverse mapping of constraining mechanisms based on phenotypes. This work proposes the scientific rules, or core structures, of biomolecular systems as binding and catalysis, with catalysis determining the direction of change, and binding regulating catalysis rates. In this chapter we further formulate a systems theory for biomolecular systems. Since binding's regulation of catalysis has reaction orders constrained in polyhedral sets, a biomolecular system can therefore be considered as a class of control systems, where the dynamics has fixed catalysis stoichiometry with controllers adjusting the exponents (or reaction orders) of the catalysis fluxes. This formulates a systems theory for biomolecular systems as flux exponent control (FEC). By formulating into a control system, FEC makes engineering hard limits or laws from control theory applicable to biomolecular dynamics including metabolism, and motivates discovery of further laws.

Let us now discuss this difficulty of knowing detailed mechanisms in the specific context of metabolic regulation. To illustrate concretely, let us take a simple enzymatic catalysis as an example:

$$E + S \rightleftharpoons C \xrightarrow{k} E + P.$$

Here the enzyme E catalyzes the conversion of substrate S into product P. This catalysis happens via an intermediate complex C formed by the enzyme binding with the substrate, and this binding reaction happens fast, reaching binding equilibrium. Written as a metabolic reaction, this has the following form:

$$(S_{\text{tot}}, P_{\text{tot}}) \xrightarrow{v=kC} (S_{\text{tot}} - 1, P_{\text{tot}} + 1),$$

so the change caused by this catalysis reaction is one less substrate, and one more product

molecule, while the rate or flux v of this reaction is $v = kC$, the catalysis rate constant k multiplying the concentration of intermediate complex C.

Given this metabolic network in cells, experimentally we can observe the concentrations of substrate and product molecules at the end of some duration and see the decrease in substrate is the same as the increas in product, therefore deducing the stoichiometry of $(-1, +1)$ for substrate and product molecules. However, the rate of this catalysis reaction over time, or how the rate depends on substrate and product concentrations, is still intractible to observe at scale in general. This is because observing this rate requires observing a time trajectory of substrate and product concentrations. The time trace of metabolites can be done for a selected few chemicals via isotope tracing or spectrometry, but time traces of many metabolites require chromotography and mass spectrometry at every time step, which becomes prohibitively expensive to do at scale. Furthermore, to have a model on regulation of reaction flux, i.e. how flux v depends on substrate and metabolite concentrations, we would require many time traces that cover a wide range of metabolite concentrations, which grows exponentially with the number of metabolites involved. Making the situation worse, the flux v also depends on enzyme concentration E_{tot}, while resolving enzyme concentrations over time requires separate experimental methods that are still hard to do jointly with metabolite concentration time traces at scale. Together, these difficulties result in the sparsity of data for metabolic fluxes.

This sparsity then creates difficulty for the typical modeling approach where the mechanisms for catalysis are known or hypothesized and equations such as in Michaelis-Menten are derived for the rates. This is because for the mechanistic models to describe a system experimentally observed, we need to fit to data many mechanistic parameters that arise in the modeling process. But for a nontrivial metabolic network, the number of such parameters is too large to fit to a sparse set of data that is feasible to obtain experimentally. This problem of under-determination also makes it hard for the mechanistic model to generalize to situations different from the ones in fitted data.

In order to resolve the under-determination problem due to sparse data, a constraint-based approach has been developed to model metabolism. The constraint-based approach dominated recent progress on computational models of large scale metabolic networks [85]. Constraint-based approach is a mechanistic modeling approach providing sufficient maps from mechanisms to phenotypes. But instead of relying on knowing all the mechanisms in a system to demonstrate a given phenotype, i.e. to build a model from a point in mechanism space to a point in phenotype space, it takes known mechanisms as constraints and unknown mechanisms as free to vary, and look at the set of all feasible phenotypes.

This is especially appropriate for metabolism, where data on mechanisms is almost always sparse. For metabolism, a natural split is between stoichiometry and flux regulations, since the former is relatively easier to know while mechanisms of the latter is much harder. Therefore, constraint-based methods take the sparse mechanistic data such as stoichiometry and supply it as constraints on reaction fluxes. Then, either the set of all feasible fluxes can be analyzed, or optimization for certain objective functions such as growth maximization or ATP regeneration can be used to find specific points of interest in flux space (Figure 4.2). One such approach, dynamic flux balance analysis (dFBA) [60], has been very successful in modeling large scale metabolic networks. The recent work [66] illustrates that dFBA could capture complex behaviors of a microbial consortia such as hysteresis in response to environmental nutrient shifts, which is hypothesized to underlie the switching between beneficial and detrimental gut microbiome compositions.

Although it holds promise as a general model for metabolism, dFBA has severe limitations in applying to metabolism dynamics of interacting cells and populations. dFBA cannot model dynamics intrinsic to metabolic regulations. This is because dFBA assumes the intracellular metabolic fluxes are faster than external changes such as growth and nutrient shifts. This makes in and out fluxes of metabolites always balanced and at steady state, which makes the constraint-based problem computationally solvable. But it also makes dFBA incapable of capturing potentially important transient dynamics intrinsic to metabolism, such as overshoots, undershoots, lags, and temporary arrests that can be essential for cell survival. In short, dFBA considers metabolic changes as static and instantaneous responses to slow variations in external environments, often on the time scale of hours to days. In comparison, many significant metabolic dynamics in cell physiology and the gut microbiome, for example, happens within minutes to hours [3, 33]. In addition, as the strength of a constraint-based method comes from the set of constraints it could use, dFBA only incorporates the stoichiometry of metabolic reactions as a constraint, so it could be considered as overly unconstrained to include un-biological actions such as instantaneous changes of metabolic flux (see Figure 4.2). This causes predictions of dFBA to be erroneous without time-consuming hand-tuning and curating by experts with extensive experimental data on the microbe modeled.

Another approach that tackles metabolic regulation was invented in [25], which uses glycolytic oscillation as an example to formulate the engineering hard limits or laws to map phenotypes back to mechanisms in the reverse, or necessary, direction. This approach builds on well-understood models of the glycolysis metabolic network from extensive experimental data, and asks what is unavoidable if the metabolic regulation is done by

arbitrary controllers, instead of the specific biological mechanisms. This could be done for glycolytic oscillation because it is at the opposite extreme of typical problems in metabolism: a small network with extensive experimental data and well established mechanistic models. Indeed, glycolytic oscillation, where metabolite concentrations (e.g. ATP and NADH) oscillate in the glycolysis pathway, has been widely observed and studied from yeast to human muscle since 1960s both theoretically and experimentally (e.g. [16, 49, 51]). The feedbacks of autocatalysis and allosteric control of ATP on the PFK enzyme were thought necessary and sufficient for glycolytic oscillation, confirmed by mechanistic models, extensive simulations, and exhaustive experiments. So what was left to be understood was the deeper "why" questions and the full generality of this oscillation behavior. By showing that oscillatory behavior was unavoidable even if the metabolic regulation was performed by arbitrary controllers that maintain a steady flux, the paper [25] showed that oscillations are necessary side effects of robustness and efficiency tradeoffs. Specifically, it showed that by combining a law on conservation of robustness in control theory called Bode's integral formula with the autocatalytic stoichiometry of glycolysis, a universal rule of metabolic regulation can be obtained that includes glycolytic oscillation as a subset: Any regulatory circuit that must robustly maintain metabolite concentrations despite fluctuations in supply and demand will inevitably have significant oscillations in some conditions, and autocatalysis as well as efficiency aggravate this.

The approach in [25] based on laws from control theory is a significant success in deriving rules of metabolic regulation, and mapping phenotypes back to mechanisms in the necesssary direction. However, the particular problem formulation in [25] began with a mechanistic model, which required that the metabolic network is small and extensively studied by experiments and mechanistic modelling. This is rare for metabolic interactions of interest of microbial communities in human microbiomes or soil rhizospheres. In other words, the general systems theory that formulates metabolic regulation into a control system that allows control-theory analysis is not yet understood. In [25], the placement of the arbitrary controller at the allosteric coefficient is a careful choice motivated by domain knowledge about the glycolysis pathway and experimentally validated feedback mechanisms. The severe robustness-efficiency tradeoff will be ameliorated if the controller is placed at some other parameters, such as the reaction rate constants. Therefore, we would like to formulate a systems theory for metabolic networks and study rules of regulation for this system by converting it into a control system. This requires a fundamental understanding of what class of control systems describe the regulation of metabolic networks.

Summarizing our discussion of existing approaches, we would like a theoretical framework to understand rules of metabolic regulation that has the best of both worlds: it should be constraint-based like dFBA so that it can incorporate sparse data, and it should be a systems theory with dynamics formalizing [25] so that it can bridge control theory laws and hard limits to derive rules and tradeoffs on metabolic regulation.

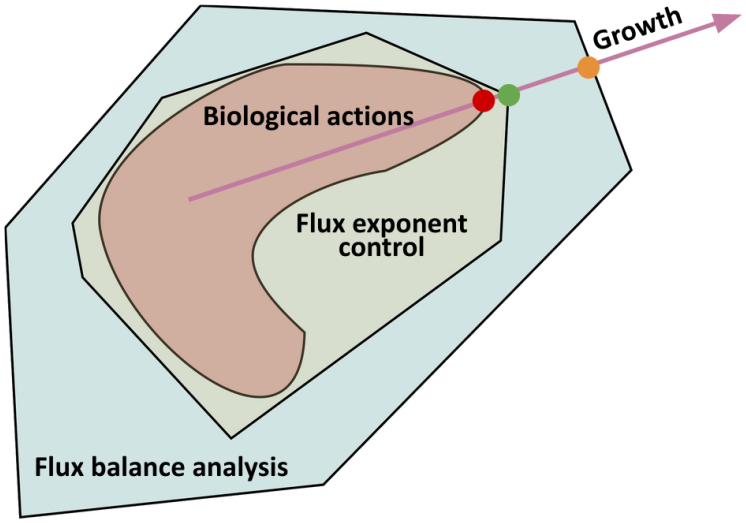

Figure 4.2 Cartoon illustrating three constraint-based methods. The arrow represents the optimization objective: e.g. growth. The red set describes the actual set of biological actions that a cell can take. The red dot then represents the optimal growth rate the cell can achieve. The light blue outer-most set is the set of actions constrained by FBA. It is only constrained by stoichiometry, therefore includes biological actions as a strict subset. The yellow dot is the optimal action expected by FBA, which deviates from the biological action (red dot), and has higher growth rate. The light green set denotes the set of actions constrained by FEC, a strict super set of biological actions and a strict subset of FBA. The green dot is optimal control action predicted by FEC, which is closer to the biological action (red dot) compared to FBA (yellow dot).

In this work, we propose one such approach called flux exponent control (FEC). Viewed as a constraint-based approach, FEC does not make the steady state assumption as in dFBA, while adding in an additional constraint on how cells control metabolic fluxes (see Figure 4.2). Namely, FEC is motivated by our understanding that biomolecular systems consist of binding reactions' regulation of catalysis, and the full profile of such regulations is parameterized by polyhedral sets constraining the reaction orders, or flux exponents (see Chapters 2 and 3). Therefore, it is a fundamental constraint from the binding and catalysis structure of biomolecular systems that cells control metabolic fluxes by adjusting their exponents, hence the additional constraint for FEC. As a constraint-based approach, FEC therefore has tighter constraints than dFBA, which only uses the stoichiometry of metabolism, yielding regulatory actions closer to biological ones (see Figure 4.2). On the other hand, FEC can be viewed as a systems theory formalization that scales-up the hard-limits approach invented in [25] to pose the regulation of any metabolic network

as a dynamical control problem and integrates naturally with tools from control theory. In particular, FEC answers why the controllers are placed at allosteric coefficients when analyzing glycolytic oscillation in [25]. Allosteric coefficients represents reaction orders in the mechanistic model of glycolysis used in [25], so this is justified by FEC that only such placements of controllers are biological. Together, FEC improves over dFBA as a constraint-based method that allows dynamics and studies fundamental tradeoffs and rules of metabolic regulation. FEC also formalizes the the hard-limits approach in [25] by posing controller placements at flux exponents as a general rule and systematically converts regulations of any metabolic network to a control system. As a result, FEC is a systems theory for metabolic regulations that provides improved necessary and sufficient maps between mechanisms and phenotypes.

The progression of this chapter goes as follows. Section 4.2 illustrates the main features of FEC using a simple model of glycolysis. Section 4.3 formulates the general structure of metabolic dynamics, and how FEC converts it into a control problem. Section 4.4 introduces some tools from control theory and adapts them to metabolic control problems from FEC. Control theory can be used to obtain hard limits and laws on that constrain all possible regulations done on a metabolic system. Section 4.5 poses regulation of metabolic fluxes as an optimal control problem as a way to explore metabolic dynamics. It discusses how to computationally solve such optimal control problems using a popular method in control theory called model predictive control (MPC). Section 4.6 uses optimal controllers solved by MPC to investigate rules of metabolic regulation in specific examples of metabolic networks, capturing important biological behaviors such as glycolytic oscillation and cell growth arrest under stress.

4.2 Glycolysis as an illustrative example of flux exponent control

In this section, we walk through how to apply flux exponent control (FEC) to a lumped model of glycolysis to illustrate the main features of FEC.

A simple model of glycolysis is introduced in Section 1.4 of Chapter 1. Also see Figure 1.13. Instead of considering the detailed steps of reactions in glycolysis, we consider two lumped reactions that capture the structure of autocatalysis. This yields the following dynamics for the concentrations of metabolites:

$$\frac{d}{dt}\begin{bmatrix} x_1 \\ x_2 \end{bmatrix} = \begin{bmatrix} 1 & -1 \\ -q & 1+q \end{bmatrix}\begin{bmatrix} v_1 \\ v_2 \end{bmatrix} + \begin{bmatrix} 0 \\ -1 \end{bmatrix} w. \tag{4.1}$$

This is of the form $\frac{d}{dt}\boldsymbol{x} = \boldsymbol{S}\boldsymbol{v} + \boldsymbol{S}^w\boldsymbol{w}$, where $\boldsymbol{x}$ is the vector of metabolite concentrations, $\boldsymbol{S}$ is the metabolic stoichiometry matrix, $\boldsymbol{v}$ is the vector of internal metabolic fluxes, and $\boldsymbol{S}^w$ is the metabolic stoichiometry matrix of external fluxes $\boldsymbol{w}$. Here x_2 is ATP, or energy charge, and x_1 is a lumped intermediate of the glycolysis pathway, such as fructose 1,6-bisphosphate. The first reaction with flux v_1 consumes q units of ATP and produce one unit of intermediate. We can take q to be 1 as a value that match the stoichiometry of ATP production in glycolysis. This reaction represents the activation of glucose by ATP to produce glycolysis intermediates. We assume glucose is overabundant, and therefore does not influence the fluxes. The second reaction with flux v_2 consumes one unit of intermediate and produces $1 + q$ units of ATP. This reaction represents the net production part of the glycolysis pathway. Together, looping through the two reactions once results in a net production of one unit of ATP. We also include an external disturbance with flux w that consumes one unit of ATP. This corresponds to the maintenance energy cost of the cell, which can increase under environmental disturbances such as heat shocks.

When the regulatory mechanisms of the fluxes are known in detail, we can specify exactly how v_1 and v_2 are regulated, as static functions or dynamic processes that depend on (x_1, x_2). Although we do know some of the mechanisms in this case because glycolysis has been studied for decades, let us assume we do not have this information to illustrate how to deal with a generic metabolic network.

One constraint-based approach to make progress is flux control. Since we do not know how any of the fluxes are regulated, flux control considers all the fluxes as arbitrarily regulated by the cell. This gives the following formulation:

$$\frac{d}{dt}\begin{bmatrix} x_1 \\ x_2 \end{bmatrix} = \begin{bmatrix} 1 & -1 \\ -q & 1+q \end{bmatrix}\begin{bmatrix} u_1 \\ u_2 \end{bmatrix} + \begin{bmatrix} 0 \\ -1 \end{bmatrix} w. \tag{4.2}$$

Here we simply substituted the flux variables (v_1, v_2) with control variables (u_1, u_2) that the cell can adjust. Flux control as a constraint-based approach then says that (u_1, u_2) can take arbitrary trajectories as controlled by the cell, if no further information about the fluxes is given. This often results in systems with trivial behavior. For example, here we can do a change of variable by defining new control variables $u_1' = u_1 - u_2$, and $u_2' = (1+q)u_2 - qu_1$ to achieve a trivial dynamics:

$$\frac{d}{dt}\begin{bmatrix} x_1 \\ x_2 \end{bmatrix} = \begin{bmatrix} u_1' \\ u_2' \end{bmatrix} + \begin{bmatrix} 0 \\ -1 \end{bmatrix} w. \tag{4.3}$$

Since the cell can adjust u_1' and u_2' arbitrarily, the metabolite concentrations (x_1, x_2) can also be made arbitrary. In other words, flux control is often underconstrained to capture metabolic dynamics.

One way to make progress despite that flux control is underconstrained is by focusing on the steady state fluxes. This results in the constraint-based approach of flux balance analysis (FBA). In this case, we obtain the following at steady state:

$$0 = \begin{bmatrix} 1 & -1 \\ -q & 1+q \end{bmatrix} \begin{bmatrix} u_1^* \\ u_2^* \end{bmatrix} + \begin{bmatrix} 0 \\ -1 \end{bmatrix} w^*. \tag{4.4}$$

Here (u_1^*, u_2^*) and w^* are steady state fluxes. We see that the steady state condition results in a constraint on the steady state fluxes by metabolic stoichiometry. In this case, the stoichiometry matrix is invertible, and therefore determines the internal fluxes in terms of the external flux uniquely at steady state.

This may seem magical, that by looking at steady state fluxes, we have gone from having no constraints to work with to having strong constraints. The deeper reason is that when FBA looks at steady state fluxes, it is implicitly assuming that the steady state fluxes are achieved, which requires the cell to maintain a stable homeostasis. This is not guaranteed at all when the fluxes are dynamic. For example, the system can be oscillatory without ever reaching a steady state. It can also crash into a disaster state that the cell dies.

Fundamentally, flux control cannot answer questions about stability because it eliminates the intrinsic dynamics of metabolism by assuming all fluxes are adjustable. One evidence of this in the glycolysis case is that glycolytic intermediates oscillate under stress, from yeast to mouse muscle cells [16, 49, 51]. This is due to the intrinsic instability of autocatalytic stoichiometry (also see Section 1.4). This implies that metabolic fluxes have intrinsic dynamics that are not modifiable by cells' regulation. Mathematically, if the fluxes are static functions, then this implies the fluxes are not fully controlled ($\boldsymbol{v} = \boldsymbol{u}$), but rather partially controlled ($\boldsymbol{v} = \boldsymbol{v}(\boldsymbol{x}, \boldsymbol{u})$).

Flux exponent control (FEC) exactly formalizes which part is controlled and which part is not. FEC is based on our previous study on binding's regulation of catalysis in Chapter 2 and Chapter 3. Since cells regulate metabolic fluxes through binding reactions, while binding reactions adjust fluxes' exponents, or reaction orders, within a constrained polyhedral set, we conclude that cells regulate fluxes' exponents. This is the content of the FEC rule. Mathematically, this means we split each metabolic flux in the following way:

$$v_j = v_j^0 x_1^{H_{j1}^A} \cdots x_n^{H_{jn}^A} u_1^{H_{j1}^B} \cdots u_{n_u}^{H_{jn_u}^B} =: v_j^0 \boldsymbol{x}^{\boldsymbol{H}_j^A} \circ \boldsymbol{u}^{\boldsymbol{H}_j^B} = v_j^0 \exp\Big\{ \boldsymbol{H}_j^A \log \boldsymbol{x} + \boldsymbol{H}_j^B \log \boldsymbol{u} \Big\}. \tag{4.5}$$

The above equation writes the decomposition of the flux of reaction j in several different notations. The first notation writes each term explicitly. The second notation is the most succinct. The third notation makes it clear that the control actions are on the flux exponents.

The flux is decomposed into three parts: (1) a constant reference flux magnitude v_j^0; (2) the passive dependence on metabolite concentrations $x_1^{H_{j1}^A} \cdots x_n^{H_{jn}^A} =: \boldsymbol{x}^{\boldsymbol{H}_j^A} =: \exp\Big\{\boldsymbol{H}_j^A \log \boldsymbol{x}\Big\}$, where $\boldsymbol{H}_j^A$ is the jth row vector of a matrix $\boldsymbol{H}^A$; (3) the active regulation depending on control actions $u_1^{H_{j1}^B} \cdots u_{n_u}^{H_{jn_u}^B} =: \boldsymbol{u}^{\boldsymbol{H}_j^B} =: \exp\Big\{\boldsymbol{H}_j^B \log \boldsymbol{u}\Big\}$. Here $\circ$ denotes component-wise product between two vectors, and exponential $\exp$ is applied component-wise. The matrix $\boldsymbol{H}^A$ specify the passive exponent or reaction order, capturing how the metabolic reactions would proceed if there is no regulatory mechanisms in place. The matrix $\boldsymbol{H}^B$ specify which control variables $\boldsymbol{u}$ influence which fluxes.

Back to the glycolysis example, we may propose the following natural split of the fluxes:

$$v_1 = v_1^0 x_2 u_1, \quad v_2 = v_2^0 x_1 u_2. \tag{4.6}$$

This corresponds to having $\boldsymbol{H}^B$ as identity matrix so that there is one exponent control variable for each flux, and having $\boldsymbol{H}^A$ with $H_{12}^A = H_{21}^A = 1$ and other entries zero. This is because reaction v_1 consumes x_2, therefore higher x_2 should naturally increase the flux v_1 without active regulation. Similarly, reaction v_2 consumes x_1, therefore higher x_1 should naturally increase the flux v_2. We then choose the exponent of this increase to be 1 as a default choice, simply because first order dependence is the most common. The entries H_{11}^A and H_{22}^A are zero here because these two reactions are almost always irreversible from thermodynamic considerations, therefore not inhibited by product molecules.

Together, we have the following FEC formulation of glycolysis fluxes:

$$\frac{d}{dt}\begin{bmatrix} x_1 \\ x_2 \end{bmatrix} = \begin{bmatrix} 1 & -1 \\ -q & 1+q \end{bmatrix} \begin{bmatrix} v_1^0 x_2 u_1 \\ v_2^0 x_1 u_2 \end{bmatrix} + \begin{bmatrix} 0 \\ -1 \end{bmatrix} w. \tag{4.7}$$

We see that when the control variables (u_1, u_2) are constant, the system has a passive dynamics that is linear and unstable, since x_1 and x_2 positively influence each other (also see Section 1.4). So FEC retains the intrinsic dynamics of metabolism by placing control variables on the exponents. On top of this formulation, further constraints can be added if more information is known. For example, we may upper bound u_1 by 1 if we know the maximum flux of v_1 and set it to v_1^0. We may also constrain the rate of change in the control variables, if we believe the regulatory mechanisms are slow. We could even require the control actions to keep x_2 above a certain level, if we consider there exists a minimum level of ATP concentration needed to keep cells alive.

Given the FEC formulation of a metabolic network, we can perform several types of analysis. First, since FEC formulates a metabolic network as a control system, we can use control theory tools to study the hard limits on system performance. This is exemplified by the

work [25], where Bode's theorem on conservation of robustness is used to explain glycolytic oscillations as inevitable side effects of the tradeoff between steady-state error and system fragility (which causes oscillations). Second, we may be interested in finding particular regulatory behaviors of the system when the regulation is optimal for a certain objective. This can help us interpret various regulatory strategies in different scenarios. For example, we may consider optimizing for keeping the ATP concentration steady at a reference level. Once an objective is formulated, solving for the optimal control variables and the system behavior becomes an optimal control problem. This is investigated in Section 4.5 and some simulation result is discussed in Section 4.6.

A third way to use FEC is to relate control actions with underlying binding networks, since control of flux exponents biologically correspond to binding networks' regulation of catalysis fluxes. We can explicitly illustrate this here since mechanisms of the flux regulations in glycolysis is well studied, so plausible models of the underlying binding networks exist. For example, [25] proposed the following simple models of the fluxes based on knowledge about catalyzing enzymes' allosteric feedback:

$$v_1 = v_1^0 x_2 u_1 = v_1^0 x_2 \frac{1}{1 + x_2^{2h}}, \qquad v_2 = v_2^0 x_1 u_2 = v_2^0 x_1 \frac{1}{1 + x_2^{2g}}. \tag{4.8}$$

In other words, both control variables u_1 and u_2 implement negative feedback based on the ATP concentration x_2, with allosteric coefficients $2h$ and $2g$, respectively. These rational function forms of u_i could have mechanistic origins from binding networks. For example, u_1 may come from the following binding network:

$$2X_2 + E_1 \rightleftharpoons E_1', \tag{4.9}$$

where E_1 is the enzyme catalyzing flux v_1, and E_1' is an inactive form of the enzyme. When X_2 is overabundant compared to E_1, we have the following expression for the flux of the first reaction:

$$v_1 = v_1^0 x_2 \frac{1}{1 + \frac{x_2}{k_1}^2}, \tag{4.10}$$

where k_1 is the dissociation constant in the above binding reaction of E_1 with two X_2. This binding network implements the control action in [25] with $h = 1$. This simple example illustrates how we can relate control variables with biological mechanisms of binding networks.

This concludes our illustration of FEC through the glycolysis example. In the next section, we begin our study of constraint-based methods from the layered architecture of metabolism.

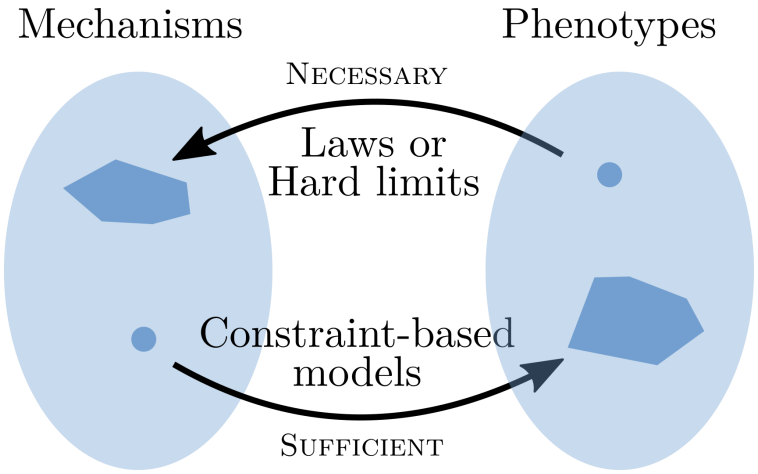

Figure 4.3 Cartoon illustrating constraint-based models and hard-limits or laws as two approaches in mapping between mechanisms and phenotypes. For a class of phenotypes, laws or hard limits can specify a criteria that many mechanisms can be used to satisfy it. As examples, many codes and hardware can implement certain channel capacity in communication networks, and many electronic circuits can implement certain performance criteria of a signal processing input-output map. For a class of mechanisms, described as a constraint-based model where some mechanisms are fixed and other mechanisms are free to vary, many phenotypes or system behaviors can be achieved. As an example, cars have some common features fixed as constraints, with the rest left to vary, resulting in a wide range of mileage, speed, safety, and comfort.

4.3 Metabolic regulation as control of flux exponents

The two approaches to study rules of metabolic regulation, namely constraint-based approach as in FBA and hard-limits approach as in [25], represent two perspectives on the space of plausible metabolic regulations. In particular, they represent two different mappings between the spaces of mechanisms and phenotypes (see Figure 4.3). The hard-limits approach was motivated by glycolysis, a case extensively studied both experimentally and computationally, so that mechanisms of regulation are known. Hence the question that the hard-limits approach focused on was answering "why" the regulatory mechanisms were made that way, by investigating the space of alternative regulatory mechanisms. In essence, the control-theory approach is devoted to understanding the "laws", or universal properties in terms of hard limits, that any system with certain key structure will obey, independent of any further details. This constitutes a "necessary" mapping from a point in phenotype space to a set in mechanism space. Indeed, [25] used the conservation of robustness as a law that connects autocatalytic stoichiometry on the mechanism side with the phenotype that severe oscillations are inevitable as a side effect of steady-state adaptations. Although formulating the case study on glycolysis in [25] using this hard-limits approach relied on knowing relatively complete mechanistic details, the result was hard limits that are universal for supply-and-demand adaptations in metabolism.

The constraint-based approach, on the other hand, was motivated by sparse data available to characterize metabolism dynamics for whole-cell metabolism modeling, such as for bacterial growth and human metabolism. Therefore the questions that the constraint-based approach focused on was how to effectively use the sparse data available to constrain reality, i.e. constrain the space of plausible metabolic fluxes. This is like a "sufficient" mapping from a point in mechanism space to a feasible set in phenotype space. For example, given the known stoichiometry of the glycolysis pathway and some upper and lower bounds on the fluxes based on rough maximum numbers of enzymes per cell, then flux balance analysis (FBA), a constraint-based approach, yields a set of possible steady state fluxes the cell can have, such as ATP production rate, that are constrained by this mechanism. For a point in the set of feasible fluxes, the glycolysis mechanism is sufficient to allow it to happen, although whether it can actually happen depends on the details not included in the constraint-based model, such as actual enzyme numbers and catalysis rates.

Although these two approaches were developed from different motivations, they yield complimentary insights for the same problem, therefore should be integrated in a cohesive fashion. In the following, we take the constraint-based approach as the main perspective to develop our formulation for modeling metabolism dynamics. But once a control system is formulated, we compliment the story with the hard-limits or laws perspective. Since constraint-based modeling is fundamentally rooted in the layered architecture of metabolism, we introduce this next.

Stoichiometry-flux split in layered architecture of metabolism enables flux control as a constraint-based approach

Layered architecture of metabolism and the stoichiometry-flux split. Constraint-based modeling splits the mechanisms of a metabolic system into two parts: a slow-varying known part of which we have solid knowledge, and a fast-varying unknown part of which we have little knowledge. Then the known part is taken as constraints, and the unknown part is allowed to vary freely. All feasible behaviors of the system are then the set of behaviors that the system can achieve by varying the unknown parts, with the known parts held fixed. Fundamentally, for this split to be effective conceptually and mathematically, the system of concern needs to have a natural layered architecture so that the lower layer, the layer that already exists and is to be controlled, is known and fixed, and the higher layer, the layer controlling the lower layer, is unknown and varies. This split requires both a time-scale separation of dynamics at each layer, and a corresponding structural split in the organization of the system into layers. Such layered architectures may be generally viewed

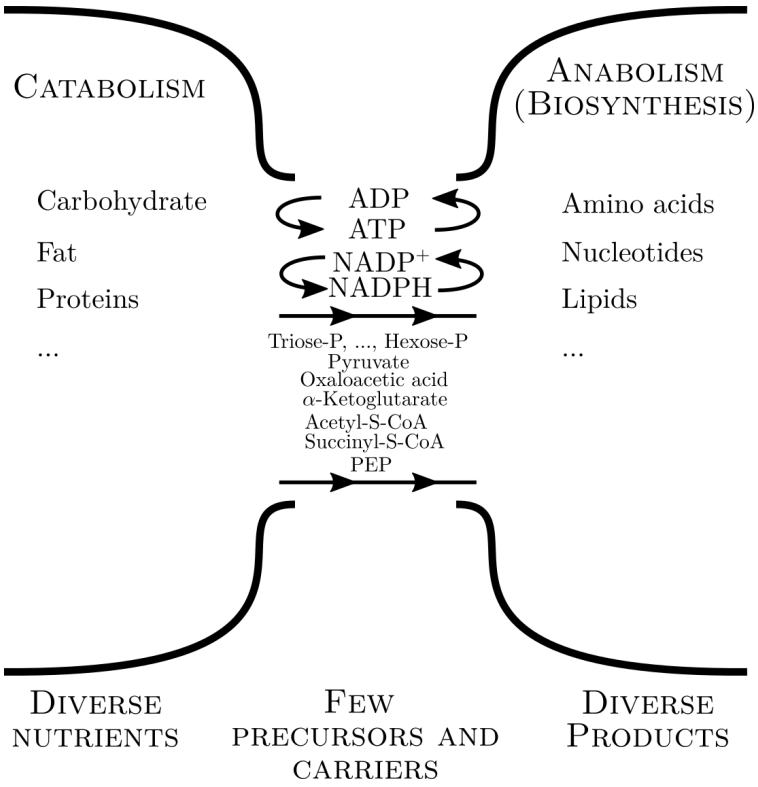

Figure 4.4 Diagram showing the bowtie shape of metabolite stoichiometry in microbial metabolism. Adapted from Figure 1 of [13], also reproduced as Figure 2.1 in [59].

as a result of adaptation to achieve optimal system performance at diverse timescales using components that are limited by severe tradeoffs such as ones on speed-accuracy [38, 79, 80].

Cells use an architecture built on metabolic reactions to achieve diverse behaviors across several timescales, from consumption and secretion of molecules and response to environmental signals, to growth and death, to differentiation and cell-cell communications. This motivates us to view the metabolic architecture of a cell as interconnected layers with separating time scales. For the purpose of this work on constraint-based modeling of metabolism dynamics, we split metabolic regulation into three layers: the bottom metabolic stoichiometry layer, the middle enzyme regulation layer, and the top gene expression layer.

For the bottom layer, the stoichiometry of metabolic reactions describe the number of metabolite molecules consumed and produced in each reaction (see Figure 4.4). The reaction fluxes involved are catalyzed by enzymes with millisecond to second timescale for catalysis rate. In contrast, the metabolism stoichiometry, i.e. what chemical reactions can happen in metabolism, varies on a much slower timescale, therefore can be considered fixed. Indeed, since metabolic reactions in cells happen largely because of the existence of corresponding enzymes, the timescale for modifying the stoichiometry is the timescale

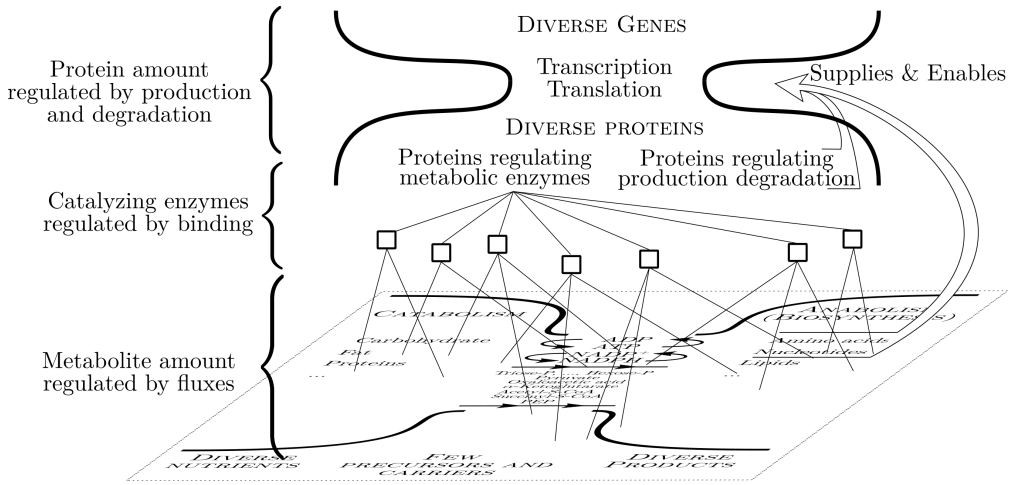

Figure 4.5 Diagram showing the layered architecture of microbial metabolism. Metabolism can be roughly viewed as consisting of three layers, from bottom up. The bottom layer is the stoichiometry of metabolic reactions, capturing how metabolite amounts are regulated by reaction fluxes. The middle layer is the proteins' regulation of metabolic enzymes, capturing how reaction fluxes are regulated by protein binding (squares) The top layer is transcription translation (TXTL), capturing how protein concentrations are regulated by production and degradation. The gene expression layer viewed as a controller for the lower layers has an hourglass shape, connecting diverse genes with diverse proteins via a thin waist of transcription and translation machinery, which has building blocks such as amino acids and nucleotides supplied by the bottom layer.

for generating new enzymes catalyzing new reactions or deleting existing enzymes. This largely come from mutations and evolution. While loss of function can happen on a timescale of tens of hours in bacteria, gain of function to catalyze new reactions often takes much longer, limited either by the generation of the right collection of mutations or by selection pressure to propagate the new function. Exceptions might be horizontal gene transfers, which can happen on tens of hours timescale similar to loss of function. So we conclude that the timescale for modifying the stoichiometry layer is more than tens of hours, with loss of function and horizontal gene transfers on the faster end, but overall much slower than the timescale for metabolic fluxes. Therefore the stoichiometry layer can be viewed as having fixed stoichiometry, with quickly varying fluxes regulated by higher layers (see Figure 4.5 and Figure 4.6).

This separation of timescales between the stoichiometry of bottom layer and fluxes regulated by higher layers is at the heart of existing constraint-based approaches to metabolism. Namely, instead of arbitrary dynamics of varying metabolite concentrations in a metabolic network, this layered architecture motivates a stoichiometry-flux split. Mathematically, the metabolite concentration dynamics without any further knowledge can be written as a generic nonlinear dynamical system,

$$\frac{d}{dt}\boldsymbol{x}(t) = \boldsymbol{f}(\boldsymbol{x}(t), \boldsymbol{w}(t)), \tag{4.11}$$

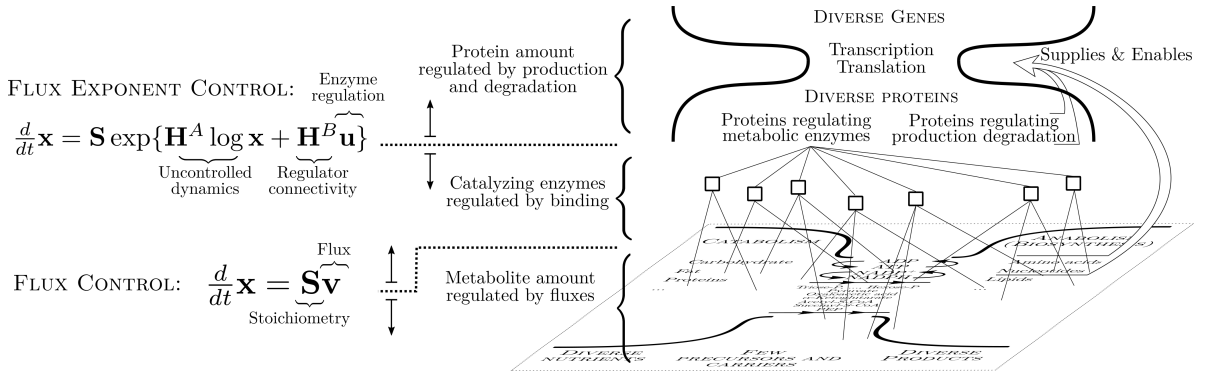

Figure 4.6 Illustration of how the two constraint-based approaches, flux control and flux exponent control, relate to the split in the layered architecture of metabolism. For simplicity, the terms for external exchange fluxes $\boldsymbol{w}$ are omitted.

where $\boldsymbol{x}(t) \in \mathbb{R}^n_{>0}$ is the concentration of metabolite in the cell, $\boldsymbol{w}(t) \in \mathbb{R}^{m_w}_{>0}$ is exchange fluxes with external environments, and $\boldsymbol{f} : \mathbb{R}^n_{>0} \times \mathbb{R}^{n_w}_{>0} \to \mathbb{R}^n$ is the change in metabolite concentrations. We do not write the system as an autonomous one like $\frac{d}{dt}x = \boldsymbol{f}(\boldsymbol{x})$ because exchange with external environments is often essential to maintain any steady state of a metabolic system. As an example, for glucose fermentation in bacteria, $\boldsymbol{x}$ may include internal metabolites such as ATP, fructose biphosphate, pyruvate, and internal glucose, while $\boldsymbol{w}$ may include glucose import flux and lactate export flux. See Figure 4.7 for the control diagram describing this general unstructured formulation. With the stoichiometry-flux split, we can further write

$$\frac{d}{dt}\boldsymbol{x}(t) = \boldsymbol{f}(\boldsymbol{x}(t), \boldsymbol{w}(t)) = \boldsymbol{S}\boldsymbol{v}(\boldsymbol{x}(t)) + \boldsymbol{S}^w\boldsymbol{w}(t), \tag{4.12}$$

where $\boldsymbol{S} \in \mathbb{R}^{n\times m}$ is the cell internal metabolism stoichiometry matrix, m is the number of internal metabolic reactions, and $\boldsymbol{v}(\boldsymbol{x}(t)) \in \mathbb{R}^m_{>0}$ is the fluxes of the m internal reactions, varying with metabolite concentrations through regulatory mechanisms such as enzyme allostery and gene regulation. Here $\boldsymbol{S}^w \in \mathbb{R}^{n\times m_w}$ is the stoichiometry for the external exchange fluxes. Note that we required the internal and external fluxes $\boldsymbol{v}$ and $\boldsymbol{w}$ to be positive, so for reversible reactions, the forward and reverse fluxes are represented separately. This is important to fully capture the dynamics in fluxes such as futile cycles, which cannot be distinguished by just the net fluxes.

Based on timescale separation, this stoichiometry-flux split captures an essential structure of metabolism that makes experimental measurements and modelling much easier. Without this split, to write down the metabolite dynamics requires detailed knowledge about $\boldsymbol{f}(\boldsymbol{x})$, i.e. how the change in metabolite concentrations depend on metabolite concentrations. Without further structures, this require measurements for transient changes with the metabolic system initiating at all possible metabolite concentrations $\boldsymbol{x} \in \mathbb{R}^n_{>0}$. This is too

costly to obtain experimentally. In contrast, with this split, we can obtain knowledge for the stoichiometry $\boldsymbol{S}$ and the flux regulation $\boldsymbol{v}(\boldsymbol{x})$ separately. In particular, the stoichiometry $\boldsymbol{S}$ can be easily determined based on bulk end-point measurements. The regulation of flux $v_i(\boldsymbol{x})$ can also be measured independent of the other fluxes, if this metabolic reaction can be perturbed and measured in an isolated fashion. Therefore, the stoichiometry-flux split greatly facilitates mechanistic measurements and modelling by capturing an essential structure of metabolism, which corresponds to a timescale separation in the layered architecture of metabolism.

Flux control from stoichiometry-flux split. We can develop a constraint-based modeling approach based on this stoichiometry-flux split. Naturally, the stoichiometry, which varies slowly, is taken as constraints, while the fluxes, which vary quickly, are allowed to vary. So we call this constraint-based approach *flux control*, since the free-to-vary fluxes can be considered as control knobs on this metabolic system (see Figure 4.7). Indeed, existing constraint-based approaches can all be considered as flux control. While further constraints and relations, such as ones based on thermodynamics or kinetic measurements, may be added to the fluxes, the variables to vary are always the fluxes. A generic description of flux control can therefore be written as follows:

$$\frac{d}{dt}\boldsymbol{x}(t) = \boldsymbol{S}\boldsymbol{u}(t) + \boldsymbol{S}^w\boldsymbol{w}(t), \quad \boldsymbol{u}(0:T) \in \mathcal{U}_{(0:T)}. \tag{4.13}$$

Here $\boldsymbol{u}(t) \in \mathbb{R}^m_{>0}$ is the control variable, or the variable to vary, representing metabolic fluxes. Since the fluxes can vary with time, any constraints we put on the fluxes should be constraints on time trajectories of fluxes. Here $\boldsymbol{u}(0:T)$ denotes the time trajectory of fluxes in the time interval of concern $[0, T]$, and $\mathcal{U}_{(0:T)}$ denotes the constraint on the flux trajectories, or the set of allowed flux trajectories. Without any knowledge constraining the fluxes, we would take $\mathcal{U}_{0:T}$ to be any function mapping $[0, T] \to \mathbb{R}^m_{\geq 0}$, or some trajectory space with regularities such as ones with finite L_2 norm.

One powerful aspect of constraint-based approaches is that they allow investigation into the set of all possible behaviors. We notice that although this flux control formulation incorporated the stoichiometry-flux split, if we do not have severe constraints on flux trajectories from $\mathcal{U}_{(0:T)}$, then the metabolite trajectories $\boldsymbol{x}(0:T)$ can be quite arbitrary. This is because the stoichiometry matrix $\boldsymbol{S} \in \mathbb{R}^{n\times m}$ is often of wide rectangular shape, i.e. $n < m$, or the number of metabolite species less than the number of reactions. As a result, $\boldsymbol{S}$ almost always has full row rank, which allows the control by fluxes $\boldsymbol{u}$ to make arbitrary trajectories of $\boldsymbol{x}$ achievable. More explicitly, we can view Eqn (4.13) as a control system with trivial plant dynamics, so the system is controllable, i.e. $\boldsymbol{x}$ can be controlled by $\boldsymbol{u}$

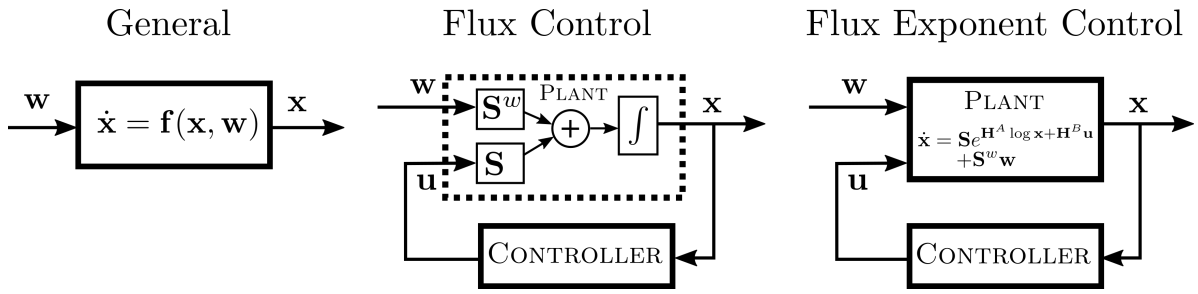

Figure 4.7 Control diagrams for several formulations of metabolism dynamics. The left is the unstructured general description of metabolite concentration dynamics, with input as external exchange fluxes $\boldsymbol{w}$ and output as metabolite concentrations $\boldsymbol{x}$. The middle one is the flux control formulation, with stoichiometry explicitly represented, and internal fluxes considered as control variable $\boldsymbol{u}$. The state variable $\boldsymbol{x}$ has trivial plant dynamics that is a direct integration of inputs. The right one is the flux exponent control formulation, with exponents of internal fluxes as control variable $\boldsymbol{u}$. The state variable $\boldsymbol{x}$ has nontrivial plant dynamics representing the uncontrolled internal fluxes.

to achieve arbitrary values at arbitrary time, if $\boldsymbol{S}\boldsymbol{S}^\intercal$ is full rank. This is very likely since $\boldsymbol{S}$ is wide rectangular. Here plant is a control theory term referring to the uncontrolled dynamics, or the process to be controlled.

One approach, *flux balance analysis (FBA)*, makes the flux control formulation more useful by restricting our attention to *steady-state fluxes*. This assumes steady states exist and are achieved, which is highly plausible for metabolism as homeostasis is one of the hallmarks of biological systems. This steady state assumption is applicable whenever the phenomenon of concern is much slower than cell metabolism, i.e. approximately hours or longer. By making this steady state assumption, Eqn (4.13) becomes

$$\mathbf{0} = \boldsymbol{S}\boldsymbol{u} + \boldsymbol{S}^w\boldsymbol{w}, \quad \boldsymbol{u} \in \mathcal{U}_{\text{ss}}. \tag{4.14}$$

This equation comes from Eqn (4.13) simply by setting $\frac{d}{dt}\boldsymbol{x} = 0$ at steady state. Here $\boldsymbol{u} \in \mathbb{R}^m_{\geq 0}$ is the steady state fluxes, $\boldsymbol{w}$ is steady state exchange fluxes, and the constraint set has become static as well, $\mathcal{U}_{\text{ss}} \subset \mathbb{R}^m_{\geq 0}$. Another simplification is often used in this steady state case. In metabolism, often both the forward and reverse directions of a reaction can happen with nontrivial rates. For dynamics, it is important to keep the forward and reverse directions separate, as a net flux could correspond to different pairs of forward and reverse fluxes. This is also important to capture "futile cycles" and energy consumption. However, focusing on steady state, these issues can no longer be captured, and thus a pair of forward and reverse reactions can be combined to one reaction without loss of generality, and their fluxes can be combined to one net flux. This can be captured by writing only one direction of each forward-reverse pair in the stoichiometry matrix $\boldsymbol{S}$, and allowing the fluxes $\boldsymbol{u} \in \mathbb{R}^m$ to be negative. This also makes the constraint set allowing negative fluxes by default, $\mathcal{U} \subset \mathbb{R}^m$.

Now we look at how the FBA formulation in Eqn 4.14 constrains the set of all possible steady state fluxes. Since FBA focuses on steady states, we can no longer capture metabolite concentrations. This is because $\boldsymbol{x}$ disappears in Eqn (4.14), as steady state concentrations are set by flux regulations $\boldsymbol{v}(\boldsymbol{x})$, which are assumed to be unknown, or set as control variables $\boldsymbol{u}$, in flux control. Instead, the steady state assumption enables a natural constraint relating steady state internal and external fluxes $\boldsymbol{u}$ and $\boldsymbol{w}$, that $\boldsymbol{S}\boldsymbol{u} = -\boldsymbol{S}^w\boldsymbol{w}$. There are several ways to view this relation. For example, we can view exchange fluxes $\boldsymbol{w}$ as measurable, therefore fixed and used as constraints on internal fluxes $\boldsymbol{u}$. This reduces $\boldsymbol{u}$'s degrees of freedom from m, the number of reactions, to $m - r$, where r is the rank of $\boldsymbol{S}$. Indeed, if we only focus on the linear equation in Eqn 4.14 and ignore the constraint set $\mathcal{U}_{\text{ss}}$ for a moment, we can write the general solution of the linear equation as

$$\boldsymbol{u} = -\boldsymbol{S}^\dagger \boldsymbol{S}^w \boldsymbol{w} + \boldsymbol{u}^\perp, \quad \text{for any } \boldsymbol{u}^\perp \in \ker \boldsymbol{S}.$$

Here $\boldsymbol{S}^\dagger$ is the pseudo-inverse of $\boldsymbol{S}$, and $\ker \boldsymbol{S}$ is the kernel of $\boldsymbol{S}$, i.e. the space of vectors $\boldsymbol{u}$ such that $\boldsymbol{S}\boldsymbol{u} = 0$. If r is the rank of $\boldsymbol{S}$, then $\ker \boldsymbol{S}$ has dimension $m - r$. So $\boldsymbol{u}$ is constrained to have the specific solution part $\boldsymbol{S}^\dagger \boldsymbol{S}^w \boldsymbol{w}$ fixed, and only vary the $\boldsymbol{u}^\perp$ part in $\ker \boldsymbol{S}$, which is $m - r$ dimensional rather than m dimensional that $\boldsymbol{u}$ began with. If $m = r$, which could happen for small or simplified metabolic systems, then $\boldsymbol{u}$ is uniquely determined.

Further constraints on $\boldsymbol{u}$ that can be implemented through $\mathcal{U}_{\text{ss}}$ would require knowledge beyond stoichiometry. One example of a general constraint is upper and lower bounds on the steady state fluxes based on estimates on the maximum number of enzymes per gram of cell weight, and the maximum enzyme catalysis activity. In fact, 1000 milli-molar per gram of cell dry weight per hour ($\text{mM}\,\text{g}^{-1}\,\text{h}^{-1}$) is widely used as a generic upper bound on flux magnitude [85]. Similar to this, any knowledge about the fluxes from experimental measurements, such as upper bounds on rate of certain nutrient uptake, can be incorporated as constraints through $\mathcal{U}_{\text{ss}}$. Another class of general constraints on fluxes $\boldsymbol{u}$ are based on energy dissipation and thermodynamics of the metabolic reactions involved. This is discussed in more detail in the next subsection. An important class of qualitative constraints from thermodynamic arguments is the irreversibility or direction of fluxes. Thermodynamics dictates that only reactions with a negative Gibbs free energy can happen. The Gibbs free energy of the jth reaction can be written as $\Delta G_j = \Delta G_j^0 + RT \log Q$. ΔG_j^0 is the standard free energy change of this reaction under some standard condition such as pH 7, 1 atmospheric pressure, and 1 molar concentrations, so this part is independent of concentrations. Q is the reaction quotient, calculated as the ratio between a numerator from multiplying product concentrations to exponents of their stoichiometric coefficients, divided by a denominator from the same procedure for reactants. R is molar gas constant,

T is temperature, and $\log$ is natural log. So ΔG_j is the sum of the standard part independent of concentrations, and the reaction quotient part that increases with product concentrations and decreases with reaction concentrations. Therefore, for a given reaction, if ΔG_j is always negative based on standard free energy and the range of reactant and product concentrations for scenarios of concern, then we can claim the flux v_j always flow in the forward direction, i.e. $v_j > 0$. Since the reaction quotient is under $\log$, the influence of concentrations on the reaction free energy is limited. So if the standard free energy is very negative, then this usually guarantees the flux is irreversible. Therefore irreversibility of reactions serve as a general class of easy to obtain constraints on the fluxes.

Altogether, the set of all possible steady state fluxes in FBA formulation (Eqn (4.14)) can be written as

$$\left\{\boldsymbol{u} \in \mathcal{U}_{\text{ss}} \subset \mathbb{R}^m : \boldsymbol{u} = \boldsymbol{S}^\dagger \boldsymbol{S}^w \boldsymbol{w} + \boldsymbol{u}^\perp,\ \ \boldsymbol{u}^\perp \in \ker \boldsymbol{S}\right\}. \tag{4.15}$$

Then steady state behaviors of interest can be further explored through optimization, such as fluxes under maximum biomass production in aerobic or anaerobic environments with different nutrients as carbon sources, or limits on ATP or redox potential regeneration. With a good curated model of stoichiometry $\boldsymbol{S}$ and constraint set $\mathcal{U}_{\text{ss}}$, the FBA formulation has been successfully applied to whole-metabolism models of a wide range of microbes.

Flux control fails to capture internal dynamics of metabolism. However, there is one severe restriction in the FBA or the flux control formulation in general: the lack of internal dynamics. Many important metabolic behaviors and interactions are dynamic or due to transient dynamics, such as microbial growth arrest under nutrient or environmental shock and Crabtree or Warburg effects [3]. In turn, essential features of these dynamics are due to limits from internal dynamics. One essential aspect of steady state behavior is whether a given steady state is stable, i.e. adapts back from small perturbations. Stability, however, can only be determined from dynamics. Now looking back at FBA, it is unable to capture dynamics since the founding assumption of FBA is metabolism has reached a stable steady state. This is not remedied by going back to the flux control formulation, however. The reason is that the flux control formulation splits all metabolic fluxes into just two types, external exchanges and internal controls (see Figure 4.7). In other words, all internal fluxes are assumed to be controllable, and the metabolite dynamics is simply integrating the controlled fluxes. As a result, the "plant", or the metabolic process to be controlled, is trivial. Therefore metabolism has no internal dynamics, and all dynamics is determined solely by the controller. If we make an analogy from mechanics, mechanical objects have internal dynamics which we often call "inertia". This is because mechanical control actions are limited to forces, or accelerations, which directly alters speed or moments, but only

indirectly acts on position. So assuming all internal dynamics are from the controller is like assuming a mechanical object has no inertia, or the mass or momentum can be directly controlled as well.

In order to put back the internal dynamics, in addition to the internal-external split of fluxes, we need to further split the dynamics of internal fluxes into plant dynamics and controller dynamics. Plant is a control theory term that refers to the part of the system that is intrinsic and cannot be controlled. In the next subsection, we show that there is significant difficulty in splitting internal plant and controller dynamics in terms of fluxes, while it is simple and clear in terms of flux exponents. More fundamentally, the known/unknown split and timescale separation in the layered architecture of metabolism motivates a further binding-catalysis split in addition to stoichiometry-flux split. This leads us to the flux exponent control formulation of metabolism that includes internal dynamics (see Figure 4.7). This is discussed in the subsection after the thermodynamic constraint subsection.

Example 10 (Simple glycolysis)**.** Throughout this section, we use a simplified description of glycolysis based on [25] to illustrate the concepts and methods introduced. Glycolysis is one of the most well-studied metabolic pathways and is present in almost all cells. It transforms glucose to pyruvate, generating ATP and redox potential in the process. In [25], to explain glycolytic oscillations as a result of hard limits in controlling the glycolysis pathway, a simplified description of glycolysis is developed. Instead of capturing the detailed metabolites and enzymatic reactions, [25] focused on ATP or energy charge regeneration, and simplified the glycolysis pathway to two lumped reactions: one consuming ATP to activate glucose, producing an intermediate molecule, and one consuming the intermediate to produce more ATP. In fact, this architecture can serve as a universal lumped description of all autocatalytic processes [17].

In this lumped description of glycolysis, there are two metabolite species, X_1 and X_2, which correspond to intermediates and ATP in glycolysis. There are two reactions: v_1 consumes q amounts of ATP (X_2) and produces one intermediate (X_1) through activation of glucose, and v_2 consumes intermediate and produces $1+q$ ATP, resulting in a net increase of 1 unit of ATP. Note that in the actual glycolysis pathway, 2 ATP molecules are consumed to activate glucose, and 4 ATP molecules are regenerated at the end, resulting in a net increase of 2 ATP molecules. So one unit for ATP here is 2 molecules. Similar normalization is applied throughout, making this formulation general for all autocatalytic pathways. There is also external exchanges with the environment, including glucose supply and ATP consumption by other parts of the cell. Because [25] focused on glycolytic oscillations, which happens in a glucose rich environment, the glucose supply is assumed abundant. So

we are left with one exchange flux, the consumption of ATP. Follow the stoichiometry-flux split in Eqn (4.13), the flux control formulation can be written as

$$\frac{d}{dt}\begin{bmatrix} x_1 \\ x_2 \end{bmatrix} = \begin{bmatrix} 1 & -1 \\ -q & q+1 \end{bmatrix}\begin{bmatrix} v_1 \\ v_2 \end{bmatrix} + \begin{bmatrix} 0 \\ -1 \end{bmatrix} w.$$

This is the description of the bottom stoichiometry-flux layer when the glycolysis pathway is considered as a layered architecutre. [25] also gives detailed models of how v_1 and v_2 are regulated by feedback from ATP, based on mechanistic understanding of the relevant enzymes involved, e.g. phosphofructokinase is allosterically activated by ADP and AMP and inhibited by ATP. Such information about enzymes and their allosteric regulation constitute the middle layer. How these enzymes are produced and degraded constitutes the top layer, which is not considered here or in [25] because the timescale of glycolytic oscillation is tens of seconds, so the top layer can be considered constant.

To have useful constraints on behavior, we focus on steady states and apply the FBA formulation. The solution set of FBA in Eqn (4.15) yields

$$\begin{bmatrix} 1 & -1 \\ -q & 1+q \end{bmatrix}\begin{bmatrix} v_1^* \\ v_2^* \end{bmatrix} = \begin{bmatrix} 0 \\ 1 \end{bmatrix} w^* \quad \Longrightarrow \quad \begin{bmatrix} v_1^* \\ v_2^* \end{bmatrix} = \begin{bmatrix} 1+q & 1 \\ q & 1 \end{bmatrix}\begin{bmatrix} 0 \\ 1 \end{bmatrix} w^* = \begin{bmatrix} w^* \\ w^* \end{bmatrix}.$$

So we see that the internal fluxes (v_1, v_2) are completely determined by the external flux w. To be specific, internal fluxes has 2 degrees of freedom, and the constraint from a rank-2 stoichiometry matrix at steady state eliminates 2 degrees of freedom, results in unique solution. This is an illustration of the power of constraint-based modelling. The stoichiometry of the reactions involved, when known, act as hard constraints on cell behavior, as unassailable as universal laws such as conservation of mass, so we can strongly constrain internal fluxes based on measurements of external fluxes.

That we obtain unique solution of internal steady state fluxes here is of course not common. Extra degrees of freedom on steady state internal fluxes is necessary for the cell to have "choices" and perform adjustments based on environments at steady state. Unique solution happens here because we used lumped descriptions, while a more detailed stoichiometry matrix is often wide, therefore not full rank. To illustrate what happens when there are extra degrees of freedom at steady state, consider adding another reaction with flux v_3, which we can term growth, that just consumes ATP, but can be regulated by the cell, therefore constitute an internal flux.

$$\frac{d}{dt}\begin{bmatrix} x_1 \\ x_2 \end{bmatrix} = \begin{bmatrix} 1 & -1 & 0 \\ -q & q+1 & -1 \end{bmatrix}\begin{bmatrix} v_1 \\ v_2 \\ v_3 \end{bmatrix} + \begin{bmatrix} 0 \\ -1 \end{bmatrix} w.$$

Now the cell has an extra knob v_3 to tune. To make the numbers simple, let us take $q = 1$, which is the same as the actual stoichiometry of glycolysis that 2 ATP molecules, or 1 unit of X_2, is consumed in v_1. At steady state, the solution set of FBA in Eqn (4.15) then yields

$$\begin{bmatrix} v_1^* \\ v_2^* \\ v_3^* \end{bmatrix} = \frac{1}{3}\begin{bmatrix} 1 \\ 1 \\ -2 \end{bmatrix} w^* + \begin{bmatrix} 1 \\ 1 \\ 1 \end{bmatrix} c = \begin{bmatrix} \frac{1}{3}w^* + c \\ \frac{1}{3}w^* + c \\ -\frac{2}{3}w^* + c \end{bmatrix},$$

where c is a real constant that parameterizes the solution set. So we see that the steady state fluxes v_i^* can be split into two parts, the part determined by external fluxes which depend on w^*, and the part regulated internally which depend on c. In particular, we see that any internal adjustment to increase growth consumption of ATP v_3^* will necessarily require simultaneous increase of ATP and intermediate productions v_1^* and v_2^* in same amount. This is again hard constraints on all biological actions the cell can take, directly from stoichiometry.

Just based on the stoichiometry, all the internal fluxes are unbounded since c can take any real number. We can further bound this by adding constraints from knowledge other than the stoichiometry. First, we can bound c to a finite range by specifying upper and lower bounds of v_j as $1000\ \mathrm{mmol\,g^{-1}\,h^{-1}}$, where gram is cell dry weight. Second, we can constrain v_1 to a relatively narrow range if we can measure the intake of glucose for the scenarios of concern. For example, intake of glucose on the order of $10\ \mathrm{mmol\,g^{-1}\,h^{-1}}$ is often used in FBA simulations for bacterial growth [60, 85]. Lastly, we can determine the v_1 and v_2 as positive for physiological ranges of ATP concentration. This is because under physiological ranges, ATP concentration is about 10^8 fold higher than equilibrium, therefore serves as a very strong driving force. This guarantees the free energy of v_1 is very negative always. Then v_2 is very negative because phosphorylated glucose are high energy compared to pyruvate, so the free energy again is very negative. Together, these conditions can strongly constrain the value that c can take. △

Thermodynamic constraints on metabolic fluxes

According to thermodynamics, the Gibbs free energy of a reaction establishes a constraint on whether a reaction can happen on average, independent of kinetic processes [35, 81, 106]. Specifically, the second law of thermodynamics dictates that any process has to cause a net increase in entropy overall, which becomes a net decrease in Gibbs free energy for systems with reactions inside under constant pressure and temperature. For metabolic systems exchanging metabolites with environments, the Gibbs free energy can increase,

but a similar constraint holds on the cost to do so. Although the second law only holds on average and allows certain trajectories in an ensemble at a microscopic scale to deviate from it, since we are mostly concerned with metabolic processes on a bulk scale, the second law holds in a tight sense.

The reader might also bring up the issue of equilibrium assumption of many thermodynamic relationships, since it is often argued that biology is far away from equilibrium and therefore thermodynamic laws do not apply. It should be clarified that thermodynamic quantities, such as entropy, enthalpy, Gibbs free energy, heat, and temperature are all well-defined on a bulk scale regardless of equilibrium or not. The thermodynamic relationships that require equilibrium are mostly the differential ones based on the equilibrium manifold, such as $dG = SdT + \mu dN + Vdp$ for Gibbs free energy that we often see in textbooks. This is because such differential relations are well-defined only on the equilibrium manifold, i.e. set of equilibrium states characterized by entropy maximization. As a result, these differential relations are only applicable to reversible processes, so that the trajectories stay on the equilibrium manifold. Nonequilibrium states, i.e. states not on the equilibrium manifold, are reached by irreversible processes, characterized by positive entropy production. Since for all states for bulk systems, equilibrium or not, the laws of thermodynamics hold in a tight sense and the thermodynamic quantities are well defined, we can relate equilibrium and nonequilibrium states, and bound irreversible processes by reversible ones plus entropy production. For example, heat from an irreversible process can be split into a reversible part and an entropy production part, $\frac{dQ}{dt} = \dot{Q}_{\text{rev}} + T\sigma$, where σ denotes entropy production rate, and $\dot{Q}_{\text{rev}}$ is the heat generation rate of this process in a reversible way, therefore we use $\dot{}$ to emphasize this part is on the equilibrium manifold [106].

For our context of a metabolic system with exchange of metabolites with external environments under constant temperature and pressure, the Gibbs free energy is the natural thermodynamic quantity to study. We derive a formula for the dissipation of Gibbs free energy for irreversible processes in bulk below, which models after Equation 10 in [106]. We begin with entropy change of the system. For a reversible process, $\Delta S = \frac{Q_{\text{rev}}}{T}$, where ΔS is change in entropy, Q_{rev} is the heat produced by the system in a reversible way, and T is temperature. Since metabolic systems are open to taking in and secreting out molecules with the environment, we also need to account for the entropy included in the molecules in these material exchanges. However, in our existing formulation such as Eqn (4.12), the metabolite concentrations $\boldsymbol{x}$ are all internal metabolites, i.e. metabolites considered as part of the system. The external metabolites that are taken in or secreted out are not included. For example, if we consider glucose is abundantly supplied, then it is not included as one of

internal metabolites $\boldsymbol{x}$, but instead is an external metabolite. Let us denote $\boldsymbol{x}^{\text{ext}} \in \mathbb{R}^{n_e}$ as the vector of external metabolite concentrations, and $\overline{s}_i^{\text{ext}}$ as the partial molar entropy carried by the ith external metabolite, assuming the unit of concentration (and flux) is molar. Since the fluxes $\boldsymbol{v}$ and $\boldsymbol{w}$ could include intake or secretion of external metabolites, we denote $\boldsymbol{S}^{\text{ext}}$ and $\boldsymbol{S}^{\text{ext},w}$ as the extended part of their stoichiometry regarding external metabolites. s_{ij}^{ext} is positive means the jth reaction with flux v_j assimilates s_{ij}^{ext} numbers of molecules of external metabolite X_i^{ext}. Then the entropy production of the external environment from intake and secretion of external metabolites by the system is $-(\overline{\boldsymbol{s}}^{\text{ext}})^\intercal(\boldsymbol{S}^{\text{ext}}\boldsymbol{v} + \boldsymbol{S}^{\text{ext},w}\boldsymbol{w})$. The negative sign is because influx of metabolites in the system is outflux of metabolites in the environment, while positive entries of $\boldsymbol{S}^{\text{ext}}$ means intake by the system. Lastly, we include the entropy change from entropy production rate σ due to irreversibility, we have

$$\frac{dS}{dt} = \frac{\dot{Q}_{\text{rev}}}{T} - (\overline{\boldsymbol{s}}^{\text{ext}})^\intercal\Big(\boldsymbol{S}^{\text{ext}}\boldsymbol{v} + \boldsymbol{S}^{\text{ext},w}\boldsymbol{w}\Big) + \sigma. \tag{4.16}$$

The second law corresponds to $\sigma \geq 0$, with equality achieved only for reversible processes. Since Gibbs free energy is defined by $G = H - TS$, where H is enthalpy, we also split entropy change in a similar way based on the first law of thermodynamics:

$$\frac{dH}{dt} = \dot{W} + \dot{Q}_{\text{rev}} - (\overline{\boldsymbol{h}}^{\text{ext}})^\intercal\Big(\boldsymbol{S}^{\text{ext}}\boldsymbol{v} + \boldsymbol{S}^{\text{ext},w}\boldsymbol{w}\Big), \tag{4.17}$$

where $\overline{h}_i^{\text{ext}}$ is the partial molar enthalpy carried by the ith metabolite, and $\dot{W}$ is rate of work or power done on the system. $\dot{W}$ is nonzero for microbes performing photosynthesis therefore absorbing significant power from environment. Since our main focus is on chemotrophs, $\dot{W}$ is negligible, so we ignore this term. Now subtracting $T\frac{dS}{dt}$ from $\frac{dH}{dt}$ yields our expression for Gibbs free energy change:

$$\frac{dG}{dt} = -(\boldsymbol{\mu}^{\text{ext}})^\intercal\Big(\boldsymbol{S}^{\text{ext}}\boldsymbol{v} + \boldsymbol{S}^{\text{ext},w}\boldsymbol{w}\Big) - T\sigma, \tag{4.18}$$

where $\mu_i^{\text{ext}} = \overline{h}_i^{\text{ext}} + T\overline{s}_i^{\text{ext}}$ is the chemical potential of the ith external metabolite. Note that chemical potential μ_i^{ext} is the same as the molar Gibbs free energy of the ith external metabolite species [27]. We can relate this to free energy changes due to internal fluxes on internal metabolites, since conservation of energy (the first law) dictates that the free energy change from these external interactions must be the same as that from internal fluxes. This means

$$\frac{dG}{dt} = \boldsymbol{\mu}^\intercal(\boldsymbol{S}\boldsymbol{v} + \boldsymbol{S}^w\boldsymbol{w}) = -(\boldsymbol{\mu}^{\text{ext}})^\intercal\Big(\boldsymbol{S}^{\text{ext}}\boldsymbol{v} + \boldsymbol{S}^{\text{ext},w}\boldsymbol{w}\Big) - T\sigma. \tag{4.19}$$

Here μ_i is the chemical potential of the ith internal metabolite. We can re-write this equation by considering the free energy change of both internal and external metabolites

involved. Adding $(\boldsymbol{\mu}^{\text{ext}})^\intercal(\boldsymbol{S}^{\text{ext}}\boldsymbol{v} + \boldsymbol{S}^{\text{ext},w})\boldsymbol{w}$ to both sides of the above equation, we obtain the following inequality:

$$(\boldsymbol{\mu}^{\text{full}})^\intercal\left(\boldsymbol{S}^{\text{full}}\boldsymbol{v} + \boldsymbol{S}^{\text{full},w}\boldsymbol{w}\right) := \begin{bmatrix}\boldsymbol{\mu}\\ \boldsymbol{\mu}^{\text{ext}}\end{bmatrix}^\intercal\left(\begin{bmatrix}\boldsymbol{S}\\ \boldsymbol{S}^{\text{ext}}\end{bmatrix}\boldsymbol{v} + \begin{bmatrix}\boldsymbol{S}^{w}\\ \boldsymbol{S}^{\text{ext},w}\end{bmatrix}\boldsymbol{w}\right) = -T\sigma \leq 0. \tag{4.20}$$

Here the full superscript means both internal and external metabolites are included in the respective variables. This inequality means that when both internal and external metabolites are considered for the reactions, the fluxes necessarily dissipates free energy. Note that Eqn (4.20) holds in general, without steady state assumptions. Therefore this inequality is a constraint that can be applied to the fluxes even when they vary dynamically. Later we will apply this to individual reaction fluxes which yields stronger constraints that relate free energy with direction of fluxes.

Coming back to Eqn (4.19), we can turn it into a constraint on the steady state fluxes. At steady state, free energy change is zero, so

$$0 = -\boldsymbol{\mu}^\intercal(\boldsymbol{S}\boldsymbol{v} + \boldsymbol{S}^{w}\boldsymbol{w}) = -(\boldsymbol{\mu}^{\text{ext}})^\intercal\left(\boldsymbol{S}^{\text{ext}}\boldsymbol{v} + \boldsymbol{S}^{\text{ext},w}\boldsymbol{w}\right) - T\sigma. \tag{4.21}$$

Note that the first equality is also implied by that the internal metabolite dynamics reach steady state, so that $\boldsymbol{S}\boldsymbol{v} + \boldsymbol{S}^{w}\boldsymbol{w} = 0$ (Eqn (4.14)). Since internal metabolite concentrations tend to vary significantly, we can denote $\boldsymbol{\mu} = \boldsymbol{\mu}(\boldsymbol{x})$ to make explicit the dependence of chemical potential on concentrations for internal metabolites.

$$\text{External free energy constraint: } (\boldsymbol{\mu}^{\text{ext}})^\intercal\left(\boldsymbol{S}^{\text{ext}}\boldsymbol{v} + \boldsymbol{S}^{\text{ext},w}\boldsymbol{w}\right) = -T\sigma \leq 0. \tag{4.22}$$

This inequality can be considered as an extra constraint on the internal and external fluxes at steady state in FBA (Eqn (4.14)). This is useful if the chemical potential of external metabolites $\boldsymbol{\mu}^{\text{ext}}$ is known. If equality is achieved in Equation (4.22), then the metabolic system is in equilibrium, with reactions happen in a reversible fashion. This means the fluxes are infinitely slow. This might be desirable when nutrient is poor, but undesirable when nutrient is available since slow consumption may cause microbes to be out-competed by other species. On the other hand, a very large entropy production rate σ would imply significant free energy is spent on driving the reactions fast, and but not much energy is stored in the product. This might be desirable when nutrient is overly abundant, but undesirable when efficiency in nutrient utilization is important (also see [106]).

While Eqn (4.22) can derive a value for entropy production rate σ based on free energy dissipation, quantitatively relating σ to actual speed of the reaction fluxes is hard. This is because it requires knowing the detailed mechanisms of chemical driving, especially the

equilibrium kinetic rates of the relevant reaction. For example, if we want to relate entropy production rate with a reaction driven by ATP coupling, then we need to know the kinetic rate constant of the catalytic enzyme when there is no ATP in the system. Even when the kinetic mechanisms are measured and known, analysis of the resulting network of states is nontrivial, and is still part of cutting edge research in biophysics [72] [Hong Qian etc]. However, any rough estimates from such kinetic considerations of entropy production would be helpful, since it relates the timescale of reaction fluxes to entropy production rates in the free energy relations. In particular, the entropy production rate in Eqn (4.22) can be considered as an upper bound on the available entropy used to accelerate any particular chemical driving mechanism. So instead of developing an analysis with exact physical underpinnings, below we introduce the rudimentary ideas in nonequilibrium steady states analysis and try to obtain coarse relations between flux rates and entropy production rate. The following are based on methods in [72].

To relate entropy production rate with kinetic mechanisms of molecular reactions, nonequilibrium steady states analysis often focus on one molecule, and consider reactions as state transitions of this molecule. This is valid if the other species involved are much more abundant than the molecule of concern. At equilibrium, the molecule transits between states with rates that follow detailed balance. Specifically, let k_{ij} denote the equilibrium rate of transition from state j to i, and G_i the energy of state i, then $k_{ij}e^{-G_j} = k_{ji}e^{-G_i}$. The equilibrium probabilities of each state therefore are just proportional to negative exponential of their energies: $p_j^{\text{eq}} \propto e^{-G_j}$. When there is driving, such as by chemical coupling, on transition from j to i, then the rate increases from k_{ij} by an amount Δq_{ij} to reach the new rate $q_{ij} = k_{ij} + \Delta q_{ij}$. The chemical potential required by this driving is defined as $\Delta\mu_{ij} = k_B T \log \frac{q_{ij}}{k_{ij}}$, where k_B is Boltzmann constant. Then the entropy production rate simply caused by driving the transition from j to i out of equilibrium is defined as $\sigma_{ij}T = k_B T J_{ij} \log \frac{q_{ij}p_j}{q_{ji}p_i}$, where $J_{ij} = q_{ij}p_j - q_{ji}p_i$ is the probability current or flux of the molecule through this transition, and p_i and p_j are possibly nonequilibrium probabilities of the molecule in state i and j respectively. [72] shows that for a transition path γ through multiple states, the equilibrium parts cancel out, so that only the driven part remains, resulting in relation $\sigma_\gamma T = \sum_{(ij)\in\gamma} J_{ij}\Delta\mu_{ij}$. In particular, for a path with only one driving step with strength $\Delta\mu_\gamma$, we have $\sigma_\gamma T = J_\gamma \Delta\mu_\gamma$. Now we can relate this to our bulk scale by changing perspective from single molecules transitioning between states to concentrations of this species transitioning between different forms. This changes the probability flux J_γ to concentration flux v_j for metabolic reaction j, if γ corresponds to the path of state transition of a molecule through the jth reaction, with other reactants and products assumed abundant. Similarly, $\Delta\mu_\gamma$ becomes $\Delta\mu_j$, the elevated potential for driving the jth

reaction. As a result, we have $\sigma_j T = v_j \Delta\mu_j$. This relates the entropy production rate with the flux v_j through the potential $\Delta\mu_j$ used in driving. Since $\Delta\mu_j$ is about how equilibrium kinetic rates are elevated by energy coupling to higher nonequilibrium rates, we now have a relation between entropy production rates, flux magnitude, and kinetic rate amplification. If we know the ratio between entropy production rates and flux magnitudes, for example, then that will bound the kinetic rate amplification, or vice versa. As another example, if kinetic rate amplifications $\Delta\mu_j$ and total entropy production rate σT are known, then this results in $\sum_j v_j^* \Delta\mu_j + \sum_j w_j^* \Delta\mu_j^* = \sigma T$, another constraint on the steady state fluxes.

We can view energy considerations of the fluxes more generally. We can consider the FBA Eqn (4.14) as the condition for *mass balance* at steady state, arising from a fundamental limitation of what cells can do: atoms cannot be created or destroyed. In addition to mass balance, other balances exist, such as energy, charge, redox (proton), and osmotic pressure [59]. Then Eqn (4.22) can be considered as the constraint from *energy balance*, arising from the fundamental limitation that energy is conserved. While law on energy conservation is as strict as the law on mass balance, the resulting constraint (Eqn (4.22)) requires more detailed knowledge, namely chemical potential $\boldsymbol{\mu}^{\text{ext}}(\boldsymbol{x}^{\text{ext}})$ and entropy production rate σ, that are harder to measure or bound than the stoichiometry. While chemical potential $\boldsymbol{\mu}^{\text{ext}}(\boldsymbol{x}^{\text{ext}})$ can be estimated based on formula for ideal solutions, which we describe below, the entropy production rate requires studies of mechanistic systems in nonequilibrium steady states that is still cutting edge research [72]. One way to make Eqn (4.22) easier to apply is to assume the entropy production rate is relatively small, so we just use the lower bound $(\boldsymbol{\mu}^{\text{ext}})^\intercal(\boldsymbol{S}^{\text{ext}}\boldsymbol{v} + \boldsymbol{S}^{\text{ext},w}\boldsymbol{w}) \geq 0$. In a similar fashion, Eqn (4.20) with negligible $T\sigma$ implies $\boldsymbol{\mu}^\intercal(\boldsymbol{S}\boldsymbol{v} + \boldsymbol{S}^w\boldsymbol{w}) = (\boldsymbol{\mu}^{\text{ext}})^\intercal(\boldsymbol{S}^{\text{ext}}\boldsymbol{v} + \boldsymbol{S}^{\text{ext},w}\boldsymbol{w})$, that the internal and external Gibbs energy dissipation are equal. This condition is used in [81] as another constraint on steady state fluxes in FBA formulation with success in explaining the Crabtree effect [3] from an energy dissipation perspective.

In order to calculate chemical potential $\boldsymbol{\mu}^{\text{ext}}(\boldsymbol{x}^{\text{ext}})$ to make Eqn (4.22) useful, we need a formula relating $\boldsymbol{\mu}^{\text{ext}}$ to measurable quantities and the metabolite concentrations. One way to estimate this is to use the formula of chemical potential for ideal solutions or gas: $\mu_i^{\text{ext}} = \mu_i^{\text{ext},0} + RT \log x_i^{\text{ext}}$. Here the external metabolite concentration x_i^{ext} in the formula is measured in molar units. T is temperature, R is the molar gas constant, and $\log$ is natural log. $\mu_i^{\text{ext},0}$ is the chemical potential of the ith metabolite under a standard condition. This standard condition is usually chosen to be the one mostly commonly measured in experiments such as one atm pressure, 25 Celsius, pH 7 or concentrations at 1 molar. Since chemical potential is molar Gibbs free energy, this standard chemical potential can also

be estimated by using the standard free energy change of formation of the ith external metabolite, often denoted $\Delta_f G_i$. This is the free energy change from a metabolite's atomic components into the molecular form under a standard condition. This estimation process is rather coarse since it assumes ideal solution and uses free energy of formation which ignores energy of solvation for example, but it provides a first order estimate that is easy to obtain and has been successfully used in works applying thermodynamic constraints on FBA such as [81].

In addition to free energy dissipation for the overall system, Eqn (4.19) and Eqn (4.20) with the second law can be applied to each reaction flux to determine the reversibility or direction of (possibly dynamic) fluxes. Eqn (4.20) for Gibbs free energy dissipation for the jth reaction flux v_j can be written as

$$\text{Flux direction constraint: } \begin{bmatrix} \boldsymbol{\mu} \\ \boldsymbol{\mu}^{\text{ext}} \end{bmatrix}^{\intercal} \begin{bmatrix} \boldsymbol{S}_j \\ \boldsymbol{S}_j^{\text{ext}} \end{bmatrix} v_j =: \mu_j^v v_j = -T\sigma_j < 0, \tag{4.23}$$

where $\boldsymbol{S}_j$ is the jth columns of the stoichiometry matrix $\boldsymbol{S}$, similarly define $\boldsymbol{S}_j^{\text{ext}}$, and $\mu_j^v = \sum_{i=1}^{n} s_{ij}\mu_i + \sum_{i=1}^{n_e} s_{ij}^{\text{ext}}\mu_i^{\text{ext}}$ is the chemical potential of the jth reaction (the same as the Gibbs free energy change of the jth reaction often denoted $\Delta_r G_j$). σ_j is the entropy projection rate from the jth reaction v_j. By the second law, $\sigma_j > 0$ for irreversible processes, and $\sigma_j = 0$ only when the process is reversible, i.e. infinitely slow. Hence, for non-negligible reaction speed, Eqn (4.23) relates free energy of the reaction with its direction. Since the reaction potential of this reaction μ_j^v depends on metabolite concentrations, this can be viewed as a relationship between concentrations, reaction potential, and flux direction. If the reaction potential is negative, i.e. the products have lower free energy than the reactants, then the reaction can have a net flux in the forward direction. As a resulting constraint, if we know that the reaction potential of reaction j is always negative in the scenarios concerned, depending on factors such as the range of metabolite concentrations, then the steady state flux v_j can be considered irreversible. In terms of the constraint set $\mathcal{U}_{\text{ss}}$, the irreversibility of the jth reaction constrain the flux u_j to be non-negative, $u_j \geq 0$. On the other hand, if the scenarios considered could vary the free energy of the jth reaction between positive and negative values, then we cannot place sign constraints on u_j.

It should be cautioned that a positive net flux of a path of reactions does not require the net flux of every step to be positive. In other words, it should not be a hard constraint that every step in a metabolic system has positive flux. This is because, for a path of reactions consisting of multiple steps to have a net forward flux, it is sufficient to have the net forward steps dominating over the net reverse or net zero steps. As an example, if an intermediate step $A \rightleftharpoons B$ is at equilibrium, so the net flux is zero, we can still generate net forward flux

through this reaction by continuously adding in A and removing B, but keeping their ratio at equilibrium. Therefore, the requirement that certain fluxes are irreversible should only be applied to key steps of reactions where we know significant driving is applied to make it irreversible. If no such information is available, irreversibility should be only applied to overall input-output paths of reactions, based on our knowledge or requirement that there is an overall input to output net flux.

We could also use Eqn (4.23) in the other direction, to use requirement that v_j is irreversible or the driving force of entropy production rate above a certain number to constrain the metabolite concentrations allowed. For example, using ideal solution relations for chemical potential $\mu_i = \mu_i^0 + RT \log x_i$, we have $\mu_j^v = \mu_j^{v,0} + 2.3RT \log_{10} \prod_{i=1}^n x_i^{s_{ij}} \prod_{i=1}^n (x_i^{\text{ext}})^{s_{ij}^{\text{ext}}}$, where $\mu_j^{v_0} = \sum_{i=1}^n s_{ij}\mu_i^0 + \sum_{i=1}^n s_{ij}^{\text{ext}}\mu_i^{\text{ext},0}$. So if we require $\mu_j^v \geq b_j$, where b_j is some lower bound we set to guarantee sufficient driving force for the jth reaction, or $b_j = 0$ to guarantee at least the net flux is in the forward direction, we can have

$$\prod_{i=1}^n x_i^{s_{ij}} \prod_{i=1}^n (x_i^{\text{ext}})^{s_{ij}^{\text{ext}}} \geq 10^{\frac{\mu_j^{v,0} - b_i}{2.3RT}}.$$

Here $2.3RT$ and base 10 are chosen for convenience with hand calculations. For example, $2.3RT$ is about $5.7\ \text{kJ}\,\text{mol}^{-1}$, which gives a conversion between chemical potential and concentration fold changes.

Example 11 (Simple glycolysis, continued)**.** Now we consider quantitative constraints from thermodynamics to further restrict the fluxes from first principles. To account for free energies, we need to include the external metabolites ignored when describing internal metabolite dynamics. External metabolites are glucose consumed in v_1, denote as x_1^{ext}, and waste secreted in v_2, denote as x_2^{ext}. Let μ_1^{ext} denote the chemical potential of glucose, and μ_2^{ext} denote the chemical potential of waste. The exchange flux w does not involve external metabolites, since we consider it as the consumption of ATP or energy charge by the cell. So the free energy dissipation in Eqn (4.19) for this system is

$$\frac{dG}{dt} = -\begin{bmatrix}\mu_1^{\text{ext}} \\ \mu_2^{\text{ext}}\end{bmatrix}^{\mathsf{T}} \left(\begin{bmatrix} -1 & 0 \\ 0 & 1 \end{bmatrix} \begin{bmatrix} v_1 \\ v_2 \end{bmatrix} + \begin{bmatrix} 0 \\ 0 \end{bmatrix} w \right) - \sigma T = \mu_1^{\text{ext}} v_1 - \mu_2^{\text{ext}} v_2 - \sigma T.$$

At steady state, this becomes the inequality in Eqn (4.22),

$$-\mu_1^{\text{ext}} v_1^* + \mu_2^{\text{ext}} v_2^* = -\sigma T \leq 0 \quad \Longrightarrow \quad \mu_1^{\text{ext}} v_1^* \geq \mu_2^{\text{ext}} v_2^*.$$

To use this to constrain the fluxes, we need to estimate the chemical potentials of glucose and waste. The standard free energy of formation for glucose is $-793.74\ \text{kJ}\,\text{mol}^{-1}$ [26]. If

we take the waste as two molecules of pyruvate, then the standard free energy of formation for pyruvate is $-420.28\ \mathrm{kJ\,mol^{-1}}$. We can take the glucose and pyruvate concentrations as $1\ \mathrm{mM}$ and $100\ \mu\mathrm{M}$ respectively. Since $\log_{10} = 2.3\log$ and $2.3RT \approx 5.72\ \mathrm{kJ\,mol^{-1}}$, we estimate $\mu_1^{\mathrm{ext}} \approx \mu_1^{\mathrm{ext},0} + 2.3RT\log_{10} x_1^{\mathrm{ext}} = -793.74 + 5.72 \cdot \log_{10} 10^{-3} = -810.9\ \mathrm{kJ\,mol^{-1}}$, and $\mu_2^{\mathrm{ext}} \approx 2 \cdot (-420.28 + 5.72\log_{10} 10^{-4}) = -886.32\ \mathrm{kJ\,mol^{-1}}$. This gives our approximate bound that

$$v_1^* \leq 1.09 v_2^*.$$

This bound is vacuous when only v_1 and v_2 are the internal fluxes, because in this case we know $v_1^* = v_2^* = w^*$ from steady state condition. But at least we see the bound and the steady state solution is consistent, showing that the unique steady state solution is plausible energetically.

We can use a coarse application of dissipation in nonequilibrium steady states to relate entropy production rate, flux magnitudes, and kinetic rate amplification. Put in $v_1^* = v_2^* = w^*$ at steady state, we have

$$\sigma T = \mu_1^{\mathrm{ext}} v_1^* - \mu_2^{\mathrm{ext}} v_2^* = (\mu_1^{\mathrm{ext}} - \mu_2^{\mathrm{ext}}) w^*.$$

Also recall our discussion that $\sigma_j T = v_j \Delta\mu_j$ which relates entropy production rate of reaction j and the driving potential $\Delta\mu_j$ for reaction j. If we consider only the forward direction of reaction j is driven, which makes sense here because the two reactions are roughly irreversible based on free energy estimates, we have $\Delta\mu_j = k_B T \log \frac{q_j^+}{k_j^+}$, where q_j^+ is the nonequilibrium forward reaction rate after driving, and k_j^+ the equilibrium kinetic rate of this forward step. So we have $\Delta\mu_j = \frac{\sigma_j T}{v_j} \leq \frac{\sigma T}{v_j}$, since $\sigma = \sum_j \sigma_j$. To apply these nonequilibrium formulations to our setting, we need to choose which species we focus on to represent the reactions as state transitions of molecules of this species. We can choose the multiple states of this species to be glucose, intermediate, and waste. Let us focus on the transition from glucose to intermediate. We have $\frac{\sigma T}{v_j^*} = \mu_1^{\mathrm{ext}} - \mu_2^{\mathrm{ext}}$, so $\Delta\mu_j \leq \mu_1^{\mathrm{ext}} - \mu_2^{\mathrm{ext}}$. Put in the numerical values in molar units, we see $\frac{q_j^+}{k_j^+} \leq \exp\left\{\frac{\mu_1^{\mathrm{ext}} - \mu_2^{\mathrm{ext}}}{RT}\right\} \approx 10^{13}$. k_j^+ is equilibrium rate of transition out of glucose. If we assume the enzymes in glycolysis are not catalytically active when there is no driving force, e.g. ATP to ADP ratio is about 1 to 10^8, then k_j^+ can be considered as the spontaneous rate of decomposition rate of glucose, which is estimated to be about per 100 years [115]. 13 orders faster corresponds to about per 0.3 millisecond, which is on the right orders of magnitude for glycolysis rate. If this relation is applied to an example where steady state fluxes can vary, then for fixed $\Delta\mu_j$ we can in turn obtain $\sum_j v_j^* \Delta\mu_j = \sigma T$ as a further constraint on the steady state fluxes. From this rough estimate,

we see how entropy production rate can relate to nonequilibrium kinetic rates or the flux magnitudes.

We can also determine directionality of the fluxes by using Eqn (4.23). Namely, we need to calculate $\boldsymbol{\mu}_j^v$. For v_1, the reaction from glucose and ATP to intermediate (two glyceraldehyde-3-phosphate, or G3P molecules), has a lumped free energy changed $\boldsymbol{\mu}_1^v = -53.73\ \mathrm{kJ\,mol^{-1}}$. This is calculated from summing the first fives steps of glycolysis under the physiological concentrations of red blood cells (see page 584 of [48]). For this default scenario, indeed $\mu_1^v < 0$, and is very negative. Therefore we can confidently consider v_1 to be irreversible and always positive. We can also consider how variations in metabolite concentrations are related to directionality. To get a context for the numbers, $2.3RT$ is about 5.7 $\mathrm{kJ\,mol^{-1}}$ at $25°\mathrm{C}$, so a 10-fold change in metabolite concentrations will change μ_1^v by $5.7\ \mathrm{kJ\,mol^{-1}}$. So to make μ_1^v close to zero, we need to vary metabolite concentrations a total of 10^9 folds, which is highly unlikely. On the other hand, given our discussion on driving nonequilibrium steady states, a very negative μ_1^v is necessary to keep the reaction rates in physiological range, which tends to be much larger than their equilibrium rates for the steps that phosphorylate sugar. So we may require μ_1^v to be more negative than -51.3 $\mathrm{kJ\,mol^{-1}}$, and see how this constrains the variations of concentrations. Here -51.3 is chosen because this is $9 \times 2.3RT$, so it gives a driving force equivalent to 10^9 folds of concentration difference, or the same folds of kinetic rate changes away from equilibrium. The metabolite concentrations used in $\mu_1^v = -53.73\ \mathrm{kJ\,mol^{-1}}$ that are relevant to this lumped reaction are glucose at $5.0\ \mathrm{mM}$, G3P at $0.019\ \mathrm{mM}$, and ATP at $1.85\ \mathrm{mM}$. We assume the other metabolites, such as phosphate group at $1.0\ \mathrm{mM}$ and ADP at $1.4\ \mathrm{mM}$, are kept constant. Then the deviation from $\mu_1^v = -53.73\ \mathrm{kJ\,mol^{-1}}$ but still higher than 51.3 leaves a margin of 2.4 $\mathrm{kJ\,mol^{-1}}$, which translates to 2.6 fold variation in concentrations in total. So $\frac{\tilde{\Delta}x_{\mathrm{glu}}\tilde{\Delta}x_{\mathrm{atp}}^2}{\tilde{\Delta}x_{\mathrm{g3p}}^2} \leq 2.6$, where $\tilde{\Delta}$ denote the fold-change of corresponding concentrations from their physiological concentrations mentioned previously, such as $\tilde{\Delta}x_{\mathrm{glu}} = \frac{[\mathrm{Glucose}]}{5.0\mathrm{mM}}$. Such bounds hold for transient concentrations as well $\triangle$

Flux exponent control from binding-catalysis split in layered architecture of metabolism incorporates internal dynamics

As a constraint-based approach, the flux control formulation splits the metabolite concentration dynamics into internal fluxes and external fluxes. We began with the model with external fluxes $\boldsymbol{w}$ and internal fluxes $\boldsymbol{v}(\boldsymbol{x})$ regulated by metabolites in Eqn (4.12), and argued that since $\boldsymbol{v}(\boldsymbol{x})$ is fast varying and unknown, we could replace it with control

variables $\boldsymbol{u}$ in the flux control formulation in Eqn (4.13). Considered as an open system, i.e. a system subject to external disturbances $\boldsymbol{w}$, the flux control formulation turns an open system with only internal dynamics $\boldsymbol{v}(\boldsymbol{x})$, to an open system with only internal control actions $\boldsymbol{u}$. This has the disadvantage of ignoring any internal uncontrollable dynamics in metabolism, like inertia in a mechanical system. So we would like to consider metabolism as an open system with both internal uncontrollable and controllable dynamics.

This is exactly how a system is typically formulated in control theory, so we introduce some of the relevant terminology. *Plant* refers to the part of a system that is influenced by external variable $\boldsymbol{w}$ and controlled by internal control variable $\boldsymbol{u}$, with state variable $\boldsymbol{x}$ as output. In other words, the dynamics of the plant is how the system would evolve when the control variables take a standard value, therefore representing the "uncontrolled" behavior of the system. This uncontrolled behavior of the plant with no feedback is also called the *open loop* dynamics of the system. *Controller* refers to how the control variable $\boldsymbol{u}$ is determined based on the state variable $\boldsymbol{x}$ of the plant, which is the metabolite concentration $\boldsymbol{x}$ in our case. The *system*, often called the *closed loop system* to be explicit, is then formed by interconnecting the plant and the controller, so that the overall system response from external variable $\boldsymbol{w}$ to state variable $\boldsymbol{x}$ is different from that of the plant, due to controller actions. In the context of metabolism, we can write this more explicitly. The plant is $\frac{d}{dt}\boldsymbol{x} = \boldsymbol{f}(\boldsymbol{x}, \boldsymbol{u}, \boldsymbol{w})$, capturing how metabolite concentrations vary with control action $\boldsymbol{u}$ and external variable $\boldsymbol{w}$. The controller is a map from $\boldsymbol{x}$ to $\boldsymbol{u}$, which we can assume to be a static function rather than a dynamic process if the controller dynamics is much faster than the plant dynamics. With slight abuse of notation, we denote this static controller function $\boldsymbol{u}(\boldsymbol{x})$. If the control variable $\boldsymbol{u}$ does not vary based on state $\boldsymbol{x}$, i.e. the controller is not interconnected with the plant, then the dynamics from $\boldsymbol{w}$ to $\boldsymbol{x}$ is the open loop dynamics. The closed loop system dynamics has the controller interconnected with the plant, which is $\frac{d}{dt}\boldsymbol{x} = \boldsymbol{f}_{\text{cl}}(\boldsymbol{x}, \boldsymbol{w}) = \boldsymbol{f}(\boldsymbol{x}, \boldsymbol{u}(\boldsymbol{x}), \boldsymbol{w})$.

Geared with control theory concepts, we see that the flux control formulation has only a controller in the system, while the plant is trivial, in the sense that it just integrates the input (see Figure 4.7). Our goal of finding a constraint-based formulation improving over flux control then corresponds to formulating metabolism dynamics as a control system with an explicit split between plant and controller, in a way that both the plant and the controller have nontrivial dynamics. To begin with, we respect the stoichiometry-flux split while allowing control variables in regulation of internal fluxes. This simply means instead of $\boldsymbol{v}(\boldsymbol{x})$ or $\boldsymbol{u}$ as internal fluxes, we write $\boldsymbol{v}(\boldsymbol{x}, \boldsymbol{u})$, to capture that the internal dynamics of metabolism has a nontrivial plant part from $\boldsymbol{v}$'s dependence on $\boldsymbol{x}$, while allowing control

actions by $\boldsymbol{v}$'s dependence on $\boldsymbol{u}$. This yields the following equation for the plant:

$$\frac{d}{dt}\boldsymbol{x}(t) = \boldsymbol{f}(\boldsymbol{x}(t), \boldsymbol{u}(t), \boldsymbol{w}(t)) = \boldsymbol{S}\boldsymbol{v}(\boldsymbol{x}(t), \boldsymbol{u}(t)) + \boldsymbol{S}^w\boldsymbol{w}(t). \tag{4.24}$$

With this formulation of a plant that is based on the stoichiometry-flux split, if the system has a static controller $\boldsymbol{u}(\boldsymbol{x})$, then the closed loop system is

$$\frac{d}{dt}\boldsymbol{x} = \boldsymbol{f}_{\text{cl}}(\boldsymbol{x}, \boldsymbol{w}) = \boldsymbol{S}\boldsymbol{v}_{\text{cl}}(\boldsymbol{x}) + \boldsymbol{S}^w\boldsymbol{w}, \tag{4.25}$$

where $\boldsymbol{v}_{\text{cl}}(\boldsymbol{x}) = \boldsymbol{v}(\boldsymbol{x}, \boldsymbol{u}(\boldsymbol{x}))$. Similar to previous discussions of general control systems, the assumption of static controller here means the map from $\boldsymbol{x}$ to control action $\boldsymbol{u}$ is fast compared to changes in the fluxes. This needs to be carefully argued rather than guaranteed, since we have not specified the mechanism underlying $\boldsymbol{u}$'s regulation of $\boldsymbol{v}$. Now to make Eqn (4.24) into a useful control system formulation of metabolism, the difficulty is in how to formulate the explicit split between plant's internal dynamics and controller actions, i.e. how to construct an explicit split between $\boldsymbol{v}$'s dependence on $\boldsymbol{x}$ and that on $\boldsymbol{u}$.

As a first try in separating plant and controller in regulation of fluxes, we could extend the flux control formulation. This means we split the fluxes into three parts: external exchange fluxes $\boldsymbol{w}$, internal plant fluxes $\boldsymbol{v}$ that are not directly controlled, and internal controller fluxes $\boldsymbol{u}$ that are varied by cells' regulation. Extending the flux control formulation in Eqn (4.13), we write

$$\frac{d}{dt}\boldsymbol{x}(t) = \boldsymbol{S}^A\boldsymbol{v}(\boldsymbol{x}(t)) + \boldsymbol{S}^B\boldsymbol{u}(t) + \boldsymbol{S}^w\boldsymbol{w}(t). \tag{4.26}$$

Here the new term that captures internal dynamics of the plant is $\boldsymbol{S}^A\boldsymbol{v}(\boldsymbol{x})$, where $\boldsymbol{S}^A$ includes the stoichiometry for reactions that are not directly controlled, and $\boldsymbol{v}(\boldsymbol{x})$ is the vector of fluxes of these reactions, capturing how they are regulated based on metabolite concentrations. So we can call $\boldsymbol{v}$ the plant fluxes, and $\boldsymbol{u}$ the controller fluxes.

Although Eqn (4.26) does extend the flux control formulation to include dynamics of the plant, this split of internal fluxes into plant and controller fluxes is impractical and unbiological. On one hand, we are again back to facing the experimental difficulty of characterizing $\boldsymbol{v}(\boldsymbol{x})$ that motivated us to do the constraint-based flux control formulation in the first place. These plant fluxes $\boldsymbol{v}(\boldsymbol{x})$ are just as difficult to characterize as any other fluxes. Namely, we need to climb up the layered architecture of metabolism (see Figure 4.5) through experimental investigations to characterize all the molecular mechanisms involved. This makes writing down $\boldsymbol{v}(\boldsymbol{x})$ in Eqn (4.26) impractical from the perspective of sparse data in metabolism.

On the other hand, a reaction's flux often has both a controlled and uncontrolled part that are not additive, therefore cannot be split into two separate fluxes. From a cell's

perspective, the fluxes are catalyzed by enzymes, and regulated by proteins, cofactors and metabolites binding to the enzymes. This means, "no control" would naturally correspond to the enzyme not regulated by binding, and "control" means inhibition or activation through binding. These two parts control the same flux not in an additive way, but rather complicated and multiplicative in nature. As a simple example, rational functions of MWC or Hill form are often used to describe allosteric regulation of enzyme activity. Say $v(x) = v_{\max}\frac{1}{1+x^2}$ describes how one flux is regulated, with $\frac{1}{1+x^2}$ capturing the fraction of the catalyzing enzyme's activity varying with normalized regulating metabolite concentration x, forming a second-order inhibition. The uncontrolled flux may be considered as the flux at $x = 0$, so $v = v_{\max}$, while the controlled flux is multiplying the factor $\frac{1}{1+x^2}$ to the uncontrolled flux. This simple example illustrates that the controlled-uncontrolled split in cells' regulation of fluxes is not in terms of separate plant and controller fluxes. From the perspective of constraint-based modeling, $\boldsymbol{u}$ represents all the actions that a cell can take biologically. Therefore a plant and controller split in terms of fluxes is unbiological as a representation of cells' actions.

To find a biological representation of cells' actions with a natural split of plant and controller dynamics, we need to respect cells' regulatory architecture of metabolism on a layer higher than the fluxes and stoichiometry. This motivates us to look back at the layered architecture of metabolism (see Figure 4.5). On top of the bottom stoichiometry layer, the metabolic fluxes are catalyzed by enzymes, which in turn are regulated by binding of metabolites, cofactors, and proteins, or transformation of molecular states by covalent modifications such as phosphorylation or methylation. Such regulatory actions often happen on a seconds to minutes timescale. These catalyzing enzymes together with regulation of these enzymes' activities by binding form the middle layer (see Figure 4.5). Here we use binding to describe regulations by binding and state transformations altogether, since state transformations can be considered as binding in an extreme scenario. This is in accordance with our definition of binding networks with state transformations in Chapter 3.

The middle enzyme layer is also regulated at a slower timescale, which we designate as a higher layer, the top gene expression layer, in our coarse description of metabolism architecture. The gene expression layer regulates protein amount by production and degradation processes, often on the tens of minutes timescale. The production process of this layer has an hourglass shape with a thin waist of conserved and non-diverse transcription-translation machinery, connecting diverse genes with diverse proteins produced. This protein production process is enabled by energy and building blocks such as nucleic acids and amino acids supplied by the bottom stoichiometry-flux layer, and the fast timescale

regulatory mechanisms such as transcription factors of the middle enzyme-binding layer. It is arguable there is a similar hourglass shape for degradation in eukaryotes, where the ubiquitin-proteosome system serves the thin waist connecting diverse signals to diverse proteins degraded. But ubiquitin-like systems are not widely present in bacteria.

Now with this description of the higher up layers of flux regulation in metabolism, we can consider how to capture more structure in the flux regulation $\boldsymbol{v}(\boldsymbol{x})$. The flux control formulation as a constraint-based approach split metabolite concentration dynamics $\boldsymbol{f}(\boldsymbol{x}, \boldsymbol{w})$ into stoichiometry and fluxes $\boldsymbol{S}\boldsymbol{v}(\boldsymbol{x})$. In terms of layers in metabolism architecture, this corresponds to splitting between the bottom stoichiometry-flux layer and the higher layers regulating the fluxes (see Figure 4.6). Now we can move up the layered architecture to incorporate more structure in the fluxes $\boldsymbol{v}(\boldsymbol{x})$. Respecting the middle layer structure that the fluxes are catalyzed by enzymes and the enzyme activities are regulated by binding, we can split the middle layer between catalytic enzymes and their binding regulations, where latter is from protein activity of the top layer and metabolites of the bottom layer. In short, we can all this *binding-catalysis split*, where catalysis refers to the catalytic enzymes determining the stoichiometry, or directions of change, and binding refers to the regulation of enzyme activity.

To mathematically formulate the binding-catalysis split in the regulation of fluxes, we need to parameterize binding's regulation of catalysis as a set in some appropriate space. Recall from Chapter 3 that the regulation of enzyme catalysis via binding reactions can be considered as regulating the reaction orders, or log derivatives, of $\boldsymbol{v}$'s dependence on $\boldsymbol{x}$, constrained in a polyhedral set. The polyhedral constraint on reaction orders comes from the stoichiometry of the binding network, which is part of the slow-varying structures of the middle layer. So the binding-catalysis split is mathematically parameterized as controlling reaction orders of catalysis fluxes, with polyhedral constraint on reaction orders from slow varying part, and dynamic control of reaction orders in the polyhedral set from fast varying part. This can be posed as a *rule* of life, that cells regulate metabolic fluxes by adjusting their exponents, or reaction orders. We call this rule *flux exponent control* (FEC). Because the middle binding-catalysis layer also interacts with the bottom stoichiometry-flux layer and the top macro-molecule production-degradation layer by metabolite feedback and protein level variation, further slow varying structures arise from these interactions in terms of which fluxes are controlled and based on concentrations of which metabolites.

Now we try to explicitly incorporate the binding-catalysis split into the control system formulation of metabolism. Reaction orders are log derivatives, capturing the local behavior of fluxes at a given metabolite concentration $\boldsymbol{x}$. So to conveniently bridge with the FEC

rule that binding's regulation of catalysis is parameterized as adjusting reaction orders in a polyhedral set, we want to log-linearize the system in Eqn (4.24) and Eqn (4.25) around a reference point $(\boldsymbol{x}^0, \boldsymbol{u}^0, \boldsymbol{w}^0)$ to consider the local dynamics. Since the FEC rule that reaction orders are constrained in a polyhedral set naturally correspond to the closed loop setting, we log-linearize Eqn (4.25) first.

$$\frac{d}{dt}\tilde{\delta}\boldsymbol{x} = \boldsymbol{\Lambda}_{\boldsymbol{x}^0}^{-1}\boldsymbol{S}\boldsymbol{\Lambda}_{\boldsymbol{v}^0}\boldsymbol{H}^{\mathrm{cl}}\tilde{\delta}\boldsymbol{x} + \boldsymbol{\Lambda}_{\boldsymbol{x}^0}^{-1}\boldsymbol{S}^{w}\boldsymbol{\Lambda}_{\boldsymbol{w}^0}\tilde{\delta}\boldsymbol{w} + \boldsymbol{\Lambda}_{\boldsymbol{x}^0}^{-1}\boldsymbol{f}_{\mathrm{cl}}^0. \tag{4.27}$$

Here $\tilde{\delta}$ denotes fold-change variation relative to the reference point, such as $\tilde{\delta}x_i = \frac{\delta x_i}{x_i^0} = \frac{x_i - x_i^0}{x_i^0}$. This is the same as log-differential in the infinitesimal case, so that $\tilde{\delta}x_i = d\log x_i$ when x_i is close to x_i^0. $\boldsymbol{H}^{\mathrm{cl}}$ is the log derivative, or reaction order, of closed loop fluxes $\boldsymbol{v}_{\mathrm{cl}}$ to metabolites $\boldsymbol{x}$, so $H_{ij}^{\mathrm{cl}} = \frac{\partial \log v_{\mathrm{cl},i}}{\partial \log x_j}$. $\boldsymbol{f}_{\mathrm{cl}}^0 := \boldsymbol{f}_{\mathrm{cl}}(\boldsymbol{x}^0, \boldsymbol{w}^0)$ is the change in metabolite concentration at the reference point in closed loop. Here $\boldsymbol{x}$ and $\boldsymbol{w}$ are naturally positive variables as they correspond to concentrations and fluxes, so taking $\log$ makes sense. To avoid issue with taking $\log$ of variables with units, we can consider a standard unit for concentrations and fluxes, and all the concentration and flux variables are numerical values relative to these standard units.

The FEC rule parameterizing the binding-catalysis split then says that binding regulates the reaction order $\boldsymbol{H}^{\mathrm{cl}}$ within some polyhedral set $\mathcal{P}$, so $\boldsymbol{H}^{\mathrm{cl}} \in \mathcal{P}$. In the closed loop system in Eqn (4.25) or its log-linearization in Eqn (4.27), the binding regulation is already included in the system, so reaction order $\boldsymbol{H}^{\mathrm{cl}}(\boldsymbol{x})$ varies with changes in $\boldsymbol{x}$, so binding's regulation can be considered as a map from $\boldsymbol{x}$ to $\boldsymbol{H}^{\mathrm{cl}}$. We want to break this open to have an explicit control variable $\boldsymbol{u}$, mapped from $\boldsymbol{x}$ via a controller, that adjusts the reaction order $\boldsymbol{H}^{\mathrm{cl}}$. This means breaking the map from $\boldsymbol{x}$ to $\boldsymbol{H}^{\mathrm{cl}}$ into the composition of two maps: a map from $(\boldsymbol{x}, \boldsymbol{u})$ to $\boldsymbol{H}^{\mathrm{cl}}$, composed with another map from $\boldsymbol{u}$ to $\boldsymbol{x}$. This split of the closed system in Eqn (4.25) should agree with the plant system in Eqn (4.24) at least in terms of log-linearization. So we can compare their log-linearized expressions for suggestions on how to do the split. Log-linearize the plant (Eqn (4.24)) yields the following:

$$\frac{d}{dt}\tilde{\delta}\boldsymbol{x} = \boldsymbol{\Lambda}_{\boldsymbol{x}^0}^{-1}\boldsymbol{S}\boldsymbol{\Lambda}_{\boldsymbol{v}^0}\left(\boldsymbol{H}^{A}\tilde{\delta}\boldsymbol{x} + \boldsymbol{H}^{B}\tilde{\delta}\boldsymbol{u}\right) + \boldsymbol{\Lambda}_{\boldsymbol{x}^0}^{-1}\boldsymbol{S}^{w}\boldsymbol{\Lambda}_{\boldsymbol{w}^0}\tilde{\delta}\boldsymbol{w} + \boldsymbol{\Lambda}_{\boldsymbol{x}^0}^{-1}\boldsymbol{f}^0. \tag{4.28}$$

Here $\boldsymbol{H}^A$ is the log derivative, or reaction order, of open loop fluxes $\boldsymbol{v}$ to $\boldsymbol{x}$, so $H_{ij}^A = \frac{\partial \log v_i}{\partial \log x_j}$. Similarly, $\boldsymbol{H}^B$ is the reaction order of $\boldsymbol{v}$ to $\boldsymbol{u}$. $\boldsymbol{f}^0 := \boldsymbol{f}(\boldsymbol{x}^0, \boldsymbol{u}^0, \boldsymbol{w}^0)$ is the change in metabolite concentration at the reference point in open loop. To take $\log$ for $\boldsymbol{u}$, we temporarily assume $\boldsymbol{u}$ is positive as well. Since $\boldsymbol{u}$ should eventually represent how reaction orders are adjusted in a polyhedral set, positive or real are simply two equivalent parameterizations.

A comparison of Eqn (4.27) with Eqn (4.28) shows that the closed loop and open loop reaction orders are related by $\boldsymbol{H}^{\mathrm{cl}}\tilde{\delta}\boldsymbol{x} = \boldsymbol{H}^{A}\tilde{\delta}\boldsymbol{x} + \boldsymbol{H}^{B}\tilde{\delta}\boldsymbol{u}$. Now if we close the loop with a

controller map from $\boldsymbol{u}$ to $\boldsymbol{x}$ that is static $\boldsymbol{u}(\boldsymbol{x})$, then we can log-linearize the controller map at $\boldsymbol{x}^0$ as well to obtain $\boldsymbol{H}^K$, the log derivative of $\boldsymbol{u}$ to $\boldsymbol{x}$: $\boldsymbol{H}^K_{ij} = \frac{\partial \log u_i(\boldsymbol{x}^0)}{\partial \log x_j}$. So the closed loop reaction orders should relate to the open loop reaction orders under static feedback via $\boldsymbol{H}^{\text{cl}}\tilde{\delta}\boldsymbol{x} = \boldsymbol{H}^A\tilde{\delta}\boldsymbol{x} + \boldsymbol{H}^B\boldsymbol{H}^K\tilde{\delta}\boldsymbol{x}$, which is just the following equality on the reaction orders:

$$\boldsymbol{H}^{\text{cl}} = \boldsymbol{H}^A + \boldsymbol{H}^B\boldsymbol{H}^K. \tag{4.29}$$

We see that this relationship between closed loop and open loop gains is in complete analogy to the static feedback in linear systems. Recall that the FEC parameterization of regulation by binding is reaction orders are varied in response to changing metabolite concentrations within a polyhedral set $\boldsymbol{H}^{\text{cl}}(\boldsymbol{x}) \in \mathcal{P}$. We see that the equality between the reaction orders naturally maps this polyhedral constraint on reaction orders to constraint on the controller gain $\boldsymbol{H}^K$. It is constrained in the set

$$\boldsymbol{H}^K \in \mathcal{P}^K := \left\{\boldsymbol{H}^K : \boldsymbol{H}^B\boldsymbol{H}^K \in \mathcal{P} - \boldsymbol{H}^A\right\}. \tag{4.30}$$

Crucially, the polyhedral constraint on reaction orders that originates from the stoichiometry of underlying binding reactions is naturally converted to polyhedral constraints on the controller gain.

The comparison of closed loop and open loop dynamics give us a clear idea for how to split the control actions and the plant internal dynamics in the log-linearized case. We would like to bring this split from the local dynamics back to the global dynamics, formulating a plant-controller split for Eqn (4.24). We can get the full flux regulation back from its log-linearization via integration. Take a scalar flux in closed loop $v_i^{\text{cl}}(\boldsymbol{x})$. It relates to its reaction orders by $\frac{\partial \log v_i^{\text{cl}}}{\partial \log \boldsymbol{x}} = \boldsymbol{H}_i^{\text{cl}}$, where $\boldsymbol{H}_i^{\text{cl}}$ is the ith row of $\boldsymbol{H}^{\text{cl}}$. In other words, $\boldsymbol{H}_i^{\text{cl}}$ is the gradient of $\log \boldsymbol{v}_i^{\text{cl}}$ in $\log \boldsymbol{x}$ coordinates. Consider a path γ from a reference point $\boldsymbol{x}^0$ to $\boldsymbol{x}$. Then we can integrate over this path to obtain $\log v_i^{\text{cl}}(\boldsymbol{x}) - \log v_i^{\text{cl}}(\boldsymbol{x}^0) = \int_\gamma \boldsymbol{H}_i^{\text{cl}}(\boldsymbol{x}) \cdot d\log \boldsymbol{x}$. For the choice of reference point, we can choose it to be the standard concentration units, so that $\boldsymbol{x}^0 = \mathbf{1}$, a vector of ones. We denote the standard flux $v_{\text{std},i}^{\text{cl}} := v_i^{\text{cl}}(\mathbf{1})$. So we can express $v_i^{\text{cl}}(\boldsymbol{x}) = v_{\text{std},i}^{\text{cl}} e^{\int_\gamma \boldsymbol{H}_i^{\text{cl}} \cdot d\log \boldsymbol{x}}$, where γ is any path that goes from $\mathbf{1}$ to $\boldsymbol{x}$. Alternatively, we can choose $\boldsymbol{x}^0$ to be the saturating concentration, since fluxes in metabolism, like many biological quantities, eventually saturates out with metabolite concentrations going towards infinity. This means we can choose $\boldsymbol{x}^0$ large enough in every coordinate such that the flux no longer responds to variations in $\boldsymbol{x}$, so the reaction order is zero $\boldsymbol{H}_i^{\text{cl}} = 0$ and the flux $\boldsymbol{v}_i^{\text{cl}}(\boldsymbol{x}^0)$ no longer changes, taking value of a well-defined saturated flux, which we denote $v_{\text{sat},i}^{\text{cl}}$. With the reference point at saturating concentrations, we have $v_i^{\text{cl}}(\boldsymbol{x}) = v_{\text{sat},i}^{\text{cl}} e^{\int_\gamma \boldsymbol{H}_i^{\text{cl}} \cdot d\log \boldsymbol{x}}$, where γ is any path that goes from a saturating concentration to $\boldsymbol{x}$.

We see that in the closed loop case, the result of integrating reaction orders is not simple because the reaction order $\boldsymbol{H}^{\mathrm{cl}}$ depends on $\boldsymbol{x}$. With the system split into plant and controller, we know the closed loop reaction order relates to the open loop reaction order with static controller feedback via $\boldsymbol{H}^{\mathrm{cl}} = \boldsymbol{H}^A + \boldsymbol{H}^B\boldsymbol{H}^K$. So we can resolve this issue in the open loop case by having $\boldsymbol{H}^A$ and $\boldsymbol{H}^B$ as constants and delegate all dependence on $\boldsymbol{x}$ into the controller feedback. In other words, with $\boldsymbol{x}$ dependence explicit, we want $\boldsymbol{H}^{\mathrm{cl}}(\boldsymbol{x}) = \boldsymbol{H}^A + \boldsymbol{H}^B\boldsymbol{H}^K(\boldsymbol{x})$. We will later show the interpretation of $\boldsymbol{H}^A$ and $\boldsymbol{H}^B$ and how to determined them so that it makes sense they are constants. Let us for now focus on mathematically integrate the flux from reaction orders in the open loop case. We know $\frac{\partial \log v_i}{\partial \log(\boldsymbol{x},\boldsymbol{u})} = \begin{bmatrix}\boldsymbol{H}_i^A & \boldsymbol{H}_i^B\end{bmatrix}$. Integrating over a path from a ference point $(\boldsymbol{x}^0, \boldsymbol{u}^0)$ to $(\boldsymbol{x}, \boldsymbol{u})$, we obtain

$$\begin{aligned}\log v_i(\boldsymbol{x},\boldsymbol{u}) - \log v_i^0 =& \int_\gamma \Big(\boldsymbol{H}_i^A d\log \boldsymbol{x} + \boldsymbol{H}_i^B d\log \boldsymbol{u}\Big)\\ =& \boldsymbol{H}_i^A(\log \boldsymbol{x} - \log \boldsymbol{x}^0) + \boldsymbol{H}_i^B(\log \boldsymbol{u} - \log \boldsymbol{u}^0),\end{aligned}$$

where $v_i^0 := v_i(\boldsymbol{x}^0, \boldsymbol{u}^0)$ is the reference flux. Let us choose the reference concentration $\boldsymbol{x}^0$ to be the standard unit of concentrations so that $\boldsymbol{x}^0 = \mathbf{1}$, a vector of ones, and the reference control action $\boldsymbol{u}^0$ to be $\mathbf{1}$ as well. These together define the standard reference flux $v_{\mathrm{std},i}^0 := v_i(\boldsymbol{x}^0, \boldsymbol{u}^0) = v_i(\mathbf{1}, \mathbf{1})$. This yields

$$v_i(\boldsymbol{x},\boldsymbol{u}) = v_{\mathrm{std},i}^0 \exp\Big\{\boldsymbol{H}_i^A \log \boldsymbol{x} + \boldsymbol{H}_i^B \log \boldsymbol{u}\Big\} = v_{\mathrm{std},i}^0 \boldsymbol{x}^{\boldsymbol{H}_i^A}\boldsymbol{u}^{\boldsymbol{H}_i^B},$$

where we use the notation $\boldsymbol{x}^{\boldsymbol{H}_i^A} := x_1^{H_{i1}^A} x_2^{H_{i2}^A} \dots x_n^{H_{in}^A}$. In vector form, we have

$$\boldsymbol{v}(\boldsymbol{x},\boldsymbol{u}) = \boldsymbol{\Lambda}_{\boldsymbol{v}_{\mathrm{std}}^0} \exp\Big\{\boldsymbol{H}^A \log \boldsymbol{x} + \boldsymbol{H}^B \log \boldsymbol{u}\Big\} = \boldsymbol{v}_{\mathrm{std}}^0 \circ \boldsymbol{x}^{\boldsymbol{H}^A} \circ \boldsymbol{u}^{\boldsymbol{H}^B}. \tag{4.31}$$

Here exponential is applied component-wise to a vector, and $\boldsymbol{\Lambda}_{\boldsymbol{v}_{\mathrm{std}}^0}$ is the diagonal matrix with the standard reference flux $\boldsymbol{v}_{\mathrm{std}}^0$ on the diagonal. The operation $\circ$ denote Hadamard or element-wise product. $\boldsymbol{x}^{\boldsymbol{H}^A}$ denotes the vector with $\boldsymbol{x}^{\boldsymbol{H}_i^A}$ as the ith element. $\boldsymbol{u}^{\boldsymbol{H}^B}$ is similarly defined. Note that for a static controller with map $\boldsymbol{u}(\boldsymbol{x})$, the standard reference flux in open and closed loop are related by $\boldsymbol{v}_{\mathrm{std}}^0 = \boldsymbol{v}(\boldsymbol{x}^0, \boldsymbol{u}^0) = \boldsymbol{v}(\boldsymbol{x}^0, \boldsymbol{u}(\boldsymbol{x}^0)) = \boldsymbol{v}^{\mathrm{cl}}(\boldsymbol{x}^0) = \boldsymbol{v}_{\mathrm{std}}^{\mathrm{cl}}$. So we can simply use $\boldsymbol{v}_{\mathrm{std}}^0$ to denote the standard reference flux that is well-defined in both closed loop and open loop cases, whenever a controller is specified.

As a simple example to illustrate this plant-controller split of fluxes in open and closed loop, consider a flux with all variables scalar: $v^{\mathrm{cl}}(x) = v_{\max}\frac{x}{K+x}$. This is a typical Michaelis-Menten type behavior of an enzyme catalyzed flux, with x the concentration of substrate, K the Michaelis constant indicating the half-flux substrate concentration, and $v_{\max}$ the maximum flux dependent on the number of enzymes. We want to describe this flux as

the interconnection of a open loop plant with a controller. So we choose $H^B = 1$ to allow control action, and choose the passive, or uncontrolled plant dynamics to be proportional to substrate, so $H^A = 1$. Therefore Eqn (4.31) in this case becomes $v^{\text{cl}}(x) = v^0_{\text{std}} x u(x)$, relating closed loop and interconnection of open loop with controller. The standard reference flux in this case is $v^0_{\text{std}} = v(x^0, u^0) = v^{\text{cl}}(x^0, u(x^0)) = \frac{v_{\max}}{1+K}$. If we change the unit of concentration, such as taking K as the unit, then this is transform $x \mapsto Kx$, so $v^{\text{cl}}(x) = v_{\max} \frac{x}{1+x} = v^0_{\text{std}} x u(x)$, where $u(x) = \frac{1}{1+x}$ and $v^0_{\text{std}} = \frac{v_{\max}}{2}$. We see that this gives a natural split between internal dynamics of the plant and the controller action, so we can break open the closed loop to ask questions about what if alternative controllers are used. In this case, we simply write the open loop flux as $v(x, u) = v^0_{\text{std}} x u$, which is the same as the closed loop flux but with u's dependence on x removed. Then alternative controllers, i.e. static or dynamic maps from x to u, can be connected to this open loop flux.

Although Eqn (4.31) gives an explicit split between internal dynamics of the plant, i.e. $\boldsymbol{v}$'s dependence on $\boldsymbol{x}$, and regulation by controller, i.e. $\boldsymbol{v}$'s dependence on $\boldsymbol{u}$, what is the biological meaning of the extra structure involved and how can it be determined in a mechanistic fashion? Just like the stoichiometry matrices $\boldsymbol{S}$ and $\boldsymbol{S}^w$ are the structures of the bottom stoichiometry-flux layer in the architecture of metabolism (see Figure 4.8 and Figure 4.5), passive reaction orders $\boldsymbol{H}^A$, controller placements $\boldsymbol{H}^B$, and the controller sparsity pattern $\mathcal{S}^{\boldsymbol{xu}}$ are the structures of the middle binding-catalysis layer. These structures of the middle layer are constant and mechanistic, just like the stoichiometry.

Let us first describe the meaning of the passive reaction order $\boldsymbol{H}^A$. Mathematically, since the local behavior satisfies $\boldsymbol{H}^{\text{cl}} = \boldsymbol{H}^A + \boldsymbol{H}^B \boldsymbol{H}^K$, the passive reaction order $\boldsymbol{H}^A$ is the reaction order of the fluxes when there is no control regulation, $\boldsymbol{H}^K = 0$. Biologically, since the controller captures regulation of enzyme activity by binding with metabolites (including the reactants themselves) and proteins, the passive reaction order can be considered as how the reaction flux would proceed if the catalyzing enzyme is a "pure" or "ideal" catalyst that has only catalytic activity but no regulation. For example, since an enzyme often consists of several functional domains that are modular to varying degrees, we can imagine making it "ideal" by removing the regulatory domains of the catalyzing enzyme, but with the catalytic activity kept intact. While this is likely very hard to do in reality if at all, we can do so theoretically in a straight-forward fashion. Since enzymes, as catalysts, only speed up reactions, the reaction order $\boldsymbol{H}^A$ should reflect how a reaction's flux naturally depend on reactants and products. For a simple reaction, i.e. a reaction with no intermediate steps, this dependence is exactly captured by the law of mass action. For a reaction with intermediate steps, which is unavoidable for catalysis, the dependence can be more involved since

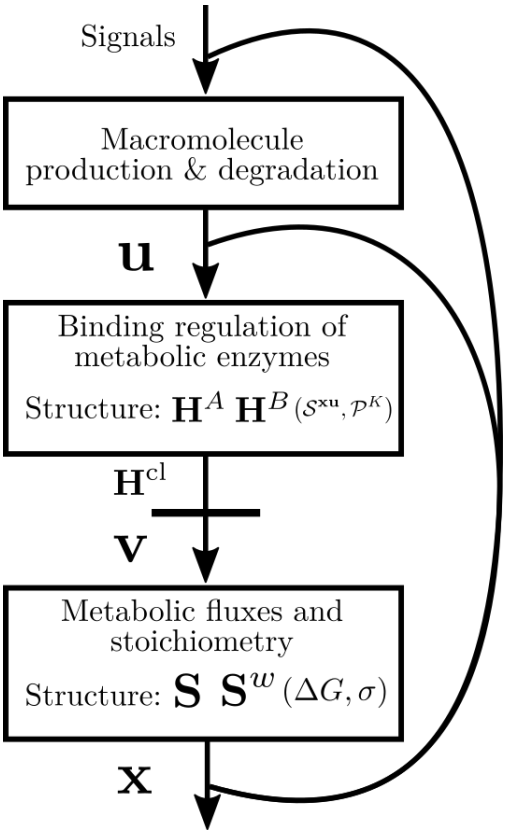

Figure 4.8 A control diagram representation of the layered architecture of metabolism (see Figure 4.5. The three rectangular boxes correspond to the three layers. $\boldsymbol{x}$ is metabolite concentrations, $\boldsymbol{v}$ is metabolic reaction fluxes, $\boldsymbol{H}^{\mathrm{cl}}$ is closed loop reaction orders or exponents of the fluxes, $\boldsymbol{u}$ is binding's regulation of fluxes through exponents or reaction orders. That fluxes $\boldsymbol{v}$ are regulated through exponents $\boldsymbol{H}^{\mathrm{cl}}$ is the rule of flux exponent control (FEC). The middle layer has hard structures $\boldsymbol{H}^A$, passive reaction orders, and $\boldsymbol{H}^B$, controller placements, and soft structures (in parenthesis) $\mathcal{S}^{\boldsymbol{xu}}$, controller sparsity pattern, and $\mathcal{P}^K$, constraints on controller gain.

the enzyme binding with metabolites needs to be considered. But we can imagine that an ideal catalyst would speed up the reaction without adding any intermediate steps, therefore the reaction would still proceed with mass action rates. Qualitatively, a reaction's passive flux always increases with reactant concentrations, and decreases with product concentrations. This is unchanged from infinitely slow reactions in the thermodynamic limit, to fast reactions catalyzed by efficient enzymes. This can be captured in the passive reaction order $\boldsymbol{H}^A$ by positive values for reactants, and negative values for products. If the reaction is largely irreversible based on the thermodynamic relationship between free energy and metabolite concentrations, then we can let the negative reaction orders for products be zeros. To assign quantitative values to the reaction orders, mass action says the value should be the same as the number of molecules consumed or produced as specified in stoichiometry. This is often 1 for reactants, and -1 for products if reversible; take these values as default. We caution that since lumped reactions are often used in writing down

the stoichiometry of metabolism, the reaction orders should be assigned based on the smallest steps, since mass action only applies to simple reactions. For example, while a lumped reaction may be $2A \to B$, the individual steps may be $A \to B'$ and $A + B' \to B$. From the lumped reaction, wrongly applying mass action to it would say reaction order to A is 2. But from the individual steps, we see that if B' concentration is kept much lower than A, so the $A + B' \to B$ step is saturated by A, then the overall reaction order of B's production to A is 1. The bottom line, of course, is to experimentally investigate the smallest reaction steps involved in a reaction to obtain how the reaction order depends on all metabolites involved in the intermediate steps, so that appropriate passive reaction orders can be assigned at each step. This accumulation of mechanistic knowledge on $\boldsymbol{H}^A$ is similar to that on stoichiometry $\boldsymbol{S}$. $\boldsymbol{H}^A$ might be hard to obtain in complex cases such as electron bifurcation in the electron transport chain. So mathematical tools that rigorously relate reaction orders for lumped and detailed reactions are urgently needed.

The other structures of the middle layer are the controller placements $\boldsymbol{H}^B$ and controller sparsity pattern $\mathcal{S}^{\boldsymbol{xu}}$. These have to do with how the metabolites $\boldsymbol{x}$ are used to regulate the fluxes $\boldsymbol{v}$ through their reaction orders $\boldsymbol{H}^{\mathrm{cl}}$. Specifically, $\boldsymbol{x}$ is mapped to control action $\boldsymbol{u}$ through controller map with sparsity pattern $\mathcal{S}^{\boldsymbol{xu}}$, and then $\boldsymbol{u}$ is mapped to reaction orders $\boldsymbol{H}^{\mathrm{cl}}$ with placements according to $\boldsymbol{H}^B$. Abstractly in control theory terms, $\mathcal{S}^{\boldsymbol{xu}}$ is the sensor sparsity, namely which metabolites are sensed by a control variable u_ℓ, and $\boldsymbol{H}^B$ is the actuator pattern, namely a control variable u_ℓ acts on which reaction orders. We can also interpret this biologically. Since the map from $\boldsymbol{x}$ to $\boldsymbol{H}^{\mathrm{cl}}$ represents how binding regulates enzyme activity, we can interpret $\boldsymbol{u}$ as any intermediate variables in this mapping, if there is any. The regulation from metabolites to reaction orders can be a direct map without intermediates, such as in enzyme allostery, or an indirect map with intermediates, such as through protein binding or phosphorylation and methylation. In the indirect case, $\boldsymbol{u}$ can represent the intermediate regulatory proteins. Then the structure in the map from $\boldsymbol{u}$ to reaction orders, captured by $\boldsymbol{H}^B$, is the interaction structure on which fluxes are influenced by the same protein. Correspondingly, the structure in the map from $\boldsymbol{x}$ to $\boldsymbol{u}$ is captured by the controller sparsity pattern $\mathcal{S}^{\boldsymbol{xu}}$, describing which metabolites influence which regulatory proteins. In the direct case such as enzyme allostery, a metabolite x_i directly acts on reaction orders of a flux v_j, so the step of mapping through a control variable u_ℓ is simply mathematically representing this direct action. Then u_ℓ for this allostery should only depend on the regulatory metabolite x_i, and u_ℓ should only influence the reaction order of flux v_j. Mathematically, this means the controller sparsity $\mathcal{S}^{\boldsymbol{xu}}$ has row ℓ with only one nonzero entry at i, and the ℓth column of $\boldsymbol{H}^B$ has only one nonzero entry at j, which can be 1 by choice.

Quantitative specification of $\mathcal{S}^{\boldsymbol{xu}}$ is simple if the controller is static, which we discuss here, while a dynamic controller would require more sophisticated tools from control theory, which we defer to next subsection. Although $\mathcal{S}^{\boldsymbol{xu}}$ does not appear explicitly in Eqn (4.31) but instead constrain controller maps, it is an important feature for metabolism and a severe constraint on possible biological actions. It is therefore important to determine the controller sparsity pattern, especially for large metabolic networks. We discuss how to incorporate this structure as constraints on metabolism dynamics in the next section, since dealing with it requires a bit more control theory technicality on distributed control. For a static controller with map $\boldsymbol{u}(\boldsymbol{x})$, $\mathcal{S}^{\boldsymbol{xu}}$ simply restricts the possible dependences of $\boldsymbol{u}$ on $\boldsymbol{x}$. So $\mathcal{S}^{\boldsymbol{xu}}$ is a matrix in $\{0,1\}^{n\times n_u}$ with all entries zero or one, where n is the number of metabolites and n_u is the dimension of control variables. This is the same dimension as derivative $\frac{\partial \boldsymbol{u}}{\partial \boldsymbol{x}}$ or log derivative $\frac{\partial \log \boldsymbol{u}}{\partial \log \boldsymbol{x}}$ of $\boldsymbol{u}$ to $\boldsymbol{x}$, and can be seen as a "mask" restriction on them, that $\frac{\partial \log x_i}{\partial \log u_j}$ can be nonzero only if $\mathcal{S}^{\boldsymbol{xu}}_{ij} = 1$. For the direct regulation by enzyme allostery, the row of $\mathcal{S}^{\boldsymbol{xu}}$ for that control action will have all zeros except a one at the entry corresponding to the allosteric metabolite. For indirect regulation, the row of $\mathcal{S}^{\boldsymbol{xu}}$ captures which metabolites influence the regulatory proteins represented by the control action. Although biologically the direct and indirect cases seem distinct, their mathematical meaning are the same: the ones in ℓth row of $\mathcal{S}^{\boldsymbol{xu}}$ captures which metabolites are sensed and eventually influence the control variable u_ℓ. To apply this sparsity pattern to a dynamic controller then requires propagation of this sparsity to dynamic trajectories, which is discussed in the next subsection.

Now we discuss quantitative specification of $\boldsymbol{H}^B$. Viewed from Eqn (4.31), the jth column of $\boldsymbol{H}^B$ specifies which fluxes are co-influenced by the jth control action u_j. Since $\boldsymbol{H}^B$ appears as product $\boldsymbol{H}^B \log \boldsymbol{u}$, we can multiply each column of $\boldsymbol{H}^B$ by a scalar and absorb that scalar into $\log \boldsymbol{u}$. So if the jth column of $\boldsymbol{H}^B$ has only one nonzero entry, say the H^B_{ij} entry, we can always make it $H^B_{ij} = 1$, which specifies that u_j only influences flux v_i. This is guaranteed for the direct regulation case, since u_j is just a representation of the allosteric metabolite acting on the catalyzing enzyme, which is one-to-one coupled by molecular structure of the enzyme. For the indirect regulation case, it is possible that a column of $\boldsymbol{H}^B$ may have more than one nonzero entry, so that one control variable u_j influences two or more fluxes simultaneously. This means that one regulatory protein can bind with multiple enzymes for example, with H^B_{ij} representing the relative strength of how the binding of this protein to the enzyme adjusts the reaction orders of the ith reaction.

Lastly, there is a polyhedral set $\mathcal{P}^K$ constraining the controller gain $\boldsymbol{H}^K$, which we discussed in the static controller case in Eqn (4.30). This polyhedral constraint comes from

stoichiometry of the underlying binding network that regulates the catalytic enzymes, as formulated in Chapter 3. Since the stoichiometry of the binding network also varies on a rather slow timescale, this polyhedral constraint $\mathcal{P}^K$ is also constant and mechanistic.

It might appear that these four structures are a lot to specify or determine. However, just like for the bottom layer, stoichiometry is always needed to formulate the problem, while free energy and concentration relations from thermodynamics can enhance the model but not necessary, these four structures can also be split according to whether they are always needed. Out of the four structures, passive reaction orders $\boldsymbol{H}^A$ and controller placements are hard structures $\boldsymbol{H}^B$, in the sense that they are always assumed known in the regulation of fluxes in Eqn (4.31). If they are not known, some value have to be specified for them to use Eqn (4.31). On the other hand, the controller sparsity pattern $\mathcal{S}^{\boldsymbol{xu}}$ and constraint on controller gain $\mathcal{P}^K$ are soft structures, in the sense that if they are not known, they can be left out so that no constraints are imposed. If the controller sparsity pattern is not known, then we allow the controller to be dense so any metabolite can be used to determine any control variable. If the controller gain constraint is not known, then we can allow the gain to be unconstrained. To avoid pathology, we can then simply require control actions to have generic regularities such as smoothness or smaller magnitudes corresponding to coarse notions of smaller energy cost. There is a deeper reason to the hard-soft split of the four structures. With the flux dynamics split into plant and controller, we see that the passive reaction orders and the controller placements are structures of the plant, while the sparsity pattern and constraints on gain are structures of the controller. To specify a control problem, we always need to specify the plant, therefore hard, while the controller is unknown or to be designed, therefore soft. Biologically, the plant corresponds to coarse information about the metabolic enzymes, namely the stoichiometry of the reactions they catalyze (for $\boldsymbol{H}^A$) and whether they are regulated by binding (for $\boldsymbol{H}^B$). The controller, on the other hand, includes all the complexity in regulation of enzyme activity by binding from metabolites and proteins, and state transformation such as phosphorylation and methylation. The processes represented by the controller is less known and harder to characterize experimentally than those of the plant. For example, to specify $\mathcal{P}^K$ requires information about the binding network regulating the enzymes. As a result, the soft constraints $\mathcal{S}^{\boldsymbol{xu}}$ and $\mathcal{P}^K$ are often difficult to specify compared to the hard constraints $\boldsymbol{H}^A$ and $\boldsymbol{H}^B$. Fortunately, this is consistent with the hard-soft split in this formulation, so that the soft constraints that are difficult to specify can be left unconstrained.

This completes our discussion of how to formulate the fluxes $\boldsymbol{v}$ as control systems with both internal plant dynamics and controller actions. We did this via the rule of flux exponent

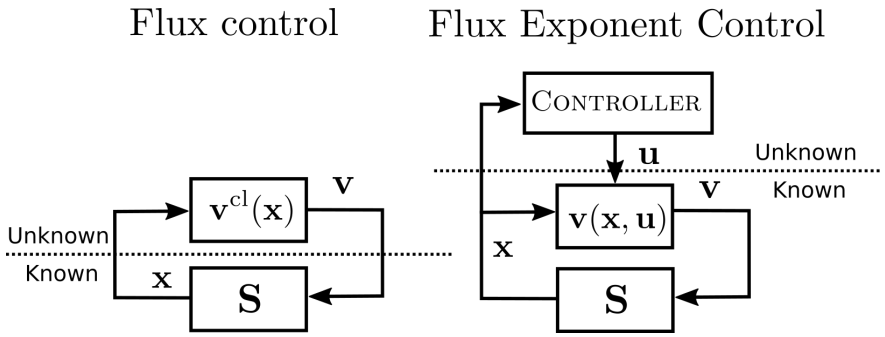

Figure 4.9 Control diagram comparison between flux control and flux exponent control in closed loop.

control (FEC) based on results from Chapter 3 that binding regulates enzyme activity by adjusting the reaction orders within a polyhedral set. This results in the control diagram in Figure 4.8 that fluxes $\boldsymbol{v}$ are regulated through a control action $\boldsymbol{u}$, mapped from metabolites $\boldsymbol{x}$ via a controller, to adjust the reaction orders $\boldsymbol{H}^{\mathrm{cl}}$. Mathematically, this is described by Eqn (4.31), which we derived by comparing closed loop and open loop formulations in local behaviors. The structures of this regulation from metabolites $\boldsymbol{x}$ to reaction orders $\boldsymbol{H}^{\mathrm{cl}}$ come from the middle binding and catalysis layer in architecture of metabolism (see Figure 4.5 and 4.8), namely passive reaction orders $\boldsymbol{H}^{A}$, controller placements $\boldsymbol{H}^{B}$, controller sparsity pattern $\mathcal{S}^{\boldsymbol{xu}}$, and constraints on controller gain $\mathcal{P}^{K}$. These structures are constant, mechanistic, and can be systematically determined based on their biological meaning, just like stoichiometry of the bottom layer.

With the fluxes formulated into a control system via FEC, we can now integrate this into the stoichiometry-flux structure of the bottom layer to have a control system for the full metabolism dynamics. Plug $\boldsymbol{v}(\boldsymbol{x},\boldsymbol{u})$ from Eqn (4.31) into the flux control formulation in Eqn (4.24), we obtain the following:

$$\frac{d}{dt}\boldsymbol{x} = \boldsymbol{S}\boldsymbol{\Lambda}_{\boldsymbol{v}^0}\exp\Big\{\boldsymbol{H}^{A}\log\boldsymbol{x} + \boldsymbol{H}^{B}\log\boldsymbol{u}\Big\} + \boldsymbol{S}^{w}\boldsymbol{w}, \tag{4.32}$$

where $\boldsymbol{v}^0$ is short-hand for the standard reference flux $\boldsymbol{v}^0_{\mathrm{std}}$, and the controller map from $\boldsymbol{x}$ to $\boldsymbol{u}$ is constrained by the sparsity pattern $\mathcal{S}^{\boldsymbol{xu}}$ and the polyhedral constraint on gain $\mathcal{P}^{K}$, if these constraints are available.

This is the full flux exponent control (FEC) formulation of metabolism dynamics as a constraint-based approach. Compared to the flux control formulation based on the stoichiometry-flux split of the bottom layer in metabolism architecture, FEC incorporates the binding-catalysis split of the middle layer as well (see Figure 4.9 and Figure 4.6). In flux control, the stoichiometry $\boldsymbol{S}$ is assumed slow-varying and known, and is therefore taken as constraints, while fluxes $\boldsymbol{v}$ are assumed fast-varying from unknown regulations of higher

layers, and therefore are taken as control variables. In FEC, further structures in fluxes $\boldsymbol{v}$ from the middle layer is incorporated. In addition to stoichiometry, passive reaction orders $\boldsymbol{H}^A$, controller placements $\boldsymbol{H}^B$, controller sparsity pattern $\mathcal{S}^{\boldsymbol{xu}}$, and constraints on controller gain $\mathcal{P}^K$, are further slow-varying structures that can be revealed and incorporated as constraints on biological actions whenever available. The control variables $\boldsymbol{u}$ that are fast-varying by unknown regulation from metabolites and proteins in other layers on the enzyme activity in the middle layer correspond to regulations on the reaction orders.

Compared to flux control, FEC as a constraint based approach for metabolism dynamics is more biological and naturally dynamic. Flux control as a dynamic formulation has difficulty in finding useful constraints. FEC significantly improves this via the FEC rule, that flux exponents are controlled, rather than the fluxes themselves. This yield the exponent-control form that is already restrictive, and further impose structural constraints such as passive reaction orders $\boldsymbol{H}^A$ and controller placements $\boldsymbol{H}^B$. By adding structural constraints from the middle layer, the set of control actions allowed in FEC is smaller compared to that in flux control, therefore closer to the exact set of biological actions, enabling better predictions overall (see Figure 4.2). So the set of flux trajectories allows in FEC is more biological than that of flux control. Flux control also ignores all intrinsic dynamics of metabolism, akin to ignoring inertia in mechanics, because all internal fluxes are controlled this formulation and the plant just trivially integrates input (see Figure 4.7). This is resolved by FEC, which is based on an explicit split between internal dynamics and controller actions in the flux dynamics (Eqn (4.31)). Specifically, the "inertia" of metabolism is captured in one of the structures of the middle layer: passive reaction orders $\boldsymbol{H}^A$ that govern internal dynamics when there is no control action. Therefore compared to flux control, FEC naturally captures the internal dynamics of metabolism through a dynamic structural foundation. So FEC qualitatively improves over flux control on dynamics and biological constraints.

FEC also improves over FBA on steady state analysis. To impose useful constraints, flux control gives up dynamics and makes the steady state assumption to obtain the FBA formulation. That flux control has no internal plant dynamics makes FBA fundamentally about steady state fluxes rather than metabolites, so metabolite concentrations cannot be obtained from FBA. FEC improves over FBA on this, since setting Eqn (4.32) at steady state yields an equation relating $\boldsymbol{x}$, $\boldsymbol{u}$ and $\boldsymbol{w}$. So metabolite concentrations at steady state can be obtained, as well as how they vary with external exchanges and control actions. Static controllers $\boldsymbol{u}(\boldsymbol{x})$ can also be easily incorporated in such analysis to compare different control

strategies. More importantly, FEC allows us to ask about whether a steady state is stable. FBA investigates steady states assuming they are stable based on biological common sense that homeostasis is often reached. However, the proper functioning of dynamic regulatory mechanisms of metabolism are exactly what makes homeostasis a reality. In other words, FBA cannot investigate what happens if metabolic systems are perturbed out of proper functioning regimes where a particular homeostasis is guaranteed. Questions about strong perturbations that push metabolic systems to their extremes cannot be answered by FBA. In contrast, because of the dynamic nature of FEC, questions about whether a steady state is stable or whether metabolism adapts to certain disturbances at steady state can be formulated and answered systematically. So FEC qualitatively improves over FBA on steady state analysis as well by making questions about metabolite concentrations and stability analyzable.

To demonstrate the power of FEC requires us to analyze dynamic properties of systems of the form in Eqn (4.32). This requires analytical and computational tools from control theory, which we introduce next.

Before we end, inspection of the FEC formulation in Eqn (4.32) from a mathematical perspective may motivate a question about why the external interaction variable $\boldsymbol{w}$ cannot act on the internal fluxes in a way similar to controllers $\boldsymbol{u}$. In terms of layered architecture, this corresponds to external interactions not only in the bottom stoichiometry-flux layer, but also the middle binding-catalysis layer. Biologically, this means concentrations of enzymes, proteins, cofactors, and other allosteric metabolites in the middle layer can be directly adjusted externally. This is possible but rare biologically, since most regulatory metabolites and proteins are kept inside cells, therefore not accessible externally through chemical means. Other external perturbations that can directly access internal metabolites and proteins are often uniform and slow-varying, such as temperature and osmotic pressure. Therefore allowing $\boldsymbol{w}$ to act on flux exponents constitute a rather different kind of problem for metabolism that naturally occur in cells. Viewed as questions to ask theoretically, placing $\boldsymbol{w}$ on flux exponents corresponds to asking what if enzyme regulations are perturbed. This is useful in modelling the effect of mutations on enzymes or regulatory proteins, including varying binding constants, allosteric activities, and knock-outs. Together, placing $\boldsymbol{w}$ at flux exponents form an interesting class of questions that we do not address here, but is a fascinating direction worthy of further investigations.

Example 12 (Simple glycolysis, continued)**.** The simple glycolysis in FEC formulation is

$$\frac{d}{dt}\begin{bmatrix} x_1 \\ x_2 \end{bmatrix} = \begin{bmatrix} 1 & -1 \\ -q & 1+q \end{bmatrix} \begin{bmatrix} v_1^0 & 0 \\ 0 & v_2^0 \end{bmatrix} \exp\left\{ \begin{bmatrix} 0 & 1 \\ 1 & 0 \end{bmatrix} \begin{bmatrix} \log x_1 \\ \log x_2 \end{bmatrix} + \begin{bmatrix} 1 & 0 \\ 0 & 1 \end{bmatrix} \begin{bmatrix} \log u_1 \\ \log u_2 \end{bmatrix} \right\} + \begin{bmatrix} 0 \\ -1 \end{bmatrix} w.$$

This may seen overly complicated. Write the fluxes together, we have a a compact form:

$$\frac{d}{dt}\begin{bmatrix} x_1 \\ x_2 \end{bmatrix} = \begin{bmatrix} 1 & -1 \\ -q & 1+q \end{bmatrix} \begin{bmatrix} v_1^0 x_2 u_1 \\ v_2^0 x_1 u_2 \end{bmatrix} + \begin{bmatrix} 0 \\ -1 \end{bmatrix} w.$$

Here v_1 has passive part x_2 because x_2, ATP, is reactant of v_1, and this flux is considered irreversible because of large driving force. Similarly, v_2 has passive part x_1 because x_1, the intermediate, is a reactant for the second flux. △

Summary

Constraint-based approach is a powerful method to model metabolism dynamics since mechanistic data is often sparse. Constraint-based models are inherently based on splits of structures in the layered architecture of metabolism. Slow-varying structures are usually known and incorporated into the problem formulation as constraints, and fast-varying variables are usually unknown and formulated as control actions. Metabolic behaviors are analyzed by characterizing the set of all possible trajectories from feasible control actions, or finding points in feasible controls that optimizes certain objectives. Flux control, and its steady state variant flux balance analysis (FBA), are based on stoichiometry-flux split in the bottom layer. Stoichiometry is used as constraints, and fluxes are control actions. Flux control cannot capture dynamic properties of metabolism due to the lack of internal dynamics not directly controlled. Flux exponent control (FEC) fixes this by incorporating further structures from the middle binding-catalysis layer. Metabolic fluxes are catalyzed by enzymes, whose activities are regulated by binding from metabolites and proteins. Based on Chapter 3, such regulations are parameterized by adjustments of flux exponents, or reaction orders, in a polyhedral set. This enables a further split of flux dynamics into control actions and internal dynamics of a plant not directly controlled. Therefore FEC captures internal dynamics of metabolism and is more biological than flux control by incorporating further structural constraints, such as passive reaction orders and controller placements.

To analyze metabolic systems formulated by FEC, we need theoretical tools for dynamics from control theory. We introduce them and adapt them to the FEC setting in the next section.

4.4 Tools, hard limits, and laws from control theory

Dynamics and transient behaviors are important to understand and engineer metabolic systems. However, data on mechanisms is often sparse in metabolism, motivating us

to move beyond traditional detailed mechanistic models which require full specification of molecular parts involved, but instead use constraint-based approaches which take the known mechanisms as constraints and let unknown parts vary freely. In Section 4.3, we proposed a constraint-based approach called flux exponent control (FEC) that is designed for capturing metabolism dynamics. To make such models useful, we need tools to analyze dynamic behaviors of metabolic models from FEC. In this section, we introduce and adapt tools from control theory for this purpose. In addition, as discussed in Section 4.1, to have knowledge about necessity relating phenotypes back to mechanisms that is complimentary to sufficiency, we need a systems theory, as well as hard limits and laws in it. FEC can be considered as a systems theory for metabolism dynamics, with the space of all possible metabolic systems corresponding to the set of all tuples $(\boldsymbol{S}, \boldsymbol{S}^w, \boldsymbol{H}^A, \boldsymbol{H}^B, \boldsymbol{\Phi}^{\boldsymbol{xu}})$. The tuple captures possible stoichiometry $(\boldsymbol{S}, \boldsymbol{S}^w)$, passive reaction orders $\boldsymbol{H}^A$ and controller placements $\boldsymbol{H}^B$, and controllers $\boldsymbol{\Phi}^{\boldsymbol{xu}}$ mapping $\boldsymbol{x}$ to $\boldsymbol{u}$, as they appear in Eqn (4.32). This provides a systems theory foundation for us to obtain hard limits and laws governing the space of all metabolic systems, akin to conservation of energy, mass and momentum governing mechanical systems. Since models from FEC are control systems, we naturally hope we can use tools from control theory to derive relevant hard limits and laws.

With this said, although we have a strong motivation to adapt control theory for metabolic systems from FEC, it is unfortunate that existing tools from control theory are not tailor-made for biological systems, and many important biological structures are not respected. This means although existing control theory tools are useful and important, and can be fruitfully applied, as we do in this section, there is still a long way to go in inventing new control theoretical tools that are best suited for biological systems. One example of biological structure not well respected by existing control theory tools is that biological variables are positive, and they vary by production and degradations. Due to both mathematical simplicity and the historical reason that control theory originated from studying mechanical and electrical systems, most powerful control theory tools are based on linear systems and real variables. Extending these results to nonlinear systems is rather complicated, because it heavily relies on the structure of nonlinear systems to be studied. This mindset of linear systems plus weak nonlinearity worked well in mechanical and electrical engineering since there is natural linearity in a wide range of the relevant physics, variables such as position, velocity and voltage naturally take real values, and deviations from linearity can be actively avoided by engineering the system to perform in the linear regime. I argue that this is not suitable for biological systems, because the natural variables such as counts and concentrations are almost always positive, and they

vary via production and degradation processes with positive fluxes that saturate at high concentrations. Hence positive variables and nonlinearity with distinct structures play a fundamental role. In particular, we can not simply consider biological systems as a positive system from exponentiating a linear system. Indeed, from a linear system $\frac{d}{dt}\boldsymbol{z} = \boldsymbol{A}\boldsymbol{z}$, exponentiation yields $\frac{d}{dt}\boldsymbol{x} = \boldsymbol{\Lambda}_{\boldsymbol{x}}\boldsymbol{A}\log\boldsymbol{x}$ where $z_i = \log x_i$, and $\boldsymbol{\Lambda}_{\boldsymbol{x}}$ denotes a diagonal matrix with $\boldsymbol{x}$ on the diagonal. This is very different from varying $\boldsymbol{x}$ by production and degradation processes, such as $\frac{d}{dt}x_i = f_i^+(\boldsymbol{x}) - f_i^-(\boldsymbol{x})$, where f_i^+ denote processes producing x_i, and f_i^- denote processes degrading x_i (also see Chapter 5). Much work still needs to be done in developing control theory tools respecting biological structures. The work in Chapter 5 may be seen as a humble attempt towards this direction, trying to incorporate the positive variable, production-degradation, and regulation-by-reaction-orders structures into a dissipative control framework.

Instead of developing new control theory tools respecting structures of metabolism dynamics, this section aims at introducing existing tools that are relevant and adapting them to the context of metabolism. In particular, this means we focus on local behaviors around steady states by log-linearization, to avoid capturing structures in biological nonlinearities. This is perhaps unsatisfying, but at least this can act as an illustration of what control theory can bring to the table. We discuss four aspects. (1) Stability: beyond steady states, the first important property is whether a given steady state is stable. This concept, extended to control systems with external inputs, also captures adaptation to disturbances. (2) System responses and internal structures: metabolic systems, like general control systems, are described both externally in terms of response to inputs, and internally in terms of system structures. Control theory rigorously relates the two, therefore allowing comparison of responses between different systems. This may provide a rigorous foundation to relate lumped and detailed metabolic networks. (3) Hard limits and laws governing system responses: given a system's internal structure, often hard limits and laws on its performance can be determined. We illustrate this by introducing the conservation of robustness or Bode's integral formula. (4) Sparsity and controller gain constraints: as discussed in Section 4.3, metabolic regulations are often localized and satisfy sparse patterns, since one reaction's flux is often regulated by just a few key metabolites. This corresponds to a sparsity constraint on controller responses, which corresponds to distributed control in control theory. This problem is hard, and becomes feasible to solve only with a recent breakthrough in control theory called system level synthesis (SLS).

The discussion we provide here is necessarily not comprehensive. So here are a few excellent books on foundations of control theory. [31] introduces control theory in the

context of biomolecular circuits. [12] is a standard introduction to control systems. [39] emphasizes robustness and fundamental limits from frequency-domain analysis and focuses on single-input-single-output systems. [41] introduces a rigorous foundation for linear control systems as linear operators, and discusses robust control and relevant computation through convex optimization.

Structural stability by combining stoichiometry with birth-death structure

When analyzing the behavior of a system, the first behaviors of interest are often the steady states. This means we consider the system interacting with external environments, and ask how would the system respond to changes in external inputs through internal regulations after the transients peter out. In the metabolism context, this means we use the closed loop formulation as in Eqn (4.12) (reproduced below) so that internal regulations by controllers are included, and the stoichiometry-flux split is applied. Note that closed loop is explicitly denoted to emphasize internal regulations are included.

$$\frac{d}{dt}\boldsymbol{x} = \boldsymbol{f}^{\mathrm{cl}}(\boldsymbol{x}, \boldsymbol{w}) = \boldsymbol{S}\boldsymbol{v}^{\mathrm{cl}}(\boldsymbol{x}) + \boldsymbol{S}^{w}\boldsymbol{w}. \tag{4.33}$$

Here $\boldsymbol{x} \in \mathbb{R}^{n}_{>0}$ is the vector of metabolite concentrations, $\boldsymbol{v} \in \mathbb{R}^{m}_{>0}$ is the vector of internal metabolic reaction fluxes, $\boldsymbol{w} \in \mathbb{R}^{m_w}$ is the vector of exchanges fluxes with environment, and $\boldsymbol{S} \in \mathbb{R}^{n\times m}$, $\boldsymbol{S}^{w} \in \mathbb{R}^{n\times m_w}$ are stoichiometry vectors for internal and exchange reactions.

Steady state fluxes. At steady state, metabolites $\boldsymbol{x}$ does not vary, so the above equation yields a relation between internal and external steady state fluxes, just as in the flux balance analysis (FBA) formulation in Eqn (4.14), with solution set in Eqn (4.15), reproduced below.

$$\boldsymbol{S}\boldsymbol{v}^{\mathrm{cl},*} = \boldsymbol{S}^{w}\boldsymbol{w}^{*} \quad \Longrightarrow \quad \boldsymbol{v}^{\mathrm{cl},*} \in \mathcal{V}^{\mathrm{cl},*}(\boldsymbol{w}^{*}) := \left\{-\boldsymbol{S}^{\dagger}\boldsymbol{S}^{w}\boldsymbol{w}^{*} + \boldsymbol{v}^{\mathrm{cl},\perp} : \boldsymbol{v}^{\mathrm{cl},\perp} \in \ker \boldsymbol{S}\right\}. \tag{4.34}$$

Here $*$ is used to denote these fluxes are at steady state. This gives us a set of steady state internal fluxes $\mathcal{V}^{\mathrm{cl},*}(\boldsymbol{w}^{*})$ that is allowed by a given external steady state flux $\boldsymbol{w}^{*}$.

However, this only relates internal and external steady state fluxes, with no mentioning of metabolite concentrations. Also, these steady state fluxes can happen in reality only if they are stable, which is assumed rather than studied in the above equation. Whether steady states are stable corresponds to whether the metabolites $\boldsymbol{x}$ come back to a steady state value $\boldsymbol{x}^{*}$ from small perturbations. So we need to study internal flux regulations $\boldsymbol{v}^{\mathrm{cl}}(\boldsymbol{x})$.

Local stability of fixed points from additive linearization. We denote $\boldsymbol{x}^{*}$ as the steady state metabolite concentrations, and it then satisfies $\boldsymbol{f}^{\mathrm{cl}}(\boldsymbol{x}^{*}, \boldsymbol{w}^{*}) = \boldsymbol{S}\boldsymbol{v}^{\mathrm{cl}}(\boldsymbol{x}^{*}) + \boldsymbol{S}^{w}\boldsymbol{w}^{*} = 0$. Since the phrase "steady state" carries a hint that it is also stable, we use the more neutral

term *fixed points* to refer to points $\boldsymbol{x}^*$ that satisfy the above for a given $\boldsymbol{w}^*$. Note that because we have external input $\boldsymbol{w}^*$, the fixed point $\boldsymbol{x}^*$ depends on $\boldsymbol{w}^*$ implicitly through the above equation. As a necessary condition for $\boldsymbol{x}^*$ to be a fixed point, from Eqn (4.34) we require $\boldsymbol{v}^{\mathrm{cl}}(\boldsymbol{x}^*)$ to satisfy $\boldsymbol{v}^*\mathrm{cl}(\boldsymbol{x}^*) \in \mathcal{V}^{\mathrm{cl},*}(\boldsymbol{w}^*)$. So when considering stability of a fixed point, we hold $\boldsymbol{w}^*$ constant.

Stability of this fixed point then refers to whether the system in Equation (4.33) with $\boldsymbol{w} = \boldsymbol{w}^*$ held fixed will evolve back to $\boldsymbol{x}^*$ when starting at $\boldsymbol{x}$ very close to $\boldsymbol{x}^*$. This can be determined from linearization of the system.

$$\frac{d}{dt}\delta\boldsymbol{x} = \boldsymbol{A}^{\mathrm{cl}}\delta\boldsymbol{x} + \boldsymbol{S}^{w}\delta\boldsymbol{w} = \boldsymbol{S}\boldsymbol{V}^{\mathrm{cl}}\delta\boldsymbol{x} + \boldsymbol{S}^{w}\delta\boldsymbol{w}, \tag{4.35}$$

where $\delta\boldsymbol{x} = \boldsymbol{x} - \boldsymbol{x}^*$ is the additive difference around the fixed point $\boldsymbol{x}^*$, and similarly $\delta w = \boldsymbol{w} - \boldsymbol{w}^*$. $\boldsymbol{A}^{\mathrm{cl}} = \boldsymbol{S}\boldsymbol{V}^{\mathrm{cl}} \in \mathbb{R}^{n\times n}$ is the derivative of $\boldsymbol{f}$ with respect to $\boldsymbol{x}$ evaluated at $\boldsymbol{x}^*$, and $\boldsymbol{V}^{\mathrm{cl}}(\boldsymbol{x}) \in \mathbb{R}^{m\times n}$ is the derivative of $\boldsymbol{v}^{\mathrm{cl}}$ to $\boldsymbol{x}$ evaluated at $\boldsymbol{x}^*$.

Stability corresponds to the case when $\boldsymbol{w}$ is held fixed at $\boldsymbol{w}^*$, so $\delta\boldsymbol{w} = 0$, and stability only depends on $\boldsymbol{A}^{\mathrm{cl}}$. Nonzero $\delta\boldsymbol{w}$ is used to study how the dynamics of metabolite concentrations locally respond to exchange fluxes, which is discussed later in system responses. The relevant result on stability from control theory states that the fixed point $\boldsymbol{x}^*$ is stable if $\boldsymbol{A}^{\mathrm{cl}}$ is Hurwitz, i.e. its eigenvalues all have negative real parts. That $\boldsymbol{A}$ is Hurwitz is equivalent to there exists a positive definite matrix $\boldsymbol{P}$ such that the following Lyapunov inequality is satisfied:

$$\boldsymbol{P}\boldsymbol{A}^{\mathrm{cl}} + \left(\boldsymbol{A}^{\mathrm{cl}}\right)^{\mathsf{T}}\boldsymbol{P} < 0,$$

where < 0 means the matrix is negative definite. This gives an easy-to-compute test for stability for one fixed point when the numerical values of $\boldsymbol{A}^{\mathrm{cl}}$ is known. As noise, rate variations and uncertainty are widely present in metabolism, we also want to test stability for fixed points from a range of conditions. However, in metabolism, $\boldsymbol{A}^{\mathrm{cl}} = \boldsymbol{S}\boldsymbol{V}^{\mathrm{cl}}$, so while stoichiometry $\boldsymbol{S}$ has a constant numerical value, $\boldsymbol{A}^{\mathrm{cl}}$ also depends on how the fluxes $\boldsymbol{x}$ responds to changes in metabolite concentrations $\boldsymbol{x}$ around the fixed point captured in the derivative matrix $\boldsymbol{V}^{\mathrm{cl}}$, and this matrix varies significantly with details on $\boldsymbol{v}(\boldsymbol{x})$ and $\boldsymbol{x}^*$. In other words, it is hard to place useful ranges on the numerical value of derivatives $\boldsymbol{V}^{\mathrm{cl}}$ to systematically test for stability of fixed points in a range of scenarios.

Taking inspiration that the fluxes are regulated by adjusting reaction orders in a polyhedral set, and the reaction orders are most likely integer values which correspond to vertices (see Chapter 3), we would like to relate stability to reaction orders. Reaction orders are often naturally bounded within an interpretable range, so this could give us a way to derive

stability of fixed points that is invariant to perturbations and rate changes. See Chapter 5 and [117] for this idea applied to generic biomolecular systems with production and degradation.

Structural stability from fold-change linearization. To relate reaction orders of fluxes to stability of fixed points, we log-linearize (or fold-change linearize) the system in Eqn (4.33) since reaction orders are log derivatives. The result is the same as the closed loop local dynamics in Eqn (4.27) when formulating FEC, except now the reference point is a fixed point.

$$\frac{d}{dt}\tilde{\delta}\boldsymbol{x} = \boldsymbol{\Lambda}_{\boldsymbol{x}^*}^{-1}\boldsymbol{S}\boldsymbol{\Lambda}_{\boldsymbol{v}^*}\boldsymbol{H}^{\mathrm{cl}}\tilde{\delta}\boldsymbol{x} + \boldsymbol{\Lambda}_{\boldsymbol{x}^*}^{-1}\boldsymbol{S}^{w}\boldsymbol{\Lambda}_{\boldsymbol{w}^*}\tilde{\delta}\boldsymbol{w}. \tag{4.36}$$

Here $\tilde{\delta}x_i = \frac{\delta x_i}{x_i^*} = \frac{x_i - x_i^*}{x_i^*}$ is the fold-change or multiplicative deviation from x_i^*, and $\tilde{\delta}\boldsymbol{w}$ is similarly defined. $\boldsymbol{H}^{\mathrm{cl}} = \frac{\partial \log \boldsymbol{v}^{\mathrm{cl}}}{\partial \log \boldsymbol{x}}$ is the reaction order, or log derivative, of $\boldsymbol{v}^{\mathrm{cl}}$ to $\boldsymbol{x}$.

Again, for stability of the fixed point, we hold $\boldsymbol{w}$ constant at $\boldsymbol{w}^*$, so $\tilde{\delta}\boldsymbol{w} = 0$. Stability of $\boldsymbol{x}^*$ therefore only depends on whether $\boldsymbol{\Lambda}_{\boldsymbol{x}^*}^{-1}\boldsymbol{S}\boldsymbol{\Lambda}_{\boldsymbol{v}^*}\boldsymbol{H}^{\mathrm{cl}}$ is Hurwitz. We want to relate this to the reaction orders $\boldsymbol{H}^{\mathrm{cl}}$ in a more direct fashion, since the reaction orders tend to be structural like the stoichiometry matrix, but varies slowly in a range.

To use flux reaction orders to determine stability of fixed points requires us to relate fluxes more directly to net changes of metabolites. In particular, the production-degradation or birth-death structure in changes of metabolite concentrations is emphasized in Chapter 5. It is shown that birth and death orders, or reaction orders of production and degradation processes governing each metabolite, can be used to determine the stability of fixed points independent of rate details. So we should relate flux reaction orders with birth and death orders by splitting reactions into ones that produce x_i and ones that degrade x_i.

We can further split $\boldsymbol{\Lambda}_{\boldsymbol{x}^*}\boldsymbol{S}\boldsymbol{\Lambda}_{\boldsymbol{v}^*}\boldsymbol{H}^{v}$ at a fixed point by utilizing the birth-death structure. Split $\boldsymbol{S} = \boldsymbol{S}^{+} - \boldsymbol{S}^{-}$, so that $\boldsymbol{S}^{\pm}$ are non-negative matrices, with $s_{ij}^{+} = s_{ij}$ if $s_{ij} > 0$, else zero, and $s_{ij}^{-} = |s_{ij}|$ if $s_{ij} < 0$, else zero. Similarly split $\boldsymbol{S}^{w} = \boldsymbol{S}^{w,+} - \boldsymbol{S}^{w,-}$. Then the concentration dynamics of each metabolite species can be written as

$$\frac{d}{dt}\boldsymbol{x} = \boldsymbol{f}^{\mathrm{cl},+}(\boldsymbol{x},\boldsymbol{w}) - \boldsymbol{f}^{\mathrm{cl},-}(\boldsymbol{x},\boldsymbol{w}) := \Big(\boldsymbol{S}^{+}\boldsymbol{v}(\boldsymbol{x}) + \boldsymbol{S}^{w,+}\boldsymbol{w}\Big) - \Big(\boldsymbol{S}^{-}\boldsymbol{v}(\boldsymbol{x}) + \boldsymbol{S}^{w,-}\boldsymbol{w}\Big),$$

with $f_i^{\mathrm{cl},\pm} = \boldsymbol{S}_i^{\pm}\boldsymbol{v} + \boldsymbol{S}_i^{w,\pm}\boldsymbol{w}$, where $\boldsymbol{S}_i^{\pm}$ is the ith row of $\boldsymbol{S}^{\pm}$, and similarly for $\boldsymbol{S}^{w,\pm}$. At steady state, $f_i^{\mathrm{cl},+}(\boldsymbol{x}^*,\boldsymbol{w}^*) = f_i^{\mathrm{cl},-}(\boldsymbol{x}^*,\boldsymbol{w}^*)$. So we can define the turnover timescales of average life time of each x_i molecule as

$$\tau_i^* := \frac{x_i^*}{f_i^{\mathrm{cl},\pm}(\boldsymbol{x}^*,\boldsymbol{w}^*)}.$$

We see that for production of degradation process, there are several contributing reaction fluxes, internal and external:

$$f_i^{\mathrm{cl},\pm} = \sum_{j=1}^{m} s_{ij}^{\pm} v_j^{\mathrm{cl}}(\boldsymbol{x}^*) + \sum_{j=1}^{m_w} s_{ij}^{w,\pm} w_j.$$

So we can define the fraction of production or degradation changes that each reaction flux contributes.

$$\theta_{ij}^{\pm} := \frac{s_{ij}^{\pm} v_j^{\mathrm{cl}}(\boldsymbol{x}^*)}{f_i^{\mathrm{cl},\pm}(\boldsymbol{x}^*, \boldsymbol{w}^*)}, \qquad \theta_{i0}^{\pm} := 1 - \sum_{j=1}^{m} \theta_{ij}^{\pm} = \frac{\sum_{j=1}^{m_w} s_{ij}^{w,\pm} w_j^*}{f_i^{\mathrm{cl},\pm}(\boldsymbol{x}^*, \boldsymbol{w}^*)}.$$

So θ_{ij}^{+} is the fraction of production of x_i contributed by internal flux v_j, and θ_{i0}^{+} is the faction of x_i's production contributed by external exchange fluxes. For each i and $\sigma \in \{-, +\}$, the set of variables $\left\{\theta_{ij}^{\sigma} : j = 0, 1, \ldots, m\right\}$ are non-negative and sum to one, therefore they are convex coefficients that parameterize a simplex. We can use the fractions of the internal fluxes $\left\{\theta_{ij}^{\pm} : i = 1, \ldots, n;\ j = 1, \ldots, m\right\}$ to form matrices $\boldsymbol{\Theta}^{\pm} \in \mathbb{R}^{n \times m}$, with $\Theta_{ij}^{\pm} = \theta_{ij}^{\pm}$. $\boldsymbol{\Theta}^{\pm}$ captures the fraction of production and degradation fluxes of each metabolite contributed by each internal flux. Note that since the fractions of external fluxes $\theta_{i0}^{\pm}$ are not included in these matrices, their rows sum to a number less than 1, and could be strictly less than 1. With these parameterization, we can write

$$\boldsymbol{\Lambda}_{\boldsymbol{x}^*}^{-1} \boldsymbol{S} \boldsymbol{\Lambda}_{\boldsymbol{v}^*} \boldsymbol{H}^{\mathrm{cl}} = \boldsymbol{\Lambda}_{\boldsymbol{\tau}^*}^{-1} \boldsymbol{\Theta} \boldsymbol{H}^{\mathrm{cl}} =: \boldsymbol{\Lambda}_{\boldsymbol{\tau}^*}^{-1} \boldsymbol{H}^{\mathrm{bd}}, \tag{4.37}$$

where $\boldsymbol{\Theta} := \boldsymbol{\Theta}^{+} - \boldsymbol{\Theta}^{-}$, $\boldsymbol{H}^{\mathrm{bd}} := \boldsymbol{\Theta} \boldsymbol{H}^{\mathrm{cl}}$ is the birth-death order determined from flux orders $\boldsymbol{H}^{\mathrm{cl}}$ and the fractions of fluxes contributed to production and degradation processes. Fixed point stability is determined by this matrix $\boldsymbol{\Lambda}_{\boldsymbol{\tau}^*}^{-1} \boldsymbol{H}^{\mathrm{bd}}$, which consists of two parts, the time constants $\boldsymbol{\Lambda}_{\boldsymbol{\tau}^*}$ and the birth-death orders $\boldsymbol{H}^{\mathrm{bd}}$. Like in analysis of generic birth-death systems in Chapter 5 and [117], this split coincides with a separation of the part that varies significantly with noise and rates, namely the time constants, and the part that varies slowly, namely the birth death orders. This motivates us to find a sufficient condition for stability independent of the time constants, which we call structural stability. A simple test for this is diagonal stability (see [117] and Chapter 5): there exists a positive diagonal matrix $\boldsymbol{P}$ such that

$$\boldsymbol{P} \boldsymbol{H}^{\mathrm{bd}} + \left(\boldsymbol{H}^{\mathrm{bd}}\right)^{\intercal} \boldsymbol{P} < 0, \tag{4.38}$$

where < 0 means the matrix is negative definite. If $\boldsymbol{H}^{\mathrm{bd}}$ is diagonal stable, then for any positive vector $\boldsymbol{\tau}^*$, the matrix $\boldsymbol{\Lambda}_{\boldsymbol{\tau}^*}^{-1} \boldsymbol{H}^{\mathrm{bd}}$ is Hurwitz, therefore the fixed point is stable. Note that the inequality for diagonal stability differs from the Lyapunov inequality only in requiring $\boldsymbol{P}$ to be diagonal. Similar to the Lyapunov inequality, the inequality for diagonal stability is a linear matrix inequality (LMI), which can be computed efficiently at scale.

Instability can also be found using similar LMIs, but instead of positive diagonal $\boldsymbol{P}$, we ask for $\boldsymbol{P}$ with all but some diagonal entries negative. If there exists any such $\boldsymbol{P}$, then $\boldsymbol{\Lambda}_{\boldsymbol{\tau}^*}^{-1}\boldsymbol{H}^{\mathrm{bd}}$ is unstable for all $\boldsymbol{\tau}^*$. See [117] for details.

We emphasize the significance of this sufficient condition in two aspects. First, instead of dealing with $\boldsymbol{A}^{\mathrm{cl}}$ and flux derivatives $\boldsymbol{V}^{\mathrm{cl}}$ that are hard to parameterize in a range, we can determine stability based on birth-death orders $\boldsymbol{H}^{\mathrm{bd}}$ which varies slowly in interpretable ranges. For more on interpretation of reaction order ranges, see Section 5.1 in Chapter 5. Second, we can determine stability of steady state metabolite concentrations without knowing the concentrations! This is because $\boldsymbol{H}^{\mathrm{bd}}$ only depends on steady state fluxes (which determine $\boldsymbol{\Theta}^{\pm}$) and flux reaction orders. Recall that knowledge about steady state metabolite concentrations require knowing $\boldsymbol{v}(\boldsymbol{x})$, which is hard, while knowledge about steady state fluxes can be significantly constrained from stoichiometry, as in Eqn (4.34). This is powerful in the sense that it allows a determination of steady state stability regardless of hard-to-know details, in the spirit of necessity mapping phenotypes to mechanisms.

Beyond the birth-death orders, we see that the local dynamics of a metabolic system is has more structure than a birth-death system studied in Chapter 5. Namely, the local dynamics is split into three parts instead of two: the timescales $\boldsymbol{\Lambda}_{\boldsymbol{\tau}^*}$, the flux fractions $\boldsymbol{\Theta}$, and the flux orders $\boldsymbol{H}^{\mathrm{cl}}$. These are determined all by different parts of the system. At steady state, $\boldsymbol{\tau}^*$ is just the average life-time of the metabolites, which only depends on overall production and degradation rates and steady state concentrations. $\boldsymbol{\Theta}$ is the fraction of production or degradation of each metabolite contributed by each flux. This does not depend on the total turn-over rate, and is only nontrivial for entries with more than one flux competing for the production or degradation of the same metabolite. Lastly, $\boldsymbol{H}^{\mathrm{cl}}$ is the reaction orders of each flux, consisting of passive reaction orders and regulations by controllers. So we see this split clearly separates how the dynamics depends on different parts of the system, on different timescales, different physical components, and on different layers in the overall architecture. Motivated by the study of stability independent of timescales, an interesting questions is the formulation of stability independent of both timescales and flux fractions.

Before we end, we can write the full log-linearized dynamics in this birth-death order as follows:

$$\frac{d}{dt}\tilde{\delta}\boldsymbol{x} = \boldsymbol{\Lambda}_{\boldsymbol{\tau}^*}^{-1}\left[\boldsymbol{\Theta}\boldsymbol{H}^{\mathrm{cl}}\tilde{\delta}\boldsymbol{x} + \boldsymbol{\Theta}^{w}\tilde{\delta}\boldsymbol{w}\right]. \tag{4.39}$$

Here $\boldsymbol{\Theta}^{w,\pm}$ are fractions of external exchange fluxes in the production and degradation processes, with $\theta_{ij}^{w,\pm} := \frac{s_{ij}^w w_j^*}{f_i^{\mathrm{cl},\pm}}$, and $\boldsymbol{\Theta}^{w} := \boldsymbol{\Theta}^{w,+} - \boldsymbol{\Theta}^{w,-}$. Rewriting into this form proceeds from $\left(\boldsymbol{\Lambda}_{\boldsymbol{x}^*}^{-1}\boldsymbol{S}^{w}\boldsymbol{\Lambda}_{\boldsymbol{w}^*}\right)_{ij} = \frac{s_{ij}^w w_j^*}{x_i^*} = \frac{f_i^{\mathrm{cl},\pm}}{x_i^*}\frac{s_{ij}^w w_j^*}{f_i^{\mathrm{cl},\pm}} = \frac{1}{\tau_i^*}\theta_{ij}^{w,\pm}$. Note that $\sum_{j=1}^{m_w}\theta_{ij}^{w,\pm} = \theta_{i0}^{\pm}$, and

$\sum_{j=1}^{m_w} \theta_{ij}^{w,\pm} + \sum_{j=1}^{m} \theta_{ij}^{\pm} = 1$.

Example 13 (Simple glycolysis, continued)**.** The simple glycolysis model we have been discussing so far is part of the glycolytic oscillations minimal model in [25]. In [25], this simple model is analyzed to demonstrate several points, including a bound on steady state error from stability, and a general tradeoff between steady-state accuracy and robustness that explains glycolytic oscillation as a necessary side effect. However, the analysis was done based on a mechanistic specification of how the fluxes are regulated:

$$\frac{d}{dt}\begin{bmatrix} x_1 \\ x_2 \end{bmatrix} = \begin{bmatrix} 1 & -1 \\ -q & q+1 \end{bmatrix}\begin{bmatrix} v_1 \\ v_2 \end{bmatrix} + \begin{bmatrix} 0 \\ -1 \end{bmatrix} w, \qquad \begin{bmatrix} v_1 \\ v_2 \end{bmatrix} = \begin{bmatrix} \frac{2x_2^a}{1+x_2^{2h}} \\ \frac{2kx_1}{1+x_2^{2g}} \end{bmatrix}.$$

Here x_1 is intermediate, x_2 is ATP, v_1 is the flux from glucose and intermediate to ATP (involving enzyme PFK), v_2 is the flux from intermediate to ATP and waste (involving enzyme PK), and w is an external disturbance flux that consumes ATP, such as a maintenance cost. This simple model is the same as what we have been using, except that a detailed form is specified for $v_1(\boldsymbol{x})$ and $v_2(\boldsymbol{x})$, based on information from mechanistic details on how the catalyzing enzymes, namely PFK and PK, are allosterically regulated.

However, we argue from a constraint-based perspective that all the points made in [25] do not require this detailed knowledge about how $v_1(\boldsymbol{x})$ and $v_2(\boldsymbol{x})$ are regulated. Instead, from the FEC rule based on general features of layered architectures of metabolism, we can perform these analysis and obtain the same results but at higher conceptual generality. FEC, as a constraint-based approach, formalizes the methods in [25] used to analyze the glycolystic oscillation example, and enables application of such analysis to general metabolic systems. In particular, no knowledge about how the catalyzing enzymes are allosterically regulated is necessary for our analysis based on the FEC framework. As a result, the results in [25], such as the tradeoff between steady state accuracy and system robustness, recast via our FEC framework, constitutes general rules that hold for lumped models of arbitrary autocatalytic metabolic processes.

Below, we illustrate how to apply FEC formulation to this example, and show that the analysis and relevant results in [25] can be done solely based on the FEC formulation, without knowing anything about $v_1(\boldsymbol{x})$ and $v_2(\boldsymbol{x})$.

The flux control formulation without knowing anything about how v_1 and v_2 are regulated is

$$\frac{d}{dt}\begin{bmatrix} x_1 \\ x_2 \end{bmatrix} = \begin{bmatrix} 1 & -1 \\ -q & 1+q \end{bmatrix}\begin{bmatrix} v_1 \\ v_2 \end{bmatrix} + \begin{bmatrix} 0 \\ -1 \end{bmatrix} w.$$

At steady state, the stoichiometry matrix constrains how internal fluxes are related to external fluxes. In this case, as shown previously, $v_1^* = v_2^* = w^*$. This can be obtained just by the stoichiometry, which is generic for any lumped autocatalytic process.

Preparing for studying stability later on, we can look at how the fluxes relate to the birth-death dynamics of each species. We see that the only flux producing x_1 is v_1, the only flux degrading x_1 is v_2, and the only flux producing x_2 is v_2. Both v_1 and w degrade x_2, so $\theta_{21}^- = \frac{qv_1^*}{qv_1^*+w^*} = \frac{q}{1+q}$. So we have

$$\boldsymbol{\Theta}^+ = \begin{bmatrix} 1 & 0 \\ 0 & 1 \end{bmatrix},\ \boldsymbol{\Theta}^- = \begin{bmatrix} 0 & 1 \\ \frac{q}{1+q} & 0 \end{bmatrix},\ \boldsymbol{\Theta}^{w,+} = \begin{bmatrix} 0 \\ 0 \end{bmatrix},\ \boldsymbol{\Theta}^{w,-} = \begin{bmatrix} 0 \\ \frac{1}{1+q} \end{bmatrix}.$$

So $\boldsymbol{\Theta}^{\pm}$, the fractional contribution of each flux to the production and degradation of metabolites, is determined directly from stoichiometry as well. In more general cases the steady state fluxes are not uniquely determined, so their values will show up in $\boldsymbol{\Theta}^{\pm}$. But the flux fractions $\boldsymbol{\Theta}^{\pm}$ are always determined solely by fluxes.

Next, we want to delve into the regulation of the fluxes to study how the system can be regulated. The first question is, are regulations necessary in the first place? Can we have a well-performing autocatalytic system without sophisticated feedback regulations?

To study regulations, we apply the FEC formulation to split the flux dynamics into a plant, or passive part, and a controller. Again, this is completely generic without knowing anything about $v_1(\boldsymbol{x})$ and $v_2(\boldsymbol{x})$.

$$\begin{aligned} \frac{d}{dt}\begin{bmatrix} x_1 \\ x_2 \end{bmatrix} &= \boldsymbol{S}\boldsymbol{\Lambda}_{\boldsymbol{v}^0} \exp\Big\{\boldsymbol{H}^A \log \boldsymbol{x} + \boldsymbol{H}^B \log \boldsymbol{u}\Big\} + \boldsymbol{S}^w \boldsymbol{w} \\ &= \begin{bmatrix} 1 & -1 \\ -q & 1+q \end{bmatrix} \begin{bmatrix} v_1^0 & 0 \\ 0 & v_2^0 \end{bmatrix} \exp\left\{ \begin{bmatrix} 0 & a_1 \\ a_2 & 0 \end{bmatrix} \begin{bmatrix} \log x_1 \\ \log x_2 \end{bmatrix} + \begin{bmatrix} 1 & 0 \\ 0 & 1 \end{bmatrix} \begin{bmatrix} \log u_1 \\ \log u_2 \end{bmatrix} \right\} + \begin{bmatrix} 0 \\ -1 \end{bmatrix} w. \end{aligned}$$

The choices for $\boldsymbol{H}^A$ and $\boldsymbol{H}^B$ follow from general rules discussed previously, and are explained later in this example. This looks rather complicated, but appear much simpler once we put the expression for the fluxes together:

$$\frac{d}{dt}\begin{bmatrix} x_1 \\ x_2 \end{bmatrix} = \begin{bmatrix} 1 & -1 \\ -q & 1+q \end{bmatrix} \begin{bmatrix} v_1^0 x_2^{a_1} u_1 \\ v_2^0 x_1^{a_2} u_2 \end{bmatrix} + \begin{bmatrix} 0 \\ -1 \end{bmatrix} w.$$

Whether a fixed point is stable only depends on the internal dynamics of the plant locally around the fixed point. The stability is determined by whether the local dynamics matrix $\boldsymbol{A}^{\mathrm{cl}}(\boldsymbol{x}^*) = \boldsymbol{\Lambda}_{\boldsymbol{x}^*}^{-1} \boldsymbol{S} \boldsymbol{\Lambda}_{\boldsymbol{v}^*} \boldsymbol{H}^{\mathrm{cl}}$ (of the log-linearized of fold-change variable) is Hurwitz. Since we can split reaction orders into passive ones and controller ones $\boldsymbol{H}^{\mathrm{cl}} = \boldsymbol{H}^A + \boldsymbol{H}^B \boldsymbol{H}^K$,

we can ask what would happen without any control action, so that $\boldsymbol{H}^{\mathrm{cl}} = \boldsymbol{H}^{A}$. Here, the passive reaction orders satisfy

$$\boldsymbol{H}^{A} = \begin{bmatrix} 0 & a_1 \\ a_2 & 0 \end{bmatrix}, \; a_1, a_2 > 0.$$

Here a_1 is reaction order of v_1 in x_2, and a_2 is reaction order of v_2 in x_1. These are positive because x_2 is reactant for v_1, while x_1 is reactant for v_2. A typical value for them is $a_1 = a_2 = 1$. That v_1 does not depend on x_1 and v_2 does not depend on x_2 is because these two reactions are irreversible due to very negative reaction free energies (see previous subsection). In [25], it was denoted $a_1 = a$ some positive variable, and $a_2 = 1$.

Now we can study how the system would behave without any control action. We first follow our approach combining stoichiometry and birth-death structure to conveniently split the local dynamics matrix into timescales, flux fractions, and reactions orders by $\boldsymbol{A}^{\mathrm{cl}}(\boldsymbol{x}^*) = \boldsymbol{\Lambda}_{\boldsymbol{x}^*}^{-1} \boldsymbol{S} \boldsymbol{\Lambda}_{\boldsymbol{v}^*} \boldsymbol{H}^{\mathrm{cl}} = \boldsymbol{\Lambda}_{\boldsymbol{\tau}^*} \boldsymbol{\Theta} \boldsymbol{H}^{\mathrm{cl}} = \boldsymbol{\Lambda}_{\boldsymbol{\tau}^*} \boldsymbol{H}^{\mathrm{bd}}$. For the case with no regulation, $\boldsymbol{H}^{\mathrm{cl}} = \boldsymbol{H}^{A}$, so

$$\boldsymbol{H}^{\mathrm{bd}} = \boldsymbol{\Theta} \boldsymbol{H}^{a} = \begin{bmatrix} 1 & -1 \\ -\frac{q}{1+q} & 1 \end{bmatrix} \begin{bmatrix} 0 & a_1 \\ a_2 & 0 \end{bmatrix} = \begin{bmatrix} -a_2 & a_1 \\ a_2 & -\frac{q}{1+q} a_1 \end{bmatrix}.$$

A necessary condition for stability by the Routh-Hurwitz criterion in this 2d case is that the determinant of the dynamics matrix is positive. Since determinant pass through matrix products, we calculate $\det \boldsymbol{\Lambda}_{\boldsymbol{\tau}^*} > 0$, $\det \boldsymbol{\Theta} = \frac{1}{1+q} > 0$, so $\det \boldsymbol{A}^{\mathrm{cl}}$ has the same sign as $\det \boldsymbol{H}^{\mathrm{cl}}$. For no control, $\boldsymbol{H}^{\mathrm{cl}} = \boldsymbol{H}^{A}$, has determinant $-a_1 a_2 < 0$. So any fixed point is unstable for all $\boldsymbol{\tau}^*, a_1, a_2 > 0$. Actually we can go even further. Just adding a feedback control action from x_1 to v_1, or just from x_2 to v_2, do not help with stability, because they do not change the fact that $\det \boldsymbol{H}^{A} = -a_1 a_2 < 0$.

As an answer to the first question, regulations are needed because the passive dynamics of autocatalysis is unstable. Not only is feedback regulation on the fluxes needed to have stable steady states at all, we also know such feedback regulations has to modify the diagonals of reaction order $\boldsymbol{H}^{\mathrm{cl}}$ simultaneously, or even better, push one of the a_i to negative.

The next question is, is there any sacrifice we have to make to stabilize the fluxes? More generally, are there some hard limits on what regulations can do? Are there fundamental tradeoffs that cannot be sidestepped no matter how delicately the enzymes are allosterically regulated or methylated based on signaling?

This takes us to analyze what would happen if we add in controller feedback, so $\boldsymbol{H}^{B} \boldsymbol{H}^{K}$ is no longer zero. There is not reason to disallow regulation of either of the fluxes, so we consider $\boldsymbol{H}^{B} = \mathbf{I}_2$ the identity matrix, to allow allosteric feedback for both enzymes

catalyzing v_1 and v_2. For feedback regulation, x_1 and x_2 are distinct based on their position in the stoichiometry or the metabolic network topology. For autocatalysis, x_2 is the metabolite amplified and consumed for many other purposes, like ATP in glycolysis. Therefore, feedback regulation from x_2 is important to construct, for purposes beyond this system, such as coordinating x_2 usage in other systems. As a result, molecular mechanisms to sense x_2 are likely easier to obtain as well, such as by adapting x_2-allostery domains of other proteins. So based on this motivation from autocatalytic stoichiometry, we consider x_2 regulates v_1 and v_2, which corresponds to nonzero H^K_{12} and H^K_{22} entries.

$$\boldsymbol{H}^K = \begin{bmatrix} 0 & h^k_{12} \\ 0 & h^k_{22} \end{bmatrix}.$$

The more general case of allowing all $\boldsymbol{H}^K$ entries to be nonzero can of course be fruitfully analyzed, but we avoid that here to keep within the domain of [25]. In [25], mechanistic information about the enzymes catalyzing the two lumped reactions are used to directly write down $u_1(x_2) = \frac{1}{1+x_2^{2h}}$ and $u_2(x_2) = \frac{1}{1+x_2^{2g}}$, capturing that PFK and PK are allosterically regulated by ATP, ADP and/or AMP so that increase in ATP cause decrease in activity. So $-h$ corresponds to h^k_{12} in our generic formulation and $-g$ corresponds to h^k_{22}. While any such mechanistic information always help formulating control of metabolic fluxes, when such information is not available, as is almost always the case, we can generate hypothesis to simplify our considerations based on stoichiometry as our discussion above.

With the feedback regulation we have

$$\boldsymbol{H}^{\text{cl}} = \begin{bmatrix} 0 & a_1 + h^k_{12} \\ a_2 & h^k_{22} \end{bmatrix}.$$

As discussed previously, a necessary condition for stability is $(a_1 + h^k_{12})a_2 < 0$, which requires $a_1 + h^k_{12} < 0$. We can go further to obtain the necessary and sufficient condition for stability using Routh-Hurwitz criterion, as is done in [25]. This results in $0 > h^k_{12} + a_1 > \frac{1+q}{q}\left(h^k_{22} - \frac{\tau_2^*}{\tau_1^*}a_2\right)$, therefore a lower bound on $a_1 + h^k_{12}$. This relates to steady state error. The steady state fluxes satisfy $v_1^* = v_2^* = w^*$ just by constraints from stoichiometry. Therefore the steady state concentrations satisfy $w^* = v_1^0(x_2^*)^{a_1}u_1^* = v_2^0(x_1^*)^{a_2}u_2^*$. We see how variation in w^* will propagate to x_1^* and x_2^* depending on how the control actions vary at steady state since $u_1^* = u_1(\boldsymbol{x}^*)$ and $u_2^* = u_2(\boldsymbol{x}^*)$. In particular, we can perform an infinitesimal fold-change around the steady states, and we have $\tilde{\delta}w = a_1\tilde{\delta}x_2 + \tilde{\delta}u_1 = a_2\tilde{\delta}x_1 + \tilde{\delta}u_2$. Now put in the controller gain, that $\tilde{\delta}u_1 = h^k_{12}\tilde{\delta}x_2$, and we have $\tilde{\delta}w = (a_1 + h^k_{12})\tilde{\delta}x_2$. So the steady state error from disturbance w to ATP concentration x_2 in terms of fold-change has magnitude $a_1 + h^k_{12}$. This can be directly seen from the closed loop reaction orders, since

this is exactly equal to H_{12}^{cl}. So together, requiring the system to be stable forms a lower bound on the steady state error that $\left|\frac{\tilde{\delta}x_2}{\tilde{\delta}w}\right| = \left|h_{12}^k + a_1\right|^{-1} \geq \left|\frac{1+q}{q}\left(\frac{\tau_2^*}{\tau_1^*}a_2 - h_{22}^k\right)\right|^{-1}$. So from the controller's perspective, steady state error can be decreased if we increase the controller gain of u_2, i.e. make h_{22}^k more negative. We see that we may also desire τ_2^*, the timescale of ATP turnover, to be much larger (slower) than τ_1^*, that of the intermediate. Since the steady state fluxes are determined by external demand w^* therefore not adjustable, this means increasing x_2^* the ATP pool size so as to increase τ_2^*. But this might be not feasible to do due to other limitations such as the energy consumption of maintaining a larger pool. Lastly, it is also desirable that q is smaller, which means finding nutrient sources so that less ATP molecules are consumed when producing the intermediates. We see that there are multiple ways to mitigate this lower bound on steady state error, and they corresponds to making changes at different physical components of the system, which corresponds to different layers in metabolism architecture and different timescales. If we restrict our regulation to the top layer for protein production and degradation that can regulate the middle layer, then only changing τ^* is feasible. If we allow modifying the middle layer so that controller gain is modifiable, then h_{22}^k can be varied. If we allow mutations and enzyme evolution which happen on a much slower timescale so that totally different reactions can be used, then q and a_2 can be modified.

This result that stability tradeoffs with steady state error is the same as the one obtained in [25], but in terms of different quantities. However, we did not use any knowledge of $\boldsymbol{v}(\boldsymbol{x})$, i.e. how the fluxes are regulated. One confirmation of this is that we have never stated what the steady state concentrations x_1^* and x_2^* would be, because finding them would require detailed knowledge of $\boldsymbol{v}(\boldsymbol{x})$, which we assumed we do not have. Instead, we are able to relate $\boldsymbol{x}^*$ with $\boldsymbol{u}^*$, $\boldsymbol{w}^*$ and $\boldsymbol{v}^0$ through generic FEC formulations, and as we have shown the hard limits on steady state error can be obtained just from this. △

Comparison of responses between different metabolic systems

Metabolic systems can be described in terms of both its response to external exchange fluxes, and the stoichiometry and regulatory structure it is composed of. In other words, a metabolic system can be described mechanistically by specifying the internal structures, or by specifying responses to external fluxes in a phenotypic fashion. Relating internal structures and system response is one universal feature of control system theory. The internal structure description is called a *state space* specification in control theory, and the phenotypic description is called an *input output* specification. For linear systems, the relation between state space and input-output descriptions is thoroughly studied (see

Chapter 4 in [41]). Since such results relate internal structures such as stoichiometry, passive reaction orders, and controller placements, with external responses such as responses to control actions and disturbances, this enables us to compare different metabolic systems in a rigorous fashion. Existing tools from control theory also allow different metrics to be used when comparison systems. For example, we can ask about the difference in metabolite concentrations' local response to disturbances between a metabolic network with lumped stoichiometry and one with detailed stoichiometry. The system response is captured as a linear operator. If we want to compare average responses, then the $\mathcal{H}_2$ norm on this space of linear operators can be used. If we want to compare worst case responses, then $\mathcal{H}_\infty$ norm can be used. If we want to compare how hard are the systems to be stabilized, then the gap metric can be used. See [39] for an introduction on relevant norms, and [102] and Chapter 17 of [121] for relevant results. Beyond comparisons, we can capture uncertainty in model descriptions in robust control, so that results can be obtained for classes of metabolic systems, rather than exact specifications. This can serve as one step towards results on necessity.

Conservation of robustness as a hard limit on metabolic system response

Once FEC formulates regulation of metabolism as a control system, theoretical tools can be used to investigate properties for the set of all possible solutions. Similar to the FBA case focused on steady state fluxes, the set of all possible solutions is often severely constrained by structures in metabolism and can be fruitfully analyzed to gain general insights into metabolic regulation. More importantly, such hard limits or laws on system behavior constitute results on necessity rather than sufficiency (see Section 4.1), so that conclusions relating mechanisms and phenotypes can be made independent of details. The control theoretical tools focusing on properties of all possible controller is usually termed fundamental limitations or limits of performance. They can be obtained based on analytical methods [99], or by numerical algorithms [21]. One class of results on fundamental limitation of particular importance is the conservation of robustness, since it illustrates a nearly universal tradeoff between accuracy and robustness. This law on conservation of robustness is also called Bode's integral formula. It was originally derived for single-input-single-output systems, and now has generalizations into multiple-input-multiple-output linear and certain nonlinear systems [99]. In [25], Bode's integral formula is used to derive a severe tradeoff between steady state error and fragility to oscillations that holds for arbitrary regulations to explain how glycolytic oscillations is a necessary side effect of adapting to changing supply and demand. This tradeoff is made worse by the autocatalytic stoichiometry of glycolysis in regeneration of ATP, so more severe oscillations

happen due to adapting to supply and demand. Bode's integral formula is also used in [58] to showcase a hard design tradeoff between speed, accuracy, and robustness in engineering synthetic gene regulatory circuits, especially the antithetic integral controller conceptualized to achieve robust perfect adaptation and experimentally implemented in bacterial and mammalian cells [10, 22]. Bode's integral formula is also considered one of the core phenomenon in robust control, and simple tutorials have been developed to illustrate it through stick balancing [70], as well as time-domain explanations [69].

Sparsity in metabolic regulation

FEC has enabled a systematic formulation of problems in metabolism regulation. By capturing the structures in metabolism, FEC also requires advances in control theoretical tools to handle these structures in an integrated fashion. Of particular importance is the sparsity and locality in how the controller, or regulation of fluxes, relate to the states, or metabolite concentrations. Other constraints that we would also like to include are delay and noise in communication, and uncertainty and error in models and from data. However, systems with pre-specified network sparsity and controllers with localized structure are hard problems that were previously thought intractable. A recent breakthrough called system level synthesis (SLS) [8] made handling these constraints computationally feasible at scale. SLS provides a formulation where problems with sparse controllers are convex, therefore solvable at scale [111, 112]. Furthermore, the localization property of the system passes down to the optimization problem itself, such that a large problem can be broken into small pieces and solved in a distributed fashion. The SLS formulation has already been leveraged for problems in biology and neuroscience [71, 96, 105]. The SLS parametrization also gives rise to distributed and localized MPC (DLMPC) [4–6].

4.5 Explore behaviors of interest via optimization

As a constraint-based approach, FEC has a powerful application to study the space of all feasible behaviors by formulating dynamic regulation of metabolism as controller design in a system. As a systems theory, FEC can utilize control theory tools to derive hard limits and laws based on structures of metabolic systems that hold for all possible controllers. However, beyond the general results that are often a bit abstract, we are also interested in exploring specific biological behaviors under particular scenarios. This would require us to explore specific points in the space of all feasible behaviors. Hence we utilize the tool of optimization to pick out particular points of interest.

Optimization of FBA problems. To pick out points or behaviors of interest by optimization under a particular scenario constitutes specifying an objective function for what the behavior should do, and a set of constraints that capture the scenario. This is well-developed for FBA, so we use it as an illustration. A general formulation of an optimization problem for FBA, which focuses on steady state internal fluxes $\boldsymbol{v}$, is the following:

$$\begin{aligned} \min_{\boldsymbol{v}} \quad & L(\boldsymbol{v}) \\ \text{s.t.} \quad & \boldsymbol{S}\boldsymbol{v} + \boldsymbol{S}^w\boldsymbol{w} = 0, \\ & \boldsymbol{v} \in \mathcal{V}_{\text{ss}}. \end{aligned} \tag{4.40}$$

Here L is the objective function, often called loss or cost so it is minimized. Equivalently, the optimization can be formulated in terms of gain or reward, so it is maximized. The variable to be optimized over is the steady state flux $\boldsymbol{v} \in \mathbb{R}^m$. The first constraint that $\boldsymbol{S}\boldsymbol{v} + \boldsymbol{S}^w\boldsymbol{w} = 0$ is simply the steady state equation relating the internal and external fluxes (Eqn (4.14)). The second constraint is a set-constraint on $\boldsymbol{v}$, which may cover irreversibility, maximum and minimum flux magnitudes, or other more sophisticated constraints such as from thermodynamics or growth laws. The external disturbance flux $\boldsymbol{w}$ is at steady state, and is thus considered a constant coefficient to the problem.

In practice, to make the optimization problem Eqn (4.40) feasible to solve computationally at scale, linear constraints are used to define $\mathcal{V}_{ss}$ and linear or quadratic objective functions $\boldsymbol{L}(\boldsymbol{v})$ are used. Because the steady state constraint is linear in $\boldsymbol{v}$, this keeps the set of feasible points from constraints linear. Then depending on whether the objective is linear or quadratic, the optimization problem is a linear program or a quadratic program. Both can be solved at scale for systems with tens of thousands of fluxes.

We illustrate a few common objectives used in FBA [60, 84, 85]. The most typical one is biomass production. This is often used to relate FBA predictions with growth rates of microbial populations in culture. To capture biomass production, an artificial reaction with stoichiometry $\boldsymbol{s}_{\text{biomass}} \in \mathbb{R}^n$ and flux v_{biomass} is added to the stoichiometry matrix $\boldsymbol{S}$ and internal fluxes $\boldsymbol{v}$. The biomass reaction stoichiometry corresponds to a vector with positive entry for pretty much every metabolite, with $s_{\text{biomass},i}$ as negative of the fractional weight of the ith metabolite in a gram of dry weight of the cell. Negative means this biomass production reaction proceeds to consume these metabolites. Then an objective $L(\boldsymbol{v}) = -\boldsymbol{c}^\intercal\boldsymbol{v} = -v_{\text{biomass}}$ can be used, with $\boldsymbol{c} \in \mathbb{R}^m$ such that only the entry corresponding to biomass production flux v_{biomass} is 1, and all other entries zero. The negative sign is because we want to maximize biomass production while the problem is formulated as minimization. Note that the biomass stoichiometry vector is well-defined as a constant

vector for steady state growth of a microbial population, while exponential growth may not be at steady state [64].

Estimates on growth under different nutrient scenarios can then be defined through constraints. For example, oxygen uptake can be constrained to be below a certain maximum rate. If the maximum rate is set to be zero, then we have completely anaerobic growth. Nutrients uptake rate can also be bounded by creating an upper bound on the uptake flux. This can allow, for example, the study of varying maximum glucose uptake rate on oxygen consumption, or the other way around on varying maximum oxygen consumption over maximum glucose uptake rate. Other constraints, when considered relevant, can be incorporated, such as ATP maintenance cost. This can be considered as a minimum flux on the ATP regeneration reaction. For example, for simple models of E. *coli* metabolism, a minimum ATP maintenance flux of 8.39 $\mathrm{mmol\,g^{-1}\,h^{-1}}$ is often used [60, 84].

Another class of common objectives are maximizing the flux of a single reaction, often the production of a metabolite, such as maximizing ATP regeneration. This is used to estimate the capacity for cells to perform certain reactions. For example, by maximizing the flux corresponding to ATP regeneration ATP + H_2O $\longrightarrow$ ADP + H^+ + P_i, we obtain the potential, or maximum capability, of a cell to regenerate energy in this scenario. Other common choices of single reactions to maximize for estimation of capacity are redox balance restoration by maximizing NADH to NAD+ conversion, and target metabolites of interest when engineering a microbe for fermentation. This is implemented in $L(\boldsymbol{v})$ in a similar way to biomass, with $L(\boldsymbol{v}) = -\boldsymbol{c}^\intercal \boldsymbol{v}$, and c_j is 1 only for the flux to maximize, and zero for all other fluxes.

Lastly, the sum of all fluxes' magnitude is often used as a generic energy cost of the cell. This can be written as a sum of absolute values $\sum_j |v_j| = \|\boldsymbol{v}\|_1$, the ℓ_1 norm, or a sum of squared values $\sum_j v_j^2 = \|\boldsymbol{v}\|_2$, the Euclidean norm. Minimizing $L(\boldsymbol{v}) = -\|\boldsymbol{v}\|$ for some norm then roughly correspond to minimizing the energy cost of the cell, since any net flux with relevant speed needs to be driven and therefore costs energy. As derivatives to this, finding efficient production of a metabolite can be formulated as maximizing the target flux divided by the energy flux, of the form $L(\boldsymbol{v}) = -\frac{v_j}{\|\boldsymbol{v}\|}$.

Optimization of FEC problems. For optimization of dynamic metabolic regulation problems formulated by FEC, the problem is now dynamic instead of static. Static problems have natural spaces for the variable to be optimized over. For example, the variables to be solved in FBA are steady state fluxes that can be nicely formulated as a vector in $\mathbb{R}^n$. For dynamic problems such as FEC, there is not a definitive space that parameterizes all the possible control actions $\boldsymbol{u}$. The key issue is whether we consider the control actions

$\boldsymbol{u}$ as the central object, or the controller that generates the control actions as the central object. In terms of the optimization problem formulation, it corresponds to whether the cost function is central, or the dynamic constraints such as stability is central.

If we consider the control actions $\boldsymbol{u}$ as central, then the space for the variable to be solved is the space of dynamic trajectories of the control variable $\boldsymbol{u}$ that regulate flux exponents. Naturally, they are functions mapping the time horizon $[0, T]$, where T can be infinite, to control actions in $\mathbb{R}^{n_u}$. To make them computable, we often represent these trajectories at time steps with step size Δt, and $N\Delta t = T$ with N the number of steps. So trajectories $\boldsymbol{u}(0 : N)$ live in space $\mathbb{R}^{n_v \times N}$. The size of the optimization problem is therefore much larger. With an objective function $L(\boldsymbol{x}(0 : T), \boldsymbol{u}(0 : T))$ specified, this becomes an optimal control problem by defining the value function $V(\boldsymbol{x}, t) = \min_{\boldsymbol{u}(0:t)} L(\boldsymbol{x}(0 : t), \boldsymbol{u}(0 : t))$. A formulation that solves this with necessary and sufficient solutions is the Hamilton-Jacobi-Bellman (HJB) equations. Such problems are hard to solve for large problems since HJB equation is a partial differential equation. The result is a control action $\boldsymbol{u}$ that is specified in terms of the value function $V(\boldsymbol{x}, t)$. The advantage of this $\boldsymbol{u}$- or cost-focused optimal control approach is that the plant dynamics of $\boldsymbol{x}$ considered can be nonlinear. The disadvantage is that the closed loop dynamics, i.e. dynamics after the controller is incorporated, is not guaranteed to be stable. Stability guarantees are analyzed after the controller is solved, or analyzed for particular classes of problems such as linear quadratic regulators (LQR). Even worse, because the controller is virtualized away as an algorithm that output control action $\boldsymbol{u}$ based on the value function $V(\boldsymbol{x}, t)$, any structural constraints on the controller, such as sparsity, localization and delays, cannot be incorporated.

The other approach that take the controller as the central object resolves these issues by explicitly representing the controller map K from $\boldsymbol{x}$ trajectories to $\boldsymbol{u}$ trajectories. As a result, the variable to be optimized over is no longer trajectories of control action $\boldsymbol{u}$, but the controller maps K. Therefore, a mathematical parameterization of the space of all controller maps is needed. In particular, the controller is always desired to be stabilizing, i.e. the closed loop is stable. The parameterization of the space of stabilizing controllers is a very hard problem for general nonlinear plant dynamics, therefore this approach is mostly developed for linear systems. While classical methods such as Youla parameterization does express the space of stabilizing controllers for linear systems, incorporating constraints such as sparsity, localization and delay is hard in these cases. Namely, the resulting optimization problem for controller design is highly nonconvex. A recent advance to resolve these problems, system level synthesis (SLS), parameterizes stabilized closed loop system response maps from $\boldsymbol{w}$ to $\boldsymbol{x}$ and from $\boldsymbol{x}$ to $\boldsymbol{u}$ for a given plant, and backs out a

controller K from these system response maps. This method makes the design of sparse and localized controllers with delays fully convex and therefore computable at scale.

While SLS makes controller design with structural constraints solvable at scale, it is still largely restricted to linear problems. FEC problems are fully nonlinear, therefore requiring nonlinearity to be respected in optimal control formulation. It is true that the nonlinearity in FEC problems are strongly structured, so that flux $\boldsymbol{v}$ in terms of $\boldsymbol{x}$ and $\boldsymbol{u}$ is a monomial $\boldsymbol{v} = \boldsymbol{v}^0 \circ \boldsymbol{x}^{\boldsymbol{H}^A} \circ \boldsymbol{u}^{\boldsymbol{H}^B}$ like in geometric programs, while the stoichiometry-flux $\boldsymbol{S}\boldsymbol{v}$ is like in linear programs. But this combination of structures is still new, with no existing optimization frameworks that handle control problems with such structures directly. It is a fascinating direction of research to find numerical algorithms that handle geometric programs on top of linear programs in a dynamic control setting. So without a specialized algorithm, we resort to general optimization frameworks that handles both stability and sparsity constraints like in controller design while allowing nonlinearity to be respected like in optimal control.

One candidate that performs this is model predictive control (MPC) [73]. Model predictive control is an optimal control method, but the control action is solved and applied at each single step. At every step, based on an approximation (e.g. linearization) of the full model, an optimal control action is computed for a horizon into the future. Then only the first step of the predicted control action is applied. At the next step, a new approximate model is used to compute a new control action, then repeat. MPC has the advantage of optimal control that it respects the nonlinearity of the plant. It also has the advantages of controller design that controller constraints from every time step, where a simpler problem (e.g. linear) is solved so that stability can be guaranteed and structural constraints such as sparsity and delay can be applied, can be propagated to the overall control trajectory. For example, recent work on combining MPC and SLS allows MPC computations in a localized fashion [6].

Hence we formulate FEC problems as optimal control problems, and try to solve them via MPC methods. The optimal control problem of FEC in continuous time is the following:

$$\begin{aligned}
\min_{\boldsymbol{u}(0:+\infty)} \quad & \int_0^{+\infty} \ell(\boldsymbol{x}(t), \boldsymbol{u}(t)) dt \\
\text{s.t.} \quad & \frac{d}{dt}\boldsymbol{x}(t) = \boldsymbol{S}\boldsymbol{v}^0 \circ \boldsymbol{x}(t)^{\boldsymbol{H}^A} \circ \boldsymbol{u}(t)^{\boldsymbol{H}^B} + \boldsymbol{S}^w \boldsymbol{w}(t), t > 0, \\
& \boldsymbol{x}(t) \in \mathbb{X}, \qquad t > 0, \\
& \boldsymbol{u}(t) \in \mathbb{U}, \qquad t > 0.
\end{aligned} \tag{4.41}$$

Here the time horizon is considered infinite, and the objective function is the integral of a

per-time loss over this infinite time horizon. The variable to be minimized over is therefore the control action trajectory $\boldsymbol{u}(0:+\infty)$. The first constraint is the dynamic equation from FEC formulation. The second constraint is on metabolite concentrations $\boldsymbol{x}$, that it needs to be in the set $\mathbb{X} \subset \mathbb{R}^n_{>0}$ for all time. This can include lower bounds on ATP concentration for example. The third constraint is on control actions $\boldsymbol{u}$, that it needs to be in $\mathbb{U} \subset \mathbb{R}^{n_u}_{>0}$ all the time. This can capture actuator saturations coming from that binding regulation has reaction orders bounded in polyhedral sets, which translates into constraints on controller gains.

Now MPC formulation to solve this problem considers a local problem at each time step. At time t, the system has evolved to state $\boldsymbol{x}(t)$ and applied controlled action $\boldsymbol{u}(t)$ and disturbance $\boldsymbol{w}(t)$. Now to find the next control action by MPC, we study the local behavior of the system log-linearized around this point $(\boldsymbol{x}(t), \boldsymbol{u}(t), \boldsymbol{w}(t))$. We denote the log-linearized variables $\tilde{\delta}\boldsymbol{x}, \tilde{\delta}\boldsymbol{u}, \tilde{\delta}\boldsymbol{w}$. Based on the log-linearized model, we predict what would happen into a horizon into the future, and based on this horizon we solve for the desired control action at the next time step. Denote the time horizon predicted into the future based on the log-linearized model as T, and the step size as Δt, then the number of time steps in the predicted horizon is N with $N\Delta t = T$. An optimal control problem for this time horizon based on log-linearized models around $(\boldsymbol{x}(t), \boldsymbol{u}(t), \boldsymbol{w}(t))$ is then the following:

$$
\begin{aligned}
\min_{\tilde{\delta}\boldsymbol{u}(0:N)} \quad & \ell_f(\boldsymbol{x}^{\text{pred}}(N), \boldsymbol{u}^{\text{pred}}(N) + \sum_{k=1}^{N} \ell(\boldsymbol{x}^{\text{pred}}(k), \boldsymbol{u}^{\text{pred}}(k)) \\
\text{s.t.} \quad & \boldsymbol{\Lambda}_{\boldsymbol{x}(t)} \frac{\tilde{\delta}\boldsymbol{x}(k+1) - \tilde{\delta}\boldsymbol{x}(k)}{\Delta t} = \boldsymbol{f}(t) + \boldsymbol{S}\boldsymbol{\Lambda}_{\boldsymbol{v}(t)} \Big(\boldsymbol{H}^A \tilde{\delta}\boldsymbol{x} + \boldsymbol{H}^B \tilde{\delta}\boldsymbol{u} \Big), \; k = 0, \ldots, N-1, \\
& \boldsymbol{x}^{\text{pred}}(k) \in \mathbb{X}, \qquad\qquad k = 0, \ldots, N-1, \\
& \boldsymbol{u}^{\text{pred}}(k) \in \mathbb{U}, \qquad\qquad k = 0, \ldots, N-1.
\end{aligned}
\tag{4.42}
$$

Here ℓ_f is cost of the last point, which may be varied to help with properties such as stability. $\boldsymbol{x}^{\text{pred}}$ and $\boldsymbol{u}^{\text{pred}}$ are predicted state and control trajectories based on the log-linearized variables, defined by $x_i^{\text{pred}}(k) := x_i(t)\tilde{\delta}x_i(k)$ for $i = 1, \ldots, n$ and $u_i^{\text{pred}}(k) := u_i(t)\tilde{\delta}u_i(k)$ for $i = 1, \ldots, n_u$. Since these predicted variables depend on the predicted control actions used, they are actually shorthand notation for more explicit expressions: $x_i^{\text{pred}}(k)$ is shorthand for $x_i^{\text{pred}}(k; \tilde{\delta}u(0:N), t)$, since it depends on the time t we log-linearized around and the local control $\tilde{\delta}u(0:N)$ we choose. Similarly, $\tilde{\delta}\boldsymbol{x}(k)$ and $u_i^{\text{pred}}(k)$ are also shorthand for $\tilde{\delta}\boldsymbol{x}(k; \tilde{\delta}u(0:N), t)$ and $u_i^{\text{pred}}(k; \tilde{\delta}u(0:N), t)$ respectively. The initial state to begin with in this local problem is $\tilde{\delta}\boldsymbol{x}(0) = 0$, which means $\boldsymbol{x}^{\text{pred}}(0) = \boldsymbol{x}(t)$. The first constraint is just the

log-linearized dynamics at the point $(\boldsymbol{x}(t), \boldsymbol{u}(t), \boldsymbol{w}(t))$, where $\boldsymbol{v}(t) = \boldsymbol{v}^0 \circ \boldsymbol{x}(t)^{\boldsymbol{H}^A} \circ \boldsymbol{u}(t)^{\boldsymbol{H}^B}$, and $\boldsymbol{f}(t) = \boldsymbol{S}\boldsymbol{v}(t) + \boldsymbol{S}^w\boldsymbol{w}(t)$. Note that in the local problem in Eqn (4.42), there is no appearance of local disturbance $\tilde{\delta}\boldsymbol{w}$ because the disturbance cannot be predicted.

We denote the optimal solution to the problem in Eqn (4.42) by $\tilde{\delta}\boldsymbol{u}^{t,*}(0:N)$, to highlight that this is from a local problem at time t. Then the controller action we apply at time t is $\boldsymbol{u}(t) = \boldsymbol{u} \circ \tilde{\delta}\boldsymbol{u}^{t,*}(0)$. With this control action, the full system, the first constraint in Eqn (4.41), is evolved one step forward to $t + \Delta t$. Then the local problem log-linearized at $t + \Delta t$ is considered to find the control action for this time step.

This completes our discussion of how to use optimal control solved by MPC to explore interesting metabolism dynamics formulated as FEC problems. Because of the nonlinearity of FEC problems, the current MPC computation is rather time-consuming because log-linearization needs to be done at every time step. There are several ways to ameliorate this. One way is to use explicit MPC [4], where the solution of a local MPC problem can be solved as an explicit solution, so that iteration at each time step is just plugging in a formula. This can significantly speed up the computation, but explicit solutions so far only exist for limited types of local problems. Another way is to combine MPC with SLS, so that sparsity and locality of metabolic regulation can be utilized. This is indeed a very promising future, since distributed and localized computation can provide computational speed up of several orders [5, 6]. Lastly, the structure in FEC problems, namely a geometric program on top of a linear program, may be fruitfully exploited to avoid linearization in the first place. In particular, if the FEC problem without state and control action constraints can be directly solved via optimization, then this can be readily generalized to include constraints via multi-parameteric programming, similar to how MPC generalizes solutions of optimal control in linear systems without constraints to ones with constraints.

4.6 Case studies of computational exploration

Glycolytic oscillations. Simple glycolysis, or generic lumped models of autocatalysis, has been our main example used in illustrating the constraint-based approaches and the FEC formulation. It also has an interested dynamic phenomenon, glycolytic oscillation, that is well-studied from a control theory perspective [25]. It is understood that the system oscillates due to radical control actions, implemented by allosteric regulation of enzymes, that adapts to changing supply and demands. This minimization of steady state error causes oscillation when hit by large disturbance, made even more severe by the autocatalysis stoichiometry that is intrinsically unstable.

FEC promises that just based on the stoichiometry of this system, we have a parameterization of all possible regulations the cell can do on glycolysis. Then by simply asking for controllers that aggressively attenuates steady state error, we should be able to recover oscillatory response, with no information other than the stoichiometry.

In particular, we consider the following local problem from log-linearization of the FEC formulation of simple glycolysis at every time step.

$$\begin{aligned}
\min_{\tilde{\delta}\boldsymbol{u}(0:N)} \quad & \sum_{k=1}^{N} (\boldsymbol{x}^{\text{pred}}(k) - \boldsymbol{x}^0)^\intercal \boldsymbol{Q} (\boldsymbol{x}^{\text{pred}}(k) - \boldsymbol{x}^0) + \tilde{\delta} u(k)^\intercal \boldsymbol{R} \tilde{\delta}\boldsymbol{u}(k) \\
\text{s.t.} \quad & \boldsymbol{\Lambda}_{\boldsymbol{x}(t)} \frac{\tilde{\delta}\boldsymbol{x}(k+1) - \tilde{\delta}\boldsymbol{x}(k)}{\Delta t} = \boldsymbol{f}(t) + \boldsymbol{S}\boldsymbol{\Lambda}_{\boldsymbol{v}(t)} \Big(\boldsymbol{H}^A \tilde{\delta}\boldsymbol{x} + \boldsymbol{H}^B \tilde{\delta}\boldsymbol{u} \Big), \, k = 0, \dots, N-1, \\
& x_2^{\text{pred}}(k) \geq 0.6 \qquad\qquad k = 0, \dots, N-1.
\end{aligned} \tag{4.43}$$

In the objective we used a typical quadratic cost on the states and control actions. The cost on states means we want to regulate the fluxes so that the metabolite concentrations are close to the reference concentration $\boldsymbol{x}^0$. The cost on control actions means we want to minimize the amount of energy we spend in moving the reaction orders and adjusting the fluxes. Here x_1 is concentration of the intermediate, and x_2 is concentration of ATP. The relevant matrices are

$$\boldsymbol{S} = \begin{bmatrix} 1 & -1 \\ -q & 1+q \end{bmatrix}, \; \boldsymbol{H}^A = \begin{bmatrix} 0 & 1 \\ 1 & 0 \end{bmatrix}, \; \boldsymbol{H}^B = \mathbf{I}_2, \; \boldsymbol{S}^w = \begin{bmatrix} 0 \\ -1 \end{bmatrix}. \tag{4.44}$$

We obtain the simulation result in Figure 4.10. First we see that the MPC solutions of FEC, with only information on the stoichiometry, can capture the hallmark oscillatory behavior in glycolysis. This is remarkable in the sense that we have supplied no mechanistic information about the system other than the stoichiometry matrix. In other words, since glycolytic oscillation is fundamentally due to the intrinsically unstable metabolism dynamics, FEC can indeed successfully split intrinsic dynamics of the metabolism from the enzymatic regulations. Next, we compare how the oscillatory behavior changes with varying parameters. In the mechanistic model plotted on the left from [25], decreasing feedback gain g of ATP on v_2 or v_{PK} that consumes intermediate to make ATP causes an increase in oscillations. Decreasing gain should correspond to smaller variations in control action when metabolites varies, and hence should correspond to increasing controller cost. Since u_2 regulates v_2, decreasing g should have similar effect as increasing R_{22}. Indeed, we see that in Figure 4.10, that increasing R_{22} cause larger oscillations in trajectories solved by MPC. Similarly, increasing feedback gain h on v_1 or v_{PFK} that consumes ATP to make

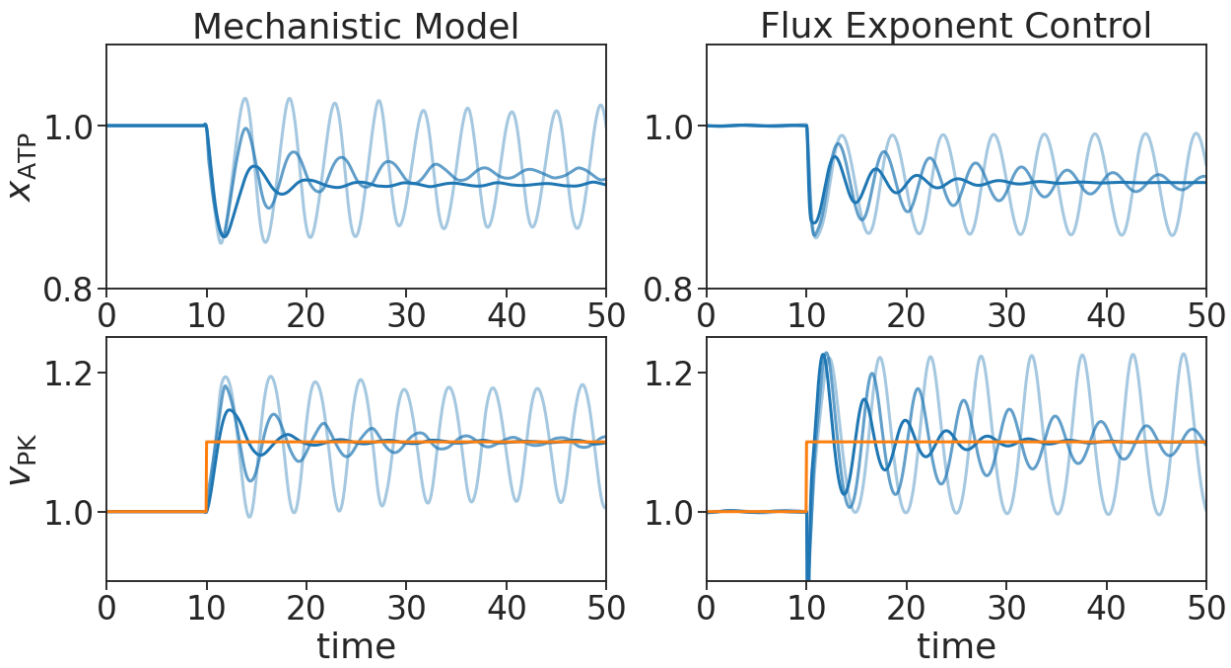

Figure 4.10 Comparison of simulations of the mechanistic model proposed in [25] for glycolytic oscillation (left), the regulatory trajectories from flux exponent control with solved by MPC (right), and the prediction of steady state fluxes by FBA (orange line). x_{ATP} is concentration of ATP, also denoted x_2 in the text. v_{PK} is flux for the reaction consuming intermediate and producing ATP, also denoted v_2 in the text. The parameter values used for the mechanistic model, in the notations of [25], are $a = 1$, $q = 1$, $k = 1.1$, $g = 0.3$ and h take values $2.5, 2.8, 3.1$ corresponding to trajectories from dark to light blue, with increasing oscillation magnitude. The disturbance w is 1 from $t = 0$ to $t = 10$, and jumps to 1.1 from $t = 10$ onward. The parameters used for the flux exponent control are $v_1^0 = 2, v_2^0 = 2.2$ to match with the mechanistic model steady state fluxes, $\Delta t = 0.03$, $T = 0.6$ or $N = 20$, initial states are $x_1(0) = \frac{1}{1.1}$ and $x_2(0) = 1$, and $u_1(0) = u_2(0) = -0.695$ to match the steady state values. When w is 1, the reference state values $\boldsymbol{x}^0$ are the same as the initial values. When w jumpts to 1.1, the reference state values are changed to $x_1^0 = 0.93$ and $x_2^0 = 0.98$ to match with change in steady state values of the mechanistic model. The cost parameters are $\boldsymbol{Q} = \mathrm{diag}(0.3, 0.08)$ and $\boldsymbol{R}$ take values $\mathrm{diag}(0.4, 0.05)$, $\mathrm{diag}(0.4, 0.25)$ and $\mathrm{diag}(0.4, 0.45)$ corresponding to the three trajectories from dark to light blue, i.e. increasing oscillation magnitude. Other parameters such as stoichiometry are given in the text.

intermediate causes increase in oscillation. However, when we decrease R_{11} in FEC, which should relate to increasing h, we observe a decrease in oscillation magnitude instead of an increase. We posit that this is because h specifically represents how u_1 responds to x_2, which corresponds to a sparsity constraint on the controller. But this sparsity constraint is not implemented in our current formulation, and therefore u_1 and u_2 in the MPC solution may also respond to x_1, causing the difference in the effect of limiting controller gain between the mechanistic model and MPC solutions. To incorporate the sparsity constraint, either output-feedback should be used with x_2 considered as output, or SLS needs to be incorporated into the MPC formulation to restrict controller sparsity.

This glycolytic oscillations example shows that the binding-catalysis split that FEC is based on can capture the split between intrinsic, or passive, dynamics of metabolic fluxes, and the

active regulations of binding on enzyme activities. This enables us to describe important dynamic phenomena of metabolic systems using only very sparse structural information, such as the stoichiometry matrix.

4.7 Summary and future directions

To study principles and rules governing ecological systems and communities of microbial species, we need to quantitatively understand metabolism at the core of interactions within and between cells and populations. Traditional mechanistic modelling methods require extensive and detailed data on all the mechanisms relevant for a metabolic phenomenon of interest. While extensive mechanistic data are available for model organisms, well-studied pathways, and common metabolites, data is highly concentrated in those cases and becomes extremely sparse outside of the well-studied realms. To resolve this sparse data issue, constraint-based modeling can be used, where we take the known mechanisms as constraints, and let unknown mechanisms vary freely. This way, we can either study the set of all possible behaviors constrained by the known mechanisms, or study particular behaviors by searching points of interest through optimization. Constraint-based approaches are fundamentally rooted on the layered architecture of metabolism and beyond, that structures of each layer are well-separated in time-scales so that slow-varying parts, also often easier to characterize experimentally, can be taken as constraints, while fast-varying parts are often unknown and allowed to vary. This is especially successful for flux control based on stoichiometry-flux split in the bottom layer of metabolism, exemplified by flux balance analysis (FBA) that focuses on steady states. However, while flux control is well-suited to study steady state metabolism, it does not capture the intrinsic dynamics of metabolism. As a result, flux control is unable to study dynamic phenomenon such as stability of steady state, oscillations, and fragility to large disturbances or shocks. To split the intrinsic dynamics of metabolism with the regulations of fluxes, we proposed the binding-catalysis split at the middle layer of metabolism architecture, that fluxes are catalyzed by enzymes, which are in turn regulated by binding reactions and state transformations. Such regulations are characterized by their adjustment of reaction orders of the fluxes constrained in polyhedral sets (see Chapter 3). This formulates the rule of flux exponent control (FEC), that cells regulate fluxes' exponents. FEC enabled a natural split between intrinsic dynamics of metabolic fluxes and their regulation by binding of catalyzing enzymes. As a constraint-based approach, FEC improves over flux control by adding in an extra biological constraint on metabolism, that fluxes are regulated through exponents. This makes FEC strictly more powerful than flux control formulations since it

can incorporate more constraints. In fact, FEC can be used for steady state analysis just like FBA, with now can incorporate regulation of fluxes by enzymatic activity. The unique advantage of FEC to study dynamics of metabolism is demonstrated through the study of glycolytic oscillations. We show that by supplying just the autocatalytic stoichiometry of glycolysis, FEC can capture the intrinsically unstable dynamics of the fluxes which results in the tendency to oscillate. More generally, FEC combined with control theory can serve as a systems theory for metabolism. Metabolic systems defined by FEC are characterized by stoichiometry, fluxes' passive reaction orders, and how flux reaction orders are controlled. In particular, control theory can be used to analyze hard limits and fundamental tradeoffs that hold for all possible controllers on a given metabolic system, regardless of details. This is one example of how hard limits and laws on top of systems theory can be used to derive necessity relationships between mechanisms and phenotypes.

Beyond metabolism in a single cell, FEC has great potential to study metabolic interactions across scales in microbial communities and ecosystems. As an example, FBA is successfully used in [66] to capture the hysteresis in the population interaction between two bacterial species, connecting intracellular metabolism with inter-population metabolite exchanges. Given experiments in [66] were done on days timescale to guarantee metabolism reached steady state, FEC should be able to capture the hystersis phenomenon and further behavior on faster time scales, including whether the hysteresis states are stable from internal metabolism, and how the community would respond to sudden shocks in nutrients or oxygen.

More generally, FEC opens the door to quantitatively reasoning about metabolic behaviors in a dynamic fashion. This may have far-reaching implications on what we can target by drugs or engineer in synthetic organisms. For example, if instead of an antibiotic targeting a protein, we design antibiotics targeting the regulatory architecture of microbes. Then since the architecture is much harder to evolve and may not be found via the greedy small steps that evolution often takes, such architecture-targeted antibiotics should encounter much less antimicrobial resistance. As another example, if instead of inserting a gene to make a microbe more fit in an static environment, we engineer a regulatory architecture in the microbe to become more fit in responses to dynamic perturbations in the environment. Then this microbe could gain a niche in the time domain, and therefore may persistently survive in an environment without constantly providing the microbe with growth advantage.

As a conclusion, FEC characterizes a structural split between intrinsic dynamics of metabolism and flux regulations. This enables both a constraint-based approach to model

metabolism dynamics, and a systems theory to study hard limits and laws. There is much more to be studied both on the FEC formulation itself, and on its application to wide ranges of metabolic problems across scales.

Chapter 5

Dynamics and control of production and degradation via reaction orders

Biomolecular systems are characterized by the fundamental structure that catalysis determines the direction of change, and catalysis rates are regulated by binding reactions. In turn, the full regulatory profile of binding reactions can be characterized in terms of reaction orders bounded in a polyhedral set. Therefore, reaction orders act as a bridge between regimes of bioregulation at the binding reaction timescale and dynamics of production and degradation at the catalysis timescale. Given that reaction orders are accessible descriptions of bioregulation, we want to analyze and design system properties of interest at the catalysis timescale via reaction orders. While reaction orders from binding networks are studied in Chapter 3, and several steady-state and local properties such as hypersensitivity, local stability, and robust perfect adaptation are discussed in Chapter 2 and [117], we focus on regional and global dynamic properties such as stability, multistability, and oscillations in this chapter.

Biomolecular systems are nonlinear in general, therefore require tools of nonlinear dynamical and control system theories. Popular approaches tackle nonlinear dynamical systems with a linear system lens, such as approximating nonlinear systems via (possibly high dimensional) linear approximations (typical linear stability analysis, Koopman operators), or bounding complicated general behaviors via linear systems (e.g. differential dissipativity [45], contraction analysis, integral quadratic constraints). Reaction order polyhedra promotes an approach for the class of biomolecular dynamical systems that is distinct from the typical linear view. One structure highlighted by reaction order polyhedra is that the full behavior can be considered as convex combinations of the vertices. Each vertex

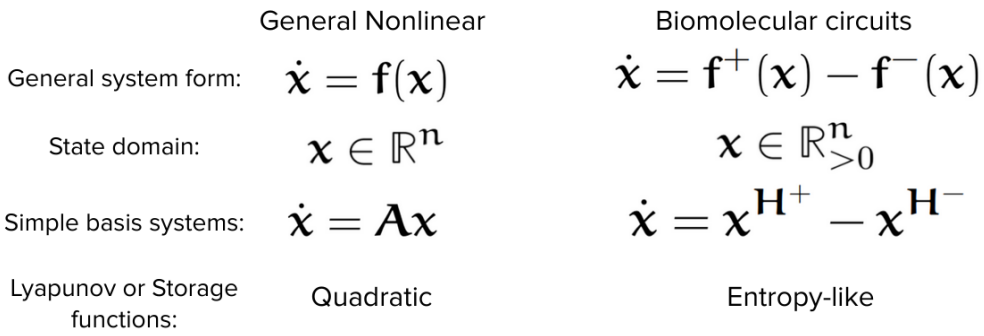

Figure 5.1 Comparison of the typical approach in treating nonlinear systems via linear systems as the basis of analysis, and the approach promoted by reaction orders to treat biomolecular systems with simple birth death systems as the basis of analysis.

corresponds to catalysis rates that are in monomial form. An implication of this is that, instead of bounding complicated general behaviors via linear systems, it could be more natural to do so via monomial systems. Indeed, reaction order polyhedra, together with other structures of biomolecular systems, suggest another class of dynamical systems, called simple birth death systems, with similar accessible analysis as linear systems, that can play the role of basis of analysis for a class of nonlinear systems. See Figure 5.1 for a comparison. We develop the formulation of biomolecular system dynamics and simple birth death systems in Section 5.1.

With the goal of tackling general biomolecular system dynamics via simple birth death systems, we need tools that can take a property of the simple birth death systems, corresponding to vertices of reaction order polyhedra that are valid approximations in certain regions of state space, and extend it to cover the general system dynamics. Motivated by the work on differential dissipativity and dominance analysis [45] and network dissipative systems [11], we take the approach of characterizing dissipative properties of component systems in terms of storage functions (Lyapunov functions for input-output behavior), and use component storage functions to cover the general systems formed as a network of component systems. In particular, we design a class of entropy-like storage functions and corresponding dissipative framework to tackle the structures of biomolecular systems, namely that the variables are positive and reaction orders dictate dissipative properties. We review the background on storage functions and dissipativity following [77] and [113], with slight generalization to explicitly include the dependence on the point of reference to suit our need for varying fixed points and multistability, in the appendix section 5.6. We begin the study of dissipativity in scalar birth death systems in Section 5.2. Dissipativity for networks of such scalar systems is studied in Section 5.3, culminating in a test for system dissipativity in terms of certifying the positivity of certain

entropy-like functions.

5.1 Dynamics of biomolecular systems

The dynamics of biomolecular systems describe how concentrations of molecular species evolve over time. The natural state variables are therefore the concentrations of species. These state variables are necessarily positive as they physically correspond to concentrations. Changes to species' concentrations happen through chemical reactions with production and degradation or transport processes such as dilution and transport in or out of compartments. We begin by describing the dynamics of biomolecular systems in chemical reactions using the formalization of chemical reaction networks (CRNs), and subsume dynamics from transport processes into the same description. A published work relevant to the discussion in this section and local stability and adaptation analysis is [117].

From chemical reaction networks to birth death systems

We begin by introducing the definition of birth death systems. We do so through chemical reaction networks (CRNs) [44, 55]. We remark that although the CRN formulation used here is the same as in Chapter 3 for binding networks, the reactions here are catalysis reactions rather than binding reactions, therefore on a slower timescale, and usually effectively not reversible. This warrants the use of different notations for most quantities. For example, the stoichiometry of the catalysis reactions can play a significant role for dynamics, which is distinct from stoichiometry of binding networks that effectively determine the polyhedral set bounding reaction orders. The reader should keep in mind that the chemical species on the catalysis time scale correspond to totals in binding reaction time scale, so each species at catalysis timescale here is a total of several species in binding timescale. However, to keep the notation familiar to readers from control and systems theory, we keep the use of $\boldsymbol{x}$ as state variables, which correspond to (total) species concentrations here.

A CRN is a collection of reactions of the form,

$$s_{1j}^{-}X_1 + \cdots + s_{nj}^{-}X_n \xrightarrow{k_j} s_{1j}^{+}X_1 + \cdots + s_{nj}^{+}X_n$$

where X_i, $i = 1, \ldots, n$ denote chemical species, $j = 1, \ldots, m$ index reactions, $s_{ij}^{-}, s_{ij}^{+} \in \mathbb{Z}_{\geq 0}$ denote the number of X_i molecules consumed as reactant or produced as product in reaction j, and $k_j \in \mathbb{R}_{>0}$ is reaction rate constant of reaction j. We denote $\boldsymbol{S}_j^{-} = \begin{bmatrix} s_{1j}^{-} & \cdots & s_{nj}^{-} \end{bmatrix}^{\mathsf{T}}$ as the reactant vector for reaction j, and similarly define $\boldsymbol{S}_j^{+}$ for product vector. We define $\boldsymbol{S}_j = \boldsymbol{S}_j^{+} - \boldsymbol{S}_j^{-}$ as the stoichiometry vector of reaction j, and collect them as columns to form the stoichiometry matrix $\boldsymbol{S} = \begin{bmatrix} \boldsymbol{S}_1 & \cdots & \boldsymbol{S}_m \end{bmatrix} \in \mathbb{Z}^{n \times m}$.

An alternative way to write the chemical reactions that highlights the catalysis nature of the reaction is the following:

$$\boldsymbol{X} \xrightarrow{v_j(\boldsymbol{x})} \boldsymbol{X} + \boldsymbol{S}_j, \tag{5.1}$$

where $\boldsymbol{X} = (X_1, \ldots, X_n)$ is the vector denoting the species, $\boldsymbol{v}(\boldsymbol{x}) : \mathbb{R}^n_{\geq 0} \to \mathbb{R}^m_{\geq 0}$ is the rate vector, with $v_j(\boldsymbol{x})$ the rate or flux or propensity of reaction j, capturing how the rate of reactions depend on concentrations.

The changes caused by the chemical reactions can either be interpreted as discrete jumps in molecule counts, or continuous variations in molecule concentrations. The deterministic rate equation of the CRN captures the continuous change in concentrations as follows:

$$\dot{\boldsymbol{x}} = \boldsymbol{S}\boldsymbol{v}(\boldsymbol{x}), \tag{5.2}$$

where $\dot{\boldsymbol{x}}$ is short for derivative with respect to time $\frac{d}{dt}\boldsymbol{x}(t)$, $x_i \in \mathbb{R}_{>0}$ is the concentration of species X_i.

A commonly used specification for $v_j(\boldsymbol{x})$ is the law of mass action, which has been used in a wide range of scenarios [109]. It says $v_j(\boldsymbol{x}) = k_j \boldsymbol{x}^{\boldsymbol{\alpha}_j}$, where we denote $\boldsymbol{x}^{\boldsymbol{\alpha}_j} = \prod_{i=1}^n x_i^{\alpha_{ij}}$ Importantly, if a reaction is an elementary reaction, namely there are no intermediate steps, then its rate is governed by the law of mass action [cite Ken Dill]. However, since we are interested in catalysis reactions in a biological context, the presence of intermediates is almost always significant. The law of mass action can still be valid, but no longer because the reaction is elementary and there are no intermediates, but rather because the catalysis reaction is in a regime with effective rate law taking a monomial form like mass action. For example, in Section 3.6, the non-saturating regime that corresponds to the $(1, 1)$ vertex yields a catalysis rate taking mass action form. Not all regimes take the form of mass action of course, so non-mass-action rate laws are often used for catalysis reactions, either derived with intermediates considered or formulated to empirically capture observed data. Our previous study of binding reactions is one way of formulating the rate law, via specific assumptions about the underlying binding reactions regulating the catalysis process. Other rate laws such as Hill functions and MWC often take the form of rational functions to account for saturation. These are discussed in more detail in the next subsection.

We can encode more structure into the reaction dynamics in Eq (5.2). Since concentrations of biomolecules change by production and degradation, we could group the reaction fluxes in terms of whether they increase or decrease X_i's concentration:

$$\dot{x}_i = f_i(\boldsymbol{x}) =: f_i^+(\boldsymbol{x}) - f_i^-(\boldsymbol{x}) \tag{5.3}$$

$$:= \sum_{j:s_{ij}>0} s_{ij} v_j(\boldsymbol{x}) - \sum_{j:s_{ij}<0} |s_{ij}| v_j(\boldsymbol{x}), \tag{5.4}$$

where we have collected terms from reactions producing x_i into $f_i^+(\boldsymbol{x})$ and terms from reactions degrading x_i into $f_i^-(\boldsymbol{x})$.

We remark that by collecting the reactions into groups that produce or degrade X_i, and focus our analysis on production and degradation rates $f_i^\pm$ instead of reaction rates v_j, we are effectively ignoring the structure in the stoichiometry matrix $\boldsymbol{S}$, or decide it is not important for the question of concern. Examples of effects encoded in the stoichiometry are conservation laws (e.g. to produce each B molecule, one A molecule needs to be consumed), and dynamical constraints such as coupled production/degradation (e.g. $A \to B + C$ so B and C are always produced simultaneously) and autocatalysis (to produce A, it needs to be consumed first). Ignoring stoichiometry is often justified when the question of concern has little coupling between species or has many ways to perform the same production or degradation, such as in gene regulation where each gene is often assumed to be expressed independently (although coupled expression in gene operons and clusters may still play significant roles in some cases). For metabolism, almost the opposite is true. Dynamics are fast, coupling is strong as a highly specialized enzyme is used to perform one type of reaction, and constraints on dynamics such as autocatalysis are at the core of metabolism regulation. Thus, for metabolism, the effect of stoichiometry should be emphasized instead of ignored. Indeed, in Chapter 4, we formulate metabolism dynamics with the stoichiometry at the center. We conclude that by grouping the reactions into production and degradation fluxes, although this procedure is mathematically valid with no approximation, we are making a choice to focus on bioregulation in scenarios with little coupling between species and close to steady states.

The physical interpretation of the variables x_i as concentrations dictate that they remain positive, therefore the positive orthant is forward invariant. A necessary and sufficient condition is $f_i(\boldsymbol{x}) > 0$ whenever $x_i = 0$. It is also natural to assume that each species has at least one production reaction and at least one degradation reaction. This yields the following definition for birth-death systems.

Definition 5.1.1. A *birth-death system* is a dynamical system of the form (5.3) where the production and degradation rates $f_i^\pm : \mathbb{R}^n_{>0} \to \mathbb{R}_{>0}$ are analytic and globally positive, and $f_i(\boldsymbol{x}) = f_i^+(\boldsymbol{x}) - f_i^-(\boldsymbol{x}) > 0$ whenever $\boldsymbol{x}$ approaches the boundary of the positive orthant, i.e. there exists i such that $x_i \to 0^+$.

Note that although CRNs are used here to introduce the context, a birth-death system can be introduced without reference to any CRNs. For example, the birth and death of a population of bacteria or animals may also be written as a birth-death system, while

there may not be any mass-action CRN corresponding to it. It is helpful to keep this generality in mind, even though all the concepts and tools we develop below are motivated by biomolecular reactions and systems of binding and catalysis in particular.

The definition of a birth-death system above describes a closed dynamical system that evolves over time by itself. However, many important features and properties of biological systems have to do with external disturbances, such as adaptation and robustness. Hence we generalize the definition to birth-death control systems by treating some species or rates as inputs that are controlled externally.

Definition 5.1.2. A *birth-death control system* is

$$\begin{aligned} \dot{\boldsymbol{x}} &= \boldsymbol{f}(\boldsymbol{x}, \boldsymbol{u}) = \boldsymbol{f}^{+}(\boldsymbol{x}, \boldsymbol{w}) - \boldsymbol{f}^{-}(\boldsymbol{x}, \boldsymbol{w}), \\ \boldsymbol{y} &= \boldsymbol{h}(\boldsymbol{x}, \boldsymbol{w}), \end{aligned} \tag{5.5}$$

where $\boldsymbol{x} \in \mathbb{R}^n_{>0}$ is state, often concentrations of species internal to the system, $\boldsymbol{w} \in \mathbb{R}^d_{>0}$ is disturbance input, often concentrations of species external to the system, and $\boldsymbol{y} \in \mathbb{R}^p$ is output, encoding objective of control. The analytic functions $\boldsymbol{f}^{\pm} : \mathbb{R}^n_{>0} \times \mathbb{R}^d_{>0} \to \mathbb{R}^n_{>0}$ are production and degradation rates, and $\boldsymbol{h} : \mathbb{R}^n_{>0} \times \mathbb{R}^d_{>0} \to \mathbb{R}^p_{>0}$ is output function.

The definition of a birth-death system emphasizes the structure that the concentration of each species is regulated by two processes, production and degradation. Understanding the dynamics of a birth-death system then comes down to characterizing how production and degradation rates $f_i^{\pm}(\boldsymbol{x})$ depend on the concentrations $\boldsymbol{x}$. In the biomolecular systems context, production and degradations are catalysis reactions regulated by networks of binding reactions (see Chapter 2 and 3, also the next subsection). This regulation is characterized by the reaction order, or log derivative, of production and degradation processes $\frac{\partial \log f_i^{\pm}(\boldsymbol{x})}{\partial \log \boldsymbol{x}}$ that are constrained in polyhedral sets. A polyhedron can be formed through convex combinations its vertices and rays. Therefore the polyhedral shape of reaction orders suggests that the full behavior of production and degradation processes $f_i^{\pm}$ could be seen as combinations of the regimes at the vertices and rays. Indeed, when the corresponding asymptotic conditions for the vertices and rays are satisfied, the behavior of a production or degradation process is essentially the same as the simple monomials at the vertices (see Section 3.6). The vertices are of special importance, as they are robustly valid for a large portion of state space (space of concentrations), and the approximate expression for production and degradation rates $f_i^{\pm}(\boldsymbol{x})$ take the simple form of a monomial, with constant reaction orders or log derivatives. Extending this to all production and degradation fluxes, we see that a general birth-death system could be seen as having

several regimes partitioning the state space, each corresponding to a simple system with production and degradation fluxes taking constant reaction orders and monomial form. When the state is in a region where a regime is valid, the system dynamics is approximately one such simple system. When the state is in between regimes, the system dynamics is roughly an interpolation between neighboring regimes, hence the following definition for the simple systems for a regime.

Definition 5.1.3. Given a birth death system, the *production order* of species X_i with respect to species X_j at $\boldsymbol{x}$ is defined as $H_{ij}^+(\boldsymbol{x}) := \frac{\partial \log f_i^+}{\partial \log x_j}(\boldsymbol{x})$. The production order of X_i refers to the vector of production orders to all $\boldsymbol{x}$, denoted as $\boldsymbol{H}_i^+(\boldsymbol{x}) := \frac{\partial \log f_i^+}{\partial \log \boldsymbol{x}}(\boldsymbol{x})$, a row vector in $\mathbb{R}^n$. The production order matrix of the birth death system at $\boldsymbol{x}$ refers to the matrix $\boldsymbol{H}^+(\boldsymbol{x}) \in \mathbb{R}^{n\times n}$. The *degradation orders* H_{ij}^-, vectors $\boldsymbol{H}_i^-$ and matrix $\boldsymbol{H}^-$ are similarly defined from degradation fluxes f_i^-. The *birth-death order matrix* is defined as $\boldsymbol{H} = \boldsymbol{H}^+ - \boldsymbol{H}^-$.

Definition 5.1.4. A *simple birth-death system* is a birth-death system with constant production and degradation orders. In other words, the production and degradation rates take the form $f_i^\pm(\boldsymbol{x}) = k_i^\pm \boldsymbol{x}^{\boldsymbol{\alpha}_i^\pm}$, where $\boldsymbol{\alpha}_i^\pm \in \mathbb{R}^n$ is a constant vector, and $k_i^\pm > 0$ is a positive constant.

Simple birth-death systems have the advantage that the order of their production and degradation rates can be directly read off from the exponent vector of the rate functions, since they are monomials. Beyond the simple case, production and degradation orders often take values in a convex polyhedron. The polyhedral shape can arise in various ways, from an underlying binding network regulating the flux, the sum of multiple reaction fluxes, or other modelling assumptions such as rates with saturating behavior and take of rational-function form. We discuss them next as a general context for the reason underlying polyhedral sets bounding production and degradation orders.

Reaction orders of production and degradation

Here we consider several scenarios we often encounter in biomolecular systems, and show in each case the production and degradation orders are bounded in some polyhedral set. This also provides some intuition in relating reaction orders (log derivatives) to biological behaviors. As illustration in the following, we use $f_i^+(\boldsymbol{x})$, the production rate of X_i, since the same results hold for degradation fluxes.

Production rate consisting of only one reaction. We first consider the case that the production flux f_i^+ consists of just one catalysis reaction. If we denote $J_i^+ = \{j = 1, \ldots, m : s_{ij} > 0\}$ as the set of indices for reactions that increased X_i concentration, then this case corresponds

to $J_i^+ = \{j^*\}$ has exactly one element for some j^*. So $f_i^+ = \sum_{j\in J_i^+} s_{ij}v_j(\boldsymbol{x}) = s_{ij^*}v_{j^*}(\boldsymbol{x})$ consists of just one reaction.

If the only reaction increasing X_i concentration has a rate of monomial form, i.e. $f_i^+(\boldsymbol{x}) = k_j^+\boldsymbol{x}^{\boldsymbol{\alpha}_j^+}$, then the production order $H_{i\ell}^+(\boldsymbol{x}) \equiv \alpha_{j\ell}^+$ is constant, $\ell = 1, \ldots, n$. In other words, the production order vector $\boldsymbol{H}_i^+$ is the exponent vector $\boldsymbol{\alpha}_j^+$, independent of the rate constant k_j^+ or concentration $\boldsymbol{x}$. This case corresponds to simple birth death system. This case could happen when X_i has only one production reaction with rate of mass-action form. Then $\boldsymbol{\alpha}_j^+$ is the reactant stoichiometry vector for that reaction. Another possibility is that there is only one dominant regime, so the rate is monomial but not necessarily mass-action. For example, consider $E + S \xrightarrow{k} E + P$, where the enzyme E catalyzes production of P from substrate S. Mass action would say the rate of P's production is kES. But if the catalysis has a significant intermediate state C formed from enzyme binding with substrate (e.g. from transition state theory [cite Ken Dill]), then from our analysis in Section 3.6 we know when there are overabundant substrates so that the enzymes are saturated, the catalysis rate could be independent of substrate, with rate kE, where E here denote total concentration of enzyme. This rate law is not mass action, but still monomial.

Alternatively, the only reaction that increase X_i concentration may have a rate consisting of several regimes, so it is more complicated than a monomial. The most important effect that is missed in a monomial rate and accounted for with several regimes is saturation, that when a reactant's concentration is too high, the reaction rate does not vary with changes in this reactant's concentration. A wide class of rate laws accounting for this take the form of rational functions. This can be derived from different models of detailed intermediate states in the catalysis process, such as in Michaelis-Menten approximations, Langmuir approximations [cite Ken Dill], single-molecule state counting of statistical mechanics in biophysics such as MWC [cite Rob and Ken Dill], or Markov chain theory for generic single-molecule state transitions [cite Gunawardena]. Rate law of rational function form can also arise from phenomenological modeling that capture observed data empirically, such as in Hill functions and the Monod model for population growth [cite]. All in all, in these cases the production rate f_i^+ is often a rational function of the following form:

$$f_i^+(\boldsymbol{x}) = k_i^+ \frac{c'\boldsymbol{x}^{\boldsymbol{\alpha}'}}{\sum_{q\in Q_i^+} c_q \boldsymbol{x}^{\boldsymbol{\alpha}_q}}, \tag{5.6}$$

where Q_i^+ is a finite set indexing the terms summed in the denominator, coefficients c' and c_q are positive. Each term often correspond to a state of the enzyme molecule catalyzing this reaction, and all but the state corresponding to numerator term are not active. Then Q_i^+ is a list of all the states the enzyme molecule can take, and $c_q\boldsymbol{x}^{\boldsymbol{\alpha}_q}$ is the weight of state j,

which is proportional to the probability the enzyme molecule is in that state. The form of the weight is often motivated by equilibrium arguments such as the Boltzmann distribution so that c_q captures the enthalpy contribution and $\boldsymbol{x}^{\boldsymbol{\alpha}_q}$ captures the entropy contribution (see [cite Ken Dill and Rob] for more detail). The production order in this case can be calculated to be

$$H_{i\ell}^+(\boldsymbol{x}) = \sum_{q\in Q_i^+} \lambda_q(\boldsymbol{x})(\alpha'_\ell - \alpha_{q\ell}), \qquad \lambda_q(\boldsymbol{x}) = \frac{c_q \boldsymbol{x}^{\boldsymbol{\alpha}_q}}{\sum_{q\in Q_i^+} c_q \boldsymbol{x}^{\boldsymbol{\alpha}_q}}, \tag{5.7}$$

where λ_q is the relative weight of the qth term, or probability of the enzyme molecule to be in state q. In this case, production order of X_i is the convex combination of each state's reaction order minus the active state's reaction order:

$$\boldsymbol{H}_i^+(\boldsymbol{x}) \in \operatorname{conv}\left\{\boldsymbol{\alpha}' - \boldsymbol{\alpha}_q : q \in Q_i^+\right\} = \boldsymbol{\alpha}' - \operatorname{conv}\left\{\boldsymbol{\alpha}_q : q \in Q_i^+\right\}. \tag{5.8}$$

The exact position in this polytope is determined by the convex coefficients $\lambda_q(\boldsymbol{x})$, which corresponds to the probability to be in each state.

While $\boldsymbol{H}_i^+(\boldsymbol{x})$ is bounded in this polytope, can it reach all points in the polytope by adjusting concentrations $\boldsymbol{x}$? Assume $\boldsymbol{\alpha}_q$ are all vertices of the polytope. If not, then take only vectors $\boldsymbol{\alpha}_q$ corresponding to vertices. Then $\boldsymbol{H}_i^+(\boldsymbol{x})$ can reach all points in the polytope by adjusting $\boldsymbol{x}$ if and only if $\left\{\boldsymbol{\alpha}_q : q \in Q_i^+\right\}$ is affinely independent. In other words, if the set of vectors $\left\{\boldsymbol{\alpha}_q - \boldsymbol{\alpha}_{q_0} : q \in Q_i^+ \backslash \{q_0\}\right\}$ is linearly independent, where q_0 can be any one element of Q_i^+. This can be easily seen as follows. $\frac{\lambda_q}{\lambda_{q_0}} = \frac{c_q}{c_{q_0}} \boldsymbol{x}^{\boldsymbol{\alpha}_q - \boldsymbol{\alpha}_{q_0}}$, so $\log \frac{\lambda_q}{\lambda_{q_0}} - \log \frac{c_q}{c_{q_0}} = (\boldsymbol{\alpha}_q - \boldsymbol{\alpha}_{q_0})^\intercal \log \boldsymbol{x}$. Collect all $\left|Q_i^+\right| - 1$ such equations, we have a linear system of equation $\boldsymbol{A} \log \boldsymbol{x} = \boldsymbol{b}$, where $\boldsymbol{A} \in \mathbb{R}^{(\left|Q_i^+\right|-1)\times n}$ has $\boldsymbol{\alpha}_q - \boldsymbol{\alpha}_{q_0}$ as row vectors, and $\boldsymbol{b}$ has $\log \frac{\lambda_q}{\lambda_{q_0}} - \log \frac{c_q}{c_{q_0}}$ as entries. For $\boldsymbol{H}_i^+(\boldsymbol{x})$ to reach every point by adjusting $\boldsymbol{x}$ means for all possible $\lambda_q > 0$, $\sum_q \lambda_q = 1$, this linear system of equations has a solution $\log \boldsymbol{x}$. This linear system of equation has a solution if and only if $\boldsymbol{b}$ is in the column span of $\boldsymbol{A}$. Since $\boldsymbol{b}$ can range over all $\mathbb{R}^{\left|Q_i^+\right|-1}$ by varying λ_q, we need $\mathbb{R}^{\left|Q_i^+\right|-1}$ to be the column span of $\boldsymbol{A}$. This corresponds to rows of $\boldsymbol{A}$, or vectors $\boldsymbol{\alpha}_q - \boldsymbol{\alpha}_{q_0}$, are linearly independent. This is also necessary since we are only considering $\boldsymbol{\alpha}_q$ that correspond to vertices.

We give a couple examples to illustrate this. Consider $f_i^+ = \frac{1}{1+x+x^2}$. We see that H_i^+ can reach the full polytope, the interval $(-2, 0)$, by varying x. But the α_q's are $\{0, 1, 2\}$, not affinely independent. This is because we need to exclude terms that are not vertices first. This means we should only consider α_q's in set $\{0, 2\}$. This is affinely independent, and therefore the full polytope is reachable. Let us consider another example where the full polytope is genuinely not reachable. $f_i^+(x_1, x_2) = \frac{1}{1+x_1+x_2+x_1x_2}$. The $\boldsymbol{\alpha}_q$'s are

$\{(0,0),(0,1),(1,0),(1,1)\}$, the vertices of a square, not affinely independent. There are λ_q's not reachable for non-negative $\boldsymbol{x}$. For example, if we fix $\lambda_{(0,0)} = \lambda_{(1,1)} = \frac{1}{3}$, where the subscript of λ denote the $\boldsymbol{\alpha}$ they correspond to, then we have $x_1 + x_2 + x_1x_2 = 2$, and $x_1x_2 = 1$. So we have $x_1x_2 = 1$ and $x_1 + x_2 = 1$. This system of equation does not have a real solution for x_1, x_2, and is therefore not reachable.

We conclude that whether the bounding polyhedron of production order is fully reachable is nontrivial even in this simple case. If we want to keep reachability simple, we need to give ourselves more freedom than just varying $\boldsymbol{x}$. For example, if we allow c_q to be varied in addition to $\boldsymbol{x}$, corresponding to adjusting the enthalpy of the states of the enzyme, then the bounding polytope of the production order is always fully reachable in this case. Similar statements are true for more sophisticated cases, such as when the reaction rate is governed by binding reactions or when multiple reactions are involved in production. In those cases, reachability by adjusting $\boldsymbol{x}$ is more complicated to characterize, and often large portions of the bounding polyhedron are not reachable. Reachability becomes accessible, however, if we allow more knobs to tune, such as modifying equilibrium constants and identity of the species involved. Intuitively, if enough knobs are allowed such that each convex coefficient can be tuned independent of other ones, then reachability is achieved.

It is worth noting that the polytope $\operatorname{conv}\left\{\boldsymbol{\alpha}_q : q \in Q_i^+\right\}$ is the Newton polytope of the denominator polynomial of f_i^+. A polynomial's Newton polytope has the exponents of each term in the polynomial as vertices. Newton polytopes are considered to capture fundamental properties of roots of polynomials in algebraic geometry [cite Sturmfels]. They are also fruitful tools in analysis and optimization of polynomial equations, dynamical systems, and CRNs [15, 34, 78].

When there are more than one active state, the numerator contains more than one term. This can be treated in the same way as the production rate f_i^+ consisting of multiple reactions, one for each active state. We consider this later in this subsection.

A more general way for multiple regimes to happen in one catalysis reaction is when this catalysis reaction is regulated by a network of binding reactions. This is studied in detail in Chapter 3. For binding networks, the production order is also constrained in a polyhedron, but not necessarily bounded. One simple example is repression. Consider an enzyme catalyzing the production of P from substrate S, $E + S \to E + P$, with rate proportional to the enzyme E. Now add a repressive ligand L that binds with enzyme E to form an inactive complex E', $E + L \rightleftharpoons E'$. This binding network with E as active species is studied in Section 3.6, and the reaction order of E to total enzyme and total ligand concentrations are unbounded, although constrained in a stripe-shaped polyhedron (see Eq (3.41)). This

also illustrates the binding network considers more general cases than rational-function forms that consider states of the enzyme molecule. In this case, just considering states of the enzyme molecule assumes ligand concentration as fixed, and enzyme transits in states E and E', giving a rational function with two terms in the denominator. But when ligand binds tightly with the enzyme, and ligand concentration is close to the enzyme concentration, then the binding and unbinding of enzyme will affect ligand concentration, so the assumption in enzyme-state model no longer holds. This is when the reaction order becomes unbounded.

Production rate consisting of multiple reactions. When there are multiple reactions, i.e. J_i^+, the set of reactions that produce X_i, has more than one element, we have $f_i^+ = \sum_{j\in J_i^+} s_{ij} v_j(\boldsymbol{x})$. Then generically we can write

$$H_i^+(\boldsymbol{x}) = \frac{\partial \log f_i^+}{\partial \log \boldsymbol{x}} = \sum_{j\in J_i^+} \lambda_j(\boldsymbol{v}) \frac{\partial \log v_j(\boldsymbol{x})}{\partial \log \boldsymbol{x}}, \quad \lambda_j(\boldsymbol{v}) = \frac{s_{ij} v_j(\boldsymbol{x})}{\sum_{j\in J_i^+} s_{ij} v_j(\boldsymbol{x})}. \tag{5.9}$$

So the production order is a weighted average of the order of each reaction involved, with the weight determined by the magnitude of the flux v_j. Therefore, if the order of the jth reaction is bounded in a polyhedron P_j, then production order H_i^+ is bounded in the larger polyhedron P formed via convex combination of these polyhedra $P = \operatorname{conv}\{P_j : j \in J_i^+\}$. Of course this only guarantees that the polyhedron P contains all possible values the production order H_i^+ can take, while not all points in P are necessarily reachable by H_i^+. Let us consider several special cases to see how this may play out.

If the flux of each reaction $v_j = k_j \boldsymbol{x}^{\boldsymbol{\alpha}_j}$ is a monomial, then f_i^+ is a polynomial in $\boldsymbol{x}$ with positive coefficients: $f_i^+(\boldsymbol{x}) = \sum_{j\in J_i} s_{ij} k_j \boldsymbol{x}^{\boldsymbol{\alpha}_j}$. Then

$$H_{i\ell}^+(\boldsymbol{x}) = \sum_{j\in J_i^+} \lambda_j(\boldsymbol{x}) \alpha_{j\ell}, \quad \lambda_j(\boldsymbol{x}) = \frac{s_{ij} k_j \boldsymbol{x}^{\boldsymbol{\alpha}_j}}{\sum_{j\in J_i^+} s_{ij} k_j \boldsymbol{x}^{\boldsymbol{\alpha}_j}}. \tag{5.10}$$

In this case each component reactions' order is constant $\boldsymbol{\alpha}_j$, and $\boldsymbol{H}_i^+$ is constrained in the polytope $P = \operatorname{conv}\{\boldsymbol{\alpha}_j : j \in J_i^+\}$, which is also the Newton polytope of the polynomial that defines f_i^+. The production order $\boldsymbol{H}_i^+$ can reach every point in this polytope by adjusting the concentrations $\boldsymbol{x}$ in the positive orthant.

If the flux of each reaction is a rational function with one term in the numerator, we have

$$v_j = k_j \frac{c_q^j \boldsymbol{x}^{\boldsymbol{\alpha}'^j}}{\sum_{q\in Q_j} c_q^j \boldsymbol{x}^{\boldsymbol{\alpha}_q^j}}, \quad \frac{\partial \log v_j}{\partial \log \boldsymbol{x}} = \sum_{q\in Q_j} \lambda_q^j(\boldsymbol{x})(\boldsymbol{\alpha}'^j - \boldsymbol{\alpha}_q^j), \;\; \lambda_q^j(\boldsymbol{x}) = \frac{c_q^j \boldsymbol{x}^{\boldsymbol{\alpha}_q^j}}{\sum_{q\in Q_j} c_q^j \boldsymbol{x}^{\boldsymbol{\alpha}_q^j}}.$$

Then the production order can be calculated to be

$$\boldsymbol{H}_i^+(\boldsymbol{x}) = \sum_{j\in J_i^+} \sum_{q\in Q_j} \lambda_j(\boldsymbol{v}) \lambda_q^j(\boldsymbol{x})(\boldsymbol{\alpha}'^j - \boldsymbol{\alpha}_q^j).$$

We can constrain production order $\boldsymbol{H}_i^+$ by the polytope P formed from convex combination of each reaction's order polytope $P_j = \boldsymbol{\alpha}'^j - \mathrm{conv}\left\{\boldsymbol{\alpha}_q^j : q \in Q_j\right\}$ that $P = \mathrm{conv}\left\{P_j : j \in J_i^+\right\} = \mathrm{conv}\left\{\boldsymbol{\alpha}'^j - \boldsymbol{\alpha}_q^j : j \in J_i^+, q \in Q_j\right\}$. We caution, however, that this bounding polytope can be very conservation, so that large portions of it are not reachable by production order $\boldsymbol{H}_i^+$ via adjusting concentraions $\boldsymbol{x}$. If $\{\lambda_j(\boldsymbol{v})\}_{j\in J_i^+}$ and $\left\{\lambda_q^j(\boldsymbol{x})\right\}_{q\in Q_j, j\in J_i^+}$ can take all values in their respective simplexes, i.e. they can be adjusted independently, then all points in this polytope P can be reached by $\boldsymbol{H}_i^+$. However, this is rather unlikely when some of the variables $\boldsymbol{x}$ are shared across different states in the same reaction in coefficients λ_q^j, or across several reactions in coefficients λ_j, which is necessary for the states and reactions to interact. As a simple example, consider $f_i^+(x) = \frac{1+x}{1+x+x^2}$. We may treat this as the sum of two active states, $\frac{1}{1+x+x^2}$ and $\frac{x}{1+x+x^2}$. The polytope for them are intervals $(-2, 0)$ and $(-1, 1)$ respectively. So with the above procedure, we would conclude the bounding polytope for the two active states together is $(-2, 1)$. However, we can calculate the log derivative in this case to be $-\frac{x^2(2+x)}{(1+x+x^2)(1+x)}$, which is bounded in $(-1, 0)$ for positive x. This is much smaller than the bounding interval $(-2, 1)$. But a tight bounding polytope does exist. It is $(-1, 0)$. So we see while the procedure discussed above to define a bounding polytope P by convex combining each reaction's P can work, it is often conservative. Finding a tight polyhedral set bounding production and degradation orders is important but nontrivial in the general case. One approach that may not scale well is via computer simulations, utilizing methods developed in Chapter 3.

In summary, production and degradation orders are often constrained in polyhedral sets, which can be derived in various modeling scenarios of increasing complexity. For production and degradation rates taking the form of polynomials and rational functions or coming from one reaction's binding network, it is often possible to determine whether the polyhedral set is reachable by adjusting species concentrations. Reachability is harder to determine for the general case when multiple reactions are involved in the production and degradation fluxes. So it is important to check via analysis or computation whether a polyhedral set bounding the production and degradation orders is overly conservative in these more complicated cases.

Dynamics from transport processes

Some dynamics of biomolecular systems in cells come from transport processes such as dilution and transport in and out of a compartment. We provide a basic discussion about some transport processes here, emphasizing that transport processes can often be treated as chemical reactions, therefore naturally subsumed into the framework of birth-death

systems.

Transport in and out of compartments. If a molecular species A is transported in and out of compartments, we can treat A inside and outside of the compartment as two separate species, A_i and A_o respectively. Then the transport out of a compartment is catalysis reaction $A_i \to A_o$. Transport into the compartment is $A_o \to A_i$. If the transport processes are fast and reach steady state, we can treat this as a state transition in binding reaction $A_i \rightleftharpoons A_o$.

Dilution due to biological growth. Many biomolecular circuits in systems and synthetic biology do not contain degradation reactions. Instead, the production of molecules are balanced by dilution due to increase in reaction volume from cell growth. Here we briefly show that dilution can be captured as a degradation reaction in birth-death systems for a homogeneous population of cells, but it has distinct structures.

For a homogeneous population of cells where each cell has the same volume and number of molecules, denote each cell's volume by v_0, and the number of cells by N. Let $X_i^{\rm tot} = x_i v_0 N$ denote the total number of X_i molecules in this population, then

$$\dot{x}_i = \frac{d}{dt}\frac{X_i^{\rm tot}}{N v_0} = \frac{1}{N v_0}\dot{X}_i^{\rm tot} - \frac{X_i^{\rm tot}}{v_0 N^2}\dot{N}. \tag{5.11}$$

Let $f_i^{\pm}$ denote the production and degradation rates for species i in every cell due to chemical reactions. So the rate of change for the total count of X_i is $\dot{X}_i^{\rm tot} = f_i(\boldsymbol{x}) v_0 N$. Let $f^{\rm g}(\boldsymbol{x})$ denote the growth rate of the population, assumed independent of N and v_0, then $\dot{N} = f^g(\boldsymbol{x})N$. Hence,

$$\dot{x}_i = f_i^+(\boldsymbol{x}) - f_i^-(\boldsymbol{x}) - f^g(\boldsymbol{x}) x_i. \tag{5.12}$$

We see that this is still a birth-death system, with dilution considered as a term in degradation. However, dilution has the unique structure that it adds the same term times x_i for each species i. So dilution from biological growth with growth rate independent of population size can be modeled as a degradation reaction $X_i \to \emptyset$, and the rate for this catalysis reaction is the growth rate $f^g(\boldsymbol{x})x_i$.

Local stability of birth death systems

We have formulated generic biomolecular processes in terms of birth-death systems. Later in this chapter we investigate regional and global dynamical properties of birth-death systems. As a starting point to understand some basic features of birth-death systems, as well as a reference for comparison with more general results, here we summarize how local stability of birth death systems relates to the birth-death order matrix. The key message

is that the local stability property determined by the birth-death order is structural, i.e. independent of rate constants. A sufficient condition for structural local stability is a linear matrix inequality (LMI) that can be easily computed given a birth-death order matrix $\boldsymbol{H}$. This topic is studied in [117]. We review the core results here.

Since local stability of a fixed point in a dynamical system is determined by the linearization at that fixed point, we relate linearization to production and degradation orders. To do so, we note the following relation between linear derivatives and log derivatives:

$$\frac{\partial f_i^{\pm}(\boldsymbol{x})}{\partial x_j} = \frac{\partial \log f_i^{\pm}(\boldsymbol{x})}{\partial \log x_j} \frac{f_i^{\pm}(\boldsymbol{x})}{x_j} = H_{ij}^{\pm} \frac{f_i^{\pm}(\boldsymbol{x})}{x_i} \frac{x_i}{x_j} = H_{ij}^{\pm} \frac{x_i}{\tau_i^{\pm}(\boldsymbol{x}) x_j}, \tag{5.13}$$

where $\tau_i^{\pm}(\boldsymbol{x}) := \frac{x_i}{f_i^{\pm}(\boldsymbol{x})}$ are time-scales of X_i's production and degradation [87, 118]. In matrix form, this is

$$\frac{\partial \boldsymbol{f}(\boldsymbol{x})}{\partial \boldsymbol{x}} = \boldsymbol{\Lambda}_{\boldsymbol{x}} \left(\boldsymbol{\Lambda}_{\boldsymbol{\tau}^+}^{-1} \boldsymbol{H}^+ - \boldsymbol{\Lambda}_{\boldsymbol{\tau}^-}^{-1} \boldsymbol{H}^- \right) \boldsymbol{\Lambda}_{\boldsymbol{x}}^{-1}, \tag{5.14}$$

where $\boldsymbol{\Lambda}_{\boldsymbol{x}^*}$ denotes the diagonal matrix with vector $\boldsymbol{x}^*$ on the diagonal. At a fixed point $\boldsymbol{x}^*$, we have $\boldsymbol{f}^+(\boldsymbol{x}^*) = \boldsymbol{f}^-(\boldsymbol{x}^*)$, so we could define $\boldsymbol{\tau} := \boldsymbol{\tau}^+(\boldsymbol{x}^*) = \boldsymbol{\tau}^-(\boldsymbol{x}^*)$ as the vector of steady-state time-scales at fixed point $\boldsymbol{x}^*$. Therefore, we have

$$\boldsymbol{A} := \frac{\partial \boldsymbol{f}}{\partial \boldsymbol{x}}(\boldsymbol{x}^*) = \boldsymbol{\Lambda}_{\boldsymbol{x}^*} \boldsymbol{\Lambda}_{\boldsymbol{\tau}}^{-1} \boldsymbol{H} \boldsymbol{\Lambda}_{\boldsymbol{x}^*}^{-1}, \tag{5.15}$$

relating linearized dynamics $\boldsymbol{A}$ to birth-death order matrix $\boldsymbol{H}$ at the fixed point $\boldsymbol{H} = \boldsymbol{H}(\boldsymbol{x}^*)$.

Stability of the fixed point depends on the real part sign of the eigenvalues of $\boldsymbol{A}$, that if they are all negative, a condition called Hurwitz, then the fixed point is stable. We see $\boldsymbol{A}$ has the same eigenvalues as $\boldsymbol{\Lambda}_{\boldsymbol{\tau}}^{-1} \boldsymbol{H}$ since they are similar. This shows that we have split the local dynamics at a fixed point $\boldsymbol{A}$ into two parts, (1) the birth-death order $\boldsymbol{H}$ structurally constrained from underlying regulatory networks, and (2) the time-scales $\boldsymbol{\Lambda}_{\boldsymbol{\tau}}$ that depends on rate constants and concentrations. This mirrors the general property of reaction orders or log derivatives that take a monomial kx^{α} and retain the exponent α while throwing away the constant k.

Therefore, from the birth-death order $\boldsymbol{H}$ at the fixed point, we can determine structural stability, i.e. stability independent of timescales $\boldsymbol{\tau}$. This means $\boldsymbol{\Lambda}_{\boldsymbol{\tau}} \boldsymbol{H}$ is Hurwitz for all positive vectors $\boldsymbol{\tau}$. A sufficient condition for this that can be easily tested computationally is for $\boldsymbol{H}$ to be diagonally stable. A matrix $\boldsymbol{H}$ is *diagonally stable* if there exists a positive diagonal matrix $\boldsymbol{P}$ such that

$$\boldsymbol{P}\boldsymbol{H} + \boldsymbol{H}^{\intercal}\boldsymbol{P} < 0, \tag{5.16}$$

where < 0 for matrices denote negative definiteness.

The birth-death order can also be used to determine structural instability. One result is that if $\boldsymbol{H}$ has no purely imaginary eigenvalues and there exists a diagonal matrix $\boldsymbol{P}$ with at least one negative entry such that Eq (5.16) holds, then $\boldsymbol{x}^*$ is structurally unstable, i.e. $\boldsymbol{\Lambda}_{\boldsymbol{\tau}}\boldsymbol{H}$ is unstable (not Hurwitz) for all positive vectors $\boldsymbol{\tau}$.

From these results on determining local stability from birth-death order matrix, we see several features that hint at general features of analysis based on reaction orders. First, the property certified by the birth-death order is structural, i.e. independent of rates. This is seen in the split of linearized dynamics into two parts in Eq (5.15). One interesting implication of this is that for a given region, stability of a fixed point could be determined from birth-death order in this region without knowing whether there exists any fixed points in this region. So the existence of fixed points and their stability are now independent, and one can be used to asked questions about the other. Second, while production and degradation processes both play a role in the general dynamics of a birth death system, the local stability can be determined using only the birth-death order $\boldsymbol{H}$. This means, for example, $\dot{x} = x - x^2$ and $\dot{x} = 1 - x$ are considered the same. Lastly, an easy-to-compute sufficient test for local stability from birth-death order takes the form of a linear matrix inequality in Eq (5.16). This test for local property can be related and generalized to tests in regional and global properties that we study next. With a sense of the typical features of dynamical properties analyzed from reaction orders, we delve into the study of regional and global properties through reaction orders using dissipative theory in the next section.

5.2 Dissipativity in positive scalar birth death systems

In dissipative theory, the behavior of a system is encoded in how the system responds to inputs and outputs captured in terms of storage functions and supply rates (see Section 5.6 for a more detailed overview with generalization to include reference points explicitly to suit our needs). Motivated by physical theories of thermodynamics and statistical mechanics, the storage function captures energy stored internally in a system's states, and the supply rate captures interaction processes of the system with the external environment such as work and heat. The notion of dissipativity then tries to capture how the second law of thermodynamics dictates increasing entropy as a force deriving a thermodynamic system to equilibrium. An equivalent statement of the second law is that the amount of work that can be extracted from a system cannot be more than what is put in. This is the formulation used to define dissipativity of a system, that the amount of energy added to the storage function cannot be more than that provided from the supply rates. Properties such as stability or invariant sets can then be determined from dissipativity. Structures

of system dynamics, physical interpretation of input and output variables, and system properties to be studied should be reflected in the use of different supply rates and storage functions. As an example, for dissipativity in mechanical and electrical systems with canonical physical notions of energy, the input and output variables are chosen to be pairs of force and potential gradient such as resistance and current, force and velocity, or torque and angle velocity. The supply rate is the product of input and output to yield power. The storage function is then quadratic, encoding energy or potential. In this work, we define storage functions and supply rates of special form that are tailor-made for biomolecular systems, so as to have a notion of dissipativity.

Another powerful feature of dissipative theory is to allow the study of a large system as the interconnection of smaller component systems [11, 77]. The dissipative properties can be characterized for each component system, and then dissipativity of the full system can be studied by taking into account the interconnections of component systems. Specifically, the storage function of component systems can be used to formulate the storage function of the full system, demonstrating dissipativity relative to supply rates of interest for the full system. Because of this, we can begin our study with the smallest possible component system: a scalar or one-dimensional birth-death system.

Supply rate for biomolecular systems

To begin with our study of dissipativity for biomolecular systems, we first need to define the notion of dissipativity in our case, namely what is the supply rate that a system is dissipative to. Let us focus on the single-input-single-output (SISO) case, where output y and input u are scalars. We consider the following class of supply rates:

$$s^{\pm}(\overline{u},\overline{y};\varepsilon,p) = \pm p(\overline{y})\left(\overline{u}-\overline{y}^{\pm\varepsilon}\right)\log\overline{y}, \tag{5.17}$$

where $p:\mathbb{R}_{>0}\to\mathbb{R}_{>0}$ is a positive function, $\varepsilon\in\mathbb{R}$, $\overline{u}=\frac{u}{u'}$, $\overline{y}=\frac{y}{y'}$, and u', y' are reference input output values. We often omit some of the arguments to write $s^{\pm}(\overline{u},\overline{y};\varepsilon)$, $s^{\pm}(\overline{u},\overline{y})$, or $s^{\pm}(\varepsilon)$ when those arguments are not relevant to the discussion.

There are several parameters in the supply rate. The meaning and importance of these parameters will become clear in later discussions. We provide an introduction here to guide the reader. There are two versions of the supply rate, s^{+} and s^{-}. This is because birth-death systems have production and degradation terms, so the input can go into production, or degradation. Where the input enters change the behavior captured by dissipativity, therefore we provide two versions, s^{+} for control in production, and s^{-} for control in degradation, explicitly in the supply rate. The input and output arguments to

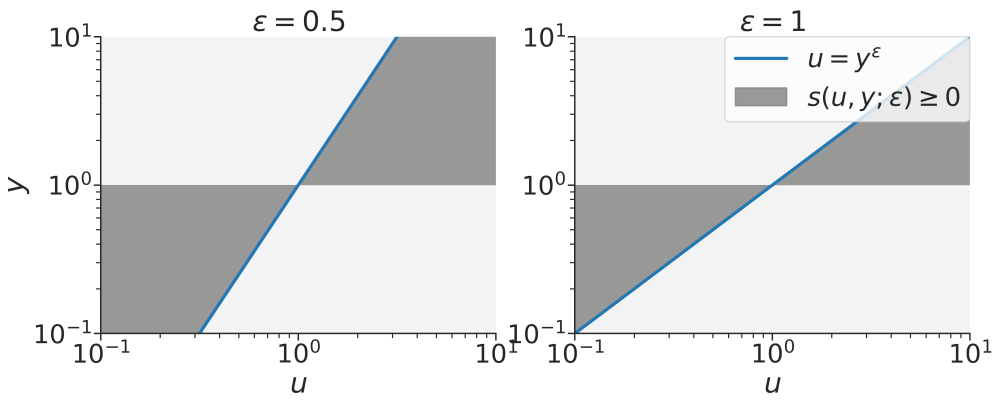

Figure 5.2 Plot showing the restriction of positive supply rate $s(u, y; \varepsilon) \geq 0$ on the values of (u, y). The grey region is where this inequality is satisfied, for $\varepsilon = 0.5$ (Left) and $\varepsilon = 1$ (Right). The blue line is $u = y^{\varepsilon}$.

the supply rate are $\overline{u}$ and $\overline{y}$, the ratio of actual input and output values relative to some reference values. The reason ratios instead of exact values are used is because of the fold-change nature of reaction orders, that reaction orders cannot capture properties due to exact values or linear changes, but rather fold changes. Implied by this, the default or no-control input is $\overline{u} = 1$, rather than $u = 0$ that is typically used in dissipative theory. This also provides us a way to derive different dissipativity properties in reference to different points, and talk about regions that allow dissipativity in reference to points in them. This is useful when studying systems with multistability, for example. The positive function p shifts the overall value of the supply rate without changing how the input and output are related. This is therefore akin to the unit for power. Mathematically, this is often taken to be a monomial in $\overline{y}$ to certify dissipativity of a suitable scale. The ε parameter captures the level of dissipativity encoded in reaction order. Larger ε, more dissipativity, corresponds the intuition that the system dissipates energy faster. This means, given positive supply rate $s(u, y) > 0$, the output of a more-dissipative system with higher ε should be more restricted. Indeed, this can be seen in Figure 5.2, which illustrates that with non-negative supply rate $s \geq 0$, a larger ε corresponds to more severe restriction on (u, y) values. As we will see later, a larger ε corresponds to stronger dissipativity, therefore more "stabilizing". We note that the restriction on $(\log u, \log y)$ space from this supply rate is exactly the same as the restriction on (u, y) from the dissipativity notion of output-strict passivity with supply rate $s(u, y) = uy - \varepsilon y^2$ used for dissipative systems inspired by linear properties (see Chapter 1 of [11]).

We can also provide a more physical interpretation for the choice of supply rate in Eq (5.17), although the form of the supply rate was designed purely based on the mathematical need to capture constraints on dynamics from reaction orders (see Example 14). Supply rate

is motivated by the physical concept of work or power, i.e. energy's rate of change. The supply rates typically used in mechanical and electrical systems are from well-understood pairs of generalized force and velocity, with the supply rate defined as force times velocity. Some examples are pressure and change in volume, surface tension and change in area, torque and angular velocity, voltage and current. Such force and velocity pairs are further extended in thermodynamics and statistical mechanics to include changes through heat and molecular concentrations. The pair for heat is temperature and change in entropy, while the pair for concentrations is chemical potential μ and change in molecular concentration c. For gas and solutions under simplifying ideal assumptions, chemical potential is proportional to $\log \frac{c}{c^0}$, where c^0 is some reference concentration. Hence the supply rate for concentration changes is chemical potential multiplying concentration, of the form $\log \frac{c}{c^0} dc$, where dc is an infinitesimal change in concentrations. Considering the change in concentrations dc as input u, and concentration c as output y, then we have a form similar to the supply rate in Eq (5.17). The parameter ε can be interpreted as akin to fugacity or thermodynamic activity coefficients that adjusts the actual energy effect from change in concentrations of a particular species.

One important property required of supply rate is that it is non-positive with no-control input, achieving value zero at the point of reference. This corresponds to the intuition that with no external input, any output of the system deviating from a reference value can only drain energy (negative supply rate). This is important if we want to use dissipativity to show stability. We show that the supply rate we just defined satisfies these conditions in the following lemma.

Lemma 5.2.1. *The SISO supply rate function in Eqn* (5.17) *satisfies* $s^{\pm}(1, \overline{y}; \varepsilon) \leq 0$ *for all* $\overline{y} > 0$ *for* $\varepsilon \geq 0$*, with equality only at* $\overline{y} = 1$ *if* $\varepsilon > 0$*.*

Proof. We show it for s^+, as the case for s^- is similar. Note that this supply rate can be rewritten as $s^+(\overline{u}, \overline{y}) = (\overline{u} - 1) \log \overline{y} - (\overline{y}^{\varepsilon} - 1) \log \overline{y}$. For $\varepsilon > 0$, expression $(x^{\varepsilon} - 1) \log x \geq 0$ holds for all $x \geq 0$ with equality only at $x = 1$ (shown below). Therefore, if $\varepsilon > 0$, $s^+(1, \overline{y}) \leq 0$ for all $\overline{y} > 0$, with equality only at $\overline{y} = 1$.

(more details on $(x^{\varepsilon} - 1) \log x \geq 0$): Derivative of $(x^{\varepsilon} - 1) \log x$ is $\varepsilon x^{\varepsilon - 1} \log x + x^{\varepsilon - 1} - x^{-1} = x^{-1}(x^{\varepsilon} \log x^{\varepsilon} + x^{\varepsilon} - 1)$, since $x \log x \geq x - 1$, the derivative is bounded between $2x^{-1}(x^{\varepsilon} - 1)$ and $2x^{-1} x^{\varepsilon} \log x^{\varepsilon}$. For $\varepsilon > 0$, in both bounds $x \leq 1$ yields negative values, $x \geq 1$ yields positive values, so $(x^{\varepsilon} - 1) \log x$ decreases in $0 < x \leq 1$, increases in $1 \leq x$. Since $(x^{\varepsilon} - 1) \log x$ has value 0 at $x = 1$, it is non-negative, with value 0 only at $x = 1$. For $\varepsilon = 0$, this is true trivially. So, $(x^{\varepsilon} - 1) \log x \geq 0$ for all $x > 0$, with equality only at $x = 1$, if $\varepsilon > 0$. □

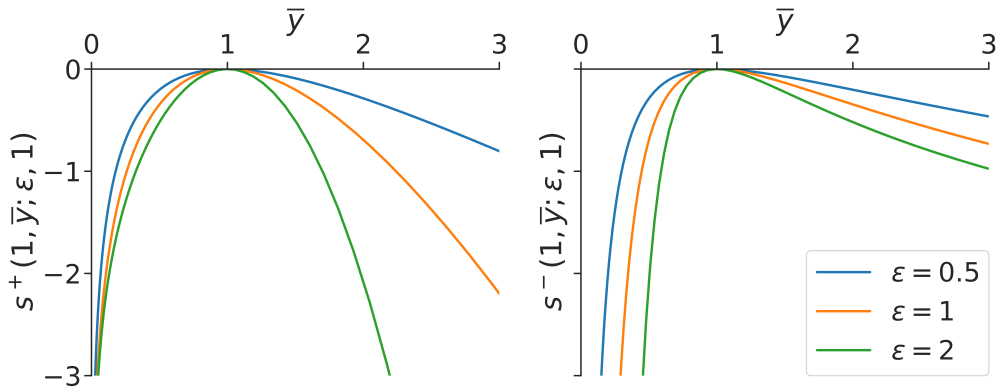

Figure 5.3 Plot for the supply rate s^+ (left) and s^- (right) with no-control input $\overline{u} = 1$ and pre-factor $p = 1$, with varying ε.

With the result of this lemma, we can apply Theorem 5.6.8 (part (1)) to this supply rate. So if a system is dissipative with respect to supply rate $s^{\pm}$ at x^* for some $\varepsilon > 0$, then x^* is asymptotically stable. We can also see the overall shape of the supply rate function in Figure 5.3. We see that with increasing ε, the sharpness of the function increases.

Another nice property for this class of supply rates is that we have the following point-wise inequality showing that supply rates with larger ε have larger magnitude globally.

$$s^{\pm}(\overline{u},\overline{y};\varepsilon,p) \leq s^{\pm}(\overline{u},\overline{y};\varepsilon',p), \quad \forall \overline{u},\overline{y} \in \mathbb{R}_{>0} \qquad \text{if } \varepsilon \geq \varepsilon'. \tag{5.18}$$

Next, we take a scalar birth-death control system and show that dissipativity with respect to supply rates $s^{\pm}$ correspond to conditions on birth-death orders.

Dissipativity in scalar birth-death control systems

In the theory of network dissipative systems, an important structure is that the system studied is control affine. We follow this and begin with the scalar control affine system of the following form,

$$\dot{x} = f(x) + g(x)u, \qquad y = h(x), \tag{5.19}$$

where state x, control input u, and output y are positive, i.e. they take values in $\mathbb{R}_{>0}$. Control affine means the control input u enters in first order. To study dissipativity for biomolecular systems, we would like to connect the control affine structure with the production and degradation processes we see in birth death systems (Definition 5.1.2). This motivates the following definition.

Definition 5.2.2 (Scalar birth-death control affine system)**.** Given a positive scalar control affine system $\dot{x} = f(x) + g(x)u$, $y = h(x)$, with $f, g, h : \mathbb{R}_{>0} \to \mathbb{R}$ continuously differentiable,

and h globally positive and strictly increasing. If in addition, either $f > 0$ and $g < 0$ globally, or $f < 0$ and $g > 0$ globally, we call this system a **(scalar) birth-death control affine system**. In particular, we can denote the positive term as f^+, and negative term as $-f^-$. The system is called **control in production** if it can be written as $\dot{x} = f^+(x)u - f^-(x)$. It has **control in degradation** if it can be written as $\dot{x} = f^+(x) - f^-(x)u$.

Note that birth-death control affine system is both a control affine system (Definition 5.19), and a birth-death control system (Definition 5.1.2).

Remark 5.2.3. One assumption encoded in our definition is that h is strictly increasing in x. What is actually important is that the output y and x have a one-to-one correspondence, i.e. h is invertible, so that the behavior of the state x is always "observable" from the output y. As h is a one-dimensional function and continuous, this means h is either strictly increasing or strictly decreasing. As a convention, we choose h to be strictly increasing, we $h(x) = x$ as a simple default option. There are cases when choosing h to be decreasing can cause trouble in interconnections (see Example 18). It might be tempting to also ask about monotonicity of $f^{\pm}$. Those do not tend to matter, it turns out, which is important to allow multistability in 1D case. What is important is the monotonicity of a multiplicative combination of f^+, f^-, and h, which determines a sufficient condition for dissipativity (see Lemma 5.2.8). △

Now we investigate dissipativity of a scalar birth death control affine system with respect to the supply rate in Eq (5.17). See Section 5.6 for a more detailed introduction to dissipative control that provides a more comprehensive perspective. As a summary, there are three elements in what it means for a system to be dissipative. First, the *supply rate*. For this, our choice is the one in Eq (5.17), with parameter ε affecting whether dissiption inequality holds true. Second, the *state region* $\mathcal{X}$ of x that the system is dissipative in. For this, as we are dealing with scalar systems with positive variables, the state region $\mathcal{X}$ is often an open interval $(x_{\min}, x_{\max})$ in $\mathbb{R}_{>0}$. Third, the *reference point* (x', u') that the system is dissipative relative to. This is perhaps the least common or intuitive, as the reference point is often assumed to be $(0, 0)$ in dissipative control. However, for our need to study multistability and capture dissipativity from reaction orders, it is crucial to include the reference points explicitly. Hence, after we determine the supply rate $s(\varepsilon)$ and some interval as the state region $\mathcal{X}$, we still need to determine the reference points (x', u') that are *admissible*, i.e. reference points that allow our system to be dissipative with the chosen supply rate $s(\varepsilon)$ in the state interest $\mathcal{X}$.

Now we define dissipativity, which relates a system's dynamics to supply rate via the idea

of storage functions. We define this now. Let state region $\mathcal{X}$ be an open interval in $\mathbb{R}_{>0}$. Fix parameters $\varepsilon > 0$, and $p : \mathbb{R}_{>0} \to \mathbb{R}_{>0}$ for the supply rate function $s^{\pm}$. A continuously differentiable function $V : \mathcal{X} \times \mathcal{X}' \to \mathbb{R}$ is a **virtual storage function** with respect to the supply rate $s^{\pm}(\overline{u}, \overline{y}; \varepsilon, p)$ and the reference point $(x', u') \in \mathbb{R}_{>0} \times \mathbb{R}_{>0}$ if and only if

$$\frac{d}{dt}V(x(t); x') \leq s^{\pm}(\overline{u}, \overline{y}; \varepsilon, p), \quad \forall x \in \mathcal{X}, u \in \mathbb{R}_{>0}, \tag{5.20}$$

where the quantification over $x \in \mathcal{X}$ is understood as affecting $y = h(x)$ and $\overline{u} = \frac{u}{u'}$, $\overline{y} = \frac{y}{y'}$, $y' = h(x')$. This inequality in Eq (5.20) is also called the **dissipation inequality**. If the virtual storage function V further satisfies that it is non-negative for all $x \in \mathcal{X}$, then it is called a **storage function**.

For a given system, it is **dissipative** with supply rate $s^{\pm}(\varepsilon, p)$, state region $\mathcal{X}$ and reference point (x', u') if there exists function $V(x, x')$ that is a storage function, i.e. it is non-negative over $x \in \mathcal{X}$ and satisfy inequality (5.20) for supply rate $s^{\pm}(\varepsilon, p)$ and reference point (x', u').

Let us analyze the dissipation inequality condition in the case of control in production, where we use s^{+}. Writing out the expression for $\frac{d}{dt}V$ and $s^{\pm}$, we have

$$\frac{d}{dt}V = \dot{x}\frac{\partial V(x; x')}{\partial x} = \Big(f^{+}(x)u - f^{-}(x)\Big)\frac{\partial V(x; x')}{\partial x} \leq p(\overline{y})(\overline{u}\log\overline{y} - \overline{y}^{\varepsilon}\log\overline{y}). \tag{5.21}$$

Collect terms in $\overline{u}$, we have

$$\left(-\frac{\partial V(x; x')}{\partial x}f^{-}(x) + p(\overline{y})\overline{y}^{\varepsilon}\log\overline{y}\right) + \overline{u}\Big(f^{+}(x)u' - p(\overline{y})\log\overline{y}\Big) \leq 0. \tag{5.22}$$

Since this inequality needs to hold for all $u > 0$, which corresponds to all $\overline{u} = \frac{u}{u'} > 0$, this inequality is equivalent to the following two inequalities:

$$-\frac{\partial V}{\partial x}f^{-} + p(\overline{y})\overline{y}^{\varepsilon}\log\overline{y} \leq 0, \quad \frac{\partial V}{\partial x}f^{+}u' - p(\overline{y})\log\overline{y} \leq 0. \tag{5.23}$$

Since $f^{\pm}(x)$ are positive, this can be expressed as bounds on derivative of V:

$$\frac{1}{f^{-}(x)}p(\overline{y})\overline{y}^{\varepsilon}\log\overline{y} \leq \frac{\partial V(x; x')}{\partial x} \leq \frac{1}{f^{+}(x)u'}p(\overline{y})\log\overline{y}. \tag{5.24}$$

Therefore, the condition for the existence of a virtual storage function V for $x \in \mathcal{X}$ then becomes

$$\frac{f^{+}(x)u'}{f^{-}(x)}\overline{y}^{\varepsilon}\log\overline{y} \leq \log\overline{y}, \quad x \in \mathcal{X}. \tag{5.25}$$

Note that this condition is independent of $p(\overline{y})$. In a moment we show that the same is true for control in degradation. This means, for a fixed scalar birth-death control affine system,

if there exists a continuously differentiable virtual storage function $V_p(x, x')$ for supply rate $s^{\pm}(\varepsilon, p)$ for some positive function p, then there exists continuously differentiable virtual storage functions $V_{p'}(x, x')$ for $s^{\pm}(\varepsilon, p')$ for all positive functions p'. At first blush this suggests that there is little value in considering supply rates $s^{\pm}(\overline{u}, \overline{y}; \varepsilon, p)$ with p other than $p(\overline{y}) \equiv 1$. However we show in Section 5.3 that for suitable compositions of dissipative scalar birth-death systems, the degree of freedom in choosing p can be of great use in finding Lyapunov functions for the stability of the composed system.

Remark 5.2.4. We used s^+ for control in production, and s^- for control in degradation. What happens if we switch them around? If we used s^- and asked for conditions s.t. control in production case is dissipative w.r.t s^-, we will get a virtual storage function V with bounds on its derivative $\partial_x V$ s.t. $-p(\overline{y})\frac{\overline{y}^{\varepsilon}\log\overline{y}}{f^-} \leq \partial_x V \leq -p(\overline{y})\frac{\log\overline{y}}{f^+}$. Note that both upper and lower bounds are positive for $\overline{y} > 1$, negative for $\overline{y} < 1$. Now, since $V(x'; x') = 0$ by definition, this implies V is globally non-positive. So V cannot be a storage function unless it is zero everywhere. For a nontrivial V, it is a virtual storage function (meaning it dissipates over time) that is bounded above, with unique maximum at x'. Therefore, for constant input $u \equiv u'$, V might certify x' is unstable. Indeed, for a function $V(x; x')$ satisfying $V(x; x') \leq 0$ and $\frac{d}{dt}V(x(t); x') \leq 0$, if for any $\alpha < 0$, sublevel sets $V_\alpha := \{x : V(x; x') \leq \alpha\}$ have a positive distance from x', then x' is not asymptotically stable. If in addition, for any $\delta > 0$, there exists $\nu(\delta) > 0$ s.t. $\frac{d}{dt}V(x(t); x') \leq -\nu(\delta) < 0$ for all trajectories with $\|x(t) - x'\| \geq \delta$, and for all $r > 0$, there exists $\alpha < 0$ s.t. V_α contains a point $\|x - x'\| > r$, and this then certifies x' is not Lyapunov stable either. This is similarly true if we use s^+ for control in degradation. △

Now we repeat the above for control in degradation, using s^-. The differential condition is

$$\partial_x V(f^+ - f^- u) \leq p(\overline{y})\Big(\overline{y}^{-\varepsilon}\log\overline{y} - \overline{u}\log\overline{y}\Big), \tag{5.26}$$

where $\partial_x V$ is shorthand for the partial derivative of V with respect to x. Requiring this condition to be true for all $u > 0$, we have

$$\partial_x V f^+ - p(\overline{y})\overline{y}^{-\varepsilon}\log\overline{y} \leq 0, \qquad -\partial_x V f^- u' + p(\overline{y})\log\overline{y} \leq 0. \tag{5.27}$$

Again, this becomes a bound on the derivative of V:

$$\frac{1}{f^-(x)u'}p(\overline{y})\log\overline{y} \leq \partial_x V(x; x') \leq \frac{1}{f^+(x)}p(\overline{y})\overline{y}^{-\varepsilon}\log\overline{y}, \tag{5.28}$$

and the condition for the existence of such virtual storage function becomes

$$\frac{f^+(x)}{f^-(x)u'}\overline{y}^{\varepsilon}\log\overline{y} \leq \log\overline{y}. \tag{5.29}$$

We summarize the above into the following proposition.

Theorem 5.2.5 (dissipation inequality)**.** *For a scalar birth-death control system, given x' and u', there exists a continuously differentiable virtual storage function in an interval $\mathcal{X} \subset \mathbb{R}_{>0}$ for supply rate $s^{\pm}(\varepsilon, p)$ with some positive function $\overline{y} \mapsto p(\overline{y})$ iff it exists for supply rate $s^{\pm}(\varepsilon, p')$ with any positive function p' iff the following is true for all $x \in \mathcal{X}$:*

$$\begin{cases} \frac{f^+(x)u'}{f^-(x)}\overline{y}^{\varepsilon}\log\overline{y} \leq \log\overline{y}, & \text{for control in production, using } s^+; \\ \frac{f^+(x)}{f^-(x)u'}\overline{y}^{\varepsilon}\log\overline{y} \leq \log\overline{y}, & \text{for control in degradation, using } s^-. \end{cases} \tag{5.30}$$

Furthermore, for a chosen p, the virtual storage function satisfies the following bounds on its derivative for $x \in \mathcal{X}$:

$$\begin{cases} \frac{p(\overline{y})\overline{y}^{\varepsilon}}{f^-(x)}\log\overline{y} \leq \partial_x V(x;x') \leq \frac{p(\overline{y})}{f^+(x)u'}\log\overline{y}, & \text{for control in production, using } s^+; \\ \frac{p(\overline{y})}{f^-(x)u'}\log\overline{y} \leq \partial_x V(x;x') \leq \frac{p(\overline{y})\overline{y}^{-\varepsilon}}{f^+(x)}\log\overline{y}, & \text{for control in degradation, using } s^-. \end{cases} \tag{5.31}$$

We emphasize that Theorem 5.2.5 says the choice of $p : \mathbb{R}_{>0} \to \mathbb{R}_{>0}$ does not affect dissipativity. In other words, the two parameters in supply rate, ε and p, can be considered in a hierarchical fashion. Dissipativity with respect to $s(\varepsilon)$ can be determined independent of p, and p can be chosen later to find a suitable virtual storage function V. There are important questions (such as stability of a closed-loop interconnected system) which benefit from the ability to choose the form of p. We explore such benefits in-depth in Section 5.3.

For a given candidate virtual storage function, Eq (5.31) is equivalent to the dissipation inequality in Eq (5.20) for this function. Eq (5.30) is equivalent to there exists a virtual storage function. So Eq (5.30) is more appropriate for our general use of deriving whether a system is dissipative or not. Therefore, from here on we refer to this equation as the **dissipation inequality**.

The dissipation inequality (Eq (5.30)) can be used to constrain what the virtual storage functions V can be, as well as what pairs of reference points (x', u') can take, if the dissipative inequality is satisfied at x'.

Proposition 5.2.6. *For a scalar birth-death control affine system satisfying the dissipation inequality (5.31) for $x \in \mathcal{X}$ at x', where $\mathcal{X} \subset \mathbb{R}_{>0}$ is an open interval. If $x' \in \mathcal{X}$, then the following are true.*

1. *$\partial_x V(x';x') = 0$. Recall we also have $V(x';x') = 0$ by definition.*
2. *$u' = \frac{f^-(x')}{f^+(x')}$ for control in production, $u' = \frac{f^+(x')}{f^-(x')}$ for control in degradation. This means any (x', u') pair where $x' \in \mathcal{X}$ and the dissipation inequality (5.31) is satisfied has x' as a fixed point with constant input $u \equiv u'$.*

3. *$V(x;x')$ is non-negative for $x \in \mathcal{X}$ and equal to zero only at $x = x'$. This means if V is a storage function.*

Proof. 1. By direct evaluation at $x = x'$, we see the upper and lower bounds of $\partial_x V$ are both zero.

2. Consider both $x \to x'^-$, approaching x' from the negative side, and $x \to x'^+$, approaching x' from the positive side, we see the dissipation inequality (5.31) becomes an equality. For example, if control in production, $x < x'$ implies $\log \overline{y} < 0$, since h is strictly monotonically increasing. So the inequality becomes $\frac{1}{f^-(x)}\overline{y}^{\varepsilon} \geq \frac{1}{f^+(x)u'}$. Taking the limit of $x \to x'^-$, we obtain $\frac{1}{f^-(x')} \geq \frac{1}{f^+(x')u'}$. Similarly, in the $x > x'$ case taking the limit $x \to x'^+$ obtains $\frac{1}{f^-(x')} \leq \frac{1}{f^+(x')u'}$. Together, we have $u' = \frac{f^-(x')}{f^+(x')}$.

3. For x in the connected component of $\mathcal{X}$ containing x', x can be reached by a continuous path from x' in $\mathcal{X}$. So $V(x;x') = \int_{x'}^{x} \partial_x V(s;x')ds \geq 0$, since $V(x';x') = 0$ by definition. Now, since $\partial_x V(x;x') < 0$ for $x < x'$, and $\partial_x V(x;x') > 0$ for $x > x'$, we know $V(x;x') \geq V(x';x') = 0$ with equality only when $x = x'$.

□

To get some concrete experience with dissipativity and storage functions, let us look at what the conditions (5.30) and (5.31) look like for a scalar birth death control affine systems that are also simple.

Example 14 (simple birth death control affine systems)**.** A scalar simple birth death system is given by

$$\dot{x} = f^+(x) - f^-(x) = k^+ x^{\alpha^+} - k^- x^{\alpha^-}.$$

We make this a control affine system by add in control input u and output $y = h(x) = x^{\beta}$ for some $\beta > 0$.

$$\dot{x} = \begin{cases} k^+ x^{\alpha^+} u - k^- x^{\alpha^-}, & \text{if control in production;} \\ k^+ x^{\alpha^+} - k^- x^{\alpha^-} u, & \text{if control in degradation.} \end{cases} \tag{5.32}$$

We consider $\mathcal{X} = \mathbb{R}_{>0}$, so x can take all positive values. With our assumption for y, we see y can also take all values in $\mathbb{R}_{>0}$.

As for points of reference (x', u'), for any $x' \in \mathcal{X}$, by Proposition 5.2.6, u' satisfies

$$(u')^{\sigma} \frac{f^+(x')}{f^-(x')} = (u')^{\sigma} \frac{k^+}{k^-} x'^{\alpha^+ - \alpha^-} = 1,$$

where $\sigma = 1$ for control in production, $\sigma = -1$ for control in degradation. So for a given x', the constant coefficients k^+ and k^- determine u'.

With this in mind, the existence condition for a virtual storage function from (5.30) becomes the same for control in production and control in degradation:

$$\overline{y}^{\frac{\alpha^+-\alpha^-}{\beta}+\varepsilon}\log\overline{y} \leq \log\overline{y},$$

where $\varepsilon \in \mathbb{R}$ is a parameter which partially defines the supply rate associated with the storage function. Since the above inequality holds for all $\overline{y} > 0$ if and only if $\varepsilon \leq -\frac{\alpha^+-\alpha^-}{\beta}$, we have the following result.

For $x \in \mathcal{X} = \mathbb{R}_{>0}$, the system in Eq (5.32) is dissipative with respect to $s^{\pm}(\varepsilon)$ at some $x' > 0$ if and only if $\varepsilon \leq -\frac{\alpha^+-\alpha^-}{\beta}$. Also, that the system is dissipative at one $x' > 0$ implies it is dissipative for all $x' > 0$.

The bounds on virtual storage functions for a chosen $p(\overline{y}) = \overline{y}^{\varepsilon^0}$ from Eqn (5.31) is

$$\begin{cases} \frac{\tau(x')}{x'}\overline{x}^{(\varepsilon^0+\varepsilon)\beta-\alpha^-}\beta\log\overline{x} \leq \partial_x V \leq \frac{\tau(x')}{x'}\overline{x}^{\varepsilon^0\beta-\alpha^+}\beta\log\overline{x}, & \text{for control in production,} \\ \frac{\tau(x')}{x'}\overline{x}^{\varepsilon^0\beta-\alpha^-}\beta\log\overline{x} \leq \partial_x V \leq \frac{\tau(x')}{x'}\overline{x}^{(\varepsilon^0-\varepsilon)\beta-\alpha^+}\beta\log\overline{x}, & \text{for control in degradation.} \end{cases}$$

where we defined timescale constants $\tau(x') := \frac{x'}{k^-x'^{\alpha^-}} = \frac{x'}{u'k^+x'^{\alpha^+}}$ for control in production, $\tau(x') := \frac{x'}{k^+x'^{\alpha^+}} = \frac{x'}{u'k^-x'^{\alpha^-}}$ for control in degradation.

The biggest ε we can take is $\varepsilon = \frac{\alpha^--\alpha^+}{\beta}$. Take this choice, then the upper and lower bounds of $\partial_x V$ become equal. So for control in production, we have the following when $\varepsilon = \frac{\alpha^--\alpha^+}{\beta}$.

$$\partial_x V = \frac{\tau(x')}{x'}\overline{x}^{\varepsilon^0\beta-\alpha^+}\beta\log\overline{x}.$$

Integrating this with $V(x';x') = 0$ yields the following storage function for control in production. Define $a = 1 + \varepsilon^0\beta - \alpha^+$, then depending on whether $a = 0$ or not, we have

$$V(x;x') = \begin{cases} \frac{\tau(x')\beta}{a^2}(\overline{x}^a\log\overline{x}^a - \overline{x}^a + 1), & a = 1+\varepsilon^0\beta-\alpha^+ \neq 0; \\ (\tau(x')\beta)\frac{(\log x)^2}{2}, & a = 0. \end{cases} \tag{5.33}$$

For the case $a = 1 + \varepsilon^0\beta - \alpha^+ = 0$, we have $\partial_x V = \frac{\tau(x')}{x'}\frac{1}{\overline{x}}\log\overline{x}$, which integrates to $\frac{\tau(x')\beta}{2}(\log\overline{x})^2$. Note that we could choose ε^0 arbitrarily, so for any given $\alpha^{\pm}$ and β, we could choose to avoid $a = 0$ or make exactly $a = 0$ by choosing ε^0.

The storage function has the form of an entropy-like function (see Section 6.6 of [43] for a discussion in the context of semidefinite programming). Indeed, entropy from microscopic

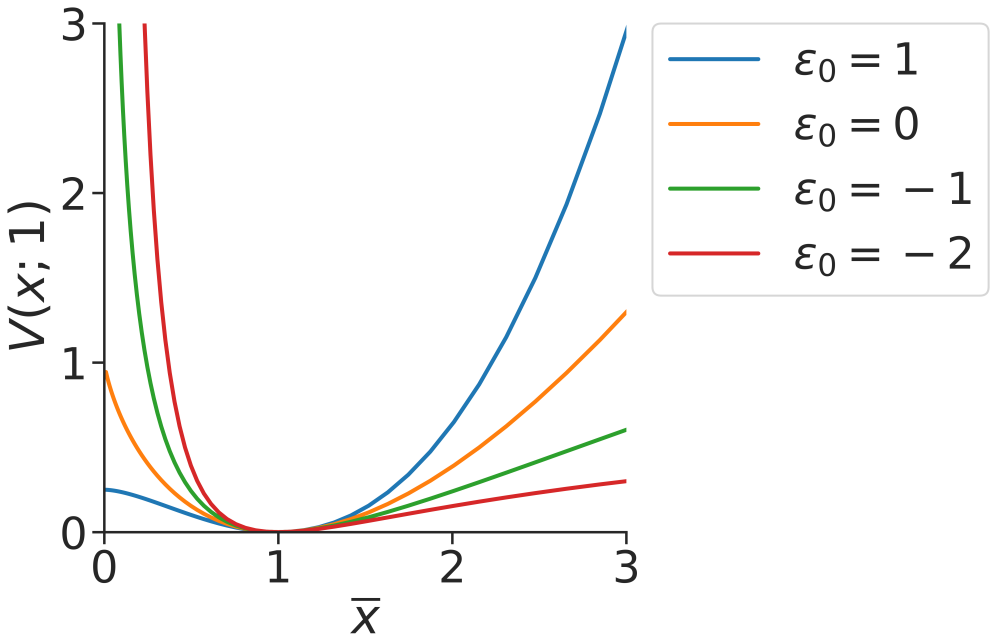

Figure 5.4 Plot for storage function in Eq (5.33) with $x' = u' = \beta = 1$ for various ε^0. For $\varepsilon^0 < -1$, V grows to $+\infty$ as $\overline{x} \to 0$, but is finite as $\overline{x} \to +\infty$. For $\varepsilon^0 > -1$, V is finite at $\overline{x} \to 0$, but grows to infinity as $\overline{x} \to +\infty$. For $\varepsilon^0 = -1$, V grows to infinity at both limits.

states is defined as $\log W$, where W is the number of microscopic states. W often consists of factorial factors of the form $N!$ for some positive integer N. Approximating the discrete sum as an integral would yield $\log N! = \sum_{x=1}^{N} \log x \approx \int_1^N \log x dx = N \log N - N + 1$, with error of order $O(\sqrt{N})$ for large N. An entropy-like function of the form $\sum_i x_i \log \frac{x_i}{x_i'} - x_i$ is also used as a Lyapunov functions for detailed balance (or more generally, complex balanced) chemical reaction networks [44, 119].

Different a yield storage functions V with different boundary behaviors. If $a > 0$, then $V(x; x') \to \frac{\tau(x')\beta}{a^2}$ as $x \to 0$, and $V \to +\infty$ as $x \to +\infty$. So V is finite on $x \to 0$ boundary, but infinite on $x \to +\infty$ boundary. If $a < 0$, then it is the other way around, that V is finite on the $+\infty$ boundary, but infinite on the 0 boundary. If $a = 0$, then V goes to infinity on both boundaries. So we can choose different ε^0, which in turn change a and thus the boundary behavior of storage function V, when we have different goals in mind. For example, if we want to certify the fixed point x' is globally stable when $u \equiv u'$, then we need V to grow to infinity on both boundaries, so we should choose $\varepsilon^0 = -1$, i.e. $a = 0$.

The storage function V above with $x' = u' = \beta = 1$ and $\alpha^+ = 0$, i.e. constant or zeroth order production, is plotted in Figure 5.4 for several different choices of ε^0. △

From this example, we see that for the case of a scalar simple birth death control affine

system, dissipativity with respect to $s(p, \varepsilon)$ is independent of prefactor $p(\overline{y})$, and only depends on how ε compares to birth-death order $H = \alpha^+ - \alpha^-$ and output order β. The storage function obtained in this case has entropy-like form, with properties adjustable by choosing prefactor $p(\overline{y})$ in supply rate. Now we study how this generalizes to non-simple scalar systems.

Dissipativity from birth-death order

The motivation for our study of dissipativity is to generalize our local analysis of biomolecular system dynamics using birth-death orders to regional and global analysis. Therefore, we would like to characterize a condition for a system's dissipativity determined by the birth-death order.

To do so, let us first inspect how to relate reaction orders to in the dissipation inequality in Eq (5.30). We see that the dissipation inequality condition is expressed in terms of variable $\overline{y} = \frac{y}{y'}$, instead of state x. Since reaction orders are log derivatives with respect to x, we would like to establish a clear relationship between x and the variable z defined as $z = \log \overline{y} = \log \frac{h(x)}{h(x')}$, with x' and u' held fixed.

Lemma 5.2.7 (x and z)**.** *For fixed $x', u' > 0$, define $z = \log \overline{y} = \log \frac{h(x)}{h(x')}$ for $x > 0$, where h is positive, continuously differentiable, and strictly increasing. Then x can be expressed as $x = h^{-1}(e^z h(x'))$, and x strictly increases in z.*

Proof. The expression for x in terms of z is easily derived by $x = h^{-1}(y) = h^{-1}(\overline{y} h(x')) = h^{-1}(e^z h(x'))$. To see x strictly increases in z, we apply inverse function theorem to have $\frac{d}{dz} h^{-1}(e^z h(x')) = (h'(h^{-1}(e^z h(x'))))^{-1}$, where h' denote the derivative of h. Since h is strictly increasing, $h' > 0$ always, so its reciprocal is positive always. □

So for fixed (x', u'), $x \in \mathbb{R}_{>0}$ and $z \in \mathbb{R}$ are strictly increasing re-parameterizations of each other. We can view this as defining $x = x(z)$ as a strictly increasing function of z, with $x(0) = x'$. We can also view this as defining a function $z = z(x)$ strictly increasing in x with $z(x') = 0$.

Now, with this variable z, we can express the dissipation inequality in Eq (5.30) in the following equivalent form

$$\text{Eq (5.30) hold at } x > 0 \quad \Longleftrightarrow \quad z(x)\varphi(z(x)) \leq z(x), \tag{5.34}$$

where $\varphi(z)$ is short hand for $\varphi(z; u', \varepsilon)$ defined by

$$\varphi(z; u', \varepsilon) = (u')^\sigma \frac{f^+(x(z))}{f^-(x(z))} e^{\varepsilon z}, \tag{5.35}$$

where $\sigma = +1$ for control in production and $\sigma = -1$ for control in degradation. We show that inequality of the form in Eq 5.34 has a sufficient condition from log derivative properties in the following lemma, paving the way to connect dissipation inequality with birth-death orders.

Lemma 5.2.8. *If $\varphi : \mathbb{R} \to \mathbb{R}_{>0}$ satisfies $\varphi(0) = 1$ and is continuously differentiable, then*

$$\frac{d \log \varphi(z)}{dz} \leq 0, \forall z \in \mathbb{R} \qquad \Longrightarrow \qquad z\varphi(z) \leq z, \forall z \in \mathbb{R}.$$

Proof. For inequality $z\varphi(z) \leq z$ to hold for all $z \in \mathbb{R}$, it is equivalent to $\varphi(z) \geq 1$ for $z < 0$, $\varphi(z) \leq 1$ for $z > 0$. A sufficient condition for this is that $\varphi(z)$ is monotonically decreasing for all $z \in \mathbb{R}$. Since $\log$ is a monotonically increasing function, that $\varphi(z)$ is monotonically decreasing is equivalent to the derivative of $\log \varphi(z)$ being non-positive, i.e. $\frac{d \log \varphi(z)}{dz} \leq 0$. □

Note that one important assumption in this lemma is that $\varphi(0) = 1$. This is valid for φ if the reference point x' we are interested in is in an interval $\mathcal{X}$ that the system is dissipative. From Proposition 5.2.6, if the dissipation inequality is satisfied at x', then the φ function has the property $\varphi(0) = (u')^\sigma \frac{f^+(x')}{f^-(x')} = 1$. However, if we are interested in reference points x' outside of a dissipative region, then this does not hold. We will see later (Proposition 5.2.12) that we can also characterize dissipativity in that case.

With the sufficient condition from Lemma 5.2.8 in mind, we want to relate derivative of $\log \varphi(z)$ to birth-death orders. Recall from Definition 5.1.1 that the production and degradation orders are $H^\pm := \frac{d \log f^\pm(x)}{d \log x}$, and the birth-death order is $H = H^+ - H^-$. We define the *output order* as $H^o := \frac{d \log h(x)}{d \log x}$. We have the following lemma relating derivative of $\log \varphi$ to the birth-death order.

Lemma 5.2.9. *Given fixed $x', u' > 0$, and function $\varphi(z) = (u')^\sigma \frac{f^+(x(z))}{f^-(x(z))} e^{\varepsilon z}$, $\sigma \in \{+1, -1\}$. We have*

$$\frac{d \log \varphi(z)}{dz} = \eta(x(z)) + \varepsilon, \tag{5.36}$$

where η is defined in terms of the birth-death order and the output order:

$$\eta(x) = \left(\frac{d \log f^+(x)}{d \log x} - \frac{d \log f^-(x)}{d \log x} \right) \left(\frac{d \log h(x)}{d \log x} \right)^{-1} =: \frac{H^+ - H^-}{H^o} = \frac{H}{H^o}, \tag{5.37}$$

where x is used as shorthand for $x(z)$.

Proof. We calculate by chain rule

$$\begin{aligned}\frac{d\log\varphi(z)}{dz} =& \frac{d\sigma\log u'}{dz} + \frac{d\log f^+(x(z))}{dz} - \frac{d\log f^-(x(z))}{dz} + \frac{d\varepsilon z}{dz}\\ =& \varepsilon + \frac{d\log x(z)}{dz}\left(\frac{d\log f^+}{d\log x}(x(z)) - \frac{d\log f^-}{d\log x}(x(z))\right).\end{aligned}$$

Recall that $x(z) = h^{-1}(y(z)) = h^{-1}(e^z h(x'))$. We note a few useful facts. If we denote h' as the derivative of function h, then $(h^{-1})'(y) = \frac{1}{h'(x)}$ where $x = h^{-1}(y)$. Also, the derivative of y with respect to z is just y itself: $\frac{dy(z)}{dz} = \frac{de^z h(x')}{dz} = e^z h(x') = y(z)$. Lastly, log derivative and derivative are related by $\frac{d\log h(x)}{d\log x} = \frac{h(x)}{x}\frac{dh(x)}{dx} = \frac{y}{x}\frac{dh(x)}{dx}$. Equipped with these facts, we calculate

$$\frac{d\log x(z)}{dz} = \frac{1}{x}\frac{dh^{-1}(y(z))}{dz} = \frac{1}{x}\left(\frac{dh(x)}{dx}\right)^{-1}\frac{dy(z)}{dz} = \frac{y}{x}\left(\frac{dh(x)}{dx}\right)^{-1} = \left(\frac{d\log h(x)}{d\log x}\right)^{-1},$$

where we omitted explicit dependence of x and y on z when not necessary. □

Put these two lemma together, we obtain a sufficient point-wise condition for the dissipation inequality to be satisfied based on birth-death order. For a scalar birth-death control affine system (Definition 5.2.2), if the dissipation inequality (Eq (5.30)) is satisfied at some reference point x', then for any point x, point $x > 0$ if

$$\eta(x) \leq -\varepsilon. \tag{5.38}$$

This concludes our effort in translating the dissipation inequality characterizing dissipativity into conditions on reaction orders in the scalar case. The point-wise condition is based on function $\eta(x)$, which is in turn calculated from birth-death orders. This allows us to find regions where we have some dissipativity condition satisfied. For these regions, we can then use dissipative conditions to constrain the system's dynamics on them. This is what we study next.

Dissipative regions and regional stability and multistability

We have formulated a nice point-wise sufficient condition for a point x to satisfy dissipation inequality with respect to supply rate $s(\varepsilon)$ in terms of a function η based on birth-death orders. This condition can then define dissipative regions that we can say something about a system's dynamics in them.

Definition 5.2.10 (Dissipative region)**.** Given a scalar birth-death system with control in either production or degradation (Definition 5.2.2), let η be given by (5.37). For $\varepsilon > 0$, the **ε-dissipative region** of this system is the set $\mathcal{X}_\varepsilon = \{x : \eta(x) \leq -\varepsilon\}$.

Remark 5.2.11. It should be noted that $\eta(x) \leq -\varepsilon$, the condition used to define the dissipative regions $\mathcal{X}_\varepsilon$, is independent of x' and only depends on x. This is rather surprising as the dissipation inequality depends on both x and x'. The reason x' dependence disappears is that the condition $\eta(x) \leq -\varepsilon$ is a sufficient condition for the dissipation inequality (5.30) using Lemma 5.2.8, involving log derivatives. Factors involving u' and x' disappears in log derivatives because log derivatives only depend on fold change, not exact magnitude. Again, the intuition is that the log derivative of $f(x) = kx^\alpha$ with respect to x yields α, independent of k. This property allows us to characterize dissipative regions without knowing what reference points we want to study. For example, instead of fixing all the parameters in a system, calculate the fixed point, and then ask whether this fixed point is stable; we can characterize dissipative regions without knowing any of the parameters, and specify under what conditions will a fixed point exist in a dissipative region, therefore stable. This mindset naturally integrates system design with system analysis. △

So the dissipative region $\mathcal{X}_\varepsilon$ is defined independent of reference points (x', u'). But the definition of dissipativity depends on (x', u'). The natural next question to characterize system dissipativity then is, if we take $s(\varepsilon)$ as the supply rate, an open interval $(x_{\min}, x_{\max})$ contained in $\mathcal{X}_\varepsilon$ as the state region, then what are the reference points (x', u') that are *admissible*? Recall that a reference point is admissible if the system can be dissipative with this reference point while holding the supply rate and state region fixed as chosen. One admissible case we are already familiar with from Proposition 5.2.6 is that (x', u') satisfies $x' \in \mathcal{X}_\varepsilon$ and $\varphi(0, u') = 1$, with the latter condition equivalent to x' is a fixed point for constant input $u \equiv u'$. In this case, the system is dissipative with respect to $s(\varepsilon)$ at (x', u') in any open interval subset of $\mathcal{X}_\varepsilon$ that contains x'. We make this formal in the following proposition and include other cases. It turns out, the admissible reference points (x', u') for state region that is an open interval in $\mathcal{X}_\varepsilon$ can have x' outside of the state region. This is because $\mathcal{X}_\varepsilon$ is defined via the the sufficient condition from Lemma 5.2.8 which yield monotonicity.

Proposition 5.2.12 (Dissipativity in a region)**.** *Given a scalar birth-death control affine system (Definition 5.2.2) with ε-dissipative region $\mathcal{X}_\varepsilon$. Fix $s(\overline{u}, \overline{y}; \varepsilon)$ as the supply rate, and an open interval $(x_{\min}, x_{\max})$ subset of $\mathcal{X}_\varepsilon$ as the state region. Take $\varphi(z; u', \varepsilon)$ as the function defined in Eq (5.35). A reference point (x', u') is **admissible**, i.e. the system is dissipative in the state region $(x_{\min}, x_{\max})$ with the fixed supply rate $s(\varepsilon)$ and this reference point, if (x', u') satisfies one of the following*

conditions.

$$\begin{cases} x' \in (x_{\min}, x_{\max}), & \varphi(z(x'); u', \varepsilon) = \varphi(0; u') = 1; \\ x' \geq x_{\max}, & \varphi(z(x_{\max}); u', \varepsilon) \geq 1; \\ x' \leq x_{\min}, & \varphi(z(x_{\min}); u', \varepsilon) \leq 1. \end{cases} \tag{5.39}$$

Proof. We consider $\sigma = +1$, the control in production case, as control in degradation is entirely analogous.

For $x' \in (x_{\min}, x_{\max})$, as shown in Proposition 5.2.6, it is necessary to choose $u' = \frac{f^+(x')}{f^-(x')}$ to satisfy dissipation inequality (Eq (5.30)). For this choice of u', we know $\varphi(z) = u' \frac{f^+(x(z))}{f^-(x(z))} e^{\varepsilon z}$ satisfies $\varphi(0) = 1$, so it satisfies the assumptions of Lemma 5.2.8. Therefore $\partial_z \log \varphi(z) \leq 0$ is a sufficient condition for the dissipation inequality in Eq (5.30). Now $\partial_z \log \varphi(z) \leq 0$ is equivalent to $\eta(x) \leq -\varepsilon$, satisfied in $\mathcal{X}_\varepsilon$.

Now we consider $x' \geq x_{\max}$. Since h is strictly increasing, $h(x') > h(x_{\max})$, so $\log \overline{y} < 0$. So we can cancel $\log \overline{y} < 0$ on both sides of dissipation inequality (5.30) to arrive at an equivalent condition, $\frac{f^+(x)}{f^-(x)} \left(\frac{h(x)}{h(x')} \right)^{\varepsilon} u' \geq 1$. This is equivalent to $\varphi(z(x)) \geq 1$ in terms of the variable z. For any $x \in (x_{\min}, x_{\max})$, we have $\eta(x) \leq -\varepsilon < 0$, i.e. $\partial_z \log \varphi(z) \leq 0$, so φ is decreasing in z in this interval, which also means it is decreasing in x in this interval (Lemma 5.2.7). Therefore an equivalent condition for $\varphi(z(x)) \geq 1$ for all $x \in (x_{\min}, x_{\max})$ is that $\varphi(z(x_{\max})) \geq 1$.

The case for $x' \leq x_{\min}$ is similar. □

From this proposition, we see that once we find the dissipative region $\mathcal{X}_\varepsilon$ of a system and choose an interval in it as the state region, there are many admissible reference points (x', u') that the system is dissipative to. These reference points separates into two cases by x' is in the dissipative region or not. This in turn dictates different dynamic behaviors in the state region when the input is constant $u \equiv u'$. As we show below, if x' is in the dissipative region, then the storage function certifies the stability of x' in an interval. If x' is outside of the dissipative region, then the storage function certifies the system will evolve out of the dissipative region towards x'.

Proposition 5.2.13 (Dynamics from dissipative region)**.** *For a scalar birth-death control affine system with ε-dissipative region $\mathcal{X}_\varepsilon$ with $\varepsilon > 0$, for any open interval $(x_{\min}, x_{\max}) \subset \mathcal{X}_\varepsilon$, the following are true. Take function $\varphi(z; u', \varepsilon)$ defined in Eq 5.35.*

1. *For (x', u') satisfying $x' \in (x_{\min}, x_{\max})$ and $\varphi(0; u', \varepsilon) = 1$, for constant input $u \equiv u'$, any trajectory starting in $(x_{\min}, x_{\max})$ asymptotically converges to x'.*

2. *For (x', u') satisfying $x' \geq x_{\max}$ and $\varphi(z(x_{\max}); u', \varepsilon) \geq 1$, for constant input $u \equiv u'$, any trajectory starting in $(x_{\min}, x_{\max})$ will leave $\mathcal{X}$ through $x_{\max}$ in finite time.*
3. *For (x', u') satisfying $x' \leq x_{\min}$ and $\varphi(z(x_{\min}; u') \leq 1$, for constant input $u \equiv u'$, any trajectory starting in $(x_{\min}, x_{\max})$ will leave $\mathcal{X}$ through $x_{\min}$ in finite time.*

Proof. By Proposition 5.2.12, dissipation inequality Eq 5.30 is satisfied for all $x \in (x_{\min}, x_{\max})$ with these reference points (x', u'). So there exists a virtual storage function $V(x; x')$ such that $\frac{d}{dt}V(x(t), x') \leq s(\overline{u}, \overline{y}; \varepsilon) \leq 0$ for all $x \in (x_{\min}, x_{\max})$ and $u > 0$. This implies different dynamics for each case.

For case 1, since x' is in the state region, by Proposition 5.2.6, the virtual storage function V is a storage function, i.e. globally non-negative with $V(x; x') = 0$ only when $x = x'$. If the current state $x(t)$ of the system is inside $(x_{\min}, x_{\max})$, then V will decrease over time converging to the unique lower bound at x'. Indeed, $\frac{d}{dt}V(x(t), x') \leq s(1, \overline{y}; \varepsilon) \leq 0$, with the equality achieved only when $x = x'$ for both inequalities, since h is invertible.

For case 2, $x' \geq x_{\max}$, then $V(x; x')$ is still be defined for $x \in (x_{\min}, x_{\max})$, but it involves complications. By definition, $V(x'; x') = 0$, but since x' may not be connected to the state region $(x_{\min}, x_{\max})$, we cannot find the value of $V(x; x')$ by integrating from $x = x'$. On the other hand, since $\overline{y} < 1$ for all $x \in (x_{\min}, x_{\max})$ because h is strictly increasing, by inequality (5.31), we know $\partial_x V(x; x') < 0$ for $x \in (x_{\min}, x_{\max})$. So starting from $x_{\max}$, we can find values of $V(x; x')$ for all $x \in (x_{\min}, x_{\max})$ by integrating, which implies $V(x; x') > V(x_{\max}; x')$ for all $x \in (x_{\min}, x_{\max})$. Therefore, V decreases over time on the interval $(x_{\min}, x_{\max})$ means the state trajectory goes toward $x_{\max}$. Indeed, for constant input $u \equiv u'$, we have $\frac{d}{dt}V(x(t); x') \leq s(1, \overline{y}; \varepsilon) \leq s(1, \frac{h(x_{\max})}{h(x')}; \varepsilon) < 0$. This implies any trajectory $x(t)$ starting in $(x_{\min}, x_{\max})$ will go toward $x_{\max}$. Furthermore, $(x(t), x_{\max})$ is compact and $\frac{d}{dt}V$ is bounded away from zero with a margin, so $x(t)$ will reach and go beyond $x_{\max}$ in finite time. The case for $x' \leq x_{\min}$ is similar. □

In summary, this dissipative analysis framework based on birth-death orders describes all dynamic behaviors a system can have in terms of two things, the ε-dissipative region and admissible reference points. Given a scalar birth death system, we have split all parameters' effect on system dynamics into two parts. One part is parameters' influence on the topology of ε-dissipative regions $\mathcal{X}_\varepsilon$. The number of connected components could change, varying from mono-stability to multi-stability. The other part is parameters' influence on admissible reference points (x', u'), so that dissipativity certify stability of x' in $\mathcal{X}_\varepsilon$ or certify finite time escape from $\mathcal{X}_\varepsilon$ towards x' outside of $\mathcal{X}_\varepsilon$. Let us see how this plays out in a few examples.

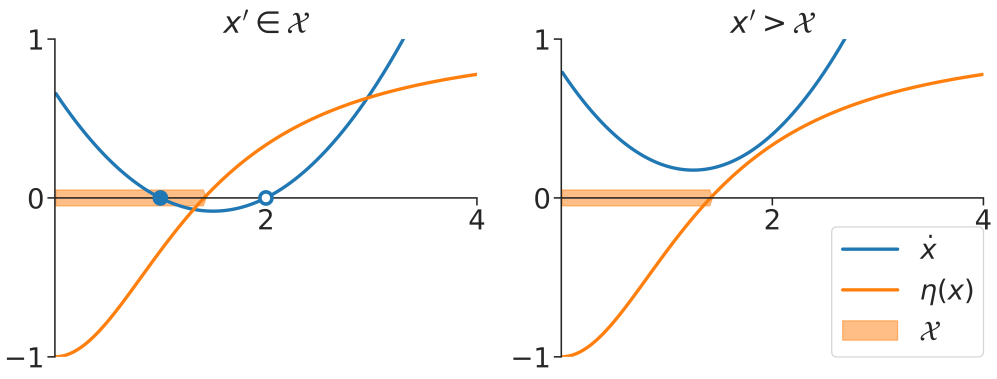

Figure 5.5 Plot for Example 15. $\dot{x} = f^+(x)u' - f^-(x)$ (blue) is the time derivative of this control in production system. $\eta(x)$ (orange) is based on birth-death order, which determines the dissipative region $\mathcal{X} = \{x : \eta(x) < 0\}$ (orange region) for infinitesimal dissipativity, i.e. $\varepsilon \to 0^+$. Solid blue circle indicates stable fixed point. Empty blue circle indicates unstable fixed point. **(Left)** The case when the reference point (x', u') satisfy $x' \in \mathcal{X}$, so dissipativity certifies stability of x' in $\mathcal{X}$. **(Left)** The case when the reference point (x', u') satisfy $x' > \mathcal{X}$, so dissipativity certifies system trajectory will leave $\mathcal{X}$ in finite time. Parameters are $\gamma = 1, \alpha = 2$, and $u' = 1/3$ for left, and $u' = 0.4$ for right.

Example 15 (two fixed points, one stable)**.** We consider a scalar birth-death system with control in production $\dot{x} = (\alpha + x^2)u - \gamma x$, $h(x) = x$, with constant coefficients $\alpha, \gamma > 0$. Here $f^-(x) = -\gamma x$ and $f^+(x) = \alpha + x^2$. See Figure 5.5 for graphical illustration of this system and the following analysis.

Let us first inspect the dissipative regions determined by birth-death orders. The production, degradation, and output orders are $H^+(x) = 2\frac{x^2}{\alpha+x^2} \in (0, 2)$ increasing in x, and $H^- = H^o = 1$. Therefore $\eta(x) = H^+(x) - 1 \in (-1, 1)$, increasing in x. So without any further analysis, we know the ε-dissipative region $\mathcal{X}_\varepsilon$ for $\varepsilon \in (0, 1)$ will be an open interval around small x. Indeed, the condition $\eta(x) \leq -\epsilon$ defining ε-dissipative region then is $x^2 \leq \frac{1-\varepsilon}{1+\varepsilon}\alpha$, so we have $\mathcal{X}_\varepsilon = (0, \sqrt{\frac{1-\varepsilon}{1+\varepsilon}\alpha})$. We see that the topology of $\mathcal{X}_\varepsilon$ does not change with respect to parameters. It is always an open interval. Let us consider the limit $\varepsilon \to 0$ corresponding to supply rate with infinitesimally small $\varepsilon > 0$. Then the corresponding dissipative region, which is also our choice of the state region for dissipativity, is $\mathcal{X} = (0, \sqrt{\alpha})$.

Now we find admissible reference points. For (x', u') such that $x' \in \mathcal{X}$ and $\varphi(0, u') = u'\frac{f^+(x')}{f^-(x')} = u'\frac{\alpha+(x')^2}{\gamma x'} = 1$, i.e. $u' = \frac{\gamma x'}{\alpha+(x')^2}$, our theory states that for constant input $u \equiv u'$, the point x' is stable in the interval $\mathcal{X}$. The expression of u' in terms of x' increases in x', so in order for x' to be in $\mathcal{X}$, i.e. $x' < \sqrt{\alpha}$, we need $u' < \frac{\gamma}{2\sqrt{\alpha}}$. Another we to see this is by solving x' in terms of u', which has real solution if $u' < \frac{\gamma}{2\sqrt{\alpha}}$, and the solution is $x'_\pm(u') = \frac{1}{2}\left(\frac{\gamma}{u'} \pm \sqrt{(\frac{\gamma}{u'})^2 - 4\alpha}\right)$, with $x'_- < \sqrt{\alpha}$ always. So we can view in this both ways, either we begin with x' in $\mathcal{X}$ and find admissible $u'(x')$ satisfy $u'(x') < \frac{\gamma}{2\sqrt{\alpha}}$, or we begin with $u' < \frac{\gamma}{2\sqrt{\alpha}}$ and find $x'_-(u') \in \mathcal{X}$ is admissible. The conclusion is the same, x' is a stable

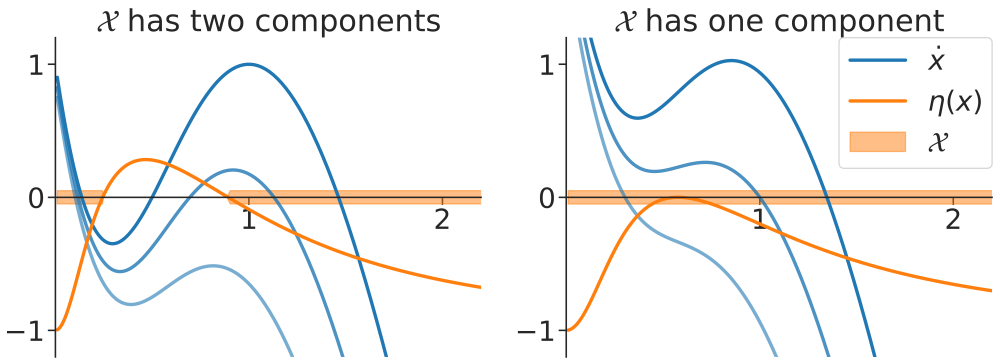

Figure 5.6 Plot for Example 16. $\dot{x} = f^+(x)u' - f^-(x)$ (blue) is the time derivative of this control in production system for constant input $u \equiv u'$. Curves with lighter blue color corresponds to $\dot{x}$ with smaller u'. $\eta(x)$ (orange) is based on birth-death order, which determines the dissipative region $\mathcal{X} = \{x : \eta(x) < 0\}$ (orange region) for infinitesimal dissipativity, i.e. $\varepsilon \to 0^+$. **(Left)** The case when α is small, so $\mathcal{X}$ has two connected components. **(Right)** The case when α is large, so $\mathcal{X}$ has one connected component. Parameters are $\alpha = 0.05$, $\gamma = 10$, $u' \in \{20, 18.5, 17\}$ for left, and $\alpha = 0.125$, $\gamma = 10$, $u' \in \{17.5, 16, 14.5\}$ for right.

fixed point in $\mathcal{X}$ for constant input $u \equiv u'$ with a storage function certifying this. We see that varying parameters α and γ change the location of reference point (x', u') and the length of state region $\mathcal{X}$, but not the qualitative behavior.

For (x', u') with $x' \geq x_{\max} = \sqrt{\alpha}$ and $\varphi(z(x_{\max}); u', \varepsilon = 0) \geq 1$, our theory states that for constant input $u \equiv u'$, any trajectory starting in $\mathcal{X} = (0, \sqrt{\alpha})$ would leave through its upper limit $\sqrt{\alpha}$. The condition for u' to be admissible in this case is $u' \geq \frac{\gamma}{2\sqrt{\alpha}}$. This corresponds to there being no fixed point.

So we see that admissible reference points (x', u') for state region $\mathcal{X} = (0, \sqrt{\alpha})$ has two cases. (1) $x' < \sqrt{\alpha}$ is a stable fixed point for constant input $u \equiv u'$ satisfying $u' < \frac{\gamma}{2\sqrt{\alpha}}$. (2) $u' > \frac{\gamma}{2\sqrt{\alpha}}$ is too large so the system has no fixed point, and reference point $x' \geq \sqrt{\alpha}$ can be used to capture that system trajectory would leave the dissipative region $\mathcal{X} = (0, \sqrt{\alpha})$ from $\sqrt{\alpha}$ in finite time. △

Example 16 (bistable). Consider $\dot{x} = f^+(x)u - f^-(x) = \left(\alpha + \frac{x^2}{1+x^2}\right)u - \gamma x$, a scalar birth-death system with control in production, and use $h(x) = x$, where $\gamma, \alpha > 0$ are positive coefficients. See Figure 5.6 for a graphical illustration of this system and the analysis below.

The birth-death orders are $H^- = H^o = 1$, while

$$H^+(x) = 2\left(\frac{\frac{x^2}{1+x^2}}{\alpha + \frac{x^2}{1+x^2}}\right)\left(\frac{1}{1+x^2}\right) \in (0, 2),$$

increasing in x and then decreasing in x. So $\eta(x) = H^+(x) - 1 \in (-1, 1)$, first increasing in x then decreasing in x. Let $\mathcal{X} := \{x : \eta(x) < 0\}$ be the dissipative region for infinitesimal

$\varepsilon \to 0^+$. Then $\mathcal{X}$ has two cases. When α is small $\alpha \ll 1$, then as x increases, $\eta(x)$ begins at -1, increases to a positive value, then decreases back to -1. So $\mathcal{X}$ has two disconnected regions. When α is large, then $\eta(x)$ never reach above 0, so $\mathcal{X}$ is the whole positive line. In the small α case, there can be two stable fixed points, one in each of the two connected components of dissipative region $\mathcal{X}$. In the large α case, there is only one fixed point that is globally stable. All these conclusions are automatically certified with a storage function by integration from Eq (5.31).

In the large α case, $\mathcal{X}$ is the full positive real line, and therefore any reference point is a globally stable fixed point. This excludes the possibility of multiple fixed points. In the small α case, $\mathcal{X}$ has two components, so if there are two possible reference points x_1' and x_2' for the same u', each in one of the component of $\mathcal{X}$, then we have bistability, and each fixed point has a storage function certifying its regional stability. However, it is still possible that there is only one fixed point. For example, see the left of Figure 5.6 for $\dot{x}$ with the lightest blue color, corresponding to smaller u'. In this case we see although $\mathcal{X}$ has the same two components (this is independent of u'), the system has shifted from bistability to monostability, and dissipativity in $\mathcal{X}$ certifies the fixed point x' is stable in the left component, and trajectories in the right component will go toward left direction. But the certificate from the storage function is not guaranteed to be valid in the middle segment not covered by $\mathcal{X}$. This is the sacrifice we made by taking a sufficient condition for dissipativity based on monotonicity and birth-death orders. So our approach has the advantage that $\eta(x)$ is easy to obtain, does not depend on all parameters (only α here), and give strong constraints on system behavior in the dissipative region $\mathcal{X}_\varepsilon$. But the behaviors close to the intersection of parameter regimes could be too complicated to be fully captured by the dissipative region, such as the middle segment not included in $\mathcal{X}$ for the case with small α but adjusting u' transitions between mono- and bi-stability. This trading exactness for robustness and simplicity or tractability is a common theme of analysis based on reaction orders. △

System from self-connection

So far when we want to study the dynamical properties such as stability of a system using dissipative control, we take the control input to be constant $u \equiv u'$ to make it a closed system. An alternative way is to take a control system and connect its output y with its input u to obtain a closed system. This works as a prelude to general interconnections.

For scalar systems $\dot{x} = f(x)+g(x)u, y = h(x)$, we could have **self-connection** $\log u = M \log y$ where $M \in \mathbb{R}$, resulting in closed loop system $\dot{x} = f(x) + g(x)h(x)^M$. With connection, a

major difference is that the interpretation of u is different. Previously, we consider u as an external input to be specified. Now, by self-connection, we have a particular specification that $u = y^M = h(x)^M$. So, conditions on (x', u') pairs now become conditions on $(x', h(x')^M)$, so a condition solely on x'.

If $V(x; x')$ is a virtual storage function with respect to supply rate $s(\overline{u}, \overline{y}; \varepsilon, p)$, then (5.20) holds for all $u > 0$. By substitution $\overline{u} \leftarrow \overline{y}^M$ and that h is strictly increasing, for all $u > 0$ means for all $y > 0$ or for all $x > 0$, so we have the following as the dissipation inequality in this case.

$$\frac{d}{dt}V \leq s(\overline{y}^M, \overline{y}; \varepsilon, p) = p(\overline{y})(\overline{y}^M - \overline{y}^\varepsilon)\log \overline{y} \quad \forall x > 0. \tag{5.40}$$

If $V(x; x')$ is a storage function with zero only when $x = x'$ and if $\frac{d}{dt}V = p(\overline{y})(\overline{y}^M - \overline{y}^\varepsilon)\log \overline{y} \leq 0$ for all $x > 0$ with zero only when $x = x'$, then $V(x; x')$ is a Lyapunov function for the closed-loop system $\dot{x} = f(x) + g(x)h(x)^M$. A sufficient condition for $\frac{d}{dt}V \leq 0$ is $\varepsilon \geq M$, although this may not be necessary since $\overline{y}$ could be bounded below 1, for example.

Therefore we could conclude that, given an open interval $\mathcal{X} \subset \mathcal{X}_\varepsilon$, $\varepsilon \geq M$, and an admissible reference point x' such that $(x', u' = h(x')^M)$, i.e. satisfies conditions of Proposition 5.2.13, the corresponding conclusions on system dynamics in $\mathcal{X}$ hold.

Example 17 (two fixed points, one stable, by self-connection)**.** Consider scalar birth-death control affine system $\dot{x} = f^+(x)u - f^-(x) = u - \gamma x$, where $\gamma > 0$ is a parameter. We consider output $y = h(x) = \alpha + x^2$, with $\alpha > 0$ a parameter, and self-connection $M = 1$ so that $u = y$. Then the resulting closed system is $\dot{x} = (\alpha + x^2)u - \gamma x$, exactly the same as the system studied in Example 15.

The birth-death orders of the open system are $H^+ = 0$, $H^- = 1$, and $H^o = 2\frac{x^2}{\alpha + x^2}$. So $\eta(x) = \frac{-1}{H^o} = -\frac{1}{2}(\frac{\alpha}{x^2} - 1)$. We take the smallest ε needed to guarantee stability, i.e. $\varepsilon = M = 1$, and find $\eta(x) \leq -M$ when $\frac{\alpha}{x^2} \leq 1$. So again we obtain the stable region $\mathcal{X} = [0, \sqrt{\alpha})$, same as in Example 15. However, it should be noted that the interpretation of this result is different from that in Example 15. The result here certifies that if there exists $x' > 0$ s.t. $\alpha + x'^2 - \gamma x' = 0$, and x' is in $[0, \sqrt{\alpha})$, then x' is stable in this region. The solution to $\alpha + x'^2 - \gamma x'$ is $x'_\pm = \frac{\gamma}{2} \pm \sqrt{(\frac{\gamma}{2})^2 - \alpha}$ if $(\frac{\gamma}{2})^2 - \alpha > 0$. x'_- is always in $[0, \sqrt{\alpha})$. Note that there is no u' involved here, in contrast with Example 15. △

We can also use self-connection as a tool to come back and inspect our assumption that h is increasing in x in the definition of scalar birth-death control affine systems. The following example illustrates what might go wrong if we use h that is decreasing in x instead of increasing.

Example 18 (self-inhibition)**.** Consider the closed-loop system $\dot{x} = \frac{1}{1+x} - x$. We can analyze stability of this system using our techniques by imagining we obtain this system from suitable self-connection of an open-loop system. Here are three such possibilities:

1. If $g(x) = 1/(1+x)$, $f(x) = -x$, $h(x) = x$, and $u \equiv 1$ ($M = 0$), then $\eta(x) = -\frac{x}{1+x} - 1$. Therefore $\eta(x) < -1 < -M = 0$ for all x, which says the fixed point is globally stable.
2. If we write $\dot{x} = u - x$, $y = 1/(1+x)$, so that the system is formed by closed loop $u = y$ ($M = 1$), we see that $\eta(x) = 1 + x^{-1}$. For self-connection we need $\eta(x) < -M$, but we see this is impossible.
3. If instead we choose $\dot{x} = u - x$, $y = 1 + x$, and self-connection $u = 1/y$ (i.e. $M = -1$), then $\eta(x) = -\frac{x}{1+x}$ and the condition is $\eta(x) < -M = 1$, which is the same as the condition without using self-connection.

This example highlights the need to choose $y = h(x)$ s.t. its monotonicity is in the right direction. Often, we should choose h to be strictly increasing in x. △

To better understand how dissipativity based on birth-death orders encoded in function $\eta(x)$ capture dynamics of the system, let us relate η to necessary and sufficient conditions of local stability in the scalar case.

Example 19 (1d local stability)**.** Consider control in production (control in degradation is similar), i.e. $\dot{x} = f^+(x)u - f^-(x)$, $y = h(x)$, where $f^{\pm}(x), h(x) > 0$ for all x and $h : \mathbb{R}_{>0} \to \mathbb{R}_{>0}$ is strictly monotonically increasing in x. Consider self-connection $u = y^M$, so the closed loop system is $\dot{x} = f^+(x)h(x)^M - f^-(x)$. Then at a fixed point x' we have $f^+(x')h(x')^M = f^-(x') := R$. Since this is a scalar system, x' is stable iff $\frac{\partial f^+ h^M}{\partial x}(x') - \frac{\partial f^-}{\partial x}(x') < 0$. Log derivative and derivative are related by $\frac{\partial \log f^-}{\partial \log x}(x') = \frac{\partial f^-}{\partial x}(x')\frac{x'}{f^-(x')} = \frac{\partial f^-}{\partial x}(x')\tau$, where $\tau := \frac{x'}{R} > 0$. Therefore, x' is a stable fixed point iff $\frac{\partial \log f^+ h^M}{\partial \log x}(x') - \frac{\partial \log f^-}{\partial \log x}(x') < 0$. This condition is equivalent to $\frac{\partial \log f^+ h^M / f^-}{\partial \log x} = \frac{\partial \log f^+}{\partial \log x} + M\frac{\partial \log h}{\partial \log x} - \frac{\partial \log f^-}{\partial \log x} < 0$. Since h is strictly increasing, its log derivative is positive. Multiplying both sides by $\left(\frac{\partial \log h}{\partial \log x}(x')\right)^{-1}$, we obtain that the condition is equivalent to $\left(\frac{\partial \log f^+}{\partial \log x}(x') - \frac{\partial \log f^-}{\partial \log x}(x')\right)\left(\frac{\partial \log h}{\partial \log x}(x')\right)^{-1} < -M$. This is exactly the condition $\eta(x') < -M$. So we see for a scalar birth death control system, the condition based on $\eta(x')$ is a necessary and sufficient condition for x' to be locally stable. △

This example highlights that η can be considered both as a function of x' and a function of x. As a function of x', it dictates whether the system is dissipative at x'. As a function of

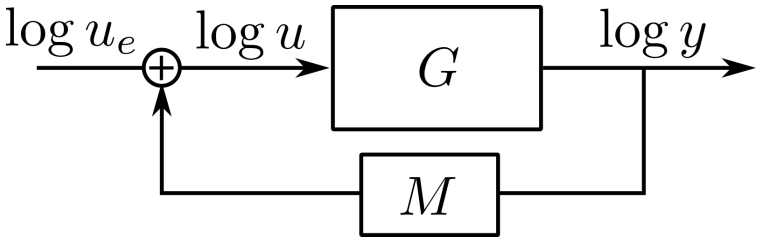

Figure 5.7 Feedback diagram for multiplicative self-connection of a scalar system. G represents the input-output scalar system, M is the feedback gain. Variables are all in log scale, so that the interconnections are multiplicative.

x, it dictates whether a trajectory starting at $x(0) = x$ will decrease according to a storage function. This is exactly our two ways of using the dissipative region to capture system dynamics in Proposition 5.2.13. If x' is inside the dissipative region, then we are treating η as a function of x'. If x is outside the dissipative region, then we are treating η as a function of $x(0)$ inside the region.

Self-connection as static feedback

We can also view self-connection as feedback interconnection for control systems (Figure 5.7). The output y is fed-back to the input u of the system, so that the new external input is now u_e and the input into the scalar control system are related by $\log u = \log u_e + M \log y$. From this perspective, the feedback interconnection creates a new input-output system from the original one, and the new system may have better dissipative properties.

The dissipation inequality for the new system becomes

$$\frac{d}{dt}V \leq s(\overline{u}_e\overline{y}^M, \overline{y}; \varepsilon, p) = p(\overline{y})(\overline{u}_e\overline{y}^M - \overline{y}^\varepsilon)\log\overline{y}, \quad \forall u_e > 0. \tag{5.41}$$

Since the positive faction $p(\overline{y})$ in front does not influence the dissipativity condition for existence of a storage function, we can factor out $\overline{y}^M$ to obtain

$$\frac{d}{dt}V \leq p(\overline{y})(\overline{u}_e - \overline{y}^{\varepsilon - M})\log\overline{y}.$$

So any ε-dissipativity condition of the original system G translates into $(\varepsilon - M)$-dissipativity condition of the system with feedback. In terms of how feedback influence input-output behavior, we see positive feedback ($M > 0$) reduces dissipativity (smaller ε), while negative feedback ($M < 0$) increases dissipativity (larger ε). This has direct parallel with positive and negative feedback for linear systems, where it is well known that negative feedback flattens the slope, which often stabilizes system dynamics, while positive feedback sharpens the slope, which open amplifies and destabilizes system dynamics.

5.3 Multiplicative networks of scalar birth-death systems

Assume we are given n scalar birth-death control affine systems, either control in production of the form $\dot{x}_i = f_i^+(x_i)u_i - f_i^-(x_i)$, or control in degradation of the form $\dot{x}_i = f_i^+(x_i) - f_i^-(x_i)u_i$. Also assume the ith system is dissipative w.r.t $s^{\sigma_i}(\overline{u}_i, \overline{y}_i; \varepsilon_i, p_i)$, where $\sigma_i \in \{+, -\}$, $\varepsilon_i > 0$, p_i is a positive function mapping $\overline{y}_i \mapsto p_i(\overline{y}_i)$. We then consider the multiplicative interconnection of these systems by

$$\log \boldsymbol{u} = \boldsymbol{M} \log \boldsymbol{y}, \tag{5.42}$$

where $\boldsymbol{M} \in \mathbb{R}^{n\times n}$ is the interconnection matrix. This forms a closed loop system:

$$\begin{cases} \dot{x}_i = f_i^+(x_i)\boldsymbol{h}(\boldsymbol{x})^{\boldsymbol{M}_i} - f_i^-(x_i), & \text{if control in production;} \\ \dot{x}_i = f_i^+(x_i) - f_i^-(x_i)\boldsymbol{h}(\boldsymbol{x})^{\boldsymbol{M}_i}, & \text{if control in degradation.} \end{cases} \tag{5.43}$$

Here $\boldsymbol{M}_i$ is the ith row of $\boldsymbol{M}$, and $\boldsymbol{h} : \mathbb{R}^n_{>0} \to \mathbb{R}^n_{>0}$ maps states $\boldsymbol{x}$ to outputs $\boldsymbol{y}$.

Certificates of dissipativity

To certify stability of the interconnected system, we could consider the candidate Lyapunov function $V = \sum_i V_i(x_i; x_i')$, where V_i is the storage function for the ith subsystem, i.e. it is nonnegative and satisfies $\frac{d}{dt}V_i(x_i(t); x_i') \le s^{\sigma_i}(\overline{u}_i, \overline{y}_i; \varepsilon_i, p_i)$.

We want to certify V is a Lyapunov function. The following is a sufficient condition:

$$\frac{d}{dt}V = \sum_i \frac{d}{dt}V_i \le \sum_i \underbrace{p_i(\overline{y}_i)\sigma_i(\overline{\boldsymbol{y}}^{\boldsymbol{M}_i}\log \overline{y}_i - \overline{y}_i^{\sigma_i\varepsilon_i}\log \overline{y}_i)}_{=s^{\sigma_i}(\overline{y}^{\boldsymbol{M}_i}, \overline{y}_i; \varepsilon_i, p_i)} \le 0, \quad \forall \boldsymbol{x}, \tag{5.44}$$

with equality achieved only at $\boldsymbol{x}$ such that $\boldsymbol{y} = \boldsymbol{y}'$. We choose p_i to only depend on $\overline{y}_i$ here to explicitly connect with properties of scalar components. But this can be modified to more flexible or more restrictive functions. See Section 5.4.

Let $z_i = -\sigma_i \log \overline{y}_i$. All $\boldsymbol{x} \in \mathbb{R}^n_{>0}$ does not necessarily maps onto all $\overline{\boldsymbol{y}} \in \mathbb{R}^n_{>0}$ or all $\boldsymbol{z} \in \mathbb{R}^n$, since h_i can be bounded, but we can take this as a sufficient condition. So this sufficient condition for the above inequality is

$$\sum_{i=1}^n p_i\Big(e^{-(\sigma_i z_i)}\Big)(e^{-(\boldsymbol{M}\boldsymbol{\Sigma})_i^\intercal \boldsymbol{z}}z_i - e^{-\varepsilon_i z_i}z_i) \ge 0, \quad \forall \boldsymbol{z} \in \mathbb{R}^n, \tag{5.45}$$

where equality is only achieved at $\boldsymbol{z} = \boldsymbol{0}$. Here $\boldsymbol{\Sigma} = \operatorname{diag}(\sigma_i)$, and we used $\boldsymbol{\Sigma}$'s inverse is $\boldsymbol{\Sigma}$ itself, so $\boldsymbol{z} = -\boldsymbol{\Sigma}\log \overline{\boldsymbol{y}}$ and $\log \overline{\boldsymbol{y}} = -\boldsymbol{\Sigma}\boldsymbol{z}$. We can rewrite the above equation in matrix format:

$$\boldsymbol{z}^\intercal \tilde{\boldsymbol{P}}\Big(e^{-\boldsymbol{M}\boldsymbol{\Sigma}\boldsymbol{z}} - e^{-\boldsymbol{E}\boldsymbol{z}}\Big) \ge 0, \tag{5.46}$$

where $\tilde{\boldsymbol{P}} := \mathrm{diag}(p_i(\exp(-\sigma_i z_i)))$, $\boldsymbol{E} = \mathrm{diag}(\varepsilon_i)$, and exponentials are applied component wise. If we take a factor $e^{\varepsilon_i z_i}$ out of each p_i, then we get

$$\boldsymbol{z}^\intercal \boldsymbol{P}\Big(e^{\boldsymbol{A}\boldsymbol{z}} - \boldsymbol{1}\Big) \geq 0, \quad \boldsymbol{A} := \boldsymbol{E} - \boldsymbol{M}\boldsymbol{\Sigma}, \tag{5.47}$$

where $\boldsymbol{P} = \mathrm{diag}(e^{-\varepsilon_i z_i} p_i(e^{-\sigma_i z_i}))$. Note that each diagonal element P_i of $\boldsymbol{P}$ is no longer the same as the positive prefactor p_i for the supply rate of the ith component system. However, since the dissipativity of each component system is independent of the choice of p_i (see Theorem 5.2.5), the prefactors p_i can always be arbitrarily chosen from the set of positive scalar functions from $\mathbb{R}_{>0}$ to $\mathbb{R}_{>0}$. This is the same for the diagonal elements of $\boldsymbol{P}$, since multiplying $x_i^{-\varepsilon_i}$ leaves the set of positive scalar functions invariant. Therefore, we can treat $\boldsymbol{P}$ as a factor that we can arbitrarily choose in the set of positive diagonal matrix functions. Once chosen, we can map it back to the prefactors p_i used in supply rates and storage functions by considering ε_i and σ_i of each component system.

So, stability of the interconnected system comes down to whether the matrix $\boldsymbol{A}$ satisfies that there exists a positive diagonal matrix function $\boldsymbol{P}(\boldsymbol{z})$ such that the above inequality in Eq (5.47) is satisfied for all $\boldsymbol{z} \in \mathbb{R}^n$. In the following proposition, we define the set of $\boldsymbol{A}$ matrices that satisfy this, and characterize some operations that leave this set invariant.

Proposition 5.3.1. *Let $\mathcal{A}$ denote the following set of matrices:*

$$\mathcal{A} = \Big\{\boldsymbol{A} \in \mathbb{R}^{n\times n} : \exists \boldsymbol{P}(\boldsymbol{z}) \in \mathcal{P},\ s.t.\ \boldsymbol{z}^\intercal \boldsymbol{P}(\boldsymbol{z})(e^{\boldsymbol{A}\boldsymbol{z}} - \boldsymbol{1}) \geq 0,\ \ \forall \boldsymbol{z} \in \mathbb{R}^n\Big\} \tag{5.48}$$

where $\mathcal{P} = \{\mathrm{diag}(P_i(z_i)), P_i : \mathbb{R} \to \mathbb{R}_{>0}\}$ is the set of positive diagonal functions from $\mathbb{R}^n$ to $\mathbb{R}^{n\times n}$. Then $\boldsymbol{A} \in \mathcal{A}$ implies $\boldsymbol{A}\boldsymbol{\Theta} + \boldsymbol{D} \in \mathcal{A}$, for all positive diagonal matrices $\boldsymbol{\Theta}$ and $\boldsymbol{D}$.

Proof. Denote $\boldsymbol{A}' = \boldsymbol{A}\boldsymbol{\Theta} + \boldsymbol{D}$. We know there exists $\boldsymbol{P}(\boldsymbol{z}) = \mathrm{diag}(p_i(z_i)), p_i > 0$ s.t. $\boldsymbol{z}^\intercal \boldsymbol{P}(\boldsymbol{z})(e^{\boldsymbol{A}\boldsymbol{z}} - \boldsymbol{1}) \geq 0$ for all $\boldsymbol{z}$. Change of variable $\boldsymbol{w} = \boldsymbol{\Theta}^{-1}\boldsymbol{z}$, and let $\tilde{\boldsymbol{P}}(\boldsymbol{w}) = \mathrm{diag}(\tilde{p}_i(w_i))$ where $\tilde{p}_i(w_i) = \theta_i p_i e^{-d_i w_i} > 0$. Then

$$\boldsymbol{w}^\intercal \tilde{\boldsymbol{P}}(\boldsymbol{w})(e^{\boldsymbol{A}'\boldsymbol{w}} - \boldsymbol{1}) = \boldsymbol{z}^\intercal \boldsymbol{\Theta}^{-1}\boldsymbol{\Theta}\boldsymbol{P}(\boldsymbol{z})\Big(e^{(\boldsymbol{A}'-\boldsymbol{D})\boldsymbol{\Theta}^{-1}\boldsymbol{z}} - e^{-\boldsymbol{D}\boldsymbol{\Theta}^{-1}\boldsymbol{z}}\Big) \geq \boldsymbol{z}^\intercal \boldsymbol{P}(\boldsymbol{z})(e^{\boldsymbol{A}\boldsymbol{z}} - \boldsymbol{1}) \geq 0,$$

for all $\boldsymbol{w} \in \mathbb{R}^n$. The second to last inequality we used $-d_i\theta_i^{-1} < 0$, so $z_i e^{-d_i\theta_i^{-1} z_i} \leq z_i$. □

Remark 5.3.2. Although we motivated our definition of $\mathcal{A}$ from our goal of studying the dynamics of a system from interconnecting of scalar birth-death systems, the set $\mathcal{A}$ is well-defined in a pure matrix theory sense. This means, we can view the study of matrices in $\mathcal{A}$ as a fundamental property of matrices, similar to diagonalizability, Hurwitz, diagonal stability, etc. Any characterization of this fundamental property, either by obtaining specific

examples or by theorems characterizing internal structures of this set, can be immediately applied to our goal. This is a result of the network formulation where we considered Lyapunov functions of the interconnected system as simply the sum of component systems. This is also the result of our use of birth-death orders that separates more detailed parameter dependences into reference points. △

Before we delve further into properties of the set $\mathcal{A}$, let us put all of our constructions so far into a theorem form for certifying stability of an interconnected system in terms of dissipativity of component systems. Nothing needs to be proved, since this is just putting all of our constructions in one setting.

Theorem 5.3.3 (Stability)**.** *Given n scalar birth-death control affine systems where the ith system G_i has dissipative property that, for any reference point $(x_i', u_i') \in \mathcal{X}' \times \mathcal{U}'$, G_i is dissipative with supply rate $s^{\sigma_i}(\overline{u}_i, \overline{y}_i; \varepsilon_i, p_i)$ and state region $\mathcal{X}_i$, certified by storage function $V_i(x_i; x_i')$, where $\sigma_i = +$ if control in production and $\sigma_i = -$ if control in degradation. Let G denote the system formed by interconnecting G_i via interconnection matrix $\boldsymbol{M} \in \mathbb{Z}^{n\times n}$. If $\boldsymbol{E} - \boldsymbol{M\Sigma} \in \mathcal{A}$, where $\boldsymbol{\Sigma} = \mathrm{diag}(\boldsymbol{\sigma})$, $\boldsymbol{E} = \mathrm{diag}(\boldsymbol{\varepsilon})$, then for any reference point $\boldsymbol{x}'$ that is admissible, i.e. $\boldsymbol{x}' \in \mathcal{X}' = \mathcal{X}_1' \times \cdots \times \mathcal{X}_n'$ and $\boldsymbol{u}' \in \mathcal{U}' = \mathcal{U}_1' \times \cdots \times \mathcal{U}_n'$, we have if $\boldsymbol{x}'$ is in $\mathcal{X} := \mathcal{X}_1 \times \cdots \times \mathcal{X}_n$, then it is locally stable in the connected component of $\mathcal{X}$ containing it, certified by Lyapunov function $V(\boldsymbol{x}; \boldsymbol{x}') = \sum_{i=1}^n V_i(x_i; x_i')$.*

So the key of certifying stability of the interconnected system is whether the matrix $\boldsymbol{A}$, capturing the interaction between interconnection and dissipativity, is in $\mathcal{A}$. Let us examine this set in a bit more detail.

Expanding $\boldsymbol{z}^\intercal \boldsymbol{P}\left(e^{\boldsymbol{Az}} - \boldsymbol{1}\right)$ at $\boldsymbol{z} = \boldsymbol{0}$, its zeroth and first order expansions are all zeros, and its second order coefficient is $\boldsymbol{P}^0\boldsymbol{A} + \boldsymbol{A}^\intercal\boldsymbol{P}^0$, where $\boldsymbol{P}^0 = \mathrm{diag}(P_i(0))$. So a necessary condition for inequality (5.47) from this expansion at $\boldsymbol{z} = \boldsymbol{0}$ is that its second order expansion is positive definite, i.e.

$$\boldsymbol{P}^0\boldsymbol{A} + \boldsymbol{A}^\intercal\boldsymbol{P}^0 > 0, \tag{5.49}$$

where > 0 denotes positive definiteness. So we have the following proposition:

Proposition 5.3.4. *$\mathcal{A} \subset \mathcal{A}^0$, where*

$$\mathcal{A}^0 := \left\{\boldsymbol{A} \in \mathbb{R}^{n\times n} : \exists \boldsymbol{P} \in \mathcal{P}^0, s.t. \boldsymbol{PA} + \boldsymbol{A}^\intercal\boldsymbol{P} > 0\right\},$$

with $\mathcal{P}^0$ is the set of diagonal matrices with positive constant diagonals.

Remark 5.3.5. The necessary condition in proposition 5.3.4 is one example of a Lyapunov inequality, widely encountered in matrix analysis and linear systems theory. This inequality

is a linear matrix inequality (LMI), which can be efficiently computed through convex optimization packages. This condition is also exactly the structural local stability condition from reaction orders as discussed at the end of Section 5.1. This necessary condition could be used to demonstrate several necessary conditions on $\boldsymbol{A} \in \mathcal{A}$. For example, $A_{ii} \geq 0$. This could be seen by first re-writing the Lyapunov inequality as $\boldsymbol{P}^{1/2}\boldsymbol{A}\boldsymbol{P}^{1/2} + \boldsymbol{P}^{1/2}\boldsymbol{A}^\intercal\boldsymbol{P}^{1/2} \geq 0$, then take $\boldsymbol{P} \in \mathcal{P}^0$ s.t. $p_i \to +\infty$ while $p_j \to 0$ for $j \neq i$. △

Below, for two simple cases of $\boldsymbol{A}$ in general dimensions, we show that they are in $\mathcal{A}$.

Example 20 (Known cases)**.** The following are a list of $\boldsymbol{A}$ that we know are in $\mathcal{A}$.

1. $\boldsymbol{A} = \mathbf{1}\mathbf{1}^\intercal$, where $\mathbf{1} \in \mathbb{R}^n$ is a vector of 1's.

   Take P_i as the constant functions $P_i = 1$, then $\sum_i (\boldsymbol{x}^{\mathbf{1}} - 1)\log x_i = (\boldsymbol{x}^{\mathbf{1}} - 1)\log \boldsymbol{x}^{\mathbf{1}} \geq 0$.

2. $\boldsymbol{A} = \mathbf{I} - \boldsymbol{\Pi}$, where $\boldsymbol{\Pi}$ is a permutation matrix for permuation map π on indices $\{1, \ldots, n\}$.

   Take $P_i = x_i^{-1}$, then

   $$\sum_i x_i^{-1}(x_i x_{\pi(i)}^{-1} - 1)\log x_i = \sum_i (x_i^{-1} - x_{\pi(i)}^{-1})\log x_i^{-1}.$$

   If we have a change of variables by $w_i = x_i^{-1}$, we obtain

   $$\begin{aligned}\sum_i (w_i - w_{\pi(i)})\log w_i &= \sum_i w_i \log w_i - \sum_i w_{\pi(i)} \log w_i \\ &= \sum_i w_{\pi(i)} w_{\pi(i)} - \sum_i w_{\pi(i)} \log w_i + \sum_i w_i - \sum_i w_{\pi(i)} \\ &= \sum_i w_i \left(\frac{w_{\pi(i)}}{w_i} \log \frac{w_{\pi(i)}}{w_i} + 1 - \frac{w_{\pi(i)}}{w_i} \right) \geq 0.\end{aligned}$$

3. $\boldsymbol{A} = A_{ii}\boldsymbol{E}_{ii} + A_{jj}\boldsymbol{E}_{jj} + A_{ij}\boldsymbol{E}_{ij} + A_{ji}\boldsymbol{E}_{ji}$, $i \neq j$, for $A_{ij}A_{ji} \leq A_{ii}A_{jj}$, $A_{ii}, A_{jj} \geq 0$, where $\boldsymbol{E}_{ij}$ is the matrix with 1 at the (i, j) entry and zero everywhere else. This claim is proved in Theorem 5.3.7.

△

Remark 5.3.6. From the statement of the theorem, we see that this dissipative framework views the dynamics of a large system in terms of cubes $\mathcal{X} = \mathcal{X}_1 \times \cdots \times X_n$ that is product of dissipative regions of component systems. Just like in the scalar case, this view separates parameters' influence on the system into two parts: the structural part from interconnection and dissipativity, encoded in $\boldsymbol{A}$, and the rate part from whether the reference point $\boldsymbol{x}'$ is

admissible. For admissible reference points $\boldsymbol{x}'$ in dissipative cube $\mathcal{X}$, we obtain stability certified by Lyapunov functions. For $\boldsymbol{x}'$ outside of the dissipative cube $\mathcal{X}$, we can say the system trajectory starting in the cube will leave the cube in finite time, but no longer sure which direction will it leave from. This is because energy stored in the storage function of one component system can be shifted into energy stored in other component systems, therefore all we know is the value of the overall Lyapunov function V will decrease, but not sure along which coordinate. △

To further explore the set $\mathcal{A}$, we can try to find classes of matrices in $\mathcal{A}$ by constructing certificates of Eq (5.47), as we did in Example 20. This requires technical constructions utilizing structural properties of the class of entropy-like functions to characterize the gap between $\mathcal{A}$ and $\mathcal{A}^0$. One major success of our effort in this direction is constructions that prove $\mathcal{A} = \mathcal{A}^0$ for the $n = 2$ case, i.e. the system is formed by interconnecting two component systems. The statement is the following proposition, but the proof is deferred to the appendix in Section 5.5 since it is technically involved. One interesting direction is to find constructions for classes of $\boldsymbol{A}$ matrices in $n = 3$ or more general cases.

Theorem 5.3.7. *For $n = 2$, $\mathcal{A} = \mathcal{A}^0 = \{\boldsymbol{A} \in \mathbb{R}^{2\times 2} : a_{12}a_{21} \leq a_{11}a_{22},\ a_{11}, a_{22} \geq 0\}$.*

Proof. This is by explicit construction of $P_i(z_i)$ for all the possible cases. See Section 5.5 for the full proof. To give a taste without delving into the technicalities, we illustrate what the argument is like when a_{12} and a_{21} have different signs and $a_{11}, a_{22} > 0$. Without loss of generality, $a_{12} < 0$ and $a_{21} > 0$. So we can take $p_1(x_1) = x_1^{-a_{11}}(x_1^{a_{21}} - 1)\frac{1}{\log x_1}$, $p_2(x_2) = x_2^{-a_{22}}(1 - x_2^{a_{12}})\frac{1}{\log x_2}$. Therefore,

$$\begin{aligned}
&p_1(x_1)(x_1^{a_{11}}x_2^{a_{12}} - 1)\log x_1 + p_2(x_2)(x_2^{a_{21}}x_1^{a_{22}} - 1)\log x_2\\
\geq &p_1(x_1)(x_1^{a_{11}}x_2^{a_{12}} - x_1^{a_{11}})\log x_1 + p_2(x_2)(x_2^{a_{21}}x_1^{a_{22}} - x_1^{a_{22}})\log x_2\\
= &(x_1^{a_{21}} - 1)(x_2^{a_{12}} - 1) + (x_1^{a_{21}} - 1)(1 - x_2^{a_{12}}) = 0.
\end{aligned}$$

□

This theorem gives a complete characterization of $\mathcal{A}$ for $n = 2$ case. This can be used to characterize dissipative regions for general two-dimensional dynamical systems with birth-death structure, as is typically the case in biomolecular systems. We demonstrate the power of this approach in the following examples.

Example 21 (2d bistable)**.** Consider the following two component systems, with their signs and corresponding η functions listed.

$$\dot{x}_1 = u_1 - \gamma_1 x_1, \quad y_1 = \alpha + \frac{x_1^2}{1+x_1^2}, \quad \sigma_1 = +, \quad \eta_1(x_1) = -\left(2\frac{\frac{x_1^2}{1+x_1^2}}{\alpha + \frac{x_1^2}{1+x_1^2}}\frac{1}{1+x_1^2}\right)^{-1};$$

$$\dot{x}_2 = u_2 - \gamma_2 x_2, \quad y_2 = x_2, \quad \sigma_2 = +, \quad \eta_2(x_2) = -1.$$

By interconnection $u_1 = y_2$, $y_2 = u_1$, encoded in the following interconnection matrix $\boldsymbol{M}$, we have the following closed loop system:

$$\boldsymbol{M} = \begin{bmatrix} 0 & 1 \\ 1 & 0 \end{bmatrix}, \quad \begin{cases} \dot{x}_1 = x_2 - \gamma_1 x_1, \\ \dot{x}_2 = \alpha + \frac{x_1^2}{1+x_1^2} - \gamma_2 x_2. \end{cases}$$

The $\boldsymbol{A} = \boldsymbol{E} - \boldsymbol{M}\Sigma$ matrix we obtain then is

$$\boldsymbol{A} = \begin{bmatrix} \varepsilon_1 & 0 \\ 0 & \varepsilon_2 \end{bmatrix} - \begin{bmatrix} 0 & 1 \\ 1 & 0 \end{bmatrix}\begin{bmatrix} 1 & 0 \\ 0 & 1 \end{bmatrix} = \begin{bmatrix} \varepsilon_1 & -1 \\ -1 & \varepsilon_2 \end{bmatrix}.$$

By Theorem 5.3.7, the condition for $\boldsymbol{A} \in \mathcal{A}$ is $\varepsilon_1\varepsilon_2 \geq 1$. The dissipative region for x_2 is always the full positive real line $\mathcal{X}_2 = (0, +\infty)$, and the largest value ε_2 can take is 1. So the condition for $\boldsymbol{A} \in \mathcal{A}$ is $\varepsilon_1 \geq 1$. This determines the dissipative region for x_1 to be $\mathcal{X}_1 = \{x_1 : \eta_1(x_1) < -1\}$. The condition $\eta_1(x_1) < -1$, after a quick algebraic check, is exactly the same as the condition for dissipativity in Example 16 and Figure 5.6. So although this system is two dimensional with different ways for the parameter γ to enter, the structural conditions for dissipativity and multistability determined by birth-death orders are exactly the same as the scalar bistable system. △

Example 22 (toggle switch)**.** One of the foundational constructions in synthetic biology is a synthetic toggle switch system achieving bistability [47]. Consider the following simple model for the toggle switch system. We begin with the two component systems that are identical, $i \in \{1, 2\}$.

$$\dot{x}_i = u_i - \gamma_i x_i, \quad y_i = \left(\alpha_i + \frac{1}{1+x_i^2}\right)^{-1}, \quad \sigma_i = +, \quad \eta_i(x_i) = -\left(2\frac{\frac{x_i^2}{1+x_i^2}}{\alpha_i + \frac{x_i^2}{1+x_i^2}}\frac{1}{1+x_i^2}\right)^{-1};$$

By interconnection $u_1 = y_2^{-1}$, $u_2 = y_1^{-1}$, encoded in the following interconnection matrix $\boldsymbol{M}$, we have the following closed loop system:

$$\boldsymbol{M} = \begin{bmatrix} 0 & -1 \\ -1 & 0 \end{bmatrix}, \quad \begin{cases} \dot{x}_1 &= \alpha_2 + \frac{1}{1+x_2^2} - \gamma_1 x_1; \\ \dot{x}_2 &= \alpha_1 + \frac{1}{1+x_1^2} - \gamma_2 x_2, \end{cases}$$

where x_1 and x_2 inhibits each other.

The region of stability corresponds to the region with $\boldsymbol{A} \in \mathcal{A}$. In this case,

$$\boldsymbol{A} = \boldsymbol{E} - \boldsymbol{M}\boldsymbol{\Sigma} = \begin{bmatrix} \varepsilon_1 & 1 \\ 1 & \varepsilon_2 \end{bmatrix}.$$

By Theorem 5.3.7, the condition for $\boldsymbol{A} \in \mathcal{A}$ is $\varepsilon_1\varepsilon_2 \geq 1$. Since $\eta_i(x_i)$ and ε_i are related by $\varepsilon_i(x_i) \leq -\varepsilon_i$, we can first fix ε_1 and ε_2, then determine the dissipative regions for each component system $\mathcal{X}_1 = \{x_1 : \eta_1(x_1) \leq -\varepsilon_1 < 0\}$, and $\mathcal{X}_2 = \{x_2 : \eta_2(x_2) \leq -\varepsilon_2 < 0\}$. Then the dissipative region for the connected system can be determined as $\mathcal{X}_1 \times \mathcal{X}_2$, which consists of rectangles, i.e. products of open intervals. See Figure 5.8 for an example. Because the rectangles come from fixed ε_1 and ε_2, the fixed points of interest could easily be outside of the rectangles. This then require us to find better pairs of $(\varepsilon_1, \varepsilon_2)$, and therefore more appropriate rectangles $\mathcal{X}_1 \times \mathcal{X}_2$, to cover the fixed points of interest.

Alternatively, to avoid fixing ε_i, we can take the conditions on ε_1 and ε_2 jointly and translate it into a two-dimensional constraint on (η_1, η_2) jointly, therefore determining a two-dimensional dissipative region $\mathcal{X} \subset \mathbb{R}^2_{>0}$, defined by

$$\mathcal{X} = \{(x_1, x_2) : \eta(x_1) < 0, \eta(x_2) < 0, \eta(x_1)\eta(x_2) \geq 1\}.$$

Such dissipative region's shape is more complicated, but covers a wider area. See the right panel of Figure 5.8 for an illustration. For any fixed points in this dissipative region, we automatically know it is locally stable with a storage function certifying its regional behavior. If we want to know how would the system trajectory evolve beginning at some point in the dissipative region, then we need to take rectangles containing this point. Then by plotting the level sets of the storage function, we know the point will go toward lower level sets when it is in the dissipative region. △

In the toggle switch example, we obtain dissipative regions based on condition of $\boldsymbol{A}(\varepsilon_1, \varepsilon_2)$ matrix formed. However, other systems can form the same $\boldsymbol{A}$ matrix, therefore our result for the toggle switch example can be applied to a class of 2d systems from interconnecting two components. We illustrate this via two examples below.

Example 23 (toggle switch via degradation)**.** In this example we construct a system with toggle switch like behavior by components that are control in degradation. Each component system is of the following form, for $i \in \{1, 2\}$.

$$\dot{x}_i = 1 - \gamma_i x_i u_i, \quad y_i = \left(\alpha_i + \frac{1}{1+x_i^2}\right)^{-1}, \quad \sigma_i = -, \quad \eta_i(x_i) = -\left(2\frac{\frac{x_i^2}{1+x_i^2}}{\alpha_i + \frac{x_i^2}{1+x_i^2}}\frac{1}{1+x_i^2}\right)^{-1}.$$

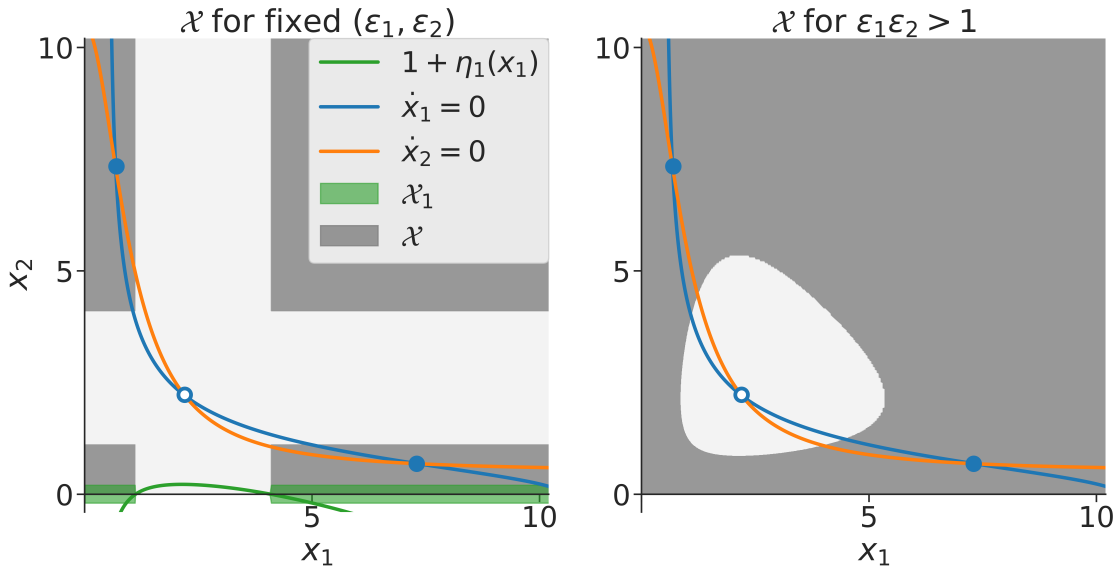

Figure 5.8 Plot for Example 22, showing how stability of fixed points relate to dissipative regions (grey). Blue and orange curves are nullclines for $\dot{x}_1 = 0$ and $\dot{x}_2 = 0$, so their intersections are fixed points of the system. We see three fixed points, with two stable fixed points (solid blue circle) in dissipative regions (grey), therefore locally stable, and one unstable fixed point (empty blud circle) outside of dissipative regions. **(Left)** A dissipative region (grey) that consists of rectangles, i.e. product of two component dissipative regions, of the form $\mathcal{X} = \mathcal{X}_1 \times \mathcal{X}_2$, with $\mathcal{X}_i = \{x_i : \eta_i(x_i) \leq -\varepsilon_i\}$. Here, ε_1 and ε_2 are chosen to be 1. The green curve at the bottom is $\eta_1(x_1) + 1$, which is negative for dissipative region $\mathcal{X}_1$. **(Right)** A dissipative region (grey) that corresponds to all (x_1, x_2) that allows $\varepsilon_1\varepsilon_2 > 1$. The resulting shape is not rectangular, but instead is a continuous region containing all but a circular region in the middle. Parameters are $\alpha_1 = \alpha_2 = 0.05$, $\gamma_1 = \gamma_2 = 0.1$.

Note that $\eta_i(x_i)$ is exactly the same as in the toggle switch example 22, since f_i^+, f_i^- and h are all the same, only where control input u_i is placed is different.

By interconnection $u_1 = y_2$, $u_2 = y_1$, encoded in the following interconnection matrix $\boldsymbol{M}$, we have the following closed loop system:

$$\boldsymbol{M} = \begin{bmatrix} 0 & 1 \\ 1 & 0 \end{bmatrix}, \quad \begin{cases} \dot{x}_1 &= 1 - \frac{\gamma_1 x_1}{\alpha_2 + \frac{1}{1+x_2^2}}; \\ \dot{x}_2 &= 1 - \frac{\gamma_2 x_2}{\alpha_1 + \frac{1}{1+x_1^2}}. \end{cases}$$

So in the full system, the net effect of interaction is the same as in the toggle switch example, that x_1 and x_2 inhibit each other. In the toggle switch case, the inhibition is via decreasing production. Here it is via increasing degradation.

We can calculate that the $\boldsymbol{A}$ matrix obtained is exactly the same as in the toggle switch example. Therefore the dissipative regions are exactly the same as in Figure 5.8. We note that the nullclines are the same as well. △

The following example further illustrates that the same $\boldsymbol{A}$ is shared by several different

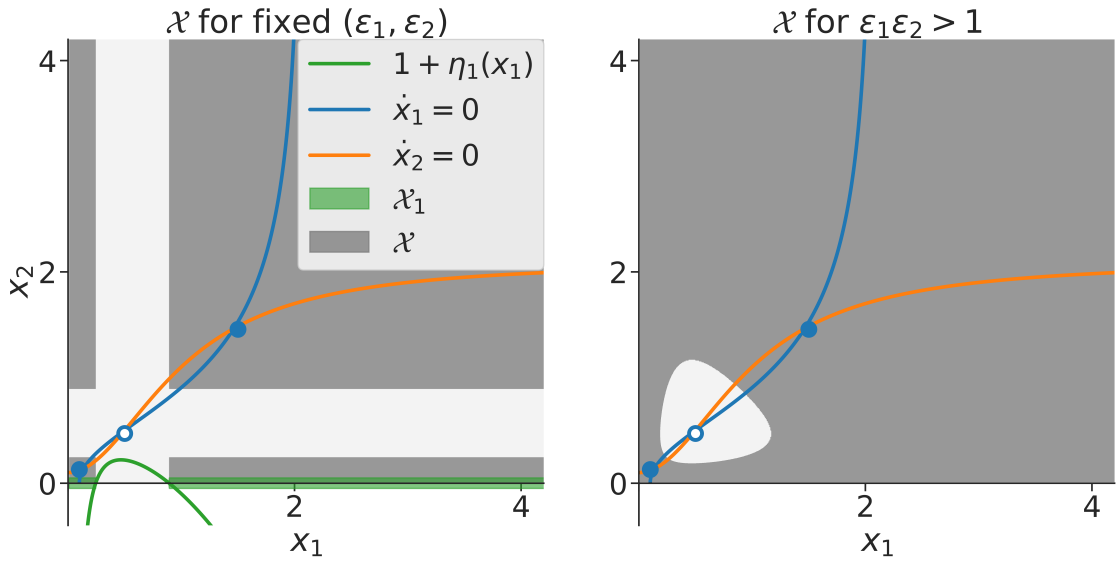

Figure 5.9 Plot for Example 24. Same format as Figure 5.8. $\varepsilon_1 = \varepsilon_2 = 1$ for $\mathcal{X}$ on the left. Parameters are $\alpha_1 = \alpha_2 = 0.05$, $\gamma_1 = \gamma_2 = 0.5$.

systems. The following example has two components activating each other instead of inhibiting each other, so the interaction graph is different from the toggle switch example. This corresponds to different $\eta_i(x_i)$, but still the same $\boldsymbol{A}(\varepsilon_1, \varepsilon_2)$.

Example 24 (mutual activation)**.** We begin with the two component systems that are identical, $i \in \{1, 2\}$.

$$\dot{x}_i = u_i - \gamma_i x_i, \qquad y_i = \alpha_i + \frac{x_i^2}{1 + x_i^2}, \qquad \sigma_i = +, \qquad \eta_i(x_i) = -2\frac{\frac{x_i^2}{1+x_i^2}}{\alpha_i + \frac{x_i^2}{1+x_i^2}}\frac{1}{1 + x_i^2}.$$

By interconnection $u_1 = y_2$, $u_2 = y_1$, encoded in the following interconnection matrix $\boldsymbol{M}$, we have the following closed loop system:

$$\boldsymbol{M} = \begin{bmatrix} 0 & 1 \\ 1 & 0 \end{bmatrix}, \qquad \begin{cases} \dot{x}_1 &= \alpha_2 + \frac{x_2^2}{1+x_2^2} - \gamma_1 x_1; \\ \dot{x}_2 &= \alpha_1 + \frac{x_1^2}{1+x_1^2} - \gamma_2 x_2, \end{cases}$$

where the interaction between x_1 and x_2 has the net effect of activating each other. This system is also capable of bistability, but instead of the two stable fixed points being one low and one high for (x_1, x_2) in toggle switch, this system has both low and both high. We illustrate this in Figure 5.9. The dissipative regions are determined via exactly the same condition as in the toggle switch example, because the $\boldsymbol{A}(\varepsilon_1, \varepsilon_2)$ matrix is exactly the same:

$$\boldsymbol{A} = \boldsymbol{E} - \boldsymbol{M}\boldsymbol{\Sigma} = \begin{bmatrix} \varepsilon_1 & 1 \\ 1 & \varepsilon_2 \end{bmatrix}.$$

△

Through these examples, it is clearly illustrated that our dissipative network approach based on birth-death orders has the advantage of clearly separating changes in system properties into different layers in the architecture of a system. The highest layer is the $\boldsymbol{A}(\varepsilon)$ matrix, which only cares about the interconnection network. It prescribes the condition that the dissipativity parameters ε needs to satisfy in order to have dissipativity or stability of the full system. A lower layer, the birth-death order layer or the $\eta_i(x_i)$ layer, contains the structural information about component systems in terms of dissipativity. It connects conditions on dissipativity parameters ε to regions in state space $\boldsymbol{x}$ of each component. This layer only cares about parameters in a system that change the topology of dissipative regions $\mathcal{X}_i$. The lowest layer, the reference point $(\boldsymbol{x}', \boldsymbol{u}')$ layer, parameterizes actual trajectories the system can have. The behavior of these trajectories are described relative to this reference point, and constrained by dissipativity in the state regions to behave in ways dictated by the storage functions.

This layered architecture makes this dissipative network approach very powerful when analyzing properties that are invariant or robust. For example, using only the $\boldsymbol{A}$ layer, we can place constraints on a systems' behavior without knowing any of its component systems or actual parameters. Another case is what we have already used in several examples, where we write down the dissipative region without knowing what the reference points or fixed points are. In other words, we can discuss properties of all possible fixed points, instead of analyzing them case by case.

Before we end, let us summarize the workflow of this dissipative network approach.

Summary of workflow

1. For given interconnection pattern $\boldsymbol{M}$, we look for dissipativity parameters ε, one point or a set of points $\varepsilon \in \mathcal{E}$, such that the resulting matrix $\boldsymbol{A}(\varepsilon)$ is in $\mathcal{A}$, i.e. it satisfies inequality (5.47) for some positive functions p_i. Along the way, we could use properties of $\mathcal{A}$ such as Proposition 5.3.1 to enlarge the set of dissipative parameters $\mathcal{E}$.

2. For each subsystem, which we assume to be a scalar birth-death control affine system, we use $\eta_i(x_i)$ to relate the set of dissipativity parameters $\varepsilon \in \mathcal{E}$ to dissipative regions. This can be done for fixed ε, we obtain $\mathcal{X} = \mathcal{X}_1 \times \cdots \times \mathcal{X}_n$ with $\mathcal{X}_i = \{x_i : \eta_i(x_i) \leq -\varepsilon_i\}$, so $\mathcal{X}$ consists of open cubes. In this cube $\mathcal{X}$, each subsystem is dissipative with supply rate $s(\overline{u}_i, \overline{y}_i; \varepsilon_i)$. Another type of $\mathcal{X}$ can be obtained for the set of dissipativity parameters $\mathcal{E}$, by $\mathcal{X} = \{\boldsymbol{x} : \exists \boldsymbol{\varepsilon}, \varepsilon_i \leq -\eta_i(x_i), \boldsymbol{\varepsilon} \in \mathcal{E}\}$. In this $\mathcal{X}$, each subsystem is

dissipative with supply rate $s(\varepsilon_i)$ such that $(\boldsymbol{\varepsilon} \in \mathcal{E}$. This $\mathcal{X}$ can be seen as the union of all possible cubes from the previous method.

3. For any fixed point in $\mathcal{X}$, we know it is locally stable with a Lyapunov function certifying it, where the Lyapunov function is the sum of storage functions of each component system. Note that these storage functions are only valid in cube-shaped regions. So multiple fixed points in $\mathcal{X}$ will be certified by multiple Lyapunov functions, each valid in a cube-shaped region containing each fix point.

Another approach to study the set $\mathcal{A}$ is to take an algorithmic approach by finding procedures that test whether any given matrix $\boldsymbol{A}$ arising from a particular example is in $\mathcal{A}$. This corresponds to computationally certify non-negativity of Eq (5.47), for candidate choices of $P_i(z_i)$. For $P_i(z_i)$ chosen as exponentials and polynomials in z_i, the class of functions to be certified for non-negativity in Eq (5.47) is entropy-like functions. This is studied in Chapter 6 of [43], for example.

5.4 Summary and future directions

In this chapter, motivated by the polyhedral structure of reaction orders in binding's regulation of catalysis, we investigated a general approach to capture dynamical properties of biomolecular systems by reaction orders, using the framework of dissipative network systems. We formulated the production-degradation structure of biomolecular systems (Definition 5.1.1), and defined a supply rate for a notion of dissipativity that naturally correspond to conditions on reaction orders (Eq (5.17)). This notion of dissipativity allows us to find dissipative regions independent of reference points (Proposition 5.2.12). For closed systems, this means stable regions independent of fixed point locations (Proposition 5.2.13). Considering a general system as interconnection of multiple component systems, we derived general conditions relating component dissipativity conditions with overall system stability (Eq (5.47)). This yields a class of matrix properties denoted by $\mathcal{A}$, corresponding to matrix $\boldsymbol{A}$ satisfying a non-negativity condition for entropy-like functions (Proposition 5.3.1).

We discuss some potential directions of future research below.

A hierarchy of scaling factors p_i

When considering a multi-variate system by interconnection of component systems, we restricted the positive function p_i in the supply rate s_i of each component system G_i to

depend only on $\overline{y}_i$, so that $s_i(\overline{u}_i, \overline{y}_i; \varepsilon_i, p_i) = p_i(\overline{y}_i)(\overline{u}_i - \overline{y}_i^{\varepsilon_i}) \log \overline{y}_i$. However, it is arguable that the positive function p_i is simply a place holder for any positive scaling, therefore can depend on other $\overline{y}_j$ variables as well. The only restriction is that p_i is independent of $\overline{u}_i$. This is possible because of Theorem 5.2.5, which showed that we can characterize each component system's dissipativity property independent of scaling factors p_i. For any choice of p_i, the component system's dissipativity with respect to $s^\sigma(\varepsilon_i, p_i)$ holds, for the same ε_i. Different choices of p_i only influences the storage function V_i obtained.

More importantly, we see that different systems in terms of interconnection of dissipative component systems result in different $\boldsymbol{A}$ matrix, and the certificates of stability of $\boldsymbol{A}$ showing that $\boldsymbol{A} \in \mathcal{A}$ depends on choices of P_i. Since choices of P_i influence properties of the component storage functions V_i and the overall Lyapunov function V, larger and smaller classes of P_i could correspond to weaker or stronger notions of stability. This prompts us to consider a hierarchy of scaling factor sets $\mathcal{P}$, which define a hierarchy of matrix sets $\mathcal{A}(\mathcal{P})$. Larger $\mathcal{P}$ such as $P_i(\boldsymbol{z})$ can depend on variables other than z_i, corresponding to the weakest notion of stability, and should have the largest $\mathcal{A}$ set. More restrictive $\mathcal{P}$, such as asking the resulting Lyapunov function to be unbounded in all directions, should result in smaller $\mathcal{A}$.

This freedom of choosing a hierarchy of $\mathcal{P}$ highlights the advantage of the supply rate and the dissipativity notion developed in this work: that component dissipativity can be determined with significant flexibility encoded in the choice of p_i to choose appropriate storage or Lyapunov functions. For example, by choosing p_i to depend on variables other than z_i, we can obtain Lyapunov functions with level sets that are not cubes.

Generalization to non-scalar component systems and multiple-input-multiple-output supply rates

In this work, we considered component systems that are scalar birth-death control affine systems. However, as we discussed in Section 5.1, the general birth-death systems have birth-death orders from networks of binding reactions. But binding reactions are naturally non-scalar. For example, consider $E + S \rightleftharpoons C \to E + P$, where one enzyme and one susbtrate binds to form a complex C. This complex C then catalyzes the conversion of a substrate S into a product P. The variables for this system is total enzyme concentration $x_E = E + C$, total substrate concentration $x_S = S + C$, and total product concentration $x_P = P$. The rate of this production of x_P, or degradation of x_S, is proportional to C, the concentration of the complexes. But this depends on both x_E and x_S (see Section 3.6 in Chapter 3) in a non-monomial way. In particular, the reaction order of C depends on both x_E and x_S in a non-separable way. Only under certain simplifying assumptions, such as

the substrate is much more than the enzyme, we can make this dependence separable, such as $C \approx x_E \frac{x_S}{x_S+K}$ for some equilibrium constant K. Then C's reaction order varies with x_S, but not x_E.

We could capture such non-scalar dependence of reaction orders in our existing framework by giving up decomposing dissipativity of the full network into individual component systems. Namely, after we form the full system via interconnections and considering mapping conditions on dissipativity parameters from stability to dissipative regions via $\eta_i(x_i)$, we need to instead consider $\boldsymbol{\eta}(\boldsymbol{x})$ altogether. The example of simple binding reaction mentioned above is one case where $\boldsymbol{\eta}(x_E, x_S)$ cannot be separated into $(\eta_E(x_E), \eta_S(x_S))$, but instead its two components are $\boldsymbol{\eta}(x_E, x_S) = (\eta_E(x_E, x_S), \eta_S(x_E, x_S))$, with each component depending on both variables. This has the advantage that we do not need a new framework, but the disadvantage is we no longer have meaningful component systems, since these components' dissipativity depend on variables from other systems.

If we want to retain the structure of forming a larger system from component systems, we need a notion of dissipativity for multiple inputs and multiple outputs (MIMO). This means a MIMO supply rate. For the simple binding example above, we need a dissipativity notion for this binding reaction with both x_E and x_S as output. The negativity of such supply rate then extends to non-negative relative entropy functions for non-scalar variables. The relative entropy cone and non-negativity certificates using lifting maps is studied in Chapter 6.6 of [43]. Obtaining a MIMO supply rate based on non-negative relative entropy functions should provide a fascinating direction for further research.

5.5 Appendix. Proof for interconnection of two component systems

Here we delve into the technical inequalities satisfied by entropy-like functions to prove Theorem 5.3.7. We begin with foundational inequalities for entropy-like functions (also heavily used in [43]).

Lemma 5.5.1. *$x^a \log x \geq x^b \log x$ for all $x > 0$ with equality only at $x = 1$ iff $a > b$.*

Proof. It is obvious that a and b cannot be equal. For $a \neq b$, the inequality can be rewritten as $(x^a - x^b) \log x = \frac{1}{a-b} x^b (x^{a-b} - 1) \log x^{a-b} \geq 0$. Let $y = x^{a-b}$ and divide by x^b, this is simplified to $\frac{1}{a-b}(y-1)\log y \geq 0$ for $y > 0$. Since $(y-1)\log y \geq 0$ with equality only at $y = 1$, i.e. $x = 1$. Now we see this inequality is true iff $a - b > 0$. □

Lemma 5.5.2. *For any $\boldsymbol{r}, \boldsymbol{s} \in \mathbb{R}^n$, $\boldsymbol{x}^{\boldsymbol{r}} \log \boldsymbol{x}^{\boldsymbol{r}-\boldsymbol{s}} \geq \boldsymbol{x}^{\boldsymbol{r}} - \boldsymbol{x}^{\boldsymbol{s}}$ for all $\boldsymbol{x} \in \mathbb{R}^n_{>0}$.*

In an alternative form, let $\boldsymbol{s} = \boldsymbol{r} - \boldsymbol{a}$, we have $\boldsymbol{x}^{\boldsymbol{r}} \log \boldsymbol{x}^{\boldsymbol{a}} \geq \frac{1}{\beta}\Big(\boldsymbol{x}^{\boldsymbol{r}} - \boldsymbol{x}^{\boldsymbol{r}-\beta\boldsymbol{a}}\Big)$.

These inequalities then allow us to show the following inequality for a class of constructed p_i. This can be used as building blocks to prove cases of Eq (5.47). Consider $\boldsymbol{a}$ as one row of matrix $\boldsymbol{A}$, then the following class of p_i constructed can modify the exponents of the terms involved in particular ways.

Lemma 5.5.3. *Fix $\boldsymbol{a} \in \mathbb{R}^n$. For any $\bar{b}_i \geq \underline{b}_i$, define $b_i := \bar{b}_i - \underline{b}_i \geq 0$. Let $p_i(x_i) := c_i \frac{x_i^{\bar{b}_i} - x_i^{\underline{b}_i}}{b_i \log x_i}$, $c_i > 0$, so $p_i : \mathbb{R}_{>0} \to \mathbb{R}_{>0}$ is continuous and positive. Then for any $\lambda, \beta \geq 0$ s.t. $\lambda + \beta b_i = c_i$, we have*

$$p_i(x_i)(\boldsymbol{x}^{\boldsymbol{a}} - 1) \log x_i \geq \Big(\boldsymbol{x}^{\boldsymbol{a}+\underline{b}_i\boldsymbol{e}_i} - \boldsymbol{x}^{\bar{b}_i\boldsymbol{e}_i}\Big) \log \boldsymbol{x}^{\lambda\boldsymbol{e}_i - \beta\boldsymbol{a}}.$$

Proof.

$$\begin{aligned}
-\frac{1}{\beta}\Big(\boldsymbol{x}^{\boldsymbol{a}+\underline{b}_i\boldsymbol{e}_i} - \boldsymbol{x}^{\bar{b}_i\boldsymbol{e}_i}\Big) \log \boldsymbol{x}^{-\beta\boldsymbol{a}} &= (\boldsymbol{x}^{\boldsymbol{a}+\underline{b}_i\boldsymbol{e}_i} - \boldsymbol{x}^{\bar{b}_i\boldsymbol{e}_i}) \log \boldsymbol{x}^{\boldsymbol{a}} \\
&= \boldsymbol{x}^{\boldsymbol{a}+\underline{b}_i\boldsymbol{e}_i} \log \boldsymbol{x}^{\boldsymbol{a}} + \boldsymbol{x}^{\bar{b}_i\boldsymbol{e}_i} \log \boldsymbol{x}^{-\boldsymbol{a}} \\
&\geq \boldsymbol{x}^{\boldsymbol{a}+\underline{b}_i\boldsymbol{e}_i} + \boldsymbol{x}^{\bar{b}_i\boldsymbol{e}_i} - \boldsymbol{x}^{\underline{b}_i\boldsymbol{e}_i} - \boldsymbol{x}^{\boldsymbol{a}+\bar{b}_i\boldsymbol{e}_i} \\
&= (\boldsymbol{x}^{\boldsymbol{a}} - 1)(x_i^{\underline{b}_i} - x_i^{\bar{b}_i}) \\
&= -b_i \frac{x_i^{\bar{b}_i} - x_i^{\underline{b}_i}}{b_i \log x_i} (\boldsymbol{x}^{\boldsymbol{a}} - 1) \log x_i.
\end{aligned}$$

Therefore

$$\beta b_i \frac{x_i^{\bar{b}_i} - x_i^{\underline{b}_i}}{b_i \log x_i} (\boldsymbol{x}^{\boldsymbol{a}} - 1) \log x_i \geq \Big(\boldsymbol{x}^{\boldsymbol{a}+\underline{b}_i\boldsymbol{e}_i} - \boldsymbol{x}^{\bar{b}_i\boldsymbol{e}_i}\Big) \log \boldsymbol{x}^{-\beta\boldsymbol{a}}.$$

Similarly,

$$\begin{aligned}
-\frac{1}{\lambda}\Big(\boldsymbol{x}^{\boldsymbol{a}+\underline{b}_i\boldsymbol{e}_i} - \boldsymbol{x}^{\bar{b}_i\boldsymbol{e}_i}\Big) \log x_i^{\lambda} &= \frac{1}{b_i}\Big(\boldsymbol{x}^{\boldsymbol{a}+\underline{b}_i\boldsymbol{e}_i} - \boldsymbol{x}^{\bar{b}_i\boldsymbol{e}_i}\Big) \log x_i^{b_i} \\
&= \frac{1}{b_i}\Big(\boldsymbol{x}^{\boldsymbol{a}+\underline{b}_i\boldsymbol{e}_i} \log x_i^{(\underline{b}_i - \bar{b}_i)} - x_i^{\bar{b}_i} \log x_i^{(\underline{b}_i - \bar{b}_i)}\Big) \\
&\geq \frac{1}{b_i}\Big(\boldsymbol{x}^{\boldsymbol{a}+\underline{b}_i\boldsymbol{e}_i} - \boldsymbol{x}^{\boldsymbol{a}+\bar{b}_i\boldsymbol{e}_i} + x_i^{\bar{b}_i} - x_i^{\underline{b}_i}\Big) \\
&= \frac{1}{b_i}(\boldsymbol{x}^{\boldsymbol{a}} - 1)(x_i^{\underline{b}_i} - x_i^{\bar{b}_i}) \\
&= -\frac{x_i^{\bar{b}_i} - x_i^{\underline{b}_i}}{b_i \log x_i} (\boldsymbol{x}^{\boldsymbol{a}} - 1) \log x_i.
\end{aligned}$$

Therefore,

$$\lambda \frac{x_i^{\bar{b}_i} - x_i^{\underline{b}_i}}{b_i \log x_i} (\boldsymbol{x}^{\boldsymbol{a}} - 1) \log x_i \geq \Big(\boldsymbol{x}^{\boldsymbol{a}+\underline{b}_i\boldsymbol{e}_i} - \boldsymbol{x}^{\bar{b}_i\boldsymbol{e}_i}\Big) \log \boldsymbol{x}^{\lambda\boldsymbol{e}_i}.$$

Summing the two inequalities, we get the desired result. □

Remark 5.5.4. We can write $p_i(x_i)$ as $c_i x_i^{\underline{b}_i} \cdot \frac{x_i^{b_i}-1}{b_i \log x_i}$, so a monomial multiplying a function of the form $\frac{x_i^{b_i}-1}{b_i \log x_i}$. Note that for any $x_i \neq 1$, when $b_i \to 0$, $\frac{1}{b_i}(x_i^{b_i}-1) = \frac{1}{b_i}(e^{b_i \log x_i}-1) \to \frac{1}{b_i}(1+b_i \log x_i - 1) = \log x_i$. Therefore, $p_i(x_i) = \lambda x_i^{\underline{b}_i}$ when $b_i = 0$. Furthermore, $\frac{x_i^{b_i}-1}{b_i \log x_i}$ is analytic in (x_i, b_i) since it is $f \circ g$ with $f : x \mapsto \frac{x-1}{\log x}$ and $g : (x_i, b_i) \mapsto x_i^{b_i}$. It is positive for all $x_i > 0$ and $b_i \geq 0$, since for $b_i > 0$ and $x_i \neq 1$, $x_i^{b_i} - 1$ and $\log x_i$ always have the same sign, while at $x_i \to 1$ or $b_i \to 0$, we get value 1. △

Lemma 5.5.3 can then be used to prove inequalities for various cases of $\boldsymbol{A}$. In particular, we focus on when $\boldsymbol{A}$ has only two nonzero rows, and each row has only two nonzero entries, so that the matrix $\boldsymbol{A}$ is effectively 2×2. We begin with relating a diagonal term A_{ii} with another term on the same column A_{ji}. These cases will all become useful when we prove Theorem 5.3.7.

Corollary 5.5.5 (Triangular)**.** *For any $A_{ii} > 0$, $A_{ji} \neq 0$, there exists $p_i(x_i) : \mathbb{R}_{>0} \to \mathbb{R}_{>0}$ s.t. $p_i(x_i)(x_i^{A_{ii}} - 1)\log x_i \geq (1 - x_i^{A_{ji}})\log x_i^{-A_{ji}} = (x_i^{A_{ji}} - 1)\log x_i^{A_{ji}}$. Indeed, we can choose*

$$\begin{cases} p_i(x_i) = \frac{A_{ji}}{A_{ii}}(x_i^{A_{ji}} - x_i^{-A_{ii}})\frac{1}{\log x_i}, & A_{ji} > 0; \\ p_i(x_i) = \frac{-A_{ji}}{A_{ii}}(1 - x_i^{A_{ji}-A_{ii}})\frac{1}{\log x_i}, & A_{ji} < 0. \end{cases}$$

$$\begin{cases} p_i(x_i) = \frac{A_{ji}}{A_{ii}-A_{ji}}(1 - x_i^{A_{ji}-A_{ii}})\frac{1}{\log x_i}, & A_{ii} > A_{ji} > 0; \\ p_i(x_i) = \frac{-A_{ji}}{A_{ii}+A_{ji}}(x_i^{A_{ji}} - x_i^{-A_{ii}})\frac{1}{\log x_i}, & -A_{ii} < A_{ji} < 0. \end{cases}$$

Proof. Apply Lemma 5.5.3. For $A_{ji} > 0$, in the first case, our choice of p_i corresponds to $\lambda = \frac{A_{ji}}{A_{ii}}$, $\overline{b}_i = A_{ji}$, $\underline{b}_i = -A_{ii}$.

In the second case. $\lambda(\overline{b}_i - \underline{b}_i) = A_{ji}$, $A_{ii} + \underline{b}_i = A_{ji}$, $\overline{b}_i = 0$. This implies $\underline{b}_i = A_{ji} - A_{ii} < 0 = \overline{b}_i$, and $\lambda = \frac{A_{ji}}{A_{ii}-A_{ji}}$. This case poses additional condition that $A_{ji} < A_{ii}$. □

The above corollary can then immediately be used to prove the triangular case, where A_{ii}, A_{ji}, and A_{jj} are nonzero, while all other terms are zero.

Corollary 5.5.6. *For $\boldsymbol{A} \in \mathbb{R}^{n \times n}$ with indices $i \neq j$ such that $A_{ii} > 0$, $A_{jj} > 0$, and $A_{ji} \neq 0$, while all other terms are zero. Then there exists positive functions p_i, p_j such that*

$$p_i(x_i)(\boldsymbol{x}^{\boldsymbol{A}_i} - 1)\log x_i + p_j(x_j)(\boldsymbol{x}^{\boldsymbol{A}_j} - 1)\log x_j \geq 0.$$

Proof. Apply Corollary 5.5.5 together with $p_j(x_j) \equiv A_{jj}$ to get

$$\begin{aligned}
&p_i(x_i)(\boldsymbol{x}^{\boldsymbol{A}_i} - 1)\log x_i + p_j(x_j)(\boldsymbol{x}^{\boldsymbol{A}_j} - 1)\log x_j \\
\geq &(x_i^{A_{ji}} - 1)\log x_i^{A_{ji}} + (x_i^{A_{ji}} x_j^{A_{jj}} - 1)\log x_j^{A_{jj}} \\
= &x_i^{A_{ji}} \log x_i^{A_{ji}} + \log x_i^{-A_{ji}} + x_i^{A_{ji}} x_j^{A_{jj}} \log x_j^{A_{jj}} + \log x_j^{-A_{jj}} \\
= &x_i^{A_{ji}} \log x_i^{A_{ji}} + x_i^{A_{ji}} x_j^{A_{jj}} \log x_j^{A_{jj}} + \log x_i^{-A_{ji}} x_j^{-A_{jj}} \\
\geq &x_i^{A_{ji}} - 1 + x_i^{A_{ji}} x_j^{A_{jj}} - x_i^{A_{ji}} + 1 - x_i^{A_{ji}} x_j^{A_{jj}} = 0.
\end{aligned}$$

□

For more general cases when considering two rows of $\boldsymbol{A}$ to satisfy Eq (5.47), we derive conditions that the two row vectors $\boldsymbol{A}_i$ and $\boldsymbol{A}_j$ need to satisfy in order for some of construction of p_i and p_j following Lemma 5.5.3 to work.

Lemma 5.5.7. *For two vectors $\boldsymbol{A}_i$ and $\boldsymbol{A}_j$, if there exists $\bar{b}_i > \underline{b}_i$, $\bar{b}_j > \underline{b}_j$ and $\lambda > 0$ s.t.*

$$\begin{aligned}
\Big\{\boldsymbol{A}_i + \underline{b}_i \boldsymbol{e}_i, \bar{b}_i \boldsymbol{e}_i\Big\} &= \Big\{\boldsymbol{A}_j + \underline{b}_j \boldsymbol{e}_j, \bar{b}_j \boldsymbol{e} - j\Big\}, \\
\Big\{(1+\lambda)\boldsymbol{A}_i + \underline{b}_i \boldsymbol{e}_i, -\lambda \boldsymbol{A}_i + \bar{b}_i \boldsymbol{e}_i\Big\} &= \Big\{\boldsymbol{A}_j + \bar{b}_j \boldsymbol{e}_j, \underline{b}_j \boldsymbol{e}_j\Big\},
\end{aligned}$$

then taking $p_i(x_i) = \lambda(x_i^{\bar{b}_i} - x_i^{\underline{b}_i})\frac{1}{\log x_i}$, $p_j(x_j) := (x_j^{\bar{b}_j} - x_j^{\underline{b}_j})\frac{1}{\log x_j}$, we have

$$p_i(x_i)(\boldsymbol{x}^{\boldsymbol{A}_i} - 1)\log x_i + p_j(x_j)(\boldsymbol{x}^{\boldsymbol{A}_j} - 1) \geq 0.$$

Proof. The assumption implies

$$\boldsymbol{x}^{\boldsymbol{A}_i + \underline{b}_i \boldsymbol{e}_i} + \boldsymbol{x}^{\bar{b}_i \boldsymbol{e}_i} - \boldsymbol{x}^{(1+\lambda)\boldsymbol{A}_i + \underline{b}_i \boldsymbol{e}_i} - \boldsymbol{x}^{-\lambda \boldsymbol{A}_i + \bar{b}_i \boldsymbol{e}_i} = -\Big(\boldsymbol{x}^{\boldsymbol{A}_j + \underline{b}_j \boldsymbol{e}_j} + \boldsymbol{x}^{\bar{b}_j \boldsymbol{e}_j} - \boldsymbol{x}^{\boldsymbol{A}_j + \bar{b}_j \boldsymbol{e}_j} - \boldsymbol{x}^{\underline{b}_j \boldsymbol{e}_j}\Big),$$

for all $\boldsymbol{x} \in \mathbb{R}^n_{>0}$. Using Lemma 5.5.3, we know $p_i(x_i)(\boldsymbol{x}^{\boldsymbol{A}_i} - 1)\log x_i \geq$ LHS, while plugging in $p_j(x_j)$ yields that LHS is equal to the term in parenthesis in the RHS. □

Another type of condition on the two rows is the following.

Lemma 5.5.8. *For $\boldsymbol{A}_i, \boldsymbol{A}_j \in \mathbb{R}^n$, if there exists $\bar{b}_i > \underline{b}_i$, $\bar{b}_j > \underline{b}_j$, s.t.*

$$\begin{aligned}
\Big\{\boldsymbol{A}_{\setminus i} + \bar{b}_i \boldsymbol{e}_i, \underline{b}_i \boldsymbol{e}_i\Big\} &= \Big\{\boldsymbol{A}_{\setminus j} + \underline{b}_j \boldsymbol{e}_j, \bar{b}_j \boldsymbol{e}_j\Big\} \\
\Big\{\boldsymbol{A}_{\setminus i} + \underline{b}_i \boldsymbol{e}_i, \bar{b}_i \boldsymbol{e}_i\Big\} &= \Big\{\boldsymbol{A}_{\setminus j} + \bar{b}_j \boldsymbol{e}_j, \underline{b}_j \boldsymbol{e}_j\Big\},
\end{aligned}$$

then for $p_i(x_i) = x_i^{-A_{ii}}(x_i^{\bar{b}_i} - x_i^{\underline{b}_i})\frac{1}{\log x_i}$, $p_j(x_j) = x_j^{-A_{jj}}(x_j^{\bar{b}_j} - x_j^{\underline{b}_j})\frac{1}{\log x_j}$ we have

$$p_i(x_i)(\boldsymbol{x}^{\boldsymbol{A}_i} - 1)\log x_i + p_j(x_j)(\boldsymbol{x}^{\boldsymbol{A}_j} - 1) \geq 0, \quad \boldsymbol{x} \in \mathbb{R}^n_{>0}.$$

Proof. The assumption implies

$$\left(\boldsymbol{x}^{\boldsymbol{A}_{\setminus i}+\bar{b}_i\boldsymbol{e}_i}+\boldsymbol{x}^{\underline{b}_i\boldsymbol{e}_i}-\boldsymbol{x}^{\boldsymbol{A}_{\setminus i}+\underline{b}_i\boldsymbol{e}_i}-\boldsymbol{x}^{\bar{b}_i\boldsymbol{e}_i}\right)+\left(\boldsymbol{x}^{\boldsymbol{A}_{\setminus j}+\bar{b}_j\boldsymbol{e}_j}+\boldsymbol{x}^{\underline{b}_j\boldsymbol{e}_j}-\boldsymbol{x}^{\boldsymbol{A}_{\setminus j}+\underline{b}_j\boldsymbol{e}_j}-\boldsymbol{x}^{\bar{b}_j\boldsymbol{e}_j}\right)=0,$$

for all $\boldsymbol{x}\in\mathbb{R}^n_{>0}$. The rest of the proof is by direct calculation after plugging in p_i, p_j. □

Now we have enough preparation to cover all the possible cases when $\boldsymbol{A}$ is effectively 2×2, i.e. it has only A_{ii}, A_{ij}, A_{ji} and A_{jj} as possibly nonzero entries. All the cases in the following proposition together constitute the proof for Theorem 5.3.7.

Proposition 5.5.9. *For two rows of $\boldsymbol{A}$, $\boldsymbol{A}_i,\boldsymbol{A}_j\in\mathbb{R}^n$ with $i\neq j$. Assume $A_{i\ell}=A_{j\ell}=0$ for $\ell\neq i,j$. There exists p_i,p_j s.t. $p_i(x_i)(\boldsymbol{x}^{\boldsymbol{A}_i}-1)\log x_i+p_j(x_j)(\boldsymbol{x}^{\boldsymbol{A}_j}-1)\log x_j\geq 0$ in the following cases with corresponding choices of p_i,p_j.*

(1) $A_{ii},A_{jj}>0$, $A_{ij}A_{ji}\leq A_{ii}A_{jj}$. *The choice of p_i has the following cases.*

(i) $A_{ij},A_{ji}<0$. *Consider $0<a_{ii}\leq A_{ii}$, $0<a_{jj}\leq A_{jj}$, s.t. $A_{ij}A_{ji}=a_{ii}a_{jj}$, and define $\lambda:=\frac{-A_{ji}}{a_{ii}}=\frac{a_{jj}}{-A_{ij}}>0$. Then take*

$$p_i(x_i)=\lambda(1-x_i^{A_{ji}-a_{ii}})\frac{1}{\log x_i},\ \ p_j(x_j)=(1-x_j^{A_{ij}-a_{jj}})\frac{1}{\log x_j};$$

(ii) $A_{ij},A_{ji}>0$. *Consider $0<a_{ii}\leq A_{ii}$, $0<a_{jj}\leq A_{jj}$, s.t. $A_{ij}A_{ji}=a_{ii}a_{jj}$, and define $\lambda:=\frac{A_{ji}}{a_{ii}}=\frac{a_{jj}}{A_{ij}}>0$. Then take*

$$p_i(x_i)=\lambda(x_i^{A_{ji}}-x_i^{-a_{ii}})\frac{1}{\log x_i},\ \ p_j(x_j)=(x_j^{A_{ij}}-x_j^{-a_{jj}})\frac{1}{\log x_j};$$

(iii) $A_{ij}<0,A_{ji}>0$. *Take*

$$p_i(x_i)=x_i^{-A_{ii}}(x_i^{A_{ji}}-1)\frac{1}{\log x_i},\ \ p_j(x_j)=x_j^{-A_{jj}}(1-x_j^{A_{ij}})\frac{1}{\log x_j};$$

(iv) $A_{ij}>0,A_{ji}<0$. *Take*

$$p_i(x_i)=x_i^{-A_{ii}}(1-x_i^{A_{ji}})\frac{1}{\log x_i},\ \ p_j(x_j)=x_j^{-A_{jj}}(x_j^{A_{ij}}-1)\frac{1}{\log x_j}.$$

(v) $A_{ij}=0$. *Take p_i as in Corollary 5.5.5, and $p_j=A_{jj}$:*

$$\begin{cases}p_i(x_i)=\frac{A_{ji}}{A_{ii}}(x_i^{A_{ji}}-x_i^{-A_{ii}})\frac{1}{\log x_i}, & A_{ji}>0;\\ p_i(x_i)=\frac{-A_{ji}}{A_{ii}}(1-x_i^{A_{ji}-A_{ii}})\frac{1}{\log x_i}, & A_{ji}<0.\end{cases}$$

(2) $A_{ii} = 0$, $A_{ij}A_{ji} < 0$, $A_{jj} > |A_{ij}|$.

$$\begin{cases} p_i(x_i) = \frac{A_{jj}-A_{ij}}{A_{ij}}(1 - x_i^{A_{ji}})\frac{1}{\log x_i}, \;\; p_j(x_j) = (1 - x_j^{A_{ij}-a_{jj}})\frac{1}{\log x_j}, & A_{ij} > 0; \\ p_i(x_i) = \frac{A_{jj}+A_{ij}}{-A_{ij}}(x_i^{A_{ji}} - 1)\frac{1}{\log x_i}, \;\; p_j(x_j) = (x_j^{A_{ij}} - x_j^{-a_{jj}})\frac{1}{\log x_j}; & A_{ij} < 0. \end{cases}$$

Proof. Let us first consider (1)-(i) and (1)-(ii) and (2). These cases can be found by considering the condition in Lemma 5.5.7. The condition $\left\{\boldsymbol{A}_i + \underline{b}_i\boldsymbol{e}_i, \overline{b}_i\boldsymbol{e}_i\right\} = \left\{\boldsymbol{A}_j + \underline{b}_j\boldsymbol{e}_j, \overline{b}_j\boldsymbol{e}_j\right\}$ has two possibilities.

(a1) $\boldsymbol{A}_i + \underline{b}_i\boldsymbol{e}_i = \boldsymbol{A}_j + \underline{b}_j\boldsymbol{e}_j$ and $\overline{b}_i\boldsymbol{e}_i = \overline{b}_j\boldsymbol{e}_j$. This implies $\overline{b}_i = \overline{b}_j = 0$, $\underline{b}_i = A_{ji} - A_{ii}$, $\underline{b}_j = A_{ij} - A_{jj}$, and $A_{i\ell} = A_{j\ell}$ for all $\ell \neq i, j$. This corresponds to condition $A_{ii} > A_{ji}$, $A_{jj} > A_{ij}$.

(a2) $\boldsymbol{A}_i + \underline{b}_i\boldsymbol{e}_i = \overline{b}_j\boldsymbol{e}_j$ and $\overline{b}_i\boldsymbol{e}_i = \boldsymbol{A}_j + \underline{b}_j\boldsymbol{e}_j$. This implies $\underline{b}_i = -A_{ii}$, $\underline{b}_j = -A_{jj}$, $\overline{b}_j = A_{ij}$, $\overline{b}_i = A_{ji}$, and $A_{i\ell} = A_{j\ell} = 0$ for all $\ell \neq i, j$. This corresponds to condition $A_{ji} + A_{ii} > 0$, $A_{ij} + A_{jj} > 0$.

The second condition $\left\{(1+\lambda)\boldsymbol{A}_i + \underline{b}_i\boldsymbol{e}_i, -\lambda\boldsymbol{A}_i + \overline{b}_i\right\} = \left\{\boldsymbol{A}_j + \overline{b}_j\boldsymbol{e}_j, \underline{b}_j\boldsymbol{e}_j\right\}$ has two cases as well.

(b1), $(1+\lambda)\boldsymbol{A}_i + \underline{b}_i\boldsymbol{e}_i = \boldsymbol{A}_j + \overline{b}_j\boldsymbol{e}_j$, $-\lambda\boldsymbol{A}_i + \overline{b}_i\boldsymbol{e}_i = \underline{b}_j\boldsymbol{e}_j$. This implies $(1+\lambda)A_{ii} + \underline{b}_i = A_{ji}$, $-\lambda A_{ij} = \underline{b}_j$, $-\lambda A_{ii} + \overline{b}_i = 0$, $(1+\lambda)A_{ij} = A_{jj} + \overline{b}_j$. For $\ell \neq i, j$, then $A_{i\ell} - A_{j\ell} = -\lambda A_{i\ell} = 0$. This corresponds to condition $A_{ji} + (1+2\lambda)A_{ii} > 0$, and $(1+2\lambda)A_{ij} - A_{jj} > 0$.

(b2), $(1+\lambda)\boldsymbol{A}_i + \underline{b}_i\boldsymbol{e}_i = \underline{b}_j\boldsymbol{e}_j$, $-\lambda\boldsymbol{A}_i + \overline{b}_i\boldsymbol{e}_i = \boldsymbol{A}_j + \overline{b}_j\boldsymbol{e}_j$. This implies $(1+\lambda)A_{ii} + \underline{b}_i = 0$, $(1+\lambda)A_{ij} = \underline{b}_j$, $-\lambda A_{ii} + \overline{b}_i = A_{ji}$, $-\lambda A_{ij} = A_{jj} + \overline{b}_j$. For $\ell \neq i, j$, $(1+\lambda)A_{i\ell} = 0$, $-\lambda A_{i\ell} = A_{j\ell}$, which implies $A_{i\ell} = A_{j\ell} = 0$. This corresponds to condition $A_{ji} + (1+2\lambda)A_{ii} > 0$, $-A_{jj} - (1+2\lambda)A_{ij} > 0$.

Now we look at possible combinations for a full cancellation.

For (a1)-(b1), the conditions come down to $\lambda A_{ii} = 0$, $(1+\lambda)A_{ij} = A_{jj}$, and $A_{ii} > A_{ji}$, $A_{jj} > A_{ij}$. $\lambda A_{i\ell} = \lambda A_{j\ell} = 0$. Since $\lambda > 0$, this corresponds to $A_{ii} = 0 > A_{ji}$, $A_{jj} > A_{ij} > 0$, i.e. (2).

For (a1)-(b2), the conditions come down to $\lambda A_{ii} = -A_{ji}$, $\lambda A_{ij} = -A_{jj}$, and $A_{ii} > A_{ji}$, $A_{jj} > A_{ij}$. $(1+\lambda)A_{i\ell} = (1+\lambda)A_{j\ell} = 0$. This implies $A_{ji}, A_{ij} < 0$, while $A_{ii}, A_{jj} > 0$, together with $\frac{A_{ji}}{A_{ii}} = \frac{A_{jj}}{A_{ij}} = -\lambda < 0$.

Considering the fact that we can use Lemma 5.5.1 to take A_{ii} and A_{jj} as lower bounds of actual A_{ii} and A_{jj}, i.e. the a_{ii} and a_{jj} as defined in the statement of the lemma. Therefore, the conditions here can be relaxed to $\lambda A_{ii} \geq -A_{ji}$, $A_{jj} \geq -\lambda A_{ij}$. Therefore $\lambda A_{ii}A_{jj} \geq -A_{ji}A_{jj} \geq \lambda A_{ji}A_{ij}$. This corresponds to (1)-(i).

For (a2)-(b1), the conditions come down to $\lambda A_{ii} = A_{ji}$, $\lambda A_{ij} = A_{jj}$, and $A_{ji} + A_{ii} > 0$, $A_{ij} + A_{jj} > 0$. This implies $A_{ii}, A_{jj}, A_{ij}, A_{ji} > 0$. Together with $\frac{A_{ji}}{A_{ii}} = \frac{A_{jj}}{A_{ij}} = \lambda > 0$. This corresponds to (1)-(ii).

For (a2)-(b2), the conditions come down to $\lambda A_{ii} = 0$, $(1+\lambda)A_{ij} + A_{jj} = 0$, and $A_{ji} + A_{ii} > 0$, $A_{ij} + A_{jj} > 0$. This implies $A_{ji} > A_{ii} = 0$, $A_{jj} > -A_{ij} > 0$. This corresponds to (2).

The cases (1)-(iii) and (1)-(iv) can be found through conditions in Lemma 5.5.8.

The condition $\left\{\boldsymbol{A}_{\setminus i} + \overline{b}_i \boldsymbol{e}_i, \underline{b}_i \boldsymbol{e}_i\right\} = \left\{\boldsymbol{A}_{\setminus j} + \underline{b}_j \boldsymbol{e}_j, \overline{b}_j \boldsymbol{e}_j\right\}$ has two cases.

(c1i). $\boldsymbol{A}_{\setminus i} + \overline{b}_i \boldsymbol{e}_i = \boldsymbol{A}_{\setminus j} + \underline{b}_j \boldsymbol{e}_j$ and $\underline{b}_i \boldsymbol{e}_i = \overline{b}_j \boldsymbol{e}_j$. This implies $\underline{b}_i = \overline{b}_j = 0$ and $\overline{b}_i = A_{ji}$, $\underline{b}_j = A_{ij}$. This corresponds to condition $A_{ji} > 0$ while $A_{ij} < 0$. $A_{i\ell} = A_{j\ell}$ for $\ell \neq i, j$.

(c2i). $\boldsymbol{A}_{\setminus i} + \overline{b}_i \boldsymbol{e}_i = \overline{b}_j \boldsymbol{e}_j$, and $\underline{b}_i \boldsymbol{e}_i = \boldsymbol{A}_{\setminus i} + \underline{b}_j \boldsymbol{e}_j$. This implies $\overline{b}_i = 0$, $\underline{b}_j = 0$, $\underline{b}_i = A_{ji}$, $\overline{b}_j = A_{ij}$. This corresponds to condition $A_{ji} < 0$ and $A_{ij} > 0$. $A_{i\ell} = A_{j\ell} = 0$ for $\ell \neq i, j$.

Then we have corresponding cases (c1j) and (c2j) for the other condition where indices i and j are interchanged. (c1j) implies $\underline{b}_j = \overline{b}_i = 0$ and $\overline{b}_j = A_{ij}$, $\underline{b}_i = A_{ji}$. (c2j) implies $\overline{b}_j = \underline{b}_i = 0$, $\underline{b}_j = A_{ij}$, $\overline{b}_i = A_{ji}$. So we see that the only compatible combinations are (c1i)-(c2j), which corresponds to (1)-(iii), and (c2i)-(c1j), which corresponds to (1)-(iv).

Case (1)-(v) is proved in Corollary 5.5.6. □

5.6 Appendix. Background on storage functions and dissipativity with fixed point dependence.

Due to historical reasons, past dissipativity notions take "a system is dissipative" to mean "a system is dissipative with respect to this specific storage function the origin". Our generalization to use dissipativity for multistability is exactly rooted in observing this, so multistability could be described as "a system is dissipative with respect to storage function s_1 and point x_1, and it is dissipative with respect to storage function s_2 and point x_2 as well". So for us it is important to keep it explicit what point is the system dissipative to. Therefore, in this section we provide a self-contained summary of the foundation of dissipativity with this in mind. This is re-doing what is done in [113] and nicely written in expository format in [77], with only a minor difference that now the reference point is explicitly written for almost all definitions, from dissipativity to storage functions.

We restrict to time-invariant systems (technically, systems where the state transition map satisfies causality, initial state consistency, semigroup property, and time invariance). For example, $\dot{x} = f(x,u)$, $y = h(x,u)$. $u(t) \in \mathbb{U}$ input value space, $u \in \mathcal{U}$ input signal

space, $y(t) \in \mathbb{Y}$ output value space, $y \in \mathcal{Y}$ output signal space, and $x(t) \in \mathbb{X}$ state space. For example, $\mathcal{U}, \mathcal{Y} = L_2$, $\mathbb{X} = \mathbb{R}^n$. For our specific purpose, we may choose $\mathbb{U} = \mathbb{R}^m_{>0}, \mathbb{Y} = \mathbb{R}^p_{>0}, \mathbb{X} = \mathbb{R}^n_{>0}$.

We start with the input/output (i/o) view, since dissipation is the natural generalization of stability from closed systems to open systems. Let G denote the i/o map of input trajectory u to output trajectory y. In order to discuss instability, we need to consider extended spaces $\mathcal{U}_e$ and $\mathcal{Y}_e$, where $\mathcal{U}_e = \{u : P_T u \in \mathcal{U}, T \geq 0\}$, P_T is truncation operator till time T. i/o stable then means bounded input gives bounded output. If we let $\mathcal{K}(G) := \{u \in \mathcal{U} : Gu \in \mathcal{Y}\}$, the set of inputs that produce bounded outputs, then i/o stability is equivalent to $\mathcal{U} = \mathcal{K}(G)$. The i/o definition of **ultimate virtual dissipation (UVD) w.r.t** s is G satisfy, $\int_0^\infty s(u(t), y(t))dt \geq 0$, for all $u \in \mathcal{K}(G)$, i.e. for all inputs that give rise to bounded outputs. G is **weakly dissipative w.r.t** s if $\int_0^T s(u(t), y(t))dt \geq -\beta$ for all T and for all u, for some constant β. G is **dissipative** if $\beta = 0$. .

Now we assume knowledge about the system state. It should be noted that we will restrict state space to a finite-time reachable and controllable set as this makes sense from the input/state/output (i/s/o) perspective. x_1 is reachable from x_0 if there exists a trajectory s.t. $x(0) = x_0$ and $x(T) = x_1$ for some u and some T. x_{-1} is controllable to x_0 if there exists a trajectory s.t. $x(-T) = x_{-1}$ and $x(0) = x_0$ for some u and some T. Thus, reachable to and controllable from forms an equivalence relationship (i.e. denote this by $\rightleftharpoons$, then $x \rightleftharpoons x$, $x_1 \rightleftharpoons x_2$ implies $x_2 \rightleftharpoons x_1$, and $x_1 \rightleftharpoons x_2 \rightleftharpoons x_3$ implies $x_1 \rightleftharpoons x_3$). Denote $[x]$ as the equivalence class of states that are reachable from and controllable to x.

Dissipativity w.r.t. s **at** x_0 is $\int_0^T s(u(t), y(t))dt \geq 0$ along all state trajectories starting from x_0. **Weak dissipativity w.r.t** s **at** x_0 is that there is a uniform lower bound for $\int_0^T s(u(t), y(t))dt \geq -\beta$ along any state trajectories starting from x_0.

Note that, in contrast to the i/o definition, dissipativity with state description is relative to one specific state x_0. This hinders the connection between i/o definitions and state definitions. i/o notions are unaware of the initial condition of the system. However, given dissipativity w.r.t one state x_0, we can deduce properties about other states. For example, if a system G is dissipative w.r.t s at x_0 then it is weakly dissipative w.r.t s at x reachable from x_0. This is because all trajectories $x \to *$ could be considered a segment of $x_0 \to x \to *$, where dissipativity implies $S(x \to *) \geq -S(x_0 \to x) =: -\beta$. Here we use $S(x_1 \to x_2)$ as a shorthand to denote the integral of supply rate for a trajectory from x_1 to x_2. So a system is weakly dissipative w.r.t s at x_0 implies it is weakly dissipative w.r.t s at any x reachable from x_0. However, it should be noted that the bound β is $\beta(x)$, which depend on the state chosen and may not have a uniform lower bound.

This is a complication that we would like to avoid. The good news is that cyclodissipativity side-steps this. Definition of **cyclodissipativity w.r.t.** s **at** x_0 is that $\int_0^T s(u(t), y(t))dt \geq 0$ along any loop state trajectory ($x(0) = x(T) = x_0$). Let $G(x)$ denote the i/o system corresponding to state system G with initial state x_0. If $G(x_0)$ is cyclodissipative w.r.t s, then $G(x)$ is cyclodissipative w.r.t s for all x that is reachable from and controllable to x_0. Since reachable from and controllable to together defines an equivalence relationship, cyclodissipativity is w.r.t. an equivalence class of states $[x_0]$, instead of one state x. So, if the state space $\mathcal{X}$ of concern is one equivalence class $[x_0]$, then the definition of cyclodissipativity could be relaxed to simply say a system G is **cyclodissipative w.r.t** s if $\int_0^T s(u(t), y(t))dt \geq 0$ along any loop state trajectory s.t. $x(0) = x(T)$.

Dissipativity and cyclodissipativity could be equivalently described in terms of storage functions. A **virtual storage function** w.r.t x_0, $V_{x_0}(x)$, is a scalar-valued function s.t. $V_{x_0}(x(t_1)) - V_{x_0}(x(t_0)) \leq \int_{t_0}^{t_1} s(u(t), y(t))dt$ for all trajectories, and $V_{x_0}(x_0) = 0$ ($V_{x_0}(x_0) = 0$ is needed as trajectories with $t_0 = t_1$ has zero supply as supply is integral of zero length. So this is necessary for required supply and available storage below to be storage functions). A **storage function w.r.t.** x_0, $V_{x_0}(x)$, is a virtual storage function with the additional property that $V_{x_0}(x) \geq 0$ for all x.

Now we define three useful specific (virtual) storage functions. The **required supply** $V_r(x_1; x_0)$ is the smallest supply ($\inf \int sdt$) over all trajectories that go from state x_0 to state x_1. $V_r(x_1; x_0) \leq \infty$ for all x_1 reachable from x_0. If we fix x_0, then we have **required supply w.r.t** x_0: $V_{r,x_0}(x)$. The **virtual available storage** $V_a^*(x_{-1}; x_0)$ is the largest negative supply ($\sup - \int sdt$) to go from x_{-1} to x_0. $V_a^*(x_{-1}; x_0) > -\infty$ for all x_{-1} controllable to x_0. The **available storage** $V_a(x)$ is the largest negative supply to go from x over all future trajectories (leaving end state free). **Note that** $V_a(x)$ **has only one argument, so it is not a relative property but a global property, which can be considered as having a lower bound, or states with "lowest energy".**

Lemma 5.6.1. *Fix supply s. We have the following characterizations:*

(1) An i/s/o system is cyclodissipative at x_0, then $V_a^*(x_0; x_0) = V_r(x_0; x_0) = 0$, and $V_r(x; x_0) \geq V_a^*(x; x_0)$ for all $x \in \mathbb{X}$. In particular, $-\infty < V_a^*(x; x_0) \leq V_r(x; x_0) < \infty$ for all x reachable to and controllable from x_0.

(2) An i/s/o system is dissipative at x_0, then $V_a(x_0) = V_{r,x_0}(x_0) = 0$ and $V_{r,x_0}(x) \geq V_a(x) \geq 0$ for all $x \in \mathbb{X}$. In particular, $0 \leq V_a(x) \leq V_{r,x_0}(x) < \infty$ for all x reachable from x_0.

(3) $V_a^*(\cdot; x_0)$, $V_r(\cdot; x_0)$ are virtual storage functions w.r.t x_0 for systems cyclodissipative at x_0. $V_a(\cdot)$ and $V_{r,x_0}(\cdot)$ are storage functions w.r.t. x_0 for systems dissipative w.r.t x_0.

(4) *An i/s/o system is cyclodissipative at x_0 iff it has $V_{x_0}(x)$, a virtual storage functions w.r.t x_0, s.t. $-\infty < V_{x_0}(x) < \infty$ for all x reachable and controllable from x_0. A system is dissipative w.r.t x_0 iff it has $V_{x_0}(x)$,a storage function w.r.t x_0, s.t. $0 \leq V_{x_0}(x) < \infty$ for all reachable x.*

Proof. (1) Consider trajectories $x(t_0) = x_0$ to $x(t_1) = x_1$ then back to $x(t_2) = x_0$, for x_1 reachable from x_0 and controllable to x_0. Cyclodissipative implies $\int_{t_0}^{t_1} sdt + \int_{t_1}^{t_2} sdt \geq 0$ for all such trajectories. Take infinimum over such trajectories, i.e. $\inf_{x_0 \to x_1}$ and $\inf_{x_1 \to x_0}$, we get $V_r(x_1; x_0) - V_a^*(x_1; x_0) \geq 0$. If we consider $x_1 = x_0$ and $t_0 = t_1 = t_2$, then integral with zero length is zero so $V_a^*(x_0; x_0) = 0$ and $V_r(x_0; x_0) = 0$. Now for x not reachable from (not controllable to) x_0, simply take $V_r(x; x_0)$ ($V_a^*(x; x_0)$) to be $+\infty$ ($-\infty$).

(2) Consider x_1 reachable from x_0, and trajectories $x(t_0) = x_0$, $x(t_1) = x_1$, with $x(t_2)$ arbitrary. Dissipative w.r.t. x_0 implies $\int_{t_0}^{t_1} sdt + \int_{t_1}^{t_2} sdt \geq 0$ for all such trajectories. Take inf over them, i.e. $\inf_{x_0 \to x_1}$ and $\inf_{x_1 \to \star}$, we get $V_r(x_1; x_0) - V_a(x_1) \geq 0$. Now since t_2 and $x(t_2)$ are arbitrary, we can consider $t_2 = t_1$. For this trajectory $\int_{t_1}^{t_2} sdt = 0$, which implies $V_a(x_1) \geq 0$ for all x_1 reachable from x_0. Now consider trajectory $t_0 = t_1 = t_2$ which gives $\int_{t_0}^{t_1} sdt = 0$, implying $V_r(x_0; x_0) \leq 0$. Together with $V_r(x_0; x_0) \geq V_a(x_0) \geq 0$, we have $V_r(x_0; x_0) = V_a(x_0) = 0$. For x not reachable from x_0, $V_r(x; x_0)$ is $+\infty$, so above are still true.

(3) Let's first show $V_r(\cdot; x_0)$ is a virtual storage function for x_0 for systems cyclodissipative w.r.t. x_0. Consider x_1, x_2 reachable by x_0. By definition, $V_r(x_2; x_0) \leq \int_{t_0}^{t_2} sdt = S(x_0 \to x_2)$ for all trajectories going from $x(t_0) = x_0$ to $x(t_2) = x_2$. Consider trajectories that pass through x_1, we have $V_r(x_2; x_0) \leq S(x_0 \to x_1) + S(x_1 \to x_2)$. Therefore $S(x_0 \to x_1) \geq V_r(x_2; x_0) - S(x_1 \to x_2)$. Take inf over the segment $x_0 \to x_1$, we have $V_r(x_1; x_0) \geq V_r(x_2; x_0) - S(x_1 \to x_2)$, which gives the dissipation inequality. Since previous paragraphs already showed $V_r(x_0; x_0) = 0$, we are done. Proof for other cases are similar.

(4) ($\Longrightarrow$) is clear as V_a, V_a^*, V_r works. ($\Longleftarrow$) If we have storage function w.r.t x_0, then any trajectory starting from x_0 satisfies $\int_{t_0}^{t_1} sdt \geq V(x(t_1); x_0) - V(x_0; x_0) = V(x(t_1); x_0) \geq 0$, so it is dissipative. If we have virtual storage function w.r.t x_0, then any loop trajectory starting and ending in x_0 satisfy $\int_{t_0}^{t_1} sdt \geq V(x_0; x_0) - V(x_0; x_0) = 0$.

□

Corollary 5.6.2. *A system is cyclodissipative w.r.t s at x_0 iff it is cyclodissipative w.r.t s at $[x_0]$.*

Proof. Cyclodissipative at x_0 iff there exists a virtual storage function $V_{x_0}(\cdot)$ s.t. $-\infty < V_{x_0}(x) < +\infty$ for all $x \in [x_0]$. For all $x_1 \in [x_0]$, consider loop trajectory starting and ending in x_1, since V_{x_0} is a virtual storage function w.r.t x_0, it satisfies $0 = V_{x_0}(x_1) - V_{x_0}(x_1) \leq \int_{t_0}^{t_1} s dt$, so cyclodissipative w.r.t x_1. □

Remark 5.6.3. Note that since cyclodissipative is w.r.t an equivalence class, we could state the characterizations in the following way: Let $\mathbb{X}_0$ be a reachable-to-controllable-from equivalence class. A system is cyclodissipative w.r.t $\mathbb{X}_0$ then $V_a^*(x_0; x_0) = V_r(x_0; x_0) = 0$ for all $x_0 \in \mathbb{X}_0$, and $-\infty < V_a^*(x; x_0) \leq V_a^*(x; x_0) < +\infty$ for all $x, x_0 \in \mathbb{X}_0 \times \mathbb{X}_0$, and $V_a^*(\cdot; x_0), V_r(\cdot; x_0)$ are virtual storage functions w.r.t x_0 for all $x_0 \in \mathbb{X}_0$.

So virtual storage functions are naturally stated with two arguments comparing two states. From now on, we define $V(x; x')$, $V : \mathbb{X} \times \mathbb{X} \to \mathbb{R}$ as a **virtual storage function** of a state system if $V(x; x) = 0$ for all x, and $V(x(t_1); x') - V(x(t_0); x') \leq \int_{t_0}^{t_1} s(u(t), y(t)) dt$ for all system trajectories. Note that the two arguments of a virtual storage function are not interchangeable, i.e. they are not symmetric. For example, V_a^* and V_r take the two arguments as start and end points of trajectories. In general, trajectories $x_1 \to x_2$ and $x_2 \to x_1$ do not have the same properties. As a another example, we know for all trajectories that go from x_0 to x_1, $V(x_1; x') - V(x_0; x') \leq S(x_0 \to x_1)$. In comparison, $V(x'; x_1) - V(x'; x_0) = (V(x'; x_1) - V(x_1; x_1)) + (V(x_0; x_0) - V(x'; x_0)) \leq S(x_1 \to x') + S(x' \to x_0)$, trajectories from x_1 to x_0 passing through x'. This inequality is not necesssarily true for $S(x_1 \to x_0)$.

In particular, if the state space $\mathbb{X}$ itself is a reachable-to-controllable-from equivalence class, then cyclodissipativity is a global property. Furthermore, this state system is cyclodissipative iff there is a virtual storage function $V(x; x')$. △

We summarize the above discussion into the following corollary.

Corollary 5.6.4. *For a system with controllable and reachable state space $\mathbb{X}$, fix a supply rate s, the following are equivalent:*

(1) it is cyclodissipative at one point in $\mathbb{X}$,

(2) it is cyclodissipative everywhere in $\mathbb{X}$,

(3) there exists a virtual storage function $V(x; x'), V : \mathbb{X} \times \mathbb{X} \to \mathbb{R}$, s.t. $-\infty < V(x; x') < +\infty$ for all $(x, x') \in \mathbb{X} \times \mathbb{X}$.

Remark 5.6.5. Note that the set of virtual storage functions and storage functions form a convex hull, with V_a, V_{r,x_0} and V_a^*, V_r as extreme elements. Namely, $\lambda V_1 + (1 - \lambda) V_2$ is a (virtual) storage function if V_1, V_2 are, for all $\lambda \in [0, 1]$. Also, if $V : \mathbb{X} \to \mathbb{R}$ is a storage

function w.r.t x_0, then $0 \leq V_a(x) \leq V(x) \leq V_{r,x_0}(x)$; if $V : \mathbb{X} \times \mathbb{X} \to \mathbb{R}$ is a virtual storage function, then $V_a^*(x;x') \leq V(x;x') \leq V_r(x;x')$ for all (x,x'). $\triangle$

Remark 5.6.6. Cyclodissipativity is natural for considering multistability, where the whole state space is cyclodissipative, then we show whether some of the points, or some regions, are dissipative (which implies stability), or not dissipative (which implies instability). $\triangle$

The i/o property UVD and the i/s/o property cyclodissipativity are equivalent in some situations. UVD implies cyclodissipativity if there is a constant input that implies non-positive supply; in particular, we translate input coordinate to let the constant input be 0. Cyclodissipativity implies UVD if bounded output implies the state eventually goes back to the initial state.

Lemma 5.6.7 (UVD and cyclodissipativity)**.** *Assume an i/o system G has a state representation Σ with initial condition x_0. Then*

(1) If there exists u^* s.t. $s(u^*, y) \leq 0$ for all y, we first shift coordinate such that $u^* = 0$, then UVD implies cyclodissipativity.

(2) If the initial state is the unique steady state, i.e. Σ satisfies $x(t) \to x_0$ as $t \to \infty$ for all trajectories with $u \in \mathcal{K}(G)$, then cyclodissipativity implies UVD.

Proof. (1) UVD means, for all $u \in \mathcal{K}(G)$, $\int_{t_0}^{\infty} s(u(t), y(t))dt \geq 0$. Consider any $x(t_0) = x_0$, and any u that brings x_0 back to $x(t_1) = x_0$, with $u(t) = 0$ for all $t > t_1$, then, $\int_{t_0}^{t_1} s(u(t), y(t))dt = \int_{t_0}^{\infty} s(u(t), y(t))dt - \int_{t_1}^{\infty} s(0, y(t))dt \geq \int_{t_0}^{\infty} s(u(t), y(t))dt \geq 0$, where the last inequality is because such u has finite support on $[t_0, t_1]$ so it is in $\mathcal{K}(G)$, so UVD property implies the inequality. Since x_0 is arbitrary, any loop satisfies the above, and therefore the system is cyclodissipative.

(2) Let the state system with initial condition x_0 be the state representation of G. Then cyclodissipativity implies $\int_{t_0}^{t_1} sdt \geq 0$ for any loop trajectory from x_0 back to x_0. Consider any trajectory with $u \in \mathcal{K}(G)$; by assumption we know $x(t_1) \to x_0$ as $t_1 \to \infty$, so there are loop trajectories infinitely close to this trajectory, so taking the limit we get $\int_{t_0}^{t_1} sdt \geq 0$, cyclodissipative implies UVD.

$\square$

Now we are ready to state how stability and instability are related to cyclodissipativity and dissipativity.

Theorem 5.6.8 (Cyclodissipative, dissipative and stability)**.** *We have the following conclusions.*

(1) Assume there exists u^*, y^* s.t. supply rate $s(u^*, y) < 0$ for all $y \neq y^*$, and $s(u^*, y^*) = 0$.

Then i/o system G is (weakly) dissipative $\implies$ G is (weakly) i/o stable (finite gain).

Assume steady state detection (SSD) condition that $y(t) = y^*$ for some interval $t \in [t_0, t_1]$ implies $x(t_0) = x^*$. Then i/s/o system G is dissipative w.r.t x^* $\implies$ x^* is asymptotically stable.

(2) Assume supply rate $s(0, y) \leq 0$. Assume i/o system G is causal and UVD.

Then G is i/o stable $\implies$ G is dissipative.

Contrapositive: G is not dissipative $\implies$ G is not i/o stable.

(3) Assume there exists u^* s.t. supply rate $s(u^*, y) \leq 0$ for all y. Assume i/s/o system G is cyclodissipative w.r.t $[x^*]$.

Then x^* is asymptotically stable $\implies$ G is dissipative w.r.t x^*.

Contrapositive: G is not dissipative w.r.t x^* $\implies$ x^* is not asymptotically stable.

Proof. (1) Consider i/s/o system G, and any trajectory $x(t_0)$ to $x(t_1)$. Dissipative w.r.t x^* means there exists storage function w.r.t x^*, V, s.t. $V(x(t_1)) - V(x(t_0)) \leq \int_{t_0}^{t_1} s(u, y)dt$. Take $u(t) = u^*$ for $t \geq t_0$, then $V(x(t_1)) - V(x(t_0)) \leq \int_{t_0}^{t_1} s(u^*, y)dt \leq 0$, so V is non-increasing along any trajectory. Since V is a storage function, it is lower bounded, so it will always go to a limit asymptotically. Let the limit be V_f, we see that for trajectory starting in any state x_f achieving $V(x_f) = V_f$, $0 = V_f - V_f \leq \int_{t_0}^{t_1} s(u^*, y(t))dt$, which together with $s(u^*, y) \leq 0$ with equality only achieved at y^* indicates that $y(t) = y^*$ for $t \geq t_0$. By SSD,this means $x(t_0) = x_f = x^*$.

(2) For all $u \in \mathcal{U}_e$, $P_T u \in \mathcal{K}(G)$, where P_T is truncation operator setting $u(t) = 0$ for $t > T$. So UVD implies $\int_0^\infty s(P_T u, GP_T u)dt \geq 0$. G is causal, i.e. $P_T G P_T = P_T G$, so $\int_0^T s(u, Gu)dt = \int_0^T s(P_T u, P_T Gu)dt = \int_0^T s(P_T u, P_T GP_T u)dt = \int_0^T s(P_T u, GP_T u)dt = \int_0^\infty s(P_T u, GP_T u)dt - \int_T^\infty s(0, GP_T u)dt \geq \int_0^\infty s(P_T u, GP_T u)dt \geq 0$, where second to last inequality is by $s(0, y) \leq 0$.

(3) Take any trajectory, G is cyclodissipative means there exists virtual storage function $V(x; x')$, s.t. $V(x(t_1); x') - V(x(t_0); x') \leq \int_{t_0}^{t_1} s(u, y)dt$. Consider $u(t) = u^*$ for $t \geq t_0$, then $V(x(t_1); x') - V(x(t_0); x') \leq \int_{t_0}^{t_1} s(u^*; y)dt \leq 0$, so $V(x(t); x')$ is non-increasing. Since x^* is asymptotically, take $x' = x^*$ and $t_1 \to \infty$, with $V(x^*; x^*) = 0$ for virtual storage functions we get $V(x(t_0); x^*) \geq 0$. Since this is true for any $x(t_0)$, we get that $V(\cdot; x^*)$ is a storage function w.r.t x^*.

□

Bibliography

[1] Leonard Adleman et al. "On the Mathematics of the Law of Mass Action". In: *A Systems Theoretic Approach to Systems and Synthetic Biology I: Models and System Characterizations*. Ed. by Vishwesh V. Kulkarni, Guy-Bart Stan, and Karthik Raman. Dordrecht: Springer Netherlands, 2014, pp. 3–46. ISBN: 978-94-017-9041-3. DOI: 10.1007/978-94-017-9041-3_1. URL: https://doi.org/10.1007/978-94-017-9041-3_1.

[2] Kathy R. Albe, Margaret H. Butler, and Barbara E. Wright. "Cellular concentrations of enzymes and their substrates". In: *Journal of Theoretical Biology* 143.2 (1990), pp. 163–195. ISSN: 0022-5193. DOI: https://doi.org/10.1016/S0022-5193(05)80266-8. URL: http://www.sciencedirect.com/science/article/pii/S0022519305802668.

[3] Elisabetta de Alteriis et al. "Revisiting the Crabtree/Warburg effect in a dynamic perspective: a fitness advantage against sugar-induced cell death". In: *Cell Cycle* 17.6 (2018). PMID: 29509056, pp. 688–701. DOI: 10.1080/15384101.2018.1442622. eprint: https://doi.org/10.1080/15384101.2018.1442622. URL: https://doi.org/10.1080/15384101.2018.1442622.

[4] Carmen Amo Alonso, Nikolai Matni, and James Anderson. "Explicit Distributed and Localized Model Predictive Control via System Level Synthesis". In: *IEEE Conference on Decision and Control* (2020).

[5] Carmen Amo Alonso and Shih-Hao Tseng. "Effective GPU Parallelization of Distributed and Localized Model Predictive Control". In: Submitted to *Proceedings of the 60th IEEE Conference on Decision and Control*. IEEE. 2021.

[6] Carmen Amo Alonso et al. "Distributed and Localized Model Predictive Control. Part I: Synthesis and Implementation". In: (2021). Submitted. URL: http://arxiv.org/abs/2110.07010.

[7] David Anderson. "Stochastic analysis of biochemical reaction networks with absolute concentration robustness. Lecture conducted from University of Utah, Salt Lake City, UT." In: (Jan. 2014).

[8] James Anderson et al. "System level synthesis". In: *Annual Reviews in Control* 47 (2019), pp. 364–393. ISSN: 13675788. DOI: 10.1016/j.arcontrol.2019.03.006. arXiv: arXiv:1904.01634v1.

[9] Yaron E. Antebi et al. "Combinatorial Signal Perception in the BMP Pathway". In: *Cell* 170.6 (2017), 1184–1196.e24. ISSN: 0092-8674. DOI: https://doi.org/10.1016/j.cell.2017.08.015. URL: https://www.sciencedirect.com/science/article/pii/S0092867417309406.

[10] Stephanie K. Aoki et al. "A universal biomolecular integral feedback controller for robust perfect adaptation". In: *Nature* 570.7762 (June 2019), pp. 533–537. ISSN: 1476-4687.

[11] Murat Arcak, Chris Meissen, and Andrew Packard. *Networks of Dissipative Systems. Compositional Certification of Stability, Performance, and Safety*. Springer, 2011. DOI: 10.1007/978-3-319-29928-0.

[12] Karl J. Åström and Richard M. Murray. *Feedback Systems: An Introduction for Scientists and Engineers*. second. Princeton University Press, 2020. URL: https://fbswiki.org.

[13] Daniel E. Atkinson. "Biochemical Function and Homeostasis: The Payoff of the Genetic Program". In: *Control Mechanisms in Development: Activation, Differentiation, and Modulation in Biological Systems*. Ed. by Russel H. Meints and Eric Davies. New York, NY: Springer US, 1975, pp. 193–211. ISBN: 978-1-4684-3255-8. DOI: 10.1007/978-1-4684-3255-8_11. URL: https://doi.org/10.1007/978-1-4684-3255-8_11.

[14] David Avis, David Bremner, and Raimund Seidel. "How good are convex hull algorithms?" In: *Computational Geometry* 7.5 (1997). 11th ACM Symposium on Computational Geometry, pp. 265–301. ISSN: 0925-7721. DOI: https://doi.org/10.1016/S0925-7721(96)00023-5. URL: https://www.sciencedirect.com/science/article/pii/S0925772196000235.

[15] Tomáš Bajbar and Oliver Stein. "Coercive polynomials: stability, order of growth, and Newton polytopes". In: *Optimization* 68.1 (2019), pp. 99–124.

[16] Martin Bier et al. "Control analysis of glycolytic oscillations". In: *Biophysical chemistry* 62.1-3 (1996), pp. 15–24.

[17] Alex Blokhuis, David Lacoste, and Philippe Nghe. "Universal motifs and the diversity of autocatalytic systems". In: *Proceedings of the National Academy of Sciences* 117.41 (2020), pp. 25230–25236. DOI: 10.1073/pnas.2013527117. eprint: https://www.pnas.org/doi/pdf/10.1073/pnas.2013527117. URL: https://www.pnas.org/doi/abs/10.1073/pnas.2013527117.

[18] Richard Blumberg and Fiona Powrie. "Microbiota, disease, and back to health: a metastable journey". In: *Science translational medicine* 4.137 (2012), 137rv7–137rv7.

[19] A. Bordbar. "Utilizing genome-scale models to enhance high-throughput data analysis : from pathways to dynamics". PhD thesis. UC San Diego, 2014.

[20] Francesco Borrelli, Alberto Bemporad, and Manfred Morari. *Predictive Control for Linear and Hybrid Systems*. Cambridge University Press, 2017. ISBN: 9781139061759. DOI: 10.1017/9781139061759.

[21] Stephen Boyd and Craig Barratt. *Linear controller design: limits of performance*. Prentice-Hall, 1991. URL: https://web.stanford.edu/~boyd/lcdbook/.

[22] Corentin Briat, Ankit Gupta, and Mustafa Khammash. "Antithetic Integral Feedback Ensures Robust Perfect Adaptation in Noisy Biomolecular Networks". In: *Cell Systems* 2.1 (2016), pp. 15–26. ISSN: 2405-4712.

[23] George Edward Briggs and John Burdon Sanderson Haldane. "A Note on the Kinetics of Enzyme Action". In: *Biochemical Journal* 19.2 (Jan. 1925), pp. 338–339. ISSN: 0006-2936. DOI: 10.1042/bj0190338. eprint: https://portlandpress.com/biochemj/article-pdf/19/2/338/773028/bj0190338.pdf. URL: https://doi.org/10.1042/bj0190338.

[24] Daniele Cappelletti et al. "Stochastic chemical reaction networks for robustly approximating arbitrary probability distributions". In: *Theoretical Computer Science* 801 (2020), pp. 64–95. ISSN: 0304-3975.

[25] Fiona A Chandra, Gentian Buzi, and John C Doyle. "Glycolytic oscillations and limits on robust efficiency". In: *Science* 333.6039 (2011), pp. 187–192.

[26] *chémeo website on high quality data of chemical properties*. https://www.chemeo.com. Accessed: 2022-05-10.

[27] Long-Qing Chen. "Chemical potential and Gibbs free energy". In: *MRS Bulletin* 44.7 (2019), pp. 520–523. DOI: 10.1557/mrs.2019.162.

[28] Boseung Choi, Grzegorz A. Rempala, and Jae Kyoung Kim. "Beyond the Michaelis-Menten equation: Accurate and efficient estimation of enzyme kinetic parameters". In: *Scientific Reports* 7.1 (Dec. 2017), p. 17018. ISSN: 2045-2322. DOI: 10.1038/s41598-017-17072-z. URL: https://doi.org/10.1038/s41598-017-17072-z.

[29] Thomas F Coleman and Alex Pothen. "The Null Space Problem I. Complexity". In: *SIAM J. Algebraic Discrete Methods* 7.4 (Oct. 1986), pp. 527–537. ISSN: 0196-5212. DOI: 10.1137/0607059. URL: https://doi.org/10.1137/0607059.

[30] Athel Cornish-Bowden. *Fundamentals of Enzyme Kinetics*. Berlin: Wiley-Blackwell, 2012.

[31] Domitilla Del Vecchio and Richard M Murray. *Biomolecular feedback systems*. Princeton University Press Princeton, NJ, 2015.

[32] Domitilla Del Vecchio, Alexander J Ninfa, and Eduardo D Sontag. "Modular cell biology: retroactivity and insulation". In: *Molecular Systems Biology* 4.1 (2008), p. 161. DOI: 10.1038/msb4100204. eprint: https://www.embopress.org/doi/pdf/10.1038/msb4100204. URL: https://www.embopress.org/doi/abs/10.1038/msb4100204.

[33] Suzanne Devkota et al. "Dietary-fat-induced taurocholic acid promotes pathobiont expansion and colitis in Il10-/- mice". In: *Nature* 487.7405 (July 2012), pp. 104–108. ISSN: 1476-4687. DOI: 10.1038/nature11225. URL: https://doi.org/10.1038/nature11225.

[34] Alicia Dickenstein et al. "Multistationarity in Structured Reaction Networks". In: *Bulletin of Mathematical Biology* 81.5 (May 2019), pp. 1527–1581. ISSN: 1522-9602.

[35] Ken A. Dill and Sarina Bromberg. *Molecular Driving Forces: Statistical Thermodynamics in Biology, Chemistry, Physics, and Nanoscience*. 2nd. Garland Science, 2010. ISBN: 978-0815344308.

[36] David Doty and Shaopeng Zhu. *Computational Complexity of Atomic Chemical Reaction Networks*. 2017. arXiv: 1702.05704 [cs.CC].

[37] David Doty and Shaopeng Zhu. "Computational complexity of atomic chemical reaction networks". In: *Natural Computing* 17.4 (Dec. 2018), pp. 677–691. ISSN: 1572-9796. DOI: 10.1007/s11047-018-9687-9. URL: https://doi.org/10.1007/s11047-018-9687-9.

[38] John C. Doyle and Marie Csete. "Architecture, constraints, and behavior". In: *Proceedings of the National Academy of Sciences* 108.Supplement 3 (2011), pp. 15624–15630. ISSN: 0027-8424. DOI: 10.1073/pnas.1103557108. eprint: https://www.pnas.org/content/108/Supplement_3/15624.full.pdf. URL: https://www.pnas.org/content/108/Supplement_3/15624.

[39] John C. Doyle, Bruce A. Francis, and Allen R. Tannenbaum. *Feedback Control Theory*. Dover Publications, 2009.

[40] Peter G. Doyle and J. Laurie Snell. *Random Walks and Electric Networks*. 2000. arXiv: math/0001057 [math.PR].

[41] Geir E. Dullerud and Fernando Paganini. *A Course in Robust Control Theory: A Convex Approach*. Springer New York, NY, 2000.

[42] David W Erickson et al. "A global resource allocation strategy governs growth transition kinetics of Escherichia coli". In: *Nature* 551.7678 (2017), pp. 119–123.

[43] H. Fawzi. "Power and limitations of convex formulations via linear and semidefinite programming lifts". PhD thesis. Massachusetts Institute of Technology, 2016.

[44] Martin Feinberg. *Foundations of Chemical Reaction Network Theory*. Springer, 2020. DOI: 10.1007/978-3-030-03858-8.

[45] Fulvio Forni and Rodolphe Sepulchre. "Differential Dissipativity Theory for Dominance Analysis". In: *IEEE Transactions on Automatic Control* 64.6 (2019), pp. 2340–2351. DOI: 10.1109/TAC.2018.2867920.

[46] Xiaojing J. Gao et al. "Programmable protein circuits in living cells". In: *Science* 361.6408 (2018), pp. 1252–1258. DOI: 10.1126/science.aat5062. eprint: https://www.science.org/doi/pdf/10.1126/science.aat5062. URL: https://www.science.org/doi/abs/10.1126/science.aat5062.

[47] Timothy S. Gardner, Charles R. Cantor, and James J. Collins. "Construction of a genetic toggle switch in Escherichia coli". In: *Nature* 403.6767 (Jan. 2000), pp. 339–342. ISSN: 1476-4687. DOI: 10.1038/35002131. URL: https://doi.org/10.1038/35002131.

[48] R. Garrett and C. M. Grisham. *Biochemistry*. 3rd. Thomson Brooks/Cole., Belmont, CA, 2005. ISBN: 978-0-534-49033-1.

[49] A Ghosh and Britton Chance. "Oscillations of glycolytic intermediates in yeast cells". In: *Biochemical and biophysical research communications* 16.2 (1964), pp. 174–181.

[50] Gilles Gnacadja. "Reachability, persistence, and constructive chemical reaction networks (part II): a formalism for species composition in chemical reaction network theory and application to persistence". In: *Journal of Mathematical Chemistry* 49.10 (Sept. 2011), p. 2137. ISSN: 1572-8897. DOI: 10.1007/s10910-011-9896-2. URL: https://doi.org/10.1007/s10910-011-9896-2.

[51] Albert Goldbeter. *Biochemical oscillations and cellular rhythms: the molecular bases of periodic and chaotic behaviour*. Cambridge university press, 1997.

[52] Lee-Ad Gottlieb and Tyler Neylon. "Matrix Sparsification and the Sparse Null Space Problem". In: *Algorithmica* 76.2 (Oct. 2016), pp. 426–444. ISSN: 1432-0541. DOI: 10.1007/s00453-015-0042-6. URL: https://doi.org/10.1007/s00453-015-0042-6.

[53] Jeremy Gunawardena. "A Linear Framework for Time-Scale Separation in Nonlinear Biochemical Systems". In: *PLOS ONE* 7.5 (May 2012), pp. 1–14. DOI: 10.1371/journal.pone.0036321. URL: https://doi.org/10.1371/journal.pone.0036321.

[54] Jeremy Gunawardena. "Biology is more theoretical than physics". In: *Molecular Biology of the Cell* 24.12 (2013). PMID: 23765269, pp. 1827–1829. DOI: 10.1091/mbc.e12-03-0227. eprint: https://doi.org/10.1091/mbc.e12-03-0227. URL: https://doi.org/10.1091/mbc.e12-03-0227.

[55] Jeremy Gunawardena. "Chemical Reaction Network Theory for in-silico biologists". In: (203). URL: http://vcp.med.harvard.edu/papers/crnt.pdf.

[56] Jeremy Gunawardena. "Models in biology: 'accurate descriptions of our pathetic thinking'". In: *BMC Biology* 12.1 (Apr. 2014), p. 29. ISSN: 1741-7007. DOI: 10.1186/1741-7007-12-29. URL: https://doi.org/10.1186/1741-7007-12-29.

[57] Jeremy Gunawardena. "Time-scale separation – Michaelis and Menten's old idea, still bearing fruit". In: *The FEBS Journal* 281.2 (2014), pp. 473–488. DOI: 10.1111/febs.12532. eprint: https://febs.onlinelibrary.wiley.com/doi/pdf/10.1111/febs.12532. URL: https://febs.onlinelibrary.wiley.com/doi/abs/10.1111/febs.12532.

[58] "Hard Limits and Performance Tradeoffs in a Class of Antithetic Integral Feedback Networks". In: *Cell Systems* 9.1 (2019), 49–63.e16. ISSN: 2405-4712. DOI: https://doi.org/10.1016/j.cels.2019.06.001. URL: https://www.sciencedirect.com/science/article/pii/S2405471219301966.

[59] Franklin Harold. *The Vital Force. A Study of Bioenergetics*. W.H. Freeman, 1986. ISBN: 978-0716717348.

[60] Laurent Heirendt et al. "Creation and analysis of biochemical constraint-based models using the COBRA Toolbox v.3.0". In: *Nature Protocols* 14.3 (Mar. 2019), pp. 639–702. ISSN: 1750-2799. DOI: 10.1038/s41596-018-0098-2. URL: https://doi.org/10.1038/s41596-018-0098-2.

[61] Martin Herceg et al. "Multi-Parametric Toolbox 3.0". In: *2013 European Control Conference (ECC)*. 2013, pp. 502–510. DOI: 10.23919/ECC.2013.6669862.

[62] Joris van der Hoeven and Grégoire Lecerf. "On the Complexity Exponent of Polynomial System Solving". In: *Foundations of Computational Mathematics* 21.1 (Feb. 2021), pp. 1–57. ISSN: 1615-3383. DOI: 10.1007/s10208-020-09453-0. URL: https://doi.org/10.1007/s10208-020-09453-0.

[63] Kenneth A. Johnson and Roger S. Goody. "The Original Michaelis Constant: Translation of the 1913 Michaelis–Menten Paper". In: *Biochemistry* 50.39 (Oct. 2011), pp. 8264–8269. ISSN: 0006-2960. DOI: 10.1021/bi201284u. URL: https://doi.org/10.1021/bi201284u.

[64] Suckjoon Jun et al. "Fundamental principles in bacterial physiology—history, recent progress, and the future with focus on cell size control: a review". In: *Reports on Progress in Physics* 81.5 (Feb. 2018), p. 056601. DOI: 10.1088/1361-6633/aaa628. URL: https://doi.org/10.1088/1361-6633/aaa628.

[65] James Keener and James Sneyd. *Mathematical Physiology I. Cellular Physiology*. Springer-Verlag New York, 2009. DOI: 10.1007/978-0-387-75847-3.

[66] Tahmineh Khazaei et al. "Metabolic multistability and hysteresis in a model aerobe-anaerobe microbiome community". In: *Science Advances* 6.33 (2020). DOI: 10.1126/sciadv.aba0353. eprint: https://advances.sciencemag.org/content/6/33/eaba0353.full.pdf. URL: https://advances.sciencemag.org/content/6/33/eaba0353.

[67] Zhi Y Kho and Sunil K Lal. "The human gut microbiome–a potential controller of wellness and disease". In: *Frontiers in microbiology* 9 (2018), p. 1835.

[68] Joshua Ladau and Emiley A Eloe-Fadrosh. "Spatial, temporal, and phylogenetic scales of microbial ecology". In: *Trends in microbiology* 27.8 (2019), pp. 662–669.

[69] Yoke Peng Leong and John C. Doyle. "Effects of Delays, Poles, and Zeros on Time Domain Waterbed Tradeoffs and Oscillations". In: *IEEE Control Systems Letters* 1.1 (2017), pp. 122–127. DOI: 10.1109/LCSYS.2017.2710327.

[70] Yoke Peng Leong and John C. Doyle. "Understanding robust control theory via stick balancing". In: *2016 IEEE 55th Conference on Decision and Control (CDC)*. 2016, pp. 1508–1514. DOI: 10.1109/CDC.2016.7798480.

[71] Jing Shuang Li. "Internal Feedback in Biological Control: Locality and System Level Synthesis". In: (). To appear in IEEE American Control Conference 2022. URL: https://arxiv.org/abs/2109.11757.

[72] Milo M. Lin. "Circuit Reduction of Heterogeneous Nonequilibrium Systems". In: *Phys. Rev. Lett.* 125 (21 Nov. 2020), p. 218101. DOI: 10.1103/PhysRevLett.125.218101. URL: https://link.aps.org/doi/10.1103/PhysRevLett.125.218101.

[73] David Q. Mayne. "Model predictive control: Recent developments and future promise". In: *Automatica* 50.12 (2014), pp. 2967–2986. ISSN: 0005-1098. DOI: https://doi.org/10.1016/j.automatica.2014.10.128. URL: https://www.sciencedirect.com/science/article/pii/S0005109814005160.

[74] David H McNear Jr. "The rhizosphere-roots, soil and everything in between". In: *Nature Education Knowledge* 4.3 (2013), p. 1.

[75] Ron Milo and Rob Phillips. *Cell Biology by the numbers*. Garland Science, New York, 2015. ISBN: 9780429258770. DOI: 10.1201/9780429258770.

[76] Inomzhon Mirzaev and Jeremy Gunawardena. "Laplacian Dynamics on General Graphs". In: *Bulletin of Mathematical Biology* 75.11 (Nov. 2013), pp. 2118–2149. ISSN: 1522-9602. DOI: 10.1007/s11538-013-9884-8. URL: https://doi.org/10.1007/s11538-013-9884-8.

[77] Peter Moylan. "Dissipative systems and stability". In: *Lecture Notes in collaboration with D. Hill, University of Newcastle, www.pmoylan.org* (2014).

[78] Riley Murray, Venkat Chandrasekaran, and Adam Wierman. "Newton Polytopes and Relative Entropy Optimization". In: *Foundations of Computational Mathematics* 21.6 (Dec. 2021), pp. 1703–1737. ISSN: 1615-3383. DOI: 10.1007/s10208-021-09497-w. URL: https://doi.org/10.1007/s10208-021-09497-w.

[79] Yorie Nakahira et al. "Diversity-enabled sweet spots in layered architectures and speed accuracy trade-offs in sensorimotor control". In: *Proceedings of the National Academy of Sciences* 118.22 (2021), e1916367118. DOI: 10.1073/pnas.1916367118. eprint: https://www.pnas.org/doi/pdf/10.1073/pnas.1916367118. URL: https://www.pnas.org/doi/abs/10.1073/pnas.1916367118.

[80] Yorie Nakahira et al. "Fitts' Law for speed-accuracy trade-off describes a diversity-enabled sweet spot in sensorimotor control". In: *arXiv* (2019). arXiv: 1906.00905 [eess.SP].

[81] Bastian Niebel, Simeon Leupold, and Matthias Heinemann. "An upper limit on Gibbs energy dissipation governs cellular metabolism". In: *Nature Metabolism* 1.1 (Jan. 2019), pp. 125–132. ISSN: 2522-5812. DOI: 10.1038/s42255-018-0006-7. URL: https://doi.org/10.1038/s42255-018-0006-7.

[82] Venant Nihorimbere et al. "Beneficial effect of the rhizosphere microbial community for plant growth and health." In: *Biotechnologie, Agronomie, Société et Environnement* 15.2 (2011), pp. 327–337.

[83] Noah Olsman, Fangzhou Xiao, and John C. Doyle. "Architectural Principles for Characterizing the Performance of Antithetic Integral Feedback Networks". In: *iScience* 14 (2019), pp. 277–291. ISSN: 2589-0042. DOI: https://doi.org/10.1016/

j.isci.2019.04.004. URL: https://www.sciencedirect.com/science/article/pii/S2589004219301014.

[84] Jeffrey D. Orth, Ines Thiele, and Bernhard Ø Palsson. "What is flux balance analysis?" In: *Nature Biotechnology* 28.3 (Mar. 2010), pp. 245–248. ISSN: 1546-1696. DOI: 10.1038/nbt.1614. URL: https://doi.org/10.1038/nbt.1614.

[85] Bernhard Ø. Palsson. *Systems Biology: Constraint-based Reconstruction and Analysis*. STU - Student edition. Cambridge University Press, 2015. ISBN: 9781107038851.

[86] Pablo Parrilo. "Structured semidefinite programs and semialgebraic geometry methods in robustness and optimization". PhD thesis. California Institute of Technology, 2000.

[87] Johan Paulsson. "Models of stochastic gene expression". In: *Physics of Life Reviews* 2 (2005), pp. 157–175.

[88] Rob Phillips. *The Molecular Switch: Signaling and Allostery*. Princeton University Press, 2020.

[89] Rob Phillips et al. *Physical biology of the cell*. Garland Science, 2012.

[90] Lulu Qian, David Soloveichik, and Erik Winfree. "Efficient Turing-Universal Computation with DNA Polymers". In: *DNA Computing and Molecular Programming*. Ed. by Yasubumi Sakakibara and Yongli Mi. Berlin, Heidelberg: Springer Berlin Heidelberg, 2011, pp. 123–140. ISBN: 978-3-642-18305-8.

[91] Manuel Razo-Mejia et al. "Tuning Transcriptional Regulation through Signaling: A Predictive Theory of Allosteric Induction". In: *Cell Systems* 6.4 (Apr. 2018), 456–469.e10. ISSN: 2405-4712. DOI: 10.1016/j.cels.2018.02.004. URL: https://doi.org/10.1016/j.cels.2018.02.004.

[92] Anjan Roy, Dotan Goberman, and Rami Pugatch. "A unifying autocatalytic network-based framework for bacterial growth laws". In: *Proceedings of the National Academy of Sciences* 118.33 (2021), e2107829118. DOI: 10.1073/pnas.2107829118. eprint: https://www.pnas.org/doi/pdf/10.1073/pnas.2107829118. URL: https://www.pnas.org/doi/abs/10.1073/pnas.2107829118.

[93] AmirHosein Sadeghimanesh and Elisenda Feliu. "The Multistationarity Structure of Networks with Intermediates and a Binomial Core Network". In: *Bulletin of Mathematical Biology* 81.7 (July 2019), pp. 2428–2462. ISSN: 1522-9602.

[94] *SageMath website*. https://www.sagemath.org/. Accessed: 2022-06-07.

[95] Mark Sagoff. "Data deluge and the human microbiome project". In: *Issues in Science and Technology* 28.4 (2012), pp. 71–78.

[96] Anish A. Sarma et al. "Internal Feedback in Biological Control: Architectures and Examples". In: (). To appear in IEEE American Control Conference 2022. URL: https://arxiv.org/abs/2110.05029.

[97] Michael A. Savageau. *Biochemical systems analysis. A study of function and design in molecular biology*. English (US). ADDISON WESLEY, 1976.

[98] Thomas H Segall-Shapiro, Eduardo D Sontag, and Christopher A Voigt. "Engineered promoters enable constant gene expression at any copy number in bacteria". en. In: *Nat Biotechnol* 36.4 (Mar. 2018), pp. 352–358.

[99] Maria M. Seron, Julio H. Braslavsky, and Graham C. Goodwin. *Fundamental limitations in filtering and control*. Springer, 1997. ISBN: 978-3-4471-1244-0.

[100] Andrew B Shreiner, John Y Kao, and Vincent B Young. "The gut microbiome in health and in disease". In: *Current opinion in gastroenterology* 31.1 (2015), p. 69.

[101] VP Singh, Spencer D Proctor, and Ben P Willing. "Koch's postulates, microbial dysbiosis and inflammatory bowel disease". In: *Clinical Microbiology and Infection* 22.7 (2016), pp. 594–599.

[102] Aivar Sootla and James Anderson. "Structured Projection-Based Model Reduction With Application to Stochastic Biochemical Networks". In: *IEEE Transactions on Automatic Control* 62.11 (2017), pp. 5554–5566. DOI: 10.1109/TAC.2017.2691315.

[103] Sonia Stefanovic et al. "Interplay of Oct4 with Sox2 and Sox17: a molecular switch from stem cell pluripotency to specifying a cardiac fate". In: *Journal of Cell Biology* 186.5 (Sept. 2009), pp. 665–673. ISSN: 0021-9525. DOI: 10.1083/jcb.200901040. eprint: https://rupress.org/jcb/article-pdf/186/5/665/1343246/jcb_200901040.pdf. URL: https://doi.org/10.1083/jcb.200901040.

[104] G. Stein. "Respect the unstable". In: *IEEE Control Systems Magazine* 23.4 (2003), pp. 12–25. DOI: 10.1109/MCS.2003.1213600.

[105] Josefin Stenberg et al. "Internal Feedback in Biological Control: Diversity, Delays, and Standard Theory". In: (). To appear in IEEE American Control Conference 2022. URL: http://arxiv.org/abs/2109.11752.

[106] Urs von Stockar. "Biothermodynamics of live cells: a tool for biotechnology and biochemical engineering". In: *Journal of Non-equilibrium Thermodynamics* 35.4 (2010), pp. 415–475. DOI: doi:10.1515/jnetdy.2010.024.

[107] M. E. Stroppolo et al. "Superefficient enzymes". In: *Cellular and Molecular Life Sciences CMLS* 58.10 (Sept. 2001), pp. 1451–1460. ISSN: 1420-9071. DOI: 10.1007/PL00000788. URL: https://doi.org/10.1007/PL00000788.

[108] A.R. Tzafriri. "Michaelis–Menten kinetics at high enzyme concentrations". In: *Bulletin of Mathematical Biology* 65.6 (2003), pp. 1111–1129. ISSN: 0092-8240. DOI: https://doi.org/10.1016/S0092-8240(03)00059-4. URL: http://www.sciencedirect.com/science/article/pii/S0092824003000594.

[109] Eberthard O. Volt, Harald A. Martens, and Stig W. Omholt. "150 Years of the Mass Action Law". In: *PLOS Computational Biology* 11.1 (2015).

[110] Tong Wang et al. "Evidence for a multi-level trophic organization of the human gut microbiome". In: *PLoS computational biology* 15.12 (2019), e1007524.

[111] Y.-S. Wang, Matni. N., and J. C. Doyle. "A system-level approach to controller synthesis". In: *IEEE Transactions on Automatic Control* 64 (10 2019).

[112] Yuh Shyang Wang, Nikolai Matni, and John C. Doyle. "Separable and Localized System-Level Synthesis for Large-Scale Systems". In: *IEEE Transactions on Automatic Control* 63.12 (2018), pp. 4234–4249.

[113] Jan C. Willems. "Dissipative dynamical systems part I: General theory". In: *Archive for Rational Mechanics and Analysis* 45.5 (1972), pp. 321–351. DOI: 10.1007/bf00276493. URL: https://doi.org/10.1007/bf00276493.

[114] Amy D Willis. "Rigorous Statistical Methods for Rigorous Microbiome Science". In: *MSystems* 4.3 (2019).

[115] Richard Wolfenden and Yang Yuan. "Rates of spontaneous cleavage of glucose, fructose, sucrose, and trehalose in water, and the catalytic proficiencies of invertase and trehalas". In: *Journal of the American Chemical Society* 130.24 (June 2008), pp. 7548–7549. ISSN: 1520-5126. DOI: 10.1021/ja802206s. URL: https://doi.org/10.1021/ja802206s.

[116] Felix Wong et al. "Structural conditions on complex networks for the Michaelis–Menten input–output response". In: *Proceedings of the National Academy of Sciences* 115.39 (2018), pp. 9738–9743. ISSN: 0027-8424. DOI: 10.1073/pnas.1808053115. eprint: https://www.pnas.org/content/115/39/9738.full.pdf. URL: https://www.pnas.org/content/115/39/9738.

[117] Fangzhou Xiao, Mustafa Khammash, and John C. Doyle. "Stability and Control of Biomolecular Circuits through Structure". In: *2021 American Control Conference (ACC)*. 2021, pp. 476–483. DOI: 10.23919/ACC50511.2021.9483039.

[118] Fangzhou Xiao et al. "Coupled Reaction Networks for Noise Suppression". In: *2019 American Control Conference (ACC)*. 2019, pp. 1547–1554. DOI: 10.23919/ACC.2019.8815179.

[119] Polly Y. Yu and Gheorghe Craciun. "Mathematical Analysis of Chemical Reaction Systems". In: *Israel Journal of Chemistry* 58.6-7 (2018), pp. 733–741. DOI: https://doi.org/10.1002/ijch.201800003. eprint: https://onlinelibrary.wiley.com/doi/pdf/10.1002/ijch.201800003. URL: https://onlinelibrary.wiley.com/doi/abs/10.1002/ijch.201800003.

[120] Liping Zhao. "The gut microbiota and obesity: from correlation to causality". In: *Nature Reviews Microbiology* 11.9 (2013), pp. 639–647.

[121] K. Zhou and J.C. Doyle. *Essentials of Robust Control*. Pearson, London, UK, 1997.

[122] Ronghui Zhu et al. "Synthetic multistability in mammalian cells". In: *Science* 375.6578 (2022), eabg9765. DOI: 10.1126/science.abg9765. eprint: https://www.science.org/doi/pdf/10.1126/science.abg9765. URL: https://www.science.org/doi/abs/10.1126/science.abg9765.

[123] Gunter M. Ziegler. *Lectures on Polytopes*. Springer, 2003. DOI: 10.1007/978-1-4613-8431-1.